

# **Transition Metal Complexes Bearing Hemilabile Pincer Ligands: Towards Enhanced Catalytic Activity**

Ashwin Gopalan Nair

A thesis in fulfilment of the requirements of the degree of

**Doctor of Philosophy**



**MACQUARIE**  
University  
SYDNEY · AUSTRALIA

Department of Chemistry and Biomolecular Sciences

Macquarie University

Australia

November 2016

## Preface

---

This thesis is a report of original research undertaken by the author and is submitted for the admission to the degree of Doctor of Philosophy at Macquarie University. This work was performed in the Department of Chemistry and Biomolecular Sciences at Macquarie University and the School of Chemistry at the University of New South Wales during the period of March 2013 to August 2016. The work and results presented in this thesis are those of the author, unless otherwise acknowledged.

Sections of this work have been published:

Chapter 2:

Nair, A. G., McBurney, R. T., Walker, D. B., Page, M. J., Gatus, M. R. D., Bhadbhade, M., Messerle, B. A. *Dalton Trans.*, 2016, **45**, 14335-14342.

Chapter 3 and 4 in this work are under the process of submission for publication in a peer reviewed journal.

Sections of this work has been presented at scientific conferences:

Ru and Ni Complexes of Hemilabile Pincer Ligands Containing a Central NHC donor

Ashwin GOPALAN NAIR and Barabara A. MESSERLE

University of New South Wales, Sydney, Australia, August 2014, Poster presentation.

26<sup>th</sup> International Conference on Organometallic Chemistry,

Sapporo, Japan, July 2014, Poster presentation.

Ru and Ni Complexes of Hemilabile Pincer Ligands Containing a Central NHC donor

Ashwin GOPALAN NAIR, Michael J. Page and Barabara A. MESSERLE

University of New South Wales, Sydney, Australia, August 2014, Poster presentation

IC'13-RACI Inorganic Chemistry Divisional Conference,

Brisbane, Australia, December 2013, Poster presentation.

Transition Metal Complexes with Pincer Ligands as Highly Active Catalysts

Ashwin GOPALAN NAIR, Michael J. Page, Barney Walker and Barabara A. MESSERLE

Macquarie University, Sydney, Australia, November 2015, Oral presentation

*28<sup>th</sup> Reactive Organometallics Symposium*

Transition Metal Complexes with Pincer Ligands as Highly Active Catalysts

Ashwin GOPALAN NAIR, Michael J. Page, Barney Walker and Barabara A. MESSERLE

University of New South Wales, Sydney, Australia, November 2014, Oral presentation

*26<sup>th</sup> Reactive Organometallics Symposium*

Transition Metal Complexes containing Hemilabile Pincer Ligands as Highly Active Catalysts

Ashwin GOPALAN NAIR, Barney Walker, Mark Gatus and Barabara A. MESSERLE

University of Sydney, Sydney, Australia, December 2015, Oral presentation

*9<sup>th</sup> Australasian Organometallics Meeting (OZOM IX)*

## Acknowledgements

---

Many thanks to my supervisor Prof. Barbara Messerle (Macquarie University, Australia) for the tremendous support and outstanding supervision over the years in my project. Under her supervision, I have learned to overcome difficult challenges and attained a number of valuable skills. This project has allowed me to travel to and learn from places inside and outside Australia and has been a marvelous, challenging and irreplaceable experience.

I am grateful for the different facilities that were available at both UNSW and Macquarie Universities. The great expertise of Dr. Douglas Lawes, Dr. Donald Thomas and Dr. Erika Davies has been a wonderful help for a majority of this project. Thank you to Dr. Mohan Bhadbhade from the UNSW analytical centre for evaluation of X-ray crystal structures. I would like to acknowledge Dr. Samantha Binding and Mathew Patterson for additional help in evaluation of crystal structures. Big thanks to Dr. Christopher McRae of Macquarie university for help with GC-MS and elemental analyses.

I would like to express my gratitude to all post-doctoral fellows, Dr. Michael. J. Page, Dr. Barney Walker, Dr. Samantha Binding, Dr. Roy McBurney and Dr. Mark Gatus who have helped me over the years. A special thank you to Dr. Mark Gatus for mentoring me and going beyond the call of duty for a large section of this project. I would like to also thank Dr. Sandra Choy for providing feedback and proof reading this thesis.

To all the members of the BAM group that have been with me over the years; Andrey, Yeng, Mark, Chin, Matt P, Ralph, Vera, Sandy and Andrew, thank you for the great help over the period of the project and providing a safe and enjoyable atmosphere. A special thanks to Ralph for always being there to help and patiently dealing with my troubles.

A great thank you to all friends in my badminton group BISA, especially my coaches Bernhard Halim and Raymond Tam for supporting me for three years.

None of this would be possible without my loving parents and big brother who have given an immeasurable amount of support and love and made me what I am today. Thanks to my mother for struggling to take care of me for so many years. I would also like to express great gratitude to my father and brother for giving me so much strength over the years.

Ashwin Gopalan Nair

(November 2016)

## List of Abbreviations

---

Ar	aryl
acac	acetylacetonato
$\text{BAr}_4^{\text{F}}$	<i>tetrakis</i> [3,5- <i>bis</i> (trifluoromethyl)phenyl]borate anion
bar	reaction pressure in bar
$\text{BPh}_4$	<i>tetra</i> -phenylborate anion
bpm	<i>bis</i> (pyrazolyl)methane
br	broad (NMR)
$^t\text{Bu}$	tert-butyl
$^{\circ}\text{C}$	degrees celcius
cat	catalyst
CO	carbon monoxide
COD	1,5-cyclooctadiene
$\text{C}_2\text{D}_2\text{Cl}_4$	deuterated 1,1,2,2-tetrachloroethane
conv.	conversion (%)
$\delta$	chemical shift (ppm)
d	doublet (NMR)
DCM	dichloromethane
dppe	1,2-bis(diphenylphosphino)ethane
dppp	1,3-bis(diphenylphosphino)propane
equiv.	equivalent
ee	enantiomeric excess

ESI-MS	ElectroSpray Ionisation Mass Spectrometry
Et	ethyl
Et <sub>2</sub> O	diethyl ether
EtOAc	ethyl acetate
fwhm	full width at half maximum
GC-MS	Gas Chromatography-Mass Spectrometry
h	hour
Hz	hertz
HMBC	Heteronuclear Multiple Bond Coherence (NMR)
HSQC	Heteronuclear Single Quantum Coherence (NMR)
<i>i</i>	ipso
<sup>i</sup> Pr	isopropyl
IR	infrared
<i>J</i>	scalar coupling constant (NMR)
L	ligand
m	multiplet (NMR)
<i>m</i>	<i>meta</i>
Me	methyl
MeOH	methanol
min	minute(s)
mol	mole
mmol	millimoles

m/z	mass to charge ratio
nbd	norbornadiene
<i>NCN</i>	pincer ligands with nitrogen-carbon-nitrogen donor atoms
<i>NCN<sup>Et</sup></i>	pyrazolyl-imidazolyl-pyrazolyl ligand (ethylene linker)
<i>NCN<sup>Me</sup></i>	pyrazolyl-imidazolyl-pyrazolyl ligand (methylene linker)
NEt <sub>3</sub>	triethylamine
NHC	N-heterocyclic carbene
<i>NNN</i>	pincer ligands with Nitrogen-Nitrogen-Nitrogen donor atoms
NMR	Nuclear Magnetic Resonance
<i>o</i>	ortho
ORTEP	Oak Ridge Thermal Ellipsoid Plot (Program)
OTf	triflate
<i>p</i>	<i>para</i>
<i>PCP</i>	pincer ligands with Phosphorous-Carbon-Phosphorous donor atoms
PHOX	phosphinooxazolines
<i>PN</i>	bidentate ligands with Phosphorous-Nitrogen donor atoms
<i>PNP</i>	pincer ligands with Phosphorous-Nitrogen-Phosphorous donor atoms
<i>PNN</i>	pincer ligands with Phosphorous-Nitrogen-Nitrogen donor atoms
Ph	phenyl
ppm	parts per million
Py	pyridine
Pz	pyrazole



q	quartet (NMR)
RT	room temperature
s	singlet (NMR)
S/C	substrate to catalyst ratio
t	triplet (NMR)
THF	tetrahydrofuran
TOF	turnover frequency
Tol	toluene
Triphos	bis(2-diphenylphosphinoethyl)phenylphosphine
U.V.	Ultraviolet
VT	variable temperature

# Table of Contents

---

Preface	i
Acknowledgements	iii
List of Abbreviations	v
Table of Contents	ix
List of Figures	xvi
List of tables	xix
List of Schemes	xxi
Abstract	xxv
 Chapter 1. Introduction	
1.1. Organometallic complexes in catalysis	1
1.2. Transition metal catalyst design	3
1.2.1. The metal centre	3
1.2.1.1. Ruthenium, nickel and gold as active and air/moisture stable catalysts	3
1.2.2. Ligand properties	4
1.2.2.1. N-Heterocyclic carbenes (NHCs)	4
1.2.2.2. Nitrogen donor ligands	6
1.2.2.3. Tridentate ligands	7

1.2.2.4. Hemilabile pincer ligands	8
1.2.3. Counterions	11
1.3. Transition metal complexes in homogeneous catalysis	12
1.3.1. Transition metal catalysed H <sub>2</sub> addition to a polar unsaturated bond	12
1.3.2. Transition metal catalysed C-C bond coupling reactions	14
1.3.3. Transition metal catalysed X-H bond addition reactions	16
1.4. Objectives	20
1.5. References	23
<b>Chapter 2. Ru(II) complexes of hemilabile pincer ligands for catalysed transfer hydrogenation reactions</b>	
2.1. Introduction	27
2.1.1. Transition metal catalysed hydrogenation reaction	27
2.1.2. Ruthenium catalysed hydrogenation reactions	27
2.1.3. Transfer hydrogenation as an alternative to hydrogenation reactions	29
2.1.4. Transition metal complexes containing pincer ligands for the transfer hydrogenation of ketones	30
2.1.5. Ruthenium complexes containing pincer ligands for the transfer hydrogenation reaction	31
2.1.6. Ruthenium complexes containing hemilabile ligands	33
2.1.7. Ruthenium complexes containing hemilabile pincer ligands	35
2.1.8. Ruthenium complexes of pincer ligands with a central NHC donor	36

2.1.9. Rhodium and Iridium complexes with pincer ligands	37
2.2. Aims of this chapter	39
2.3. Synthesis of Ru(II) complexes containing a hemilabile $NCN^{Me}$ pincer ligand	40
2.3.1. Synthesis and characterisation of $[Ag(I)(NCN^{Me})_2]BPh_4$ ( <b>2</b> )	40
2.3.2. Synthesis and characterisation of $[Ru(II)(\eta^6-C_6H_6)(NCN^{Me})Cl]BPh_4$ ( <b>3</b> )	42
2.3.3. Synthesis and characterisation of $[Ru(II)(\eta^6-C_{10}H_{14})(NCN^{Me})Cl]BPh_4$ ( <b>4</b> )	44
2.3.4. Synthesis and characterisation of $[Ru(II)(H)CO(NCN^{Me})(PPh_3)_2]BPh_4$ ( <b>5</b> )	47
2.3.4.1. Isomerisation reaction of $[Ru(II)(H)CO(NCN^{Me})(PPh_3)_2]$ ( <b>5</b> )	49
2.3.4.2. Synthesis of an unexpected cubane structure $[Ru(I)Cl(PPh_3)]_4$ ( <b>6</b> )	50
2.3.5. Synthesis and characterisation of $[Ru(II)(NCN^{Me})_2]BPh_4$ ( <b>7</b> )	52
2.3.6. Comparison of solid state structures	55
2.4. Catalysed transfer hydrogenation of ketones using complexes <b>3</b> , <b>4</b> , <b>4a</b> , <b>5</b> , <b>5a</b> and <b>7</b>	57
2.5. Conclusions	64
2.6. References	66
<b>Chapter 3. Ni(II) complexes of hemilabile pincer ligands for catalysed Kumada cross coupling reactions</b>	
3.1. Introduction	70
3.1.1. Transition metal catalysed C-C bond formation reactions	70
3.1.2. Catalysts for the Kumada cross coupling reactions	71
3.1.3. The mechanisms of Kumada cross coupling reactions	75

3.1.4. Nickel complexes containing pincer ligands as catalysts for the Kumada cross coupling reaction: ligand effects	76
3.1.4.1. Electron donating ability and its effects on catalytic activity	77
3.1.4.2. Pincer ligands with strongly coordinating side arm donors	78
3.1.4.3. Pincer ligands with weakly coordinating side arms: towards hemilability	80
3.2. Aims of this chapter	83
3.3. Synthesis of Ni(II) complexes containing an $NCN^{Me}$ hemilabile pincer ligand	84
3.3.1. Synthesis, characterisation and coordination study of $[Ni(NCN^{Me})Cl].BPh_4$ ( <b>8</b> )	84
3.3.2. Coordination chemistry of $[Ni(NCN^{Me})Cl]BPh_4$	90
3.3.3. Synthesis and characterisation of $(NCN^{Me})PF_6$ ( <b>1b</b> )	93
3.3.4. Synthesis and characterisation of $[Ni(NCN^{Me})Cl]PF_6$ ( <b>9</b> )	94
3.3.5. Synthesis and characterisation of $[Ni(NCN^{Et})_2](BPh_4)_2$ ( <b>10</b> )	96
3.3.6. Comparison of the inner coordination sphere of complexes <b>8</b> , <b>9</b> and <b>10</b> .	102
3.4. Catalytic activity of Ni(II) complexes for Kumada cross coupling of aryl halides	103
3.4.1. Catalytic activity of <b>8</b> , <b>9</b> and <b>10</b> for Kumada cross coupling reactions of chlorobenzene and bromobenzene	104
3.4.2. Substrate scope of complex <b>8</b> for the Kumada cross coupling reaction	106
3.5. Conclusions	109
3.6. References	111

Chapter 4. Gold(I) and Gold(III) complexes of hemilabile pincer ligands for catalysed  
activation of alkynes

4.1.	Introduction	114
4.1.1.	Transition metal catalysed addition of X-H bonds to alkynes	114
4.1.1.1.	Transition metal catalysed hydroalkoxylation reactions	114
4.1.1.2.	Transition metal catalysed hydroamination reactions	118
4.1.2.	Transition metal complexes containing pincer ligands for catalysed addition of X-H bonds to alkynes	119
4.1.2.1.	Transition metal complexes containing pincer ligands as catalysts for hydroalkoxylation reactions	120
4.1.2.2.	Transition metal catalysts containing pincer ligands for hydroamination reactions	122
4.1.2.3.	Metal complexes containing hemilabile pincer ligands for the addition of X-H bonds to the C-C multiple bond of alkenes or alkynes	124
4.2.	Aims of this chapter	125
4.3.	Synthesis of Gold(I) and Gold(III) complexes containing an $NCN^{Me}$ hemilabile pincer ligand	127
4.3.1.	Synthesis and characterisation of $[Au(I)(NCN^{Me})Cl]BPh_4$ ( <b>11</b> )	127
4.3.2.	Synthesis and characterisation of $[Au(III)(NCN^{Me})Cl]BPh_4$ ( <b>12</b> )	128
4.3.3.	Comparison of the solid state structures of <b>11</b> and <b>12</b>	130
4.3.4.	Attempted synthesis of Au(I)/Rh(I) bimetallic complexes	132

4.4.	Catalysed hydroalkoxylation reactions using complexes <b>11</b> and <b>12</b> .	135
4.4.1.	Catalysed dihydroalkoxylation of 2-(5-hydroxypent-1-ynyl)benzylalcohol ( <b>14</b> ).	135
4.4.2.	Catalyst scope: investigating substrates with varying structure ( <b>15, 16</b> )	146
4.5.	Catalysed hydroamination reactions using complexes <b>11</b> and <b>12</b> .	148
4.5.1.	Intramolecular hydroamination reactions catalysed by complexes <b>11</b> and <b>12</b> .	149
4.5.2.	Intermolecular hydroamination reactions catalysed by complexes <b>11</b> and <b>12</b>	153
4.6.	Conclusions	156
4.7.	References	157
 <b>Chapter 5. Conclusions and Future work</b>		
5.1.	Conclusions	161
5.1.1.	Chapter 2	161
5.1.2.	Chapter 3	163
5.1.3.	Chapter 4	164
5.2.	Future work	166
 <b>Chapter 6. Experimental</b>		
General Procedures		169
6.1.	Experimental for Chapter 2	171
6.1.1.	Synthesis of Ru(II) complexes	171

6.1.2. Catalysed transfer hydrogenation reactions using Ru(II) complexes <b>3-6</b> .	177
<b>General procedure for transfer hydrogenation reactions</b>	177
6.1.3. Crystal data for chapter 2	183
6.2. Experimental for chapter 3	184
6.2.1. Synthesis of Ni(II) complexes	184
6.2.2. Catalysed Kumada cross coupling reactions using complexes <b>8, 9</b> and <b>10</b> .	187
6.2.3. Crystal data for chapter 3	193
6.3. Experimental for chapter 4	197
6.3.1. Synthesis of Au(I) and Au(III) complexes	197
6.3.2. Catalysed dihydroalkoxylation reactions using complexes <b>11</b> and <b>12</b>	198
6.3.3. Catalysed hydroamination reactions using complexes <b>11</b> and <b>12</b>	209
6.3.4. Crystal data for chapter 4	215
6.4. References:	217
<b>Appendices in CD</b>	



## List of Figures

---

Figure 1.1 General structures of imidazolyliidenes and imidazolinyliidenes .....	5
Figure 1.2 Typical N-donor ligand systems.....	7
Figure 1.3 Common motifs of pincer ligands .....	8
Figure 1.4 Varying coordination strengths of counterions.....	12
Figure 1.5 Pharmaceutical compounds containing nitrogen/oxygen heterocycles.....	17
Figure 2.1 Early examples of hydrogenation catalysts: a) Crabtrees catalyst, and b) (S)-iPr– PHOX. ....	27
Figure 2.2 Ligand selective hydrogenation of ketones. ....	28
Figure 2.3 Early Ru(II) catalysts for the transfer hydrogenation reaction, left: Schvo’s catalyst, right: Ru(II)arene complex containing a <i>PN</i> bidentate ligand. ....	30
Figure 2.4 Recent examples of catalysts for the transfer hydrogenation reaction a) [Co(II)( <i>PBP</i> )N <sub>2</sub> ], b) [Fe(II)( <i>PNP</i> )CO(H)Br], and c) [Ir(III)( <i>PNP</i> )H <sub>2</sub> ]. ....	31
Figure 2.5 Ru(II) complexes containing pincer ligands by, a) van Koten and b) Milstein. ....	32
Figure 2.6 Best catalyst for transfer hydrogenation of ketones. ....	32
Figure 2.7 Transfer hydrogenation of ketones catalysed by Ru(II) complexes with hemilabile pincer ligands.....	36
Figure 2.8 Comparison of other carbene-based ligands with pendant N-heterocyclic donor groups.. ....	38
Figure 2.9 X-ray crystal structure of the imidazolium bis-pyrazole ligand <b>1</b> . ....	40
Figure 2.10 ORTEP depiction of the structure of complex <b>2</b> with ellipsoids at 50% probability.....	42

Figure 2.11 ORTEP depiction of the structure of complex <b>3</b> showing atom labeling scheme..	44
Figure 2.12 ORTEP depiction of the structure of complex <b>4a</b> showing atom labeling scheme.	45
Figure 2.13 $^1\text{H}$ NMR spectrum of $\text{Ru(II)}(\eta^6\text{-C}_{10}\text{H}_{14})(\text{NCN}^{\text{Me}})\text{Cl}]\text{BPh}_4[\text{B}_5\text{O}_6(\text{OH})_4]$ .	46
Figure 2.14 ORTEP depiction of the structure of complex <b>5</b> showing atom labeling scheme.	49
Figure 2.15 Stacked $^1\text{H}$ NMR spectra of the hydride resonance regions at 72 °C for complexes <b>5</b> and <b>5a</b> . (H trans to pyrazole + H cis to pyrazole).	50
Figure 2.16 Molecular structure of complex <b>6</b> showing atom labeling scheme..	51
Figure 2.17 Variable temperature $^1\text{H}$ NMR spectra of $[\text{Ru(II)}(\text{NCN}^{\text{Me}})_2](\text{BPh}_4)_2$ ( <b>7</b> ) showing the isomerisation between the <i>fac</i> isomer ( <b>7</b> ) and <i>mer</i> isomer ( <b>7a</b> ).	54
Figure 2.18 Facial and meridional coordination modes of $[\text{Ru(II)}(\text{NCN}^{\text{Me}})_2](\text{BPh}_4)_2$ .	55
Figure 2.19 ORTEP depiction of the solid state structure of complex <b>7</b> at 50% probability thermal ellipsoids showing the <i>fac</i> coordination..	55
Figure 3.1 Ni(II) complexes containing pincer ligands with strongly coordinating NHC donors.	79
Figure 3.2 ORTEP depiction of complex <b>8</b> with 50 % probability ellipsoids for all non-hydrogen atoms..	86
Figure 3.3 D-orbital energy level diagrams of the d-orbital electrons arising from different conformations possible for complexes of nickel(II).	87
Figure 3.4 Variable temperature NMR (600 MHz, acetone- $\text{d}_6$ ) of complex <b>8</b> .	89
Figure 3.5 Different conformations possible for complex <b>8</b> .	90

Figure 3.6 $^1\text{H}$ NMR (500 MHz, acetone- $\text{d}_6$ , 25 °C) stacked plots of <b>8</b> reacting with hard donor ligands. (a) xylisocyanide, (b) pyridine, (c) $\text{PMe}_3$ , (d) CO, (e) complex <b>8</b> . ....	91
Figure 3.7 ORTEP depiction of complex <b>9</b> with 50 % probability ellipsoids for all non-hydrogen atoms.. ....	96
Figure 3.8 ORTEP depiction of ligand <b>1c</b> with 50% probability ellipsoids for all non-hydrogen atoms.. ....	97
Figure 3.9 Variable temperature $^1\text{H}$ NMR spectra (600 MHz, Acetone- $\text{d}_6$ ) of complex <b>10</b> ...	100
Figure 3.10 ORTEP depiction of complex <b>10</b> with 50% probability ellipsoids for all non-hydrogen atoms.. ....	101
Figure 4.1 ORTEP depiction of the solid state structure of complex <b>11</b> at 50% probability thermal ellipsoids.. ....	128
Figure 4.2 ORTEP depiction of the solid state structure of complex <b>12</b> at 50% probability thermal ellipsoids.. ....	130
Figure 4.3 ORTEP depiction of complex <b>11</b> showing the distance between pyrazole nitrogens. ....	131
Figure 4.4 $^1\text{H}$ NMR (600MHz, acetone- $\text{d}_6$ ) of complex <b>11</b> .....	133
Figure 4.5 Variable temperature $^1\text{H}$ NMR (400MHz, acetone- $\text{d}_6$ ) of heterobimetallic complex <b>13</b> .....	134
Figure 4.6 Comparison in catalytic activity of <b>12</b> with complexes in literature. <sup>32 34</sup> .....	142
Figure 5.1 Ru(II) complex bearing a ligand with a boronate pendant arm .....	166

## List of tables

---

Table 2.1 Selected bond lengths (Å) and angles (°) for <b>3</b> , <b>4a</b> , <b>5</b> , and <b>7</b> .	56
Table 2.2 Catalytic transfer hydrogenation of ketones using complexes <b>4a</b> and <b>4</b> .	63
Table 3.1 Selected bond lengths (Å) and angles (°) for <b>8</b> , <b>9</b> and <b>10</b> .	102
Table 3.2 Kumada cross coupling reactions of PhBr and PhCl with PhMgBr catalysed by <b>8</b> , <b>9</b> and <b>10</b> .	104
Table 3.3 Catalysed Kumada cross coupling of PhCl and PhBr using <b>8</b> at different catalyst loadings.	106
Table 3.4 Range of substrates catalysed by <b>8</b> for Kumada cross coupling reactions.	107
Table 4.1 Selected bond lengths(Å) and angles(°) for <b>11</b> and <b>12</b> .	131
Table 4.2 Comparison of Au(I) vs Au(III) catalysts and the effect of counterion.	139
Table 4.3 Summary of intramolecular hydroamination reactions of 4-pentyne-1-amine ( <b>17</b> ) and 5-phenyl-4-pentynamine ( <b>18</b> ) using complexes <b>11</b> and <b>12</b> .	152
Table 6.1 Quantities of acetophenone and catalyst used.	178
Table 6.2 Quantities of catalyst <b>4</b> and substrates used at 82 °C.	180
Table 6.3 Quantities of catalyst <b>4</b> and substrates used at RT.	181
Table 6.4 Quantities of catalyst <b>4a</b> and substrates used at 82 °C.	181
Table 6.5 Quantities of catalyst <b>4a</b> and substrates used at RT.	182
Table 6.6 Quantities of catalyst <b>4a</b> and substrates used for <sup>i</sup> PrOH/THF solvent mix..	182
Table 6.7 Quantities of catalyst and chlorobenzene and PhMgBr used.	189
Table 6.8 Quantities of catalyst, bromobenzene and PhMgBr used.	189
Table 6.9 Quantities of catalyst and iodobenzene and PhMgBr used.	190

Table 6.10 Quantities of catalyst and substrates used.....	190
Table 6.11 Quantities of catalyst <b>8</b> and substrates used.....	192
Table 6.12 Quantities of catalyst and substrate <b>14</b> used. ....	199
Table 6.13 Quantities of catalyst <b>12</b> , NaBAR <sup>F</sup> <sub>4</sub> and substrate <b>14</b> used. ....	201
Table 6.14 Quantities of catalyst, NaBAR <sup>F</sup> <sub>4</sub> and substrate <b>14</b> used. ....	203
Table 6.15 Quantities of catalyst, NaBAR <sup>F</sup> <sub>4</sub> , AgSbF <sub>6</sub> and substrate <b>14</b> used.....	204
Table 6.16 Quantities of catalyst and substrate <b>15</b> used. ....	206
Table 6.17 Quantities of catalyst and substrate <b>14</b> , <b>15</b> used.. ....	207
Table 6.18 Quantities of catalyst and substrate <b>16</b> used. ....	209
Table 6.19 Quantities of catalyst and substrate <b>17</b> used at RT.....	210
Table 6.20 Quantities of catalyst and substrate <b>17</b> used at 70 °C. ....	211
Table 6.21 Quantities of catalyst and substrate <b>17</b> used at 100 °C. ....	211
Table 6.22 Quantities of catalyst and substrate <b>18</b> used.. ....	212
Table 6.23 Quantities of catalyst and substrate <b>19/19a</b> used at 100 °C.....	213
Table 6.24 Quantities of catalyst and substrate <b>19/19a</b> used at 70 °C.....	214

## List of Schemes

---

Scheme 1.1 Monsanto process.....	1
Scheme 1.2 Homogeneous transition metal catalysts for the hydrogenation reaction of alkenes.. .....	63
Scheme 1.3 Regioselective hydrogenation of quinaxoline.....	102
Scheme 1.4 Pd and Rh complexes with an <i>SNS</i> hemilabile pincer ligand.....	9
Scheme 1.5 Complexes containing hemilabile pincer ligands.....	10
Scheme 1.6 Ru(II) complex with a NNP hemilabile pincer ligand.. .....	11
Scheme 1.7 Typical hydrogenation and dehydrogenative coupling reactions.. .....	13
Scheme 1.8 Transition metal catalysed hydrogenation reactions... .....	13
Scheme 1.9 Synthetic production of terpenes.. .....	14
Scheme 1.10 Conversion of steroid ethers to 6-methyl steroids.....	14
Scheme 1.11 Pd and Ni catalyzed coupling reactions.....	16
Scheme 1.12 Dihydroalkoxylation of alkyne diols and hydroamination of alkynamines.....	17
Scheme 1.13 X-H bond addition reactions catalyzed by simple metal complexes.....	18
Scheme 1.14 X-H bond addition reactions catalyzed by copper complexes.....	19
Scheme 2.1 First reported hemilabile ligand coordinated to Ru(II) and its reactivity to CO... .....	34
Scheme 2.2 Ru(II) complexes containing hemilabile monophosphite ligands.....	34
Scheme 2.3 Ru(II) complexes containing a pincer ligand with a central NHC donor.....	37
Scheme 2.4 Synthesis of imidazolium bis-pyrazole ligand <b>1</b> from chloromethylpyrazole and trimethylsilyl imidazole.. .....	40

Scheme 2.5 Synthesis of $[\text{Ag}(\text{I})(\text{NCNMe})_2]\text{BPh}_4$ ( <b>2</b> ).....	41
Scheme 2.6 Synthesis of $[\text{Ru}(\text{II})(\eta^6\text{-C}_6\text{H}_6)(\text{NCN}^{\text{Me}})\text{Cl}]\text{BPh}_4$ ( <b>3</b> ) from <b>2</b> .....	43
Scheme 2.7 Synthesis of $[\text{Ru}(\eta^6\text{-C}_{10}\text{H}_{14})(\text{NCN}^{\text{Me}})\text{Cl}]\text{BPh}_4[\text{B}_5\text{O}_6(\text{OH})_4]$ ( <b>4a</b> ).....	45
Scheme 2.8 Synthesis of $[\text{Ru}(\text{II})(\eta^6\text{-}p\text{-cym})(\text{NCN}^{\text{Me}})\text{Cl}]\text{BPh}_4$ ( <b>4</b> ).....	47
Scheme 2.9 Synthesis of $[\text{Ru}(\text{H})\text{CO}(\text{NCN}^{\text{Me}})(\text{PPh}_3)_2]\text{BPh}_4$ ( <b>5</b> ) from <b>1</b> .....	48
Scheme 2.10 Synthesis of $[\text{Ru}(\text{II})(\text{NCN}^{\text{Me}})_2](\text{BPh}_4)_2$ ( <b>7</b> ).....	52
Scheme 3.1 Kumada cross coupling as a key synthetic step in the production of (a) Aliskiren and (b) polythiophenes.....	71
Scheme 3.2 Kumada cross coupling reactions catalysed by: (a) an in situ generated bis- oxazoline Ni(II) complex, (b) a pre-prepared Ni(II) catalyst and (c) an iron(III) catalyst... .....	73
Scheme 3.3 Recent Pd(II) and Ni(II) catalysed Kumada cross coupling reactions.....	74
Scheme 3.4 Selective Kumada cross coupling reactions.....	75
Scheme 3.5 Kumada coupling mechanisms: a) conventional mechanism and b) mechanism with Ni(IV) intermediate.. ..	76
Scheme 3.6 Effect of varying electron donating abilities of ligands used in Ni(II) catalysed Kumada cross coupling reactions: (a) coupling of alkyl Grignard reagents; (b) coupling of aryl Grignard reagents.. ..	78
Scheme 3.7 Ni(II) complexes containing pincer ligands with tunable catalytic properties....	80
Scheme 3.8 Ni(II) hemilabile complexes of pincer ligands containing a single NHC donor...	82
Scheme 3.9 Ni(II) complex of a pincer ligand with a central NHC donor... ..	82
Scheme 3.10 Synthesis of $[\text{Ni}(\text{NCN}^{\text{Me}})\text{Cl}]\text{BPh}_4$ ( <b>8</b> ).....	84

Scheme 3.11 Proposed equilibrium between the square planar and tetrahedral conformations of complex <b>8</b> .....	87
Scheme 3.12 Equilibrium between the square planar and tetrahedral conformations of $\text{Ni(PPh}_3)_2\text{Cl}_2$ .....	88
Scheme 3.13 Synthesis of NCN pincer ligand $(\text{NCN}^{\text{Me}})\text{PF}_6$ ( <b>1b</b> )... ..	94
Scheme 3.14 Synthesis of $[\text{Ni}(\text{NCN}^{\text{Me}})\text{Cl}]\text{PF}_6$ ( <b>9</b> ).....	94
Scheme 3.15 Synthesis of $(\text{NCN}^{\text{Et}})\text{BPh}_4$ ( <b>1c</b> ).....	97
Scheme 3.16 Synthesis of $[\text{Ni}(\text{NCN}^{\text{Et}})_2](\text{BPh}_4)_2$ ( <b>10</b> ).....	98
Scheme 3.17 Kumada cross coupling reactions of PhBr and PhCl with PhMgBr catalysed by <b>8</b> , <b>9</b> and <b>10</b> .....	104
Scheme 4.1 Examples of Pd(II) catalysed hydroalkoxylation reactions.(a) aromatic alkynes, <sup>6</sup> (b) aromatic and alkyl substituted alkynes, <sup>7</sup> (c) disubstituted aromatic alcohols. <sup>8</sup> .....	115
Scheme 4.2 Cu(I) catalysed intramolecular hydroamination of alkynyl alcohols.....	115
Scheme 4.3 Rh(I) and (Ir) catalysts synthesised in the Messerle group for the dihydroalkoxylation reaction... ..	116
Scheme 4.4 Catalysed dihydroalkoxylation of alkyne diols.....	116
Scheme 4.5 (a) Intermolecular hydroalkoxylation catalysed by $\text{Au(PPh}_3)_3\text{Me}$ . (b) Intramolecular hydroalkoxylation catalysed by $\text{LAuNCMe}$ ... ..	117
Scheme 4.6 Au(I) catalysed intramolecular dihydroalkoxylation of alkyne diols.....	118
Scheme 4.7 Samarium catalyst for the intramolecular hydroamination of aminoalkynes... ..	118
Scheme 4.8 Rh(I) and Ir(I) catalysts for the hydroamination reaction of 4-pentyn-1-amine... ..	119



Scheme 4.9 Highly active Au(I) catalyst for the intermolecular hydroamination reaction...	119
Scheme 4.10 (a) First example of a Ru(II) catalysed intermolecular addition of allyl alcohols to acetylenes. (b) An iridium complex bearing a PCP pincer ligand for the hydroaryloxylation reaction of olefins .....	121
Scheme 4.11 Key Pd(II) intermediate stabilised by the tridentate coordination of PON or POP pincer ligands.....	122
Scheme 4.12 (a) Ir(III) catalyst with a pincer ligand for the hydroamination of 2-alkynylanilines. (b) Ti catalyst with a pincer ligand for the hydroamination of alkenes.. .....	123
Scheme 4.13 Ti catalyst used for three component intermolecular hydroamination reactions... ..	123
Scheme 4.14 Hemilabile magnesium pincer catalyst for the hydroamination of aminoalkenes.....	124
Scheme 4.15 Rh(I) catalyst containing the hemilabile pincer ligand <b>1</b> for the hydroalkoxylation of 4-pentynoic acid.....	125
Scheme 4.16 Synthesis of [Au(I)(NCN <sup>Me</sup> )Cl] ( <b>11</b> ).. ..	127
Scheme 4.17 Synthesis of [Au(III)(NCN <sup>Me</sup> )Cl] ( <b>12</b> )... ..	129
Scheme 4.18 Synthesis of a heterobimetallic Au(I)/Rh(I) complex ( <b>13</b> ).....	132

## Abstract

---

This thesis describes the synthesis of new Ag(I), Ru(II), Ni(II), Au(I) and Au(III) complexes containing an imidazolyl-pyrazolyl ligand motif ( $NCN^{Me}$ - methylene linker, and  $NCN^{Et}$ -ethylene linker). The synthesised complexes were tested as catalysts for a number of organic transformations.

Complexes  $[Ag(NCN^{Me})_2]BPh_4$  (**2**),  $[Ru(NCN^{Me})_2](BPh_4)_2$  (**7**),  $[Ru(H)CO(NCN^{Me})(PPh_3)_2]BPh_4$  (**5a**),  $[Ru(H)CO(NCN^{Me})(PPh_3)_2]BPh_4$  (**5**),  $[Ru(\eta^6-C_6H_6)(NCN^{Me})Cl]BPh_4$  (**3**),  $[Ru(\eta^6-C_{10}H_{14})(NCN^{Me})Cl]BPh_4[B_5O_6(OH)_4]$  (**4a**),  $[Ru(\eta^6-C_{10}H_{14})(NCN^{Me})Cl]BPh_4$  (**4**),  $[Ni(NCN^{Me})Cl]BPh_4$  (**8**),  $[Ni(NCN^{Me})Cl]PF_6$  (**9**) and  $[Ni(NCN^{Et})_2](BPh_4)_2$  (**10**),  $[Au(I)(NCN^{Me})Cl]$  (**11**) and  $[Au(III)(NCN^{Me})Cl_3]$  (**12**) were synthesised and fully characterised. Solid state structures of **1a**, **1c**, **2**, **3**, **4a**, **5a**, **6**, **7**, **8**, **9**, **10**, **11** and **12** were analysed using X-ray crystallography. The presence of an unusual boronate counterion  $[B_5O_6(OH)_4]$  and a new Ru(I) compound  $[RuCl(PPh_3)]_4$  were also revealed using X-ray crystallography.

Ruthenium complexes **3**, **4**, **4a**, **5**, **5a** and **7** were tested as catalysts for the transfer hydrogenation reaction of ketones. Complexes containing arene co-ligands  $[Ru(\eta^6-C_6H_6)(NCN^{Me})Cl]BPh_4$  (**3**),  $[Ru(\eta^6-C_{10}H_{14})(NCN^{Me})Cl]BPh_4[B_5O_6(OH)_4]$  (**4a**),  $[Ru(\eta^6-C_{10}H_{14})(NCN^{Me})Cl]BPh_4$  (**4**) were found to be more active catalysts for the organic transformation with  $[Ru(\eta^6-C_{10}H_{14})(NCN^{Me})Cl]BPh_4[B_5O_6(OH)_4]$  (**4a**) exhibiting the best activity showing that the boronate counterion  $[B_5O_6(OH)_4]^-$  enhances catalytic activity. The complexes achieved complete conversions for all substrates within short reaction times (< 1 hr).  $[Ru(\eta^6-C_{10}H_{14})(NCN^{Me})Cl]BPh_4[B_5O_6(OH)_4]$  (**4a**) was catalytically active for the organic transformation at room temperature.

Nickel complexes **8**, **9** and **10** were found to exhibit broad resonances in NMR spectroscopy. Analysis using UV vis spectroscopy and variable temperature NMR spectroscopy revealed that the Ni(II) complexes were diamagnetic in nature and that the broad spectra at room temperature resulted from conformational changes due to the flexible nature of the ligands. All three complexes were tested as catalysts for the Kumada cross coupling reaction of aryl halides with phenylmagnesium bromide. Complexes **8** and **9** containing a tridentate coordination of the pincer ligand were found to be more active for the organic transformation in comparison to the bidentate complex **10**. The choice of counterion was found to alter the activity for the conversion of selected chlorinated and brominated substrates. A reduction in catalyst loading resulted in reduced activity of complex **8** for the conversion of chlorobenzene, whereas a negligible effect was observed for the catalytic conversion of bromobenzene using reduced catalyst loading.

The oxidation states and structure of gold complexes **11** and **12** were determined using X-ray crystallography and UV vis spectroscopy. Both complexes were tested as catalysts for intramolecular dihydroalkoxylation reactions. Both complexes were highly active for the organic transformation, with complex (**12**) showing excellent activity, exceeding TOF values of 18,000 and maintaining high catalytic activity even at room temperature. Direct comparison of Au(I) complex **11** and Au(III) complex **12** showed that **12** was significantly more active for the organic transformation showing that catalytic activity can be altered by changing the oxidation state of the gold catalysts.

Complexes **11** and **12** proved to be highly active for the intramolecular hydroamination reactions of pentyn-4-amine and phenylpentynamine achieving complete conversions

within thirty minutes and moderate conversions for the intermolecular hydroamination reactions of aniline with phenylacetylene.

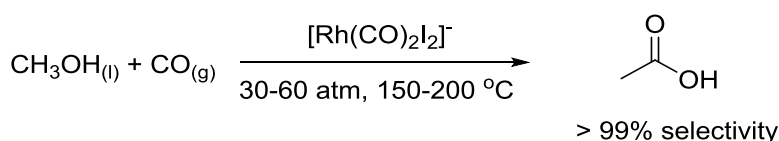
---

# Chapter 1. Introduction

---

### 1.1. Organometallic complexes in catalysis

Organometallic complexes are defined as a chemical species containing at least one bond between a metal and the carbon atom in an organic molecule, ion or substituent group.<sup>1</sup> These complexes have been studied over many years and used as catalysts to modify the routes of organic transformations. The ability of organometallic complexes to influence synthetic reactions has resulted in their use in a wide range of industrial processes. A well-known and important reaction in industry that relies on organometallic catalysts is the Monsanto process. Developed in 1966, the Rh(I) catalysed transformation is used to produce acetic acid from methanol and carbon monoxide (Scheme 1.1).<sup>2</sup>

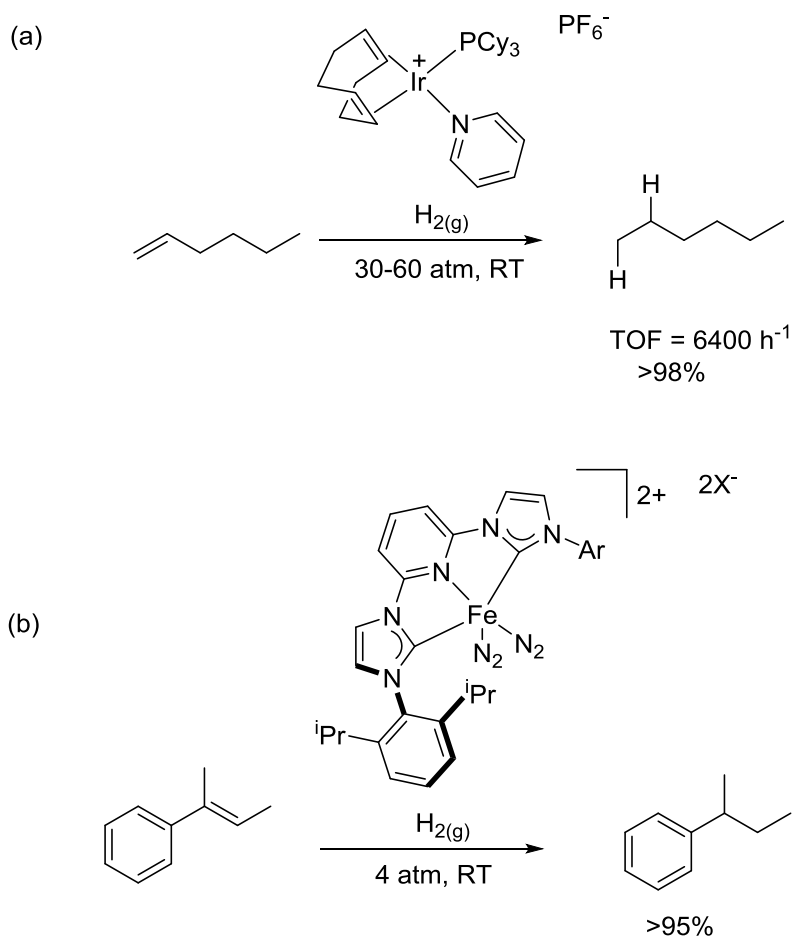


**Scheme 1.1** Monsanto process.

A catalyst is a substance that increases the rate of a reaction by lowering the activation energy without itself being consumed in the reaction.<sup>3</sup> The overall Gibbs free energy of the reaction is not altered by the catalyst, the catalyst merely accelerates the thermodynamically favoured reactions. As the catalyst remains unchanged upon completing the transformation, it can be recycled to complete more organic transformations. Catalysts can also achieve high selectivity in reactions by favouring certain reaction pathways over others.<sup>4</sup>

The production of pharmaceutical products and other high value chemicals often rely on the use of homogeneous catalysts to reduce production costs, minimise use of resources, improve reaction rates and provide milder/safer reaction conditions.<sup>5</sup> Reactions that were

inaccessible through traditional synthetic methods can also be carried out by the use of homogeneous catalysts.<sup>6</sup> For example, the hydrogenation of alkenes requires catalysts to initiate and complete the reaction. Non-catalytic approaches to hydrogenating alkenes require extremely high temperatures and pressures. Homogeneous transition metal catalysts, achieve high turnover frequency (TOF)<sup>7</sup> values (Scheme 1.2a) for the hydrogenation reactions of alkenes, and high conversions at room temperature conditions (Scheme 1.2).<sup>8</sup>



**Scheme 1.2** Homogeneous transition metal catalysts for the hydrogenation reaction of alkenes.

## 1.2. Transition metal catalyst design

Homogeneous transition metal catalysts are particularly useful for modifying the level of reactivity of an organic transformation. This is achieved by modifying different components in the structure of the catalyst, such as the coordination environment of the metal centre, the metal centre itself and the counterion used.

### 1.2.1. The metal centre

The catalytic properties of an organometallic complex are largely defined by the characteristics of the metal centre. Transition metals can exist in various oxidation states, some of which have unfilled d-orbitals which allow them to readily exchange electrons. This allows the metals to easily access substrates and makes them ideal candidates as catalysts for a wide array of organic transformations. Late transition metals are more electronegative in nature and this allows them to withdraw electrons from coordinated bonds. Therefore, unsaturated ligands bound to late transition metals are more likely to undergo nucleophilic attack.<sup>9, 10</sup>

#### 1.2.1.1. Ruthenium, nickel and gold as active and air/moisture stable catalysts

Ruthenium and nickel complexes are highly utilised in industry and since the synthesis of Grubbs' catalyst and Ni(*bis*-phosphino) dichloride complexes,<sup>11</sup> have been extensively investigated as catalysts for a number of organic transformations including hydrogenations and C-C coupling reactions. Complexes of Ru and Ni tend to be highly air and moisture stable in the +II oxidation state.<sup>12</sup> Ni(II) complexes can also be both four, five and six coordinate allowing for a wide range of coordination geometries. Different oxidation states of either ruthenium or nickel can adopt different geometries such as four coordinate



tetrahedral, square planar and six coordinate octahedral geometries. Both ruthenium and nickel are late transition metals that can access multiple oxidation states, which makes them useful as catalysts for organic transformations that involve redox changes at the metal centre during the catalytic cycle, e.g. oxidative addition and reductive elimination.

Similar to ruthenium and nickel complexes, gold complexes are highly air and moisture stable.<sup>13</sup> Gold complexes have received significant attention in catalysis due to their high levels of reactivity and wide applicability for different synthetic reactions.<sup>13</sup> Gold complexes often occur in the +I and +III oxidation states, and can hence access linear or square planar geometries. Gold(I) and gold(III) complexes have the added advantage that the complexes are diamagnetic which allows for easy characterisation of the complexes using NMR spectroscopy.

### 1.2.2. Ligand properties

The catalytic activity of a transition metal catalyst can be greatly affected by the associated ligand. The properties of ligands depend on different factors such as the coordinating strength/labity of donor atoms, type of coordination modes and steric and electronic environments. A number of ligand types are described below.

#### 1.2.2.1. N-Heterocyclic carbenes (NHCs)

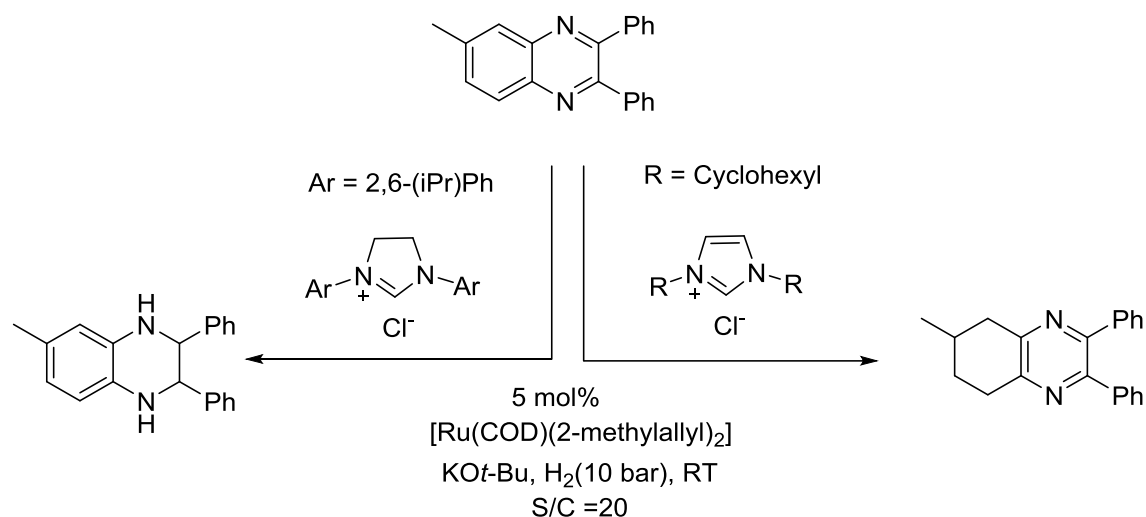
N-Heterocyclic carbenes (NHCs) consist of an  $sp^2$  hybridised six-electron carbene group embedded in an N-heterocyclic ring.<sup>14</sup> NHCs are stronger  $\sigma$  donors than phosphines, which leads to a reduced labity of the ligand and therefore results in complexes of higher thermal stability and robustness than complexes containing phosphine ligands.<sup>15</sup> Due to their potential as strongly coordinating ligands to the metal, NHC bearing transition metal

complexes have been used widely as catalysts for homogeneous and heterogeneous organic transformations.<sup>16</sup> Altering the steric and electronic properties of NHCs has proven to be significantly easier than altering the same properties of phosphines.<sup>17</sup> The most commonly employed NHCs in transition metal catalysts are imidazolylidenes and imidazolinyldenes (Figure 1.1). The coordination chemistry of NHCs bearing the imidazolylidene motif has been studied using a wide array of transition metals.<sup>17</sup> This versatility in coordination allowed transition metal complexes bearing NHC ligands to be used as catalysts in a large number of synthetic reactions, such as C-C bond formation and X-H (X = O, N) bond activation reactions.



**Figure 1.1** General structures of imidazolylidenes and imidazolinyldenes.

Variation of the electronic properties of NHCs used in transition metal complexes as shown in Figure 1.1 (imidazolylidenes compared to imidazolinyldenes) can significantly effect the selectivity of transition metal catalysed reactions. For example, the regioselective hydrogenation of quinoxaline<sup>18</sup> as shown in Scheme 1.3.



Scheme 1.3 Regioselective hydrogenation of quinaxoline.

#### 1.2.2.2. Nitrogen donor ligands

Coordination of nitrogen donor atoms to transition metals is widely known in naturally occurring processes. For example, the haem b group in haemoglobin consists of an iron ion bound to four nitrogens in the centre of a protoporphyrin ring.<sup>19</sup> A number of transition metal complexes containing nitrogen donor ligands have been synthesised with aims to mimic and even improve upon the effective catalytic activity of these biological processes and achieve higher catalytic activity for different organic transformations.<sup>20</sup> The relatively labile character of ligands containing nitrogen donor atoms compared to stronger donors such as phosphines allow the resulting transition metal catalyst to produce vacant coordination sites more readily, which is desirable for enhancing the catalytic reactivity. Typical N-donor ligand systems in transition metal complexes often include pyrazole, pyridine, pyrrole and imine groups (Figure 1.2).<sup>20</sup> These  $sp^2$  N-donors, in particular the heterocyclic systems, are less likely to undergo oxidation processes themselves which are common in phosphine donor systems.<sup>21</sup> The increased robustness of ligands containing N-

donor atoms relative to other donors have resulted in the popular use of the resulting metal complexes as catalysts for a number of different organic transformations.

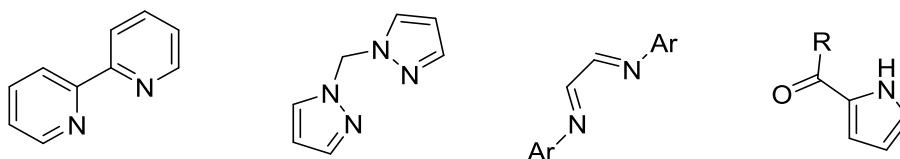


**Figure 1.2** Typical N-donor ligand systems.

### 1.2.2.3. Tridentate ligands

Tridentate pincer ligands provide an excellent platform for modifying the steric and electronic properties of a complex. Tridentate ligands are advantageous over bidentate ligands due to an increased chelate effect, which enhances the chemical stability of the resulting metal complex.<sup>12</sup> A popular class of tridentate ligands are pincers, which are commonly denoted in the form  $DYD'$ , where Y denotes the central donor atom and  $D/D'$  the two sidearm donor atoms (Figure 1.3).<sup>22, 14</sup> The central donor (Y) is most commonly a phenyl or pyridyl ring, although amide, silyl and NHC donors have also been reported.<sup>23</sup> A diverse array of side arm donor groups ( $D/D'$ ) have been used in pincer complexes, such as phosphines, phosphites, amines, amides, thioethers and NHC donors.<sup>23</sup> A short and rigid linker between the central donor and the side arm donor groups typically promotes a meridional coordination of the ligand to a metal centre, such that all three donor groups lie in the same plane, however facial coordination modes are also possible.

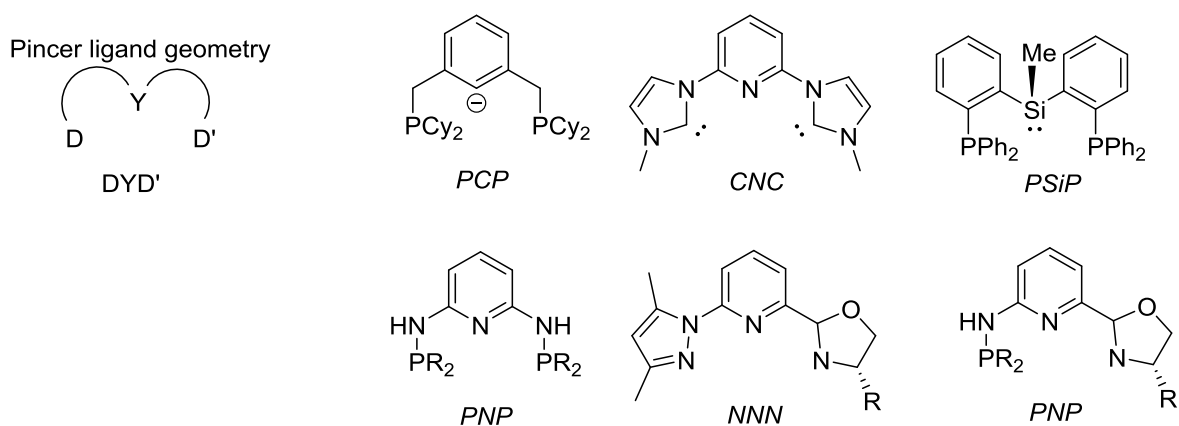
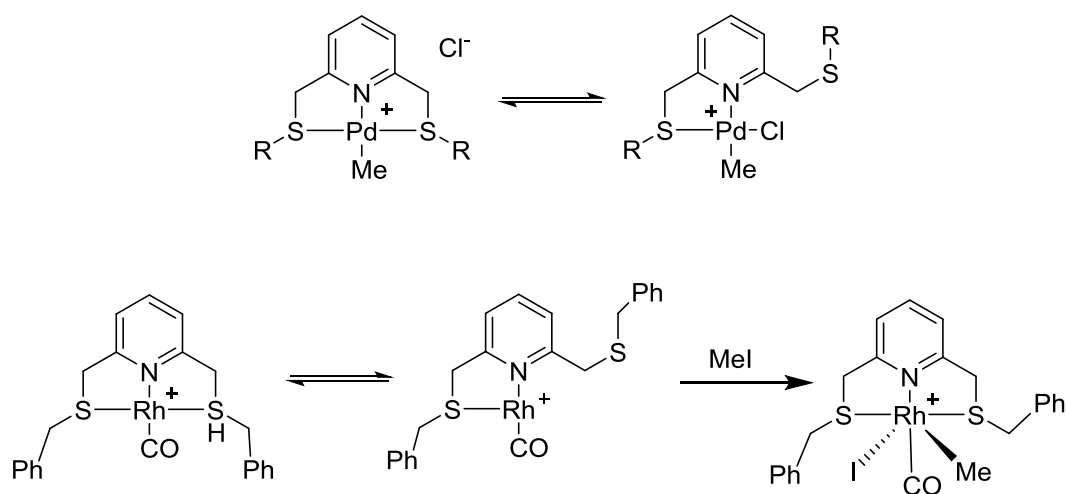


**Figure 1.3** Common motifs of pincer ligands.

A strong meridional coordination of the pincer ligand to a metal centre can result in complexes of high thermal stability. This is due to a restricted arrangement of the remaining coordination sites which can inhibit potential decomposition pathways. For example, Shaw *et al.* reported that a Ni(II) complex containing the *PCP* ligand in Figure 1.3 was stable up to 240 °C.<sup>12</sup>

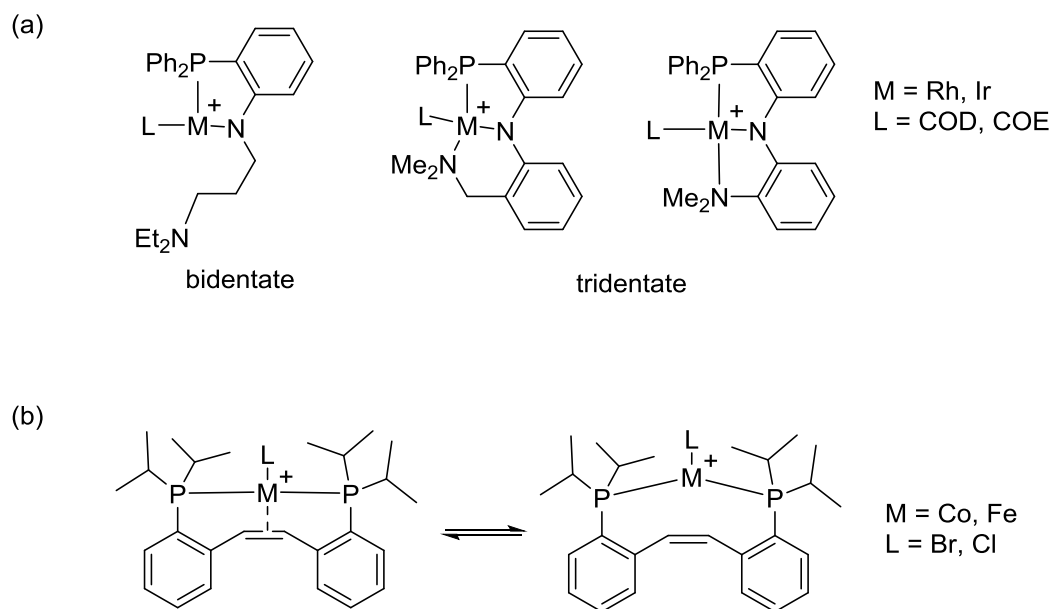
#### 1.2.2.4. Hemilabile pincer ligands

The use of weakly coordinating side arms in pincer ligands can lead to tridentate ( $\kappa^3$ ), bidentate ( $\kappa^2$ ) and even monodentate ( $\kappa^1$ ) coordination modes. For example, Canovese *et al.* observed an equilibrium between  $\kappa^2$  and  $\kappa^3$  coordination modes in a Pd complex containing an *SNS* pincer ligand with labile thioether side arms (Scheme 1.4).<sup>24</sup> The ligand system has since been investigated using different metals, for example, a Rh(I) complex containing the *SNS* ligand exhibited hemilabile character and was shown to facilitate the oxidative addition reaction of methyl iodide.<sup>24, 25a</sup>



**Scheme 1.4** Pd and Rh complexes with an SNS hemilabile pincer ligand.

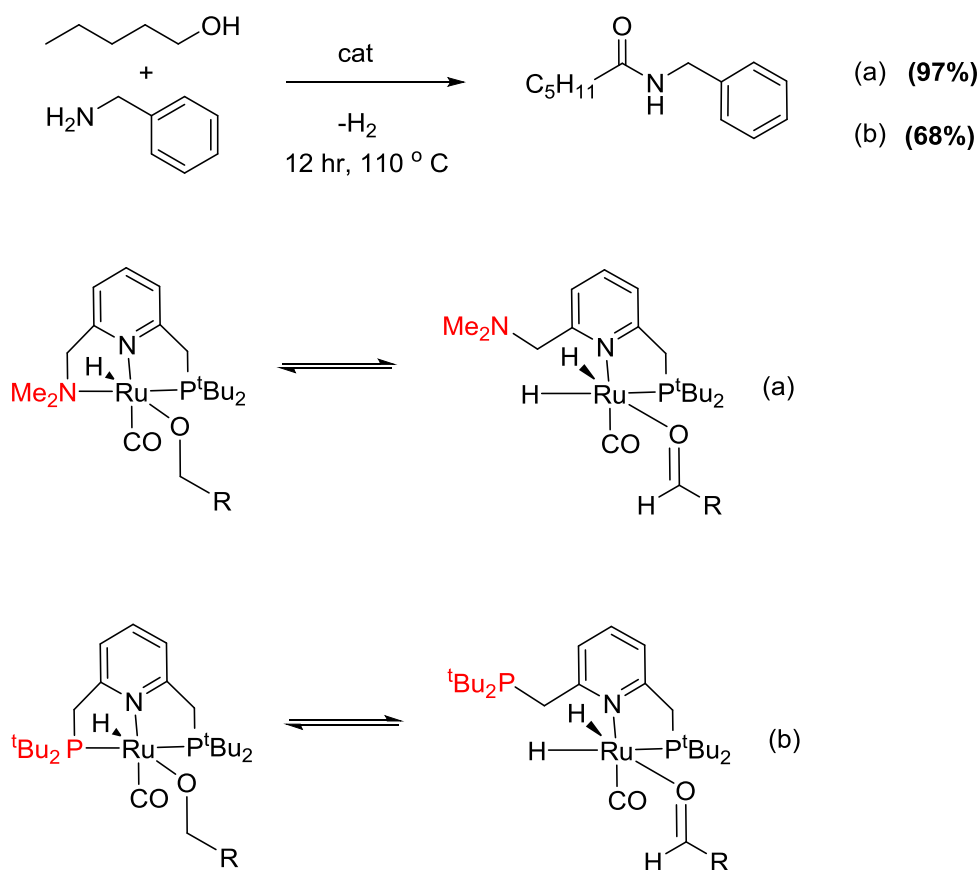
Recent work has demonstrated that the hemilability of pincer ligands is tunable through variable donor strength and spacer length/rigidity. Lindner *et al.* demonstrated this by testing the coordination chemistry of *PNN* pincer ligands with varying R substituents on the labile N donor arm and the spacer linker between the side arms donors and the central donor (Scheme 1.5a).<sup>25b</sup> Hemilability of complexes are also not limited to use of weakly coordinating heteroatom donors such as nitrogen, oxygen and sulphur. A pincer ligand containing a central alkene was reported to exhibit hemilabile character as shown in Scheme 1.5b.<sup>25c</sup>



**Scheme 1.5** Complexes containing hemilabile pincer ligands.

Transition metal complexes bearing ligands that exhibit hemilabile character have been shown to enhance catalytic activities for a number of organic transformations. Nitrogen moieties are commonly used as side arm donors in hemi-labile pincer complexes, and show increased lability compared to phosphorus donors.

A Ru(II) complex containing an *NNP* pincer ligand was reported to produce enhanced catalytic activity for the intermolecular dehydrogenative hydroamination reaction (Scheme 1.6) of alcohols and amines. In comparison, the analogous *PNP* pincer complex exhibits significantly reduced conversions of substrates to amide product.<sup>26, 27</sup>

Scheme 1.6 Ru(II) complex with a *NNP* hemilabile pincer ligand.

### 1.2.3. Counterions

In transition metal complexes, counter anions are typically used to balance the positive charge associated with the cationic metallic species. The counterions tend to exist within the coordination sphere of the metal ion.<sup>28</sup> Varying the counterion of a transition metal catalyst has been shown to alter its ability to perform organic transformations.<sup>29</sup> This can be associated with the varying coordination strengths and steric bulk of the counterion, which has the potential to alter the electrophilicity and steric effects of the resulting metal complex.



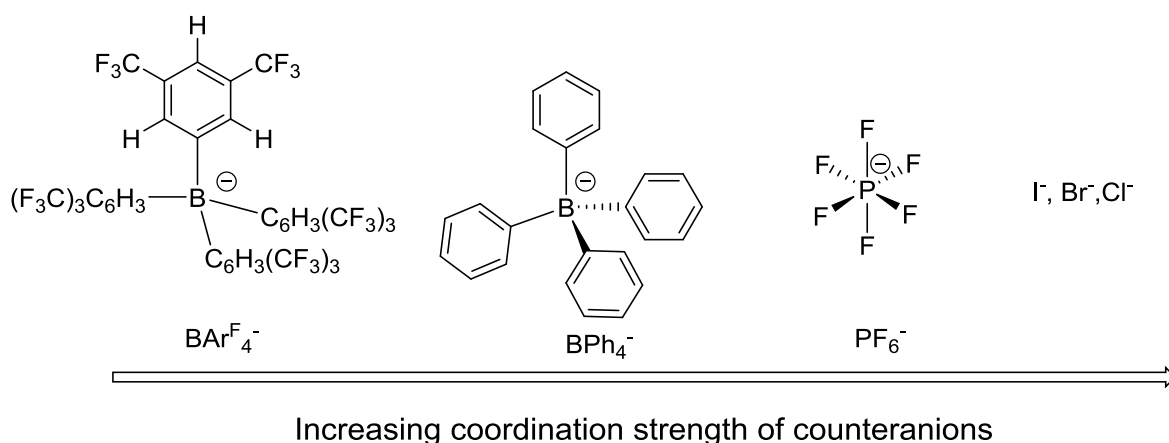


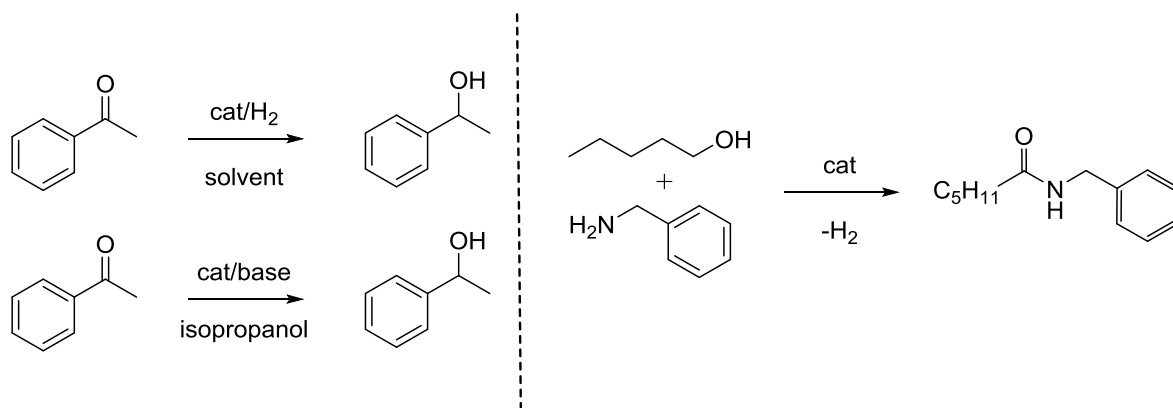
**Figure 1.4** Varying coordination strengths of counterions

Weakly coordinating counterions are commonly used in transition metal catalysts with the aim to optimise interaction between catalyst and substrates during catalysis.<sup>30</sup> Most of the weakly coordinating counterions include borates such as  $\text{BPh}_4^-$  (tetraphenylborate),  $\text{B}(\text{C}_6\text{F}_5)_4^-$  and  $\text{BARF}_4^-$  (tetrakis(-3, 5-bis(trifluoromethyl)phenyl) borate).<sup>30, 31</sup>

### 1.3. Transition metal complexes in homogeneous catalysis

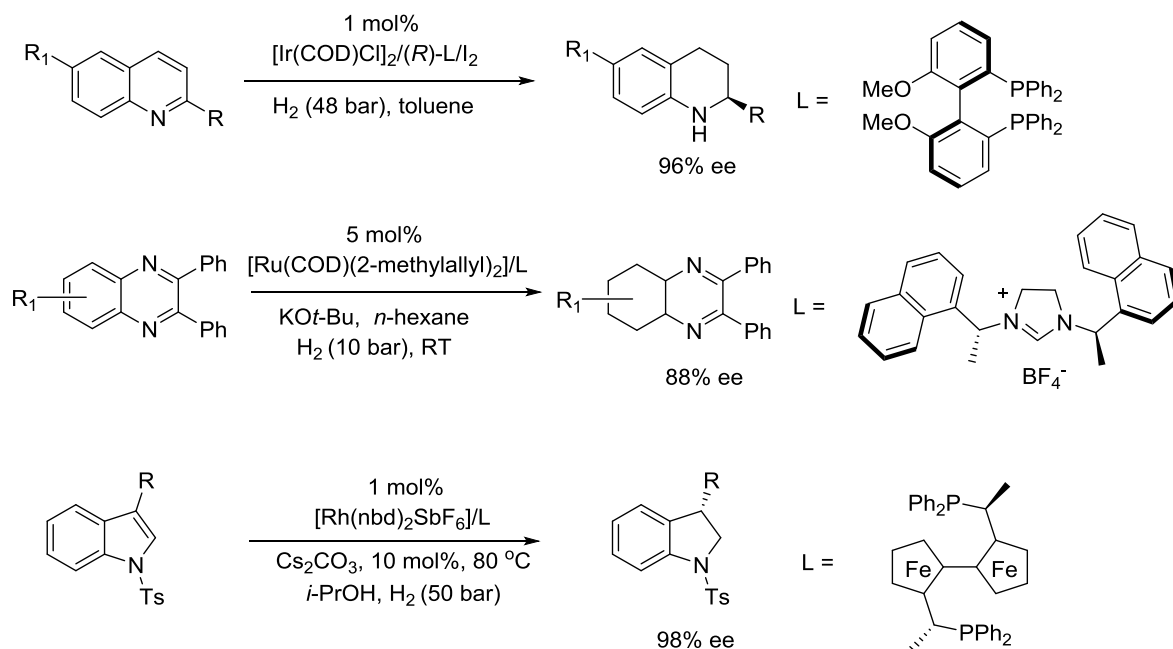
#### 1.3.1. Transition metal catalysed $\text{H}_2$ addition or removal to a polar unsaturated bond

The metal mediated addition of  $\text{H}_2$  to or removal of  $\text{H}_2$  from a polar unsaturated bond has been studied using various transition metals.<sup>32</sup> These types of reactions typically involve the hydrogenation of ketones and imines, the reductive cleavage of esters and the dehydrogenative coupling of alcohols and amines (Scheme 1.7).<sup>33, 34</sup>

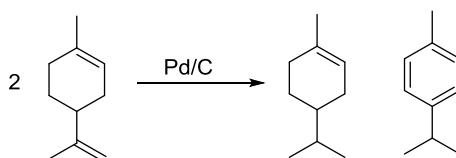


**Scheme 1.7** Typical hydrogenation and dehydrogenative coupling reactions.

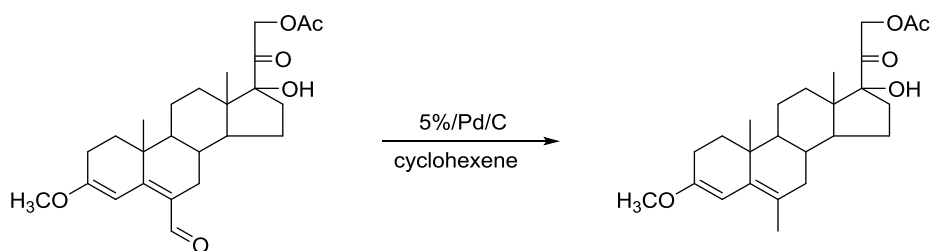
Among the  $\text{H}_2$  transfer reactions, catalysed hydrogenation and transfer hydrogenation reactions have received significant attention due to the wide number of applications in industrial scale synthesis, green chemistry and medicinal chemistry.<sup>35</sup> These catalytic hydrogenation reactions are accessible using a number of transition metals including rhodium, iridium, iron and ruthenium (Scheme 1.8).<sup>36</sup>



Transfer hydrogenation can provide a milder route to the formation of alcohols and alkanes from ketones and alkenes respectively compared to conventional hydrogenation reactions where the use of high temperatures, pressures and potentially dangerous gases such as hydrogen<sup>32</sup> can be avoided. The transfer hydrogenation process can also offer different selectivities to hydrogenation reactions,<sup>37</sup> which can be useful for the selective production of stereoisomers. Well known uses of transfer hydrogenation in industry include the synthetic production of terpenes and functionalisation of steroids (Scheme 1.9).<sup>35</sup> For example, the conversion of steroid ethers to 6-methyl steroids was achieved with high selectivity where other functional groups on the steroid remained unaffected (Scheme 1.10).<sup>38</sup>



**Scheme 1.9** Synthetic production of terpenes.

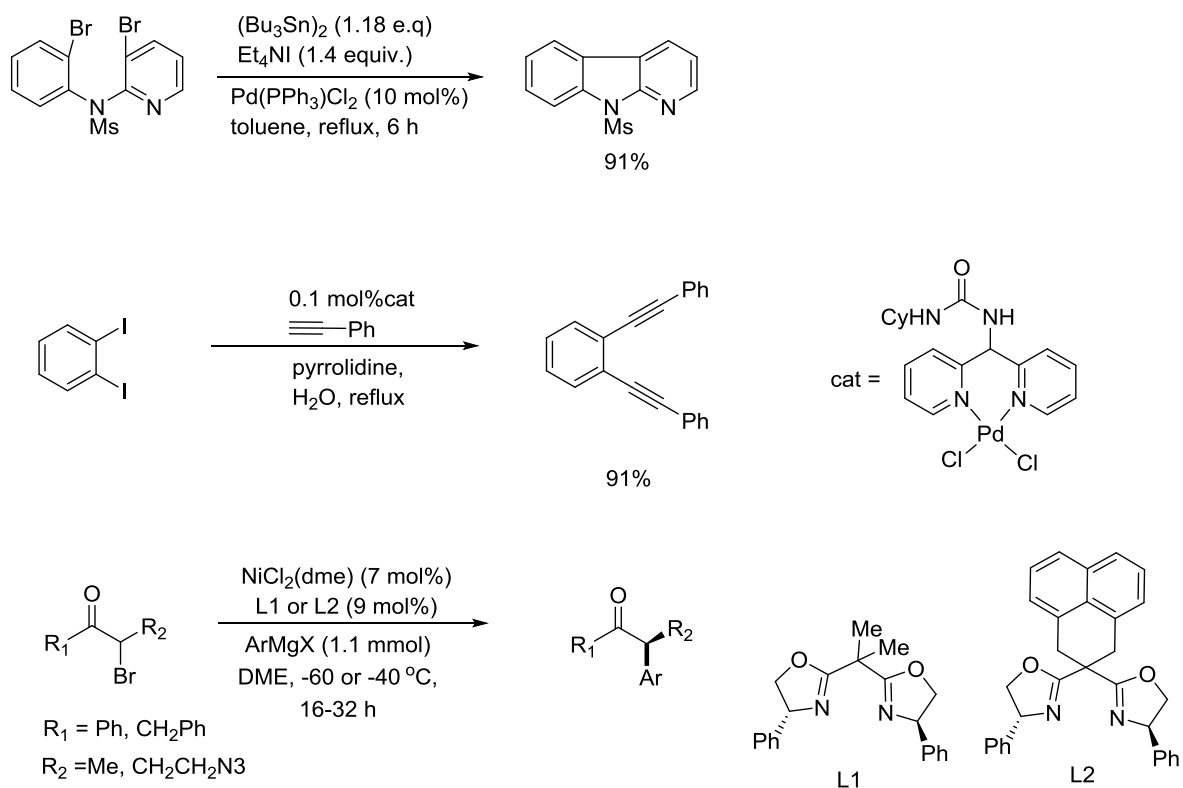


**Scheme 1.10** Conversion of steroid ethers to 6-methyl steroids.

### 1.3.2. Transition metal catalysed C-C bond coupling reactions

The formation of C-C bonds remains amongst the most vital reactions in organic synthesis and has been used for industrial processes such as crude oil refining and production of pharmaceutical drugs.<sup>39</sup> Since the introduction of transition metal catalysts to these

processes, the volume and number of different catalysed C-C coupling reactions has significantly increased over time. Typical C-C bond formation reactions include Suzuki, Negishi, Stille, Sonogashira and Kumada cross coupling reactions. Early accounts of C-C bond formation reactions involved the coupling of Grignard reagents with organic halides. Karasch and Fields first reported the enhanced coupling reaction of Grignard reagents with organic halides by utilising a cobalt catalyst.<sup>40</sup> However, the early reports of these catalysed coupling reactions resulted in the formation of significant homo-coupled products and poor yields for the desired products. Introduction of nickel and palladium based catalysts alleviated this problem; Corriu and Kumada reported nickel and palladium catalysed coupling reactions of Grignard reagents with organic halides achieving high yields.<sup>41</sup> A number of palladium and nickel catalysts have since been synthesised to catalyse different coupling reactions under a wide range of conditions of solvent, temperature and co-reagents with supporting ligands being used to control both reactivity and selectivity (Scheme 1.11).<sup>39</sup>



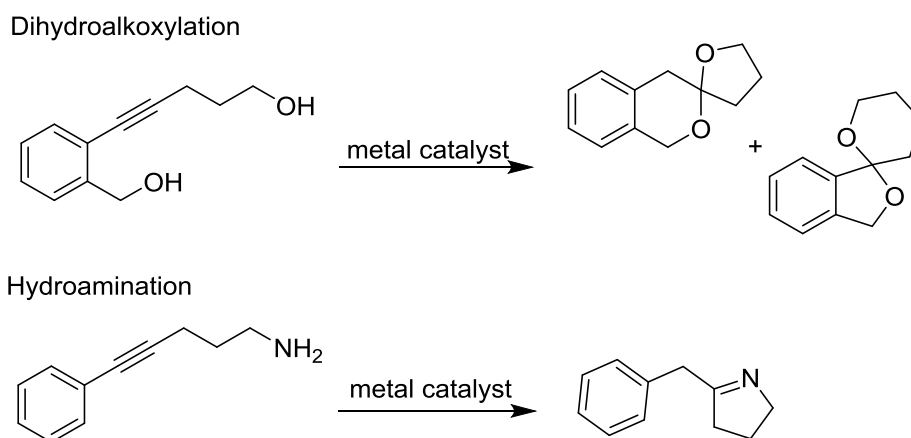
Scheme 1.11 Pd and Ni catalyzed coupling reactions.

The advantages provided by transition metal complexes such as high stereoselectivity and reduction of unwanted by-products allows for the advent of efficient methods to forge C-C bonds.

### 1.3.3. Transition metal catalysed X-H bond addition reactions

The addition of X-H ( $\text{X} = \text{N}, \text{O}, \text{S}, \text{Se}$  or  $\text{P}$ ) across an alkyne functionality, known as hydroelementation reactions, using transition metal complexes as catalysts has received significant attention in organometallic chemistry.<sup>42</sup> The great potential for hydroelementation processes to achieve 100% atom economy makes them an attractive approach to organic syntheses and green chemistry. Intramolecular reactions involving X-H bond addition are also highly efficient methods for the production of heterocycles containing nitrogen and oxygen groups.<sup>42, 43</sup> Formation of such heterocycles is critical in the

pharmaceutical industry for the production of valuable medicinal compounds. The dihydroalkoxylation reaction (Scheme 1.12) of alkyne diols produces spiroketals which are moieties commonly found in natural products such as (-)-Berkelic acid (Figure 1.5).<sup>44</sup> Similarly, the intramolecular hydroamination reaction of alkynamines (Scheme 1.12) results in the formation of nitrogen containing heterocycles which are moieties commonly found in pharmaceutical compounds such as pyrrolysine (Figure 1.5).<sup>45</sup>



**Scheme 1.12** Dihydroalkoxylation of alkyne diols and hydroamination of alkynamines.

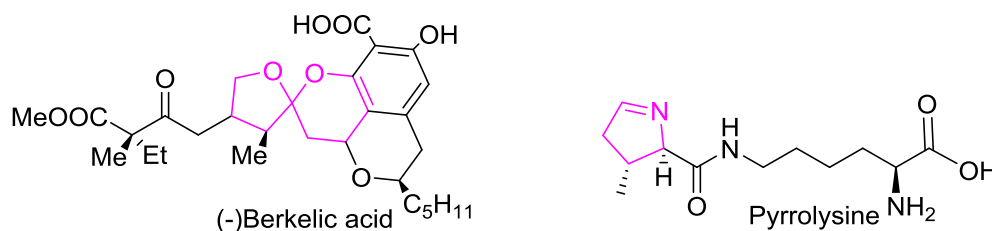
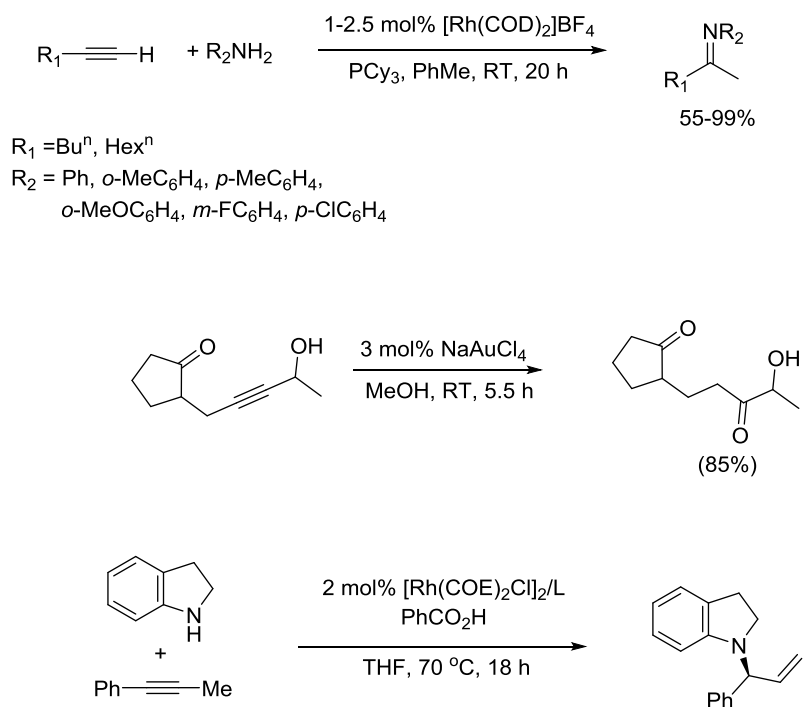


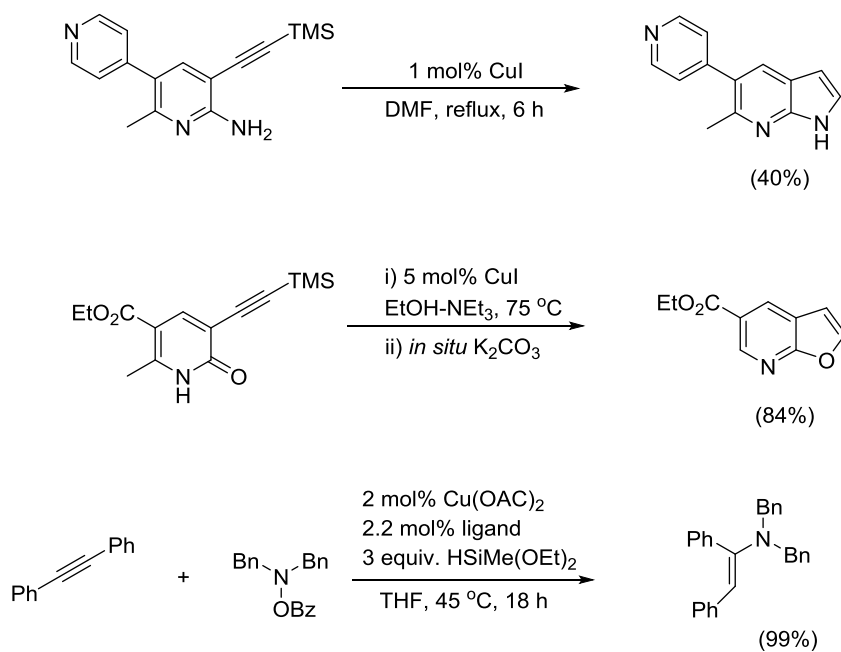
**Figure 1.5** Pharmaceutical compounds containing nitrogen/oxygen heterocycles.

The X-H bond addition reactions are able to proceed under mild conditions and are versatile as a result of the number of different transition metals that are able to catalyse the organic transformations.<sup>43, 46, 47</sup> As shown in Scheme 1.13, both the intermolecular hydroamination and intramolecular hydroalkoxylation reactions achieve high conversions at room temperature and utilise simple metal complexes to catalyse the transformations.



**Scheme 1.13** X-H bond addition reactions catalyzed by simple metal complexes.

High regioselectivity is also usually achieved with metal catalysed X-H bond addition reactions of alkynes. The broad applicability of a range of transition metals also allows the use of inexpensive transition metals such as copper (Scheme 1.14).<sup>48, 49</sup>



**Scheme 1.14** X-H bond addition reactions catalyzed by copper complexes.



#### 1.4. Objectives

Current catalytic systems which are highly active tend to have reduced stability and a combination of high stability and reactivity is rarely present. Improvements to such systems can be made by utilising tridentate systems containing both strong and weakly coordinating donors. The goals of this research project were to synthesise novel complexes using Ru, Ni, and Au, which contain a pincer ligand with a central NHC donor and labile pyrazole pendant donors, and to investigate the efficiency of these complexes as homogeneous catalysts for a variety of organic transformations. The aim was to determine whether the hemilability of the ligands can lead to higher activity of the complexes as catalysts without compromising stability, for the selected transformations. The formation of complexes containing bidentate or tridentate coordination modes was therefore targeted such that the weakly coordinated pendant arms can readily dissociate during catalysis, providing vacant coordination sites. The goals of the project were:

- To synthesise novel transition metal complexes (Ru(II), Ag(I), Ni(II), Au(I) and Au(III)) containing pincer ligands with a central imidazolium group flanked by labile pyrazole pendant arms.
- To analyse the structural properties and coordination chemistry of these novel complexes, which were carried out using a range of analytical techniques including NMR and U.V. spectroscopy.
- To investigate the catalytic activity of novel Ru(II) complexes for transfer hydrogenation reactions, Ni(II) complexes for Kumada cross coupling reactions and Au(I)/Au(III) complexes for X-H bond addition reactions.

General structure of this thesis:

### **Chapter 1 : Introduction**

This chapter describes the use of transition metal complexes as catalysts for different organic transformations and the different compositional aspects of a homogeneous catalyst that affects its reactivity. The importance of ligand design in a metal complex is presented highlighting aspects of donor types and hemilability.

### **Chapter 2: Ru(II) complexes containing hemilabile pincer ligands for catalysing transfer hydrogenation reactions:**

This chapter describes the synthesis of Ag(I) and Ru(II) complexes containing hemilabile pincer ligands. Structural analyses of the complexes were conducted using different characterisation techniques including X-ray crystallography and NMR spectroscopy. The resulting Ru(II) complexes were tested as catalysts for the transfer hydrogenation reaction of acetophenone. Optimised catalytic conditions were established and the transfer hydrogenation reaction was investigated using a range of ketone substrates.

### **Chapter 3: Ni(II) complexes containing hemilabile pincer ligands for catalysing Kumada cross coupling reactions.**

This chapter describes the synthesis of Ni(II) complexes containing hemilabile pincer ligands. The structural and electronic properties of the complexes were analysed using different coordinating donor ligands and counteranions, and their coordination chemistry investigated using different characterisation techniques. These Ni(II) complexes were tested as catalysts for the Kumada cross coupling reaction and the effect of counterions on catalytic activity was examined.

**Chapter 4: Au(I) and Au(II) complexes containing hemilabile pincer ligands for alkyne activation reactions.**

This chapter investigates the coordination chemistry of hemilabile pincer complexes containing Au(I) or Au(II) metal centres. The properties of the synthesised gold complexes including oxidation state and geometry were analysed using X-ray crystallography and U.V spectroscopy. Gold complexes of both (I) and (III) oxidation states were tested as catalysts for X-H bond addition reactions, specifically dihydroalkoxylation and hydroamination reactions. The effect of oxidation states on catalytic activity between the Au(I) and Au(III) catalysed hydroelementation reactions were analysed.

**Chapter 5: Conclusions and future work.**

Provides a summary of the work presented in the project and promising possibilities in future work as a follow up on the findings of this work.

## 1.5. References

- (1) Salzer, A. *Nomenclature of Organometallic Compounds of the Transition Elements.*; Pure Appl. Chem. **1999**, 71, 1557.
- (2) Cheung, H.; Tanke, R. S.; Torrence, G. P. "Acetic Acid" in *Ullmann's Encyclopedia of Industrial Chemistry*, Wiley-VCH, Weinheim, **2002**.
- (3) Atkins, P. *Physical chemistry*. 7<sup>th</sup> ed.; Oxford Univ. Press, **2002**.
- (4) Hartwig, J. F. *Organotransition Metal Chemistry, from Bonding to Catalysis.*; University Science Books: New York, **2010**.
- (5) (a) Cornils, B.; Herrmann, W. A.; Schlogl, R.; Wong, C. H. *Catalysis from A to Z*; 2<sup>nd</sup> ed.; Wiley-VCH, **2003**; (b) Noyori, R. *Asymmetric Catalysis in Organic Synthesis*; John Wiley and Sons, Inc, Chichester, **1994**.
- (6) Hegedus, L. S. *Transition Metals in the Synthesis of Complex Organic Molecules*, 2<sup>nd</sup> ed.; University science books; Sausalito, **1999**.
- (7) Constantin, C.; Drouet, S.; Robert, M.; Savéant, J. M. *J. Am. Chem. Soc.* **2012**, 134, 11235.
- (8) (a) Crabtree, R. H. "(1,5-Cyclooctadiene)(tricyclohexylphosphine)(pyridine)iridium(I) Hexafluorophosphate". *e-EROS Encyclopedia of Reagents for Organic Synthesis*, **2001**; (b) Chirik, P. J. *Acc. Chem. Res.* **2015**, 48, 1687.
- (9) Crabtree, R. H. *The Organometallic Chemistry of the Transition Metals*; 3<sup>rd</sup> ed.; John Wiley and Sons, Inc, Brisbane, **2001**.
- (10) Cotton, F. A.; Wilkinson, G.; Murillo, C. A.; Bochmann, M. *Advanced Inorganic Chemistry*, 6<sup>th</sup> ed.; John Wiley and Sons, Inc, New York, **1999**.

- (11) (a) Grubbs, R. H. *Handbook of Metathesis (1st ed.)*; Weinheim: Wiley-VCH. **2003**; (b) Montgomery, J.; George Thieme Verlag K G. *Science of Synthesis*, **1986**, 1, 11.
- (12) (a) Moulton, C. J.; Shaw, B. L. *Dalton Trans.* **1976**, 11, 1020; (b) Banach, L.; Guńka, P. A.; Buchowicz, W. *Dalton Trans.* **2016**, 45, 8688; (c) Chai, H.; Liu, T.; Wang, Q.; Yu, Z. *Organometallics* **2015**, 34, 5278.
- (13) (a) Hashmi, A. S. K. *Chem. Rev.* **2007**, 107, 3180; (b) Dorel, R.; Echavarren, A. M. *Chem. Rev.* **2015**, 115, 9028; (c) Pflästerer, D.; Hashmi, A. S. K. *Chem. Soc. Rev.* **2016**, 45, 1331.
- (14) Arduengo, A. J.; Harlow, R. L.; Kline, M. J. *Am. Chem. Soc.* **1991**, 113, 361.
- (15) (a) Herrmann, W. A. *Angew. Chem. Int. Ed.* **2002**, 41, 1490; (b) Wilson, D. J. D.; Couchman, S. A.; Dutton, J. L. *Inorg. Chem.* **2012**, 51, 7657.
- (16) Gaillard, S.; Cazin, C. S. J.; Nolan, S. P. *Acc. Chem. Res.* **2012**, 45, 778.
- (17) (a) Díez-González, S.; Marion, N.; Nolan, S. P. *Chem. Rev.* **2009**, 109, 3612; (b) Hopkinson, M. N.; Richter, C.; Schedler, M.; Glorius, F. *Nat. Chem.* **2014**, 510, 485; (c) Zhang, D.; Zi, G. *Chem. Soc. Rev.* **2015**, 44, 1898.
- (18) Urban, S.; Ortenga, N.; Glorius, F. *Angew. Chem. Int. Ed.* **2011**, 50, 3803.
- (19) Van Kessel "2.4 Proteins – Natural Polyamides." *Chemistry 12*. Toronto: Nelson, **2003**, 122.
- (20) (a) Togni, A.; Venanzi, L. M. *Angew. Chem. Int. Ed.* **1994**, 33, 497; (b) Wende, C.; Lüdtke, C.; Kulak, N. *Eur. J. Inorg. Chem.* **2014**, 16, 2597.
- (21) Garrou, P. E. *Chem. Rev.* **1985**, 85, 171.
- (22) (a) Lee, D. W.; Jensen, C. M. *Organometallics* **2003**, 22, 4744; (b) Younus, H. A.; Su, W.; Ahmad, N.; Chen, S.; Verpoorta, F. *Adv. Synth. Catal.* **2015**, 357, 283; (c) Lapointe, S.; Vabre, B.; Zargarian, D. *Organometallics* **2015**, 34, 3520.

- (23) Morales-Morales, D. *Chem. Soc. Rev.* **2004**, 48, 338.
- (24) Canovese, L.; Visentin, F.; Chessa, G.; Uguagliati, P.; Santo, C.; Bandoli, G.; Maini, L. *Organometallics* **2003**, 22, 3230.
- (25) Weng, W.; Parkin, S.; Ozerov, O. V. *Organometallics* **2006**, 25, 5345; (b) Lindner, R.; van den Bosch, B.; Lutz, M.; Reek, J. N. H.; van der Vlugt, J. I. *Organometallics* **2011**, 30, 499; (c) Barrett, B. J.; Iluc, V. M. *Inorg. Chem.* **2014**, 53, 7248.
- (26) Basseti, M.; Capone, A.; Salamone, M. *Organometallics* **2004**, 23, 247.
- (27) Milstein, D. *Angew. Chem. Int. Ed.* **2010**, 49, 1468.
- (28) Leeuwen, P. W. *Homogeneous catalysis: understanding the art, Springer Science & Business Media*, **2006**.
- (29) Jia, M.; Bandini, M. *ACS Catal.* **2015**, 5, 1638.
- (30) Kennedy, D. F.; Messerle, B. A.; Smith, M. K. *Eur. J. Inorg. Chem.* **2007**, 2007, 80.
- (31) Yakelis, N. A.; Bergman, R. G. *Organometallics* **2005**, 24, 3579.
- (32) (a) Stanislaus, A.; Cooper, B. H. *Catal. Rev.* **1994**, 36, 75; (b) Bagala, D. B.; Bhanagea, B. M. *Adv. Synth. Catal.* **2015**, 357, 883.
- (33) Naziruddin, A. R.; Huang, Z. J.; Lai, W. C.; Lin, W. J.; Hwang, W. S. *Dalton Trans.* **2013**, 42, 13161.
- (34) Gerard, V. K.; Ignacio, D. R. *Tetrahedron Lett.* **1999**, 40, 1401.
- (35) (a) Brieger, G.; Nestrick, T. J. *Chem. Rev.* **1974**, 74, 567; (b) Wang, D.; Astruc, D. *Chem. Rev.* **2015**, 115, 6621.
- (36) Wang, D. S.; Chen, Q. A.; Lu, S. M.; Zhou, Y. G. *Chem. Rev.* **2012**, 112, 2557.
- (37) Clapham, S. E.; Hadzovic, A.; Morris, R. H. *Coord. Chem. Rev.* **2004**, 248, 2201.
- (38) Burn, D.; Kirk, N. D.; Petrov, V. *Tetrahedron* **1965**, 21, 1619.

- (39) Cherney, A. H.; Kadunce, N. T.; Reisman, S. E. *Chem. Rev.* **2015**, *115*, 9587.
- (40) Kharasch, M. S.; Fields, E. K. *J. Am. Chem. Soc.* **1941**, *63*, 2316.
- (41) Corriu, R. J. P.; Masse, J. P. *Chem. Commun.* **1972**, *3*, 144.
- (42) Alonso, F.; Beletskaya, I. P.; Yus, M. *Chem. Rev.* **2004**, *104*, 3079.
- (43) Huang, L.; Arndt, M.; Gooßen, K.; Heydt, H.; Gooßen, L. J. *Chem. Rev.* **2015**, *115*, 2596.
- (44) Müller, T. E.; Hultsch, K. C.; Yus, M.; Foubelo, F.; Tada, M. *Chem. Rev.* **2008**, *108*, 3795.
- (45) Martinez, P. H.; Hultsch, K. C. *Tetrahedron. Lett.* **2009**, *50*, 2054.
- (46) Hartung, C. G.; Tillack, A.; Trauthwein, H.; Beller, M. *J. Org. Chem.* **2001**, *66*, 6339.
- (47) (a) Imai, K.; Imai, K.; Utimoto, K. *Tetrahedron Lett.* **1987**, *28*, 3127; (b) Chen, Q. A.; Chen, Z.; Dong, V. M. *J. Am. Chem. Soc.* **2015**, *137*, 8392.
- (48) (a) Kumar, V.; Dority, J. A.; Bacon, E. R.; Singh, B.; Lesher, G. Y. *J. Org. Chem.* **1992**, *57*, 6995; (b) Pirnot, M. T.; Wang, Y. M.; Buchwald, S. L. *Angew. Chem. Int. Ed.* **2016**, *55*, 48.
- (49) (a) Houpis, I. N.; Choi, W. B.; Reider, P. J. *Tetrahedron Lett.* **1994**, *35*, 9355; (b) Shi, S. L.; Buchwald, S. L. *Nat. Chem.* **2015**, *7*, 38.

---

Chapter 2. Ru(II) complexes of hemilabile pincer  
ligands for catalysed transfer hydrogenation  
reactions

---



## 2.1. Introduction

### 2.1.1. Transition metal catalysed hydrogenation reaction

Hydrogenation of polar, unsaturated bonds is a widely researched area in organometallic chemistry. The process is important in food, petrochemical and pharmaceutical industries. Applications of hydrogenation include the production of daily commodity items such as margarine, and commonly used chemicals such as aniline.<sup>1</sup> Some of the early, well known active catalysts for the hydrogenation reaction include Crabtree's catalyst and complexes containing the (S)-iPr-PHOX ligand developed by Braunstein (Figure 2.1).<sup>2, 3</sup>

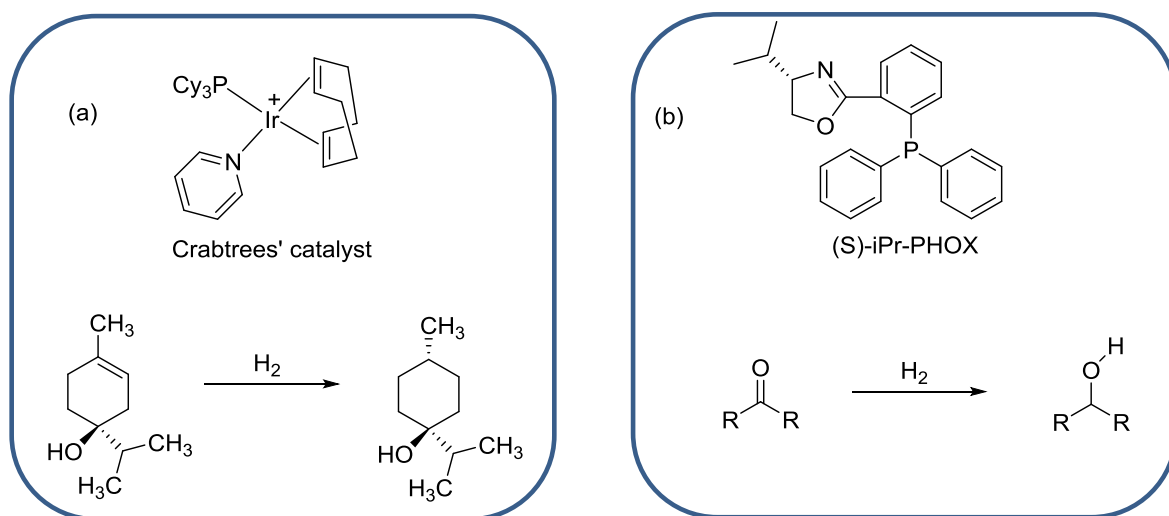


**Figure 2.1** Early examples of hydrogenation catalysts: a) Crabtree's catalyst,<sup>2</sup> and b) (S)-iPr-PHOX.<sup>3</sup>

### 2.1.2. Ruthenium catalysed hydrogenation reactions

Ruthenium(II) complexes containing pincer ligands proved to be efficient catalysts for transformations that involve the metal mediated addition (or removal) of H<sub>2</sub> to a polar unsaturated bond. This includes the reductive cleavage of esters using H<sub>2</sub>, and the dehydrogenative coupling of alcohols and amines to form amides.<sup>4</sup> Recently Ru(II) catalysts

have been used for the hydrogenation reaction of ketones where excellent yields and selectivity were achieved.<sup>5</sup> Noyori, *et al.* used a Ru(II) catalyst bearing a BINAP (2,2'-bis(diphenylphosphino)-1,1'-binaphthyl) ligand (Figure 2.2a). The structure of the ligand was shown to be essential for achieving high enantioselectivity for the alcoholic product shown in Figure 2.2a.<sup>5a</sup> Using the (*R*)-isomer instead of the (*S*)-isomer of the BINAP ligand resulted in poor enantioselectivity which was attributed to the altered sterics about metal centre. Beller *et al.* also showed similar results for the hydrogenation of secondary and tertiary amides to amines (Figure 2.2b) using a simple [Ru(acac)<sub>3</sub>]/Triphos catalyst system.<sup>5b</sup>

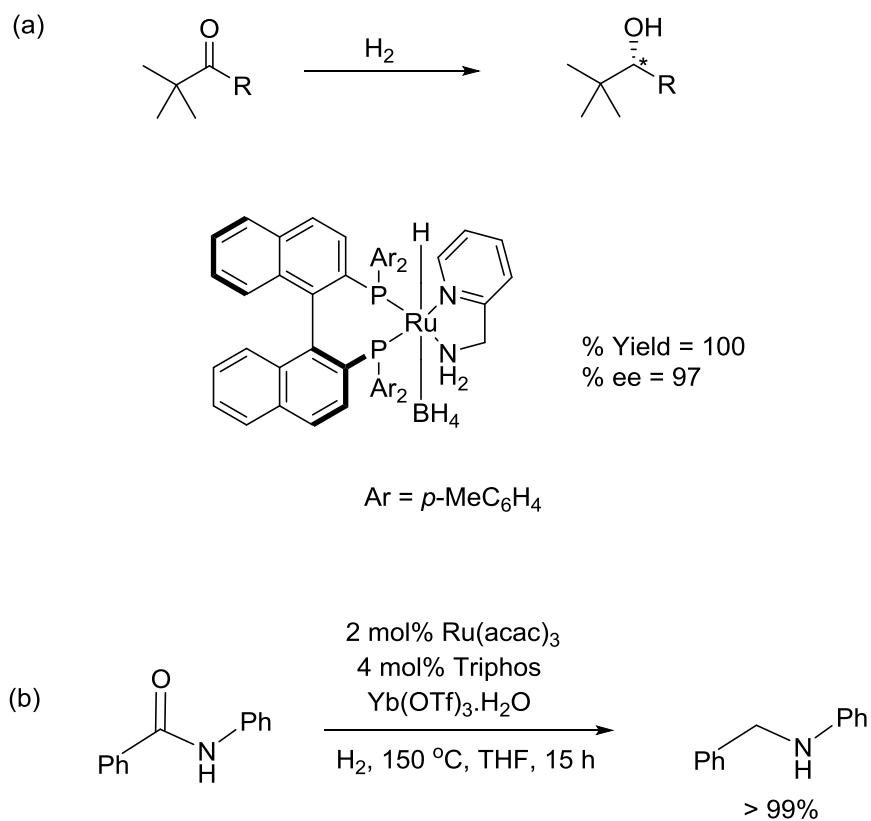


**Figure 2.2** Ligand selective hydrogenation of ketones.

### 2.1.3. Transfer hydrogenation as an alternative to hydrogenation reactions

Typical hydrogenation reactions utilise hydrogen gas as the source of hydrogen and are carried out under harsh reaction conditions, requiring the use of high temperatures and/or pressures.<sup>6</sup> This results in dangerous conditions involving potentially explosive H<sub>2</sub> gas, and as such, these reactions also require expensive apparatus to safely contain the harsh reaction conditions. An alternative to direct hydrogenations of substrates with H<sub>2</sub> is the transfer hydrogenation reaction. This reaction typically involves a proton donor (usually an alcohol) as the hydrogen source, which avoids the harsh reaction conditions involved in hydrogenation reactions, and provides a milder alternative route. The product selectivities of transfer hydrogenation reactions differ from those of the traditional hydrogenation reactions as the degree of enantioselectivity varies even under altered pressure conditions.<sup>7</sup> These reactions have been extensively studied using transition metal complexes as catalysts and Ru(II) systems have proved to be the most common and effective for the organic transformations.<sup>8</sup> Early work on Ru(II) catalysed transfer hydrogenation reactions focused on complexes containing bidentate ligands and arene co-ligands (Figure 2.3).<sup>10</sup> The earliest examples include the well-known Schvo's catalyst, which was found to operate *via* an "outer sphere mechanism" for the hydrogenation reaction.<sup>9</sup> Ru(II) complexes containing arene co-ligands were targeted in early work as catalysts for the transfer hydrogenation reaction of carbonyl bonds as shown in (Figure 2.3) as they proved to be efficient catalysts for the organic transformation.<sup>10</sup>

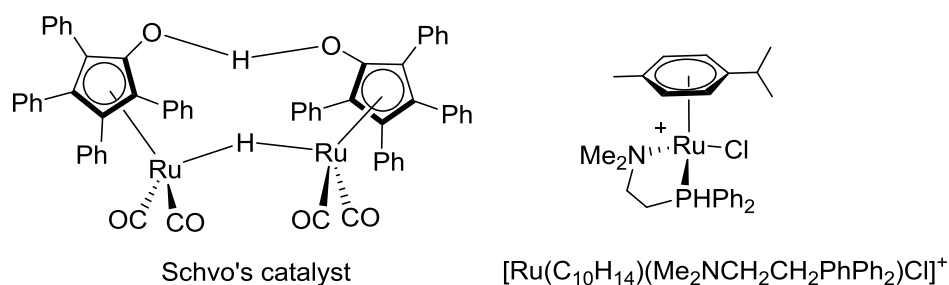


**Figure 2.3** Early Ru(II) catalysts for the transfer hydrogenation reaction, left: Schvo's catalyst,<sup>9</sup> right: Ru(II)arene complex containing a *PN* bidentate ligand.<sup>10</sup>

#### 2.1.4. Transition metal complexes containing pincer ligands for the transfer hydrogenation of ketones

Transition metal complexes containing pincer ligands have been used successfully as catalysts for promoting a wide range of transformations and evidence showed that selected coordination motifs may significantly improve catalysis rates and/or selectivities.<sup>11</sup> Much of the attention on transfer hydrogenation reactions have been focused on transition metal complexes containing pincer ligands as catalysts partly due to the increased thermal and catalytic stability of pincer complexes.<sup>12b</sup>

Pincer complexes containing different transition metals have been utilised for the transfer hydrogenation reaction, including Rh(III), Ir(III) and Ru(II) and more recently Fe(II) and Co(II) have also been investigated (Figure 2.4).<sup>12, 13, 14, 15</sup>

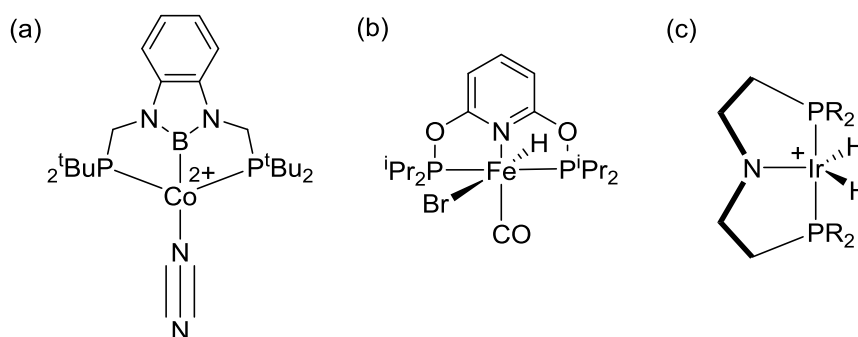


**Figure 2.4** Recent examples of catalysts for the transfer hydrogenation reaction a)  $[\text{Co(II)}(\text{PBP})\text{N}_2]^{12}$ , b)  $[\text{Fe(II)}(\text{PNP})\text{CO(H)Br}]^{13}$ , and c)  $[\text{Ir(III)}(\text{PNP})\text{H}_2]^{14}$ .

### 2.1.5. Ruthenium complexes containing pincer ligands for the transfer hydrogenation reaction

Different transition metals provide varied degree of stereoselectivity for the transfer hydrogenation of functional groups containing polar unsaturated bonds, such as ketones and imines. Among these catalysts, Ru(II) complexes containing pincer ligands proved to be the most effective catalysts for the transfer hydrogenation reaction involving carbonyl groups. The majority of such catalysts contain pincer ligands with a central aryl or pyridyl donor group with phosphine and amido side arms.<sup>4, 15</sup> For example, van Koten and co-workers have shown that Ru(II) complexes containing *NNN* and *PCP* pincer ligands are efficient transfer hydrogenation catalysts,<sup>4b</sup> while more recently Milstein and co-workers used a Ru(II) complex containing a *PNN* pincer ligand as an efficient catalyst for the coupling of alcohols and amines (Figure 2.5).<sup>15</sup>

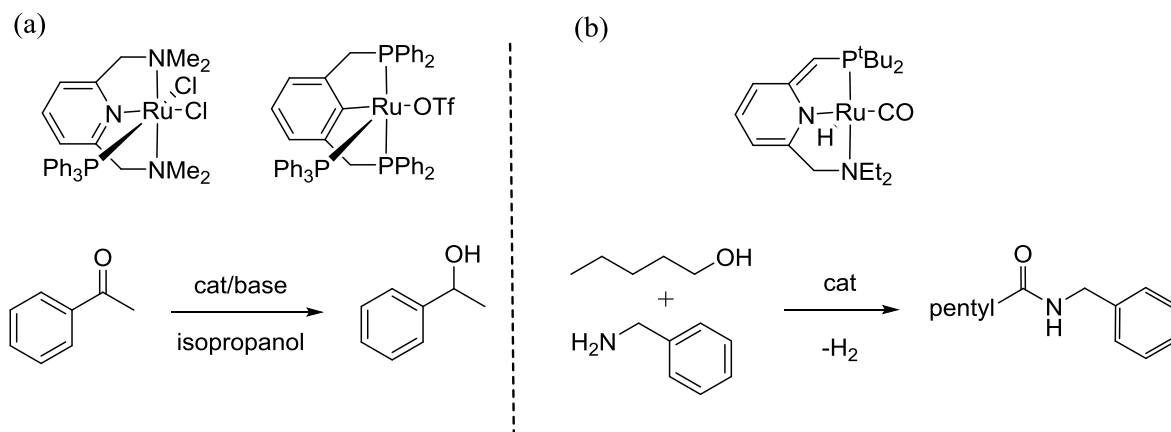


**Figure 2.5** Ru(II) complexes containing pincer ligands by, a) van Koten and b) Milstein.

Among the best catalysts for the transfer hydrogenation of ketones were reported recently by Zhenkun Yu<sup>16</sup> with turnover frequencies (TOFs) exceeding  $345600 \text{ h}^{-1}$  (Figure 2.6).<sup>16b</sup> As the asymmetric Ru(II) complex contained a combination of relatively strong (pyridine) and weak (benzimidazole and pyrazole) *N*-donor ligands, and the presence of the weakly coordinating donor atoms are likely key for effective transfer hydrogenation catalysis.

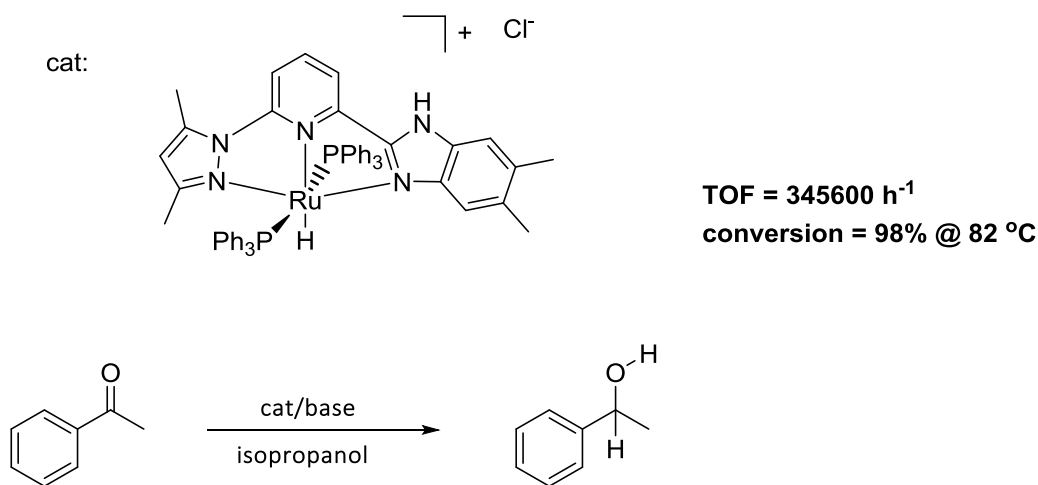


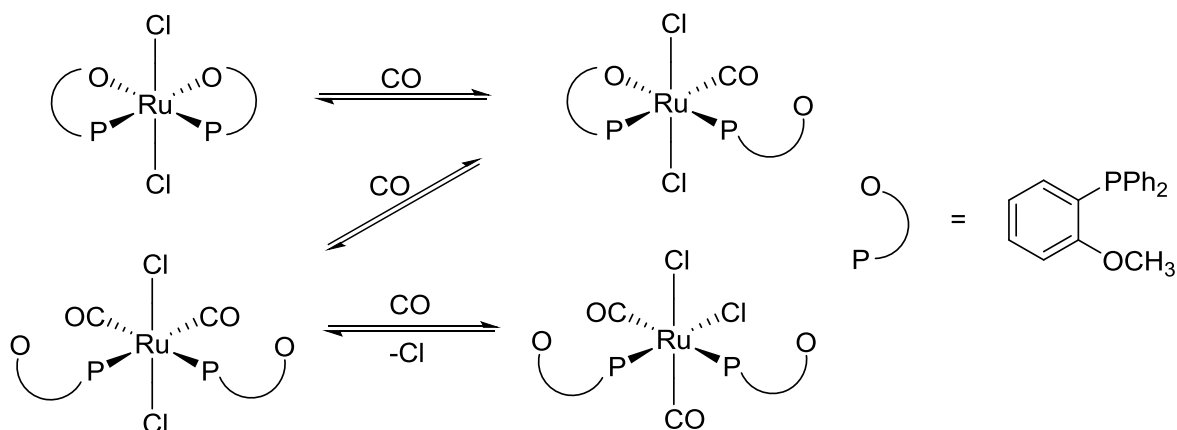
**Figure 2.6** Best catalysts for transfer hydrogenation of ketones.

The complex achieves near complete conversions within 20-30 seconds and maintains high catalytic activity under ambient conditions. However, such complexes are known to be unstable during catalysis due to the weak coordination of the ligand to the metal centre

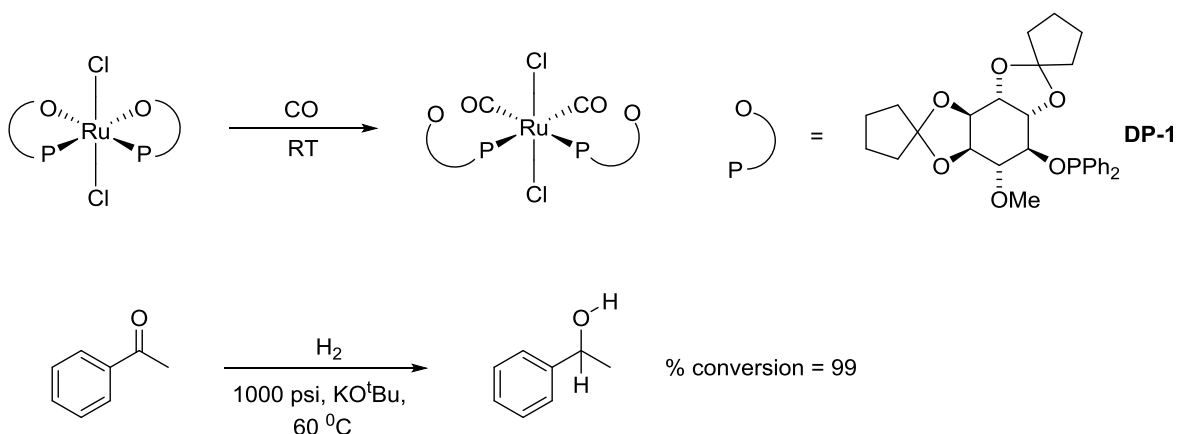
and conversion of larger quantities of substrate could be difficult.<sup>17</sup> Therefore, the utilisation of ligand motifs containing a strong central donor, such as N-heterocyclic carbenes (NHC), in combination with weakly coordinating pendent donor arms could prove to be useful for the transfer hydrogenation reaction. A central NHC donor would increase the stability of the catalyst while labile pendent donors would allow for high catalytic activity by rapid coordination/decoordination opening up vacant co-ordination sites on the metal centre to allow substrate interaction.

#### 2.1.6. Ruthenium complexes containing hemilabile ligands

In an effort to create organometallic complexes with diverse coordination modes, pincer ligands which utilise hemilability with a mix of strongly donating donors and weakly donating pendant arms that may or may not coordinate to a metal ion have received significant attention. However, few Ru(II) complexes have been reported in literature with such hemilabile character. Jeffrey and Rauchfuss, *et al.* reported the first ligand to be classified as hemilabile which was an ether-phosphine ligand, *o*-(diphenylphosphino)anisole.<sup>18</sup> The hemilabile character of the ligand was determined by monitoring the co-ordination of the ligand to a Ru(II) metal centre using IR spectroscopy (Scheme 2.1). This was achieved by recording multiple C≡O stretches which correspond to the presence of complexes bearing different numbers of metal bound CO. The data demonstrated that the oxygen donor atoms of the ligand were labile and opened up vacant sites for CO to bind to the Ru centre.



**Scheme 2.1** First reported hemilabile ligand coordinated to Ru(II) and its reactivity to CO.<sup>18</sup>



**Scheme 2.2** Ru(II) complexes containing hemilabile monophosphite ligands.

The ligand system has since been modified to produce effective catalytic systems (Scheme 2.2).<sup>19</sup> In an analogous reaction to that of the Ru(II) *o*-(diphenylphosphino)anisole complex,<sup>18</sup> addition of CO gas to the RuCl<sub>2</sub>(DP-1)<sub>2</sub> complexes (Scheme 2.2) resulted in the displacement of the oxygen donors by the CO co-ligands. The Ru(II)Cl<sub>2</sub>(DP-1)<sub>2</sub> complexes containing the hemilabile phosphinite motif proved to be superior catalysts for the asymmetric hydrogenation reaction in comparison to the analogous complexes containing strong phosphine donor atoms. This exemplified that the hemilabile character of weakly donating O-donor ligands (easily displaced by CO) on the complexes is a crucial character of effective catalysts for the asymmetric hydrogenation reaction of aromatic ketones.



### 2.1.7. Ruthenium complexes containing hemilabile pincer ligands

Xu *et al.* has also recently reported Ru(II) complexes with pincer ligands containing a strong phosphine side arm donor in combination with weakly coordinating N, S and O donor atoms.<sup>20</sup> The work demonstrated that the coordination site of the labile group/co-ligand can affect the catalytic activity of the complex bearing the pincer ligand. The Ru(II) complexes with hemilabile pincer ligands containing *PNX* (X = N, O or S) donors produced catalytic activity that varied significantly with different modes of coordination (Figure 2.7). Ru(II) complexes containing the ligand coordinated to the metal centre in a meridional (*mer*-) configuration produced greatly enhanced activity compared to complexes bearing ligands in a *fac* configuration for the hydrogenation of aromatic ketones. For example, the Ru(II) complex containing a pyridine co-ligand *trans* to the pendant phosphine donor achieves near complete conversion for the hydrogenation of acetophenone. In comparison, the analogous complex with the ligand bound to the metal centre in a (*fac*-) geometry (Figure 2.7) only achieves 10 % conversion of substrate.

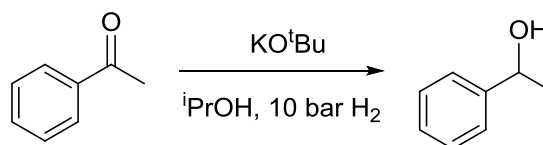
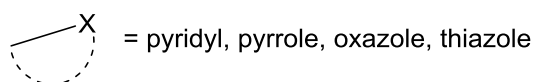
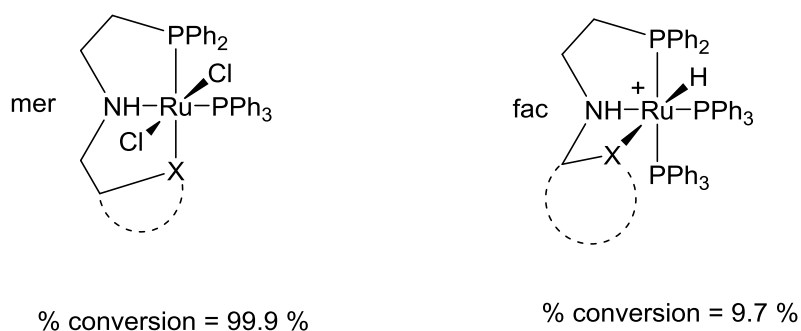
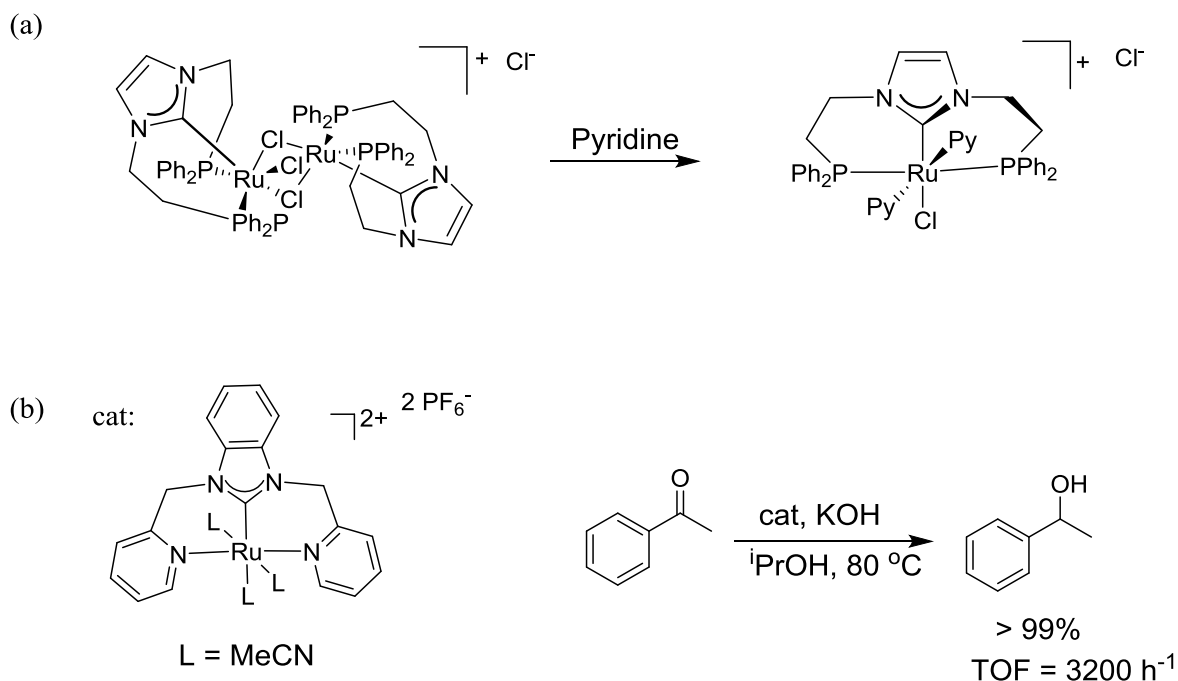


**Figure 2.7** Transfer hydrogenation of ketones catalysed by Ru(II) complexes with hemilabile pincer ligands.

#### 2.1.8. Ruthenium complexes of pincer ligands with a central NHC donor

Very little work has been reported on Ru(II) complexes bearing pincer ligands where the ligand contains a central NHC donor group. There are only three previous reports of such complexes, and in two cases, relatively strong phosphine donor side arms were present.<sup>21a</sup> A range of coordination modes were observed for these ligands depending on the co-ligands present. For example, a facial configuration of a *PCP* pincer ligand was observed in the bimetallic  $[\text{Ru(II)}_2(\text{PCP})_2\text{Cl}_3]$  complex (Scheme 2.3a). However, upon addition of pyridine the dimer is cleaved in two resulting in a  $[\text{Ru(II)}(\text{PCP})\text{Py}_2\text{Cl}]^+$  complex where a meridional coordination of the *PCP* ligand is observed (Scheme 2.3a). Recently a Ru complex bearing an *NCN* pincer ligand with a central imidazolium donor and pyridyl side arms was synthesized. A meridional coordination of the ligand to the ruthenium metal centre was observed for the complex (Scheme 2.3b)<sup>21b</sup>. The  $[\text{Ru(II)}(\text{NCN})(\text{CH}_3\text{CN})](\text{PF}_6)_2$  complex

(Scheme 2.3b) proved to be highly active for the transfer hydrogenation of aromatic ketones.



**Scheme 2.3** Ru(II) complexes containing a pincer ligand with a central NHC donor.

### 2.1.9. Rhodium and Iridium complexes with pincer ligands

Other complexes with different metals in have been reported in the literature including Pd(II), Rh(I) and Ir(I) complexes containing a central NHC donor and weakly coordinating side donor arms.<sup>22, 23</sup> A number of these complexes show superior catalytic activity in comparison to analogous complexes with strongly coordinating side arm donors. For example, an Ir(I) complex with a carbene ligand and two pendant pyridyl donor groups, hence potentially a  $\kappa^2$  or  $\kappa^3$  complex, demonstrated enhanced catalytic turnovers for transfer hydrogenation (Figure 2.8) relative to the efficiency of other Ir(I) NHC complexes.<sup>22</sup> Similar to the ligand system under investigation here, Shreeve and co-workers reported Pd(II) complexes with bidentate ligands containing the strongly donating carbene donor as

well as the weakly coordinating pyrazole donors as catalysts for the Heck and Suzuki reactions in ionic liquids, (Figure 2.8).<sup>23</sup> The hemilability of this ligand facilitated the weakly coordinating pyrazole to dissociate from the metal centre, allowing the catalyst to pass through the key Pd(0) intermediate for enhancing catalysis.

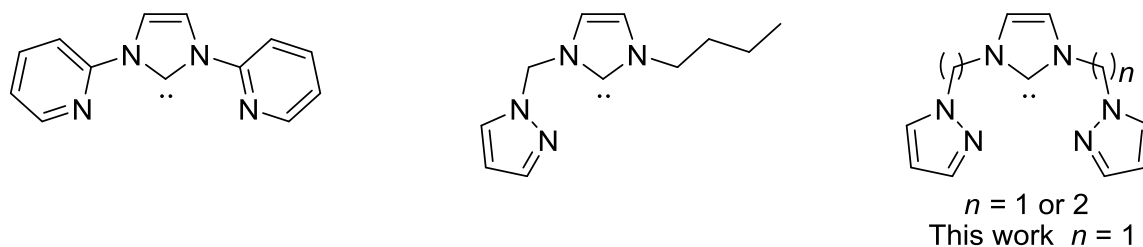


**Figure 2.8** Comparison of other carbene-based ligands with pendant N-heterocyclic donor groups. In this work,  $n = 1$ .

We have recently reported the coordination chemistry and catalytic activity of Rh(I) and Ir(I) complexes containing a pincer ligand with a central NHC and a pair of weakly coordinating pyrazole pendant donors (Figure 2.8).<sup>24</sup> As with many other hemilabile carbene containing ligands, these Rh(I) and Ir(I) complexes exhibited a diverse coordination chemistry, including the less flexible ligands ( $n = 1$ ). The Ir(I) and Rh(I) complexes with the ligand featuring a methylene bridge ( $n = 1$ ) were shown to be good catalysts for both hydroamination and hydroacyloxylation but not hydrosilylation reactions. It was found that an increase in hemilability of the pendant donors, achieved using a longer linker between the pendant donor and the central NHC donor (ethylene vs methylene bridge), resulted in much poorer catalytic activity for hydrocarboxylation reactions. A similar reactivity was observed in hydroamination reactions.

## 2.2. Aims of this chapter

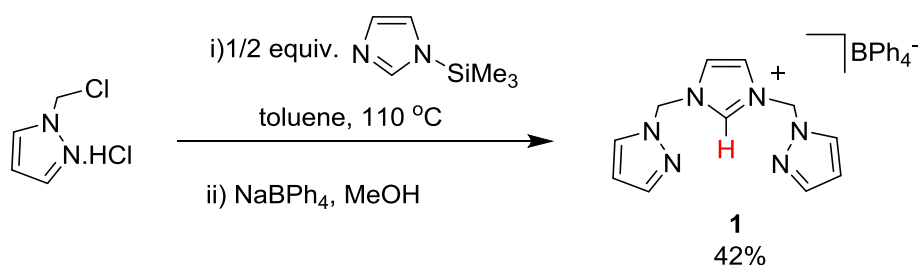
The work presented in this chapter focuses on pincer ligands containing a central *N*-heterocyclic carbene donor together with labile pendant pyrazole donors. The carbene donor should provide a strong  $\sigma$ -bond to the metal centre,<sup>11a</sup> thereby stabilising metal complexes which use this particular ligand giving access to a range of different coordination modes. Complexes of such hemilabile pincer ligands are known to display enhanced catalytic activity over analogous complexes where the pendant arms are strongly binding.

The specific aim of this chapter is to investigate the synthesis and co-ordination chemistry of a number of novel Ru(II) complexes containing a hemilabile  $NCN^{Me}$  pincer ligand and subsequently test the novel complexes as catalysts for the transfer hydrogenation reaction of ketones. The specific aims were:

- To synthesise a range of Ru(II) complexes of the  $NCN^{Me}$  pincer ligand containing different co-ordination modes with the aim of controlling the coordination mode via careful reagent selection.
- To characterise the new complexes and analyse the co-ordination chemistry using NMR spectroscopy, mass spectrometry, elemental and X-ray crystallography.
- To test the catalytic activity of all synthesised Ru(II) complexes for the transfer hydrogenation of acetophenone. To explore the scope of the catalysis for a range of ketone substrates.

2.3. Synthesis of Ru(II) complexes containing a hemilabile  $NCN^{Me}$  pincer ligand2.3.1. Synthesis and characterisation of  $[Ag(I)(NCN^{Me})_2]BPh_4$  (**2**)

The  $NCN^{Me}$  ligand **1** was synthesised according to a procedure previously published from our group. This was achieved by treating chloromethylpyrazole with half a molar equivalent of trimethylsilyl imidazole in refluxing toluene (Scheme 2.4).<sup>24</sup> After 16 hours, a viscous brown oil formed; upon anion exchange with  $NaBPh_4$ ,  $(NCN^{Me})BPh_4$  (**1**) was isolated as colourless crystals in 42% yield.



**Scheme 2.4** Synthesis of imidazolium bis-pyrazole ligand **1** from chloromethylpyrazole and trimethylsilyl imidazole.

Crystals suitable for X-ray analysis were grown by slow evaporation of a saturated acetone solution of **1**. As expected, the solid state structures confirmed the chemical structure of the ligand essentially in a linear conformation (Figure 2.9).

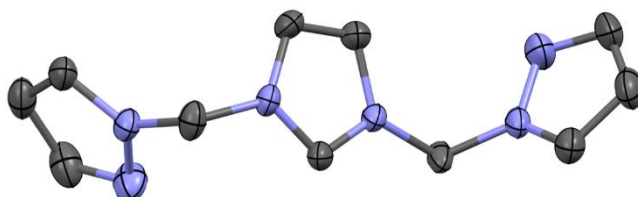


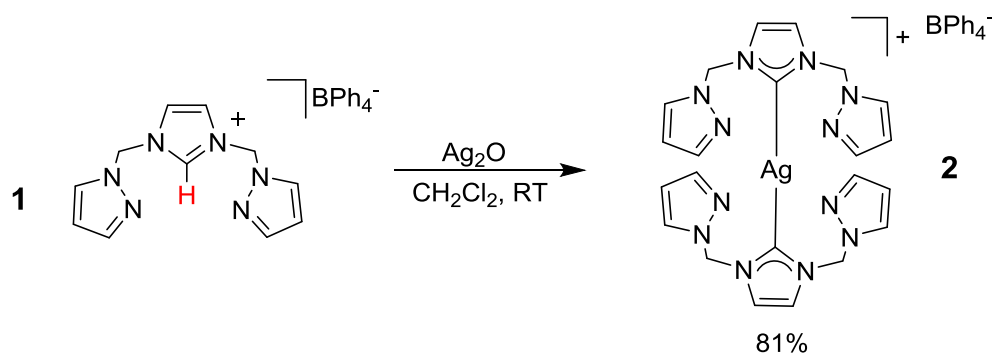
**Figure 2.9** X-ray crystal structure of the imidazolium bis-pyrazole ligand **1**. Ellipsoids shown with 50% probability, hydrogen atoms and  $BPh_4$  anion have been omitted for clarity.

Initial attempts to produce a Ru(II) complex directly using the ligand **1** were undertaken by reacting the metal precursor  $[Ru(II)(\eta^6-C_6H_6)Cl_2]_2$  with the  $NCN^{Me}$  ligand **1** in the presence of  $NEt_3$  as an external base in refluxing methanol or ethanol. The resulting mixture

contained multiple species and subsequent isolation of the desired complex was attempted by recrystallising the product from the crude mixture using dichloromethane and *n*-pentane. However, any single Ru(II) complex proved to be inseparable from the unwanted components in the crude mixture. Multiple attempts at recrystallisation reduced the number of unwanted by-products in the crude mixture, however, separation of any major product proved to be unsuccessful.

Silver transmetallation has proven to be a mild and efficient method for the synthesis of Ru(II) complexes containing carbene ligands.<sup>25</sup> Due to the versatility of Ag(I) complexes for transmetallating with many transition metals, the silver complex of ligand **1** was first targeted and isolated. This approach also avoids any problem arising from simple deprotonation of imidazolium salts that generate free carbene ligands in solution which can be extremely unstable and are prone to react/decompose.

The silver complex containing the  $NCN^{Me}$  ligand **1** was synthesised by treating **1** with excess  $Ag_2O$  in dichloromethane to produce  $[Ag(I)(NCN^{Me})_2]BPh_4^-$  (**2**) as a white solid in 81% yield (Scheme 2.5).



**Scheme 2.5** Synthesis of  $[Ag(I)(NCN^{Me})_2]BPh_4^-$  (**2**).

The  $^1H$  NMR spectrum of complex **2** exhibits eight proton resonances, five of which are attributed to the ligand protons, while the other three are due to the  $BPh_4^-$  protons. The

absence of imidazolium proton resonances indicated successful complexation of Ag(I) metal to the ligand. The 2D  $^1\text{H}$ - $^{13}\text{C}$  HMBC spectrum revealed the resonance value for the imidazolium (ImC2) carbon to be 183.9 ppm, which is characteristic of silver metal bound carbonic carbons. Only one set of proton resonances was present which suggested a symmetric structure of the silver intermediate. The ratio of integration of ligand proton resonances to  $\text{BPh}_4^-$  proton resonances was 2:1, indicating a bis-carbenic- $\kappa^1\text{-NCN}$  geometry. X-ray crystallography confirmed both the  $\kappa^1\text{-NCN}$  coordination to Ag(I) in a linear geometry as well as the symmetric structure of the *bis*-ligand monometallic complex (Figure 2.10).

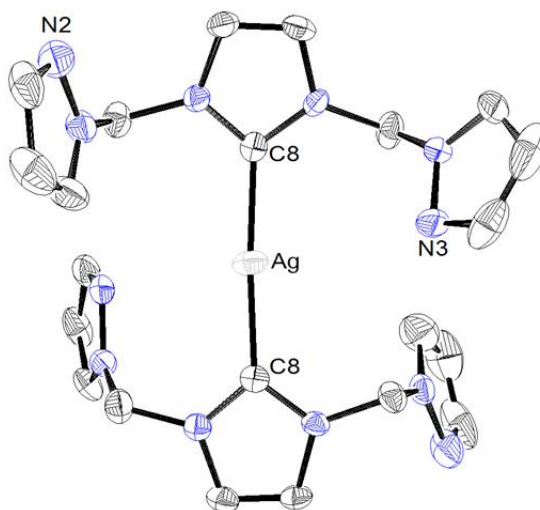
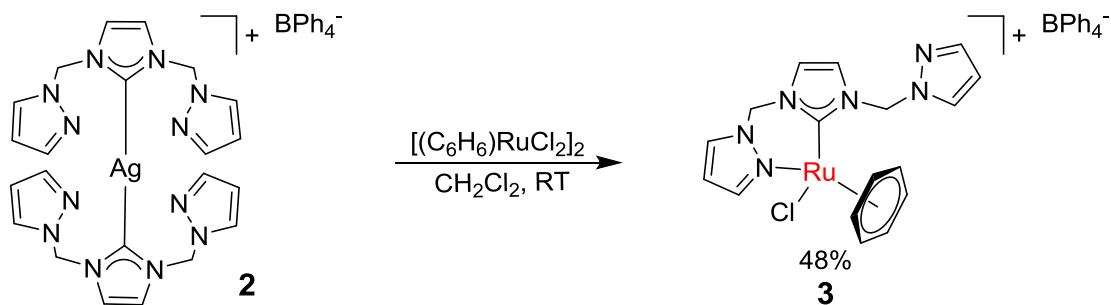


**Figure 2.10** ORTEP depiction of the structure of complex **2** with ellipsoids at 50% probability. Hydrogen atoms and  $\text{BPh}_4$  have been omitted for clarity.

### 2.3.2. Synthesis and characterisation of $[\text{Ru}(\text{II})(\eta^6\text{-C}_6\text{H}_6)(\text{NCN}^{\text{Me}})\text{Cl}]\text{BPh}_4$ (**3**)

The precursor  $[\text{Ru}(\text{II})(\eta^6\text{-C}_6\text{H}_6)\text{Cl}_2]_2$  with was reacted with one molar equivalent of **2** to afford the complex  $[\text{Ru}(\text{II})(\eta^6\text{-C}_6\text{H}_6)(\text{NCN}^{\text{Me}})\text{Cl}]\text{BPh}_4$  (**3**) as a bright yellow solid in 48% yield (Scheme 2.6).





**Scheme 2.6** Synthesis of  $[Ru(II)(\eta^6-C_6H_6)(NCN^{Me})Cl]BPh_4^-$  (**3**) from **2**.

The  $^1H$  NMR spectrum of complex **3** contains sixteen resonances. Twelve of the  $^1H$  resonances were attributed to the  $NCN$  ligand protons, one to the benzene co-ligand and three to the  $BPh_4^-$  counterion. The presence of twelve  $^1H$  resonances for the  $NCN^{Me}$  ligand **1** suggests there is asymmetry in the three dimensional structure of the complexes. Although only two resonances were expected for the methylene protons, the presence of four resonances indicated the diastereotopic nature of the methylene protons. The integration ratio of the proton resonances due to ortho Ar-H of the  $BPh_4^-$  counterion and a ligand proton resonance is 8:1 which indicates a 1:1 Ru(II) complex to  $BPh_4^-$  counterion ratio. A Cl co-ligand is likely to be co-ordinated to the Ru(II) metal centre to balance the remaining 1+ charge of the Ru(II) species. As the benzene co-ligand appears as a singlet, it indicates that it is still bound to Ru(II) in an  $\eta^6$  co-ordination, and occupies three co-ordination sites of the Ru(II) metal. Only two co-ordination sites remain on the Ru(II) metal centre which infers a bidentate co-ordination of  $NCN^{Me}$  ligand **1** to Ru(II). The expected structure containing the bidentate co-ordination geometry was confirmed using X-Ray crystal structure analysis (Figure 2.11). Mass spectrometry of the isolated yellow solid shows a single dominant signal at 443.03 m/z which is attributed to the loss of the  $BPh_4^-$  counterion. The isotope pattern of the signal matches the expected isotope pattern typical of Ru(II) complexes.

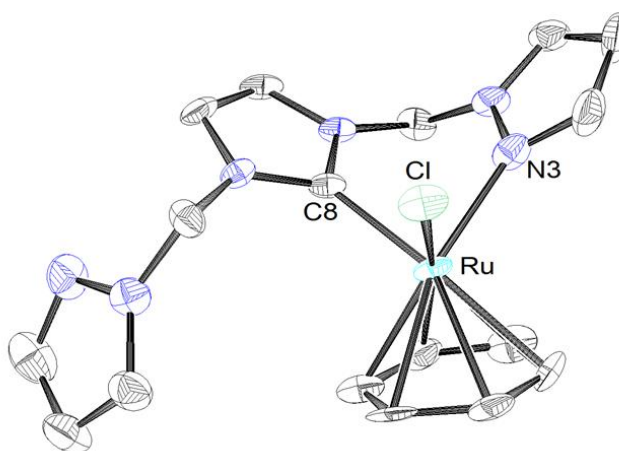
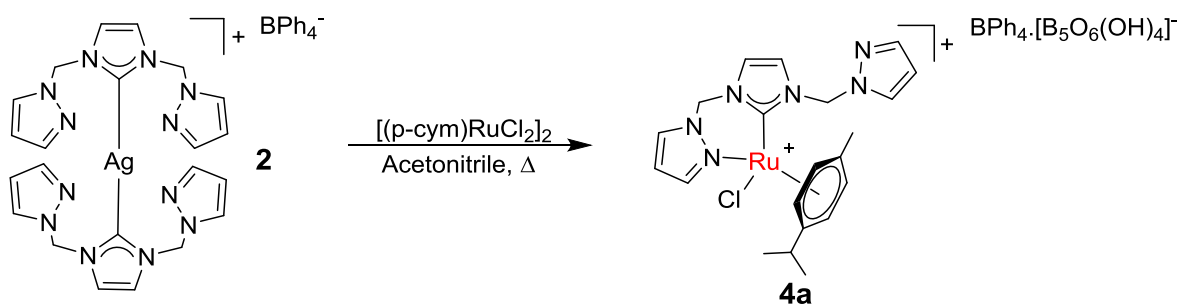


**Figure 2.11** ORTEP depiction of the structure of complex **3** showing atom labelling scheme. Hydrogen atoms and BPh<sub>4</sub><sup>-</sup> have been omitted for clarity.

### 2.3.3. Synthesis and characterisation of Ru(II)( $\eta^6$ -C<sub>10</sub>H<sub>14</sub>)(NCN<sup>Me</sup>)Cl]BPh<sub>4</sub> (**4**)

Due to the successful synthesis of complex **3** using the isolated silver intermediate **2**, the silver transmetallation route was utilised in attempts to produce the analogous complex containing the *p*-cymene co-ligand. Reaction of the precursor [Ru(II)( $\eta^6$ -*p*-cym)Cl<sub>2</sub>]<sub>2</sub> with one molar equivalent of [Ag(NCN<sup>Me</sup>)<sub>2</sub>]BPh<sub>4</sub> (**2**) (Scheme 2.7) was expected to produce the complex [Ru(II)( $\eta^6$ -*p*-cym)(NCN<sup>Me</sup>)Cl]BPh<sub>4</sub> (**4**). However, the elemental analysis of the mixture had a carbon composition 20% below the expected value (C: 65.97, H: 5.78, N: 10.26). Elucidation of the solid state structure of the mixture using X-ray crystallography revealed the presence of **4a** with only an unusual [B<sub>5</sub>O<sub>6</sub>(OH)<sub>4</sub>]<sup>-</sup> counterion (Figure 2.12). The <sup>1</sup>H NMR spectrum of the mixture showed the expected proton resonances consistent with the structure of complex **4**; similar to complex **3**, twelve proton resonances are attributed to the ligand. However, the integration ratio of *o*-BPh<sub>4</sub> proton resonances to a ligand proton resonance was approximately 0.7:1, this is approximately 14% of the expected ratio of 8:1.



Scheme 2.7 Synthesis of  $[\text{Ru}(\eta^6\text{-C}_{10}\text{H}_{14})(\text{NCN}^{\text{Me}})\text{Cl}]\text{BPh}_4\text{[B}_5\text{O}_6(\text{OH})_4\text{]}^-$  (**4a**).

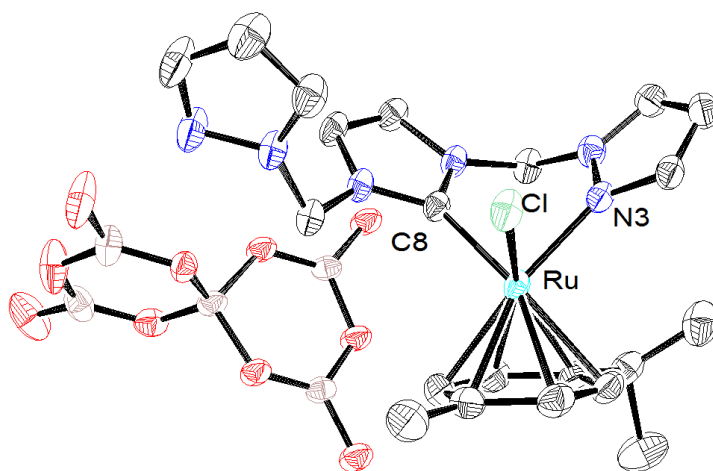
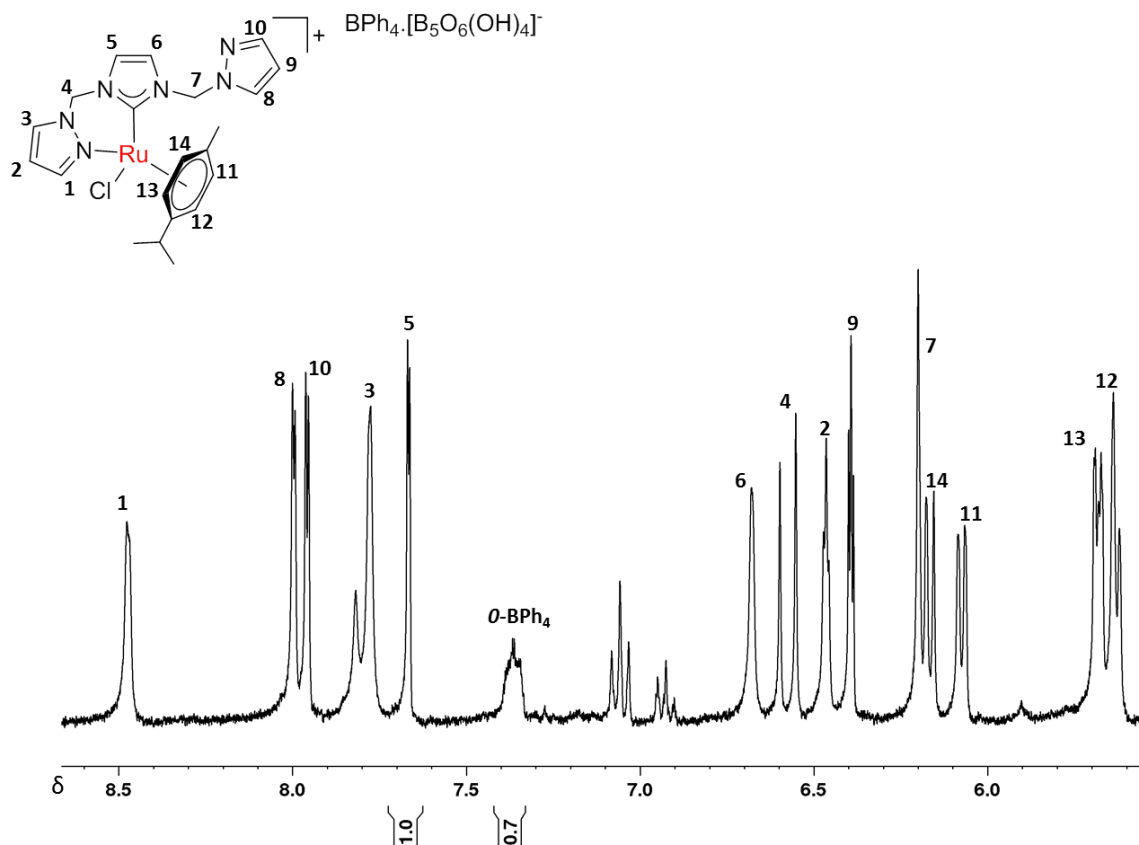


Figure 2.12 ORTEP depiction of the structure of complex **4a** showing atom labelling scheme (red: oxygen, purple: boron). Hydrogen atoms have been omitted for clarity.

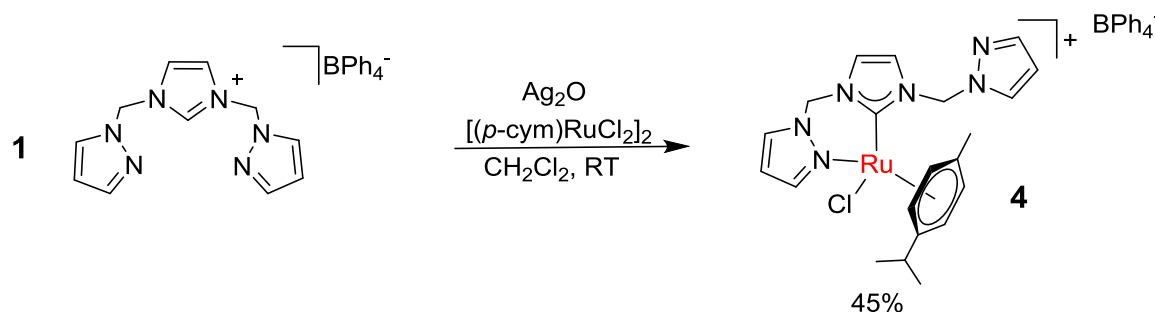


**Figure 2.13**  $^1\text{H}$  NMR spectrum of  $\text{Ru}(\text{II})(\eta^6\text{-C}_{10}\text{H}_{14})(\text{NCN}^{\text{Me}})\text{Cl}]\text{BPh}_4[\text{B}_5\text{O}_6(\text{OH})_4]$  (**4a**).

The integration ratio of ligand protons in the mixture: *o*-protons of the  $\text{BPh}_4^-$  counterion is 1: 0.7 as shown in Figure 2.13, which is equivalent to a ligand:  $\text{BPh}_4^-$  ratio of 1: 0.175. This ratio shows 14% of the counterion is  $\text{BPh}_4^-$  and that the ratio of  $[\text{B}_5\text{O}_6(\text{OH})_4]:\text{BPh}_4$  is 86:14. This counterion ratio is in close agreement with the elemental analysis. However, slightly different ratio of counterions were produced upon attempts to repeat the reaction.

An *in situ* silver transmetallation reaction was carried out in an attempt to avoid the  $\text{BPh}_4/[\text{B}_5\text{O}_6(\text{OH})_4]^-$  mixture where the  $\text{NCN}^{\text{Me}}$  ligand (**1**) was reacted with half a molar equivalent of  $[\text{Ru}(\text{II})(\eta^6\text{-}p\text{-cym})\text{Cl}_2]_2$  in the presence of  $\text{Ag}_2\text{O}$  in dichloromethane (Scheme

2.8). The reaction was successful and afforded complex **4** as an orange-yellow solid in 45% yield which does not contain the  $[\text{B}_5\text{O}_6(\text{OH})_4]^-$  anion, only  $\text{BPh}_4^-$ .



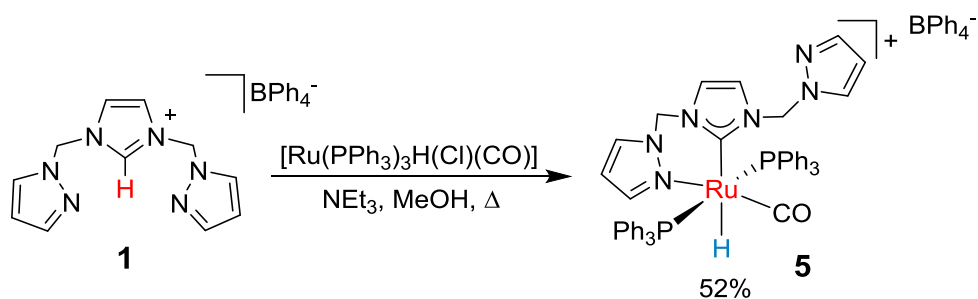
**Scheme 2.8** Synthesis of  $[\text{Ru}(\text{II})(\eta^6\text{-}p\text{-cym})(\text{NCN}^{\text{Me}})\text{Cl}]\text{BPh}_4$  (**4**).

The  $^1\text{H}$  NMR spectrum of **4** showed a similar set of proton resonances to the complex **4a** which contained the unusual counterion  $[\text{B}_5\text{O}_6(\text{OH})_4]^-$ . However, the integration ratio of  $\sigma\text{-BPh}_4^-$  proton resonances to a ligand proton resonance for complex **4** is 8:1. Elemental analysis of the complex (C: 65.86; H: 5.77; N: 9.83) confirmed the calculated values and suggested that only  $\text{BPh}_4^-$  is present as the counterion.

#### 2.3.4. Synthesis and characterisation of $[\text{Ru}(\text{II})(\text{H})\text{CO}(\text{NCN}^{\text{Me}})(\text{PPh}_3)_2]\text{BPh}_4$ (**5**)

Deprotonation of imidazolium salts using an external base such as triethylamine is a common method for the synthesis of Ru(II) NHC complexes.<sup>26</sup> If the metal precursor is also added into the reaction mixture along with the base the accumulation of the free carbene can be avoided.

Reaction of the imidazolium ligand **1** with one molar equivalent of the precursor  $[\text{Ru}(\text{II})(\text{H})\text{Cl}(\text{CO})(\text{PPh}_3)_3]$  in the presence of excess  $\text{NEt}_3$  in refluxing methanol resulted in the formation of complex **5** as a white powder in 52% yield (Scheme 2.9).



**Scheme 2.9** Synthesis of  $[\text{Ru}(\text{H})\text{CO}(\text{NCN}^{\text{Me}})(\text{PPh}_3)_2]\text{BPh}_4$  (**5**) from **1**.

The  $^1\text{H}$  NMR spectrum of complex **5** shows ten ligand proton resonances and is indicative of the asymmetric structure of complex **5**. The resonances of the protons of one of the pyrazole rings are at significantly different chemical shifts to those of the other pyrazole ring suggesting a  $\kappa^2$ -coordination (NC) of ligand **1** to the Ru(II) metal centre. Additionally, a triplet resonance due to a Ru(II) bound hydride was observed at -6 ppm ( $^2J_{\text{H-P}} = 21.9$  Hz) indicative of a hydride that is situated *cis* to two chemically equivalent phosphorous atoms which are *trans* to one another ( $^{31}\text{P}$  NMR,  $\delta = -48$  ppm,  $^2J_{\text{H-P}} = 21.9$  Hz).<sup>27</sup> Unlike complex **4**, only two resonances were assigned to the methylene protons as singlets which indicated the absence of diastereotopic coupling. The structure of complex **5** was confirmed by single crystal X-ray structure analysis (Figure 2.14), with the hydride in a *trans* configuration relative to the carbonic carbon (Im C2) and *cis* to the two  $\text{PPh}_3$  groups. The IR spectrum contained two distinct, strong signals for the Ru-H ( $1606\text{ cm}^{-1}$ ) and Ru-CO ( $1938\text{ cm}^{-1}$ ) stretches.

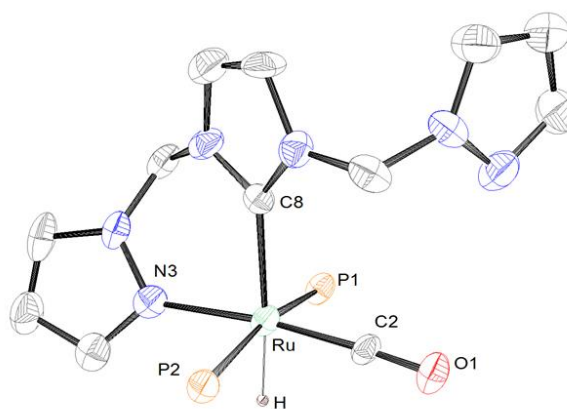


**Figure 2.14** ORTEP depiction of the structure of complex **5** showing atom labelling scheme. Hydrogen atoms have been omitted for clarity. Phenyl groups of the PPh<sub>3</sub> ligands were omitted for clarity.

#### 2.3.4.1. Isomerisation reaction of [Ru(II)(H)CO(NCN<sup>Me</sup>)(PPh<sub>3</sub>)<sub>2</sub>] (**5**):

Upon analyzing the <sup>1</sup>H NMR data of **5** a second hydride resonance and a second set of ligand peaks in the base line were observed. Variable temperature <sup>1</sup>H NMR experiments were undertaken to determine if this second set of resonances was due to the free pyrazole arm binding to the metal centre to produce a  $\kappa^3$ -coordination geometry of the pincer ligand. When the complex was heated to 70 °C in CH<sub>3</sub>CN for 24 h the second set of resonances increased in intensity. 2D NMR (NOESY, COSY) did not reveal any cross peaks between the two sets of proton resonances which would have indicated some exchange process. It was determined that the second set of proton resonances represented an isomerisation of the CO and H co-ligands (Figure 2.15). As the isomer which contains the hydride co-ligand in a *trans* position to the pyrazole nitrogen produces a distinct triplet resonance at -13 ppm; the ratio of **5** and **5a** was monitored overtime by calculating the integration ratio of the two resonances at -6 and -13 ppm. The irreversible reaction to **5a** achieves over 95% conversion after 36 hours in refluxing acetonitrile.

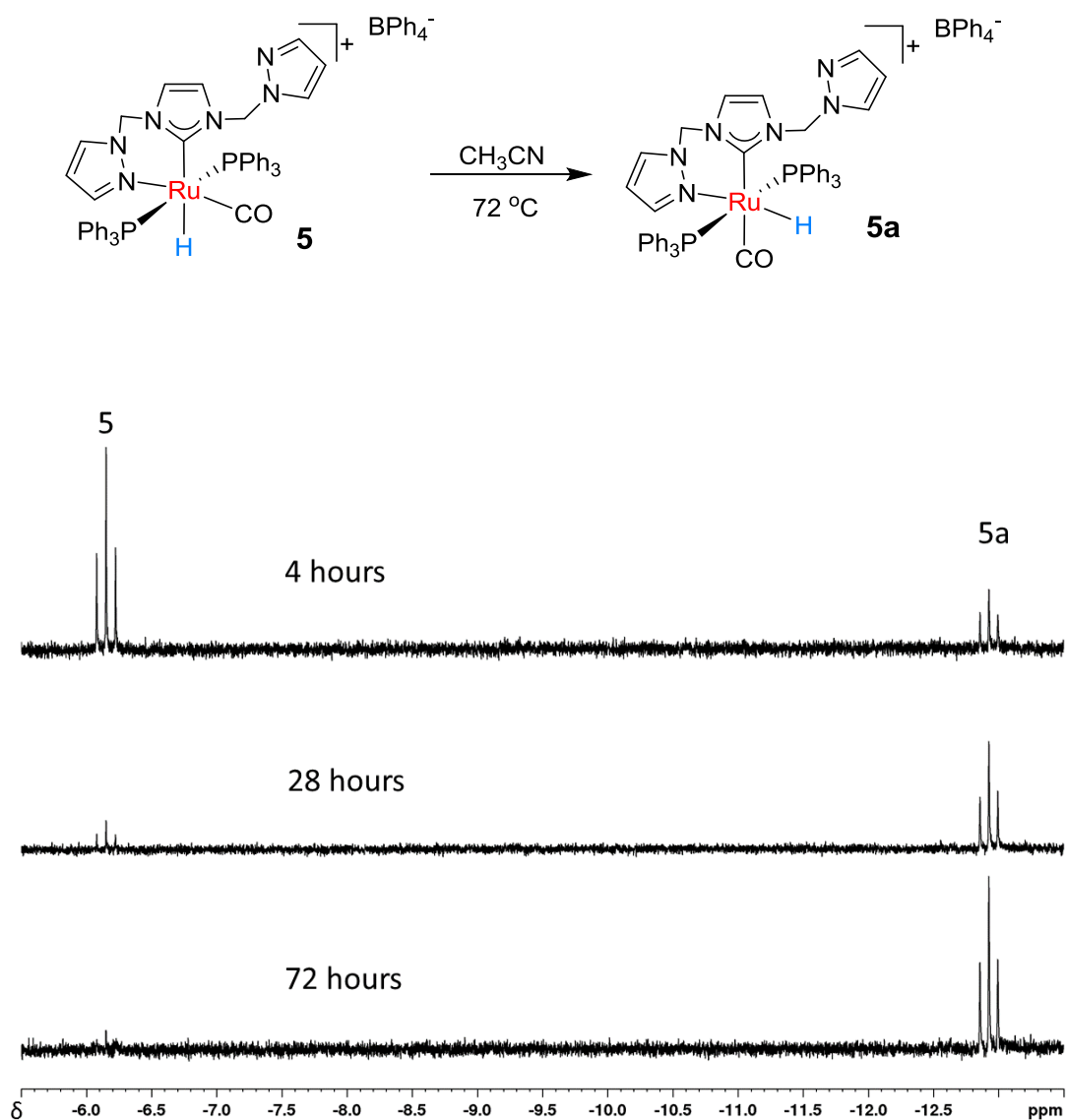


**Figure 2.15** Stacked  $^1\text{H}$  NMR spectra of the hydride resonance regions at  $72^\circ\text{C}$  for complexes **5** and **5a**. (*H trans* to pyrazole + *H cis* to pyrazole).

#### 2.3.4.2. Synthesis of an unexpected cubane structure $[\text{Ru}(\text{I})\text{Cl}(\text{PPh}_3)]_4$ (**6**)

Initial attempts to produce the complex  $[\text{Ru}(\text{II})(\text{H})\text{CO}(\text{NCN}^{\text{Me}})(\text{PPh}_3)_2]\text{BPh}_4$  (**5**) by reacting the silver intermediate  $[\text{Ag}(\text{I})(\text{NCN}^{\text{Me}})_2]\text{BPh}_4$  with one molar equivalent of  $[\text{Ru}(\text{II})(\text{H})\text{ClCO}(\text{PPh}_3)_3]$  resulted in isolation of a grey powder which was found to be a mixture of a complex with different counterions,  $[\text{Ru}(\text{II})(\text{H})\text{CO}(\text{NCN}^{\text{Me}})(\text{PPh}_3)_2]\text{X}$  (where  $\text{X} = \text{BPh}_4$  or  $\text{Cl}$ ). The  $^1\text{H}$  NMR spectrum of the mixture showed an  $\text{ortho BPh}_4^-$ :  $\text{NCN}^{\text{Me}}$  ligand proton resonance ratio



significantly lower than the expected value of 8:1 indicating that the remaining amount of counterion is likely Cl. Multiple attempts to purify complex **5** from the crude mixture by recrystallisation proved to be unsuccessful. However, single crystals suitable for X-ray crystallography were grown from the crude mixture. Elucidation of the resulting green crystals by X-ray analysis revealed an unusual distorted Ru(I) cubane structure (Figure 2.16).

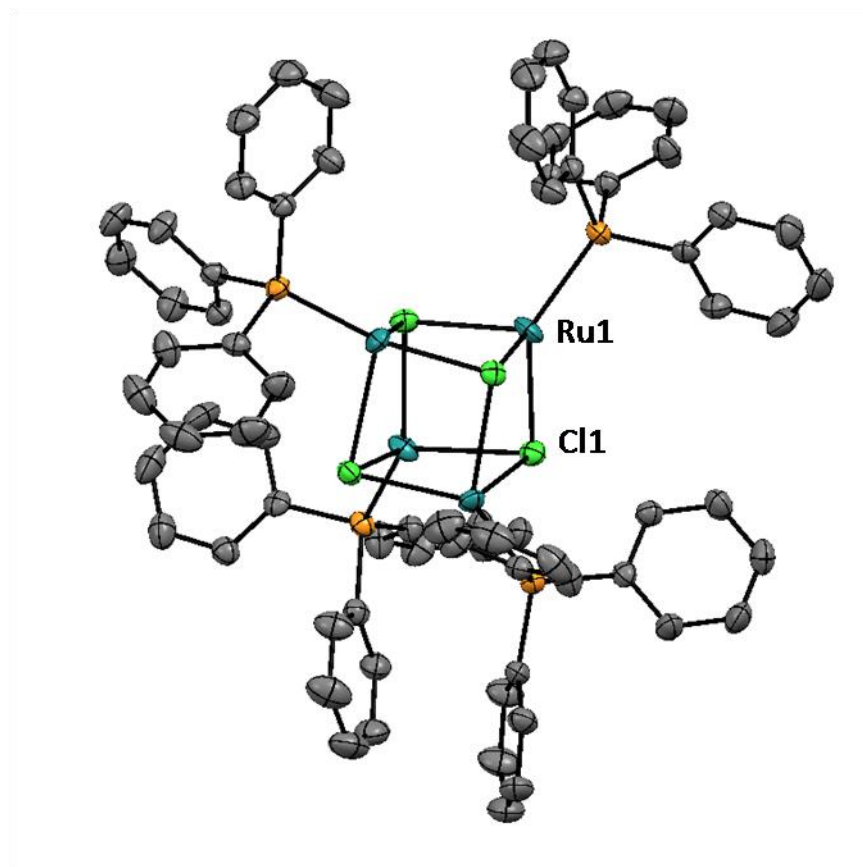


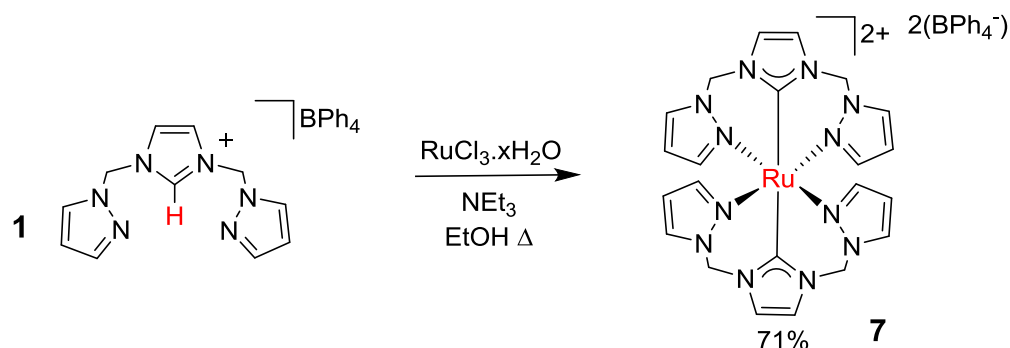
**Figure 2.16** Molecular structure of complex **6** showing atom labelling scheme. Hydrogen atoms have been omitted for clarity.

Interestingly, complex **6** has not been reported in literature and only a few Ru complexes are reported to contain an analogous cuboid structure.<sup>28</sup> The analogous  $[\text{Ru(II)Cl}(\text{Cp})]_4$  complex is a useful precursor for the production of a number of Ru(II) complexes.<sup>28a</sup> Isolation of  $[\text{Ru(I)Cl}(\text{PPh}_3)]_4$  in higher yields could prove to be important as the complex can

be utilised as a new class of ruthenium(I) precursor. As shown in Figure 2.16, the cubane structure consists of two distorted tetrahedral units of ruthenium(I) and chlorine atoms, each ruthenium ion is also coordinated to a single PPh<sub>3</sub> ligand. The Ru(I)-Cl bond distances range from 2.523 Å to 2.761 Å. These distances are closely comparable to the isostructural Ag<sub>4</sub>Cl<sub>4</sub>(PPh<sub>3</sub>)<sub>4</sub> reported in literature.<sup>28</sup> The Ru(I)-P bond distances are smaller (2.369 Å- 2.377 Å) in comparison to the Ru(I)-Cl bond distances. Interestingly, all Ru(I)-P-C angles which range from 112.75- 116.55° are larger than typical tetrahedral angles likely due to the strained cubic structure. This trend is also evident for the P-Ru(I)-Cl bond angles which range from 112.07- 139.78°.

### 2.3.5. Synthesis and characterisation of [Ru(II)(NCN<sup>Me</sup>)<sub>2</sub>](BPh<sub>4</sub>)<sub>2</sub> (**7**)

Deprotonation of the pro ligand **1** using NEt<sub>3</sub> as an external base followed by complexation with one molar equivalent of Ru(III)Cl<sub>3</sub>.xH<sub>2</sub>O in refluxing ethanol afforded complex **7** in 71% yield as a dull green solid (Scheme 2.10).



**Scheme 2.10** Synthesis of [Ru(II)(NCN<sup>Me</sup>)<sub>2</sub>](BPh<sub>4</sub>)<sub>2</sub> (**7**)

The <sup>1</sup>H NMR spectrum of complex **7** contained two sets of ligand proton resonances. Careful analysis of the prepared complex showed that these two sets of resonances could be attributed to the formation of two products or a pair of isomers (Figure 2.17). In

attempts to separate the two different species, single crystals were isolated from the green solid. Dissolution of the green solid in acetone followed by slow evaporation at room temperature in a crystallisation tube afforded multiple yellow single crystals suitable for X-ray crystallography. Upon dissolution of the isolated single crystals, the identical two sets of resonances remained. Mass spectrometry showed one strong signal at 279.08 m/z which indicated the presence of a single species and is assigned to the loss of two  $\text{BPh}_4^-$  counterions. Elemental analysis of the isolated crystals was in complete agreement with the calculated value of complex **7**, confirming that only one species was present. Variable temperature NMR studies showed the intensity of one set of proton resonances reduced upon reduction of temperature (Figure 2.17). Lowering the temperature also resulted in the reduction of fluctuation of the equivalent methylene ( $\text{CH}_2$ ) protons; which is evident from the conversion of the broad resonance between 6.0 to 6.1 ppm to a sharp (fwmh 13.7 Hz) signal. This indicates that one type of isomer is favoured at lower temperatures.

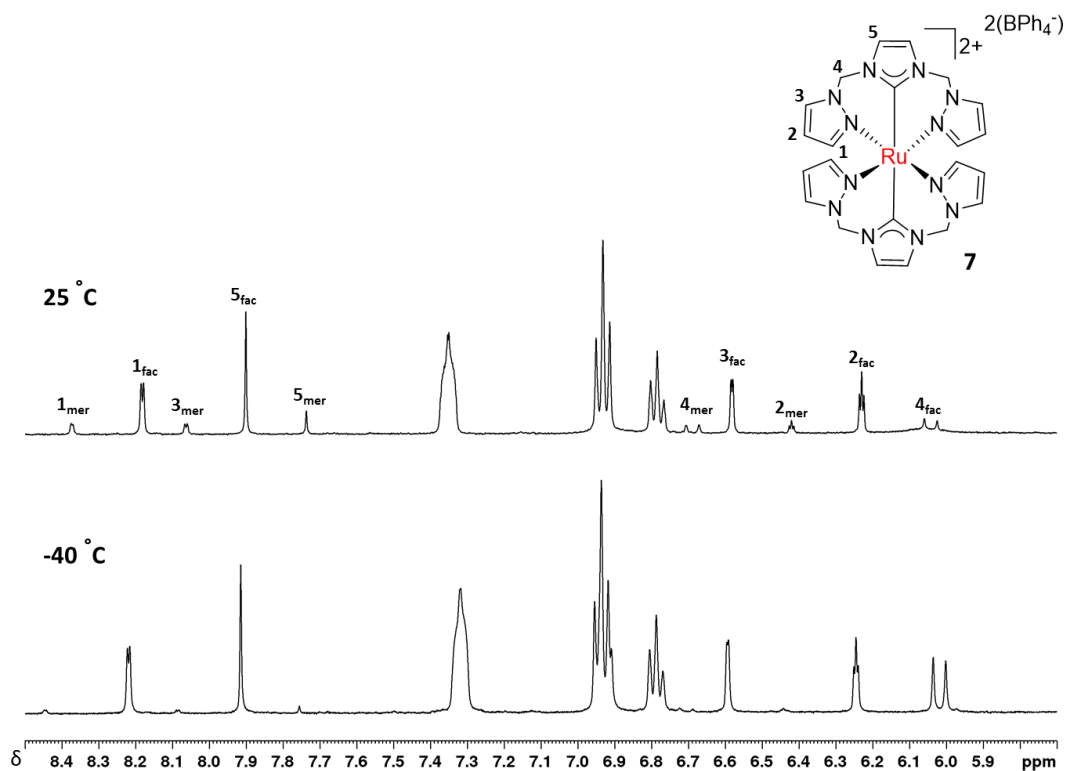


**Figure 2.17** Variable temperature <sup>1</sup>H NMR spectra of [Ru(II)(NCN<sup>Me</sup>)<sub>2</sub>](BPh<sub>4</sub>)<sub>2</sub> (**7**) showing the isomerisation between the *fac* isomer (**7**) and *mer* isomer (**7a**).

A Ru(II) bis-carbene structure was confirmed by analysis of the solid state structure using X-ray crystallography (Figure 2.19). Complex **1** can coordinate to the Ru(II) metal centre either in a facial or meridional coordination mode although only the *fac* coordination was observed by X-ray crystallography (Figure 2.18). It may be coincidental that the crystals of each isomer were indistinguishable and therefore the *mer*-isomer was not resolved by X-ray crystallography. Alternatively, the *fac* isomer could selectively crystallise but isomerises in solution.

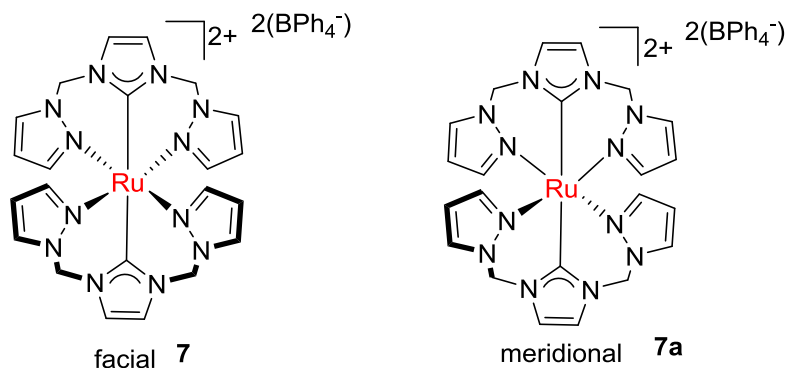


Figure 2.18 Facial and meridional coordination modes of  $[\text{Ru}(\text{II})(\text{NCN}^{\text{Me}})_2](\text{BPh}_4)_2$ .

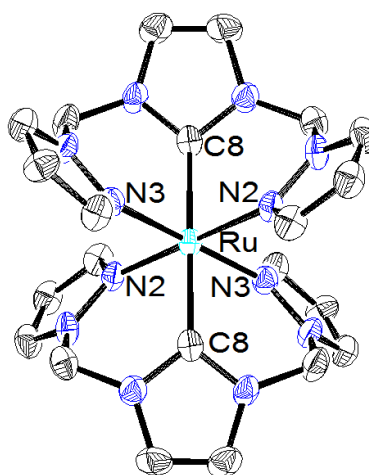


Figure 2.19 ORTEP depiction of the solid state structure of complex **7** at 50% probability thermal ellipsoids showing the *fac* coordination. Hydrogen atoms and  $\text{BPh}_4^-$  counterions have been omitted for clarity.

### 2.3.6. Comparison of solid state structures

$\text{Ru}(\text{II})$  complexes **5** and **7** adopt an octahedral geometry, with the main difference being that the  $\text{NCN}^{\text{Me}}$  ligand is bound to  $\text{Ru}(\text{II})$  in a bidentate co-ordination mode in complex **5**, while in complex **7**, the ligand adopts a tridentate co-ordination mode to the metal centre (Figure 2.18). Complex **7** is also the only species in the series that consists of a bis- NHC structure where all co-ordination sites are occupied by two ligands. The  $\text{Ru}-\text{C}(1)$  and  $\text{Ru}-\text{N}(3)$  bond lengths are slightly longer in complex **5** in comparison to the analogous bond lengths in **7**, indicating stronger bonding

interaction between Ru(II) and pyrazole in **7** as strong  $\pi$  back-donation from Ru(II) to CO in **5** weakens the Ru-pyrazole bond located in the *trans* position, see Table 2.1. The carbene carbons and pyrazole nitrogens (N2, N3) in complex **7** show no distortion from linearity as the Ru(II) ion lies on an inversion centre (C-Ru-C/N-Ru-N: 180.00(2)°). However, similar alignments in complex **5** (X-Ru-Y, where X=N, Y=C, or X=Y=P) exhibit heavy distortion from linearity (P-Ru-P: 168.77(2)°) likely due to the steric bulk of the two PPh<sub>3</sub> groups.

Atoms	<b>7</b> (Figure 2.19)	<b>5</b> (Figure 2.14)	<b>3</b> (Figure 2.11)	<b>4a</b> (Figure 2.12)
Ru(1)-C(1)	2.049(5)	2.117(6)	2.04(1)	2.046(2)
Ru(1)-C(2)	----	1.810(5)	----	----
Ru(1)-N(2)	2.076(4)	-----	-----	-----
Ru(1)-N(3)	2.088(4)	2.122(5)	2.096(7)	2.085(2)
Ru(1)-Cl	-----	-----	2.399(2)	2.408(1)
Ru(1)-P(1)	-----	2.368(1)	-----	-----
Ru(1)-P(2)	-----	2.369(1)	-----	-----
C(1)-Ru(1)-N(3)	84.2(2)	86.6(2)	83.3(3)	83.58(9)
C(1)-Ru(1)-N(2)	82.1(2)	-----	-----	-----

**Table 2.1** Selected bond lengths (Å) and angles (°) for **3**, **4a**, **5**, and **7**.

Complexes **3** and **4a** each adopt a psuedo-octahedral geometry and are similar in structure, for example, the Ru-C(1) bond lengths are the same within 1 esd. Structural similarity of complexes **3** and **4a** was further confirmed by comparison of the Ru-N(3) or Ru-Cl bond lengths, which fall within 0.01 Å of each other, as well as the C(1)-Ru-N(3) angle which differs by only 0.2° between complexes **3** and **4a**. The Ru-C1 bond lengths of complexes **3**, **4**, **4a**, **5**, **5a** and **7** are comparable to similar

Ru(II) complexes reported in the literature.<sup>29</sup> The boron counterion  $[\text{B}_5\text{O}_6(\text{OH})_4]^-$  in **4a** was identified using X-ray crystallography. The counterion is composed of a central tetrahedral boron as the apex of two six-membered rings composed of alternating boron and oxygen atoms, the counterion is terminated by four hydroxy units. The two six-membered rings in the complex are perpendicular to one another relative to the central boron atom.

As expected the crystal structure of Ag(I) complex **2** showed two  $\text{NCN}^{\text{Me}}$  ligands coordinated to the Ag(I) ion through the carbene unit. In the solid state the pendant pyrazole arms are directed toward the same face such that the complex has a centre of inversion through the silver centre. The Ag-C1 and Ag-C2 each have a bond length of 2.08 Å typical of similar silver *bis*-NHC complexes and the angle between C1-Ag-C2 is 4° off linearity (180°).<sup>30</sup> There is also slight rotation of one of the NHC ligands out of the plane relative to the other in complex **2** giving a torsion angle of 17°.

#### 2.4. Catalysed transfer hydrogenation of ketones using complexes **3**, **4**, **4a**, **5**, **5a** and **7**

Ru(II) complexes have proven to be effective catalysts for the activation of polar unsaturated bonds including transfer hydrogenation of ketones.<sup>4b</sup> The transfer hydrogenation upon use of metal catalysts such as Ru(II) does not require harsh reaction conditions. Therefore, complexes  $[\text{Ru}(\text{II})(\eta^6\text{-C}_6\text{H}_6)(\text{NCN}^{\text{Me}})\text{Cl}]\text{BPh}_4$  (**3**),  $[\text{Ru}(\text{II})(\eta^6\text{-C}_{10}\text{H}_{14})(\text{NCN}^{\text{Me}})\text{Cl}]\text{BPh}_4$  (**4**),  $[\text{Ru}(\text{II})(\eta^6\text{-C}_{10}\text{H}_{14})(\text{NCN}^{\text{Me}})\text{Cl}]\text{BPh}_4[\text{B}_5\text{H}_{10}\text{O}_4]^-$  (**4a**),  $[\text{Ru}(\text{II})(\text{H})\text{CO}(\text{NCN}^{\text{Me}})(\text{PPh}_3)_2]\text{BPh}_4$  (**5**) and  $[\text{Ru}(\text{II})(\text{NCN}^{\text{Me}})_2]\text{BPh}_4$  (**6**) were tested as catalysts for the catalysed transfer hydrogenation of ketones. A selection of substrates including aromatic and aliphatic ketones were used to test the scope of catalytic activity for the Ru(II) complexes. The reactions were carried out in refluxing *i*-PrOH using KOH as a base and a

catalyst loading of 1.5 mol% unless otherwise stated. For complete experimental details, refer to chapter 6.

Interestingly, the complexes with the pseudo-octahedral coordination geometry (**4**, **4a** and **3**) proved to be the most active for the transfer hydrogenation reaction and also gave the highest yield of hydrogenated products, see Chart 2.1. The mixed catalyst  $[\text{Ru}(\text{II})(\eta^6\text{-C}_{10}\text{H}_{14})(\text{NCN}^{\text{Me}})\text{Cl}]\text{BPh}_4[\text{B}_5\text{H}_{10}\text{O}_4]^-$  **4a** containing the unusual boron counterion achieves over 90% conversion of acetophenone to 1-phenylethan-1-ol in less than 30 minutes at 83 °C, and complete conversion within four hours. The efficacy of **4a** as a catalyst for transfer hydrogenation is comparable to some of the best Ru(II) catalysts reported for this reaction, such as  $[\text{Ru}(\text{II})(\text{OTf})(\text{PCP})\text{PPh}_3]$ .<sup>31</sup>



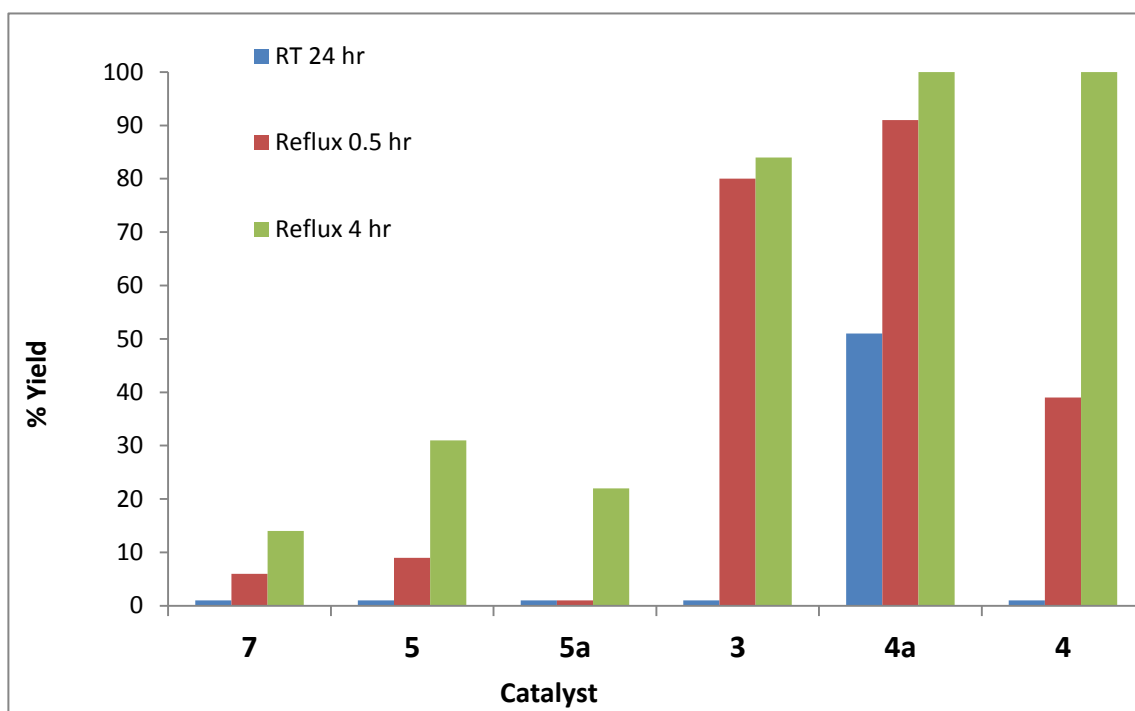
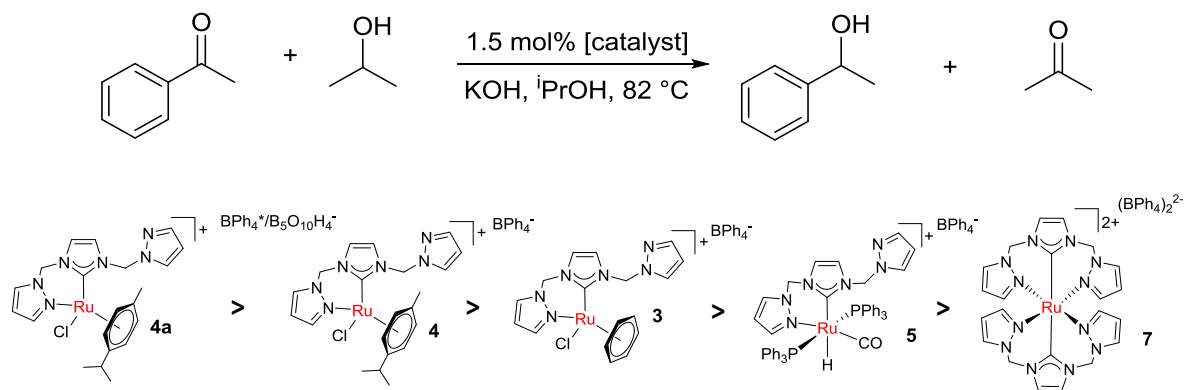


**Chart 2.1** Catalytic transfer hydrogenation of ketones. % Conversion refers to conversion of acetophenone to 1-phenylethanol-1-ol. Values in graph represent results from individual experiments.

Comparing the efficacy of complex **4a** containing the mixed borate anion with complex **4** containing pure BPh<sub>4</sub><sup>-</sup> anion, it was found that the catalyst **4a** is more active, achieving 91% conversion in 0.5 hours vs. 39% conversion for **4** (Chart 2.1). This indicates that the presence of [B<sub>5</sub>O<sub>6</sub>(OH)<sub>4</sub>]<sup>-</sup> does enhance the catalytic activity for the transfer hydrogenation reaction and is therefore non-innocent, potentially acting as a catalyst in its own right. Oxygenated four-coordinate boron compounds

have been reported previously in literature as catalysts with a moderate efficiency for the transfer hydrogenation reaction of ketones. In these reports, the boron atom is covalently linked to an organic scaffold unlike the counterion used here.<sup>32</sup> This suggests that reasonable increase in catalytic activity is a result of the pentaborate anion.

Catalysts **3** and **4a** exhibit different catalytic rates for the transfer hydrogenation of acetophenone despite the similarity in structure of the two complexes, with the only difference being the arene co-ligand (benzene, **3**, vs. *p*-cym, **4a**). Whilst complex **4** achieves complete conversion within four hours, complex **3** only reached a maximum conversion of 80% over the same period of time. The stronger electron donating properties of the *p*-cym co-ligand of complex **4** may stabilise **4** more effectively than the benzene co-ligand of complex **3**, resulting in the catalyst remaining stable for a longer period of time under the reaction condition and hence a higher conversion of the substrate.

Complex **5** catalysed the formation of the 1-phenylethan-1-ol product yielding 24% of the product after four hours at reflux, and >99% conversion after 24 hours at reflux. This slow reactivity was unexpected as the complex contains a pre-existing hydrido group which should enable a more efficient transfer hydrogenation reaction, as one of the key steps in the catalytic cycle is the transfer of a hydride from the catalyst to the substrate. It is possible that the catalytic activity is affected by the relative position of the hydride and carbonyl co-ligands on the complex, which were found to interconvert upon heating the complex in solution (*vide supra*). To test this hypothesis, complex **5** was heated to 73 °C for 24 hours to produce the isomer **5a**

with the hydrido group trans to the pyrazole. However, on testing **5a** as a catalyst for the transfer hydrogenation reaction, it achieved only 22% conversion of the substrate within four hours at 83 °C. This conversion was nearly identical to that of the *trans* isomer (**5**). Complex **5** could follow an "inner sphere mechanism" for the transfer hydrogenation reaction where an initial chloride exchange with alkoxide occurs followed by  $\beta$ -hydride elimination to give a ruthenium hydride species. However, the reaction likely proceeds at a slower rate as there is no chloride that can be lost to allow binding of the alkoxide.<sup>9</sup>

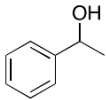
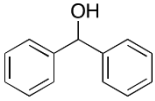
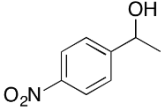
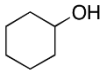
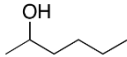
The complex with two NHC ligands **7** was expected to perform poorly for the transfer hydrogenation reaction due to the metal centre being enclosed by two pincer ligands which occupy all six available co-ordination sites. Indeed, complex **7** only promoted the transfer hydrogenation reaction to a conversion of 14% after four hours at 83 °C, and after 24 hours reached a maximum conversion of 30% (see Chart 2.1). As complex **7** is coordinatively saturated, any activity must result from the hemilability of the pyrazole side arms or decomposition to an active species.

The catalytic activity for the transfer hydrogenation of acetophenone was assessed for all Ru(II) complexes (**3**, **4**, **4a**, **5**, **5a**, and **7**) at room temperature (25 °C). Intriguingly, it was found that mixed anion complex **4a** was the only active catalyst at room temperature, resulting in a 51% conversion within 24 hours (Chart 2.1). Complexes **3**, **4**, **5**, **5a**, and **7** did not catalyse the reaction at room temperature even after 24 hours. This would suggest that the pentaborate anion does indeed play a non-innocent role in the catalysed transfer hydrogenation reaction and likely has an entirely separate mechanism from the carbene pincer based catalyst. All efforts to

isolate the pentaborate anion via salt metathesis reactions and chromatography failed, otherwise a potassium or sodium pentaborate salt would have provided an interesting set of control experiments. While most Ru(II) complexes that have been reported as catalysts for the transfer hydrogenation reaction of ketones to alcohols are effective at elevated temperatures ( $> 50\text{ }^{\circ}\text{C}$ ), there are relatively few reports of Ru(II) complexes capable of catalysing the reaction at room temperature.<sup>16</sup> The catalyst containing the pentaborate anion (**4a**) is indeed a unique system which requires further mechanistic investigation.

Whilst using complex **4** for the transfer hydrogenations it transpired that this complex was only partially soluble in the solvent/substrate propan-2-ol, and this could have led to reduced catalytic activity of the complex. Addition of THF as a co-solvent in a propan-2-ol: THF ratio of 9:1 aided solubility of the catalyst. The catalytic activity of complex **4** in either neat propan-2-ol or in the propanol-2-ol/THF mixture for the transfer hydrogenation reaction of acetophenone proved to be nearly identical (THF/iPrOH: 45% at 0.5 h,  $>99\%$  at 4 h. iPrOH: 39% at 0.5 h,  $> 99\%$  at 4h). To ensure that THF was not affecting the reactivity of the complex, complex **3** was also tested for the transfer hydrogenation reaction of acetophenone using the 9:1 propan-2-ol: THF solvent ratio. The addition of THF to the reaction mixture resulted in complete conversion of the substrate (87% after 0.5 h,  $>99\%$  at 4 h), the catalytic rate remains relatively constant in comparison to using neat propan-2-ol as solvent. It is likely that the complete conversion achieved by catalyst **3**, was a result of coordination of THF to the Ru(II) metal centre, stabilising the catalyst resting state and prolonging the lifetime of the catalyst.

The most active catalysts, **4a** and **4**, were further screened for the transfer hydrogenation reaction with a number of different ketone substrates (both aromatic and aliphatic, see Table 2.2). Both catalysts successfully catalysed the reactions at reflux and were able to achieve complete conversion of substrate for each case with the exception of the *p*-nitro-acetophenone (Table 2.2, entry 3). As was observed for the transfer hydrogenation reaction of acetophenone, catalyst **4a** was more efficient for the conversion of all substrates in comparison to **4**. Catalyst **4a** was tested for the transfer hydrogenation reaction of acetophenone, benzophenone and cyclohexanone at room temperature and reasonable yields of 51%, 41% and 59% were achieved respectively after 24 hours. (Table 2.2, entries 1, 2 and 4).

entry	product	catalyst	% conv. at time (h)			
			0.5h <sup>u</sup>	2h <sup>u</sup>	4h <sup>u</sup>	24h <sup>u</sup>
1		<b>4a</b>	91	96	>99	51
		<b>4</b>	39	82	>99	-
2		<b>4a</b>	91	91	>99	41
		<b>4</b>	69	97	>99	-
3		<b>4a</b>	0	0	0	-
		<b>4</b>	0	0	0	-
4		<b>4a</b>	92	>99	>99	59
		<b>4</b>	72	>99	>99	-
5		<b>4a</b>	51	94	>99	-
		<b>4</b>	44	78	>99	-

**Table 2.2** Catalytic transfer hydrogenation of ketones using complexes **4a** and **4**<sup>a</sup> refluxing

propan-2-ol, 1.5 mol% catalyst. <sup>b</sup> 25 °C, 1.5 mol% catalyst.

This mixed anion catalyst (**4a**) was found to be the most active catalyst for the transfer hydrogenation reaction, promoting the conversion of a range of aromatic and aliphatic ketone substrates to alcohols with high yields in reasonable times at elevated temperature. The catalysed transfer hydrogenation reaction could also be conducted at room temperature, with catalyst **4a** found to be moderately active, whereas complexes **3**, **4**, **5**, **5a** and **6** were catalytically inactive. Comparison of the catalytic activities of **4a** and **4** revealed that the presence of the  $[\text{B}_5\text{O}_6(\text{OH})_4]^-$  counterion enhanced the rate of reaction by catalysing transfer hydrogenation reactions *via* a separate mechanism from the organometallic catalyst. Few boron compounds have been reported to perform the transfer hydrogenation reaction. Kilic *et al.* has recently shown that boron compounds containing a bidentate N, O donor system can achieve high conversions for the transfer hydrogenation reaction of acetophenone.<sup>32</sup> However, the reaction requires over eight hours in refluxing isopropanol to achieve near complete conversions and the boron compounds are inactive as catalysts for transfer hydrogenation at room temperature. In comparison, complex **4a** achieves moderate conversions even at room temperature.

## 2.5. Conclusions

This chapter describes the coordination chemistry of the  $\text{NCN}^{\text{Me}}$  pincer ligand precursor **1** with Ru(II) and Ag(I) salts and investigates the activity of the resulting Ru(II) complexes as catalysts for transfer hydrogenation reactions. A series of coordination motifs were observed for the complexes in the solid state, ranging from a fully saturated tridentate Ru(II) dimer to a mono-dentate Ag(I) dimer, all of which could be preferentially synthesised by careful reagent choice. Crystallographic

analysis unexpectedly revealed a rare pentaborate anion for complex **4a**. Indeed, this mixed anion complex was found to be the most active catalyst for the transfer hydrogenation reaction, promoting the conversion of a range of aromatic and aliphatic ketone substrates to alcohols with high yields in reasonable times at elevated temperature. The catalysed transfer hydrogenation reaction could also be conducted at room temperature using catalyst **4a**. Complexes **2**, **3**, **4**, **5**, **5a** and **7** were catalytically inactive at room temperature. Comparison of the catalytic activities of the mixture **4a** and complex **4** revealed that the presence of the  $[\text{B}_5\text{O}_6(\text{OH})_4]^-$  counterion enhanced the rate of reaction, most probably by catalysing transfer hydrogenations *via* a separate mechanism from the organometallic catalyst. Despite not being amongst the most active hemilabile Ru(II) in the literature, the discovery and catalytic activity of the pentaborate anion warrants further investigation.

## 2.6. References

- (1) Patel, D. R. *J. Mol. Catal. A: Chem.* **1998**, *130*, 57.
- (2) Crabtree, R. H.; Davis, M. W. *J. Org. Chem.* **1986**, *51*, 2655.
- (3) Hu, A.; Ngo, H. L.; Lin, W. *Angew. Chem. Int. Ed.* **2004**, *43*, 2501.
- (4) (a) Nazzirudin, A. R.; Huang, Z.; Lai, W.; Lin, W.; Hwang, W. *Dalton Trans.* **2013**, *10*, 2;  
(b) Ignacio, D. R.; Stephen, B.; Milja, S. H.; Gerd, R.; Heinrich, L.; Gerard, V. K. *Inorg. Chim. Acta.* **2000**, *300-302*, 1094.
- (5) (a) Ohkuma, T.; Sandoval, C. A.; Srinivasan, R.; Lin, Q.; Wei, Y.; Muniz, K.; Noyori, R. *J. Am. Chem. Soc.* **2005**, *127*, 8288; (b) Cabrero-Antonino, J. R.; Alberico, E.; Junge, K.; Jungea, H.; Beller, M. *Chem. Sci.* **2016**, *7*, 3432.
- (6) (a) Stanislaus, A.; Cooper, B. H. *Catal. Rev.* **1994**, *36*, 75; (b) Zhang, Z.; Butt, N. A; Zhang, W. *Chem. Rev.* **2016**, *116*, 14769; (c) Wang, D. S.; Chen, Q. A.; Lu, S. M.; Zhou, Y. G. *Chem. Rev.* **2012**, *112*, 2557.
- (7) (a) Clapham, S. E.; Hadzovic, A.; Morris, R. H. *Coord. Chem. Rev.* **2004**, *248*, 2201; (b) Noyori, R.; Hashiguchi, S. *Acc. Chem. Res.* **1997**, *30*, 97.
- (8) (a) Backwall, J. E. *J. Organomet. Chem.* **2002**, *652*, 105; (b) Zassiniovich, G.; Mestroni, G.; Gladiali, S. *Chem. Rev.* **1992**, *92*, 1051; (c) Wang, D.; Astruc, D. *Chem. Rev.* **2015**, *115*, 6621.
- (9) (a) Conley, B. J.; Pennington-Boggio, M. K.; Boz, E.; Williams, T. J. *Chem. Rev.* **2010**, *110*, 2294; (b) Blum, Y.; Schvo, Y. *Isr. J. Chem.* **1984**, *24*, 144.
- (10) Standfest-Hauser, C.; Slugovc, C.; Mereiter, K.; Schmid, R.; Kirchner, K.; Xiao, L.; Weissensteiner, W. *Dalton Trans.* **2001**, *20*, 2989; (b) Nieto, I.; Livings, M. S.; Saccilll, J. B.; Reuther, L. E.; Zeller, M.; Papish, E. T. *Organometallics* **2011**, *30*, 6339.



- (11) (a) Bader, A.; Lindner, E. *Coord. Chem. Rev.* **1991**, *108*, 27; (b) Shi, P. Y.; Liu, Y. H.; Peng, S. M.; Liu, S. T. *Organometallics* **2002**, *21*, 3203; (c) Basseti, M.; Capone, A.; Salamone, M. *Organometallics* **2004**, *23*, 247; (d) Poverenov, E.; Gandelman, M.; Shimon, L. J. W.; Rozenberg, H.; Ben-David, Y.; Milstein, D. *Organometallics* **2005**, *24*, 1082; (e) Niu, J. L.; Hao, X. Q.; Gong, J. F.; Song, M. P. *Dalton Trans.* **2011**, *40*, 5135.
- (12) (a) Lin, T.-P.; Peters, J. C. *J. Am. Chem. Soc.* **2013**, *135*, 15310; (b) Lagaditis, P. O.; Schluschaß, B.; Demeshko, S.; Würtele, C.; Schneider, S. *Inorg. Chem.* **2016**, *55*, 4529.
- (13) Mazza, S.; Rosario, S.; Xile, H. *Organometallics* **2015**, *34*, 1538.
- (14) Zaheer, E.; Clarke, P. T.; Maragh, T. P.; Dasgupta, D. G.; Gusev, A. J.; Lough, K. A.-R. *Organometallics* **2006**, *25*, 4113.
- (15) (a) Milstein, D. *Top. Catal.* **2010**, *53*, 915; (b) Bagala, D. B.; Bhanage, B.M. *Adv. Synth. Catal.* **2015**, *357*, 883; (c) Younus, H. A.; Su, W.; Ahmad, N.; Chen, S.; Verpoort, F. *Adv. Synth. Catal.* **2015**, *357*, 283.
- (16) (a) Yu, Z. *Chem. Eur. J.* **2011**, *17*, 4737; (b) Chai, H.; Liu, T.; Wang, Q.; Yu, Z. *Organometallics* **2015**, *34*, 5278.
- (17) Wang, X. W.; Ning, L. *Eur. J. Inorg. Chem.* **2012**, *6*, 901.
- (18) Jeffrey, J. C.; Rauchfuss, T. B. *Inorg. Chem.* **1979**, *18*, 2658.
- (19) Slade, A. T.; Lensink, C.; Falshaw, A.; Clarka, G. R.; Wright, L. J. *Dalton Trans.* **2014**, *43*, 17163.
- (20) Xu, W.; Langer, R. *Dalton Trans.* **2015**, *44*, 16785.
- (21) Pei, L. C.; Hon, M. L. *Organometallics* **2005**, *24*, 1692; (b) Chen, C.; Lu, C.; Zheng, Q.; Ni, S.; Zhang, M.; Chen, W. *Beilstein J. Org. Chem.* **2015**, *11*, 1786.

- (22) Riener, K.; Bitzer, M. J.; Pöthig, A.; Raba, A.; Cokoja, M.; Herrmann, W. A.; Kühn, F. E. *Inorg. Chem.* **2014**, *53*, 12767.
- (23) (a) Wang, R.; Twamley, B.; Shreeve, J. M. *J. Organomet. Chem.* **2006**, *71*, 426; (b) Wang, R.; Zeng, Z.; Twamley, B.; Piekarski, M. M.; Shreeve, J. M. *Eur. J. Org. Chem.* **2007**, *4*, 655.
- (24) Mancano, G.; Page, M. J.; Bhadbhade, M.; Messerle, B. A. *Inorg. Chem.* **2014**, *53*, 10159.
- (25) Garrison, J. C.; Youngs, W. J. *Chem. Rev.* **2005**, *105*, 3978.
- (26) Gessler, S.; Randl, S.; Blechert, S. *Tetrahedron Lett.* **2000**, *41*, 9973.
- (27) Malecki, J. G.; Maron, A. *Transition Met. Chem.* **2012**, *38*, 419.
- (28) (a) Teo, B.-K.; Calabrese, J. C. *Inorg. Chem.* **1976**, *15*, 2467; (b) Barron, P. F.; Dyason, J. C.; Engelhardt, L. M.; Healy, P. C. *Inorg. Chem.* **1984**, *23*, 3766.
- (29) (a) Horn, S.; Gandolfi, C.; Albrecht, M. *Eur. J. Inorg. Chem.* **2011**, *2011*, 2863; (b) del Río, I.; Van Koten, G.; Lutz, M.; Spek, A. L. *Organometallics* **2000**, *19*, 361; (c) Poyatos, M.; Mata, A.; Falomir, E.; Crabtree, R. H.; Peris, E. *Organometallics* **2003**, *22*, 1110.
- (30) He, Z.; Zhang, S.-H.; Xue, J.-R.; Liang, Y.; Zhang, X.; Jing, L.-H.; Qin, D.-B. *J. Organomet. Chem.* **2016**, *808*, 12.
- (31) (a) Herrmann, W. A. *Angew. Chem. Int. Ed.* **2002**, *41*, 1290; (b) Bennett, M. A.; Smith, A. K. *Dalton Trans.* **1974**, *2*, 233; (c) Danopoulos, A. A.; Winston, S.; Motherwell, W. *Chem. Commun.* **2002**, *36*, 1376; (d) Steinke, T.; Shaw, B. K.; Jong, H.; Patrick, B. O.; Fryzuk, M. D. *Organometallics* **2009**, *28*, 2830; (e) Chen, C.; Qiu, H.; Chen, W. *J. Organomet. Chem.* **2012**, *696*, 4166.

- (32) (a) Kilic, A.; Aydemir, M.; Durgun, M.; Meriç, N.; Ocak, Y. S.; Keles, A.; Temel, H. *J. Fluor. Chem.* **2014**, 162, 9; (b) Kilic, A.; Kayanb, C.; Aydemirb, M.; Durapb, F.; Durguna, M.; Baysalb, A.; Tasc, E.; Gümgüm, B. *Appl. Organomet. Chem.* **2011**, 25, 390.

---

Chapter 3. Ni(II) complexes of hemilabile pincer  
ligands for catalysed Kumada cross coupling  
reactions

---

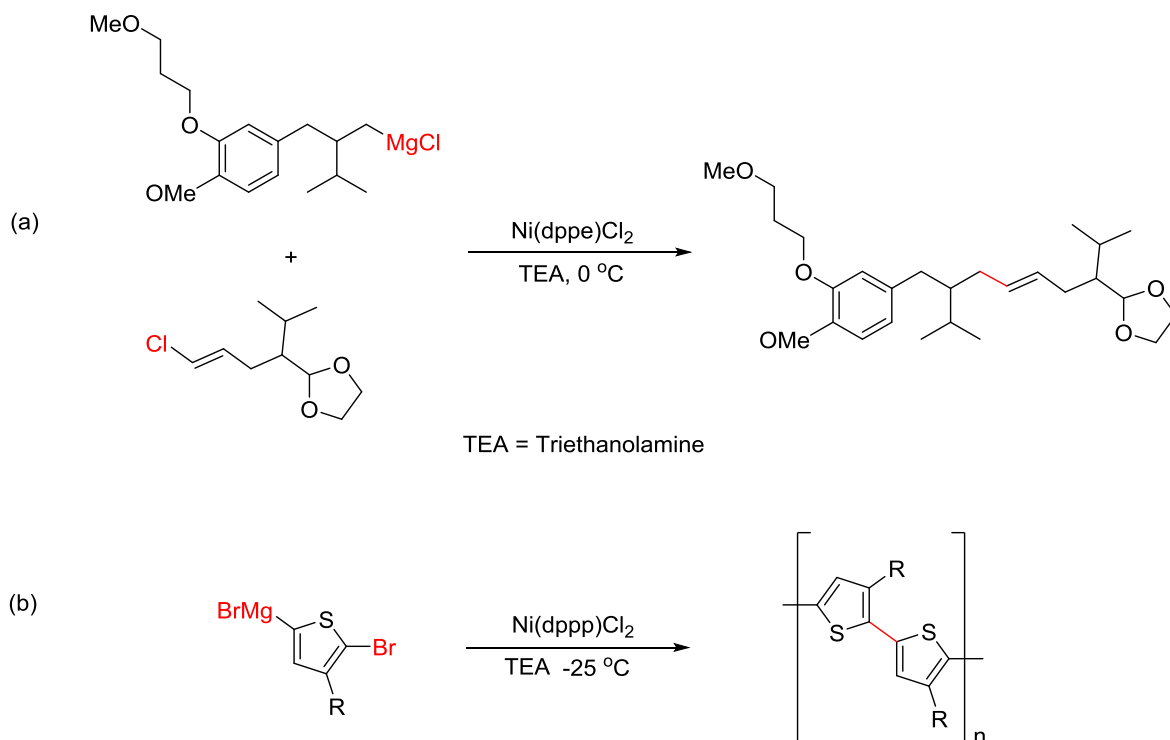
### 3.1. Introduction

#### 3.1.1. Transition metal catalysed C-C bond formation reactions

Carbon-carbon bond cross coupling reactions have been studied extensively in the field of organometallic chemistry.<sup>1</sup> Among the first reported catalytic C-C coupling reactions is the Kumada cross coupling reaction.<sup>2</sup> The reaction involves the catalysed cross coupling between a Grignard reagent and an organic halide, which results in the formation of a new C-C bond. Despite the advent of alternative reactions, such as Suzuki, Negishi, Stille or Sonogashira coupling reactions, Kumada cross coupling reactions continue to be used in industry due to the ability of the reaction to directly couple Grignard reagents to a wide variety of halide containing compounds.<sup>3</sup> The reaction provides an economic and efficient organic transformation of the Grignard reagents containing alkyl, aryl and vinyl substrates. In particular, since the reaction is not limited to  $sp^2$  carbon hybridisations, the Kumada cross coupling reaction has a higher versatility over other C-C coupling reactions.<sup>4</sup>

Kumada cross coupling reactions provide a safer route for the formation of C-C bonds, than Stille coupling reactions, which use toxic organotin compounds.<sup>5</sup> Usually, nickel complexes are utilised as catalysts in Kumada cross coupling reactions, and hence provide a cheaper alternative for the same organic transformation than alternative C-C coupling reactions which generally use more expensive metals such as palladium. Additionally, a greater range of temperatures can be employed for Kumada cross couplings than alternative coupling reactions due to the thermal stability of the Grignard reagents commonly used which allows for the successful coupling of both activated and deactivated substrates.<sup>6</sup> Reactions such as the Stille coupling typically use reagents that are susceptible to decomposition.

Kumada cross coupling reactions are also well utilised in the pharmaceutical and commercial industries, an example is in the synthesis of the drug Aliskiren (Scheme 3.1a), which is used for the treatment of hypertension.<sup>7</sup> Key steps in the synthesis of polymers such as polyalkylthiophenes also utilise the Kumada cross coupling reaction (Scheme 3.1b).<sup>8</sup>

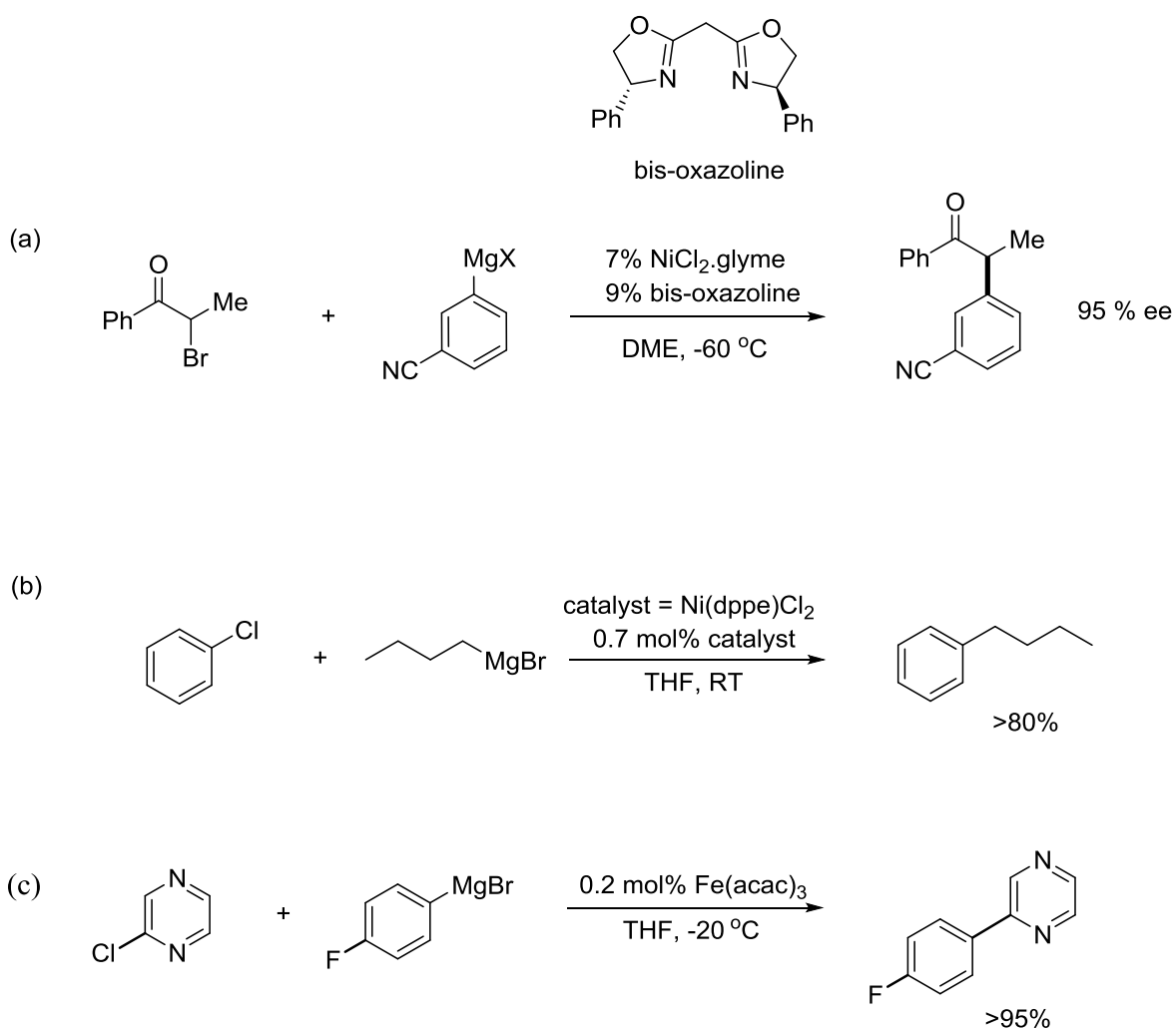


**Scheme 3.1** Kumada cross coupling as a key synthetic step in the production of (a) Aliskiren and (b) polythiophenes.

### 3.1.2. Catalysts for the Kumada cross coupling reactions

The Kumada cross coupling reaction can be catalysed by a wide range of nickel and palladium complexes. Catalytically active species can be formed *in situ* by addition of organic ligands such as bis-oxazoline to metal precursors such as  $\text{NiCl}_2$  (Scheme 3.2a).<sup>9</sup> A disadvantage to the use of an active catalyst generated *in situ* is the unknown structure of the catalytically active species in the reaction mixture, therefore reaction pathways can be hard to determine. Therefore, isolated organometallic complexes have received increased

attention as catalysts for the Kumada cross coupling reaction. Among the first reported isolated organometallic complexes used for Kumada cross coupling is Ni(dppe)Cl<sub>2</sub> (dppe = 1,2-bis(diphenylphosphino)ethylene, Scheme 3.2b).<sup>10a</sup> This catalyst achieves near complete conversions for the Kumada cross coupling reaction of butylmagnesium bromide and chlorobenzene. Compared to *in situ* generated complexes, the isolated complex requires significantly reduced catalyst loadings to achieve high conversions. New catalysts and methods have since been developed for the Kumada cross coupling reaction with aims to achieve higher conversions at lower catalyst loadings. A “continuous flow” iron-catalysed Kumada cross coupling was recently reported which achieved high conversions for fluorinated substrates at low catalyst loadings (Scheme 3.2c).<sup>10b</sup>

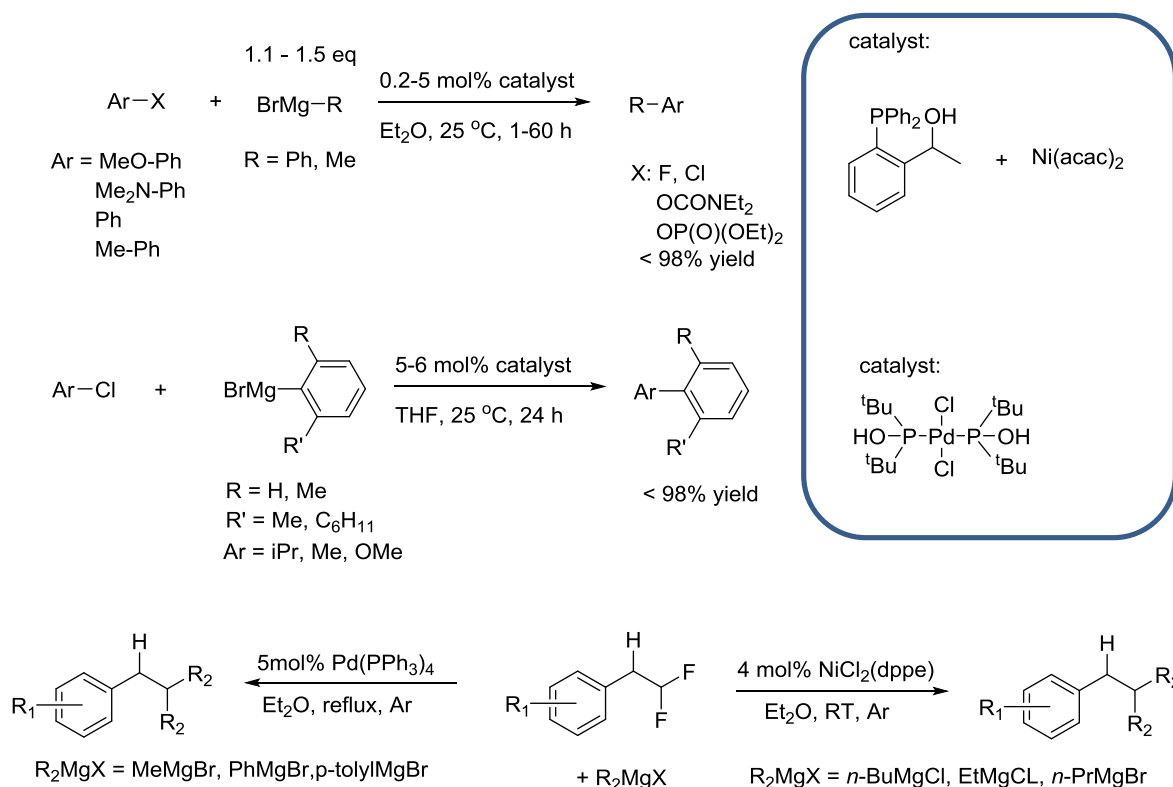


**Scheme 3.2** Kumada cross coupling reactions catalysed by: (a) an *in situ* generated bis-oxazoline Ni(II) complex, (b) a pre-prepared Ni(II) catalyst and (c) an iron(III) catalyst.

Pd(II) and Ni(II) are the most successful and commonly used metals among the organometallic catalysts used for the Kumada cross coupling reaction. Most of the initially investigated catalysts for this type of organic transformation used Pd(II), Pd(0) and Ni(II) precursors, such as  $\text{Pd}(\text{PPh}_3)_2\text{Cl}_2$ ,  $\text{Pd}(\text{PPh}_3)_4$ ,  $\text{NiCl}_2$  and  $\text{NiCl}_2\cdot\text{glyme}$ .<sup>11</sup> However, most of these early complexes were susceptible to thermal and catalytic decomposition and optimization of selectivity was required. Hence, new complexes containing modified ligand structures were synthesised in order to improve catalytic activities and selectivities. Previous reports show the versatility of Ni(II) complexes used as catalysts for the cross



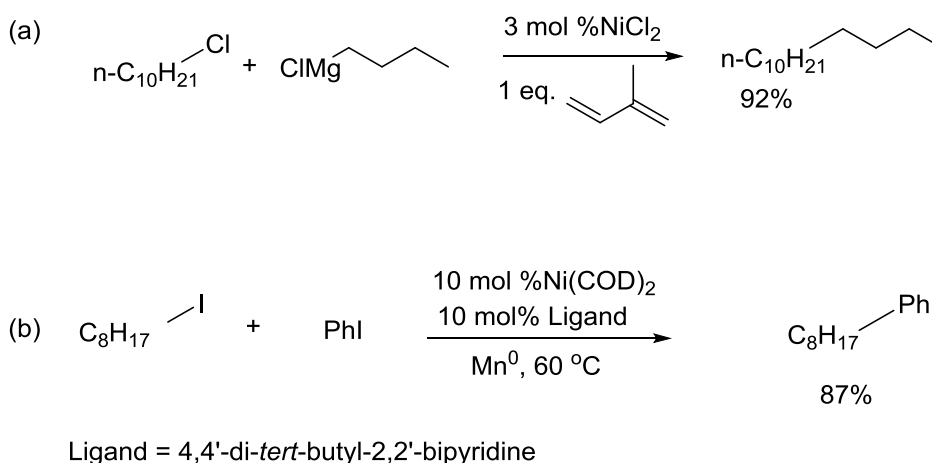
coupling reaction by using substrates with varying electronic and steric properties (Scheme 3.3).<sup>12</sup> The catalytic system showed high functional group tolerance, achieving moderate to high substrate conversions of a number of substrates containing electron withdrawing and electron donating groups. The versatility of Pd(II) complexes has also been demonstrated where similar functional group tolerance to that of nickel catalysts was observed (Scheme 3.3).<sup>12, 13</sup>



**Scheme 3.3** Recent Pd(II) and Ni(II) catalysed Kumada cross coupling reactions.<sup>12, 13</sup>

The coupling of alkyl halides with Grignard reagents is significantly more difficult than the coupling of aryl halides with Grignard reagents due to the presence of  $\beta$ -hydrogen atoms, which can interfere with the reaction causing the production of side products *via* competitive elimination processes.<sup>14</sup> However, these processes can be avoided with use of Ni(II) complexes which allows for the selective synthesis of desired products from alkyl

halides. Early examples of catalysts that suppress  $\beta$ -hydride elimination include the addition of dienes such as 1,3-butadiene to  $\text{NiCl}_2$  which resulted in the production of long alkane/alkene chains with high selectivity (Scheme 3.4a).<sup>15</sup> The addition of the diene is hypothesised to produce a Ni(IV) intermediate which prevents the elimination processes involving  $\beta$ -hydrogen atoms.<sup>15a</sup> Recent examples demonstrated that the addition of diene ligands separate to nickel precursors may not be required to eliminate the formation of by-products (Scheme 3.4b).<sup>15b</sup>

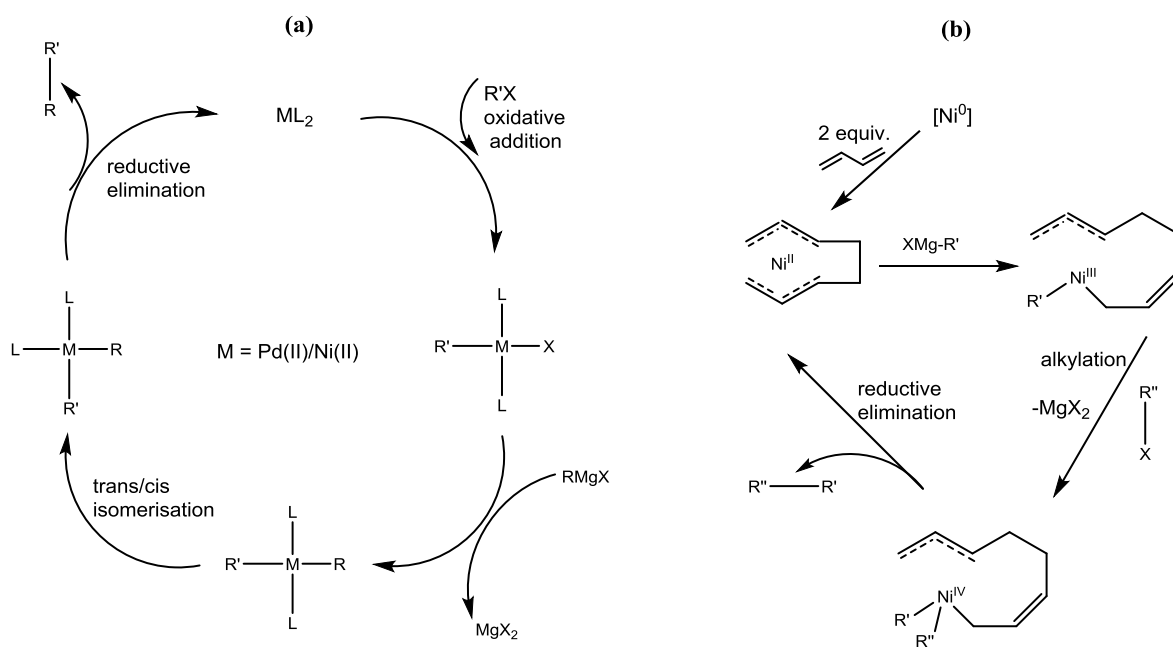


**Scheme 3.4** Selective Kumada cross coupling reactions.

### 3.1.3. The mechanisms of Kumada cross coupling reactions

There are multiple proposed mechanisms for the Kumada cross coupling reaction catalysed by nickel complexes. One common example of such a mechanism is shown in Scheme 3.5a, which proceeds *via* the standard oxidative addition-transmetallation-reductive elimination pathways utilising Ni(0)/Ni(II) oxidation states.<sup>4,16</sup> The other example of proposed mechanisms for the Ni catalysed Kumada cross coupling reaction (Scheme 3.5b) is more specific to alkyl substrates, where it is proposed that the Ni(0) centre accesses multiple oxidation states during the reaction including Ni(0), Ni(II), Ni(III) and Ni(IV).<sup>15,16</sup> This

particular mechanism is based on a reaction that utilises 1,3-butadiene. Homocoupling of the 1,3-butadiene suppresses elimination processes involving  $\beta$ -hydrogen atoms of the R groups from the organohalide or the Grignard. Although palladium catalysed Kumada cross coupling reactions are also able to proceed *via* the same proposed 0/+II mechanism as proposed in Scheme 3.5a for nickel, the disadvantage of palladium is that it is susceptible to  $\beta$ -hydrogen atom elimination processes when catalysing reactions with alkyl substrates. Use of  $\text{PdCl}_2$  for the reaction in Scheme 3.4 resulted in poor yield (38%) and by-products due to the  $\beta$ -hydrogen atom elimination processes were still observed.<sup>15</sup>



**Scheme 3.5** Kumada coupling mechanisms: a) conventional mechanism and b) mechanism with Ni(IV) intermediate.

### 3.1.4. Nickel complexes containing pincer ligands as catalysts for the Kumada cross coupling reaction: ligand effects

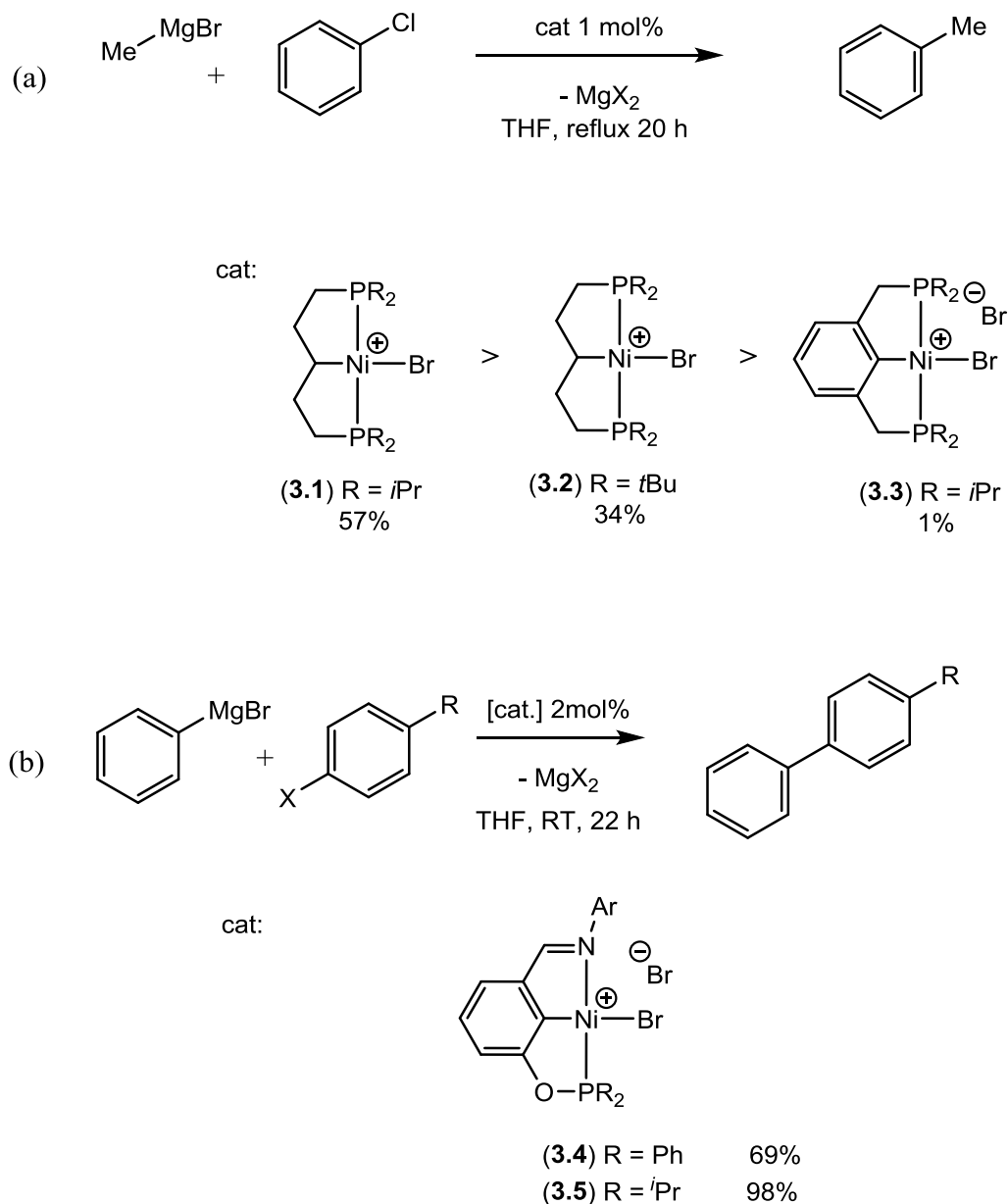
Significant attention has been focused on transition metal complexes containing pincer ligands as catalysts for C-C cross coupling reactions because complexes containing pincer

ligands can exhibit higher reactivity and increased stability over complexes containing bidentate/monodentate ligands.<sup>17, 18</sup> Ni complexes containing pincer ligands are widely used in C-C cross coupling reactions, particularly the coupling of aryl Grignards with aryl or alkyl halides (i.e. Kumada coupling).<sup>3, 19</sup>

Some of the early synthetic work in the use of complexes with pincer ligands involved the *in situ* addition of a metal precursor to a pincer ligand.<sup>1</sup> A wide array of transition metal complexes, mostly Ni(II) and Pd(II) containing pincer ligands have since been synthesised, aiming to achieve higher selectivities and/or activities for the Kumada cross coupling reaction.<sup>3</sup> The ability of the complexes bearing pincer ligands to catalyse Kumada cross coupling reactions depends on factors such as the degree of electron donation to the metal centre, and the lability of the coordinating groups to the metal centre.<sup>3</sup>

#### 3.1.4.1. Electron donating ability and its effects on catalytic activity

Castonguay and coworkers have demonstrated a correlation between the electron donating ability of the coordinating groups of a pincer ligand to a Ni(II) metal centre and the catalytic activity of the resulting complex.<sup>20</sup> The catalytic activity of complexes **3.1**, **3.2** and **3.3** (Scheme 3.6a) decreased with increasing electron donating ability of functional groups on the coordinating phosphorous or carbon atoms (**3.1** > **3.2** > **3.3**). This trend was also observed for similar pincer complexes where the authors report higher catalytic activity for complex **3.4** (Scheme 3.6b) which contains smaller electron donating isopropyl groups on the phosphorous donors in comparison to the analogous complex **3.5** containing more electron donating phenyl groups.<sup>21</sup>



**Scheme 3.6** Effect of varying electron donating abilities of ligands used in Ni(II) catalysed Kumada cross coupling reactions: (a) coupling of alkyl Grignard reagents; (b) coupling of aryl Grignard reagents.

#### 3.1.4.2. Pincer ligands with strongly coordinating side arm donors

The most common motifs of pincer ligands used for coordination to Ni(II) include a central pyridyl donor group flanked by one or more NHC groups, a selection of which (3.6, 3.7, 3.8 and 3.9) are shown in Figure 3.1.<sup>22, 23, 24, 25, 26</sup>

Complex **3.6** (Figure 3.1) has been used as a catalyst for the Kumada cross coupling reaction of aryl bromides, chlorides and fluorides,<sup>22</sup> achieving moderate to good yields for most substrates with the exception of substrates containing fluorides and some chlorides. However, the use of a Ni(II) complex containing a pincer ligand (**3.9**) with only one NHC side arm led to higher yields for the coupling reaction of *para*-tolyl magnesium bromide with aryl chlorides.<sup>23</sup> This result suggested that combining two relatively labile donor groups with a strongly coordinating NHC donor allows increased catalytic reactivity of Ni(II) compared to pincer complexes that contain two strongly coordinating NHC donors.

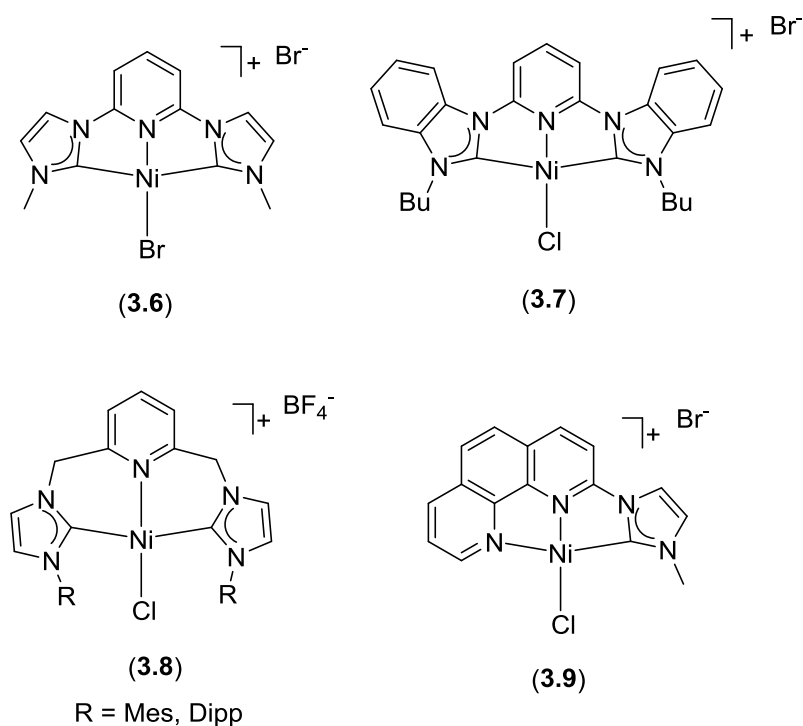
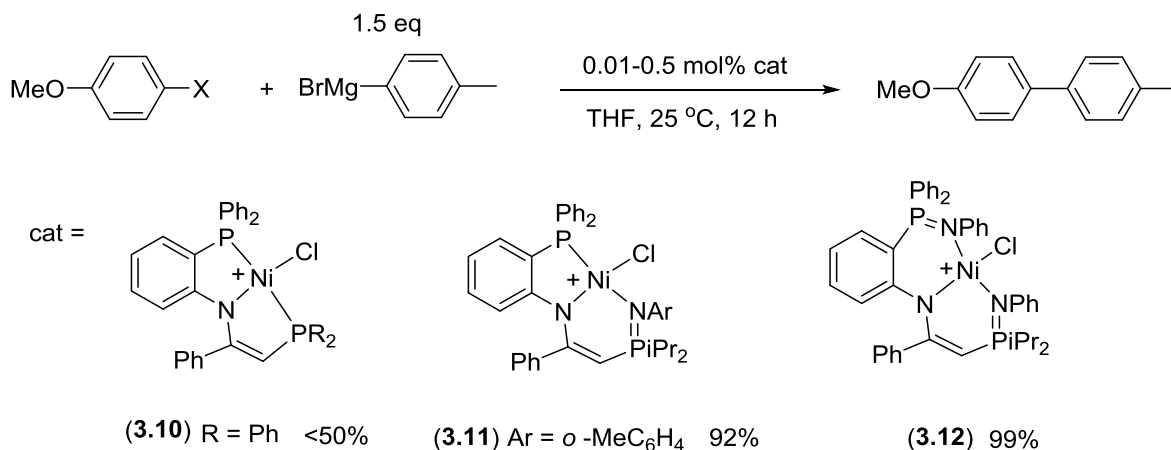


**Figure 3.1** Ni(II) complexes containing pincer ligands with strongly coordinating NHC donors.

## 3.1.4.3. Pincer ligands with weakly coordinating side arms: towards hemilability

The catalytic activity of Ni(II) complexes containing pincer ligands can be increased if strongly donating side arms are replaced with weakly coordinating side arm donors such as pyrazoles and imines. Xia Wang, Ning Liu and co-workers have demonstrated this using Ni(II) complexes containing pincer ligands of the type shown in Scheme 3.7.<sup>27</sup> The *PNP* pincer complexes (**3.10**) containing two strongly coordinating phosphine donor groups proved to be the least active catalysts in the series. The *NNN* pincer complex (**3.12**) containing two donor atoms as shown in Scheme 3.7 exhibited superior catalytic activity for the cross coupling reaction in comparison to similar *PNN* pincer complex (**3.11**) containing only one labile donor atom.



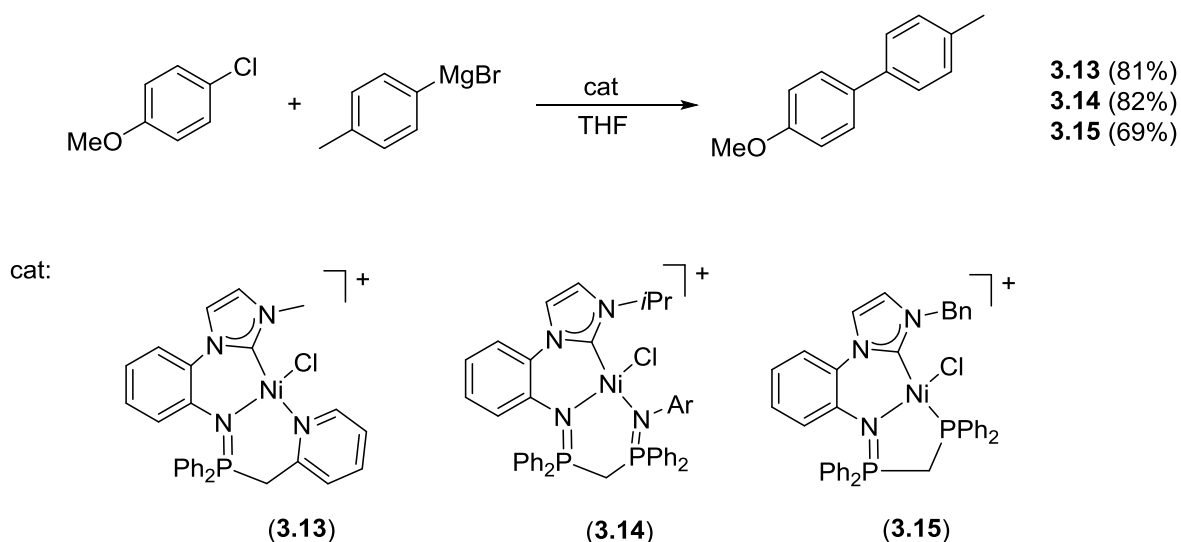
**Scheme 3.7** Ni(II) complexes containing pincer ligands with tunable catalytic properties.

Although the increased lability of selected pincer ligands proved to be effective for increasing the catalytic activity of the resulting complexes, the *PNP*, *PNN* and *NNN* pincer complexes were not stable over time when used as catalysts. Complexes containing labile donors have reduced thermal stability and are prone to destabilisation<sup>28,29</sup> at the elevated temperatures which are sometimes required for Kumada cross coupling reactions of certain alkyl and aryl chloride substrates, e.g. 1-chloro-4-methoxybenzene.<sup>6</sup> To alleviate the

reduced catalytic and thermal stability of the pincer complexes with weakly coordinating donors, introduction of a strongly coordinating central  $\sigma$ -donor group (NHC) could be an answer to the instability of the complexes.

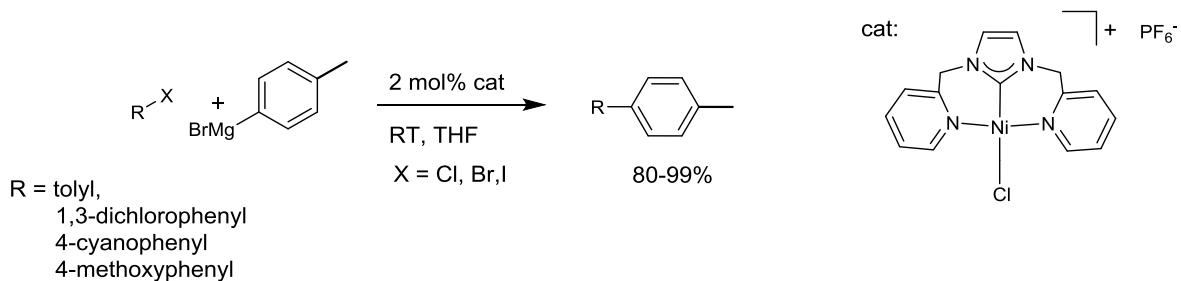
Zhang *et al.* reported the use of complexes with hemilabile pincer ligands containing  $sp^2$  nitrogen ligand donors and NHC side arm donors (**3.13**, **3.14** and **3.15**, Scheme 3.8) as catalysts for the Kumada cross coupling reaction of activated aryl halides and arylmagnesium bromides with high yields at room temperature conditions.<sup>6</sup> However, certain unactivated substrates required the use of higher temperatures to achieve successful conversions. The complexes that contained hemilabile pincer ligands also catalysed the cross coupling reactions of unactivated chloride substrates, though the reactions had to be performed at higher temperatures (80 °C). This can be attributed to the ability of the complexes containing pincer ligands to maintain their reactivity by dissociation of one or more of the weakly coordinating ligand donors to provide vacant coordination sites for substrate binding, while retaining thermal stability owing to the strong  $\sigma$ -coordination of the NHC donor. The authors report high yields for the coupling of the unactivated 1-chloro-4-methoxybenzene substrate at 80 °C while no reaction occurred at room temperature. Complexes **3.13** and **3.14** (Scheme 3.8) were more active for the cross coupling of aryl chlorides with Grignard reagents in comparison to complex **3.15**, and the increased activity was attributed to the hemilability of the ligands. Complexes **3.13** and **3.14** exhibit similar reactivity due to the presence of two labile N donor groups whereas complex **3.15** contains a phosphine donor which dissociates less readily from the Ni(II) centre during catalytic reactions than the imine donors (**3.13** and **3.14**).





**Scheme 3.8** Ni(II) hemilabile complexes of pincer ligands containing a single NHC donor.

Only a few complexes containing a central NHC donor and labile donor arms have been reported in the literature. Chao Chen *et al.* have reported the use of a Ni(II) complex containing a pincer ligand with a central NHC donor and pyridyl sidearm donors (Scheme 3.9).<sup>30</sup> The complex achieves high conversions for the Kumada cross coupling reaction of aryl halides with aryl magnesium bromide. Heteroaryl and disubstituted aryl substrates also undergo the Kumada cross coupling reaction with tolyl magnesium bromide using the same catalyst, achieving good yields. This shows the versatility of the Ni(II) complex bearing the pincer ligand to catalyse the Kumada cross coupling reaction for a range of chlorinated substrates.



**Scheme 3.9** Ni(II) complex of a pincer ligand with a central NHC donor.

### 3.2. Aims of this chapter

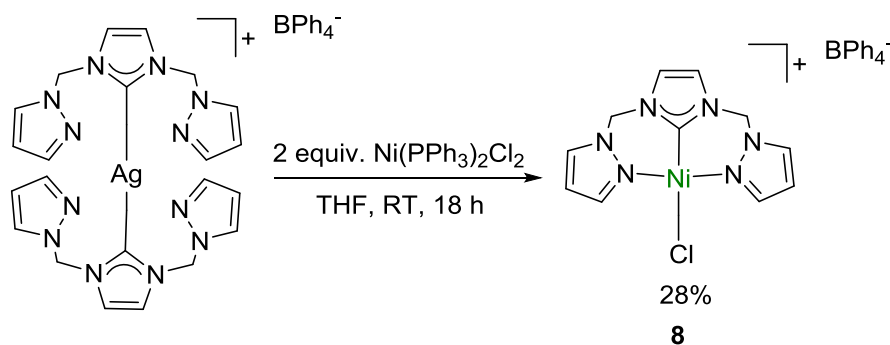
The aims of this chapter are to investigate the synthesis and coordination chemistry of a range of novel nickel(II) complexes containing hemilabile *NCN* pincer ligands, as well as their activity as catalysts for the Kumada cross coupling reaction of aryl halides. The specific goals were to:

- Prepare a range of Ni(II) complexes containing hemilabile pincer ligands composed of pyrazole-imidazolium-pyrazole motifs.
- Investigate the coordination modes of the resulting complexes with strongly coordinating co-ligands.
- Test the catalytic activities of all synthesised Ni(II) complexes for the Kumada cross coupling reaction, initially of chlorobenzene and phenylmagnesium bromide.
- Investigate the catalytic activity of the best catalyst using optimised conditions for Kumada cross coupling of a range of substituted aryl halides.

### 3.3. Synthesis of Ni(II) complexes containing an $NCN^{Me}$ hemilabile pincer ligand

#### 3.3.1. Synthesis, characterisation and coordination study of $[Ni(NCN^{Me})Cl]BPh_4$ (**8**)

The synthetic routes to the complexes presented in this chapter follow similar synthetic procedures to those used for the Ru(II) complexes presented in Chapter 2. The Ni(II) complexes of the  $NCN^{Me}$  pincer ligand **1** were synthesised by transmetallation of the  $Ag(I)NCN^{Me}$  complex (**2**) with two molar equivalents of  $Ni(PPh_3)_2Cl_2$  to yield the complex  $[Ni(NCN^{Me})Cl]BPh_4$  (**8**) as a yellow micro-crystalline solid in 28% yield (Scheme 3.10). Multiple attempts were made to increase the yield of the product including the synthesis of the complex **8** using an external base ( $NEt_3$ ). The complex was successfully isolated using this method, however, the yield did not improve. A mass balance analysis of the crude reaction mixture revealed the presence of three fractions. One fraction was isolated as the product **8**, the remaining two fractions proved to contain highly insoluble products and  $^1H$  NMR analysis of these two fractions did not yield useful information. Use of starting materials such as  $Ni(DME)Cl_2$  and  $Ni(OAc)_2 \cdot xH_2O$  resulted in an unreacted mix of starting material.



**Scheme 3.10** Synthesis of  $[Ni(NCN^{Me})Cl]BPh_4$  (**8**).

The  $^1H$  NMR spectrum obtained for complex **8** exhibited broad resonances for all protons attributed to the pincer ligand at room temperature. A single set of aromatic resonances

between 7.5 and 8.4 ppm were attributed to the protons of the pyrazolyl and imidazolyl donors. The number of resonances indicated a symmetric  $\kappa^3$ -NCN structure of the Ni(II) complex **8**.

There were significant differences between the pyrazolyl proton resonances in comparison to those observed for silver intermediate  $[\text{Ag}(\text{NCN}^{\text{Me}})_2]\text{BPh}_4$  (**2**). The pyrazolyl resonances due to protons of intermediate **2** occur at 7.60 ppm and 8.13 ppm, whereas those due to the protons of the nickel complex (**8**) occur at 8.26 ppm and 8.29 ppm respectively. The downfield shift of these pyrazolyl proton resonances indicated that the transmetallation reaction was successful in coordinating the two pyrazolyl ligand arms to the nickel center unlike in Ag(I) complex **2** where the N-donors remain unbound. The ratios of the integration of ligand proton resonances to those of the  $\text{BPh}_4$  counterion indicated that the ratio of ligand to counterion is 1:1. As the  $^1\text{H}$  NMR spectrum indicates that all ligand donors are bound to the metal centre, it is highly likely that a Cl co-ligand is also bound to the Ni metal centre.

$^{13}\text{C}\{^1\text{H}\}$  NMR and 2D NMR spectroscopy did not reveal any valuable information that explained the broad signals in the  $^1\text{H}$  NMR spectrum. There are different possibilities for the broad signals in the NMR spectrum including purity, paramagnetism and conformational flexibility of the complex **8** in solution state. Further characterisation was therefore carried out in aims to identify the cause of the broad signals in the NMR spectrum.

Crystals suitable for X-ray analysis were grown by vapour diffusion of diethyl ether into a saturated solution of **8** in acetone. X-ray crystal structure analysis confirmed the predicted four co-ordinate structure (Figure 3.2), with the Ni(II) centre possessing a square planar

geometry. The central NHC is twisted out of the square plane, such that the two methylene groups are positioned on opposite faces of the plane at a torsion angle of  $30.1^\circ$ . Mass spectrometry of complex **8** shows a dominant signal at 303.05 m/z which is attributed to the cationic fragment with formula  $[\text{Ni}(\text{NCN}^{\text{Me}})\text{OH}]^+$ .

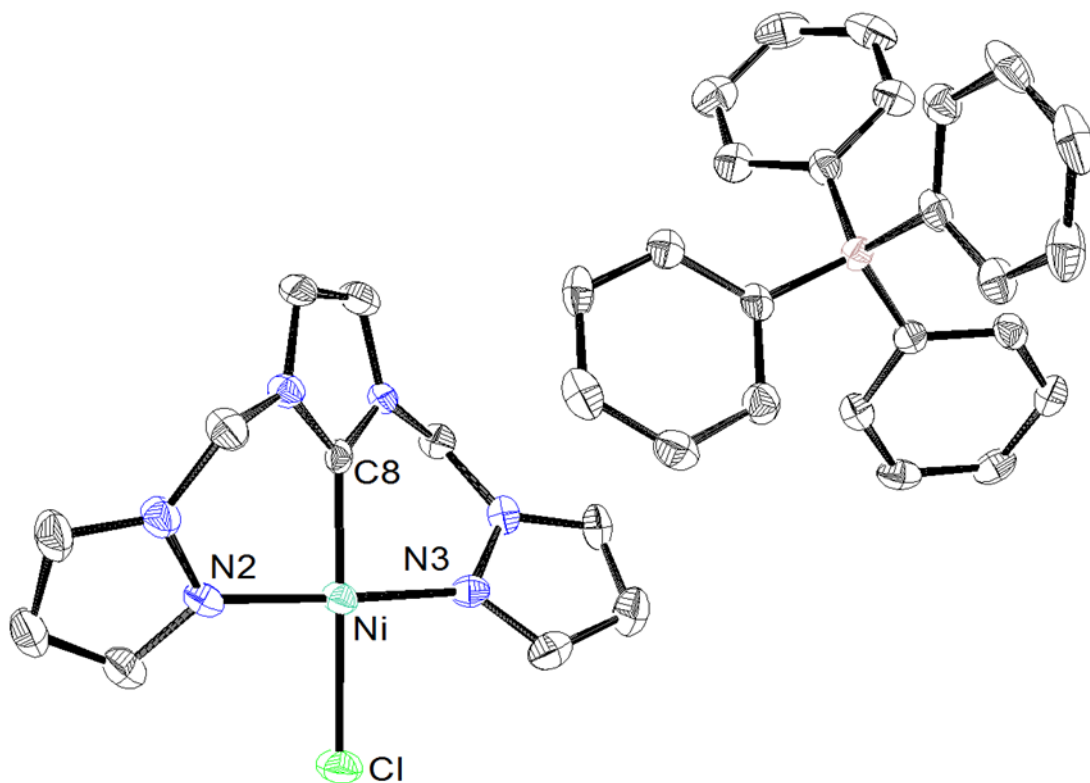


**Figure 3.2** ORTEP depiction of complex **8** with 50 % probability ellipsoids for all non-hydrogen atoms. Hydrogen atoms have been omitted for clarity.

Elemental analysis on the batch of crystals used for X-ray analysis revealed values (C, 65.54; H, 5.07; N, 13.04) nearly identical to the calculated value (C, 65.52; H, 5.03; N, 13.10) of complex **8**. However,  $^1\text{H}$  NMR analysis of the isolated crystals used for solid state structure determination of **8** and elemental analysis produced a spectrum identical to that obtained for the previously synthesised yellow powder with broad signals. The evidence indicated that the broad resonances in the NMR spectrum of **8** were not due to the presence of impurities.

Square planar Ni(II) ( $d^8$ , 16 valence  $e^-$ ) complexes are diamagnetic due to the pairing of all eight d-electrons (Figure 3.3), and typically produce a sharp, well-defined  $^1\text{H}$  NMR spectrum. However, it is possible for four co-ordinate Ni(II) complexes to undergo an isomerization reaction in the solution state, such that the complex exists in an equilibrium between square planar and tetrahedral geometries.<sup>31</sup> Since tetrahedral Ni(II) ( $d^8$ , 16 valence  $e^-$ ) complexes are paramagnetic due to two unpaired d-electrons (Figure 3.3), an equilibrium between pairs of square planar and tetrahedral geometric isomers in solution would result in broadening of the  $^1\text{H}$  NMR spectrum (Scheme 3.11). The  $\text{Ni}(\text{PPh}_3)_2\text{Cl}_2$  precursor used for the synthesis of complex **8** itself exists in such an equilibrium (Scheme 3.12).<sup>31</sup>

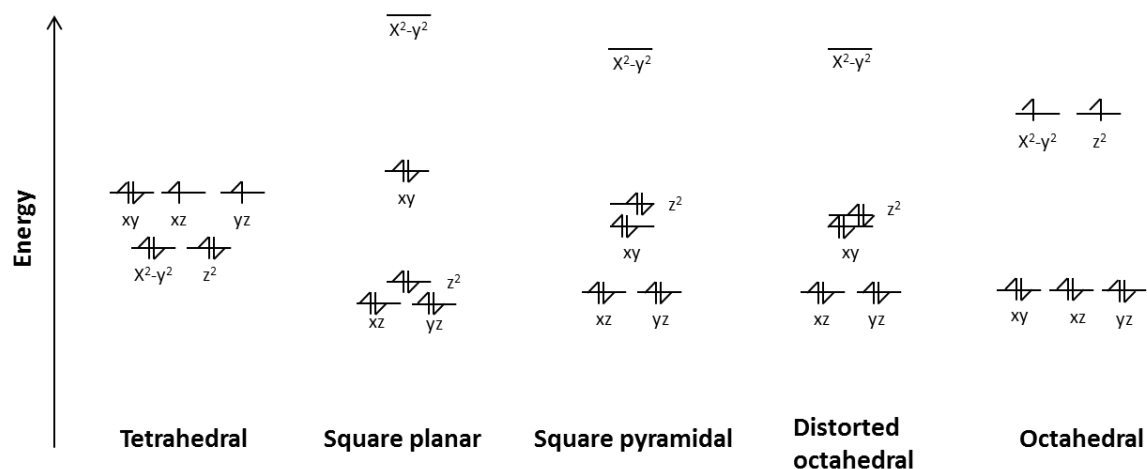
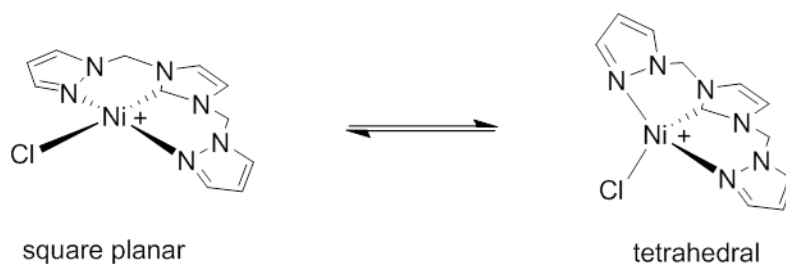


**Figure 3.3** Frontier-orbital energy level diagrams of the d-orbital electrons arising from different geometries possible for complexes of nickel(II).



**Scheme 3.11** Proposed equilibrium between the square planar and tetrahedral conformations of complex **8**.



**Scheme 3.12** Equilibrium between the square planar and tetrahedral conformations of  $\text{Ni}(\text{PPh}_3)_2\text{Cl}_2$ .<sup>31</sup>

The ligand of complex **8** can potentially undergo a conformational change, due to the flexibility of the pendant arms of the ligand, to accommodate the change in metal coordination geometry (Scheme 3.11). A tetrahedral structure of complex **8** requires a coordination of the ligand **1** to the nickel centre in a similar fashion to facial coordination observed in octahedral complexes. As presented in Chapter 2, facial coordination of ligand **1** to ruthenium(II) was shown to be possible. Complex **8** could therefore exist in an equilibrium between square planar and tetrahedral conformations. This could lead to broadened signals in the  $^1\text{H}$  NMR spectrum due to the contribution of the tetrahedral paramagnetic nickel(II) species.

Analysis of the complex using UV spectroscopy should provide clear evidence of the presence of a paramagnetic species since tetrahedral and square planar Ni(II) complexes are known to exhibit characteristic bands in UV visible spectroscopy. Tetrahedral Ni(II) complexes exhibit strong bands in the UV spectra at 400-500 nm and 600-800 nm, whereas analogous complexes containing a square planar geometry produce only one strong band at 400-500 nm.<sup>32</sup> Analysis of complex **8** in acetone solution using UV visible spectroscopy revealed the presence of only one strong band at 460 nm which is characteristic of a square planar Ni(II) compound. This suggested that the broadness observed in the  $^1\text{H}$  NMR spectrum was not a result of paramagnetism.

It is possible that the flexible ligand results in broadness of the  $^1\text{H}$  NMR spectrum. Evidence of the flexibility in the ligand is evident from the X-ray crystal structure analysis where the methylene groups are significantly bent out of plane about the Ni(II) centre and  $\text{NCN}^{\text{Me}}$  donor atoms. To test this hypothesis, complex **8** was analysed using variable temperature  $^1\text{H}$  NMR spectroscopy (Figure 3.4).

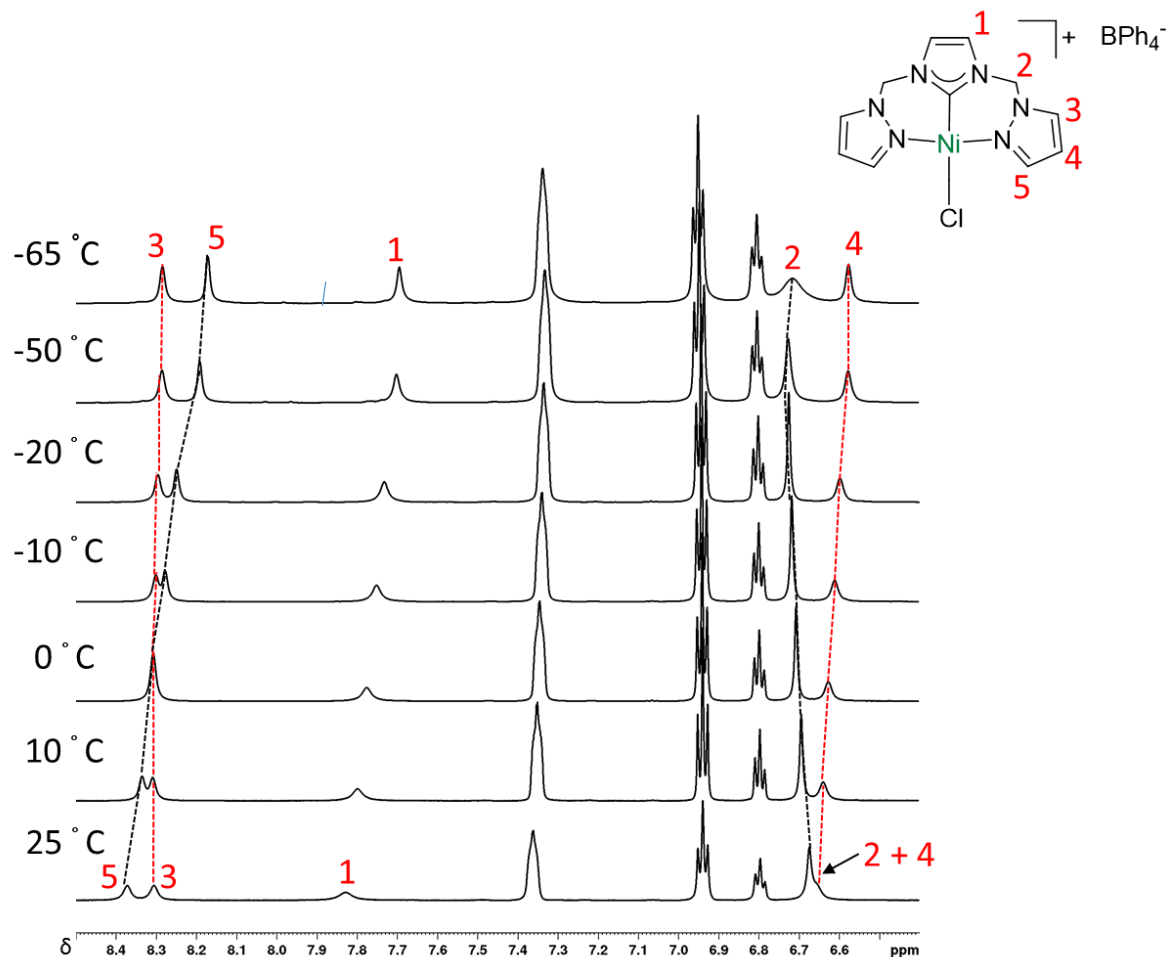


**Figure 3.4** Variable temperature NMR (600 MHz, acetone- $d_6$ ) of complex **8**.

Characterisation using  $^{13}\text{C}\{^1\text{H}\}$  NMR and 2D NMR techniques were possible at  $-65\text{ }^\circ\text{C}$ . Characterisation of complex **8** at the reduced temperature of  $-65\text{ }^\circ\text{C}$  showed the presence of eight proton resonances, five of which are attributed to the ligand, indicative of a single species with a symmetric structure. This is typical of a  $\kappa^3$  coordination of the ligand to the



nickel metal centre and the changing chemical shifts confirmed that the broadness in the  $^1\text{H}$  NMR spectrum of complex **8** resulted from conformational flexibility (Figure 3.5) of the complex rather than paramagnetism or presence of impurities.

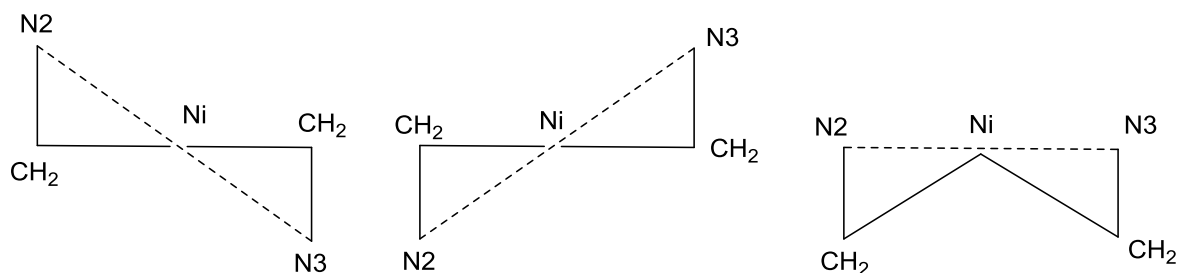


**Figure 3.5** Different conformations possible for complex **8**.

### 3.3.2. Coordination chemistry of $[\text{Ni}(\text{NCN}^{\text{Me}})\text{Cl}]\cdot\text{BPh}_4$

Four coordinate Ni(II) complexes can be converted into more conformationally stable diamagnetic square pyramidal or octahedral complexes upon additional coordination of hard-donor ligands.<sup>33</sup> Hence, NMR scale reactions of complex **8** with a range of hard donor ligands were carried out with the aim of gaining better understanding of the complex in terms of geometric character (spin state) and coordination chemistry (Figure 3.6).

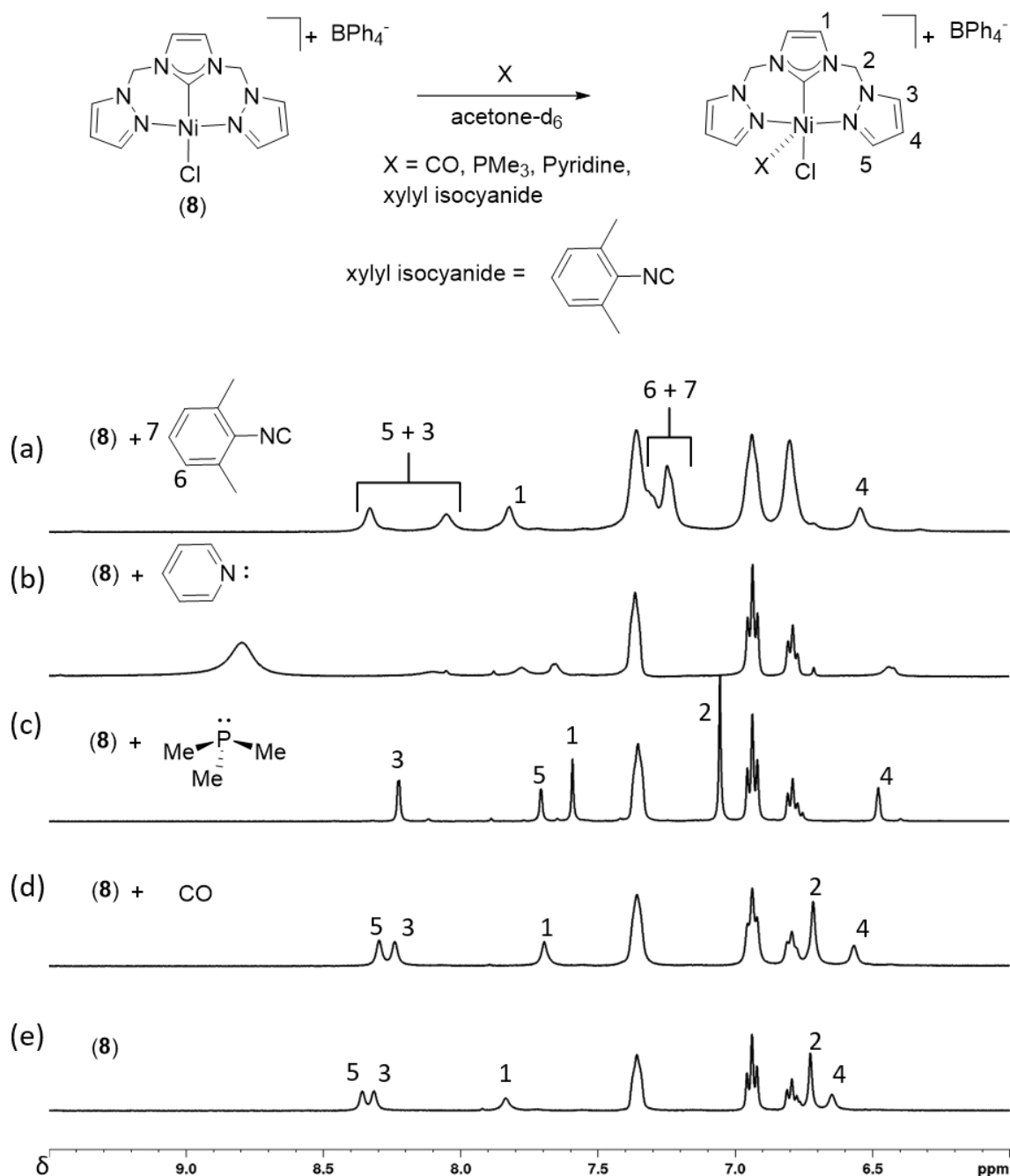


**Figure 3.6**  $^1\text{H}$  NMR (500 MHz,  $\text{acetone-d}_6$ , 25 °C) stacked plots of **8** reacting with hard donor ligands. (a) xylylisocyanide, (b) pyridine, (c)  $\text{PMe}_3$ , (d) CO, (e) four-coordinate complex **8**.

Carbon monoxide, trimethylphosphine, pyridine and xylylisocyanide were used as donor ligands to investigate their effect on the Ni(II) complex upon coordination. The  $^1\text{H}$  NMR spectra of Ni(II) complex **8** in the presence of the additional donors show clear evidence of

coordination of each except CO. The  $^1\text{H}$  NMR spectra of complex **8** before and after exposure to  $\text{CO}_{(\text{g})}$  shows little difference in the chemical shifts of proton resonances and IR ( $\nu(\text{CO})$ ) spectra were not obtained as a  $\text{CO}_{(\text{g})}$  atmosphere would be required for the analysis. Addition of pyridine and xylisocyanide resulted in successful coordination to the nickel metal centre, this was evident from significant shifts of the ligand proton resonances in comparison to the  $^1\text{H}$  NMR spectrum of the parent nickel complex **8** (Figure 3.6a and b). However, the  $^1\text{H}$  NMR spectra of **8+pyridine** and **8+xyl isocyanide** remain broad suggesting structural flexibility of these *in situ* complexes in solution. Upon addition of  $\text{PMe}_3$  to **8**, the broad  $^1\text{H}$  NMR resonances became sharp, well-defined peaks (Figure 3.6c). A single resonance at 6.2 ppm was observed in the  $^{31}\text{P}$  NMR (free  $\text{PMe}_3$  = -62 ppm) spectrum indicating successful addition of the phosphine co-ligand to the nickel metal centre. Unlike the spectrum upon addition of pyridine and xylisocyanide to **8**, the resonances in the  $^1\text{H}$  NMR spectrum of **8+PMe<sub>3</sub>** were sharp indicating that the nickel species was conformationally stable on the NMR time scale. The chemical shift of the pyrazolyl ( $\text{H}^5$ ) proton resonance moves from 8.3 ppm to 7.6 ppm which is likely due to the increased electron density on the pyrazolyl groups due to the  $\text{PMe}_3$ . A significant change in the chemical shift of the pyrazolyl ( $\text{H}^5$ ) proton resonance is expected as it lies closest in proximity to the nickel metal centre. The  $^1\text{H}$  NMR spectrum of complex **8** after the addition of  $\text{PMe}_3$  retains its  $\kappa^3\text{-NCN}$  geometry symmetry as indicated by the five distinct  $^1\text{H}$  resonances attributed to a symmetrically coordinated ligand **1**.

The integration ratio of *NCN*-ligand proton resonances to  $\text{PMe}_3$  proton resonances is 12 : 18, demonstrating that two  $\text{PMe}_3$  co-ligands are bound to the nickel metal centre. However, an octahedral geometry is unlikely since it would result in a paramagnetic

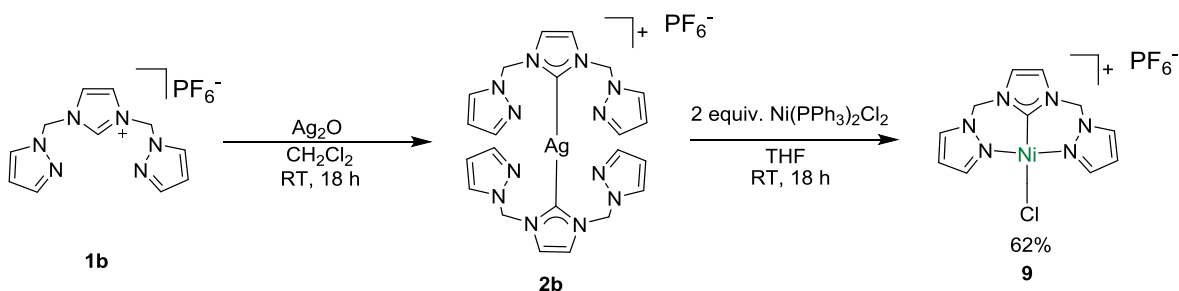
complex (Figure 3.3). It is possible that the complex exists in a distorted octahedral geometry whereby Jahn-Teller distortion causes splitting of the  $x^2-y^2$  and  $z^2$  orbitals, resulting in pairing of all d-orbital electrons (Figure 3.3). This distortion can also occur for the pyridine and xylyl isocyanide analogues, however, ligand **1** likely retains its flexibility resulting in spectra with broad resonances. Pyridine and xylyl isocyanide are sterically bulkier than  $\text{PMe}_3$  and CO. Congestion at the nickel center may also cause more fluctuation in the pincer ligand resulting in broad  $^1\text{H}$  NMR spectra. In comparison, the  $\text{PMe}_3$  bound Ni(II) species, similar to complex **3**, which also contains two phosphine co-ligands *trans* to each other, exhibits a sharp singlet resonance for the  $\text{CH}_2$  protons in the  $^1\text{H}$  NMR spectrum. The evidence shows that the flexibility of the ligand while coordinated to a metal center can be controlled by careful selection of co-ligands.

### 3.3.3. Synthesis and characterisation of $(\text{NCN}^{\text{Me}})\text{PF}_6$ (**1b**)

Complex **8** proved to be difficult to synthesise in reasonable yields and required a number of steps in purification and since the choice of counter ion used in a metal complex can significantly affect catalytic activity,<sup>34</sup> the analogous  $\text{PF}_6^-$  derivative of complex **8** was synthesised. The imidazolium ligand (**1b**) was synthesised following a similar method reported previously.<sup>35</sup> However, the counterion exchange reaction of the  $(\text{NCN}^{\text{Me}})\text{Cl}$  salt was performed with 1.2 equiv. of ammonium hexafluorophosphate instead of  $\text{NaBPh}_4$ . The pro-ligand  $(\text{NCN}^{\text{Me}})\text{PF}_6$  (**1b**) was isolated as a crystalline white solid in 56% yield (Scheme 3.13). The  $^1\text{H}$  NMR spectrum of ligand **1b** was analogous to that of ligand (**1**), exhibiting six  $^1\text{H}$  resonances with the characteristic imidazolium proton signal appearing in the expected region at 9.56 ppm.

Scheme 3.13 Synthesis of  $NCN$  pincer ligand  $(NCN^{Me})PF_6$  (**1b**)3.3.4. Synthesis and characterisation of  $[Ni(NCN^{Me})Cl]PF_6$  (**9**)

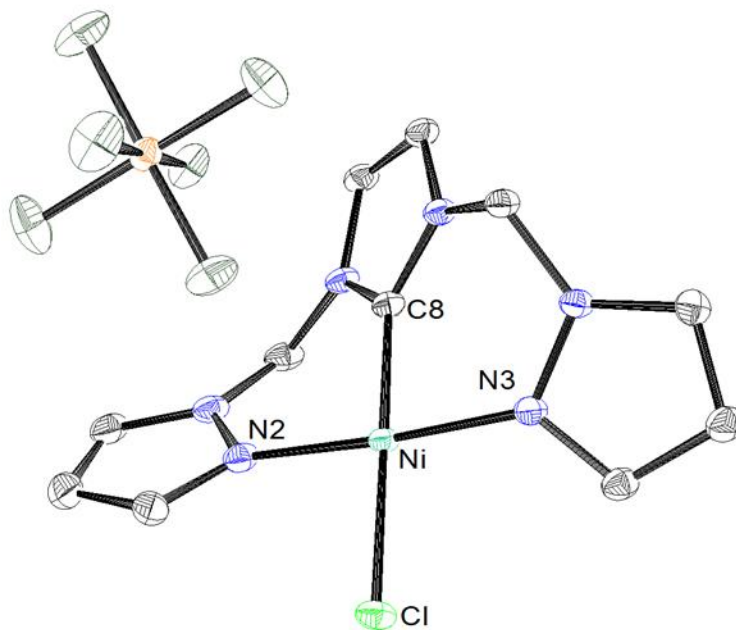
The  $NCN^{Me}$  pincer ligand **1b** was reacted with excess  $Ag_2O$  (2 equiv.) to produce  $[Ag(NCN^{Me})_2].PF_6$  as a pale brown solid (Scheme 3.14), to which  $Ni(PPh_3)_2Cl_2$  was added *in situ* to afford  $[Ni(NCN^{Me})Cl].PF_6$  (**9**) as an orange powder in 62% yield.

Scheme 3.14 Synthesis of  $[Ni(NCN^{Me})Cl]PF_6$  (**9**)

The  $^1H$  NMR spectrum of **9** was similar to the analogous Ni(II)  $BPh_4$  complex **8**, the  $^1H$  NMR spectrum of the  $PF_6^-$  derivative (**9**) exhibited five broad ligand resonances. Complex **9** could not be characterized at 25 °C using  $^{13}C$  NMR or 2D NMR techniques as the resonances were too broad. Analysis of complex **9** using UV visible spectroscopy produced a single peak at 460 nm, similar to the UV/Vis spectra of complex **8** which suggested that the broadness was not a result of any paramagnetic species. Low temperature NMR spectroscopy at -50 °C allowed characterisation of the complex to be achieved using  $^{13}C$  NMR and 2D NMR techniques.

The presence of only five resonances in the  $^1\text{H}$  NMR spectrum of **9** at  $-50\text{ }^\circ\text{C}$  suggested symmetry in the structure in the solution state and is likely to contain a  $\kappa^3\text{-NCN}$  geometry analogous to complex **8**. The resonances due to the methylene linker protons ( $\text{CH}_2$ ) and pyrazolyl protons (Pz4) are well separated in complex **9** even at  $25\text{ }^\circ\text{C}$  compared to those of complex **8** suggesting that the change in counterion altered the chemical shifts of the Ni(II) complex bearing the  $\text{NCN}^{\text{Me}}$  ligand **1**. The resonance due to  $\text{CH}_2$  protons at  $-50\text{ }^\circ\text{C}$  shows a doublet pattern typical of diastereotopic coupling which has been observed previously for the Ru(II) complexes of ligand **1**, synthesised in chapter 2.

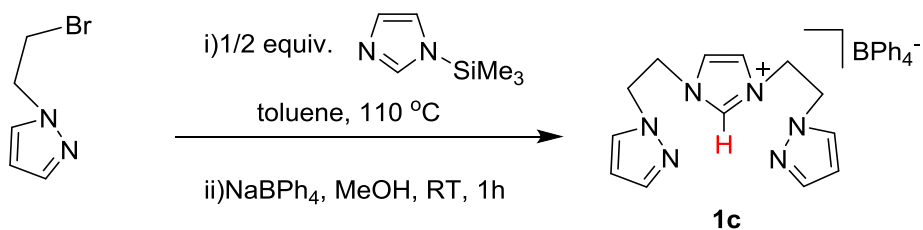
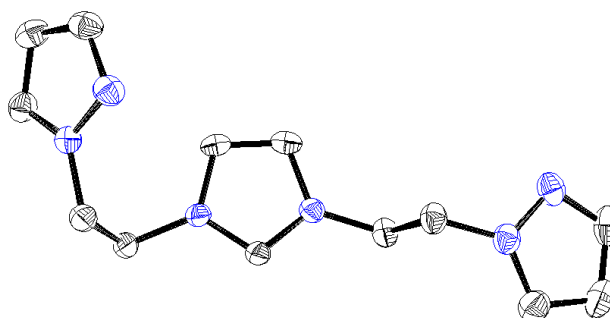
Crystals of **9** suitable for X-ray analysis were grown by vapour diffusion of diethyl ether into a saturated solution of **9** in acetone. Analysis using X-ray crystallography confirmed the expected  $\kappa^3\text{-NCN}$  symmetric structure with the Cl co-ligand terminally bound to the Ni metal centre and in a *trans* position relative to the central carbene (Figure 3.7). Mass spectrometry shows a dominant signal at  $303.05\text{ m/z}$  which was attributed to the cationic fragment with formula  $[\text{Ni}(\text{NCN}^{\text{Me}})\text{OH}]^+$ . The structure with the exemption of the counter ion proved to be isostructural to complex **8**.



**Figure 3.7** ORTEP depiction of complex **9** with 50 % probability ellipsoids for all non-hydrogen atoms. Hydrogen atoms have been omitted for clarity.

### 3.3.5. Synthesis and characterisation of $[\text{Ni}(\text{NCN}^{\text{Et}})_2](\text{BPh}_4)_2$ (**10**)

The use of a pincer ligand containing a longer alkyl linker between the central imidazolyl and pendant pyrazolyl moieties can affect the coordination of the ligand to a metal centre. Therefore, the pincer ligand  $(\text{NCN}^{\text{Et}})\text{BPh}_4$  (**1c**) was synthesised according to a previous literature procedure using bromoethylpyrazole and half an equivalent of trimethylsilylimidazole in refluxing toluene.<sup>35</sup> This was followed by counterion exchange with  $\text{NaBPh}_4$  to yield **1c** as a white solid at a yield of 72% (Scheme 3.15).<sup>35</sup> Crystals suitable for X-ray analysis were grown by slow evaporation of a saturated solution of **1c** in acetone. The X-ray analysis confirms the conformational flexibility of the ligand as expected due to the ethylene linkers with one pendant pyrazolyl arm nearly linear in conformation whereas the second pendant arm is rotated nearly 90° away from linearity (Figure 3.8).

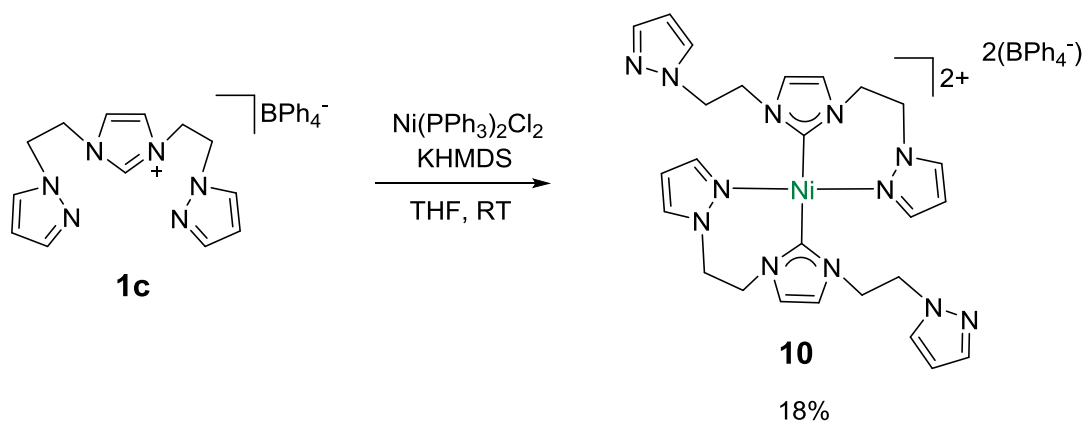
Scheme 3.15 Synthesis of  $(NCN^{Et}) BPh_4$  (**1c**).**Figure 3.8** ORTEP depiction of ligand **1c** with 50% probability ellipsoids for all non-hydrogen atoms. Hydrogen atoms and  $BPh_4$  have been omitted for clarity.

The silver complex  $[Ag(NCN^{Et})_2] \cdot BPh_4$  (**2c**) was prepared as a white solid by reaction of ligand **1c** with excess  $Ag_2O$ . The  $^1H$  NMR spectrum of the white solid contained nine proton resonances, six of which were attributed to the ligand protons and the remaining three resonances are assigned to the  $BPh_4^-$  protons. In a similar fashion to the  $^1H$  NMR spectrum of  $[Ag(NCN^{Me})_2] BPh_4$  (**2**), the absence of the imidazolium proton resonance in the  $^1H$  NMR spectrum of **2c** indicates successful complexation of silver to the ligand. The ratio of the integrals of the proton resonances indicate that the ligand to  $BPh_4^-$  ratio is 2 : 1 which is indicative of a homoleptic structure for the silver complex  $[Ag(NCN^{Et})_2] BPh_4$  (**2c**).

With the aim of synthesising a Ni(II) complex of ligand **1c** containing longer alkyl linkers linker between the central imidazole and pendant pyrazolyl moieties, two equiv. of  $Ni(PPh_3)_2Cl_2$  were added to the silver intermediate (**2c**). This approach had been used previously for the transmetallation synthesis of Ni(II) complexes **8** and **9** containing ligands



**1a** and **1b** respectively. However the reaction of **2c** and  $\text{Ni}(\text{PPh}_3)_2\text{Cl}_2$  resulted in a mixture of unreacted starting material and insoluble silver salts, so this method proved to be unsuccessful. An alternate approach to the synthesis of a Ni(II) complex with ligand **1c** was to use an external base to deprotonate the imidazolium salt (**1c**) *in situ* prior to addition of the nickel precursor ( $\text{Ni}(\text{PPh}_3)_2\text{Cl}_2$ ). Triethylamine,  $\text{K}_2\text{CO}_3$  and potassium hexamethyldisilazide (KHMDs) were tested as bases for this reaction, however only KHMDs was successful at deprotonating **1c**. The precursor  $\text{Ni}(\text{PPh}_3)_2\text{Cl}_2$  was reacted with ligand **1c** in the presence of excess KHMDs producing  $[\text{Ni}(\text{NCN}^{\text{Et}})_2](\text{BPh}_4)_2$  (**10**) as a yellow solid in 18% yield (Scheme 3.16). Many attempts were made to improve the yield of complex **10**, by altering the reaction temperatures and ligand to metal ratios. However, any deviations from the synthetic method shown in Scheme 3.16 resulted in unsuccessful reactions which did not show evidence of any single isolable species.



**Scheme 3.16** Synthesis of  $[\text{Ni}(\text{NCN}^{\text{Et}})_2](\text{BPh}_4)_2$  (**10**).

The  $^1\text{H}$  NMR spectrum of the nickel(II) complex **10** revealed that **10** exists as an asymmetric species in solution. The  $^1\text{H}$  NMR spectrum contains 19 distinct proton resonances, 16 of which were assigned to the protons of two ligands which suggested the complex had two NHC donors. The analysis of the NMR spectrum indicates that each pincer ligand of

complex **10** has only two coordinating donors and one free pyrazolyl arm giving rise to the unsymmetric structure. Two sets of proton resonances with coupling patterns that are typical of resonances due to diastereotopic proton pairs were attributed to the ethylene protons. One set consists of four multiplets within close proximity (4.35-4.72 ppm;  $^3J = 13.8$  Hz) while the second set of resonances due to diastereotopic protons contains four separate multiplet signals (5.04, 5.42, 6.11 and 7.05 ppm;  $^3J = 13.8$  Hz); which is characteristic of an asymmetric geometry of the ligand about the metal centre. The ratio of the integrals of resonances due to the ligand and BPh<sub>4</sub> indicates that the ratio of ligand to BPh<sub>4</sub> is 1:1, again indicating a likely *bis*-NHC structure. The *bis*-NHC structure was further confirmed by an absence of PPh<sub>3</sub> proton resonances in the <sup>1</sup>H NMR spectra of complex **10**, which indicates that the two phosphine co-ligands have been displaced from the nickel centre. Analysis of complex **10** by variable temperature <sup>1</sup>H NMR spectroscopy revealed the presence of another species at low concentrations (Figure 3.9). The resonance of H<sup>8a</sup> markedly shifts to high ppm at lower temperatures (Figure 3.9), this indicates a strong C-H  $\pi$ -interaction with a pyrazole from the second NCN ligand.

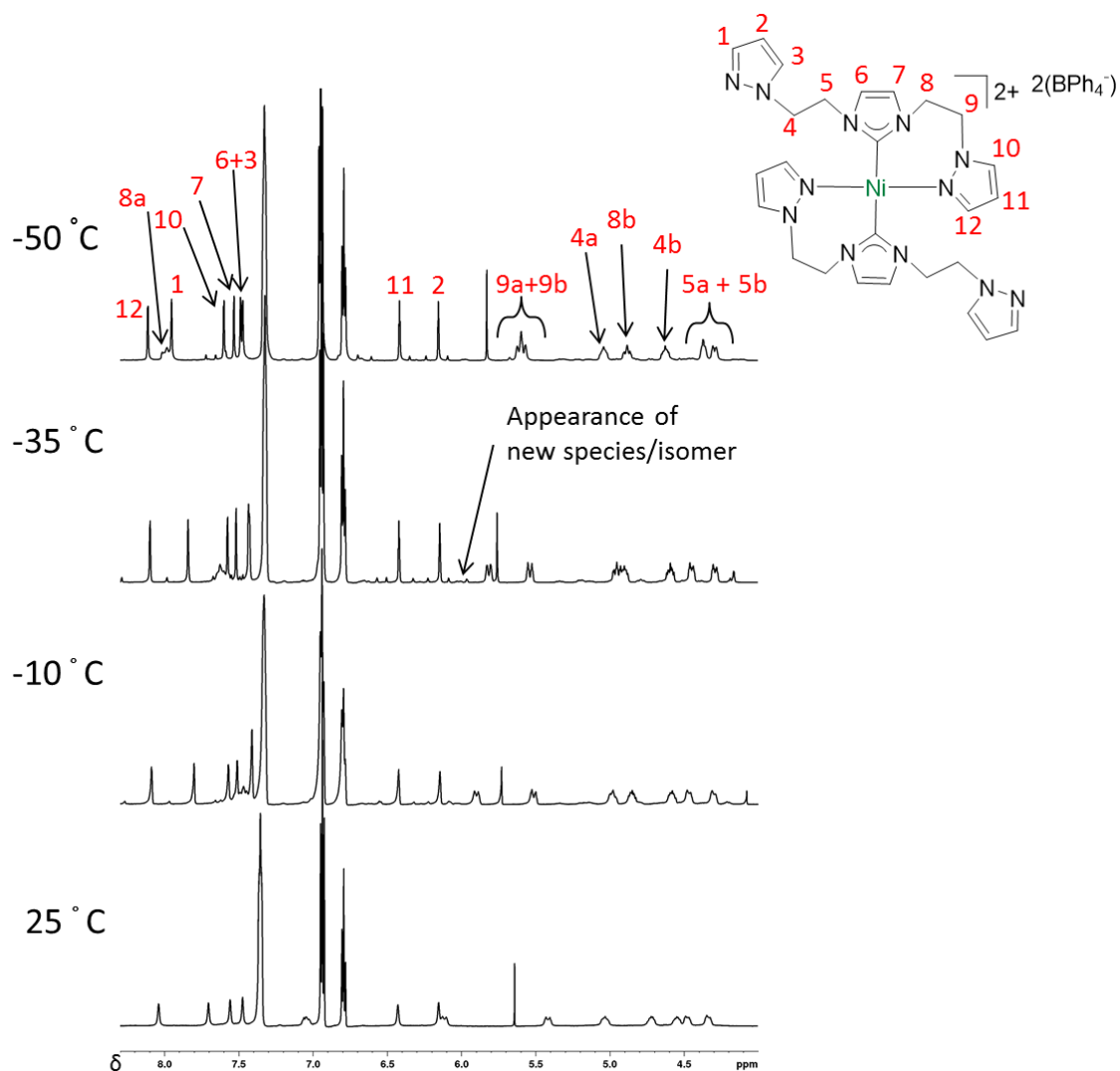


**Figure 3.9** Variable temperature  $^1\text{H}$  NMR spectra (600 MHz, acetone- $d_6$ ) of complex **10**. (a and b = diastereotopic hydrogens of ethylene linkers).

Crystals of **10** suitable for X-ray analysis were grown by vapour diffusion of diethyl ether into a saturated solution of **10** in acetone. X-ray crystal structure analysis confirmed that Ni(II) had a square planar geometry in complex (**10**) and that the *bis*-NHC ligands were asymmetrically  $\kappa^2\text{-NCN}$  coordinated (Figure 3.10). The significant shift of the resonances due to  $\text{H}^{8a}$  to higher ppm ranges as observed in  $^1\text{H}$  NMR (Figure 3.9) was confirmed by X-ray analysis to be due to C-H  $\pi$ -interaction of the proton to a pyrazolyl ring with an interaction distance of 2.845 Å. This distance is typical of C-H  $\pi$ -interactions of hydrogen atoms to an

aryl ring.<sup>36</sup> A similar *bis*-NHC geometry was reported previously by Mancano *et al.* for a complex containing ligand **1c**,<sup>35</sup> where the Ir(I) compound contained two ligands *trans* to each other similar to complex **10**. However complex **10** shows a bidentate coordination of the ligand **1c** to the metal centre whereas the Ir(I) counterpart had a monodentate coordination of the ligand to the metal centre.

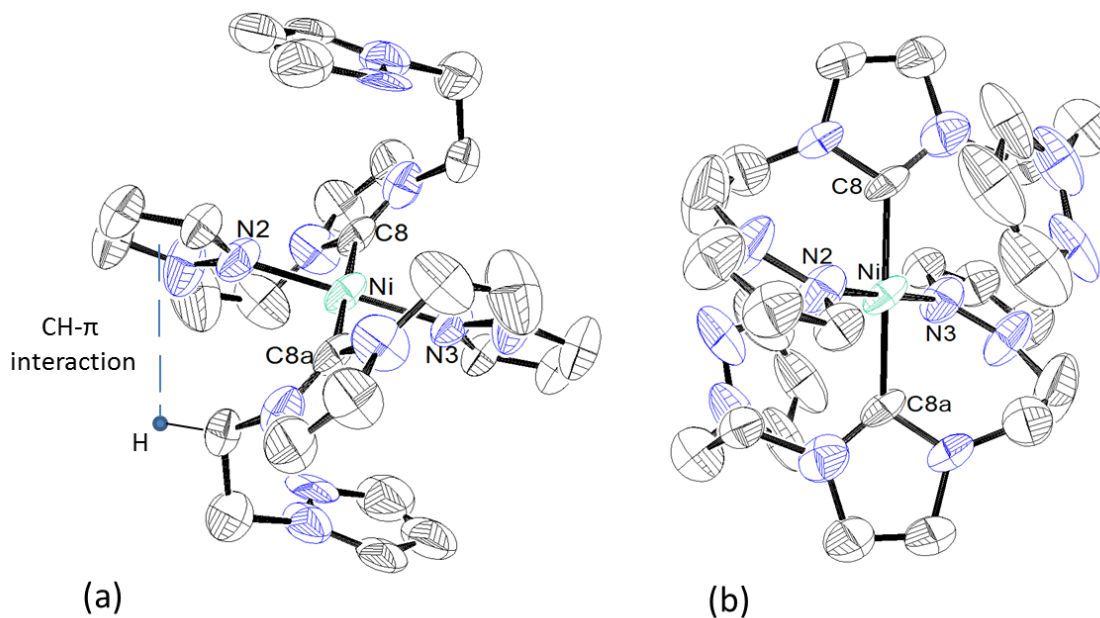


**Figure 3.10** ORTEP depiction of complex **10** with 50% probability ellipsoids for all non-hydrogen atoms. Hydrogen atoms and BPh<sub>4</sub> have been omitted for clarity. (a) Viewed along C8a-Ni-C8 axis. (b) Viewed along N2-Ni-N3 axis.

3.3.6. Comparison of the inner coordination sphere of complexes **8**, **9** and **10**.

	Atoms	<b>8</b>	<b>9</b>	<b>10</b>
Bond lengths	Ni(1)-C(8)(carbene)	1.850(4)	1.847(2)	1.899(1)
	Ni(1)-C(8a)	----	-----	1.899(1)
	Ni(1)-N(2)	1.887(3)	1.902(2)	1.909(8)
	Ni(1)-N(3)	1.908(3)	1.900(2)	1.909(8)
	Ni(1)-Cl	2.200(1)	2.220(1)	-----
Bond angles	C(1)-Ni(1)-N(3)	89.8(2)	88.6(1)	91.9(2)
	C(1)-Ni(1)-N(2)	88.2(2)	88.4(1)	88.1(2)

**Table 3.1** Selected bond lengths (Å) and angles (°) for **8**, **9** and **10**.

All three Ni(II) complexes **8**, **9** and **10** under investigation here adopt a square planar geometry, with the main difference between the structures being that there are two *NCN* ligands bound to the Ni(II) centre in a bidentate coordination mode in complex **10** (Figure 3.10) where there is only one *NCN*<sup>Me</sup> ligand bound to nickel in **8** and **9**. The bond lengths of the inner coordination sphere of complexes **8** and **9** are nearly identical as expected due to their isostructural solid state structures. Analogous Ni(II) square planar carbene complexes in the literature where the NHC ligand contains pyridine side arms have similar nickel-carbene (1.837 Å) and Ni(1)-Cl (2.236 Å) bond lengths to those of complexes **8** and **9**.<sup>30</sup> The nickel-carbene bond length in complex **10** is slightly longer than that observed for **8** and **9**. Complexes **8** and **9** contain a Cl co-ligand *trans* to the NHC carbene which has a weaker *trans* effect than an NHC carbene. Since all three complexes consist of two pyrazolyl groups *trans* to each other, the Ni(1)-N(2) and Ni(1)-N(3) bond lengths are similar in all three complexes; where the maximum variation in Ni(1)-N bond lengths is 0.012 Å. The two carbene carbons (C8 and C8a) and two pyrazolyl nitrogens (N2 and N3) in complex **10** show no distortion from linearity as the Ni atom lies in an inversion centre (C-Ni-C/N-Ni-N:

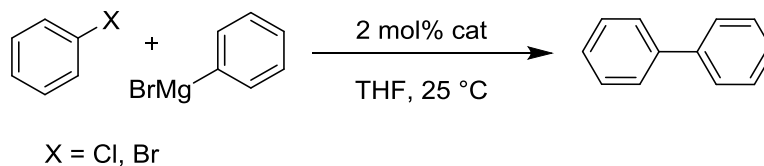
180.00(2)°). However, similar alignments in complexes **8** and **9** exhibit slight distortion from linearity (complex **8**: N-Ni-N: 176.02(2)°, complex **9**: N-Ni-N: 175.68(2)°) which is likely due to decreased ring strain in complex **10** enabled by bidentate coordination of ligand **2** to the Ni(II) metal centre. There are also significant rotations of the NHC ligands out of the square plane in all three complexes, giving a torsion angle (N3-Ni-C8-Imidazolium N5) of 30° in complexes **8** and **9** and 46° in complex **10**.

### 3.4. Catalytic activity of Ni(II) complexes for Kumada cross coupling of aryl halides

Ni(II) square planar complexes are known to be efficient catalysts for the Kumada cross coupling reaction. Among the best nickel catalyst systems for the Kumada cross coupling reaction include the addition of nickel metal ions to calixarene ligands. The catalytic systems achieve complete conversions of substrate at room temperature within 1 h, and can catalyse the reaction at catalyst loadings as low as 0.1-0.02 mol%.<sup>37</sup> However, only a few of the Ni complexes of weakly coordinating ligands such as calixarene maintain high activity at elevated temperatures without suffering catalyst decomposition.<sup>6</sup> Thus, complexes [Ni(NCN<sup>Me</sup>)Cl](BPh<sub>4</sub>) (**8**), [Ni(NCN<sup>Me</sup>)Cl](PF<sub>6</sub>) (**9**) and [Ni(NCN<sup>Et</sup>)<sub>2</sub>Cl](BPh<sub>4</sub>)<sub>2</sub> (**10**) synthesised here that contain hemilabile ligands composed of pyrazolyl and imidazolyl carbene donors, were tested as catalysts for the Kumada cross coupling reaction of aryl halides. The reactions were carried out under Schlenk conditions using distilled THF at 25 °C with a catalyst loading of 2 mol% unless otherwise stated. The glassware was flame dried and catalysts were predried under vacuum prior to the catalysis reactions. GC-MS analysis was used to monitor the reaction progress by taking aliquots at regular intervals. For complete experimental details, refer to Chapter 6.

### 3.4.1. Catalytic activity of **8**, **9** and **10** for Kumada cross coupling reactions of chlorobenzene and bromobenzene

Complexes **8**, **9** and **10** were initially tested as catalysts for the Kumada cross coupling reactions of chlorobenzene and bromobenzene and with phenylmagnesium bromide (Scheme 3.17).



**Scheme 3.17** Kumada cross coupling reactions of PhBr and PhCl with PhMgBr catalysed by **8**, **9** and **10**.

**Table 3.2** Kumada cross coupling reactions of PhBr and PhCl with PhMgBr catalysed by **8**, **9** and **10**.

entry	substrate	catalyst	%conv. (3.5 h)
<b>1</b>		<b>8</b>	87
<b>2</b>		<b>9</b>	89
<b>3</b>		<b>10</b>	40
<b>4</b>		<b>8</b>	>99
<b>5</b>		<b>9</b>	40
<b>6</b>		<b>10</b>	40

Conditions - Temperature: 25 °C. Catalyst loading: 2 mol%. Substrate: (0.5 mmol).

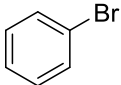
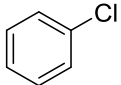
Phenylmagnesium bromide: (1.5 mmol).

Complex **10** proved to be the least active catalyst of the three catalysts tested, achieving low conversions for the Kumada cross coupling reactions of both chlorobenzene and bromobenzene. Both reactions with chlorobenzene and bromobenzene terminate at 40% conversion (entries 1 and 2, Table 3.2) which suggested that deactivation of the catalyst occurs. The deactivation and thus the reduced catalytic activity of complex **10** compared to complexes **8** and **9** is likely due to complete coordinative saturation of the nickel center by ligand **1c**. Any conversion of substrate promoted by **10** likely occurred due to the lability of the weakly coordinating pyrazolyl groups allowing substrate access to the active metal center. The pyrazolyl groups are positioned *trans* to each other along with the central NHC groups. Previous work reported in the literature has demonstrated that nickel *bis*-carbenic systems have reduced activity for the Kumada cross coupling reaction in relation to mono carbenic systems. Zhang *et al.* have synthesized Ni(I)(IMes)Br and Ni(II)(IMes)Br<sub>2</sub> complexes which were tested as catalysts for the Kumada cross coupling reaction of aryl bromides.<sup>38</sup> The Ni(I) complexes fail to achieve complete conversions with reactions terminating at 60-80% even at 3 mol% catalyst loading. Very low yields were reported for the Ni(II)(IMes)Br<sub>2</sub> systems.<sup>38</sup>

Complex **8**, containing the BPh<sub>4</sub><sup>-</sup> counterion, proved to be the most effective catalyst overall for the Kumada cross coupling reactions of chlorobenzene and bromobenzene, achieving high conversions for both substrates within 3.5 h (entries 1 and 4, Table 3.2). Due to the high conversions achieved using complex **8**, the reactions were repeated at a lower catalyst loading of 1 mol% to determine whether the catalyst maintains the activity at lower loadings.



**Table 3.3** Catalysed Kumada cross coupling of PhCl and PhBr using **8** at different catalyst loadings.

entry	substrate	Catalyst loading	%conv. (4 h)
1		1 mol%	80
2		2 mol%	87
3		1 mol%	43
4		2 mol%	>99

Conditions - Temperature: 25 °C. Catalyst loading: 1 or 2 mol%. Substrate: (0.5 mmol).

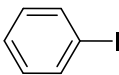
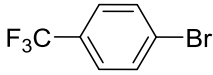
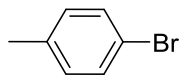
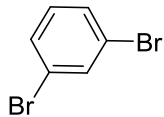
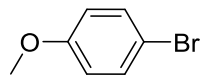
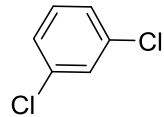
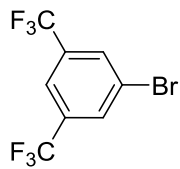
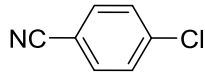
Phenylmagnesium bromide: (1.5 mmol).

Decreasing the catalytic loading of complex **8** to 1 mol% for the conversion of the chlorobenzene substrate to biphenyl resulted in a significant reduction in catalytic activity, where only 43% conversion of chlorobenzene was achieved (entries 3 & 4, Table 3.3). Surprisingly, the coupling reaction of bromobenzene using 1 mol% of **8** did not result in a significant reduction in catalytic activity compared to the reaction catalysed by 2 mol% of **8**. Catalyst loadings of 1 mol% and 2 mol% achieve 80% conversion and 87% conversion respectively (entries 1 & 2, Table 3.3). All reactions shown in Table 3.3 were reproducible. There is currently no established mechanism to explain the higher reactivity of **8** for the conversion of chlorobenzene compared to bromobenzene.

#### 3.4.2. Substrate scope of complex **8** for the Kumada cross coupling reaction

As complex **8** proved to be the most effective catalyst under investigation here for the cross coupling reactions of bromobenzene and chlorobenzene, it was tested as a catalyst for the transformation of a selection of substrates. (Table 3.4)

**Table 3.4** Range of substrates catalysed by **8** for Kumada cross coupling reactions.

entry	R-X	% conv.	entry	R-X	% conv.
1		>99	5		90
2		78	6		67(m)
3		50	7		16(d)
4		68	8		0

Conditions - Temperature: 25 °C. Catalyst loading: 2 mol%. Substrate: (0.5 mmol).

Phenylmagnesium bromide: (1.5 mmol). Time : 4h. (m = monosubstituted product, d= disubstituted product)

Of all the bromo-substrates tested (Table 3.4) for conversion to biphenyl products using **8**, the highest conversions were achieved for the substrate containing an electron withdrawing CF<sub>3</sub> substituent on the aryl ring. In comparison, substrates with mesomerically electron donating substituents (*i.e.* methoxy) and more electron donating functional groups (methyl) achieve lower conversion to product. The tolyl bromide with increased electron donating character showed reduced activity for the Kumada cross coupling reaction compared to the phenyl counterparts with the reaction terminating at 78% conversion. Increasing the catalyst loading did not improve the catalytic activity, with a higher loading of 5 mol% achieving nearly identical results (76% conversion) within 4 h. Increasing the number of functional groups resulted in lower conversions for the cross coupling; since disubstitution of CF<sub>3</sub> groups located at the *meta* positions on the aryl ring relative to the bromine resulted in a reduced substrate conversion (68%) compared to the mono-*para*

substituted  $\text{CF}_3$  reaction (90%). It was interesting to observe that the choice of halide altered the selectivity of cross coupling reactions to form biphenyl or triphenyl products. The catalysed reaction of phenylmagnesium bromide with the 1,3-dibromobenzene resulted in selective formation of the monosubstituted 1-bromo-3-phenylbenzene. However, the catalyzed reaction of the analogous 1,3-dichlorobenzene with phenylmagnesium bromide using **8** results in the selective production of the disubstituted 1,3-diphenylbenzene. This result was unexpected considering 1,3-dibromobenzene is more likely to produce the disubstituted product due to the propensity of bromide groups to be more readily substituted in comparison to chloride groups. However, as expected, substrates containing bromide groups produced higher overall yields in comparison to the substrates containing chloride groups.

### 3.5. Conclusions

This chapter describes the coordination chemistry of *NCN* pincer ligand precursors **1**, **1b** and **1c** with Ni(II) and Ag(I) metal centres and the investigation of the activity of the resulting Ni(II) complexes **8**, **9** and **10** as catalysts for the Kumada cross coupling reaction.

- Choice of ligand affected the nature of the coordination observed in the resulting complexes. Both bidentate and tridentate coordination of the *NCN* ligands to the Ni(II) metal centre were observed.
- Complex **8** containing the pincer geometry was found to be the most active catalyst for the Kumada cross coupling reaction in comparison to complexes **9** and **10**. The coordinatively saturated complex **10** was found to be nearly inactive as a catalyst for the organic transformation.
- Changing the counterion from  $\text{BPh}_4^-$  to  $\text{PF}_6^-$  (complexes **8** and **9**) resulted in reduced activity for promoting the transformation of the chlorinated substrate chlorobenzene, and similar activity for the Kumada cross coupling reaction of bromobenzene with phenylmagnesium bromide.
- Complex **8**, being the most active catalyst under investigation here was tested as a catalyst for a wide range of substrates to test functional group tolerance and ability to perform more difficult di-substitution reactions. Complex **8** catalysed the Kumada cross coupling reaction for a wide range of substrates with higher activities achieved for substrates with electronegative substituents. The investigation showed that the catalytic activity was dependent on the type of substituents present on the aryl substrates.

- Complex **8** proved to be moderately active for the Kumada cross coupling reaction compared to other Ni(II) complexes in literature. Other Ni(II) complexes containing NHC pincer ligands achieve similar conversions to those of complex **8** for the Kumada cross coupling reaction.
- The air stable complex **8** may prove to be useful in catalysed reactions such as Suzuki- Miyura cross coupling.

### 3.6. References:

- (1) Cherney, A. H.; Kadunce, N. T.; Reisman, S. E. *Chem. Rev.* **2015**, *115*, 9587.
- (2) Tamao, K.; Sumitani, K.; Kumada, M. *J. Am. Chem. Soc.* **1972**, *63*, 4374.
- (3) Wang, Z. X.; Liu, N. *Eur. J. Inorg. Chem.* **2012**, *6*, 901.
- (4) Christiane, E. I.; Wangelin, J. V. *Chem. Soc. Rev.* **2011**, *40*, 4948.
- (5) (a) Stille, J. K. *Angew. Chem. Int. Ed.* **1986**, *25*, 508; (b) Cordovilla, C.; Bartolomé, C.; J Martínez-Ilarduya, J. M.; Espinet, P. *ACS Catal.* **2015**, *5*, 3040.
- (6) (a) Zhang, C.; Wang, Z. X. *Organometallics* **2009**, *28*, 6507. (b) Garcia, P. M. P.; Di Franco, T.; Epenoy, A.; Scopelliti, R.; Hu, X. *ACS Catal.* **2016**, *6*, 258.
- (7) Li, J. J. *Modern Drug Synthesis*. **2010**, 153.
- (8) McCullough, R. D.; Lowe, R. D. *Chem. Commun.* **1992**, *1*, 70.
- (9) Lou, S.; Fu, G. C. *J. Am. Chem. Soc.* **2010**, *132*, 1264.
- (10) (a) Kumada, M. *Bull. Chem. Soc. Jpn.* **1976**, *49*, 1958; (b) Buono, F. G.; Zhang, Y.; Tan, Z.; Brusoe, A.; Yang, B. S.; Lorenz, J. C.; Giovannini, R.; Song, J. J.; Yee, N. K.; Senanayake, C. H. *Eur. J. Org. Chem.* **2016**, *15*, 2599.
- (11) Linstrumelle, G. *Tetrahedron Lett.* **1978**, *19*, 191.
- (12) (a) Yoshikai, N.; Matsuda, H.; Nakamura, E. *J. Am. Chem. Soc.* **2009**, *131*, 9590; (b) Dai, W.; Xiao, J.; Jin, G.; Wu, J.; Cao, S. *J. Org. Chem.* **2014**, *79*, 10537.
- (13) Wolf, C.; Xu, H. J. *J. Org. Chem.* **2008**, *73*, 162.
- (14) Rudolph, A.; Lautens, M. *Angew. Chem. Int. Ed.* **2009**, *48*, 2656.
- (15) (a) Terao, J.; Watanabe, H.; Ikumi, A.; Kuniyasu, H.; Kambe, N. *J. Am. Chem. Soc.* **2002**, *124*, 4222; (b) Biswas, S.; Weix, D. J. *J. Am. Chem. Soc.* **2013**, *135*, 16192.
- (16) Frisch, A.; Beller, M. *Angew. Chem. Int. Ed.* **2005**, *44*, 674.

- (17) Morales-Morales, D.; Jensen, C. M. *The Chemistry of Pincer Compounds*, 1<sup>st</sup> ed.; Elsevier. **2007**.
- (18) (a) Selander, N.; Szabo, K. J. *Chem. Rev.* **2011**, *111*, 2048; (b) van der Vlug, J. I.; Reek, J. N. H. *Angew. Chem. Int. Ed.* **2009**, *121*, 8990.
- (19) de Meijere, A.; Diederich, F. *Metal-Catalyzed Cross-Coupling Reactions*, 2<sup>nd</sup> ed., Wiley-VCH, Weinheim, **2004**.
- (20) Costanguay, A.; Beauchamp, A. L.; Zargarian, D. *Organometallics* **2008**, *27*, 5723.
- (21) Sanford, J.; Dent, C.; Masuda, J. D.; Xia, A. *Polyhedron* **2011**, *30*, 1091.
- (22) Inamoto, K. U.; Kuroda, J. I.; Sakamoto, T.; Hiroya, K. *Synthesis* **2007**, 2853.
- (23) Gu, S.; Chen, W. *Organometallics* **2009**, *28*, 909.
- (24) (a) Lundin, P. M.; Esquivias, J.; Fu, G. C. *Angew. Chem. Int. Ed.* **2009**, *121*, 160; (b) Andrew, R. H.; González-Sebastián, L.; Chaplin, A. B.; *Dalton Trans.* **2016**, *45*, 1299.
- (25) (a) Inamoto, K.; Kuroda, J. I.; Kwonb, E.; Hiroya, K.; Doi, T. *J. Organomet. Chem.* **2009**, *694*, 389; (b) Xu, M.; Li, X.; Sun, Z.; Tu, T. *Chem. Commun.* **2013**, *49*, 11539; (c) Tu, T.; Mao, H.; Herbert, C.; Xu, M.; Dötz, K. H. *Chem. Commun.* **2010**, *46*, 7796.
- (26) Kuroda, J. I.; Inamoto, K.; Hiroya, K.; Doi, T. *Eur. J. Org. Chem.* **2009**, *14*, 2251.
- (27) Wang, Z. X.; Wang, L. *Chem. Commun.* **2007**, *23*, 2423.
- (28) Jeffrey, J. C.; Rauchfuss, T. B. *Inorg. Chem.* **1979**, *18*, 2658.
- (29) Bernhammer, J. C.; Frison, G.; Huynh, H. V. *Dalton Trans.* **2014**, *43*, 8591.
- (30) Chen, C. *J. Organomet. Chem.* **2012**, *696*, 4166.
- (31) (a) Corain, B.; Longato, B.; Angeletti, R.; Valle, G. *Inorg. Chim. Acta.* **1985**, *104*, 15; (b) Brammer, L.; Stevens, E. D. *Acta Cryst. C.* **1989**, *45*, 400.

- (32) Maganas, D.; Grigoropoulos, A.; Staniland, S. S.; Chatziefthimiou, S. D.; Harrison, A.; Robertson, N.; Kyritsis, P.; Neese, F. *Inorg. Chem.* **2010**, *49*, 5079.
- (33) Breitenfield, J.; Ruiz, J.; Matthew, D. W.; Hu, X. *J. Am. Chem. Soc.* **2013**, *135*, 12004.
- (34) Jia, M.; Bandini, M. *ACS Catal.* **2015**, *5*, 1638.
- (35) Mancano, G.; Page, M. J.; Bhadbhade, M.; Messerle, B. A. *Inorg. Chem.* **2014**, *53*, 10159.
- (36) Suezawa, H.; Ishihara, S.; Umezawa, Y.; Tsuboyama, S.; Nishio, M. *Eur. J. Org. Chem.* **2004**, *2004*, 4816.
- (37) Semeril, D. *J. Mol. Catal. A: Chem.* **2005**, *239*, 257.
- (38) Zhang, K.; Sheridan, M. C.; Cooke, S.; Louie, J. *Organometallics* **2011**, *30*, 2546.



---

Chapter 4. Gold(I) and Gold(III) complexes of  
hemilabile pincer ligands for catalysed activation  
of alkynes

---

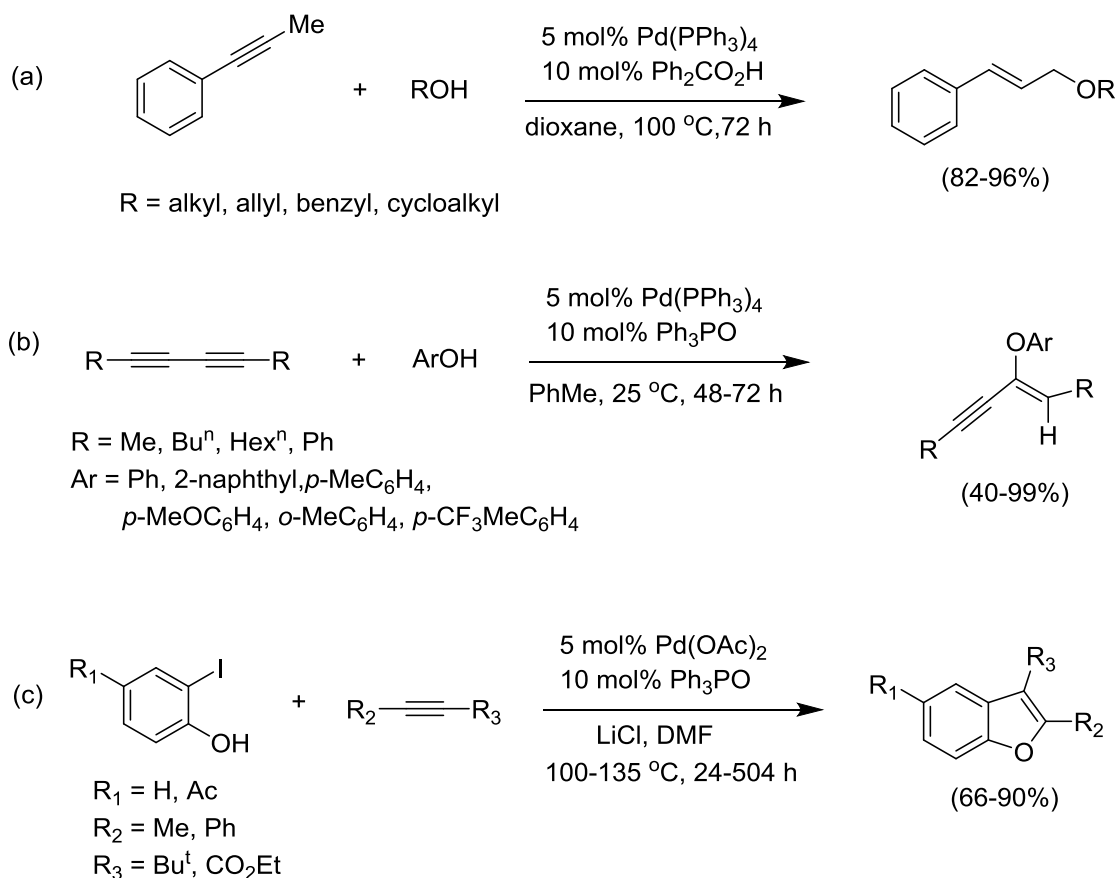
## 4.1. Introduction

### 4.1.1. Transition metal catalysed addition of X-H bonds to alkynes

The addition of X-H bonds to an alkyne functional group, where X= O, N, Si, B, or P, has proven to be important in the field of chemistry,<sup>1, 2, 3</sup> as it is an efficient and atom economical method for the synthesis of X-C bonds resulting in little to no production of wasteful by-products when compared to traditional synthetic/retrosynthetic methods.<sup>1</sup> The production of many organic compounds vital to the pharmaceutical industry often relies on the economic hydroelementation reaction as a key step in the synthetic process.<sup>4, 5</sup> Transition metal complexes have proven to be the ideal choice as catalysts for the addition reactions of X-H bonds to alkynes in comparison to main group elements, due to increased product selectivity.<sup>2</sup> The efficacy of the complexes as catalysts for the hydroalkoxylation (X = O) and hydroamination (X = N) reactions is described below.

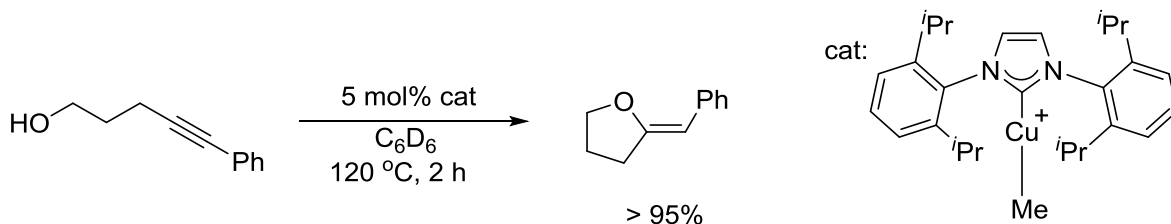
#### 4.1.1.1. Transition metal catalysed hydroalkoxylation reactions

A large number of transition metal complexes have been used for the addition of O-H bonds to alkynes (hydroalkoxylation reaction), which include Rh(I), Ir(I), Ag(I), Hg(I), Au(I), Au(III) and Pd(II).<sup>1</sup> Up to 2004, Pd(II) complexes were the preferred choice for this type of organic transformation. A selection of hydroalkoxylation reactions catalysed by Pd(II) are shown in Scheme 4.1.<sup>6, 7, 8</sup>



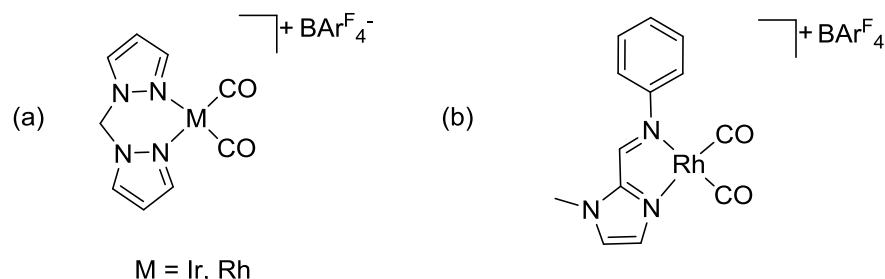
**Scheme 4.1** Examples of Pd(II) catalysed hydroalkoxylation reactions. (a) aromatic alkynes,<sup>6</sup> (b) aromatic and alkyl substituted alkynes,<sup>7</sup> (c) disubstituted aromatic alcohols.<sup>8</sup>

Other metal complexes have since been synthesised with the aims of achieving higher turnover number (TON) and turnover frequency (TOF) for the hydroalkoxylation reaction. Recently, a copper(I) NHC complex was found to be an active catalyst for the intramolecular hydroalkoxylation reaction of alkynyl alcohols, achieving near complete conversions within two hours (Scheme 4.2).<sup>9</sup>

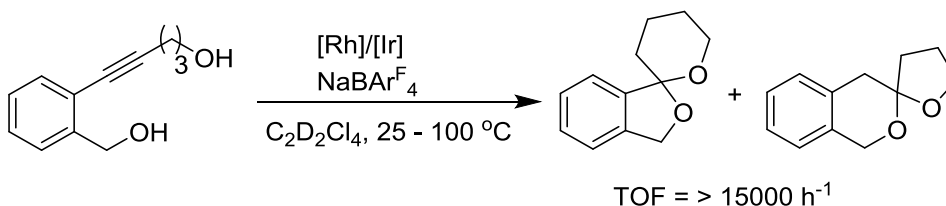


**Scheme 4.2** Cu(I) catalysed intramolecular hydroamination of alkynyl alcohols.<sup>9</sup>

Messerle *et al.* have extensively investigated the hydroalkoxylation reaction using Rh(I) and Ir(I) complexes (Scheme 4.3), in particular, the intramolecular dihydroalkoxylation reaction of alkyne diols (Scheme 4.4).<sup>10</sup> The complexes containing carbonyl co-ligands,  $[M(bpm)(CO)_2]BARF_4^-$  (M = Rh, Ir) were highly efficient catalysts for this double cyclisation reaction.<sup>10</sup>



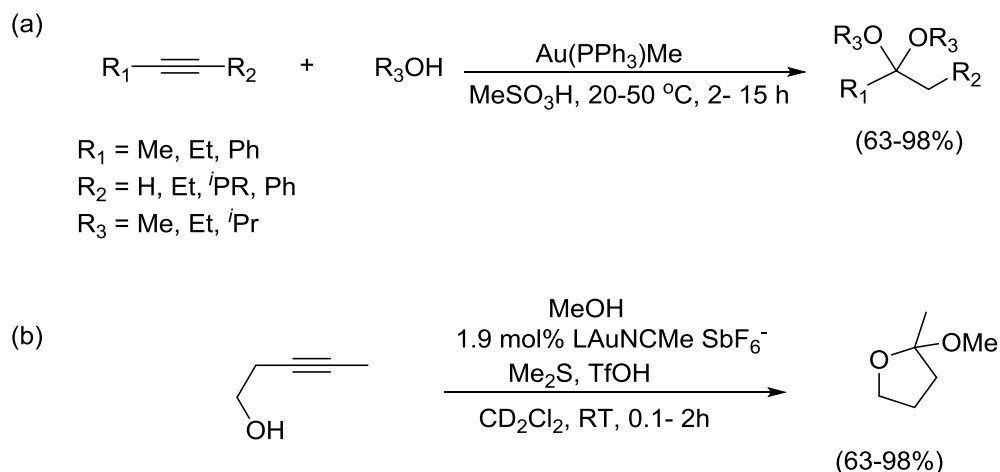
**Scheme 4.3** Rh(I) and (Ir) catalysts synthesised in the Messerle group for the dihydroalkoxylation reaction.<sup>10</sup>



**Scheme 4.4** Catalysed dihydroalkoxylation of alkyne diols.

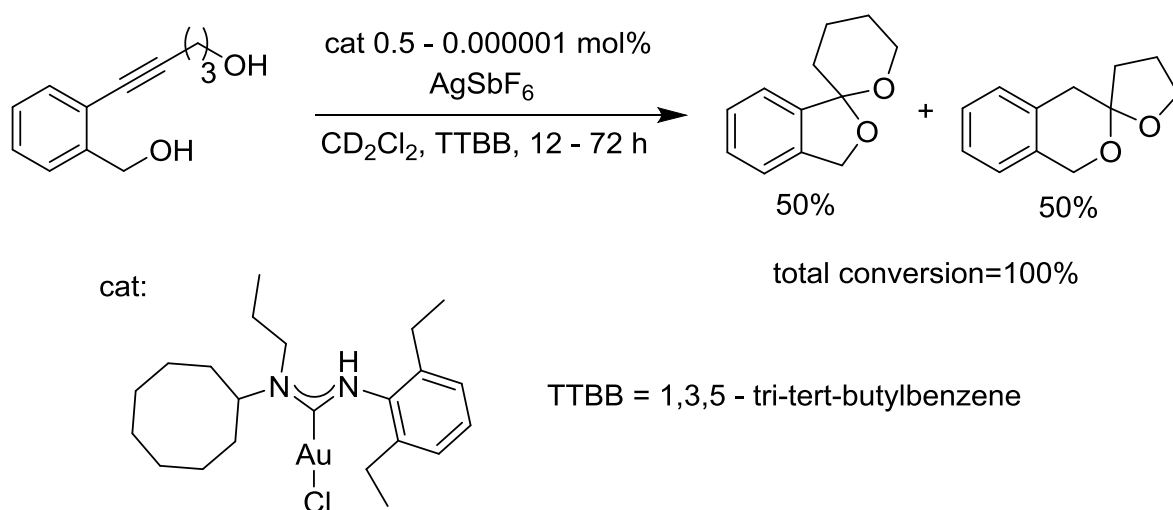
Gold complexes have received significant attention as catalysts for the activation of alkynes, including hydroalkoxylation reactions,<sup>11</sup> due to the ability of the complexes to achieve high catalytic conversions at very low catalyst loadings without being air or moisture sensitive. Teles *et al.* have reported the use of an *in situ* generated Au(I) complex from Au(PPh<sub>3</sub>)Me and methanesulfonic acid, which achieved TON values up to 10<sup>5</sup> and TOF of 5400 h<sup>-1</sup> for the intermolecular dihydroalkoxylation reaction of asymmetric alkynes (Scheme 4.5a).<sup>12a, 12b</sup> Gold complexes are also able to achieve complete conversions for the hydroalkoxylation reaction at ambient conditions within short reaction times. For example,

a gold complex containing an acetonitrile co-ligand for selected intramolecular hydroalkoxylation reactions within 12 minutes (Scheme 4.5b)<sup>12c</sup>



**Scheme 4.5** (a) Intermolecular hydroalkoxylation catalysed by Au(PPh<sub>3</sub>)Me. (b) Intramolecular hydroalkoxylation catalysed by LAuNCMe.

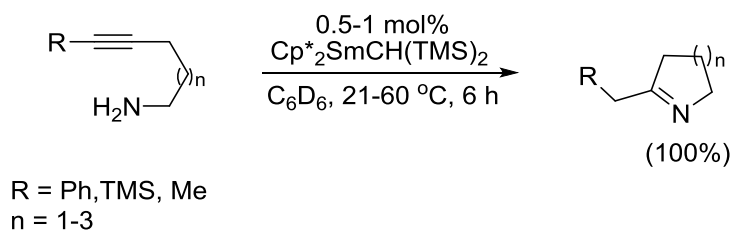
Gold complexes that are stabilised by strong donors have proven to be highly stable over longer periods of time, achieving unmatched catalytic TON (turnover numbers) values for the hydroalkoxylation reactions. Hashmi *et al.* have recently reported the use of a Au(I)-carbene complex which achieved a TON value of 970 000 for the dihydroalkoxylation reaction of alkyne diols when used as a homogeneous catalyst. Remarkably, the complex when attached to a silica based support achieved over 32 000 000 TON for the organic transformation (Scheme 4.6).<sup>11a</sup>



**Scheme 4.6** Au(I) catalysed intramolecular dihydroalkoxylation of alkyne diols.

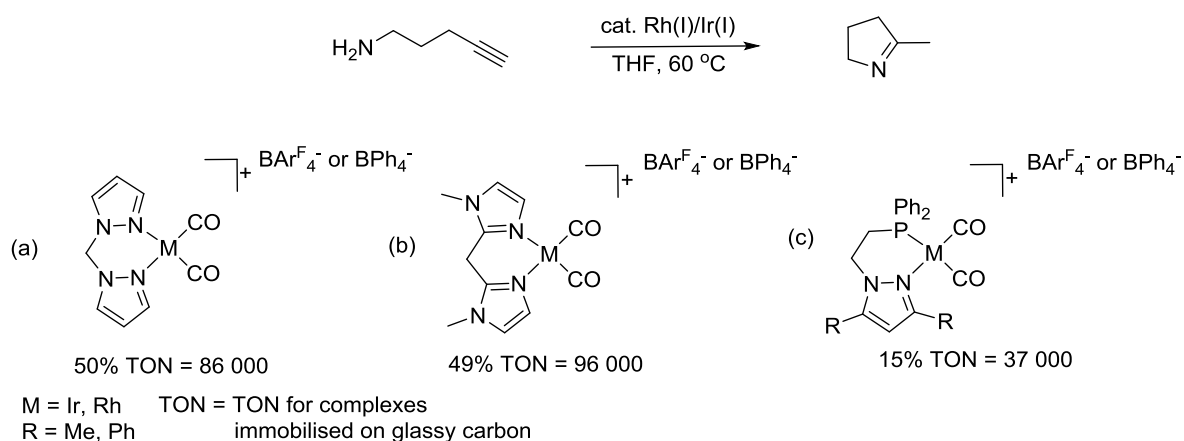
#### 4.1.1.2. Transition metal catalysed hydroamination reactions

Early examples of hydroamination reactions, the addition of an N-H bond across unsaturated C-C bonds, involved the use of lanthanide and actinide complexes.<sup>2</sup> A lanthanide complex, Cp<sub>2</sub>SmCH(TMS)<sub>2</sub> kept under rigorously inert conditions (moisture and oxygen free) was shown to be a highly active catalyst for the intramolecular hydroamination reaction of a series of aminoalkynes achieving TOF values up to 7600 h<sup>-1</sup>.<sup>13</sup>



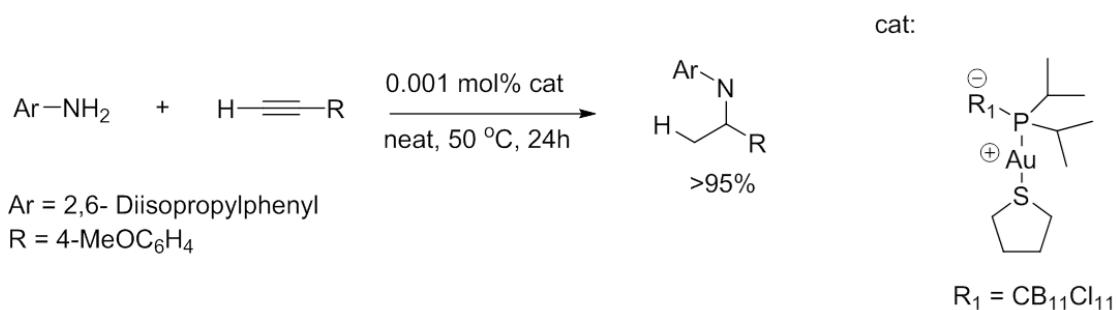
**Scheme 4.7** Samarium catalyst for the intramolecular hydroamination of aminoalkynes.<sup>13</sup>

Recently reported catalysts that are highly active for the hydroamination reaction include Rh(I) and Ir(I) complexes containing *NN* and *NP* bidentate ligands (Scheme 4.8).<sup>14</sup> Messerle *et al.* have synthesised a number of Rh(I) and Ir(I) catalysts,<sup>10, 14</sup> some of which achieved TON up to 96 000 for the intramolecular hydroamination of 4-pentyn-1-amine.<sup>14a</sup>



**Scheme 4.8** Rh(I) and Ir(I) catalysts for the hydroamination reaction of 4-pentyn-1-amine.<sup>14</sup>

The high TON values achieved by using the Rh(I) catalysts require a heterogeneous system. Simple homogeneous gold complexes catalyse hydroamination reactions at low catalyst loadings under mild conditions. Lavallo *et al.* have demonstrated the high efficiency of a boron cluster containing a zwitterionic gold complex and a phosphine donor group (Scheme 4.9). This catalyst has the highest reported TON value (95 000) for the intermolecular hydroamination reaction.<sup>15</sup>



**Scheme 4.9** Highly active Au(I) catalyst for the intermolecular hydroamination reaction.

#### 4.1.2. Transition metal complexes containing pincer ligands for catalysed addition of X-H bonds to alkynes

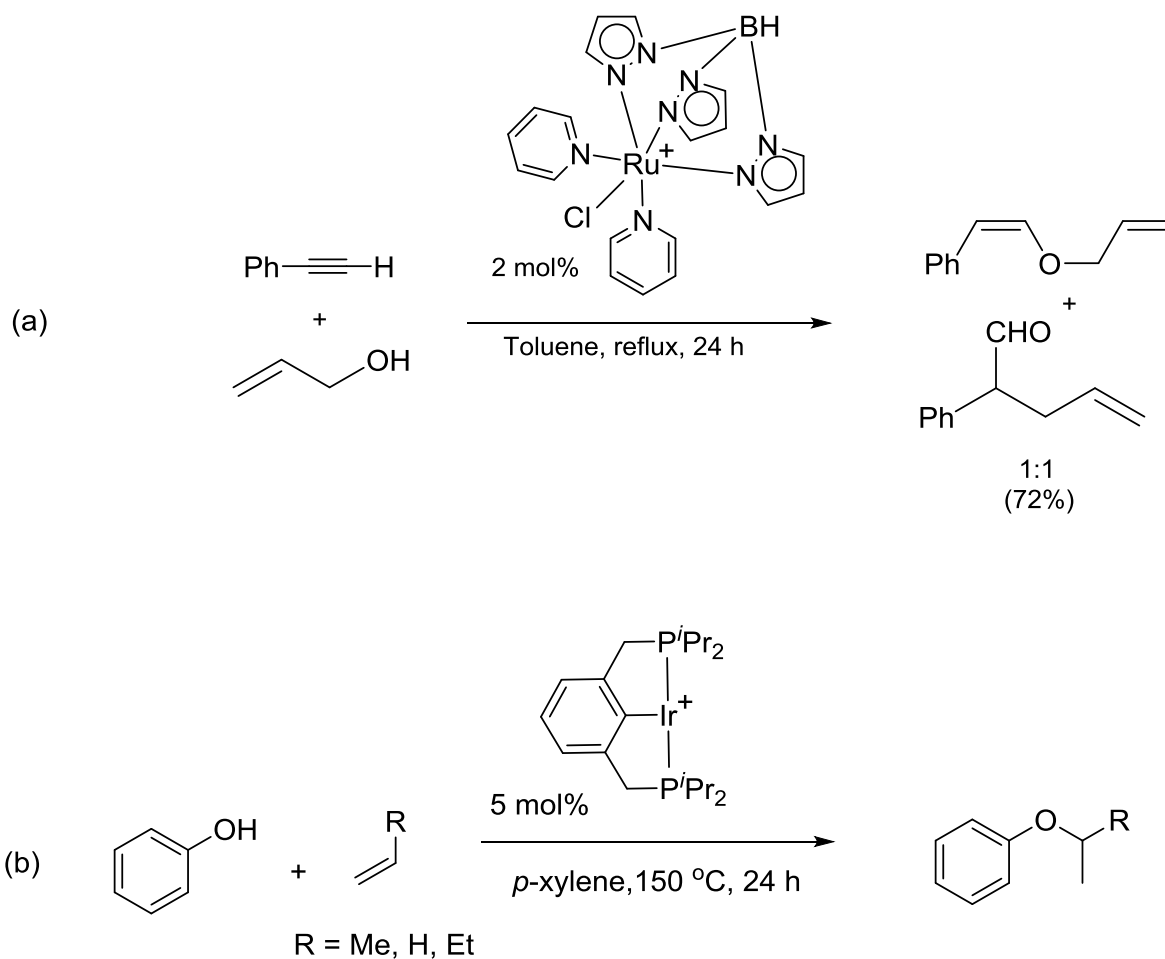
Transition metal complexes containing monodentate and bidentate ligands can be effective catalysts for X-H addition to alkynes for selected substrates as described above. However,

monodentate and bidentate complexes can suffer from reduced catalytic and thermal stability resulting in reduced activity due to decomposition of the catalysts. Transition metal complexes bearing pincer ligands tend to have increased catalytic and thermal stability owing to the  $\kappa^3$  co-ordination of the ligands allowing successful catalytic conversions even at elevated temperatures.<sup>16</sup>

#### 4.1.2.1. Transition metal complexes containing pincer ligands as catalysts for hydroalkoxylation reactions

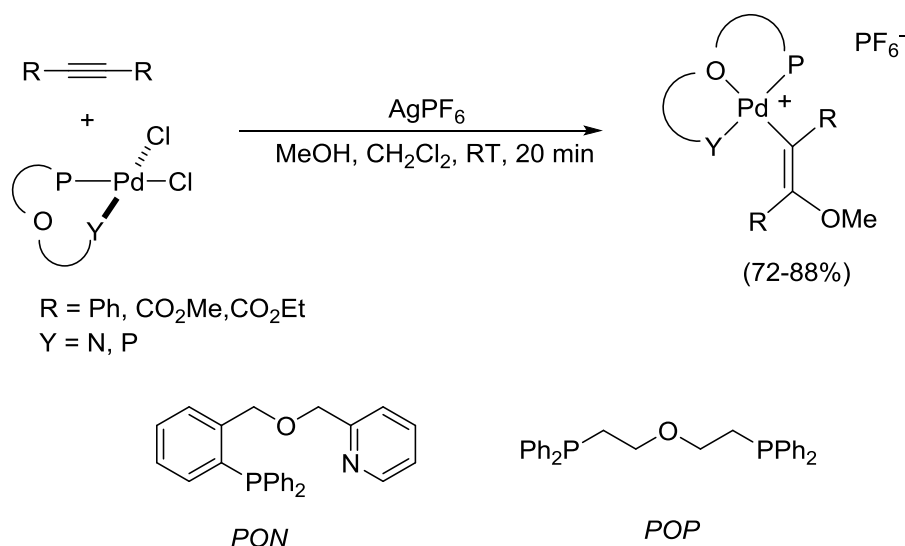
A Ru(II) complex synthesised by Kirchner *et al.* containing tridentate co-ordination of a *tris*(pyrazolyl) borate ligand to the metal centre was the first reported case for the intermolecular addition of allyl alcohols to acetylenes by ruthenium. The complex maintains stability at elevated temperatures (110 °C) over an extended period of time (24 hours), achieving a consistent ratio of 1:1 of the *cis*-allyl vinyl ether and the aldehyde shown in Scheme 4.10a.<sup>17a</sup> A significant number of pincer complexes with different metals has since been investigated as catalysts for hydroalkoxylation reactions. Goldman *et al* has recently reported the catalytic activity an iridium complex bearing a *PCP* pincer ligand for the hydroaryloxylation reaction of olefins (Scheme 4.10b).<sup>17b</sup>





**Scheme 4.10** (a) First example of a Ru(II) catalysed intermolecular addition of allyl alcohols to acetylenes. (b) An iridium complex bearing a *PCP* pincer ligand for the hydroaryloxylation reaction of olefins<sup>17</sup>

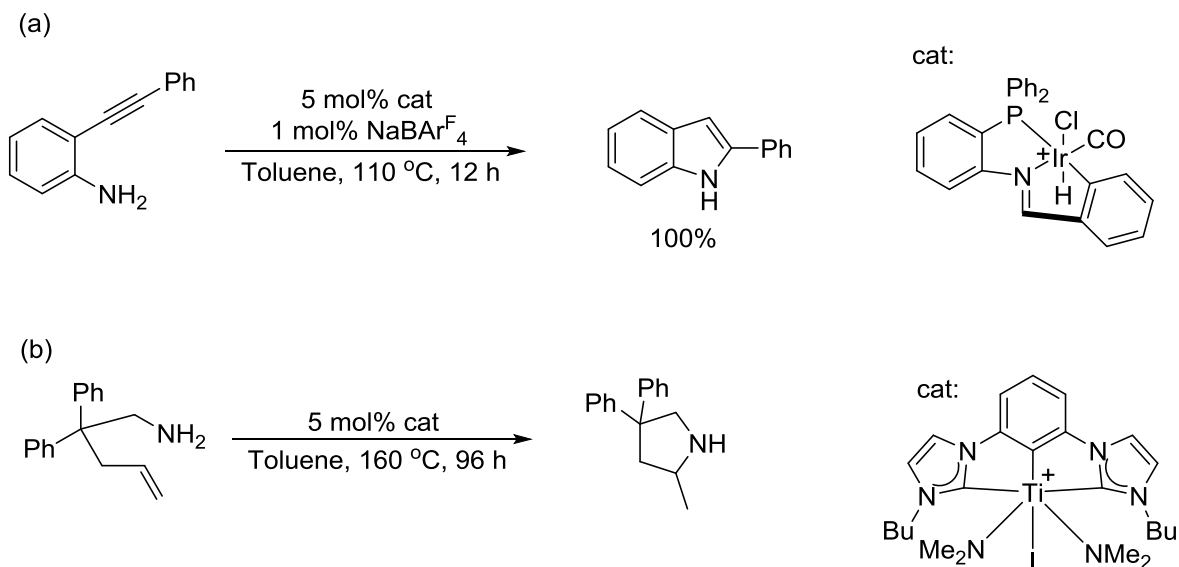
Mechanistic investigations using palladium complexes containing *PON* and *POP* tridentate ligands have provided vital information on the reaction pathway of the stereoselective addition of methanol to activated acetylenes.<sup>18</sup> This was made possible by isolating key Pd(II) intermediates in the reaction, which were stabilised by the  $\kappa^3$  chelate effect of the pincer ligands (Scheme 4.11).



**Scheme 4.11** Key  $Pd(II)$  intermediate stabilised by the tridentate coordination of *PON* or *POP* pincer ligands.<sup>18</sup>

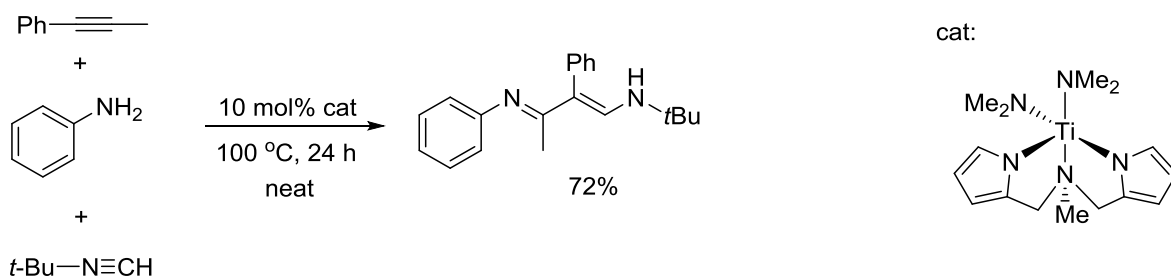
#### 4.1.2.2. Transition metal catalysts containing pincer ligands for hydroamination reactions

Transition metal complexes with pincer ligands have also been utilised as catalysts for the hydroamination reaction.<sup>19</sup> For example, an  $Ir(III)$  complex bearing a *PNC* pincer ligand proved to be an effective catalyst for the intramolecular hydroamination of 2-alkynylanilines to produce indoles (Scheme 4.12a). The catalyst achieved complete conversion of substrates, avoiding thermal decomposition at high temperatures (110 °C) for over 12 hours.<sup>19a</sup> Recent work has also expanded the investigation of complexes containing pincer ligands for the hydroamination reaction to metals such as titanium. As shown in Scheme 4.12b, a titanium complex of a *CCC* pincer ligand achieved high conversions for the intramolecular hydroamination of alkenes.<sup>19b</sup>



**Scheme 4.12** (a) Ir(III) catalyst with a pincer ligand for the hydroamination of 2-alkynylanilines. (b) Ti catalyst with a pincer ligand for the hydroamination of alkenes.<sup>19</sup>

It is difficult to achieve high yields for catalysed three component reactions, and often high temperatures are required to produce successful conversions.<sup>20</sup> A titanium complex containing a tridentate *NNN* pincer ligand achieved good conversions for the three component intermolecular hydroamination of alkynes with aromatic amines and *tert*-butyl isonitrile at temperatures of up to 100 °C, with exclusive selectivity for  $\alpha,\beta$ -unsaturated  $\beta$ -aminoimine (Scheme 4.13).<sup>21</sup>

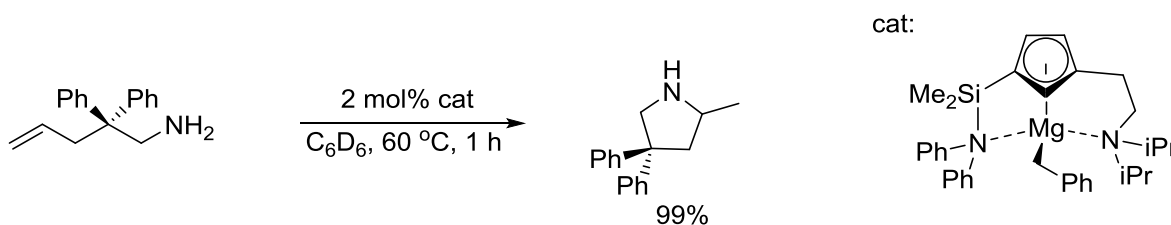


**Scheme 4.13** Ti catalyst used for three component intermolecular hydroamination reactions.<sup>21</sup>

#### 4.1.2.3. Metal complexes containing hemilabile pincer ligands for the addition of X-H bonds to the C-C multiple bond of alkenes or alkynes

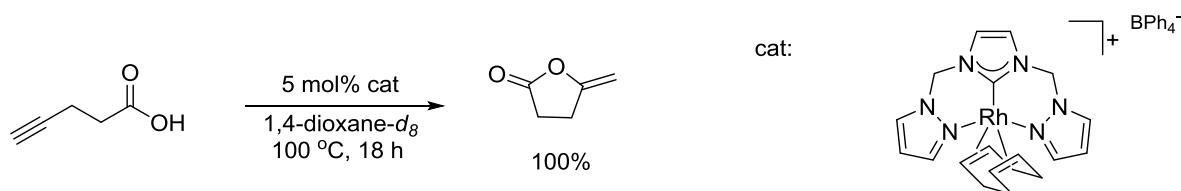
Pincer ligands that contain a combination of strong and weak donor groups (hemilabile ligands) can offer additional advantages in metal catalysis; the strong donors are able to stabilise the complex by forming a robust metal-ligand bonds while weaker donors are able to temporarily dissociate from the metal opening up reactive coordination sites during the catalytic cycle.<sup>22</sup> Therefore hemilabile pincer complexes are able to maintain catalytic and thermal stability without sacrificing high reactivity.

A hemilabile magnesium complex containing *NN* pendant donor arms and a strongly coordinating central aryl group was found to be a highly active catalyst for the intramolecular hydroamination of aminoalkenes.<sup>23</sup> The catalyst achieves complete conversion for the organic transformation within one hour (Scheme 4.14).



**Scheme 4.14** Hemilabile magnesium pincer catalyst for the hydroamination of aminoalkenes.

Messlerle *et al.* have recently synthesised Rh(I) and Ir(I) complexes containing the hemilabile pincer ligand **1** as presented in Chapter 2.<sup>24</sup> The Rh(I) complex bearing the pincer ligand **1** and a COD co-ligand achieved complete conversion for the hydroalkoxylation reaction of 4-pentynoic acid to  $\gamma$ -methylene- $\gamma$ -butyrolactone (Scheme 4.15). The catalyst remained active at elevated temperatures over an extended period of time.



**Scheme 4.15** Rh(I) catalyst containing the hemilabile pincer ligand **1** for the hydroalkoxylation of 4-pentynoic acid.

#### 4.2. Aims of this chapter

The work presented in this chapter focuses on pincer ligands containing a central *N*-heterocyclic carbene donor and labile pyrazole pendant donors. Gold complexes have proven to be highly active catalysts for a range of organic transformations, however, tend to lack thermal stability. The coordination of a gold centre to hemilabile pincer ligands should provide an advantageous combination of stable and highly active catalysts for hydroalkoxylation and hydroamination reactions.

The aim of this chapter was to investigate the synthesis and co-ordination chemistry of novel gold complexes containing an hemilabile  $NCN^{Me}$  pincer ligands, and their activity as catalysts for the dihydroalkoxylation and hydroamination reactions. The specific goals were to:

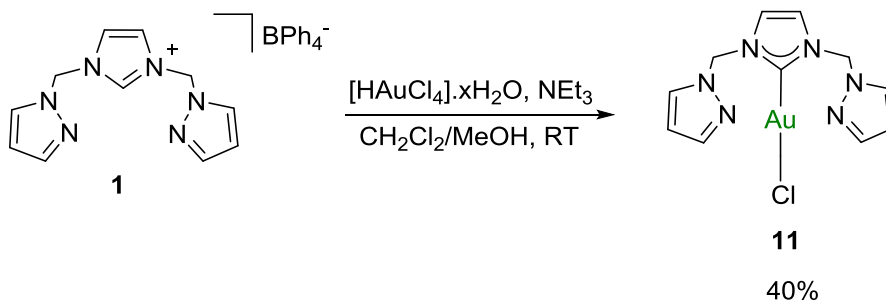
- Synthesise gold complexes containing oxidation states +I or +III using different reagents and deprotonation methods.
- Characterise and investigate coordination chemistry of these novel gold complexes using NMR spectroscopy, mass spectrometry, elemental analysis and X-ray crystallography.

- Investigate dihydroalkoxylation reactions of alkyne diols catalysed by the novel Au(I) and Au(III) complexes containing pincer ligands.
- Test the Au(I) and Au(III) complexes as catalysts for intramolecular and intermolecular hydroamination reactions.

### 4.3. Synthesis of Gold(I) and Gold(III) complexes containing an $NCN^{Me}$ hemilabile pincer ligand

#### 4.3.1. Synthesis and characterisation of $[Au(I)(NCN^{Me})Cl]BPh_4$ (**11**)

There is literature precedence for the synthesis of Au(I) carbene complexes using mild bases, such as carbonates as deprotonating agents.<sup>25</sup> Therefore, initial attempts to synthesise the Au(I) complex of ligand **1** were carried out by reacting  $Au(I)(SMe_2)Cl$  with the  $NCN^{Me}$  ligand **1** using  $NaHCO_3$  and  $K_2CO_3$  as the deprotonating agents. However, these reactions resulted in no formation of **1** leaving an unreacted mixture of reactants. It was likely that the carbonates were not sufficiently basic to deprotonate the imidazolium proton of the ligand. Triethylamine was therefore employed as an alternative deprotonating agent. Complex **11** was successfully prepared by stirring a suspension of chloroauric acid in the presence of excess triethylamine, dichloromethane, methanol and ligand **1** at room temperature for 16 hours (Scheme 4.16). The resulting reduced gold(I) complex was isolated as a grey solid. The complex can also be synthesised using a silver transmetallation route, by reacting  $Au(SMe_2)Cl$  with the silver intermediate **2** (Chapter 2) in dichloromethane. Interestingly, the yield of the desired Au(I) complex *via* the silver transmetallation route was significantly reduced compared to the earlier carbene deprotonation route. Further details are provided in the experimental section, Chapter 6.



Scheme 4.16 Synthesis of  $[Au(I)(NCN^{Me})Cl]$  (**11**).

The  $^1\text{H}$  NMR spectrum of complex **11** exhibited five resonances indicating a symmetric environment in the gold complex. All five resonances were attributed to the ligand protons. The absence of  $\text{BPh}_4^-$  proton resonances suggested that the resulting Au(I) complex was neutral in character with a terminally bound Cl to balance the +1 charge. The structure containing monodentate coordination of the *NCN* pincer ligand, and exhibiting a linear geometry typical of Au(I) complexes was confirmed using X-ray crystal structure analysis (Figure 4.1). Mass spectrometry provided further evidence of the linear conformation of the Au(I) metal centre with a single ligand showing a dominant signal at 425.0778  $m/z$ , which is attributed to the loss of the terminally bound Cl co-ligand.

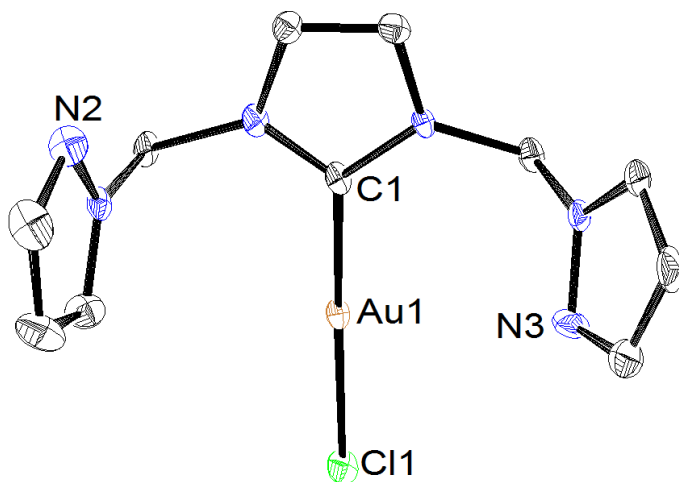


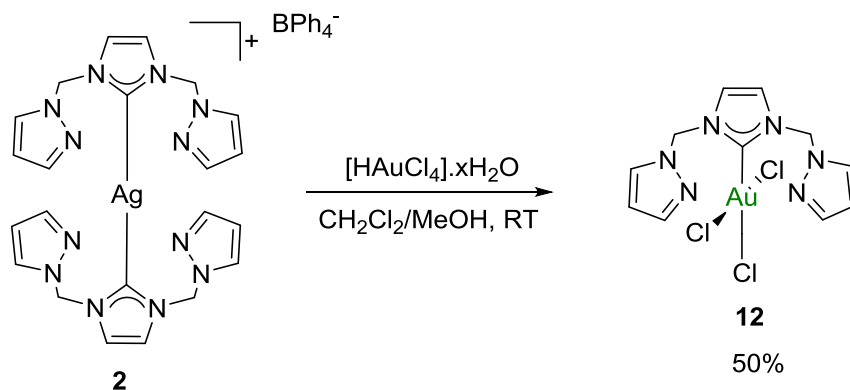
**Figure 4.1** ORTEP depiction of the solid state structure of complex **11** at 50% probability thermal ellipsoids. Hydrogen atoms have been omitted for clarity.

#### 4.3.2. Synthesis and characterisation of $[\text{Au(III)}(\text{NCN}^{\text{Me}})\text{Cl}]\text{BPh}_4$ (**12**)

Few Au(III) carbene complexes have been reported in the literature and most of those reported have been synthesised using a mercury or silver transmetallation route under mild conditions.<sup>26</sup> This method was therefore employed for the synthesis of the Au(III)



complex of ligand **1**. The Au(III) compound was prepared by transmetallation of the ligand to Au(III) from the silver intermediate  $[\text{Ag(I)}(\text{NCN}^{\text{Me}})_2]\text{BPh}_4$  (**2**) using chloroauric acid in dichloromethane (Scheme 4.17). Stirring the reaction mixture at room temperature followed by addition of pentane resulted in the isolation of  $[\text{Au(III)}(\text{NCN}^{\text{Me}})\text{Cl}]\text{BPh}_4$  (**12**) as a yellow solid.



**Scheme 4.17** Synthesis of  $[\text{Au(III)}(\text{NCN}^{\text{Me}})\text{Cl}]$  (**12**)

Similar to the  $^1\text{H}$ NMR spectrum of Au(I) complex **11**, the  $^1\text{H}$  NMR of  $[\text{Au(III)}(\text{NCN}^{\text{Me}})\text{Cl}]$  (**12**) shows that the complex is symmetric with a line of symmetry along the carbene-gold-chloride axis. Only five resonances were observed in the spectrum which were all attributed to the ligand protons. As observed for complex **11**, the absence of resonances due to protons of  $\text{BPh}_4^-$  suggested the loss of the counterion and that the 3+ charge of the Au(III) compound was balanced by three terminally bound Cl atoms. X-ray analysis of a single crystal of **12** (Figure 4.2) confirmed the expected square planar geometry of the Au(III) complex with a monodentate co-ordination of the  $\text{NCN}^{\text{Me}}$  ligand to the Au(III) metal centre *via* the carbene donor. Mass spectrometry of the isolated yellow solid revealed the presence of a dominant signal at 495.0155 m/z which was assigned to the loss of one terminally bound Cl co-ligand.

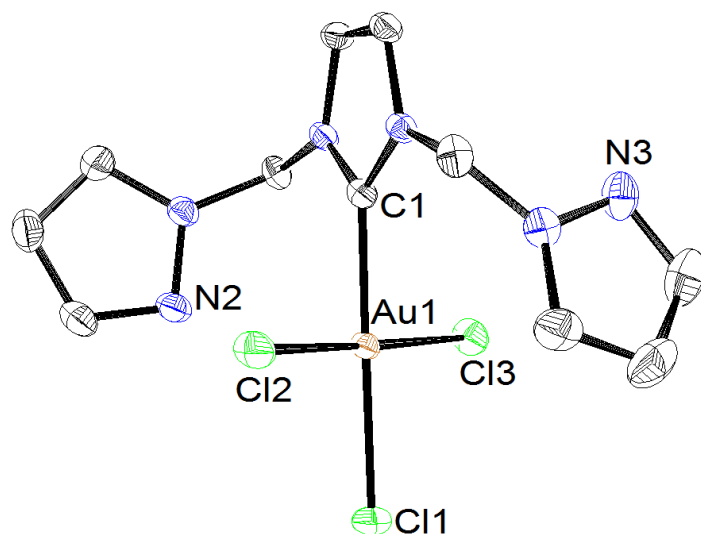


**Figure 4.2** ORTEP depiction of the solid state structure of complex **12** at 50% probability thermal ellipsoids. Hydrogen atoms have been omitted for clarity.

#### 4.3.3. Comparison of the solid state structures of **11** and **12**

The Au(I) complex **11** and Au(III) complex **12** both have similar planar structures. However, the metal centres Au(I) and Au(III) are linear and square planar respectively, see Figure 4.1 and Figure 4.2, and the Au(III) complex contains two extra Cl co-ligands. In both structures the gold ions are coordinated to the carbon atom on the NHC unit and the (C2-C3)<sub>centroid</sub>-C1-Au angle is close to linear. The slight elongation of the gold-carbene bond length in complex **12** compared to that of complex **11**, is attributed to the square planar geometry of complex **12** with combined *cis* effects from the two additional Cl atoms. The pendant pyrazole donors remain uncoordinated to both Au(I) and Au(III) centres in both **11** and **12**, N-Au distances are greater than 3.1 Å, though in the Au(III) example the N-atom from the pyrazole would be available for hemilabile binding upon displacement of a chloride ion by a suitable counterion such as NaBAR<sup>F</sup><sub>4</sub>.

Atoms	<b>11</b>	<b>12</b>
Au(1)-C(1)	1.973(5)	2.007(2)
Au(1)-Cl(1)	2.285(1)	2.3116(8)
Au(1)-Cl(2)	-----	2.2807(7)
Au(1)-Cl(3)	-----	2.2780(7)
C(1)-Au(1)-Cl(2)	-----	89.37(6)
C(1)-Au(1)-Cl(3)	-----	89.02(6)
C(2)-C(3) <sub>centroid</sub> -C(1)-Au(1)	175.57(6)	178.71(6)

**Table 4.1** Selected bond lengths(Å) and angles(°) for **11**, and **12**.

Both pendant pyrazole arms are not coplanar with the central imidazole. For complex **11** a cavity bearing an N...N distance of 6.626 Å was observed. This has the potential to coordinate a second metal center to form a bimetallic complex containing a shared ligand moiety (Figure 4.3).

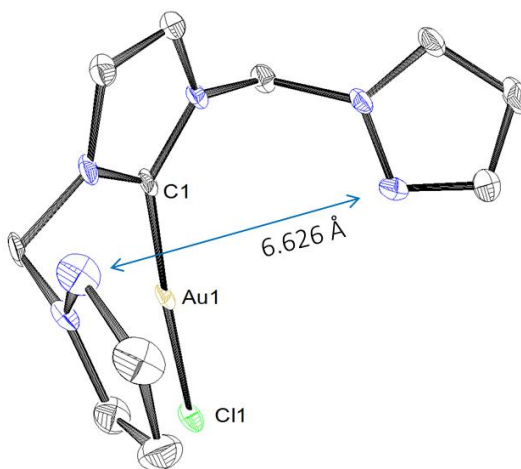
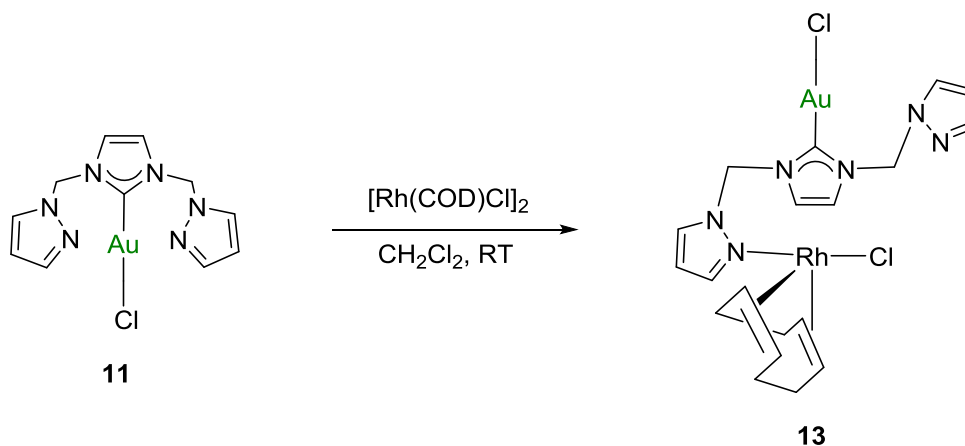


**Figure 4.3** ORTEP depiction of complex **11** showing the distance between pyrazole nitrogens.

## 4.3.4. Attempted synthesis of Au(I)/Rh(I) bimetallic complexes

As the X-ray analysis of the structure of complex **11** revealed a close proximity of the two pendent pyrazole arms, the distance between the pyrazoles provided an ideal "pocket" for an additional and different metal such as Rh(I) (Scheme 4.18).

Bimetallic complexes have been shown to enhance the catalytic activity for a number of organic transformations.<sup>10b,27</sup> Heteronuclear bimetallic complexes can also promote tandem catalytic reactions where the different metals can catalyse the different individual reaction steps respectively in a multi-step reaction.<sup>28</sup> Therefore, an attempt was made to synthesise an Au(I)/Rh(I) bimetallic complex. Complex **11** was mixed with a half molar equivalent of  $[\text{Rh}(\text{COD})\text{Cl}]_2$  in dichloromethane. Addition of pentane resulted in the isolation of complex **13** as a yellow solid. ( $^1\text{H}$  NMR of **11** shown in Figure 4.4 for comparison to **13** in Figure 4.5)



**Scheme 4.18** Synthesis of a heterobimetallic Au(I)/Rh(I) complex (**13**).

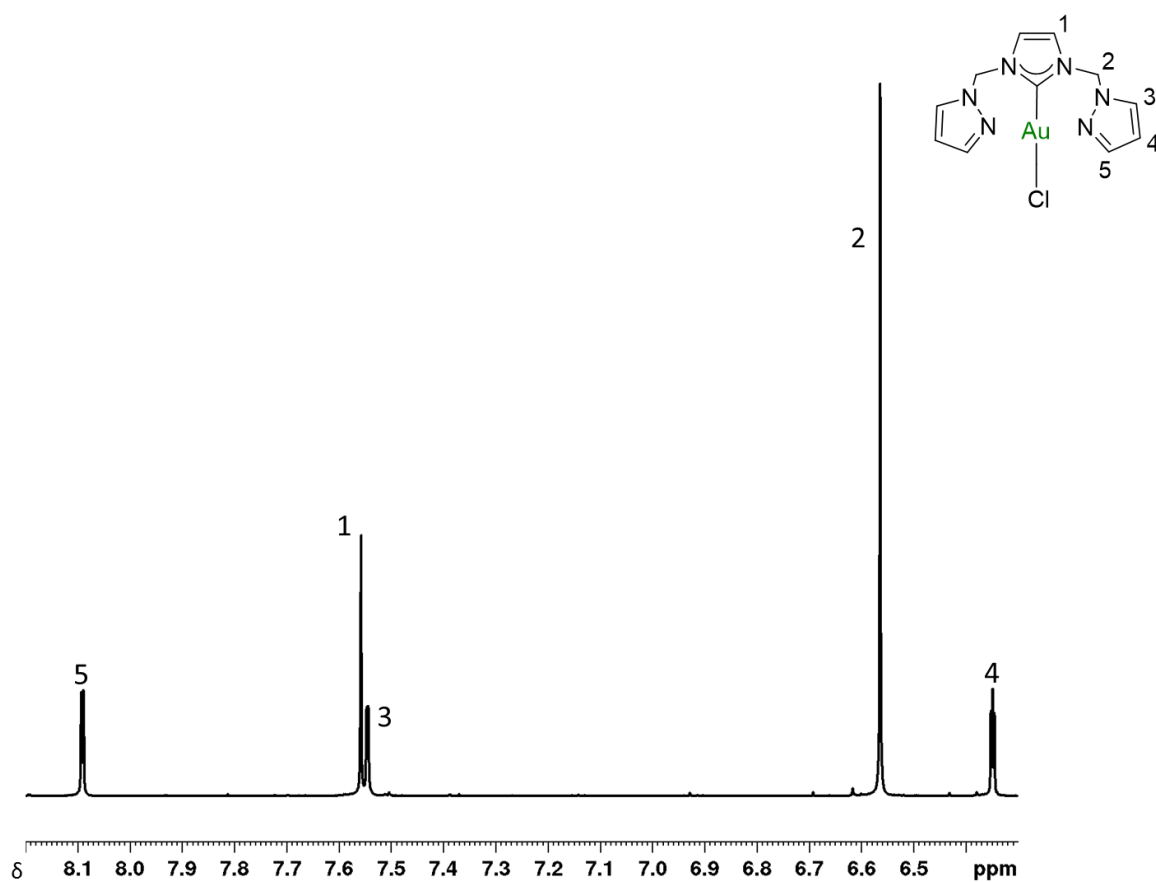
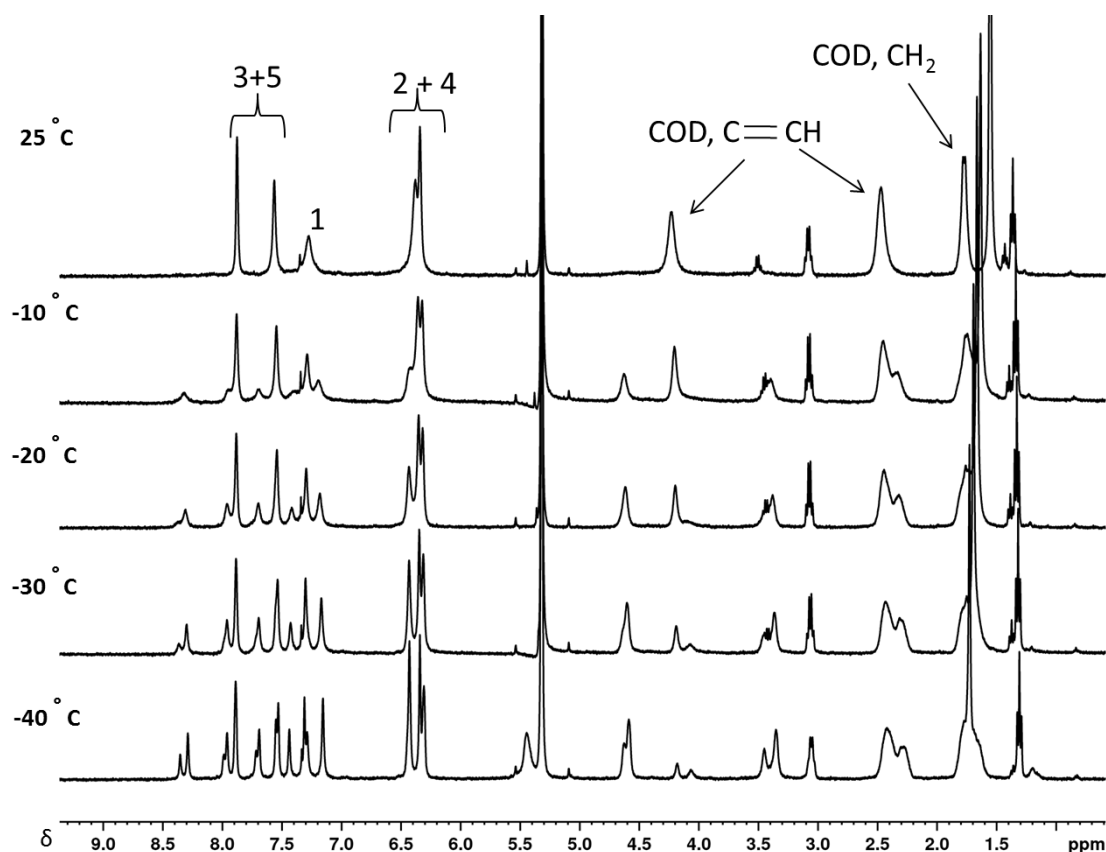


Figure 4.4  $^1\text{H}$  NMR (600 MHz,  $\text{acetone-d}_6$ ) of complex 11.



**Figure 4.5** Variable temperature  $^1\text{H}$  NMR (400MHz, acetone- $\text{d}_6$ ) of heterobimetallic complex **13**.

The  $^1\text{H}$  NMR spectrum of the complex **13** at room temperature exhibited five broad resonances that were unresolved. The broadening of the signals was attributed to fluctuonality of the  $\text{NCN}^{\text{Me}}$  ligand **1** on the NMR time scale. Analysis of the sample using variable temperature  $^1\text{H}$  NMR revealed the presence of 12 resonances between 6 and 9 ppm (Figure 4.5) which were attributed to protons on the ligand and counter ion. The asymmetry revealed by the  $^1\text{H}$  NMR suggested successful coordination of the pyrazolyl donors of the  $\text{NCN}^{\text{Me}}$  ligand to the Rh(I) metal centre. However, further characterisation proved to be difficult due to the decomposition of the complex over time even at reduced temperatures and under inert conditions.

Decomposition of the heterobimetallic complex may occur *via* dissociation of labile pyrazole nitrogen ligand donors from the rhodium. To alleviate the problem, the complex **13** was treated with abstracting agents such as NaBPh<sub>4</sub> and NaBAR<sup>F</sup><sub>4</sub> in a DCM solution, which can promote removal of a terminally bound chloride from either the Au(I) or Rh(I) centres promoting coordination of the free pyrazole pendant arm. This bidentate coordination of the ligand to the Au(I) or Rh(I) centre should significantly reduce the rate of dissociation by increasing the chelate effect of the complex. However, analysis of the reaction of **13** with NaBAR<sup>F</sup><sub>4</sub> and NaBPh<sub>4</sub> by <sup>1</sup>H NMR spectroscopy indicated the formation of an intractable mix of products. It is likely that the Cl co-ligand on the Au(I) metal can undergo abstraction, which could result in decomposition of complex **13**.

#### 4.4. Catalysed hydroalkoxylation reactions using complexes **11** and **12**.

Au(I) and Au(III) complexes have proven to be excellent catalysts for the activation of alkynes.<sup>11, 29</sup> Therefore, [Au(I)(NCN<sup>Me</sup>)Cl] (**11**) and [Au(III)(NCN<sup>Me</sup>)Cl] (**12**) were tested as catalysts for the dihydroalkoxylation reaction of the alkyne diols **14**, **15** and **16**. The reactions were carried out in C<sub>2</sub>D<sub>2</sub>Cl<sub>4</sub> at various temperatures as stated using a catalyst loading of 1 mol% unless otherwise stated. NaBAR<sup>F</sup><sub>4</sub> was also used as an additive for the catalysis reactions. For further details, refer to the experimental section in Chapter 6.

##### 4.4.1. Catalysed dihydroalkoxylation of 2-(5-hydroxypent-1-ynyl)benzylalcohol (**14**).

Gold complex **11** was an efficient catalyst for the dihydroalkoxylation of 2-(5-hydroxypent-1-ynyl)benzylalcohol **14** (Chart 4.1). On using **11** to promote dihydroalkoxylation of **14**, two isomeric spiroketal products **14a** and **14b** were observed in equivalent proportions. The isomers can be separated using methods such as HPLC, however, this work is focused only

on the catalytic conversion and selectivity of the catalyst. Previous reports have shown that regioselectivity between these two spiroketal isomers is difficult to control.<sup>10,30</sup>

The reaction was first attempted at 100 °C in C<sub>2</sub>D<sub>2</sub>Cl<sub>4</sub> using Au(I) complex **11** with a catalyst loading of 1 mol% to which was added NaBAR<sup>F</sup><sub>4</sub> (1.1 mol%) and alkyne diol **14**. The reaction was monitored at regular intervals using <sup>1</sup>H NMR spectroscopy. Catalytic efficiency was established using the TOF (h<sup>-1</sup>) calculated at the time of 50% conversion of substrate to product, as the amount of product formed per mole of catalyst per hour.

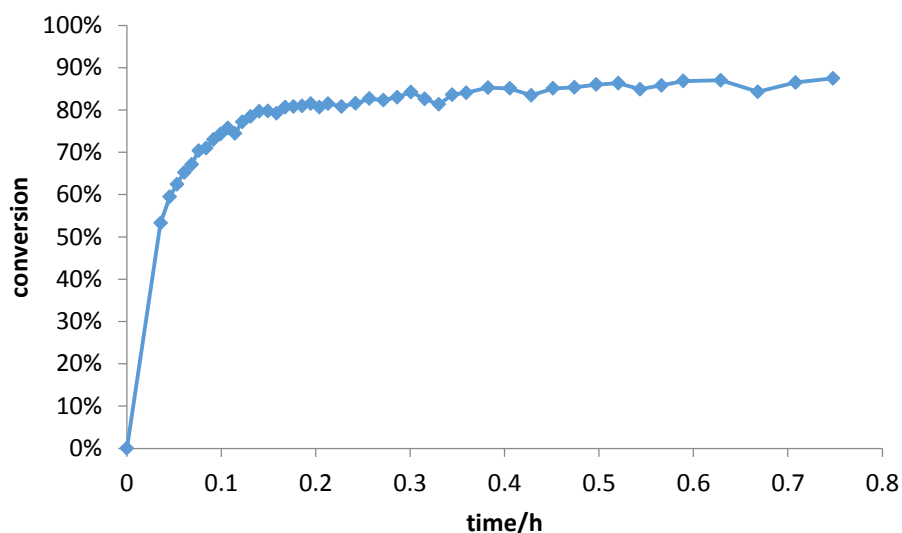
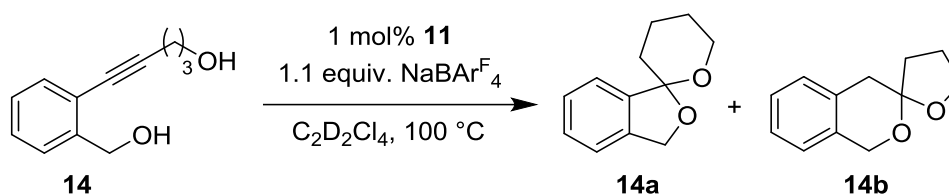


**Chart 4.1** Time course profile for the dihydroalkoxylation of **14** catalysed by **11** at 100 °C (equiv. = equivalent relative to catalyst).

The reaction of **14** catalysed by **11** at 100 °C achieves a high TOF of 1241 h<sup>-1</sup>, however, there was a reduction of the rate of conversion after 0.2 h, with a maximum of 85% conversion reached. This suggested rapid decomposition of the Au(I) catalyst which was in



agreement with the physical observation of the formation of a purple precipitate/mixture indicative of the formation of gold nanoparticles. Navarro *et al.* reported similar findings using UV spectroscopy.<sup>31</sup> Reducing the temperature to 80 °C resulted in complete conversion of the dihydroalkoxylation and the reaction reaches > 98% conversion within two min. Formation of a purple mixture at this temperature was only observed after completion of reaction. Since the catalyst is highly active at 80 °C, monitoring of the organic transformation proved to be difficult and a further reduction in temperature to 70 °C was required to attain reliable kinetic data (Chart 4.2). The Au(I) catalyst **11** promoted full conversion of **14** after 12 min at 70 °C as shown in Chart 4.2.

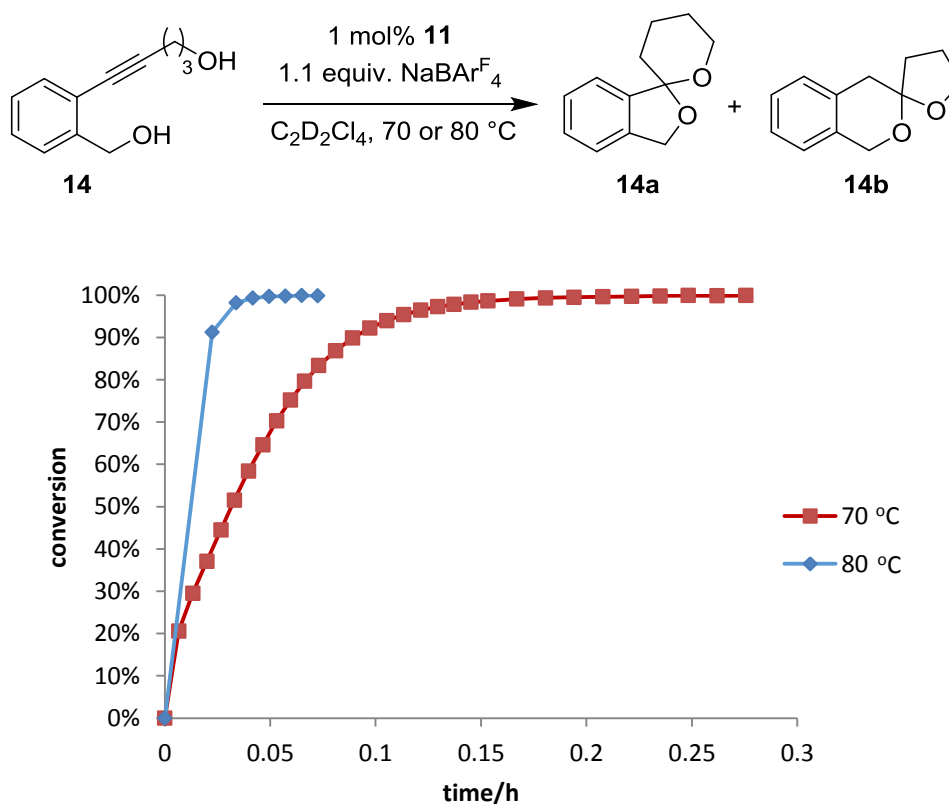


**Chart 4.2** Time course plots for the dihydroalkoxylation reaction of **14** catalysed by **11** at 70 °C and 80 °C. (equiv. = equivalent relative to catalyst).

Au(III) complex **12** was also investigated as a catalyst for the dihydroalkoxylation of alkyne diol **14**. Surprisingly, the Au(III) catalyst reached complete conversion of **14** to **14a** and **14b** by the time the first NMR spectra had been acquired (< 1 min) at 70 °C. Given the excellent activity of **12** at 70 °C, the temperature was lowered to ambient (25 °C) and the reactions repeated. Again the Au(III) complex **12** was found to be a more efficient catalyst than Au(I) complex **11**, with complexes **12** and **11** achieving complete conversion of **14** within 9.3 min and 145 min respectively (Table 4.2, entries 3 and 5, Chart 4.3). These gold(III) catalysed reactions at room temperature are the fastest reported for 2-(5-hydroxypent-1-ynyl)benzyl alcohol (**14**).<sup>10b, 11a,</sup>

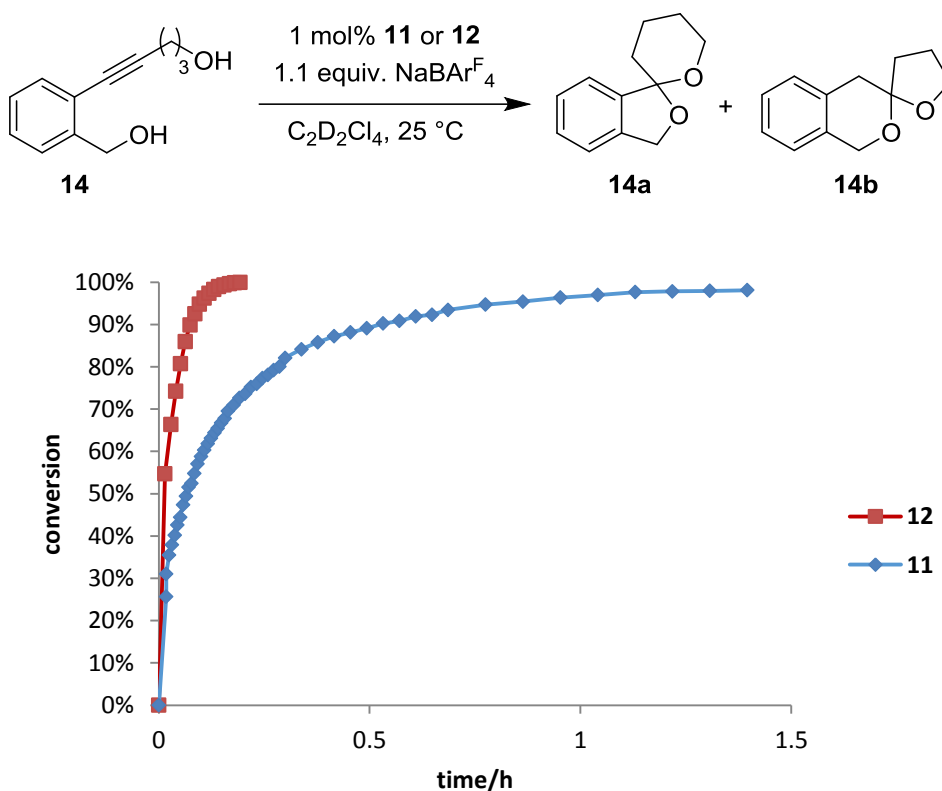
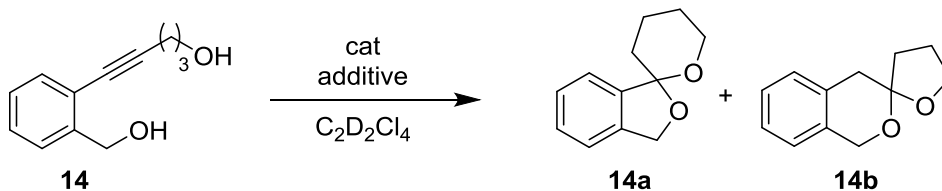


**Chart 4.3** Time course plots for the catalysed dihydroalkoxylation of **14** using **11** and **12** at 25 °C. (equiv. = equivalent relative to catalyst).

**Table 4.2** Comparison of Au(I) vs Au(III) catalysts and the effect of counterion. <sup>a</sup>Determined by <sup>1</sup>H NMR spectroscopy. <sup>b</sup>Conversion refers to substrate to combined spiroketal products a and b. <sup>c</sup> Time taken to reach stated conversion.



entry	catalyst	additive	temp, °C	conv, % <sup>b</sup>	time, min. <sup>c</sup>	TOF, h <sup>-1</sup>	TON
1	<b>11</b> (1 mol%)	NaBAR <sub>4</sub> <sup>F</sup> (1.1 mol%)	70	>99	12	>1600	99
2	<b>12</b> (1 mol%)	NaBAR <sub>4</sub> <sup>F</sup> (1.1 mol%)	70	>99	<1	>15000	99
3	<b>11</b> (1 mol%)	NaBAR <sub>4</sub> <sup>F</sup> (1.1 mol%)	25	97	145	>58	97
4	<b>12</b> (1 mol%)	-	25	98	67.8	>800	98
5	<b>12</b> (1 mol%)	NaBAR <sub>4</sub> <sup>F</sup> (1.1 mol%)	25	>99	9.3	>2100	99
6	<b>12</b> (1 mol%)	NaBAR <sub>4</sub> <sup>F</sup> (2.2 mol%)	25	>99	10.7	>4400	99
7	<b>12</b> (1 mol%)	NaBAR <sub>4</sub> <sup>F</sup> (3.3 mol%)	25	>99	5	>5200	99
8	<b>12</b> (0.1 mol%)	NaBAR <sub>4</sub> <sup>F</sup> (0.11 mol%)	25	30	2.2	-	361
9	<b>12</b> (0.01 mol%)	NaBAR <sub>4</sub> <sup>F</sup> (0.011 mol%)	25	10	3.3	-	1033
10	<b>12</b> (1 mol%)	AgSbF <sub>6</sub> (1.1 mol%)	25	93	39.9	>2000	93
11	<b>12</b> (0.1 mol%)	AgSbF <sub>6</sub> (0.11 mol%)	25	0	-	-	-

#### 4.4.2. Counterion dependence:

The impact of the amount of NaBAR<sub>4</sub><sup>F</sup> on reaction rate was also investigated (Table 4.2, entries 4-7) to establish the effect of displacing the strongly coordinating Cl<sup>-</sup> ions with a weakly coordinating counterion. Messerle *et al.* has shown that NaBAR<sub>4</sub><sup>F</sup> alone will not catalyse the dihydroalkoxylation of **14**.<sup>10b,10c</sup> However, as the amount of added NaBAR<sub>4</sub><sup>F</sup> was increased from 0 to 3.3 mol%, a marked improvement in the turnover rate was observed, Chart 4.4. A two-fold increase in TOF was observed for the reaction conducted using 2.2 mol% NaBAR<sub>4</sub><sup>F</sup> compared to that using 1.1 mol% NaBAR<sub>4</sub><sup>F</sup> additive (Table 4.2, entries 5 & 6). Furthermore, addition of 3.3 mol%. of NaBAR<sub>4</sub><sup>F</sup> increasingly enhanced the initial rate of the dihydroalkoxylation reaction. The steady enhancement in catalytic activity with

increasing  $\text{NaBAR}_4^{\text{F}}$  concentrations for the conversion of **14** to **14a** and **14b** catalysed by **12** was attributed to the increasing substitution of the coordinated chloride ions in **12** by the weakly coordinating  $\text{BAR}_4^{\text{F}}$  counter anion.

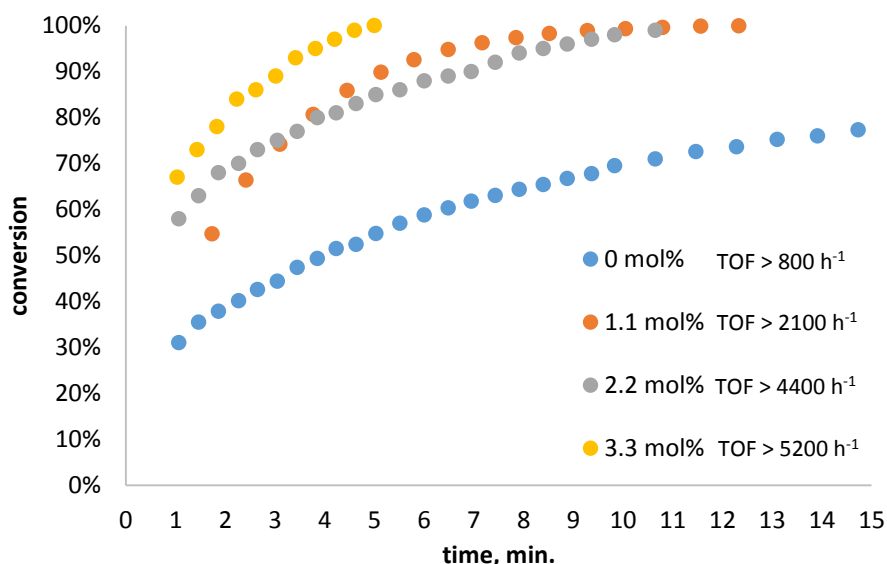


**Chart 4.4** Time course plots for varying quantity of  $\text{NaBAR}_4^{\text{F}}$  additive, see Table 4.2, entries 4-7. Reaction conditions: pre-catalyst (1 mol%), 25 °C,  $\text{C}_2\text{D}_2\text{Cl}_4$ .

To assess if this enhanced reaction rate was due to any decomplexed metal present in solution, control reactions were performed using various gold salts at room temperature.  $\text{Au}(\text{SMe}_2)\text{Cl}$  in the presence of  $\text{NaBAR}_4^{\text{F}}$  gave quantitative conversion after 15.6 min, whereas  $\text{Au}(\text{SMe}_2)\text{Cl}$  by itself gave a lower conversion (70%) after a much longer time (166 min).  $\text{HAuCl}_4$  gave no reaction at room temperature, with or without  $\text{NaBAR}_4^{\text{F}}$  present. Catalysis of similar reactions using the simple gold(I) and gold (III) salts has been reported in the literature.<sup>32</sup>

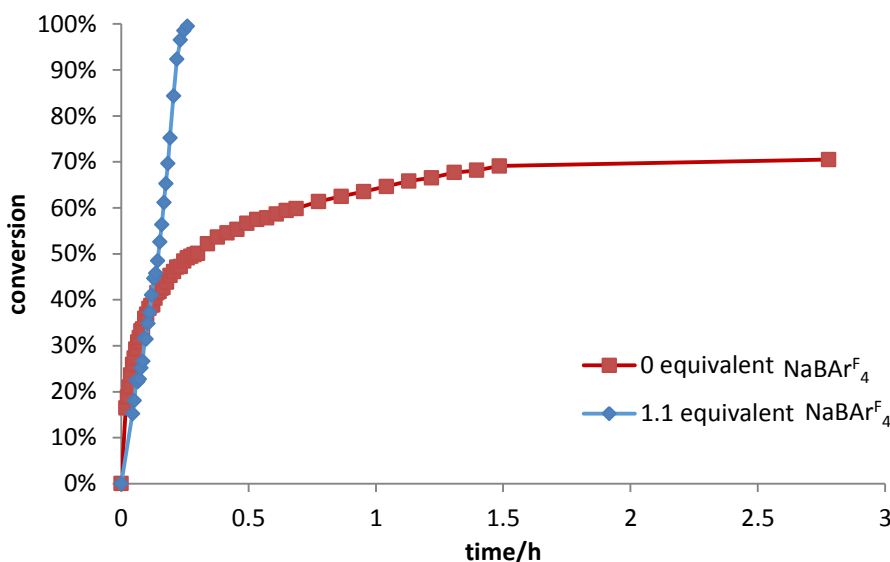
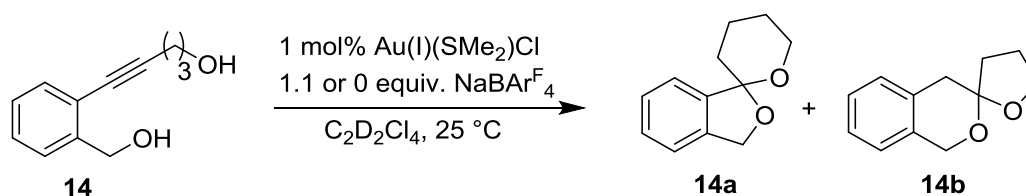


**Chart 4.5** Time course plots showing catalytic activity of Au(I)(SMe<sub>2</sub>)Cl for the conversion of **14**. (equiv. = equivalent relative to catalyst).

It was interesting to note that the rate at which the gold(III) complex (**12**) catalysed the reaction was faster than any other reported analogous reaction, especially given the absence of catalytic activity using HAuCl<sub>4</sub>. Gold complexes are well known to be the most active species for alkyne activation reactions, which are attributed to the metal's relativistic effects, high acidity and low oxyphilicity. However, the Au(III) complex **12** greatly outperforms the Au(I) counterpart **11** for the dihydroalkoxylation reaction of **14**. This is likely due to the increased Lewis acidity of the Au(III) metal centre in **12** compared to the Au(I) metal centre in **11** and the increased number of coordination sites available in **12** due to its square planar geometry, in comparison, **11** only contains one vacant coordination site due to its linear geometry. Only a few complexes in literature achieve high TOF values for

the dihydroalkoxylation reaction at lower temperatures (25 or 40 °C) and complete the reaction in a time scale of minutes. Hashmi *et al.* has reported the highest TOF values for the dihydroalkoxylation reaction, however, the reaction required 72 hours to achieve complete conversion.

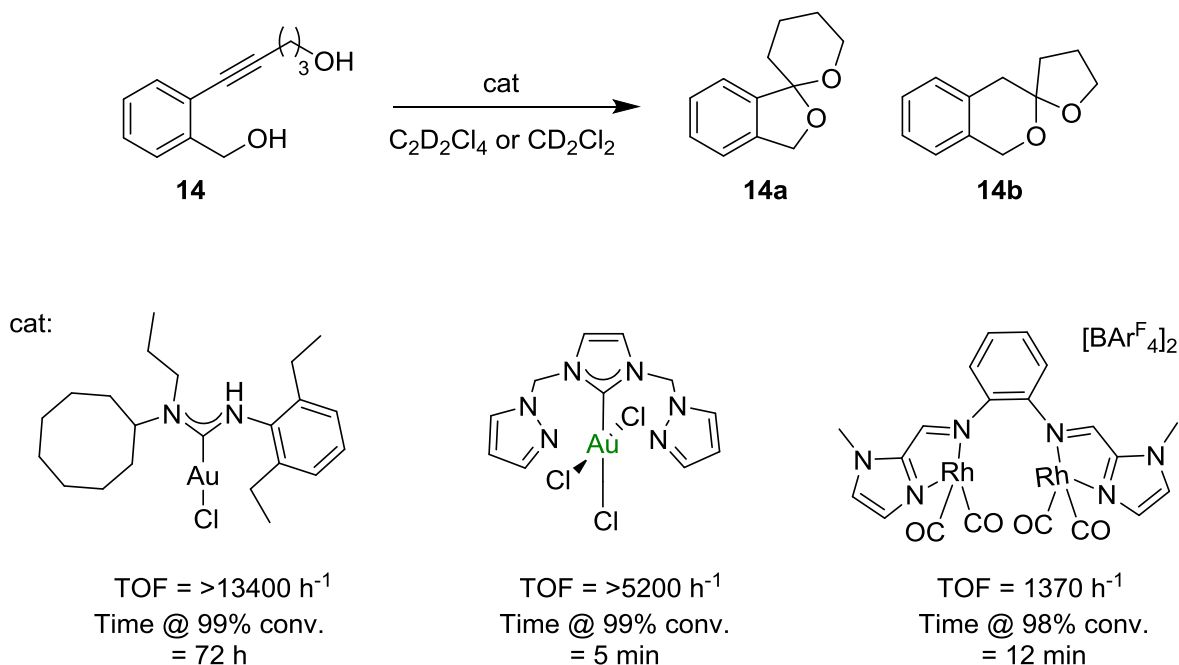


**Figure 4.6** Comparison in catalytic activity of **12** with complexes in literature.<sup>11, 33</sup>

#### 4.4.3. Oxidation state:

To investigate if the Au(III) complex **12** catalysed reaction was strictly a gold(III) catalysed process and that no redox transformation between (I) and (III) oxidation states transpired, these catalysis reactions were monitored by UV/Vis spectroscopy (Chart 4.6 and Chart 4.7). The gold(I) complex **11** gave an absorption at 258 nm and gold(III) complex **12** gave a similar absorption at 258 nm with a second absorption appearing between 270 nm to 330 nm. Over time (>6 min) a broad absorption appeared in the gold(III) spectrum between 500 nm to 580 nm, indicative of a surface plasmon resonance, most likely caused by the formation

of nanoparticles.<sup>34</sup> No such peak appeared on using the gold(I) system (**11**), even after 40 min at 25 °C.

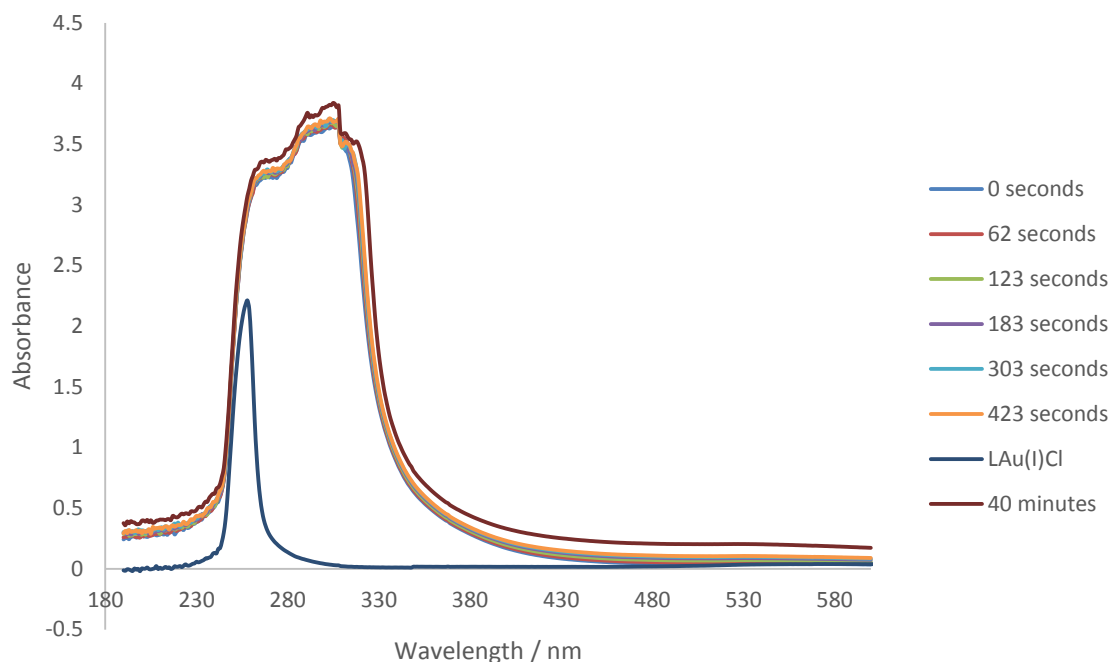


Chart 4.6 UV/Vis Spectra for Au(I) (**11**) catalysed dihydroalkoxylation of **14**

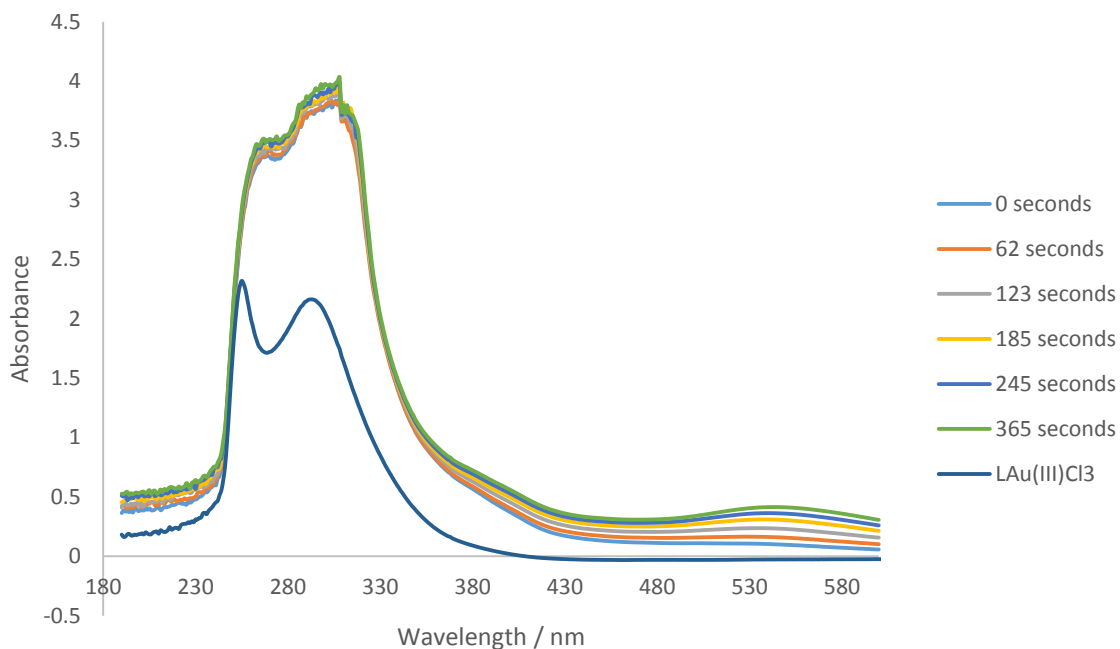


Chart 4.7 UV/Vis Spectra for Au(III) (**12**) catalysed dihydroalkoxylation of **14**

These results indicate that the gold catalysts **11** and **12** decompose to a certain extent over time. Although both spectra look similar after 62 seconds, only the spectra of **12** shows bands at 380 nm and 500 to 580 nm regions. To rule out catalysis caused by nanoparticle formation, a mercury drop test was conducted, by adding mercury to the dihydroalkoxylation reactions catalysed by both the gold(I) and gold(III) catalysts **11** and **12** for substrate **14**; using the conditions stated in Table 4.2, (entries 3 and 5) and monitored by  $^1\text{H}$  NMR spectroscopy. In both cases the reactions reached the same conversions at the same times as those conducted in the absence of mercury (Table 4.2, entries 3 and 5). This confirmed that the catalytic activities observed were promoted by complexes **11** and **12** and not due to any nanoparticles that may have formed.

#### 4.4.4. Catalyst loading dependence:

Encouraged by the results of the initial reactions and the control reactions, lower catalyst loadings of the gold(III) catalyst **12** were used to further investigate the dihydroalkoxylation reaction of **14** (Table 4.2, entries 8-11). Lowering the catalyst loadings to 0.1 mol% resulted in a significant decrease in catalytic activity, with the reaction progressing up to 30% conversion after 2.2 min (Table 4.2, entry 8). Further decreasing catalyst loading of **12** to 0.01 mol% resulted in a 10% conversion of **14** to **14a** and **14b** after 3.3 minutes. The time course plots show both reactions essentially plateau after the first NMR spectra were recorded (Chart 4.8). It would seem that the gold(III) catalyst **12** suffers from inhibition during reactions at these low catalyst loadings, possibly from either substrate or product binding.



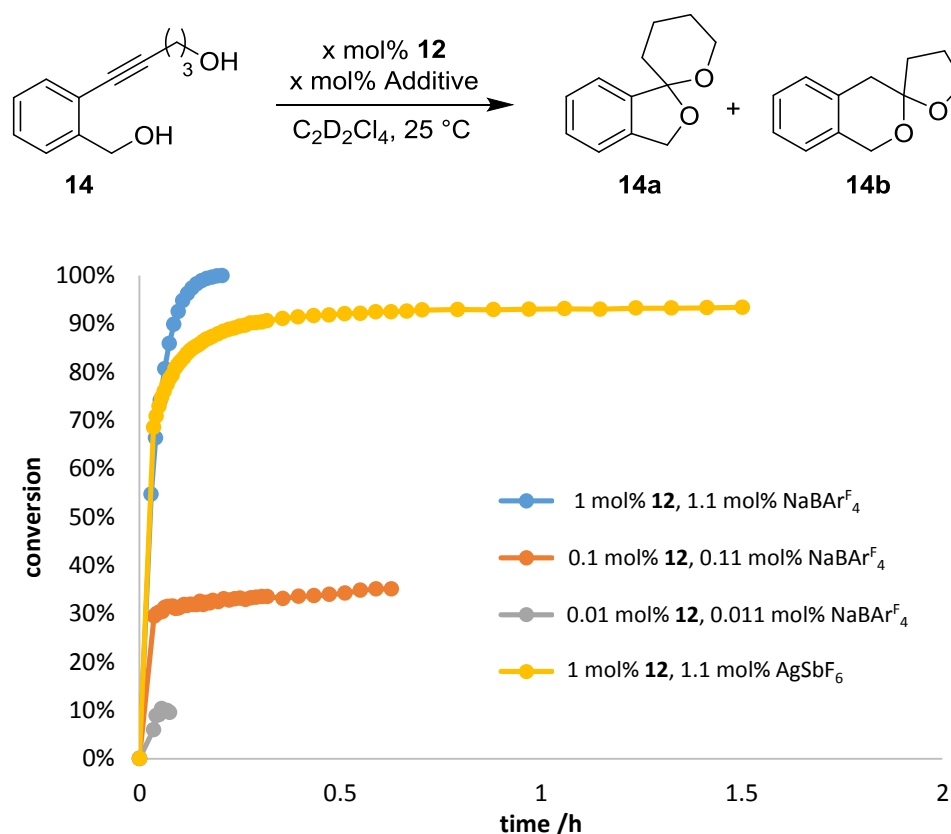


**Chart 4.8** Time vs conversion plots of the dihydroalkoxylation of **14** by **12** showing the effect of catalyst loading and counterion.

The role of the counterion proved to be vital for increasing catalytic activity, hence the dihydroalkoxylation reaction of **14** was examined using  $SbF_6^-$  instead of  $BAR_4^{F-}$  (Table 4.2, entries 10, 11). At 1 mol% of **12** the reaction proceeded to 93% conversion of **14** after almost 40 minutes, nearly four times slower than when using the  $BAR_4^{F-}$  counterion. Lowering the catalyst loading to 0.01 mol% whilst using  $SbF_6^-$  as an additive gave no conversion to spiroketal products. These results would indicate that for the dihydroalkoxylation reaction of **14**,  $BAR_4^{F-}$  outperforms  $SbF_6^-$ . Screenings of other weakly coordinating anions were deemed unnecessary given the excellent performance of  $BAR_4^{F-}$ .

## 4.4.5. Catalyst scope-investigating substrates with varying structure (15, 16)

To increase the scope of alkyne diols, substrates with different lengths of alkyl chain between the alkyne and the aliphatic alcohol were investigated. The substrate with the shorter alkyl chain 2-(4-hydroxybut-1-ynyl)benzyl alcohol (**15**) cyclised to give the 5,5-spiroketal product **15a** in a similar time (>99% conv., 15 min) to the reaction of **14** when using **12** as the catalyst (Chart 4.9). For comparison, the gold (I) catalyst **11** took almost two hours to reach quantitative conversion (96%) for the cyclisation of **14**. The use of  $\text{SbF}_6^-$  as the counterion for catalyst **12** for the cyclisation of **15** also produced similar results compared to the catalysed reaction of **14** (Chart 4.10), which is consistent with the similarity in results observed for the two substrates when using  $\text{BAR}^{\text{F}}_4^-$  as the counterion.

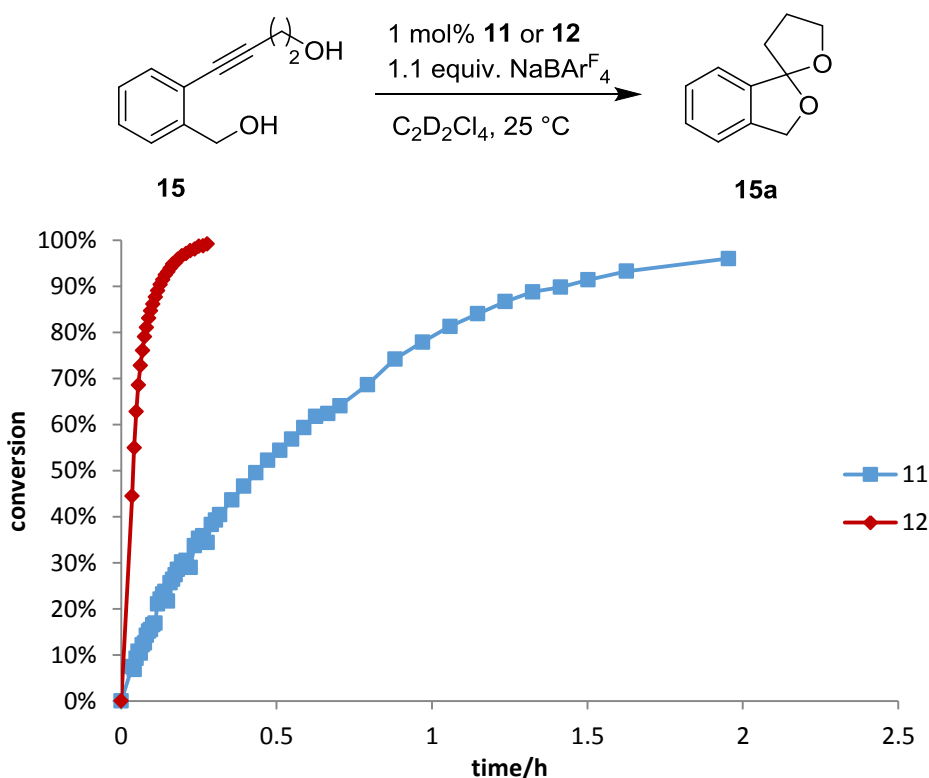


**Chart 4.9** Time vs conversion plots showing conversion of alkyne diol **15** catalysed by 1 mol% **11** and **12** at 25 °C. (equiv. = equivalent relative to catalyst).

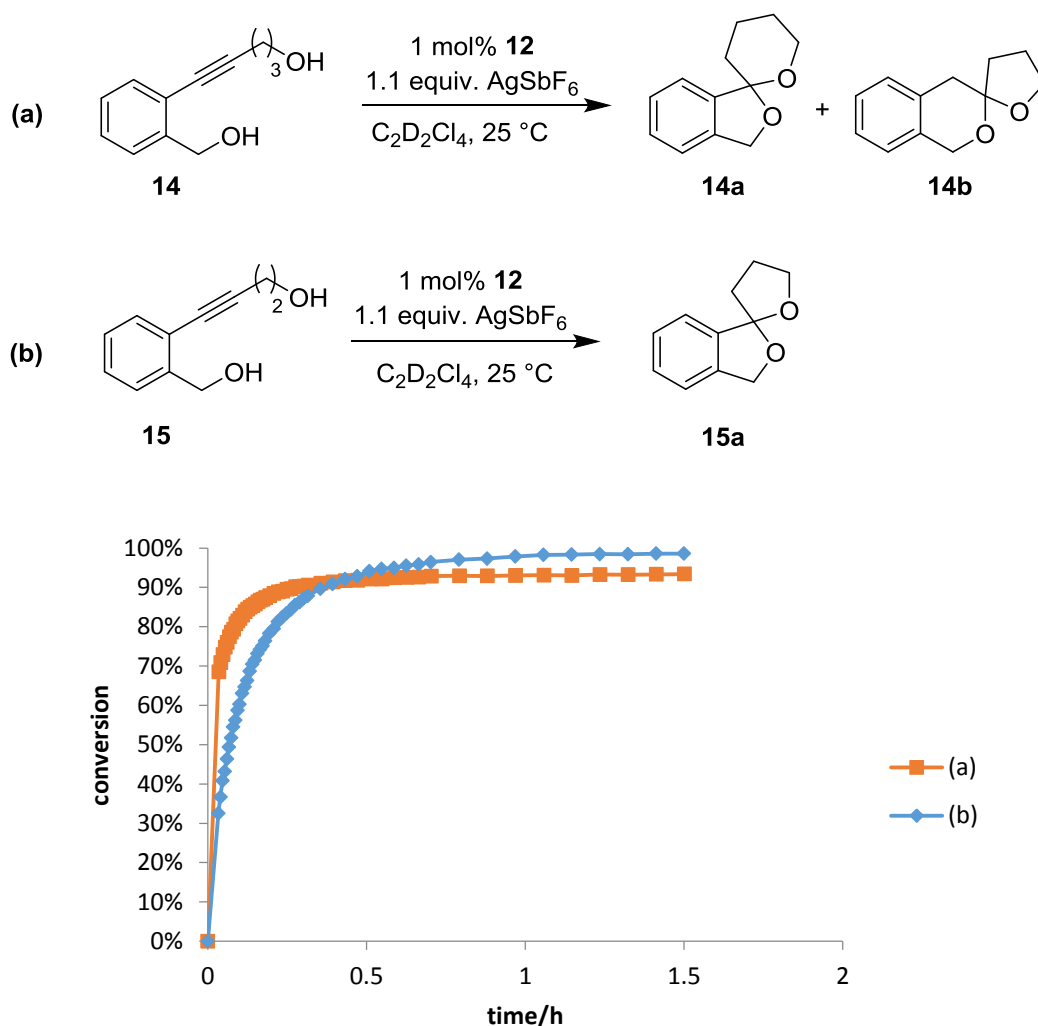


**Chart 4.10** Time vs conversion plots showing catalytic conversion of **14** and **15** using 1 mol% complex **12** and  $\text{SbF}_6^-$  as counterion at 25 °C. (equiv. = equivalent relative to catalyst).

Catalysed dihydroalkoxylation of 2-(6-hydroxyhex-1-ynyl)benzyl alcohol (**16**) gave no conversion at room temperature in the presence of the gold(III) catalyst **12**, conversion of **16** was only achieved after heating to 40 °C. Catalyst decomposition was recorded to occur at elevated temperatures from previous experiments and the transformation reactions of **16** were carried out at 40 °C rather than 70 °C. The time course plot of the gold(III) catalyst **12** shows the first data point at 38% conversion to the 6,6-spiroketal product **16a**, and no further reaction beyond this point (Chart 4.11), indicating that the catalyst had likely

decomposed or become inhibited prior to the first NMR spectrum being recorded. No reaction was observed for the gold(I) analogue (**11**) catalysed reaction of **16** at either 25 °C or 40 °C.

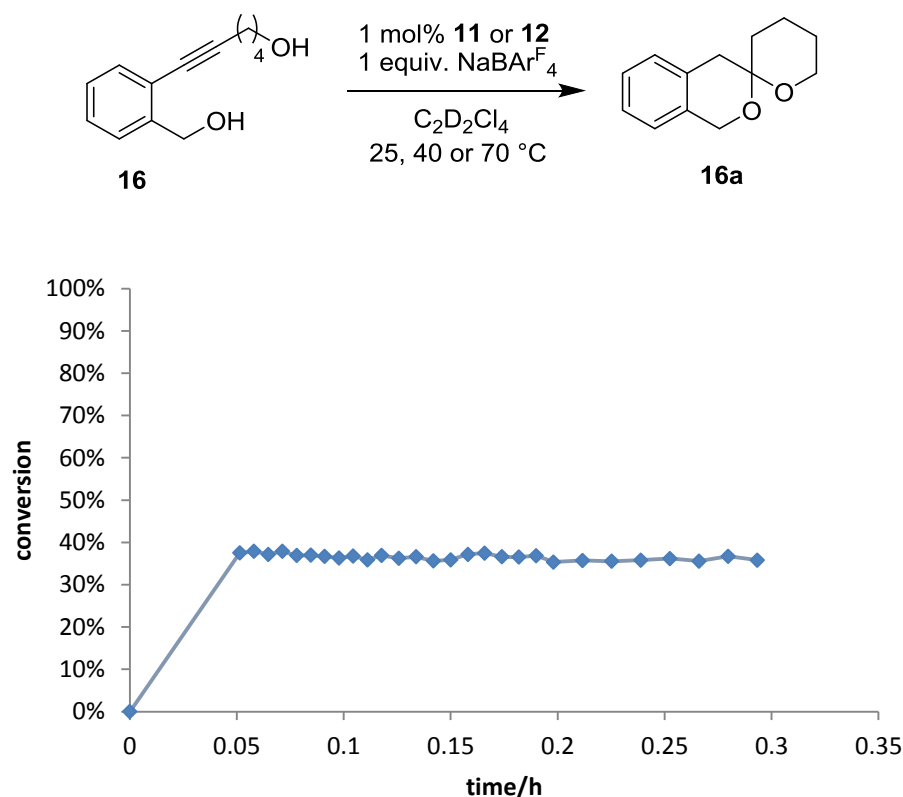


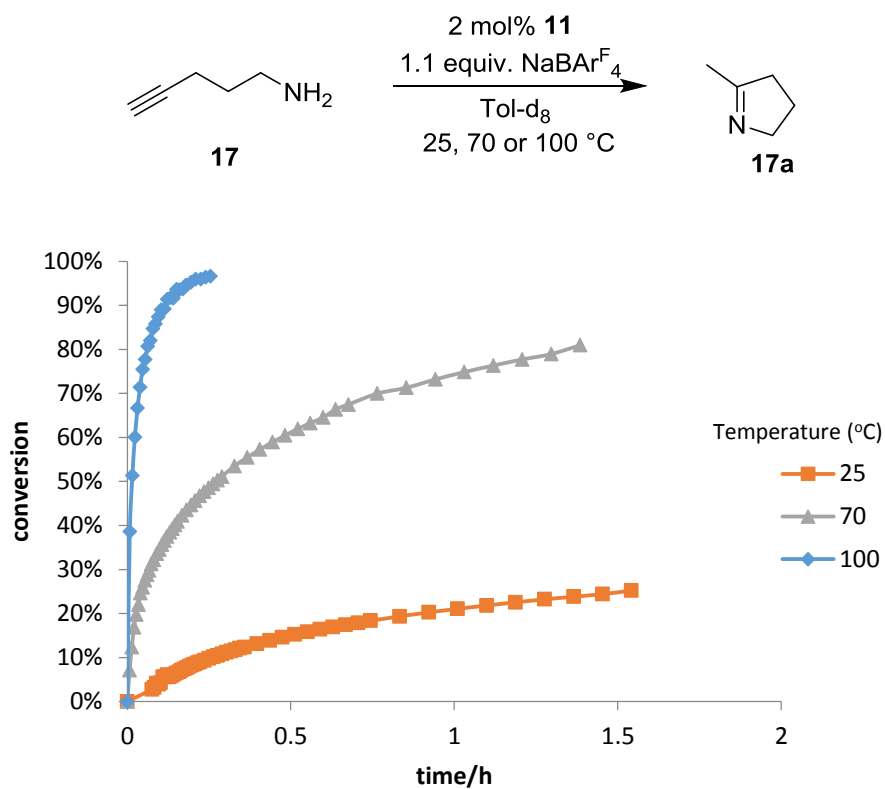
**Chart 4.11** Time vs conversion plot showing catalysis of the cyclisation of substrate **16** by 1 mol% complex **12** at 40 °C. (equiv. = equivalent relative to catalyst).

#### 4.5. Catalysed hydroamination reactions using complexes **11** and **12**.

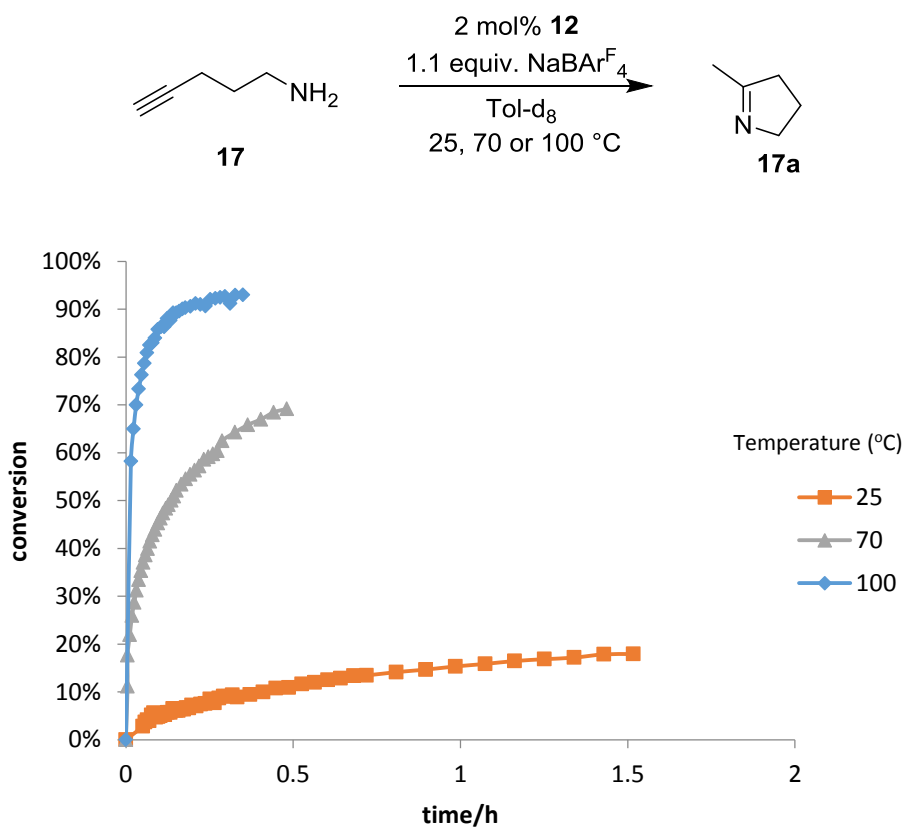
Hydroamination reactions involve the addition of an N-H bond across an unsaturated C-C bond and are typically atom economical processes.<sup>2,5</sup> Alkynes usually react faster than alkenes due to less electron density in the C=C bond, and intramolecular cyclisation outpaces intermolecular reactions.<sup>2</sup> Having shown that gold complexes containing an NCN<sup>Me</sup> ligand proved to be excellent catalysts for dihydroalkoxylation reactions, we set out to investigate their activity as hydroamination catalysts.

#### 4.5.1. Intramolecular hydroamination reactions catalysed by complexes **11** and **12**.

Initially the catalytic activity of the intramolecular cyclisation of 4-pentyn-1-amine (**17**) to 2-methyl-1-pyrroline (**17a**) at room temperature was investigated using catalysts **11** and **12**. Given the typically slower progress of hydroamination reactions compared to the dihydroalkoxylation reactions, a catalyst loading of 2 mol% was used in toluene-*d*<sub>8</sub>, and the reactions monitored using <sup>1</sup>H NMR spectroscopy. Over the course of 90 minutes, the catalysed reactions of **17** progressed slowly and a conversion of 25% was reached when using the Au(III) catalyst **12** and a maximum of 18% was reached using the Au(I) catalyst **11** (Chart 4.12 and Chart 4.13). Heating the reaction to 70 °C saw the initial reaction rate accelerate, with conversion plateauing at 69% after 30 minutes using the Au(I) complex **11**. and 81% conversion using Au(III) complex **12** after 90 minutes. Increasing the temperature to 100 °C resulted in 97% conversion after 15 minutes using complex **12** and 93% conversion after 20 minutes using complex **11**.

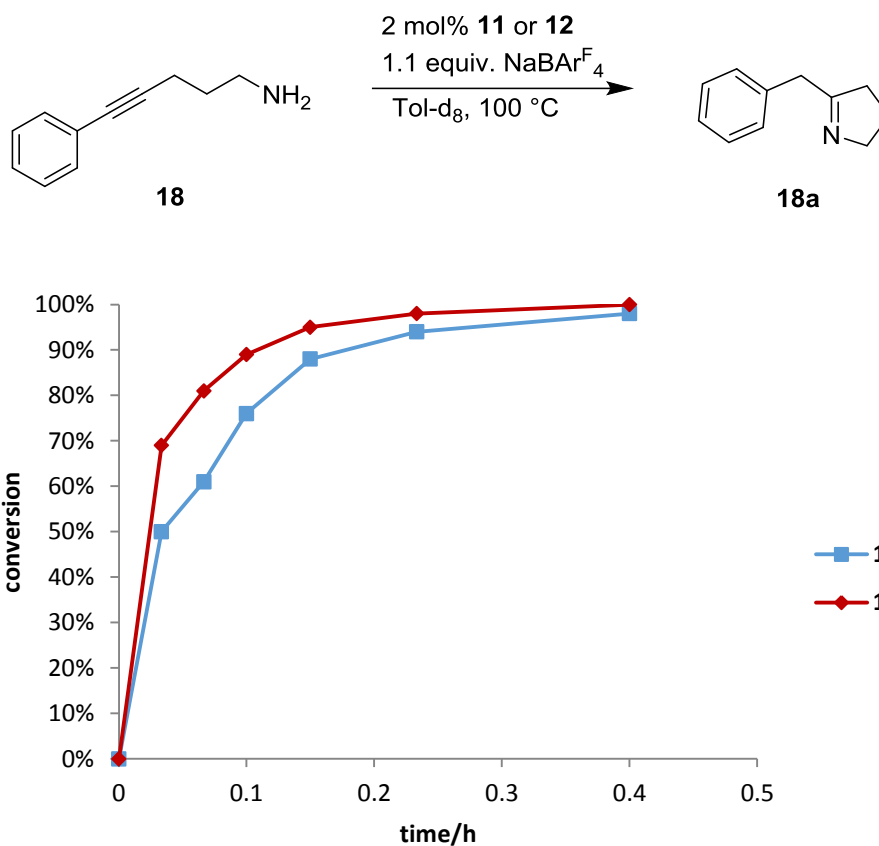
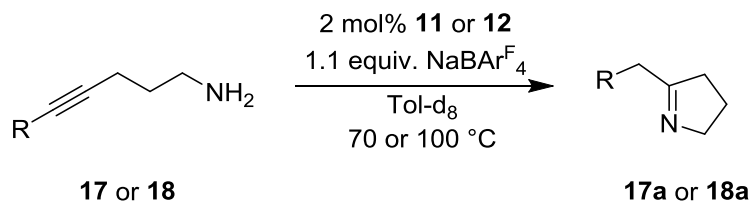


**Chart 4.12** % Time vs conversion plot for the hydroamination of **17** using 2 mol% of **11**. (equiv. = equivalent relative to catalyst).



**Chart 4.13** % Time vs conversion plots showing hydroamination of **17** using **12**. (equiv. = equivalent relative to catalyst).

The efficiency of conversion of 5-phenyl-4-pentyn-1-amine (**18**) proved to be similar to that of **17** at 100 °C with quantitative conversions on using both gold catalysts after 24 minutes. The TOFs for 5-phenyl-4-pentyn-1-amine (**18**) proved to be about half that of the substrate possessing the terminal alkyne (**17**), confirming that addition to a terminal alkyne is faster than addition to an internal alkyne.

Chart 4.14 Time course plots showing hydroamination of **18** at 100 °C using complexes **11**Table 4.3 Summary of intramolecular hydroamination reactions of **17** and **18** using complexes **11** and **12**. (equiv. = equivalent relative to catalyst).

entry	R	catalyst	temp, °C	% conv(+/-0.5%).	time, min	TOF, h <sup>-1</sup>
1	H	<b>11</b>	70	69	29	179
2	H	<b>12</b>	70	81	83	95
3	H	<b>11</b>	100	93	18	1952
4	H	<b>12</b>	100	97	15	1668
5	Ph	<b>11</b>	100	96	24	893
6	Ph	<b>12</b>	100	98	24	758



#### 4.5.2. Intramolecular hydroamination of alkenes:

Alkenes are harder to cyclise than alkynes due to the potential inability of the alkyl gold species to undergo protodeauration,<sup>35</sup> though hydroamination reactions of alkenes are known despite reports that anilines and amines inhibit the reaction.<sup>36</sup> Routes to circumvent this have included using benzyl or carbobenzyloxy protected amines,<sup>37</sup> carboxamides,<sup>38</sup> ureas,<sup>39</sup> and sulphonamides.<sup>40</sup> As such, a reaction using a primary amine, specifically the cyclisation of 2,2-diphenyl-4-penten-1-amine to 3,3-diphenylpyrrolidine was investigated at 100 °C. Even after 48 hours there was no conversion observed as determined by <sup>1</sup>H NMR spectroscopy for either gold catalysts **11** or **12**. Given the lack of reaction, further attempts at any other hydroaminations using alkene containing substrates were not carried out.

#### 4.5.3. Intermolecular hydroamination reactions catalysed by complexes **11** and **12**

Next, intermolecular hydroamination reactions were examined between phenylacetylene (**19**), pentyne (**20**) and aniline (**19a**) and benzylamine (**21**). These catalysed reactions were conducted in Tol-*d*<sub>8</sub> at 100 °C and monitored by <sup>1</sup>H NMR spectroscopy. No conversion was observed for reactions involving substrates **20** and **21** catalysed by either **11** or **12**. However, hydroamination of phenylacetylene (**19**) and aniline (**19a**) gave 30% conversion to **19b** after 60 minutes using complexes **11** and 26% conversion using complex **12** after 20 minutes. Extended reaction times at 100 °C did not improve the conversions. Though, the initial rate of conversion was certainly faster than expected given the slower nature of intermolecular reactions compared to hydroalkoxylation reactions. Having previously encountered catalyst decomposition with **11** and **12** (observation of Au nanoparticles) at elevated temperatures, the same reaction of aniline (**19a**) with phenylacetylene (**19**) was attempted but at a lower

temperature of 70 °C. Au(I) complex **11** gave 28% conversion after 1 hour, Au(III) complex **12** producing 21% conversion after 1 hour. Upon leaving the reactions for 20 hours the % conversion only increased by a few % indicating the catalyst had decomposed. Given the partial success of reacting phenylacetylene (**19**) with aniline (**19a**), hydroamination of diphenylacetylene with aniline (**19a**) was attempted, however no reaction was observed.

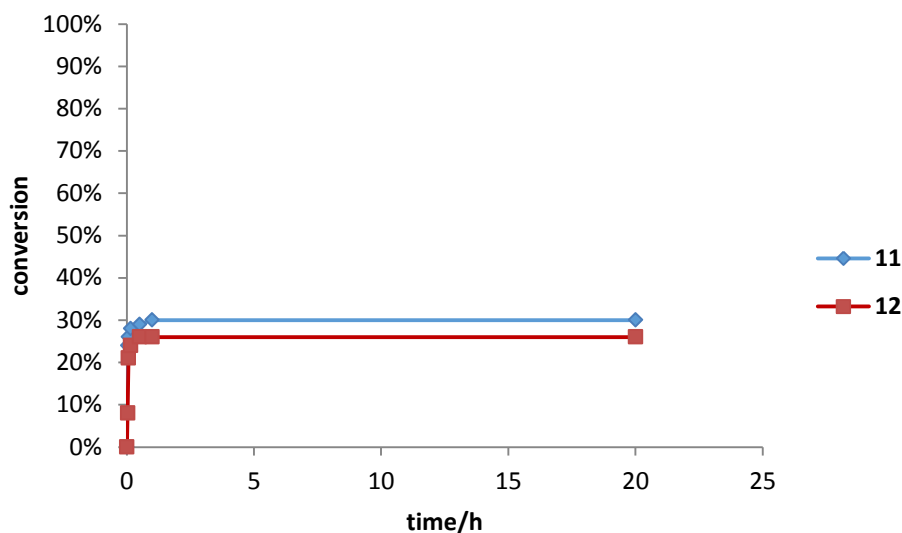
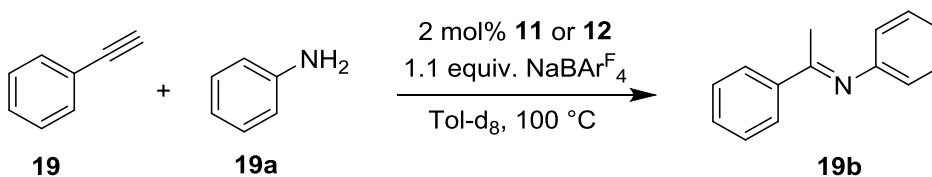


**Chart 4.15** Time course plot for the intermolecular hydroamination reaction of aniline (**19a**) and phenylacetylene (**19**) at 100 °C using complexes **11** and **12**. (equiv. = equivalent relative to catalyst).

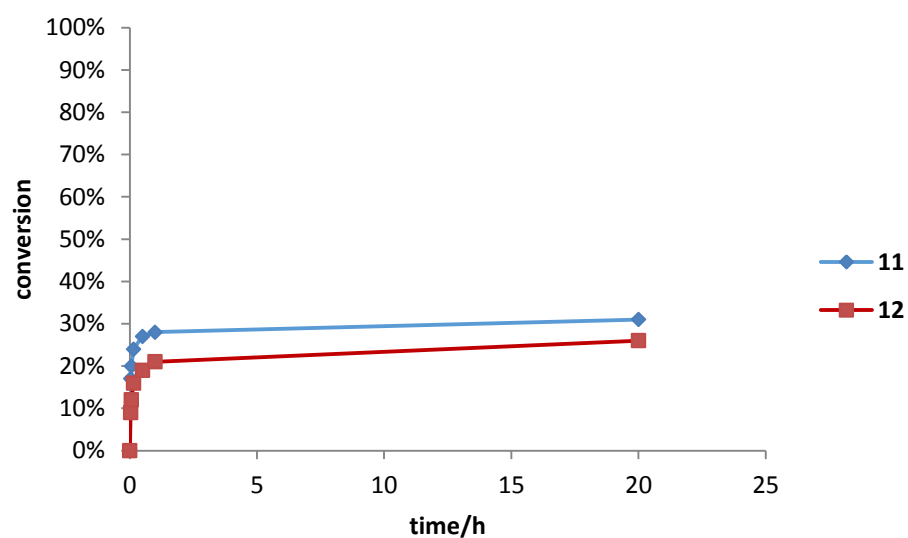
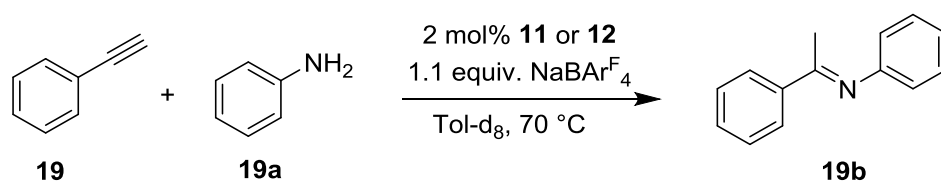


**Chart 4.16** Time course plot for the intermolecular hydroamination reaction of aniline (**19a**) and phenylacetylene (**19**) at 70 °C using complexes **11** and **12**. (equiv. = equivalent relative to catalyst).

#### 4.6. Conclusions

Gold complexes consisting of oxidation states I and III were synthesised and characterised.

It was found that a simple NHC-based gold(III) complex **12** was not only significantly faster than its gold(I) analogue, it is the fastest system reported to date at room temperature for the dihydroalkoxylation reaction of alkynyl diols under mild conditions. The next fastest system in literature are Rh(I) complexes containing bidentate imine ligands.<sup>32, 34</sup>

Control experiments proved that the dihydroalkoxylation reactions of alkynyl diols were gold(III)-catalysed processes, with no competing off-ligand reaction or contribution from gold nanoparticles.

Intramolecular hydroamination reactions of alkynes and alkenes were also studied with both catalysts performing well for the reaction with alkynes, achieving excellent conversions in less than 30 min, which places them on par with our previously reported catalysts.

Disappointingly, only one intermolecular hydroamination of aniline with phenylacetylene was found to proceed albeit in low conversion.

#### 4.7. References:

- (1) Alonso, F.; Beletskaya, I. P.; Yus, M. *Chem. Rev.* **2004**, *104*, 3079.
- (2) Huang, L.; Arndt, M.; Gooßen, K.; Heydt, H.; Gooßen, L. J. *Chem. Rev.* **2015**, *115*, 2596.
- (3) Zeng, X. *Chem. Rev.* **2013**, *113*, 6864.
- (4) Martinez, P. H.; Hultzs, K. C. *Tetrahedron Lett.* **2009**, *50*, 2054.
- (5) Müller, T. E.; Hultzs, K. C.; Yus, M.; Foubelo, F.; Tada, M. *Chem. Rev.* **2008**, *108*, 3795.
- (6) Kadota, I.; Mpaka Lutete, L.; Shibuya, A.; Yamamoto, Y. *Tetrahedron Lett.* **2001**, *42*, 6207.
- (7) Camacho, D. H.; Saito, S.; Yamamoto, Y. *Tetrahedron Lett.* **2002**, *43*, 1085.
- (8) (a) Larock, R. C.; Yum, E. K. *J. Am. Chem. Soc.* **1991**, *113*, 6689; (b) Larock, R. C.; Yum, E. K.; Refvik, M. D. *J. Org. Chem.* **1998**, *63*, 7652.
- (9) Puoy, M. J.; Cochrane, N. A.; Forman, G. C.; Gunnoe, T. B.; Cundari, T. R.; Sabat, M.; Myers, W. H. *ACS Catal.* **2012**, *2*, 2182.
- (10) (a) Messerle, B. A.; Vuong, K. Q. *Organometallics* **2007**, *26*, 3031; (b) Ho, J. H. H.; Choy, S. W. S.; Macgregor, S. A.; Messerle, B. A. *Organometallics* **2011**, *30*, 5978; (c) Timerbulatova, M. G.; Gatus, M. R. D.; Vuong, K. Q.; Bhadbhade, M.; Algarra, A. G.; Macgregor, S. A.; Messerle, B. A. *Organometallics* **2013**, *32*, 5071.
- (11) (a) Blanco Jaimes, M. C.; Böhling, C. R. N.; Serrano-Becerra, J. M.; Hashmi, A. S. K. *Angew. Chem. Int. Ed.* **2013**, *52*, 7963; (b) Biasiolo, L.; Trinchillo, M.; Belanzoni, P.; Belpassi, L.; Busico, V.; Ciancaleoni, G.; D'Amora, A.; Macchioni, A.; Tarantelli, F.; Zuccaccia, D. *Chem. Eur. J.* **2014**, *20*, 14594.

- (12) (a) Schulz, M.; Teles, J. H. *Chem. Abstr.* **1997**, 127, 121499; (b) Teles, J. H.; Brode, S.; Chabanas, M. *Angew. Chem. Int. Ed.* **1998**, 37, 1415; (c) Zhdanko, A.; Maier, M. E. *ACS Catal.* **2014**, 4, 2770.
- (13) Li, Y.; Fu, P. F.; Marks, T. *Organometallics* **1994**, 13, 439.
- (14) (a) Tregubov, A. A.; Vuong, K. Q.; Luais, E.; Gooding, J. J.; Messerle, B. A. *J. Am. Chem. Soc.* **2013**, 135, 16429; (b) Ho, J. H. H.; Wagler, J.; Willis, A. C.; Messerle, B. A. *Dalton Trans.* **2011**, 40, 11031.
- (15) Levallo, V.; Wright, J. H.; Tham, F. S.; Quinlivan, S. *Angew. Chem. Int. Ed.* **2013**, 52, 3172.
- (16) Morales-Morales, D.; Jensen, C. M. *The Chemistry of Pincer Compounds, Elsevier.* **2007**.
- (17) (a) Slugovc, C.; Schmid, R.; Kirchner, K. *Coord. Chem. Rev.* **1999**, 109, 185; (b) Haibach, M. C.; Guan, C.; Wang, D. Y.; Li, B.; Lease, N.; Steffens, A. M.; Krogh-Jespersen, K.; Goldman, A. S. *J. Am. Chem. Soc.* **2013**, 135, 15062.
- (18) Kataoka, Y.; Tsuji, Y.; Matsumoto, O.; Ohashi, M.; Yamagata, T.; Tani, K. *Chem. Commun.* **1995**, 20, 2099.
- (19) (a) Rung-Yi, L.; Surekha, K.; Akito, H.; Fumiyuki, O.; Yi-Hong, L.; Shie-Ming, P.; Shiuh-Tzung, L. *Organometallics* **2007**, 26, 1062; (b) Helgert, T. R.; Hollis, T. K.; Valente, E. J. *Organometallics* **2012**, 31, 3002; (c) Yang, Z.; Xia, C.; Liu, D.; Liu, Y.; Sugiya, M.; Imamoto, T.; Zhang, W. *Org. Biomol. Chem.* **2015**, 13, 2694.
- (20) Severin, R.; Doye, S. *Chem. Soc. Rev.* **2007**, 36, 1407.
- (21) Cao, C.; Shi, Y.; Odom, A. L. *J. Am. Chem. Soc.* **2003**, 125, 2880.
- (22) Zhang, C.; Wang, Z. X. *Organometallics* **2009**, 28, 6507.

- (23) Gallegos, C.; Camacho, R.; Valiente, M.; Cuenca, T.; Cano, J. *Catal. Sci. Technol.* **2016**, *6*, 5134.
- (24) Mancano, G.; Page, M. J.; Bhadbhade, M.; Messerle, B. A. *Inorg. Chem.* **2014**, *53*, 10159.
- (25) Collado, A.; Gomez-Suarez, A.; Martin, A. R.; Slawin, A. M. Z.; Nolan, S. P. *Chem. Commun.* **2013**, *49*, 5541.
- (26) (a) Alesso, G.; Cinellu, M. A.; Stoccoro, S.; Zucca, A.; Minghetti, G.; Manassero, C.; Rizzato, S.; Swang, O.; Ghosh, M. K. *Dalton Trans.* **2010**, *39*, 10293; (b) Dinda, J.; Nandy, A.; Rana, B. K.; Bertolasi, V.; Saha, K. D.; Bielawski, C. W. *RSC Adv.* **2014**, *4*, 60776.
- (27) Ho, J. H. H.; Hodgson, R.; Wagler, J.; Messerle, B. A. *Dalton Trans.* **2010**, *39*, 4062.
- (28) Wong, C. M.; Vuong, K. Q.; Gatus, M. R. D.; Hua, C.; Bhadbhade, M.; Messerle, B. A. *Organometallics* **2012**, *31*, 7500.
- (29) (a) Hashmi, A. S. K.; Bührle, M.; Wölfe, M.; Rudolph, M.; Wietek, M.; Rominger, F.; Frey, W. *Chem. Eur. J.* **2010**, *16*, 9846; (b) Rudolph, M.; Hashmi, A. S. K. *Chem. Soc. Rev.* **2012**, *41*, 2448.
- (30) (a) Quach, R.; Furkert, D. P.; Brimble, M. A. *Tetrahedron Lett.* **2013**, *54*, 5865; (b) Fang, W.; Pisset, M.; Guérinot, A.; Bour, C.; Bezenine-Lafollée, S.; Gandon, V. *Chem. Eur. J.* **2014**, *20*, 5439.
- (31) Navarro, J. R. G.; Lerouge, F.; Cepraga, C.; Micouin, G.; Favier, A.; Chateau, D.; Charreyre, M. T.; Lanoe, P. H.; Monnereau, C.; Chaputa, F.; Marotte, S.; Leverrier, Y.; Marvel, J.; Kamada, K.; Andraud, C.; Baldeck, P. L.; Parola, S. *Biomaterials* **2013**, *34*, 8344.
- (32) Liu, B.; De Brabander, J. K. *Org. Lett.* **2006**, *8*, 4907.

- (33) Choy, S. W. *PhD Thesis-Bimetallic Rhodium Complexes for Promoting C-X Bond Formation: Structure and Mechanism*. **2015**.
- (34) Haiss, W.; Thanh, N. T.; Aveyard, J.; Fernig, D. G. *Anal. Chem.* **2007**, 79, 4215.
- (35) LaLonde, R. L.; Brenzovich, J. W. E.; Benitez, D.; Tkatchouk, E.; Kelley, K.; Goddard, W. A.; Toste, F. D. *Chem. Sci.* **2010**, 1, 226.
- (36) Zhang, J.; Yang, C.-G.; He, C. *J. Am. Chem. Soc.* **2006**, 128, 1798.
- (37) Han, X.; Widenhoefer, R. A. *Angew. Chem. Int. Ed.* **2006**, 45, 1747.
- (38) Bender, C. F.; Widenhoefer, R. A. *Chem. Commun.* **2006**, 4143.
- (39) Bender, C. F.; Widenhoefer, R. A. *Org. Lett.* **2006**, 8, 5303.
- (40) Liu, X.-Y.; Li, C.-H.; Che, C.-M. *Org. Lett.* **2006**, 8, 2707.



---

## Chapter 5. Conclusions and Future work

---

## 5.1. Conclusions

### 5.1.1. Chapter 2

A series of novel Ag(I) and Ru(II) complexes containing pincer imidazolyl-pyrazole ligands were synthesised and characterised. Complexes  $[\text{Ag}(\text{NCN}^{\text{Me}})_2]\text{BPh}_4$  (**2**),  $[\text{Ru}(\text{NCN}^{\text{Me}})_2](\text{BPh}_4)_2$  (**6**),  $[\text{Ru}(\text{H})\text{CO}(\text{NCN}^{\text{Me}})(\text{PPh}_3)_2]\text{BPh}_4$  (**5a**),  $[\text{Ru}(\text{H})\text{CO}(\text{NCN}^{\text{Me}})(\text{PPh}_3)_2]\text{BPh}_4$  (**5**),  $[\text{Ru}(\eta^6\text{-C}_6\text{H}_6)(\text{NCN}^{\text{Me}})\text{Cl}]\text{BPh}_4$  (**3**),  $[\text{Ru}(\eta^6\text{-C}_{10}\text{H}_{14})(\text{NCN}^{\text{Me}})\text{Cl}]\text{BPh}_4 \cdot [\text{B}_5\text{O}_6(\text{OH})_4]$  (**4a**),  $[\text{Ru}(\eta^6\text{-C}_{10}\text{H}_{14})(\text{NCN}^{\text{Me}})\text{Cl}]\text{BPh}_4$  (**4**) were prepared in moderate yields.

- The solid state structures of ligands and complexes  $(\text{NCN}^{\text{Me}})\text{BPh}_4$  (**1a**),  $(\text{NCN}^{\text{Et}})\text{BPh}_4$  (**1c**),  $[\text{Ag}(\text{NCN}^{\text{Me}})_2]\text{BPh}_4$  (**2**),  $[\text{Ru}(\text{NCN}^{\text{Me}})_2](\text{BPh}_4)_2$  (**7**),  $[\text{Ru}(\text{H})\text{CO}(\text{NCN}^{\text{Me}})(\text{PPh}_3)_2]\text{BPh}_4$  (**5a**),  $[\text{Ru}(\eta^6\text{-C}_6\text{H}_6)(\text{NCN}^{\text{Me}})\text{Cl}]\text{BPh}_4$  (**3**),  $[\text{Ru}(\eta^6\text{-C}_{10}\text{H}_{14})(\text{NCN}^{\text{Me}})\text{Cl}]\text{BPh}_4 \cdot [\text{B}_5\text{O}_6(\text{OH})_4]$  (**4a**) were obtained using X-ray crystal structure analyses. Complex (**2**) showed the expected linear geometry for a Ag(I) metal centre. The Ru(II) complex (**6**) shows an octahedral geometry with a bis-tridentate coordination of ligand (**1**) about the metal centre, whereas complexes (**5a**), (**3**) and (**4a**) consist of a bidentate coordination of the ligand to the metal centre. Complexes (**3**) and (**5a**) adopt a pseudo-octahedral geometry as expected for Ru(II) complexes containing a  $\eta^6$  arene ring.
- X-ray crystal structure analysis of  $[\text{Ru}(\eta^6\text{-C}_{10}\text{H}_{14})(\text{NCN}^{\text{Me}})\text{Cl}]\text{BPh}_4 \cdot [\text{B}_5\text{O}_6(\text{OH})_4]$  (**4a**) revealed the presence of a rare boronic counterion  $[\text{B}_5\text{O}_6(\text{OH})_4]^-$ . Initial attempts in the synthesis of  $[\text{Ru}(\text{H})\text{CO}(\text{NCN}^{\text{Me}})(\text{PPh}_3)_2]\text{BPh}_4$  (**5a**) using the silver transmetallation route resulted in the formation of a new Ru(I) cubane complex  $[\text{RuCl}(\text{PPh}_3)]_4$  which could only be identified using X-ray crystal structure analysis.

- The Ru(II) complexes  $[\text{Ru}(\text{NCN}^{\text{Me}})_2](\text{BPh}_4)_2$  (**7**),  $[\text{Ru}(\text{H})\text{CO}(\text{NCN}^{\text{Me}})(\text{PPh}_3)_2]\text{BPh}_4$  (**5a**),  $[\text{Ru}(\text{H})\text{CO}(\text{NCN}^{\text{Me}})(\text{PPh}_3)_2]\text{BPh}_4$  (**5**),  $[\text{Ru}(\eta^6\text{-C}_6\text{H}_6)(\text{NCN}^{\text{Me}})\text{Cl}]\text{BPh}_4$  (**3**),  $[\text{Ru}(\eta^6\text{-C}_{10}\text{H}_{14})(\text{NCN}^{\text{Me}})\text{Cl}]\text{BPh}_4[\text{B}_5\text{O}_6(\text{OH})_4]$  (**4a**),  $[\text{Ru}(\eta^6\text{-C}_{10}\text{H}_{14})(\text{NCN}^{\text{Me}})\text{Cl}]\text{BPh}_4$  (**4**) were tested as catalysts for the transfer hydrogenation reaction of acetophenone. Complexes containing arene co-ligands  $[\text{Ru}(\eta^6\text{-C}_6\text{H}_6)(\text{NCN}^{\text{Me}})\text{Cl}]\text{BPh}_4$  (**3**),  $[\text{Ru}(\eta^6\text{-C}_{10}\text{H}_{14})(\text{NCN}^{\text{Me}})\text{Cl}]\text{BPh}_4[\text{B}_5\text{O}_6(\text{OH})_4]$  (**4a**),  $[\text{Ru}(\eta^6\text{-C}_{10}\text{H}_{14})(\text{NCN}^{\text{Me}})\text{Cl}]\text{BPh}_4$  (**4**) were found to be more active catalysts for the organic transformation with  $[\text{Ru}(\eta^6\text{-C}_{10}\text{H}_{14})(\text{NCN}^{\text{Me}})\text{Cl}]\text{BPh}_4[\text{B}_5\text{O}_6(\text{OH})_4]$  (**4a**) exhibiting the best activity.
- To investigate the scope of the catalyzed transfer hydrogenation,  $[\text{Ru}(\eta^6\text{-C}_{10}\text{H}_{14})(\text{NCN}^{\text{Me}})\text{Cl}]\text{BPh}_4[\text{B}_5\text{O}_6(\text{OH})_4]$  (**4a**) and  $[\text{Ru}(\eta^6\text{-C}_{10}\text{H}_{14})(\text{NCN}^{\text{Me}})\text{Cl}]\text{BPh}_4$  (**4**) were used as catalysts for the transfer hydrogenation reaction of a number of substrates. The complexes promoted complete conversions of all substrates in short reaction times (< 1hr).  $[\text{Ru}(\eta^6\text{-C}_{10}\text{H}_{14})(\text{NCN}^{\text{Me}})\text{Cl}]\text{BPh}_4[\text{B}_5\text{O}_6(\text{OH})_4]$  (**4a**) was also found to be active for the organic transformation at room temperature conditions.

A series of coordination motifs were observed for the Ru(II) and Ag(I) complexes in solid state, ranging from a fully saturated tridentate Ru(II) dimer to a mono-dentate Ag(I) dimer. Crystallographic analysis unexpectedly revealed a rare pentaborate anion for complex **4a**. This mixed anion complex was found to be the most active catalyst for the transfer hydrogenation reaction among the Ru(II) catalysts suggesting the pentaborate anion enhances catalytic activity. Most probably, the complex catalyses the transfer hydrogenations via a separate mechanism from the organometallic catalyst. The mixture containing the pentaborate anion was also found to be the only active catalyst for the transfer hydrogenation reaction at room temperature conditions.

### 5.1.2. Chapter 3

A series of novel Ni(II) complexes containing pincer imidazolyl-pyrazole ligands were synthesised and characterised. Complexes  $[\text{Ni}(\text{NCN}^{\text{Me}})\text{Cl}]\text{BPh}_4$  (**8**),  $[\text{Ni}(\text{NCN}^{\text{Me}})\text{Cl}]\text{PF}_6$  (**9**) and  $[\text{Ni}(\text{NCN}^{\text{Et}})_2](\text{BPh}_4)_2$  (**10**) were prepared in moderate yields.

- The solid state structures of complexes  $[\text{Ni}(\text{NCN}^{\text{Me}})\text{Cl}]\text{BPh}_4$  (**8**),  $[\text{Ni}(\text{NCN}^{\text{Me}})\text{Cl}]\text{PF}_6$  (**9**) and  $[\text{Ni}(\text{NCN}^{\text{Me}})^{\text{Et}}_2](\text{BPh}_4)_2$  (**10**) were obtained using X-ray crystal structure analyses. All complexes showed the expected square planar geometry about the metal centre and were symmetrical in structure. Complexes (**8**) and (**9**) consisted of a single pincer ligand **1a** engaged in tridentate coordination to the metal centre, whereas complex (**10**) displayed a bis-bidentate coordination of ligand **1c** to the Ni(II) metal.
- Analysis using UV spectroscopy and variable temperature NMR spectroscopy revealed that the Ni(II) complexes were diamagnetic in nature and that the broad spectra at room temperature conditions resulted from changes in conformation due to the flexible nature of the ligands.
- The Ni(II) complexes  $[\text{Ni}(\text{NCN}^{\text{Me}})\text{Cl}]\text{BPh}_4$  (**8**),  $[\text{Ni}(\text{NCN}^{\text{Me}})\text{Cl}]\text{PF}_6$  (**9**) and  $[\text{Ni}(\text{NCN}^{\text{Et}})_2](\text{BPh}_4)_2$  (**10**) were tested as catalysts for the Kumada cross coupling reaction of aryl halides.
- Changing the counterion from  $\text{BPh}_4^-$  to  $\text{PF}_6^-$  resulted in reduced selectivity for the chlorinated substrate chlorobenzene and different catalytic rates for the Kumada cross coupling reaction of bromobenzene and phenylmagnesium bromide.
- Reduction in catalytic loading resulted in reduced activity of complex **8** for the conversion of chlorobenzene whereas reduction in catalyst loading had an insignificant effect on the final catalytic conversion of bromobenzene.

The choice of ligand used affected the coordination modes observed for the Ni(II) complexes. Use of an  $NCN^{Me}$  pincer ligand **1c** with longer linker arms between pyrazole and imidazole groups resulted in a bidentate coordination (**10**) whereas a shorter linker arm produced a tridentate coordination mode of the ligand to the Ni(II) metal centre (**8** and **9**). Complex **8** containing the pincer geometry was found to be the most active catalyst for the Kumada cross coupling reaction in comparison to complexes **9** and **10**. The coordinatively saturated complex **10** was found to be nearly inactive for the organic transformation and any conversion attained was attributed to the lability of the pyrazole arms. Complex **8** catalysed the Kumada cross coupling reaction for a wide range of substrates with higher activities achieved for substrates with electronegative substituents. The investigation showed that the catalytic activity was dependent on the type of substituents present on the aryl substrates.

#### 5.1.3. Chapter 4

A series of new Au(I) and Au(III) complexes containing pincer imidazolyl-pyrazole ( $NCN^{Me}$ ) ligands were synthesised and characterised. Complexes  $[Au(I)(NCN^{Me})Cl]$  (**11**) and  $[Au(III)(NCN^{Me})Cl_3]$  (**12**) were prepared in moderate yields.

- The solid state structures of complexes  $[Au(I)(NCN^{Me})Cl]$  (**11**) and  $[Au(III)(NCN^{Me})Cl_3]$  (**12**) were obtained using X-ray crystal structure analyses. Complex (**11**) showed a linear geometry typical of an Au(I) complex with monodentate coordination of ligand **1** to the gold metal centre. Complex (**12**) shows a square planar geometry as expected for an Au(III) complex with monodentate coordination of the ligand to the metal and three Cl co-ligands occupying the remaining coordination sites.

- The oxidation states and properties of the complexes were further determined using UV spectroscopy
- Complexes  $[\text{Au(I)}(\text{NCN}^{\text{Me}})\text{Cl}]$  (**11**) and  $[\text{Au(III)}(\text{NCN}^{\text{Me}})\text{Cl}_3]$  (**12**) were tested as catalysts for the intramolecular dihydroalkoxylation reactions. Both complexes were highly active for the organic transformation with complex (**12**) showing excellent activity at very high TOF values even at room temperature conditions.
- Intramolecular and intermolecular hydroamination reactions were then tested using both complexes. Complexes (**11**) and (**12**) proved to be highly active for the intramolecular hydroamination reactions of pentyn-4-amine and phenylpentynamine and achieved moderate conversions for the intermolecular hydroamination reactions of aniline with phenylacetylene.

Unlike the Ru(II) and Ni(II) complexes containing weakly coordinating counterions, both the Au(I) and Au(III) complexes **11** and **12** were found to be neutral in nature with terminally bound chlorine atoms balancing the positive charge of the Au metal centres. The Au(III) complex **12** was found to be more active than its Au(I) analogue **11** for the intramolecular dihydroalkoxylation reaction and was attributed to the increased Lewis acidity of Au(III). It was found that the simple NHC-based gold(III) complex **12** is the fastest system reported to date at room temperature for the dihydroalkoxylation reaction of alkynyl diols under mild conditions.

## 5.2. Future work

## Chapter 2:

This chapter has shown that Ru(II) complexes bearing the imidazolyl-pyrazolyl  $NCN^{Me}$  pincer ligands and  $\eta^6$  arene co-ligands are highly active catalysts for the transfer hydrogenation reaction of ketones and that the presence of a boronate counterion  $[B_5O_6(OH)_4]^-$  can enhance catalytic activity. However, this requires further investigation to understand the systems' effect on catalytic activity as follows:

- Repeating the catalytic reactions using the Ru(II) complexes with addition of catalytic amounts of boronic acids and testing whether all reactions can be performed under room temperature conditions.
- Utilising a simple salt of  $[B_5O_6(OH)_4]^-$  to synthesise complexes containing only the boronate counteranion and investigating the catalytic activity of the complexes for different organic transformations.
- Synthesising new pincer ligands containing a boronate pendant arm and investigating the coordination chemistry of the new ligand to Ru(II) metal and examine the catalytic activity of the resulting complexes for the transfer hydrogenation reaction.

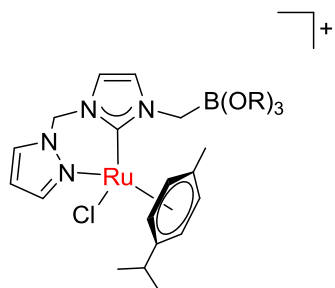


**Figure 5.1** Ru(II) complex bearing a ligand with a boronate pendant arm.

### Chapter 3:

Ni(II) complexes bearing the *NCN* pincer ligands were shown to have unusual activity for the Kumada cross coupling reactions. Complex (**8**) showed higher activity for chlorinated substrates in comparison to brominated counterparts. The complex also showed highly selectivity for disubstituted substrates. Further investigation on the catalytic activity of **8** for selected chlorinated, brominated and hetero-disubstituted substrates can reveal important information:

- Perform the catalysed Kumada cross coupling reaction of hetero-halo-disubstituted substrates using complex (**8**) to evaluate the level of selectivity of the Ni(II) complexes for the different halogen functional groups.
- The Ni(II) complexes were found to be air and moisture stable and can therefore be useful in other organic transformations which do not require rigorous air sensitive manipulations.i.e. Initial testing of complex **8** as a catalyst for the Suzuki-Miyura cross coupling reactions in the presence of air and moisture.

### Chapter 4:

This chapter has demonstrated that Au(I) and Au(III) complexes containing imidazolyl-pyrazolyl pincer ligands are highly active catalysts for intramolecular dihydroalkoxylation and hydroamination reactions. The Au(III) complex (**12**) achieves extremely high TOF values and remains highly active at room temperature conditions. However, the stability of the complex degrades overtime under catalytic conditions. Achieving bimetallic coordination by the ligand also proved to be difficult. Future work would include:



- Isolation of Au(III) complexes containing a true pincer coordination could be useful for increased stability and elongated catalytic activity. A pincer coordination of the ligand to the metal centre will result in increased thermal and catalytic stability of the complex.
- Investigation of the coordination chemistry of the pincer ligand **1c** containing the longer ethylene linker arms could prove to be useful as the flexible coordination and increased distance between the metal centres may stabilise the bimetallic complex. The bimetallic complexes should be tested as catalysts for tandem reactions where each metal could selectively catalyse a specific organic transformation.

---

## Chapter 6. Experimental

---

### General Procedures

All manipulations were carried out under a nitrogen atmosphere using standard Schlenk techniques or in a nitrogen or argon filled glovebox unless otherwise stated. Imidazolium ligand **1** was prepared according to a literature method.<sup>1</sup>  $\text{RuHCl(CO)(PPh}_3)_3$ ,<sup>3</sup>  $[\text{Ru}(\eta^6\text{-C}_6\text{H}_6)\text{Cl}_2]_2$ <sup>2</sup> and  $[\text{Ru}(\eta^6\text{-C}_6\text{H}_6)\text{Cl}_2]_2$ <sup>2</sup> were prepared according to literature procedures.<sup>2, 3</sup> Commercially available reagents were purchased from Sigma-Aldrich or Alfa Aesar Inc. and used as received.  $\text{CH}_2\text{Cl}_2$  and  $\text{CH}_3\text{CN}$  were dried on a solvent purification system and used as dispensed. Propan-2-ol and methanol were freshly distilled from calcium hydride and THF was freshly distilled using a sodium mirror.

$^1\text{H}$ ,  $^{13}\text{C}$ ,  $^{13}\text{C}\{^1\text{H}\}$  and  $^{31}\text{P}$  NMR spectra were recorded on Bruker DPX300, DMX500 and DMX400 spectrometers. Chemical shifts ( $\delta$ ) are quoted in ppm and coupling constants ( $J$ ) are given in Hz (+/- 0.5 Hz).  $^1\text{H}$ ,  $^{13}\text{C}$  and  $^{31}\text{P}$  NMR chemical shifts were referenced internally to residual solvent resonances. All NMR data was acquired and processed using TopSpin<sup>TM</sup> version 3.2 from Bruker NMR software.<sup>4</sup>

Mass spectra were acquired using a Thermo Scientific LCQ Fleet (ESI-MS) mass spectrometer, or using a Thermo Scientific LTQ Orbitrap XL instrument at the Bioanalytical Mass Spectrometry Facility at UNSW. 'M' is defined as the molecular weight of the compound or cationic fragment of interest.

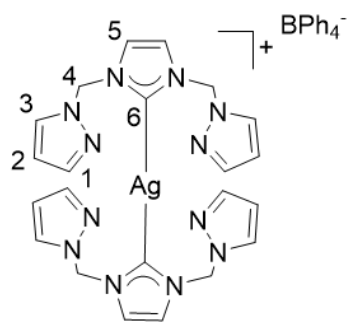
IR spectra were recorded as KBr discs using an Avatar 370 FTIR (resolution =  $1\text{ cm}^{-1}$ ) spectrometer at the University of New South Wales. Elemental analyses were carried out at the Campbell Microanalytical Lab, University of Otago, New Zealand,

Elemental Analysis Unit, The Research School of Chemistry, Australian National University and the Elemental Microanalysis Service at the Department of Chemistry and Biomolecular Sciences, Macquarie University.

Single crystal X-ray analyses were carried out at the Mark Wainwright Analytical Centre, University of New South Wales, Sydney. X-ray diffraction measurements were recorded on a Bruker Kappa APEXII CCD diffractometer using graphite-monochromated Mo-K $\alpha$  radiation ( $\lambda$ = 0.710723 Å). All structures were solved by direct methods and the full-matrix least-square refinements were carried out using SHELXL. Absorption correction was performed using Multi-scan SADABS and H-atom parameters were treated as constrained. CCDC 1480997 – 1481002 contains supplementary X-ray crystallographic data for complexes **2**, **3**, **4a**, **5** and **7**. The yields of hydrogenation products were determined using GCMS - QP2010 ULTRA.

## 6.1. Experimental for Chapter 2

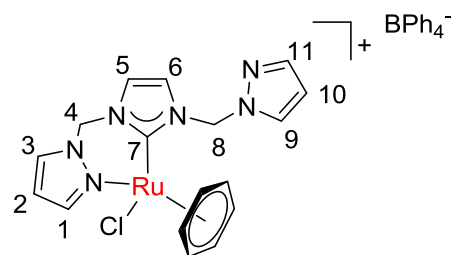
## 6.1.1. Synthesis of Ag(I) and Ru(II) complexes

Synthesis of  $[\text{Ag}(\text{NCN}^{\text{Me}})_2]\text{BPh}_4$  (2)

The imidazolium salt  $(\text{NCN}^{\text{Me}})\text{BPh}_4$  (**1**) (0.155 g, 0.287 mmol) and  $\text{Ag}_2\text{O}$  (0.090 g, 0.388 mmol) were suspended in 20 mL of dry  $\text{CH}_2\text{Cl}_2$ . The suspension was stirred for 16 hours at room temperature. The colourless solution was filtered using glass fibre (GF/C) filter paper and the

solvent removed under vacuum yielding a white precipitate.

Yield: 81%. Single crystals were grown by vapour diffusion of pentane into saturated  $\text{CH}_2\text{Cl}_2$  solution of complex **2**.  $^1\text{H}$  NMR (300 MHz,  $\text{CD}_2\text{Cl}_2$ ):  $\delta$  7.73 (d,  $^3J_{\text{H1-H2}} = 2.4$  Hz, 4H, H1), 7.58 (d,  $^3J_{\text{H3-H2}} = 1.8$  Hz, 4H, H3), 7.38 (m, 8H, *o*-BPh<sub>4</sub>), 7.20 (s, 4H, H5), 6.98 (t,  $^3J_{\text{H-H}} = 7.0$  Hz, 8H, *m*-BPh<sub>4</sub>), 6.89 (t,  $^3J_{\text{H-H}} = 7.2$  Hz, 4H, *p*-BPh<sub>4</sub>), 6.38 (dd,  $^3J_{\text{H2-H3}}/^3J_{\text{H2-H1}} = 2.1$  Hz, 4H, H2), 6.36 (s, 8H, H4) ppm.  $^{13}\text{C}$  NMR (75 MHz,  $\text{CD}_2\text{Cl}_2$ ):  $\delta$  183.9 (C6, identified through HMBC), 141.9 (C1), 136.3 (*o*-C of BPh<sub>4</sub>), 130.5 (C3), 126.1 (*m*-C of BPh<sub>4</sub>), 122.3 (*p*-C of BPh<sub>4</sub>), 122.2 (C5), 108.1 (C2), 65.3 (C4) ppm.

Synthesis of  $[\text{Ru}(\eta^6\text{-C}_6\text{H}_6)(\text{NCN})\text{Cl}]\text{BPh}_4$  (3)

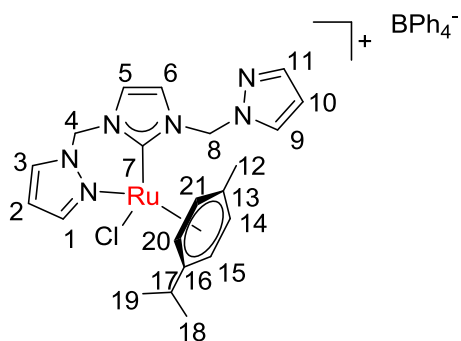
$[\text{Ag}(\text{NCN}^{\text{Me}})_2]\text{BPh}_4$  (**2**) (0.060 g, 0.068 mmol) and  $[\text{Ru}(\eta^6\text{-C}_6\text{H}_6)\text{Cl}_2]_2$  (0.034 g, 0.068 mmol) were dissolved in 20 mL of  $\text{CH}_2\text{Cl}_2$ . The mixture was stirred overnight at room temperature under an

atmosphere of argon. The resulting yellow mixture was filtered and pentane (40 mL)

was slowly added to the filtrate resulting in the precipitation of the complex  $[\text{Ru}(\eta^6\text{-C}_6\text{H}_6)(\text{NCN}^{\text{Me}})\text{Cl}]\text{BPh}_4$  (**3**) as a yellow powder.

Yield: 48%. Single crystals were grown by slow evaporation of a saturated methanol solution of **3**.  $^1\text{H}$  NMR (300 MHz,  $(\text{CD}_3)_2\text{CO}$ ):  $\delta$  8.19 (d,  $^3J_{\text{H1-H2}} = 2.2$  Hz, 1H, **H1**), 8.16 (d,  $^3J_{\text{H11-H10}} = 2.4$  Hz, 1H, **H11**), 8.14 (d,  $^3J_{\text{H3-H2}} = 2.8$  Hz, 1H, **H3**), 7.68 (d,  $^3J_{\text{H9-H10}} = 1.8$  Hz, 1H, **H9**), 7.63 (d,  $^3J_{\text{H5-H6}} = 2.2$  Hz, 1H, **H5**), 7.40 (d,  $^3J_{\text{H6-H5}} = 2.2$  Hz, 1H, **H6**), 7.37-7.30 (m, 8H, *o*-BPh<sub>4</sub>), 6.92 (t,  $^3J_{\text{H-H}} = 7.3$  Hz, 8H, *m*-BPh<sub>4</sub>), 6.86 (d,  $^2J_{\text{H4-H4}} = 13.9$  Hz, 1H, **H4**), 6.77 (t,  $^3J_{\text{H-H}} = 7.3$  Hz, 4H, *p*-BPh<sub>4</sub>), 6.75 (d,  $^2J_{\text{H8-H8}} = 13.9$  Hz, 1H, **H8**), 6.55 (dd,  $^3J_{\text{H2-H3}}/^3J_{\text{H2-H1}} = 2.4$  Hz, 1H, **H2**), 6.49 (d,  $^2J_{\text{H8-H8}} = 13.9$  Hz, 1H, **H8**), 6.40 (dd,  $^3J_{\text{H10-H9}}/^3J_{\text{H10-H11}} = 2.4$  Hz, 1H, **H10**), 6.21 (s, 6H, Ru-C<sub>6</sub>H<sub>6</sub>), 6.08 (d,  $^2J_{\text{H4-H4}} = 13.9$  Hz, 1H, **H4**) ppm.  $^{13}\text{C}\{^1\text{H}\}$  NMR (75 MHz,  $(\text{CD}_3)_2\text{CO}$ ):  $\delta$  177.8 (**C7**), 165.9-164.0 (q,  $^1J_{\text{C-B}} = 48.9$  Hz, *ipso*-C of BPh<sub>4</sub>), 149.4, (**C1**), 142.1 (**C9**) 137.0 (*o*-C of BPh<sub>4</sub>), 135.4 (**C3**), 132.2 (**C11**), 126.1 (*m*-BPh<sub>4</sub>), 124.1 (**C5**), 122.3 (*p*-BPh<sub>4</sub>& **C6**), 108.8 (**C2**), 107.7 (**C10**), 89.7 (Ru-C<sub>6</sub>H<sub>6</sub>), 64.9 (**C8**), 63.3 (**C4**) ppm. Elemental Analysis found: C, 64.69; H, 5.42; N, 10.85. Calc for Ru<sub>1</sub>C<sub>41</sub>H<sub>38</sub>N<sub>6</sub>B<sub>1</sub>: C, 64.83; H, 5.44; N, 10.80. ESI MS: (m/z 443.03) [**3**-BPh<sub>4</sub>]<sup>+</sup> amu.

#### Synthesis of $[\text{Ru}(\eta^6\text{-C}_{10}\text{H}_{14})(\text{NCN}^{\text{Me}})\text{Cl}]\text{BPh}_4$ (**4**)



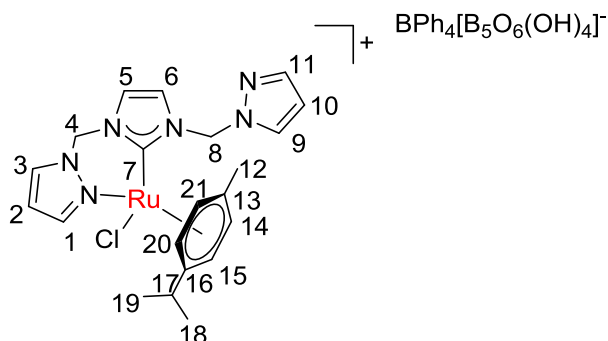
$\text{Ag}_2\text{O}$  (0.100 g, 0.432 mmol),  $\text{NCN}^{\text{Me}}\cdot\text{BPh}_4$  (**1**) (0.061 g, 0.120 mmol) and  $[\text{Ru}(\eta^6\text{-C}_{10}\text{H}_{14})\text{Cl}_2]_2$  (0.035 g, 0.056 mmol) were dissolved in 20 mL of dry  $\text{CH}_2\text{Cl}_2$ . The mixture was left stirring overnight

at room temperature under an  $\text{N}_2$  atmosphere. The resulting dark suspension was

filtered using glass fibre (GF/C) filter paper producing a yellow filtrate which was reduced to 10 mL. 40 mL of diethyl ether was slowly added to the solution to precipitate  $[\text{Ru}(\eta^6\text{-C}_{10}\text{H}_{14})(\text{NCN}^{\text{Me}})\text{Cl}]\text{BPh}_4$  as a yellow powder.

Yield: 51%.  $^1\text{H}$  NMR (400 MHz,  $\text{CD}_2\text{Cl}_2$ ):  $\delta$  7.87 (br d, 1H, **H1**), 7.77 (d,  $^3J_{\text{H9-H10}} = 2.4$  Hz, 1H, **H9**), 7.71 (br d, 1H, **H3**), 7.40 (br t, 8H, *o*-BPh<sub>4</sub>), 7.09 (d,  $^3J_{\text{H11-H10}} = 2.6$  Hz, 1H, **H11**), 7.06 (t,  $^3J_{\text{H-H}} = 7.5$  Hz, 8H, *m*-BPh<sub>4</sub>), 6.95 (t,  $^3J_{\text{H-H}} = 7.5$  Hz, 5H, *p*-BPh<sub>4</sub> & **H5**), 6.64 (d,  $^3J_{\text{H6-H5}} = 2.0$  Hz, 1H, **H6**), 6.53 (d,  $^2J_{\text{H4-H4}} = 13.8$  Hz, 1H, **H4**), 6.42 (m, 1H, **H2**), 6.38 (m, 1H, **H10**), 6.09 (d,  $^2J_{\text{H4-H4}} = 13.8$  Hz, 1H, **H4**), 5.90 (d,  $^3J_{\text{H20-H21}} = 6.2$  Hz, 1H, **H20**), 5.78 (d,  $^3J_{\text{H14-H15}} = 6.1$  Hz, 1H, **H14**), 5.47 (d,  $^3J_{\text{H21-H20}} = 6.2$  Hz, 1H, **H21**), 5.24 (d,  $^3J_{\text{H15-H14}} = 6.1$  Hz, 1H, **H15**), 4.75 (d,  $^2J_{\text{H8-H8}} = 14.1$  Hz, 1H, **H8**), 4.64 (d,  $^2J_{\text{H8-H8}} = 14.1$  Hz, 1H, **H8**), 2.64 (sept,  $^3J_{\text{H17-H18}}/^3J_{\text{H17-H19}} = 7.0$  Hz, 1H, **H17**), 2.07 (s, 3H, **H12**), 1.22-1.21 (2 x d,  $^3J_{\text{H18-H17}}/^3J_{\text{H19-H17}} = 2.1$  Hz, 6H, **H18** & **H19**) ppm.  $^{13}\text{C}\{^1\text{H}\}$  NMR (100 MHz,  $\text{CD}_2\text{Cl}_2$ ):  $\delta$  177.7 (**C7**), 164.8-163.4 (q,  $^1J = 49.3$  Hz *ipso*-C of BPh<sub>4</sub>), 148.4 (**C1**), 142.2 (**C11**), 136.4 (*o*-C of BPh<sub>4</sub>), 134.8 (**C3**), 131.2 (**C9**), 126.3 (*m*-C of BPh<sub>4</sub>), 123.4 (**C5**), 122.7 (*p*-C of BPh<sub>4</sub>), 121.2 (**C6**), 112.5 (**C16**), 108.6 (**C2**), 107.8 (**C10**), 102.6 (**C13**), 89.1 (**C20**), 86.9 (**C21**), 86.6 (**C14**), 84.3 (**C15**), 64.5 (**C8**), 61.8 (**C4**), 31.9 (**C17**), 23.7 (**C19**), 21.4 (**C18**), 18.9 (**C12**) ppm. Elemental Analysis found: C, 65.86; H, 5.77; N, 9.83 %. Calcd. for  $\text{Ru}_1\text{C}_{45}\text{H}_{46}\text{N}_6\text{B}_1$ : C, 65.97; H, 5.78; N, 10.26. ESI MS: (m/z 499.19) [**4**-BPh<sub>4</sub>]<sup>+</sup> amu.

### Synthesis of $[\text{Ru}(\eta^6\text{-C}_{10}\text{H}_{14})(\text{NCN}^{\text{Me}})\text{Cl}]\text{BPh}_4[\text{B}_5\text{O}_6(\text{OH})_4]$ (**4a**)

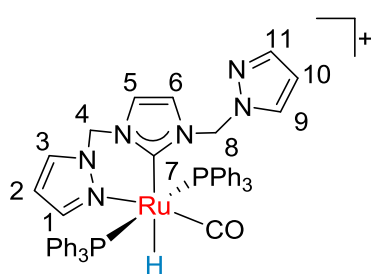


$[\text{Ag}(\text{NCN}^{\text{Me}})_2]\text{BPh}_4$  (**2**) (0.050 g, 0.056 mmol) and  $[\text{Ru}(\eta^6\text{-C}_{10}\text{H}_{14})\text{Cl}_2]_2$  (0.035 g, 0.056 mmol) were dissolved in 20 mL of dry  $\text{CH}_2\text{Cl}_2$ . The mixture was left

stirring overnight at room temperature under an  $\text{N}_2$  atmosphere. The resulting yellow mixture was filtered using glass fibre (GF/C) filter paper and the filtrate reduced to 10 mL. 40 mL of diethylether was slowly added to the solution to precipitate  $[\text{Ru}(\eta^6\text{-C}_{10}\text{H}_{14})(\text{NCN}^{\text{Me}})\text{Cl}]\text{BPh}_4[\text{B}_5\text{O}_6(\text{OH})_4]$  as a yellow powder.

Yield: 51%. Elemental Analysis found: C, 40.05; H, 4.08; N, 11.64. Calc. for  $[\text{Ru}(\eta^6\text{-C}_{10}\text{H}_{14})(\text{NCN}^{\text{Me}})\text{Cl}]14\%\text{BPh}_4.86\%[\text{B}_5\text{O}_6(\text{OH})_4]$ : C, 40.01; H, 4.44; N, 11.49. ESI MS: ( $m/z$  499.19)  $[\mathbf{4a}\text{-BPh}_4/\text{B}_5\text{O}_6(\text{OH})_4]^+$  amu.

### Synthesis of $[\text{Ru}(\text{H})\text{CO}(\text{NCN}^{\text{Me}})(\text{PPh}_3)_2]\text{BPh}_4$ (**5**)



$(\text{NCN}^{\text{Me}})\text{BPh}_4$  (**1**) (0.040 g, 0.073 mmol) and  $[\text{Ru}(\text{H})(\text{CO})\text{Cl}(\text{PPh}_3)_3]$  (0.070 g, 0.073 mmol) were suspended in 20 mL of dry MeOH and  $\text{NEt}_3$  (1 mL).

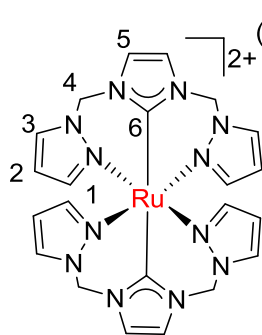
The mixture was refluxed for 2 hours. The

resulting pale yellow mixture was filtered using glass fibre (GF/B) filter paper. The beige filtrate was dried *in vacuo* to precipitate  $[\text{Ru}(\text{H})\text{CO}(\text{NCN}^{\text{Me}})(\text{PPh}_3)_2]\text{BPh}_4$  as a white solid. The crude product was washed with diethyl ether (2 x 20 mL) and dried under vacuum.



Yield: 40%. Single crystals were grown by vapour diffusion of diethyl ether into saturated dichloromethane solution of **5**.  $^1\text{H}$  NMR (300 MHz,  $(\text{CD}_3)_2\text{CO}$ ):  $\delta$  7.60 (d,  $^3J_{\text{H1-H2}} = 1.8$  Hz, 1H, **H1**), 7.57 (d,  $^3J_{\text{H5-H6}} = 2.1$  Hz, 1H, **H5**), 7.49 (d,  $^3J_{\text{H6-H5}} = 2.1$  Hz, 1H, **H6**), 7.48-7.30 (m, 40H, *o*-BPh<sub>4</sub>PPh<sub>3</sub>, **H3**, **H9**), 6.92 (t,  $^3J_{\text{H-H}} = 7.2$  Hz, 9H, *m*-BPh<sub>4</sub>, **H11**), 6.77 (br m,  $^3J_{\text{H-H}} = 7.2$  Hz, 4H, *p*-BPh<sub>4</sub>), 6.26 (dd,  $^3J_{\text{H2-H1}}/^3J_{\text{H2-H3}} = 1.8$  Hz, 1H, **H2**), 5.67 (br s, 2H, **H8**), 5.53 (dd,  $^3J_{\text{H10-H9}}/^3J_{\text{H10-H11}} = 1.8$  Hz, 1H, **H10**), 5.30 (br s, 2H, **H4**), -6.03 (t,  $^2J_{\text{H-P}} = 22.0$  Hz, 1H, Ru-**H**) ppm.  $^{13}\text{C}\{^1\text{H}\}$  NMR (75 MHz,  $\text{CD}_2\text{Cl}_2$ ):  $\delta$  206.7 (Ru-CO), 189.3 (**C7**), 149.3 (**C9**), 141.6 (**C3**), 136.3 (**C1**), 134.7-133.7 (4 x **C**, PPh<sub>3</sub>) 130.7 (3 x **C**, PPh<sub>3</sub>), 130.2 (**C11**), 129.3-129.0 (3 x **C**, PPh<sub>3</sub>) 126.2 (*m*-C of BPh<sub>4</sub>) 124.7 (**C5**), 122.4 (*o*-C of BPh<sub>4</sub>), 122.0 (**C6**), 107.5 (**C2**) 107.2 (**C10**), 62.1 (**C8**), 61.8 (**C4**) ppm.  $^{31}\text{P}$  NMR (121 MHz,  $(\text{CD}_3)_2\text{CO}$ ):  $\delta$  47.7 (**P**-Ru) ppm. Elemental analysis found: C, 70.93; H, 5.51; N, 6.90. Calc. for  $\text{Ru}_1\text{C}_{72}\text{H}_{63}\text{N}_6\text{B}$ . 0.25  $\text{CH}_2\text{Cl}_2$ : C, 70.93; H, 5.23; N, 6.87. ESI-MS: (*m/z* 883.26) [**5**-BPh<sub>4</sub>]<sup>+</sup>amu. IR (Solid): Ru-H: 1606.2  $\text{cm}^{-1}$ , Ru-C=O: 1938.3  $\text{cm}^{-1}$ .

### Synthesis of $[\text{Ru}(\text{NCN}^{\text{Me}})_2](\text{BPh}_4)_2$ (**7**)



$(\text{BPh}_4)_2^{2-}$  ( $\text{NCN}^{\text{Me}}\text{BPh}_4$  (**1**) (0.050 g, 0.092 mmol) and  $\text{RuCl}_3 \cdot x\text{H}_2\text{O}$  (0.024 g, 0.092 mmol) and  $\text{NEt}_3$  (1 mL) were suspended in 15 mL of dry ethanol. The mixture was refluxed for 16 hours. The resulting dark green solid,  $[\text{Ru}(\text{NCN}^{\text{Me}})_2](\text{BPh}_4)_2$  was separated from a pale yellow solution using glass fibre (GF/C) filter paper.

Yield: 65%. Single crystals were grown by slow evaporation of a saturated acetone solution of **7**.  $^1\text{H}$  NMR (400 MHz,  $(\text{CD}_3)_2\text{CO}$ ):  $\delta$  8.14 (d,  $^3J_{\text{H1-H2}} = 2.6$  Hz, 4H, **H1**), 7.85 (s, 4H, **H5**), 7.28 (m, 16H, *o*-BPh<sub>4</sub>), 6.88 (t,  $^3J_{\text{H-H}} = 7.3$  Hz, 16H, *m*-BPh<sub>4</sub>), 6.85 (d,  $^3J_{\text{H4-H4}} = 13.7$  Hz, 4H, **H4**), 6.73 (t,  $^3J_{\text{H-H}} = 7.2$  Hz, 8H, *p*-BPh<sub>4</sub>), 6.52 (d,  $^3J_{\text{H3-H2}} = 1.6$  Hz, 4H, **H3**), 6.17 (br m, 4H, **H2**), 5.97 (d,  $^3J_{\text{H4-H4}} = 13.7$  Hz, 4H, **H4**) ppm.  $^{13}\text{C}\{^1\text{H}\}$  NMR (100 MHz,  $(\text{CD}_3)_2\text{SO}$ ):  $\delta$  195.4 (**C6**), 164.3-162.3 (q,  $^1J = 49.8$  Hz, *ipso*-C of BPh<sub>4</sub>), 147.0 (**C1**), 136.1 (**C3**), 135.5 (*o*-BPh<sub>4</sub>), 125.2 (*m*-BPh<sub>4</sub>), 121.4, (*p*-BPh<sub>4</sub>), 120.8 (**C5**), 107.2 (**C2**), 62.4 (**C4**) ppm. Elemental analysis found: C, 70.17; H, 5.50; N, 14.05. Calc. for  $\text{Ru}_1\text{C}_{70}\text{H}_{64}\text{N}_{12}\text{B}_2$ : C, 70.18; H, 5.55; N, 14.03. ESI MS: ( $m/z$  279.08) [**7**-2(BPh<sub>4</sub>)]<sup>2+</sup> amu.

Catalysed Transfer Hydrogenation reactions using Ru(II) complexes 3, 4, 4a, 5, 5a and 7.

#### General procedure for Transfer Hydrogenation reactions

The transfer hydrogenation experiments were carried out under standard schlenk conditions. The substrates (0.25 mmol), catalyst (1.5 mol%) and base (KOH, 0.045 mmol) were mixed in 10 mL of 2-propanol. The mixture was heated to reflux (82 °C) for 24 hours. 1 mL aliquots were taken at regular intervals, which were quenched with cold isopropanol (1 mL) and filtered through a plug of silica. The crude products were diluted in dichloromethane and analysed using GC-MS analysis. Selected aliquots were also analysed using  $^1\text{H}$  NMR spectroscopy. Integration of selected resonance signals were compared in quantitative ratio between substrates and products. The GC-MS product yield values were consistently within 2% of the  $^1\text{H}$  NMR analysed yield values.

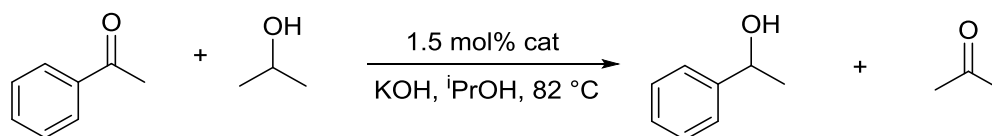
GC-MS analyses were performed on a Shimadzu QP2010 Plus gas chromatograph-mass spectrometer. A BP20 column was used, and the oven temperature was ramped from 50 to 220 °C at a rate of 10 °C min<sup>-1</sup>. Ultra high purity grade helium was used as the carrier gas. The screw-cap autosampler vials used were obtained from Agilent Technologies and were fitted with PTFE/silicone septa and 0.2 mL micro inserts. The identification of products was confirmed using GC-MS spectroscopy and  $^1\text{H}$  NMR spectroscopy, and the conversion of substrate to product(s) was monitored by GC-MS by comparing the peak areas of the product(s).

**Catalysed Transfer Hydrogenation of Acetophenone to form Acetophenol using Ru(II) complexes 3, 4, 4a, 5, 5a and 7.**

The catalysed transfer hydrogenation of acetophenone to form acetophenol at 80 °C was investigated using complexes;  $[\text{Ru}(\text{NCN}^{\text{Me}})_2](\text{BPh}_4)_2$  (**7**),  $[\text{Ru}(\text{H})\text{CO}(\text{NCN}^{\text{Me}})(\text{PPh}_3)_2]\text{BPh}_4$  (**5a**),  $[\text{Ru}(\text{CO})\text{H}(\text{NCN}^{\text{Me}})(\text{PPh}_3)_2]\text{BPh}_4$  (**5**),  $[\text{Ru}(\eta^6\text{-C}_6\text{H}_6)(\text{NCN}^{\text{Me}})\text{Cl}]\text{BPh}_4$  (**3**),  $[\text{Ru}(\eta^6\text{-C}_{10}\text{H}_{14})(\text{NCN}^{\text{Me}})\text{Cl}]\text{BPh}_4$  (**4**),  $[\text{Ru}(\eta^6\text{-C}_{10}\text{H}_{14})(\text{NCN}^{\text{Me}})\text{Cl}]\text{BPh}_4 \cdot [\text{B}_5\text{O}_6(\text{OH})_4]^-$  (**4a**). A typical reaction was performed as follows:

The catalyst was weighed in air and transferred to a schlenk flask. The flask was then filled with an inert atmosphere, 10 mL of 2-propanol added followed by subsequent addition of acetophenone (0.25 mmol) and base (KOH, 0.045 mmol). The mixture was heated to reflux (82 °C) for 24 hours. Refer to chapter 2, section 2.5 for final results.

**Table 6.1** Quantities of acetophenone and catalyst used.



Catalyst	Catalyst loading (mol %)	Mass of catalyst (mg)	Mass of Acetophenone (mg)
$[\text{Ru}(\eta^6\text{-C}_6\text{H}_6)(\text{NCN}^{\text{Me}})\text{Cl}]\text{BPh}_4$ ( <b>3</b> )	1.5	2.8	30 (0.02 mL)
$[\text{Ru}(\eta^6\text{-C}_{10}\text{H}_{14})(\text{NCN}^{\text{Me}})\text{Cl}]\text{BPh}_4$ ( <b>4</b> ).	1.5	3.0	30 (0.02 mL)
$[\text{Ru}(\eta^6\text{-C}_{10}\text{H}_{14})(\text{NCN}^{\text{Me}})\text{Cl}]\text{BPh}_4$ $[\text{B}_5\text{O}_6(\text{OH})_4]^-$ ( <b>4a</b> ).	1.5	3.2	30 (0.02 mL)

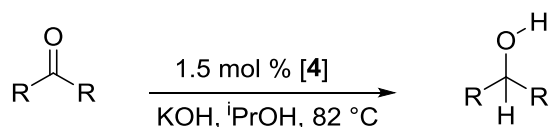
$[\text{Ru}(\text{H})\text{CO}(\text{NCN}^{\text{Me}})(\text{PPh}_3)_2]\text{BPh}_4$ <b>(5)</b>	1.5	4.2	30 (0.02 mL)
$[\text{Ru}(\text{CO})\text{H}(\text{NCN}^{\text{Me}})(\text{PPh}_3)_2]\text{BPh}_4$ <b>(5a),</b>	1.5	4.2	30 (0.02 mL)
$[\text{Ru}(\text{NCN}^{\text{Me}})_2](\text{BPh}_4)_2$ <b>(7),</b>	1.5	4.0	30 (0.02 mL)

### Catalysed transfer hydrogenation of ketones to form alcohols using Ru(II) complexes **4** and **4a**.

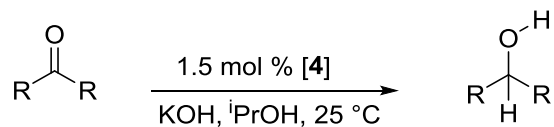
The catalysed transfer hydrogenation reaction of acetophenone, benzophenone, 4-nitroacetophenone, cyclohexanone and 2-hexanone was investigated at 25 and 82 °C using  $[\text{Ru}(\eta^6\text{-C}_{10}\text{H}_{14})(\text{NCN}^{\text{Me}})\text{Cl}]\text{BPh}_4$  (**4**) or  $[\text{Ru}(\eta^6\text{-C}_{10}\text{H}_{14})(\text{NCN}^{\text{Me}})\text{Cl}]\text{BPh}_4[\text{B}_5\text{O}_6(\text{OH})_4]$  (**4a**). A typical reaction was performed as follows:

The catalyst was weighed in air and transferred to a schlenk flask. The flask was then filled with an inert atmosphere, 10 mL of 2-propanol added followed by subsequent addition of substrate (0.25 mmol) and base (KOH, 0.045 mmol). The mixture was heated to reflux (82 °C) for 4 hours, or maintained at 25 °C for 24 hours. Refer to chapter 2, section 2.5 for final results.

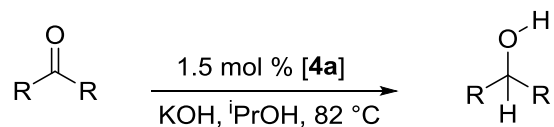
**Table 6.2** Quantities of catalyst **4** and substrates used at 82 °C.



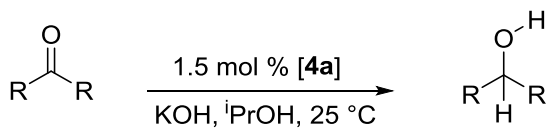
Substrate	Catalyst loading (mol %)	Mass of catalyst (mg)	Mass of substrate (mg)
Acetophenone	1.5	3.0	30 (0.02 mL)
Benzophenone	1.5	3.1	46
4-Nitroacetophenone	1.5	3.0	42
Cyclohexanone	1.5	3.0	24.5 (0.026 mL)
2-Hexanone	1.5	3.1	25 (0.031 mL)

**Table 6.3** Quantities of catalyst **4** and substrates used at RT.

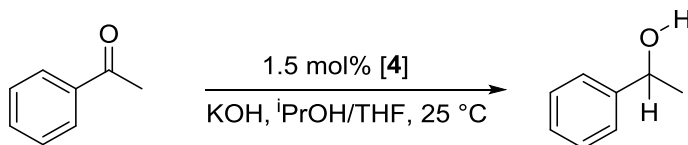
Substrate	Catalyst loading (mol %)	Mass of catalyst (mg)	Mass of Substrate (mg)
Acetophenone	1.5	3.0	30 (0.02 mL)
Benzophenone	1.5	3.0	46
4-Nitroacetophenone	1.5	3.2	43
Cyclohexanone	1.5	3.1	24.5 (0.026 mL)
2-Hexanone	1.5	3.0	25 (0.031 mL)

**Table 6.4** Quantities of catalyst **4a** and substrates used at 82 °C.

Substrate	Catalyst loading (mol %)	Mass of catalyst (mg)	Mass of Substrate (mg)
Acetophenone	1.5	3.3	30 (0.02 mL)
Benzophenone	1.5	3.4	45
4-Nitroacetophenone	1.5	3.4	43
Cyclohexanone	1.5	3.2	24.5 (0.026 mL)
2-Hexanone	1.5	3.3	25 (0.031 mL)

**Table 6.5** Quantities of catalyst **4a** and substrates used at RT.

Substrate	Catalyst loading (mol %)	Mass of catalyst (mg)	Mass of Substrate (mg)
Acetophenone	1.5	3.4	30 (0.02 mL)
Benzophenone	1.5	3.4	46
4-nitroacetophenone	1.5	3.3	44
cyclohexanone	1.5	3.2	24.5 (0.026 mL)
2-hexanone	1.5	3.3	25 (0.031 mL)

**Table 6.6** Quantities of catalyst **4a** and substrates used for *i*PrOH/THF solvent mix.

Substrate	Catalyst loading (mol %)	Mass of catalyst (mg)	Mass of Substrate (mg)
Acetophenone	1.5	3.1	30 (0.02 mL)



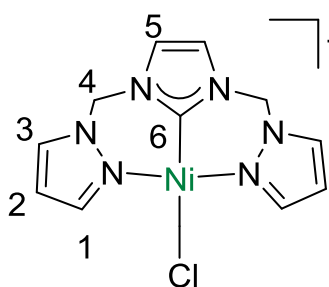
## 6.1.2. Crystal data for chapter 2

## Crystal data for ligand 1 and complexes 2, 3, 4a, 5, 6 and 7

	1	2	3	4a	5	6	7
Chemical formula	$C_{11}H_{13}N_6 \cdot C_{24}H_{20}B$	$2(C_{22}H_{24}AgN_{12}) \cdot C_{22}H_{23}AgN_{12} \cdot 3(C_{24}H_{20}B)$	$C_{17}H_{18}ClN_6Ru \cdot 3(C_{16}H_{18}ClN_7Ru) \cdot 4(C_{24}H_{20}B) \cdot 3(CH_4O)$	$C_{21}H_{26}ClN_6Ru \cdot B_5H_4O_{10}$	$C_{48}H_{43}N_6OP_2Ru \cdot C_{24}H_{20}B$	$C_{36}H_{30}Cl_2P_2Ru_2$	$C_{11}H_{12}N_6Ru_{0.5} \cdot C_{24}H_{20}B$
M (g mol <sup>-1</sup> )	548.48	2649.82	3150.53	717.08	1202.10	797.62	598.01
Crystal System	Orthorhombic	Triclinic	Triclinic	Monoclinic	Monoclinic	Orthorhombic	Monoclinic
Space Group	$P2_12_12_1$	$P\bar{1}$	$P\bar{1}$	$P2_1/n$	$P2_1/c$	$Pbcn$	$P2_1/n$
Crystal Habit							
Temperature (K)	150	150	150	150	150	150	150
a (Å)	8.5977 (3)	14.4586(6)	16.8274 (12)	11.3903 (4)	37.968 (2)	17.815 (4)	9.6717 (8)
b (Å)	17.9211 (6)	19.1802(7)	18.3619 (15)	11.8757 (4)	11.5676 (7),	20.572 (4)	15.4965 (13)
c (Å)	19.1642 (7)	24.5632(10)	24.387 (2)	23.6462 (9)	28.5760 (18)	18.093 (4)	19.8638 (18)
$\alpha$ (°)	90	99.448(2)	74.808 (4)	90	90		90
$\beta$ (°)	90	99.315(2)	89.916 (4)	101.366 (2)	92.123 (3)		91.611 (5)
$\gamma$ (°)	90	106.299(2)	81.797 (4)	90	90		90
V (Å <sup>3</sup> )	2952.82 (18)	6291.9 (4)	7192.5 (10)	3135.84 (19)	12542.0 (13)	6631 (2)	2976.0 (4)
Z	4	2	2	4	8	8	4
Radiation type	Mo K $\alpha$	Mo K $\alpha$	Mo K $\alpha$	Mo K $\alpha$	Mo K $\alpha$	Mo K $\alpha$	Mo K $\alpha$
$\mu$ (mm <sup>-1</sup> )	0.07	0.53	0.55	0.65	0.35	1.19	0.32
Crystal size (mm)	$0.46 \times 0.20 \times 0.15$	$0.26 \times 0.24 \times 0.08$	$0.12 \times 0.11 \times 0.05$	$0.21 \times 0.17 \times 0.06$	$0.23 \times 0.06 \times 0.04$	--	$0.15 \times 0.08 \times 0.05$
Tmin, Tmax	0.538, 0.746	0.692, 0.746	0.638, 0.746	0.660, 0.746	0.667, 0.746		0.636, 0.745
Refl. measured	14308	87774	112286	27698	27324	134939	20709
Unique reflections	6260	21420	25301	6813	27320	9474	5648
Obsd. Reflections	5658	13558	16486	5717	11308	9021	3092
[I > 2 $\sigma$ (I)]							
Rint	0.051	0.082	0.122	0.033	0.0000	0.053	0.111
R[F <sup>2</sup> > 2 $\sigma$ (F <sup>2</sup> )]	0.042	0.047	0.091	0.034	0.068	0.042	0.055
wR(F <sup>2</sup> )	0.105	0.117	0.240	0.094	0.172	0.152	0.133
S	1.04	1.00	1.03	1.06	0.88	1.43	1.00
Reflections used	6260	21420	25301	3796	27320	9474	5648
Parameters	379	1624	1861	413	1524	378	385
Restraints	0	482	H-atom parameters constrained	6	37	H-atom parameters constrained	122
$\Delta\rho_{max}, \Delta\rho_{min}$ (e Å <sup>-3</sup> )	0.24, -0.21	0.70, -0.70	4.71, -1.01	1.19, -0.77	1.36, -0.93	1.61, -2.95	0.50, -0.91

## 6.2. Experimental for chapter 3

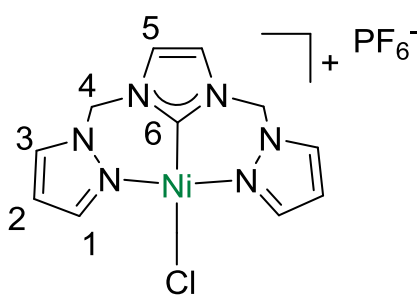
## 6.2.1. Synthesis of Ni(II) complexes

Synthesis of  $[\text{Ni}(\text{NCN}^{\text{Me}})\text{Cl}]\text{BPh}_4$  (**8**)

$[\text{Ag}(\text{NCN}^{\text{Me}})_2]\text{BPh}_4$  (**2**) (0.050 g, 0.056 mmol) and  $\text{Ni}(\text{PPh}_3)_2\text{Cl}_2$  (0.077 g, 0.118 mmol) were dissolved in 20 mL of dry THF. The mixture was left stirring overnight at room temperature under an  $\text{N}_2$

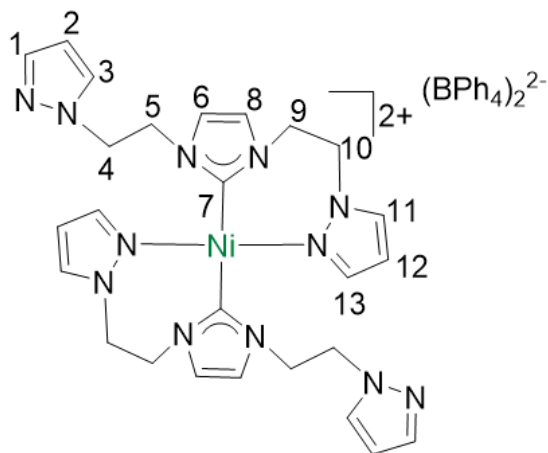
atmosphere. The resulting yellow mixture was filtered using glass fibre (GF/C) filter paper and the filtrate reduced to 10 mL. 40 mL of diethyl ether was slowly added to the solution to precipitate  $[\text{Ni}(\text{NCN}^{\text{Me}})\text{Cl}]\text{BPh}_4$  (**8**) as a yellow powder. Crystals suitable for X-ray crystallography were grown by vapour diffusion of diethyl ether into a saturated acetone (2 mL) solution of **8**.

Yield: 40%.  $^1\text{H}$  NMR (600 MHz,  $(\text{CD}_3)_2\text{CO}$ ):  $\delta$  8.29 (br d, 2H, **H3**), 8.18 (br d, 2H, **H1**), 7.70 (br s, 2H, **H5**), 7.37-7.30 (m, 8H, *o*-BPh<sub>4</sub>), 6.92 (t,  $^3J_{\text{H-H}} = 7.3$  Hz, 8H, *m*-BPh<sub>4</sub>), 6.95 (t,  $^3J_{\text{H-H}} = 7.3$  Hz, 4H, *p*-BPh<sub>4</sub>) 6.81 (br d, 4H, **H4**), 6.58 (m, 2H, **H2**).  $^{13}\text{C}\{^1\text{H}\}$  NMR (150 MHz,  $(\text{CD}_3)_2\text{CO}$ ):  $\delta$ , 164.3-163.3 (**C** ipso of BPh<sub>4</sub>), 147.6 (**C3**), 143.9 (**C6**), 136.9 (**C1**), 136.0 (*o*-**C** of BPh<sub>4</sub>), 125.6 (*m*-**C** of BPh<sub>4</sub>), 121.8 (*p*-**C** of BPh<sub>4</sub>), 122.0 (**C5**), 107.6 (**C2**), 61.9 (**C4**) ppm. Elemental analysis found: C, 65.54; H, 5.07; N, 13.04. Calc. for  $\text{NiC}_{35}\text{H}_{32}\text{B}_6\text{N}_6\text{Cl}$ : C, 65.52; H, 5.03; N, 13.10. ESI MS ( $m/z = 286.04704$ ) [**8-Cl**]<sup>+</sup>.

Synthesis of  $[\text{Ni}(\text{NCN}^{\text{Me}})\text{Cl}]\text{PF}_6$  (**9**)

$(\text{NCN}^{\text{Me}})\text{PF}_6$  (**1b**) (0.090 g, 0.242 mmol) and  $\text{Ag}_2\text{O}$  (0.150 g, 0.640 mmol) were mixed in 30 mL of dry  $\text{CH}_2\text{Cl}_2$  and the mixture was left stirring overnight at room temperature under an  $\text{N}_2$  atmosphere. Filtration of the dark mixture using glass fibre (GF/C) filter paper gave a colourless filtrate which was reduced to dryness. The resulting white powder was redissolved in 30 mL of dry THF to which  $\text{Ni}(\text{PPh}_3)_2\text{Cl}_2$  (0.158 g, 0.242 mmol) was added. The orange suspension was left stirring overnight at room temperature under an  $\text{N}_2$  atmosphere. The resulting yellow solution was filtered using glass fibre (GF/C) filter paper and the filtrate reduced to 10 mL. 40 mL of diethyl ether was slowly added to the solution to precipitate  $[\text{Ni}(\text{NCN}^{\text{Me}})\text{Cl}]\text{PF}_6$  (**9**) as a yellow powder. Crystals suitable for X-ray crystallography were grown by vapour diffusion of diethyl ether into a saturated acetone (2 mL) solution of **9**.

Yield: 62%.  $^1\text{H}$  NMR (600 MHz,  $(\text{CD}_3)_2\text{CO}$ ):  $\delta$  8.36 (br d, 2H, **H3**), 8.16 (br d, 2H, **H1**), 7.79 (br s, 2H, **H5**), 6.92 (br d, 4H, **H4**), 6.60 (m, 2H, **H2**).  $^{13}\text{C}\{^1\text{H}\}$  NMR (150 MHz,  $(\text{CD}_3)_2\text{CO}$ ):  $\delta$  147.6 (**C3**), 143.9 (**C6**), 136.9 (**C1**), 122.0 (**C5**), 107.6 (**C2**), 61.9 (**C4**) ppm. Elemental analysis found: C, 28.24; H, 2.52; N, 17.90. Calc. for  $\text{Ni}_1\text{C}_{11}\text{H}_{12}\text{P}_6\text{F}_6\text{Cl}_1$ : C, 28.27; H, 2.59; N, 17.98. ESI MS ( $m/z$  = 303.05)  $[\mathbf{9} + \text{OH}]^+$ .

Synthesis of  $[\text{Ni}(\text{NCN}^{\text{Et}})_2](\text{BPh}_4)_2$  (**10**)

$(\text{NCN}^{\text{Et}})\text{BPh}_4$  (**1c**) (0.100 g, 0.242 mmol) and KHMDS (0.150 g, 0.640 mmol) and  $\text{Ni}(\text{PPh}_3)_2\text{Cl}_2$  (0.158 g, 0.242 mmol) were mixed in 30 mL of dry THF and the resulting yellow mixture was left stirring overnight at room temperature

under an  $\text{N}_2$  atmosphere. The resulting yellow solution was filtered using glass fibre (GF/C) filter paper and the filtrate reduced to 10 mL. 40 mL of diethyl ether was slowly added to the solution to precipitate  $[\text{Ni}(\text{NCN}^{\text{Et}})_2](\text{BPh}_4)_2$  (**10**) as a yellow powder. Crystals suitable for X-ray crystallography were grown by vapour diffusion of diethyl ether into a saturated acetone (2 mL) solution of **10**.

Yield: 18%.  $^1\text{H}$  NMR (600 MHz,  $(\text{CD}_3)_2\text{CO}$ ):  $\delta$  8.11 (d,  $^3J_{\text{H}13-\text{H}12} = 2.3$  Hz, 2H, **H13**), 7.98 (br t, 2H, **H9a**), 7.84 (br d, 2H, **H1**), 7.60 (d,  $^3J_{\text{H}11-\text{H}12} = 2.3$  Hz, 2H, **H11**), 7.53 (d,  $^3J_{\text{H}8-\text{H}6} = 2.2$  Hz, 2H, **H8**), 7.49 (br d, 2H, **H6**), 7.47 (d,  $^3J_{\text{H}3-\text{H}2} = 2.2$  Hz, 2H, **H3**), 7.35-7.29 (m, 8H, *o*-BPh<sub>4</sub>), 6.94 (t,  $^3J_{\text{H}-\text{H}} = 7.3$  Hz, 8H, *m*-BPh<sub>4</sub>), 6.80 (t,  $^3J_{\text{H}-\text{H}} = 7.3$  Hz, 4H, *p*-BPh<sub>4</sub>), 6.42 (dd,  $^3J_{\text{H}12-\text{H}11}/^3J_{\text{H}12-\text{H}13} = 2.2$  Hz 4H, **H12**), 6.16 (br m, 2H, **H2**), 5.61 (br d, 2H, **H10a**), 5.58 (br d, 2H, **H10b**), 5.04 (br m, 2H, **H4a**) 4.88 (br m, 2H, **H9b**), 4.63 (br m, 2H, **H4b**), 4.37 (br m, 2H, **H5a**), 4.29 (br m, 2H, **H5b**).  $^{13}\text{C}\{^1\text{H}\}$  NMR (150 MHz,  $(\text{CD}_3)_2\text{CO}$ ):, 151.7 (**C7**), 147.6 (**C3**),  $\delta$ 142.5 (**C11**),  $\delta$ 141.9 (**C1**), 140.8 (**C10**), 136.0 (*o*-C of BPh<sub>4</sub>), 135.0 (**C13**), 131.1 (**C3**), 127 (**C8**), 125.6 (*m*-C of BPh<sub>4</sub>), 123.5 (**C6**), 121.8 (*p*-C of BPh<sub>4</sub>), 108.9 (**C12**), 105.5 (**C2**), 50.6 (**C5**), 50.0 (**C4**), 49.4 (**C9**), 48.7 (**C10**) ppm. Elemental analysis found: C, 72.07; H, 5.97; N, 13.04. Calc. for

$\text{Ni}_1\text{C}_{74}\text{H}_{72}\text{B}_2\text{N}_{12}$ : C, 73.47; H, 6.00; N, 13.89. ESI MS:  $m/z$  calculated for  $\text{Ni}_1\text{C}_{50}\text{H}_{52}\text{BN}_{12} = 889.38789$ . ESI MS: ( $m/z = 889.38823$ )  $[\mathbf{10}\text{-BPh}_4]^+$ .

### 6.2.2. Catalysed Kumada cross coupling reactions using complexes 8, 9 and 10.

#### General procedure for Kumada cross coupling reactions

THF used for catalysis reactions was distilled and dried using a sodium mirror and stored under an inert atmosphere. All substrates were purified by distillation and glassware oven-dried (120- 150°C) prior to use. The nickel complexes were pre-dried under vacuum prior to catalysis reactions. The Kumada cross coupling experiments were carried out under standard schlenk conditions. GC-MS analyses were performed on a Shimadzu QP2010 Plus gas chromatograph-mass spectrometer. A BP20 column was used, and the oven temperature was ramped from 50 to 220 °C at a rate of 10 °C min<sup>-1</sup>. UHP grade helium was used as the carrier gas. The screw-cap autosampler vials used were obtained from Agilent Technologies and were fitted with PTFE/silicone septa and 0.2 mL micro inserts. The identification of products was confirmed using GC-MS spectroscopy and <sup>1</sup>H NMR spectroscopy and the conversion of substrate to product(s) was monitored by GC-MS by comparing the peak areas of the product(s). All catalytic reactions were carried out in duplicates. A typical catalysed Kumada coupling experiment was performed as follows:

A Schlenk flask was charged with the catalyst (2 mol%) to which 10 mL of THF was cannulated in an inert atmosphere. The organohalide substrate (0.5 mmol) and phenylmagnesium bromide (1.5 mmol) were added subsequently using an air tight

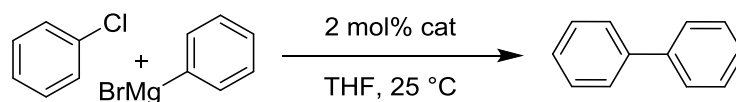
syringe. The mixture was stirred at 25 °C for 4 hours. Aliquots were taken at regular intervals, which were quenched with cold deionised H<sub>2</sub>O (1 mL) followed by the addition of Et<sub>2</sub>O (1 mL). The organic phase was extracted, dried using anhydrous MgSO<sub>4</sub> and filtered using a plug of silica. The crude products (2-3 drops of the Et<sub>2</sub>O phase) were diluted in 1 mL of dichloromethane and collected for GC-MS analysis.

The Et<sub>2</sub>O of selected reactions were also reduced to dryness under vacuum, dissolved in CD<sub>3</sub>Cl<sub>3</sub> and analysed using <sup>1</sup>H NMR spectra. Integration of selected resonance signals were compared in quantitative ratio between substrates and respective products.

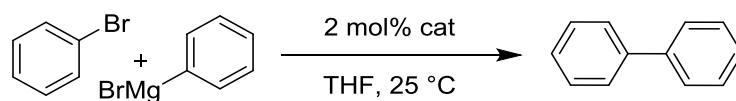
**Catalysed Kumada cross coupling reactions of aryl halides and phenylmagnesium bromide using complexes 8, 9 and 10.**

The Kumada cross coupling reaction of aryl halides with phenylmagnesium bromide was catalysed by the complex [Ni(NCN<sup>Me</sup>)Cl]BPh<sub>4</sub> (**8**), [Ni(NCN<sup>Me</sup>)Cl]PF<sub>6</sub> (**9**) or [Ni(NCN<sup>Et</sup>)<sub>2</sub>](BPh<sub>4</sub>)<sub>2</sub> (**10**). A typical reaction was performed as follows:

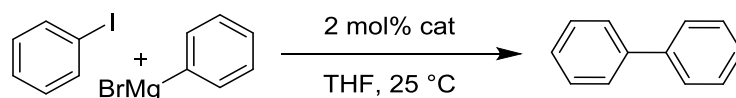
A schlenk flask was charged with the pre-dried catalyst (2 mol%) to which 10 mL of THF was cannulated in an inert atmosphere. The organohalide substrate (0.5 mmol) and phenylmagnesium bromide (1.5 mmol) were added subsequently using an air tight syringe. The mixture was stirred at 25 °C for 4 hours. Refer to chapter 3 section 3.4 for final results.

**Table 6.7** Quantities of catalyst and chlorobenzene and PhMgBr used.

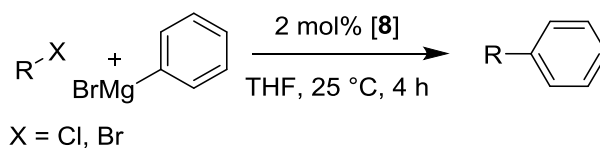
Catalyst	Catalyst loading (mol %)	Mass of catalyst (mg)	Volume of PhCl (mL)	Volume of PhMgBr (mL)
$[\text{Ni}(\text{NCN}^{\text{Me}})\text{Cl}]\text{BPh}_4$ ( <b>8</b> )	2.0	6.6	0.051	1.5
$[\text{Ni}(\text{NCN}^{\text{Me}})\text{Cl}]\text{PF}_6$ ( <b>9</b> )	2.0	4.7	0.051	1.5
$[\text{Ni}(\text{NCN}^{\text{Et}})_2](\text{BPh}_4)_2$ ( <b>10</b> )	2.0	6.0	0.025	0.75

**Table 6.8** Quantities of catalyst, bromobenzene and PhMgBr used.

Catalyst	Catalyst loading (mol %)	Mass of catalyst (mg)	Volume of PhBr (mL)	Volume of PhMgBr (mL)
$[\text{Ni}(\text{NCN}^{\text{Me}})\text{Cl}]\text{BPh}_4$ ( <b>8</b> )	2.0	6.5	0.053	1.5
$[\text{Ni}(\text{NCN}^{\text{Me}})\text{Cl}]\text{PF}_6$ ( <b>9</b> )	2.0	4.7	0.053	1.5
$[\text{Ni}(\text{NCN}^{\text{Et}})_2](\text{BPh}_4)_2$ ( <b>10</b> )	2.0	6.0	0.027	0.75

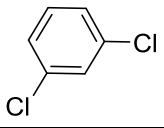
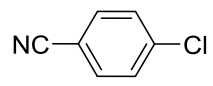
**Table 6.9** Quantities of catalyst and iodobenzene and PhMgBr used.

Catalyst	Catalyst loading (mol %)	Mass of catalyst (mg)	Volume of PhI (mL)	Volume of PhMgBr (mL)
$[\text{Ni}(\text{NCN}^{\text{Me}})\text{Cl}]\text{BPh}_4$ ( <b>8</b> )	2.0	6.5	0.056	1.5
$[\text{Ni}(\text{NCN}^{\text{Me}})\text{Cl}]\text{PF}_6$ ( <b>9</b> )	2.0	4.6	0.056	1.5

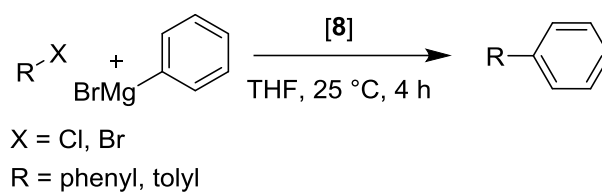
**Table 6.10** Quantities of catalyst and substrates used.

Substrate	Catalyst loading (mol %)	Mass of catalyst (mg)	Mass of substrate (mg)	Volume of PhMgBr (mL)
	2.0	6.6	85.5	1.5
	2.0	3.3	46.8	0.75
	2.0	3.3	73.1	0.75
	2.0	3.3	56.2	0.75
	2.0	3.4	83.9	0.75



	2.0	3.4	37.1	0.75
	2.0	3.3	34.4	0.75

Refer to chapter 3 section 3.4 for final results.

**Table 6.11** Quantities of catalyst 8 and substrates used.

Substrate	Catalyst loading (mol %)	Mass of catalyst (mg)	Volume(mL) or mass(mg) of Substrate	Volume of PhMgBr (mL)
Phenyl chloride	1.0	3.3	0.051 mL	1.5
Phenyl Bromide	1.0	3.3	0.053 mL	1.5
Tolyl Bromide	5.0	6.6	34.2 mg	0.6

## 6.2.3. Crystal data for chapter 3

## Crystal data for ligand 1c

p21byn\_a

## Crystal data

Chemical formula	$C_{13}H_{17}N_6 \cdot C_{24}H_{20}B$
$M_r$	576.53
Crystal system, space group	Monoclinic, $P2_1/n$
Temperature (K)	150
$a, b, c$ (Å)	11.3106 (4), 17.5185 (8), 15.8531 (6)
$\beta$ (°)	100.0240 (16)
$V$ (Å <sup>3</sup> )	3093.3 (2)
$Z$	4
Radiation type	Mo $K\alpha$
$\mu$ (mm <sup>-1</sup> )	0.07
Crystal size (mm)	$0.27 \times 0.17 \times 0.07$

## Data collection

Diffractometer	Bruker APEX-II CCD
Absorption correction	Multi-scan <i>SADABS2012/1</i> (Bruker, 2012) was used for absorption correction. $wR2(int)$ was 0.0758 before and 0.0528 after correction. The Ratio of minimum to maximum transmission is 0.8924. The 1/2 correction factor is 0.0015.
$T_{min}, T_{max}$	0.665, 0.746
No. of measured, independent and observed [ $I >$ $2s(I)$ ] reflections	27165, 6757, 5114
$R_{int}$	0.048
$(\sin \theta / \lambda)_{max}$ (Å <sup>-1</sup> )	0.640

## Refinement

$R[F^2 > 2s(F^2)],$ $wR(F^2), S$	0.044, 0.111, 1.02
No. of reflections	6757
No. of parameters	397
H-atom treatment	H-atom parameters constrained
$D\rho_{max}, D\rho_{min}$ (e Å <sup>-3</sup> )	0.25, -0.22

Computer programs: *SAINT* v8.34A (Bruker, 2013), *SHELXL* (Sheldrick, 2008), *Olex2* (Dolomanov *et al.*, 2009).

## Crystal data for complex 8

	ashwin_31oct13_a
Crystal data	
Chemical formula	$\text{C}_{11}\text{H}_{12}\text{ClN}_6\text{Ni}\cdot\text{C}_3\text{H}_6\text{O}\cdot\text{C}_{24}\text{H}_{20}\text{B}$
$M_r$	699.71
Crystal system, space group	Monoclinic, $P2_1/c$
Temperature (K)	150
$a, b, c$ (Å)	16.0883 (12), 12.3222 (8), 18.5299 (15)
$\beta$ (°)	109.158 (3)
$V$ (Å <sup>3</sup> )	3470.0 (4)
$Z$	4
Radiation type	Mo $K\alpha$
$\mu$ (mm <sup>-1</sup> )	0.68
Crystal size (mm)	$0.09 \times 0.09 \times 0.03$
Data collection	
Diffractometer	Bruker APEX-II CCD
Absorption correction	Multi-scan SADABS2012/1 (Bruker,2012) was used for absorption correction. $wR2(\text{int})$ was 0.1184 before and 0.0785 after correction. The Ratio of minimum to maximum transmission is 0.8131. The $\lambda/2$ correction factor is 0.0015.
$T_{\min}, T_{\max}$	0.606, 0.746
No. of measured, independent and observed [ $I >$ $2\sigma(I)$ ] reflections	23797, 6092, 3657
$R_{\text{int}}$	0.110
$(\sin \theta/\lambda)_{\max}$ (Å <sup>-1</sup> )	0.595
Refinement	
$R[F^2 > 2\sigma(F^2)],$ $wR(F^2), S$	0.055, 0.131, 1.01
No. of reflections	6092
No. of parameters	454
No. of restraints	18
H-atom treatment	H-atom parameters constrained
$\Delta\rho_{\max}, \Delta\rho_{\min}$ (e Å <sup>-3</sup> )	0.38, -0.39

Computer programs: *SHELXL* (Sheldrick, 2008), *Olex2* (Dolomanov *et al.*, 2009).

## Crystal data for complex 9

	p-1_a
Crystal data	
Chemical formula	$C_{11}H_{12}ClN_6Ni \cdot F_6P$
$M_r$	467.40
Crystal system,	Triclinic, $P\bar{1}$
space group	
Temperature (K)	100
$a, b, c$ (Å)	7.9770 (16), 8.7170 (17), 12.200 (2)
$\alpha, \beta, \gamma$ (°)	91.69 (3), 104.13 (3), 104.66 (3)
$V$ (Å <sup>3</sup> )	792.1 (3)
$Z$	2
Radiation type	Synchrotron, $\lambda = 0.71073$ Å
$\mu$ (mm <sup>-1</sup> )	1.57
Crystal size (mm)	$0.02 \times 0.01 \times 0.01$
Data collection	
Diffractometer	Bruker APEX-II CCD
Absorption	—
correction	
No. of measured,	16062, 4211, 3991
independent and	
observed [ $I >$	
$2\sigma(I)$ ] reflections	
$R_{int}$	0.036
$(\sin \theta/\lambda)_{max}$ (Å <sup>-1</sup> )	0.705
Refinement	
$R[F^2 > 2\sigma(F^2)],$	0.038, 0.100, 1.09
$wR(F^2), S$	
No. of reflections	4211
No. of parameters	235
H-atom treatment	H-atom parameters constrained
$D\rho_{max}, D\rho_{min}$ (e Å <sup>-3</sup> )	0.66, -0.85

Computer programs: BluIce (McPhillips, 2002), XDS (Kabsch, 1993), *SIR2004* (Burla *et al.*, 2007), *SHELXL* (Sheldrick, 2008), Olex2 (Dolomanov *et al.*, 2009).

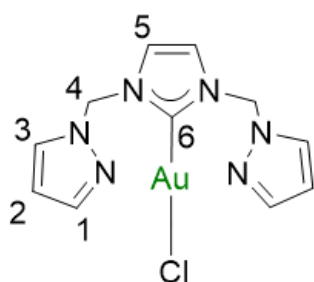
## Crystal data for complex 10

	ashwin_26aug14_0m
Crystal data	
Chemical formula	$C_{12.25}H_{14.25}N_{5.75}Ni_{0.5} \cdot C_8H_8N_4Ni_{0.5} \cdot C_{24}H_{15}B \cdot C_{24}H_{19}B$
$M_r$	1171.39
Crystal system, space group	Monoclinic, $P2/n$
Temperature (K)	150
$a, b, c$ (Å)	23.4252 (19), 12.5805 (9), 24.392 (2)
$\beta$ (°)	118.202 (3)
$V$ (Å <sup>3</sup> )	6334.9 (9)
$Z$	4
Radiation type	Mo $K\alpha$
$\mu$ (mm <sup>-1</sup> )	0.36
Crystal size (mm)	××
Data collection	
Diffractometer	Bruker APEX-II CCD
Absorption correction	Multi-scan SADABS2014/5 (Bruker,2014/5) was used for absorption correction. $wR2(int)$ was 0.1903 before and 0.0707 after correction. The Ratio of minimum to maximum transmission is 0.7724. The $1/2$ correction factor is 0.00150.
$T_{min}, T_{max}$	0.576, 0.746
No. of measured, independent and observed [ $I >$ $2\sigma(I)$ ] reflections	54182, 14136, 4841
$R_{int}$	0.177
$(\sin \theta / \lambda)_{max}$ (Å <sup>-1</sup> )	0.646
Refinement	
$R[F^2 > 2\sigma(F^2)],$ $wR(F^2), S$	0.176, 0.481, 1.80
No. of reflections	14136
No. of parameters	674
No. of restraints	705
H-atom treatment	H-atom parameters constrained
$D\rho_{max}, D\rho_{min}$ (e Å <sup>-3</sup> )	2.71, -1.22

Computer programs: *SAINT* v8.37A (Bruker, 2015), *XT* (Sheldrick, 2015), *SHELXL* (Sheldrick, 2015), *Olex2* (Dolomanov *et al.*, 2009).

## 6.3. Experimental for chapter 4

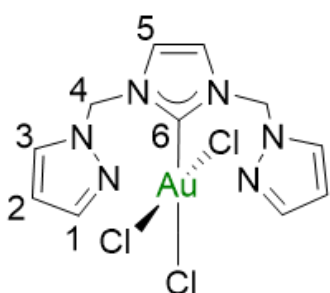
## 6.3.1. Synthesis of Au(I) and Au(III) complexes

Synthesis of Au(I)(NCN<sup>Me</sup>)Cl (11)

(NCN<sup>Me</sup>)BPh<sub>4</sub> (**1**) (0.050 g, 0.092 mmol) and NEt<sub>3</sub> (1 mL) were suspended in 20 mL of dry CH<sub>2</sub>Cl<sub>2</sub> to which [HAuCl<sub>4</sub>.xH<sub>2</sub>O] (0.036 g, 0.092 mmol) dissolved in 5 mL of methanol was added. The resulting grey-white suspension was stirred at room

temperature for 16 hours. The mixture was then filtered using a GF/C filter producing a colourless solution. The filtrate was reduced in vacuo to 10 mL and pentane (40 mL) added to precipitate a grey-white solid, the solid was washed with distilled water (25 mL), diethyl ether (25 mL) and dried in vacuo.

Yield: 40%. <sup>1</sup>H NMR (600 MHz, (CD<sub>3</sub>)<sub>2</sub>CO): δ 8.07 (d, <sup>3</sup>J<sub>H3-H2</sub> = 2.5 Hz, 2H, H3), 7.54 (s, 2H, H5), 7.53 (d, <sup>3</sup>J<sub>H1-H2</sub> = 1.5 Hz, 2H, H1), 6.55 (s, 4H, H4), 6.33 (m, 2H, H2) ppm. <sup>13</sup>C{<sup>1</sup>H} NMR (150 MHz, (CD<sub>3</sub>)<sub>2</sub>CO): δ 172.9 (C6), 141.9 (C1), 131.5 (C3), 122.6 (C5), 107.6 (C2), 65.1 (C4) ppm. Elemental analysis found: C, 30.06; H, 2.91; N, 17.62. Calc. for Au<sub>1</sub>C<sub>11</sub>H<sub>12</sub>N<sub>6</sub>Cl.0.2C<sub>5</sub>H<sub>12</sub>: C, 30.34; H, 3.06; N, 17.69. ESI MS: (m/z= 425.0778) [**11**-Cl]<sup>+</sup>.

Synthesis of Au(III)(NCN<sup>Me</sup>)Cl<sub>3</sub> (12)

[Ag(NCN<sup>Me</sup>)<sub>2</sub>]BPh<sub>4</sub> (**2**) (0.10 g, 0.11 mmol) was dissolved in 20 mL of dry CH<sub>2</sub>Cl<sub>2</sub> to which a solution of [HAuCl<sub>4</sub>.xH<sub>2</sub>O] (0.09g, 0.22mmol) in ethanol (5 mL) was added. The resulting yellow suspension was stirred at room temperature in an N<sub>2</sub>

atmosphere for 16 h. Filtration using GF/C filter paper (cannulation) produced a clear

yellow filtrate solution which was reduced in vacuo to 10 mL in volume. Pentane (40 mL) was added to the solution slowly to precipitate the complex as a yellow solid. The mixture was filtered using GF/B filter and the product dried in vacuo.

Yield: 50 %.  $^1\text{H}$  NMR (600 MHz,  $(\text{CD}_3)_2\text{CO}$ ):  $\delta$  8.08 (d,  $^3J_{\text{H3-H2}} = 2.4$  Hz, 2H, H3), 7.82 (s, 2H, H5), 7.60 (d,  $^3J_{\text{H1-H2}} = 1.6$  Hz, 2H, H1), 6.78 (s, 4H, H4), 6.37 (m, 2H, H2) ppm.  $^{13}\text{C}\{^1\text{H}\}$  NMR (150 MHz,  $(\text{CD}_3)_2\text{CO}$ ):  $\delta$  142.9 (C6), 142.4 (C3), 132.0 (C1), 125.4 (C5), 108.2 (C2), 64.4 (C4) ppm. Elemental analysis found: C, 24.86; H, 2.16; N, 15.26. Calc. for  $\text{Au}_1\text{C}_{11}\text{H}_{12}\text{N}_6\text{Cl}_3$ : C, 24.85; H, 2.28; N, 15.81. ESI MS: ( $m/z = 495.0155$ )  $[\mathbf{12-Cl}]^+$ .

### 6.3.2. Catalysed dihydroalkoxylation reactions using complexes 11 and 12

#### General method for catalysed dihydroalkoxylation reactions

A Young's NMR tube was charged with 1 mol% catalyst and 1.1 equiv. of  $\text{NaBAr}^{\text{F}}_4$ , relative to the amount of substrate. In an Argon filled glovebox, the alkyne diol substrate (0.2 mmol) was subsequently added to the Young's NMR tube, followed by 0.6 mL of  $\text{C}_2\text{D}_2\text{Cl}_4$ . The samples were frozen at  $-72^\circ\text{C}$  in an acetone/liquid  $\text{N}_2$  slush bath and thawed directly before injecting the sample into the NMR instrument for analysis. The temperature of the NMR spectrometer was calibrated using an Omega Microprocessor Thermometer (HH23) that was fitted with a K-type thermocouple immersed in ethylene glycol or ethanol. The identification of products was confirmed using  $^1\text{H}$  NMR spectroscopy with reference to literature.<sup>5</sup> Refer to chapter 4 section 4.4 for final results. All catalytic reactions were carried out in duplicate. TONs were determined by dividing the moles of substrate converted by moles of catalyst used. TOFs (error =  $\pm 1\%$ ) were determined by dividing TON by time at 50% conversion.



**Catalysed dihydroalkoxylation of **14** using Au(I) complex **11** or Au(III) complex **12**:**

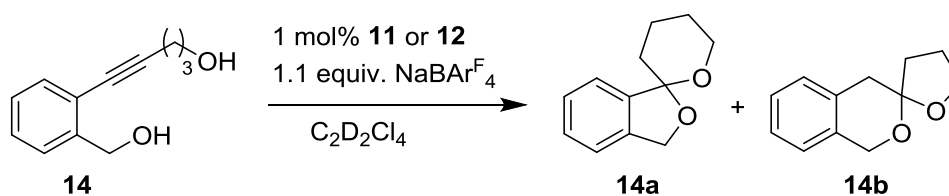
The catalysed dihydroalkoxylation reaction of **14** was catalysed by the complexes

[Au(I)(NCN<sup>Me</sup>)Cl] (**11**) and [Au(III)(NCN<sup>Me</sup>)Cl<sub>3</sub>] (**12**). A typical reaction was performed as

follows:

The Au(I) catalyst **11** or Au(III) catalyst **12** (1 mol%), NaBAR<sup>F</sup><sub>4</sub> (1.1 equiv.) and **14** (0.036 g, 0.2 mmol) were weighed in air using a 5 decimal point balance and transferred into an NMR tube fitted with a Youngs<sup>TM</sup> valve. Substrate **14** was not allowed to come in contact with the catalyst in the weighing process. The sample was brought into a nitrogen filled glovebox where C<sub>2</sub>D<sub>2</sub>Cl<sub>4</sub> (0.6 mL) was added slowly without allowing contact with substrate **14**. The samples were thoroughly mixed upon removal from the glovebox, immediately frozen at -72 °C in an acetone/liquid N<sub>2</sub> slush bath and thawed directly before injecting the sample into the NMR instrument for analysis. The reactions were monitored by <sup>1</sup>H NMR spectroscopy while maintaining a constant temperature of 100, 80, 70, 40 or 25 °C.

**Table 6.12** Quantities of catalyst and substrate **14** used.



Catalyst (loading)	Temperature(°C)	Mass of catalyst (mg)	Mass of <b>14</b> (mg)
<b>11</b> (1 mol%)	100	0.98	37
<b>11</b> (1 mol%)	80	0.94	37

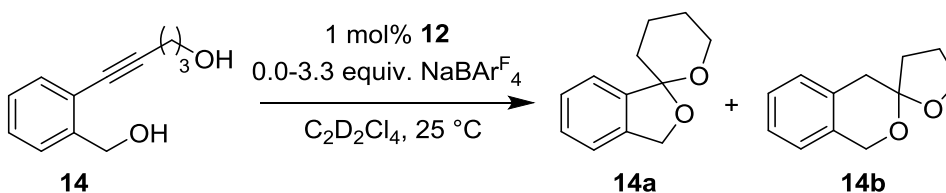
<b>11</b> (1 mol%)	70	0.96	38
<b>11</b> (1 mol%)	25	0.96	38
<b>12</b> (1 mol%)	70	1.06	38
<b>12</b> (1 mol%)	25	1.06	37

**Catalysed dihydroalkoxylation of **14** using **12**, variation in NaBAr<sup>F</sup><sub>4</sub> loading.**

The catalysed dihydroalkoxylation reaction of **14** was catalysed by the complex [Au(III)(NCN<sup>Me</sup>)Cl<sub>3</sub>] (**12**) with varying amounts of NaBAr<sup>F</sup><sub>4</sub>.

The Au(III) catalyst **12** (1 mol%), NaBAr<sup>F</sup><sub>4</sub> (0.0-3.3 equiv.) and **14** (0.036g, 0.2mmol) were weighed in air using a 5 decimal point balance and transferred into an NMR tube fitted with a Youngs<sup>TM</sup> valve. Substrate **14** was not allowed to come in contact with the catalyst in the weighing process. The sample was brought into a nitrogen filled glovebox where C<sub>2</sub>D<sub>2</sub>Cl<sub>4</sub> (0.6 mL) was added slowly without allowing contact with substrate **14**. The samples were thoroughly mixed upon removal from the glovebox, immediately frozen at -72 °C in an acetone/liquid N<sub>2</sub> slush bath and thawed directly before injecting the sample into the NMR instrument for analysis. The reaction was monitored by <sup>1</sup>H NMR spectroscopy while maintaining a constant temperature of 25 °C.

**Table 6.13** Quantities of catalyst **12**, NaBAr<sup>F</sup><sub>4</sub> and substrate **14** used.



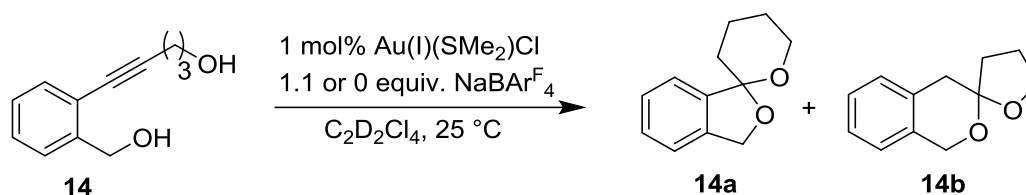
Catalyst (loading)	NaBAr <sup>F</sup> <sub>4</sub> (loading)	Mass of catalyst (mg)	Mass of NaBAr <sup>F</sup> <sub>4</sub> (mg)	Mass of <b>14</b> (mg)
<b>12</b> (1 mol%)	0.0 equiv.	1.06	0	38
<b>12</b> (1 mol%)	1.1 equiv.	1.06	1.98	38
<b>12</b> (1 mol%)	2.2 equiv.	1.04	3.98	37

12 (1 mol%)	3.3 equiv.	1.05	6.01	38
-------------	------------	------	------	----

#### Catalysed dihydroalkoxylation of **14** using Au(I)(SMe<sub>2</sub>)Cl:

The catalysed dihydroalkoxylation reaction of **14** was catalysed by the complex [Au(I)(SMe<sub>2</sub>)Cl] with varying amounts of NaBAr<sup>F</sup><sub>4</sub>. A typical reaction was performed as follows:

The Au(I) catalyst **Au(I)(SMe<sub>2</sub>)Cl** (1 mol%), NaBAr<sup>F</sup><sub>4</sub> (0.0 or 1.1 equiv.) and **14** (0.036g, 0.2mmol) were weighed in air using a 5 decimal point balance and transferred into an NMR tube fitted with a Youngs<sup>TM</sup> valve. Substrate **14** was not allowed to come in contact with the catalyst in the weighing process. The sample was brought into a nitrogen filled glovebox where C<sub>2</sub>D<sub>2</sub>Cl<sub>4</sub> (0.6 mL) was added slowly without allowing contact with substrate **14**. The samples were thoroughly mixed upon removal from the glovebox, immediately frozen at -72 °C in an acetone/liquid N<sub>2</sub> slush bath and thawed directly before injecting the sample into the NMR instrument for analysis. The reaction was monitored by <sup>1</sup>H NMR spectroscopy while maintaining a constant temperature of 25 °C.

**Table 6.14** Quantities of catalyst,  $\text{NaBAR}^{\text{F}}_4$  and substrate **14** used.

Catalyst (loading)	$\text{NaBAR}^{\text{F}}_4$ (loading)	Mass of catalyst (mg)	Mass of $\text{NaBAR}^{\text{F}}_4$ (mg)	Mass of <b>14</b> (mg)
$[\text{Au(I)(SMe}_2\text{)Cl}]$ (1 mol%)	0.0 equiv.	0.70	0	37
$[\text{Au(I)(SMe}_2\text{)Cl}]$ (1 mol%)	1.1 equiv.	0.71	1.99	37

#### Catalysed dihydroalkoxylation of **14**, kinetic studies using $\text{Au(III)}$ complex **12**:

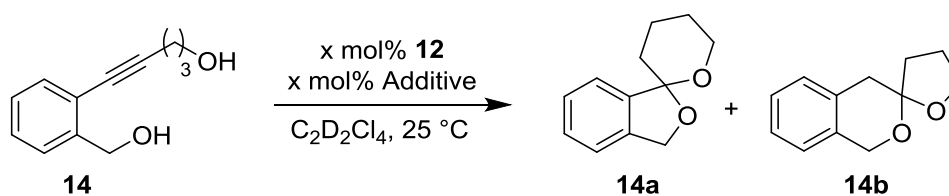
The catalysed dihydroalkoxylation reaction of **14** was catalysed by the complex

$[\text{Au(III)(NCN}^{\text{Me}}\text{)Cl}_3]$  (**12**) with varying amounts of  $\text{NaBAR}^{\text{F}}_4$  or  $\text{AgSbF}_6$ . A typical reaction was performed as follows:

The  $\text{Au(III)}$  catalyst **12** (1 mol%),  $\text{NaBAR}^{\text{F}}_4$  or  $\text{AgSbF}_6$  (1.1 equivalent) and **14** (0.036g, 0.2mmol) were weighed in air, and **14** was transferred into an NMR tube fitted with a Youngs<sup>TM</sup> valve. Sample vials containing the  $\text{Au(III)}$  catalyst **12** and  $\text{NaBAR}^{\text{F}}_4$  or  $\text{AgSbF}_6$  were introduced separately from the NMR tube containing **14** into a nitrogen filled glove box. The  $\text{Au(III)}$  catalyst **12** and  $\text{NaBAR}^{\text{F}}_4$  or  $\text{AgSbF}_6$  were dissolved in 1 mL of  $\text{C}_2\text{D}_2\text{Cl}_4$  from which 0.1 mL (0.1 mol%) and 0.01 mL (0.01 mol%) of the sample were extracted. These 0.1 mL and 0.01 mL of samples were diluted separately to a total volume of 0.6 mL of  $\text{C}_2\text{D}_2\text{Cl}_4$  and added to the NMR tubes containing the substrate **14**. The samples were thoroughly mixed upon removal from the glovebox, immediately frozen at  $-72\text{ }^\circ\text{C}$  in an acetone/liquid  $\text{N}_2$  slush bath and thawed directly before injecting the sample into the NMR instrument for analysis.

The reaction was monitored by  $^1\text{H}$  NMR spectroscopy while maintaining a constant temperature of 40 or 25 °C.

**Table 6.15** Quantities of catalyst,  $\text{NaBAr}^{\text{F}}_4$ ,  $\text{AgSbF}_6$  and substrate **14** used.



Catalyst (loading)	Additive (loading)	Mass of catalyst (mg)	Mass of Additive (mg)	Mass of 14 (mg)
<b>12 (1 mol%)</b>	$\text{NaBAr}^{\text{F}}_4$ (1.1 equivalent)	1.06	1.98	38
<b>12 (0.1 mol%)</b>	$\text{NaBAr}^{\text{F}}_4$ (0.11 equivalent)	Diluted from 1 mL of 1 mol% stock solution	Diluted from 1 mL of 1 mol% stock solution	Diluted from 1 mL of 1 mol% stock solution
<b>12 (0.01 mol%)</b>	$\text{NaBAr}^{\text{F}}_4$ (0.011 equivalent)	Diluted from 1 mL of 0.1 mol% stock solution	Diluted from 1 mL of 0.1 mol% stock solution	Diluted from 1 mL of 0.1 mol% stock solution
<b>12 (1 mol%)</b>	$\text{AgSbF}_6$ (1.1 equivalent)	1.05	0.7	37

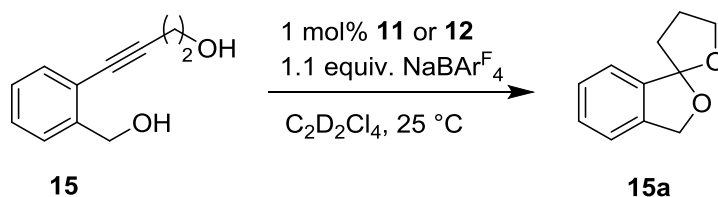
12 (0.1 mol%)	AgSbF <sub>6</sub> (0.11 equivalent)	0.3	0.2	11
---------------	---	-----	-----	----

**Catalysed dihydroalkoxylation of **15** using Au(I) complex **11** or Au(III) complex **12**:**

The catalysed dihydroalkoxylation reaction of **15** was catalysed by the complexes [Au(I)(NCN<sup>Me</sup>)Cl] (**11**) and [Au(III)(NCN<sup>Me</sup>)Cl<sub>3</sub>] (**12**). A typical reaction was performed as follows:

The Au(I) catalyst **11** or Au(III) catalyst **12** (1 mol%), NaBAR<sup>F</sup><sub>4</sub> (1.1 equiv.) and **15** (0.034g, 0.2mmol) were weighed in air using a 5 decimal point balance and transferred into an NMR tube fitted with a Youngs<sup>TM</sup> valve. Substrate **15** was not allowed to come in contact with the catalyst in the weighing process. The sample was brought into a nitrogen filled glovebox where C<sub>2</sub>D<sub>2</sub>Cl<sub>4</sub> (0.6 mL) was added slowly without allowing contact with substrate **15**. The samples were thoroughly mixed upon removal from the glovebox, immediately frozen at -72 °C in an acetone/liquid N<sub>2</sub> slush bath and thawed directly before injecting the sample into the NMR instrument for analysis. The reaction was monitored by <sup>1</sup>H NMR spectroscopy while maintaining a constant temperature of 25 °C.

**Table 6.16** Quantities of catalyst and substrate **15** used.



Catalyst (loading)	Mass of catalyst(mg)	Mass of 15 (mg)
<b>11</b> (1 mol%)	0.98	34
<b>12</b> (1 mol%)	1.05	34

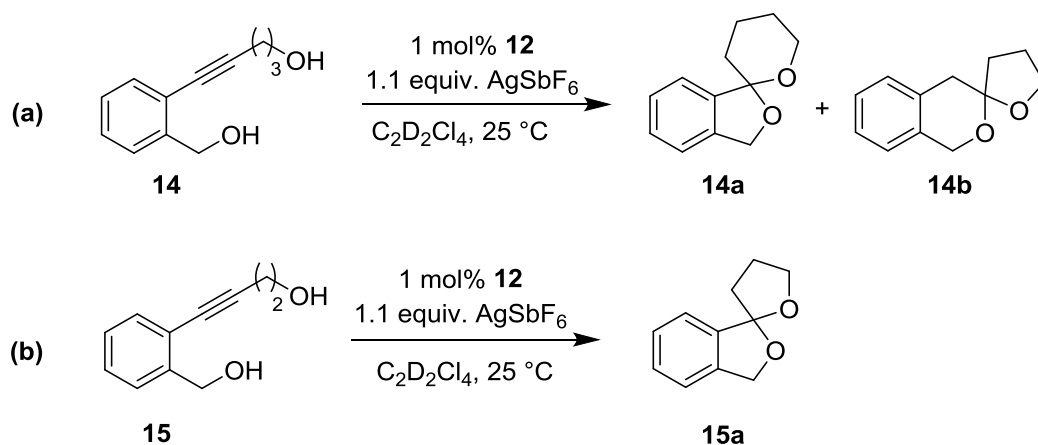


**Catalysed dihydroalkoxylation of **14** and **15** using Au(III) complex **12** and AgSbF<sub>6</sub>:**

The catalysed dihydroalkoxylation reaction of **14** and **15** was catalysed by the complex [Au(III)(NCN<sup>Me</sup>)Cl<sub>3</sub>] (**12**). A typical reaction was performed as follows:

The Au(III) catalyst **12** (1 mol%), AgSbF<sub>6</sub> (1.1 equiv.) and **14** (0.036g, 0.2mmol) or **15** (0.034g, 0.2mmol) were weighed in air using a 5 decimal point balance and transferred into an NMR tube fitted with a Youngs<sup>TM</sup> valve. Substrate **14** and **15** were not allowed to come in contact with the catalyst in the weighing process. The samples were brought into a nitrogen filled glovebox where C<sub>2</sub>D<sub>2</sub>Cl<sub>4</sub> (0.6 mL) was added slowly without allowing contact with the substrates. The samples were thoroughly mixed upon removal from the glovebox, immediately frozen at -72 °C in an acetone/liquid N<sub>2</sub> slush bath and thawed directly before injecting the sample into the NMR instrument for analysis. The reactions were monitored by <sup>1</sup>H NMR spectroscopy while maintaining a constant temperature of 25 °C.

**Table 6.17** Quantities of catalyst and substrate **14**, **15** used. Refer to Chapter 4 section 4.4 for final results.

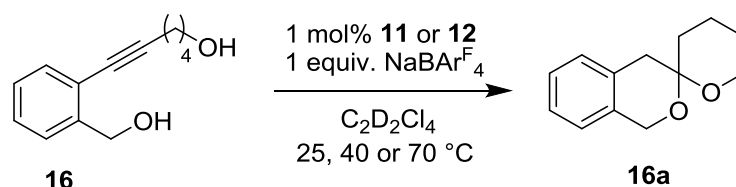


Catalyst (loading)	Mass of catalyst (mg)	Mass of 14 or 15 (mg)
<b>12</b> (1 mol%)	0.104	<b>14</b> (37)
<b>12</b> (1 mol%)	0.105	<b>15</b> (35)

#### Catalysed dihydroalkoxylation of **16** using Au(III) complexes **11** or **12**:

The catalysed dihydroalkoxylation reaction of **16** was catalysed by the complex  $[\text{Au(III)}(\text{NCN}^{\text{Me}})\text{Cl}_3]$  (**11**) or  $[\text{Au(III)}(\text{NCN}^{\text{Me}})\text{Cl}_3]$  (**12**). A typical reaction was performed as follows:

The Au(I) catalyst **11** or Au(III) catalyst **12** (1 mol%),  $\text{NaBAR}_4^{\text{F}}$  (1.1 equiv.) and **16** (0.038 g, 0.2mmol) were weighed in air using a 5 decimal point balance and transferred into an NMR tube fitted with a Youngs<sup>TM</sup> valve. Substrate **16** was not allowed to come in contact with the catalyst in the weighing process. The sample was brought into a nitrogen filled glovebox where  $\text{C}_2\text{D}_2\text{Cl}_4$  (0.6 mL) was added slowly without allowing contact with substrate **16**. The samples were thoroughly mixed upon removal from the glovebox, immediately frozen at -72 °C in an acetone/liquid  $\text{N}_2$  slush bath and thawed directly before injecting the sample into the NMR instrument for analysis. The reactions were monitored by  $^1\text{H}$  NMR spectroscopy while maintaining a constant temperature of 40 or 25 °C.

**Table 6.18** Quantities of catalyst and substrate **16** used.

Catalyst (loading)	Temperature (°C)	Mass of catalyst (mg)	Mass of 16 (mg)
11 (1 mol%)	70	0.99	38
12 (1 mol%)	25	0.105	39
12 (1 mol%)	40	0.105	38

### 6.3.3. Catalysed hydroamination reactions using complexes **11** and **12**

#### General method for hydroamination

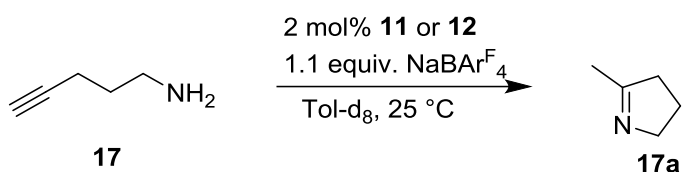
Alkynamines **17** and **18** were synthesised using literature procedures.<sup>6</sup> A Youngs<sup>TM</sup> NMR tube was charged with 2 mol% catalyst and 1.1 equiv. of NaBARF<sub>4</sub> (unless otherwise stated). The substrate (0.2mmol) was subsequently added and 0.6 mL of Tol-d<sub>8</sub> was added to the mix in an Ar atmosphere (Ar glovebox). The samples were frozen at -72 °C in an acetone/liquid N<sub>2</sub> slush bath and thawed before injecting the sample into the NMR instrument for analysis. Thermometer (HH23) that was fitted with a K-type thermocouple immersed in ethylene glycol or ethanol. The identification of products was confirmed using <sup>1</sup>H NMR spectroscopy with reference to literature.<sup>7</sup> Integration of selected resonance signals were compared in quantitative ratio between substrates and respective products.

**Catalysed hydroamination of 17 using Au(I) complex 11 or Au(III) complex 12:**

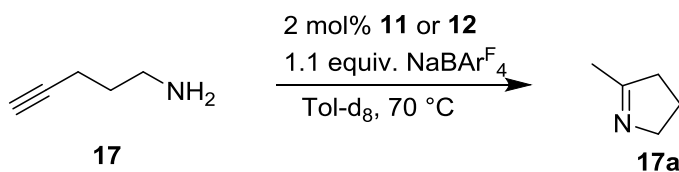
The catalysed hydroamination reaction of **17** was catalysed by the complexes [Au(I)(NCN<sup>Me</sup>)Cl] (**11**) and [Au(III)(NCN<sup>Me</sup>)Cl<sub>3</sub>] (**12**). A typical reaction was performed as follows:

The Au(I) catalyst **11** or Au(III) catalyst **12** (2 mol%), NaBAR<sup>F</sup><sub>4</sub> (1.1 equiv.) and **17** (0.0174 g, 0.2 mmol) were weighed in air using a 5 decimal point balance. The catalyst and NaBAR<sup>F</sup><sub>4</sub> were transferred into an NMR tube fitted with a Youngs<sup>TM</sup> valve and were brought into an Argon filled glovebox where Tol-d<sub>8</sub> (0.6 mL) was added. **17** (0.0174 g, 0.2 mmol) was added to the samples upon removal from the glovebox, mixed thoroughly and the NMR tubes were immediately frozen at -72 °C in an acetone/liquid N<sub>2</sub> slush bath and thawed directly before injecting the sample into the NMR instrument for analysis. The reaction was monitored by <sup>1</sup>H NMR spectroscopy while maintaining a constant temperature of 100, 70 or 25 °C.

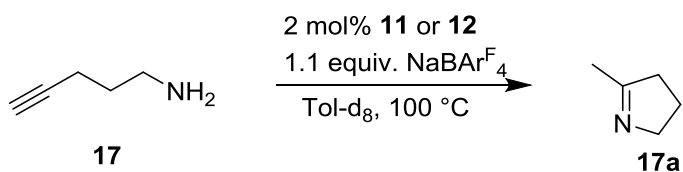
**Table 6.19** Quantities of catalyst and substrate **17** used at RT. Refer to chapter 4 section 4.5 for final results.



Catalyst (loading)	Mass of catalyst (mg)	Mass of 17 (mg)
<b>11</b> (1 mol%)	1.8	17.4
<b>12</b> (1 mol%)	2.2	17.4

**Table 6.20** Quantities of catalyst and substrate **17** used at 70 °C.

Catalyst (loading)	Mass of catalyst (mg)	Mass of <b>17</b> (mg)
<b>11</b> (1 mol%)	1.8	17.2
<b>12</b> (1 mol%)	2.2	17.4

**Table 6.21** Quantities of catalyst and substrate **17** used at 100 °C.

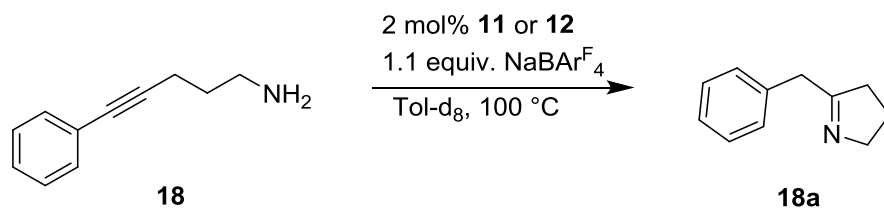
Catalyst (loading)	Mass of catalyst (mg)	Mass of <b>17</b> (mg)
<b>11</b> (1 mol%)	1.8	17.1
<b>12</b> (1 mol%)	2.2	17.2

**Catalysed hydroamination of **18** using Au(I) complex **11** or Au(III) complex **12**:**

The catalysed hydroamination reaction of **18** was catalysed by the complexes [Au(I)(NCN<sup>Me</sup>)Cl] (**11**).and [Au(III)(NCN<sup>Me</sup>)Cl<sub>3</sub>] (**12**). A typical reaction was performed as follows:

The Au(I) catalyst **11** or Au(III) catalyst **12** (2 mol%), NaBAR<sup>F</sup><sub>4</sub> (1.1 equiv.) and **18** (0.0326 g, 0.2mmol) were weighed in air using a 5 decimal point balance. The catalyst and NaBAR<sup>F</sup><sub>4</sub> were transferred into an NMR tube fitted with a Youngs<sup>TM</sup> valve and were brought into a nitrogen filled glovebox where Tol-d<sub>8</sub> (0.6 mL) was added. **18** (0.0326g, 0.2mmol) was added to the samples upon removal from the glovebox, mixed thoroughly and the NMR tubes were immediately frozen at -72 °C in an acetone/liquid N<sub>2</sub> slush bath and thawed directly before injecting the sample into the NMR instrument for analysis. The reaction was monitored by <sup>1</sup>H NMR spectroscopy while maintaining a constant temperature of 100 °C.

**Table 6.22** Quantities of catalyst and substrate **18** used. Refer to chapter 4 section 4.5 for final results.



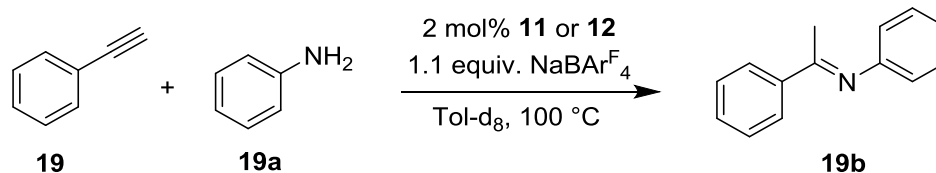
Catalyst (loading)	Mass of catalyst (mg)	Mass of <b>18</b> (mg)
<b>11</b> (1 mol%)	1.9	32.6
<b>12</b> (1 mol%)	2.2	32.6

**Catalysed hydroamination of 19 + 19a using Au(I) complex 11 or Au(III) complex 12:**

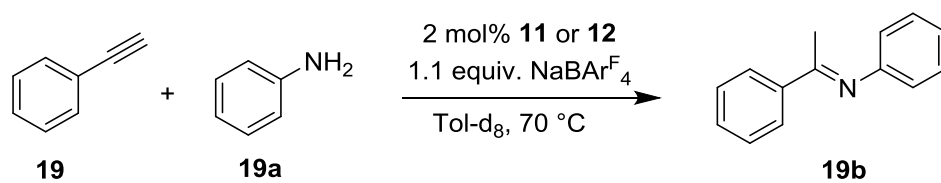
The catalysed hydroamination reaction of **19** + **19a** was catalysed by the complexes [Au(I)(NCN<sup>Me</sup>)Cl] (**11**) and [Au(III)(NCN<sup>Me</sup>)Cl<sub>3</sub>] (**12**). A typical reaction was performed as follows:

The Au(I) catalyst **11** or Au(III) catalyst **12** (2 mol%), NaBAR<sup>F</sup><sub>4</sub> (1.1 equiv.), **19** (0.0337 g, 0.2 mmol) and **19a** (0.0307 g, 0.2 mmol) were weighed in air using a 5 decimal point balance. The catalyst and NaBAR<sup>F</sup><sub>4</sub> were transferred into an NMR tube fitted with a Youngs<sup>TM</sup> valve and were brought into a nitrogen filled glovebox where Tol-d<sub>8</sub> (0.6 mL) was added. **19** (0.0337 g, 0.2 mmol) and **19a** (0.0307 g, 0.2 mmol) were added to the samples in the NMR tubes upon removal from the glovebox. This was mixed thoroughly and the NMR tubes were immediately frozen at -72 °C in an acetone/liquid N<sub>2</sub> slush bath and thawed directly before injecting the sample into the NMR instrument for analysis. The reaction was monitored by <sup>1</sup>H NMR spectroscopy while maintaining a constant temperature of 100 or 70 °C.

**Table 6.23** Quantities of catalyst and substrate **19/19a** used at 100 °C. Refer to chapter 4 section 4.5 for final results.



Catalyst (loading)	Mass of catalyst (mg)	Mass of 19 (mg)	Mass of 19a (mg)
<b>11</b> (1 mol%)	3.0	33.7	30.7
<b>12</b> (1 mol%)	3.5	33.8	30.7

**Table 6.24** Quantities of catalyst and substrate **19/19a** used at 70 °C. Refer to chapter 4 section 4.5 for final results.

Catalyst (loading)	Mass of catalyst (mg)	Mass of 189 (mg)	Mass of 19a (mg)
<b>11</b> (1 mol%)	3.0	33.7	30.6
<b>12</b> (1 mol%)	3.5	33.8	30.7



## 6.3.4. Crystal data for chapter 4

[Au(I)(NCN<sup>Me</sup>)Cl] complex 11 crystal data

Crystal data	CCDC (1495705)
Chemical formula	C <sub>22</sub> H <sub>24</sub> Au <sub>2</sub> Cl <sub>2</sub> N <sub>12</sub>
<i>M</i> <sub>r</sub>	921.35
Crystal system, space group	Monoclinic, <i>P</i> 2 <sub>1</sub> / <i>n</i>
Temperature (K)	150
<i>a</i> , <i>b</i> , <i>c</i> (Å)	10.5781 (5), 10.8458 (5), 12.0025 (5)
β (°)	101.132 (2)
<i>V</i> (Å <sup>3</sup> )	1351.11 (11)
<i>Z</i>	2
Radiation type	Mo <i>K</i> α
μ (mm <sup>-1</sup> )	11.08
Crystal size (mm)	0.40 × 0.40 × 0.40
Data collection	
Diffractometer	Bruker Kappa Apex2
Absorption correction	Multi-scan <i>SADABS</i> (Siemens, 1996)
<i>T</i> <sub>min</sub> , <i>T</i> <sub>max</sub>	0.01, 0.01
No. of measured, independent and observed [ <i>I</i> > 2.0σ( <i>I</i> )] reflections	16358, 2945, 2696
<i>R</i> <sub>int</sub>	0.064
(sin θ/λ) <sub>max</sub> (Å <sup>-1</sup> )	0.639
Refinement	
<i>R</i> [ <i>F</i> <sup>2</sup> > 2σ( <i>F</i> <sup>2</sup> )], <i>wR</i> ( <i>F</i> <sup>2</sup> ), <i>S</i>	0.029, 0.075, 0.98
No. of reflections	2937
No. of parameters	173
H-atom treatment	H-atom parameters constrained
Δρ <sub>max</sub> , Δρ <sub>min</sub> (e Å <sup>-3</sup> )	2.68, -2.67

Computer programs: Apex2 (Bruker AXS, 2006), *SHELXS* 86 (Sheldrick, 1986), *CRYSTALS* (Betteridge *et al.*, 2003), *CAMERON* (Watkin *et al.*, 1996).

**[Au(III)(NCN<sup>Me</sup>)Cl] complex 12 crystal data**

Crystal data	CCDC (1495706)
Chemical formula	C <sub>11</sub> H <sub>12</sub> AuCl <sub>3</sub> N <sub>6</sub>
<i>M</i> <sub>r</sub>	531.58
Crystal system, space group	Triclinic, <i>P</i> 1
Temperature (K)	150
<i>a</i> , <i>b</i> , <i>c</i> (Å)	8.3986 (18), 9.666 (2), 10.058 (2)
$\alpha$ , $\beta$ , $\gamma$ (°)	93.034 (9), 101.256 (8), 99.441 (9)
<i>V</i> (Å <sup>3</sup> )	786.9 (3)
<i>Z</i>	2
Radiation type	Mo <i>K</i> α
$\mu$ (mm <sup>-1</sup> )	9.86
Crystal size (mm)	0.20 × 0.20 × 0.06
Data collection	
Diffractometer	Bruker Kappa Apex2
Absorption correction	Multi-scan <i>SADABS</i> (Siemens, 1996)
<i>T</i> <sub>min</sub> , <i>T</i> <sub>max</sub>	0.55, 0.55
No. of measured, independent and observed [ <i>I</i> > 2.0σ( <i>I</i> )] reflections	16689, 3371, 3283
<i>R</i> <sub>int</sub>	0.035
(sin θ/λ) <sub>max</sub> (Å <sup>-1</sup> )	0.637
Refinement	
<i>R</i> [ <i>F</i> <sup>2</sup> > 2σ( <i>F</i> <sup>2</sup> )], <i>wR</i> ( <i>F</i> <sup>2</sup> ), <i>S</i>	0.014, 0.034, 1.01
No. of reflections	3360
No. of parameters	190
H-atom treatment	H-atom parameters constrained
Δρ <sub>max</sub> , Δρ <sub>min</sub> (e Å <sup>-3</sup> )	1.09, -0.85

Computer programs: Apex2 (Bruker AXS, 2006), *SHELXS* 86 (Sheldrick, 1986), *CRYSTALS* (Betteridge *et al.*, 2003), *CAMERON* (Watkin *et al.*, 1996).

#### 6.4. References

- (1) Mancano, G.; Page, M. J.; Bhadbhade, M.; Messerle, B. A. *Inorg. Chem.* **2014**, *53*, 10159.
- (2) Bennett, M. A.; Huang, T. N.; Matheson, T. W.; Smith, A. K. *Inorg. Synth.* **1982**, *21*, 74.
- (3) Prasanna, N.; Srinivasan, S.; Rajagopal, G.; Athappan, P. R. *Indian J. Chem., Sect A.* **2001**, *40A*, 426.
- (4) Bruker NMR Software, *Topspin* ; 3.2, **2013**.
- (5) (a) Elgafi, S.; Field, L. D.; Messerle, B. A. *Organomet. Chem.* **2000**, *607*, 97; (b) Messerle, B. A.; Vuong, K. Q. *Organometallics* **2007**, *26*, 3031.
- (6) Hultsch, K. C.; Hampel, F.; Wagner, T. *Organometallics* **2004**, *23*, 2601.
- (7) (a) Li, Y.; Marks, T. J. *J. Am. Chem. Soc.* **1996**, *118*, 9295; (b) Burling, S.; Field, L. D.; Messerle, B. A.; Rumble, S. L. *Organometallics* **2007**, *26*, 4335.

---

## Chapter 7. Appendices

---

### 7.1. X-ray crystallographic data

The X-ray diffraction measurements were carried out on a Bruker APEX II diffractometer (Graphite monochromator ( $\phi$  and  $\omega$  scans)) at 150 K Symmetry related absorption corrections using the program SADABS2 were applied and the data were corrected for Lorentz and polarisation effects using Bruker APEX2 software.<sup>1</sup> All structures were solved by direct methods and the full-matrix least-square refinements were carried out using SHELXL.<sup>2</sup> The molecular graphics were generated using Mercury or ORTEP.<sup>3</sup>

#### 7.1.1. Crystal data for ligand 1

##### Selected geometric parameters (Å)

N1A—N2A	1.355 (3)	C14—C15	1.369 (4)
N1A—C1	1.431 (3)	C15—H15	0.9500
N1A—C3A	1.340 (4)	C15—C16	1.397 (3)
N1B—C1	1.471 (3)	C16—H16	0.9500
N1B—C1B	1.322 (3)	C21—C22	1.416 (3)
N1B—C3B	1.374 (3)	C21—C26	1.400 (3)
N1C—N2C	1.351 (3)	C21—B1	1.633 (3)
N1C—C2	1.436 (3)	C22—H22	0.9500
N1C—C3C	1.348 (3)	C22—C23	1.375 (4)
N2A—C1A	1.328 (4)	C23—H23	0.9500
N2B—C1B	1.325 (3)	C23—C24	1.386 (3)
N2B—C2	1.468 (3)	C24—H24	0.9500
N2B—C2B	1.374 (3)	C24—C25	1.382 (3)
N2C—C1C	1.322 (4)	C25—H25	0.9500
C1—H1A	0.9900	C25—C26	1.387 (3)
C1—H1B	0.9900	C26—H26	0.9500
C1A—H1AA	0.9500	C31—C32	1.395 (3)
C1A—C2A	1.383 (5)	C31—C36	1.404 (3)
C1B—H1BA	0.9500	C31—B1	1.649 (3)
C1C—H1C	0.9500	C32—H32	0.9500
C1C—C2C	1.390 (4)	C32—C33	1.390 (3)
C2—H2A	0.9900	C33—H33	0.9500
C2—H2B	0.9900	C33—C34	1.376 (3)
C2A—H2AA	0.9500	C34—H34	0.9500

C2A—C3A	1.356 (4)	C34—C35	1.390 (3)
C2B—H2BA	0.9500	C35—H35	0.9500
C2B—C3B	1.343 (3)	C35—C36	1.382 (3)
C2C—H2C	0.9500	C36—H36	0.9500
C2C—C3C	1.354 (4)	C41—C42	1.393 (3)
C3A—H3A	0.9500	C41—C46	1.406 (3)
C3B—H3B	0.9500	C41—B1	1.648 (3)
C3C—H3C	0.9500	C42—H42	0.9500
C11—C12	1.399 (4)	C42—C43	1.392 (3)
C11—C16	1.396 (3)	C43—H43	0.9500
C11—B1	1.648 (3)	C43—C44	1.377 (3)
C12—H12	0.9500	C44—H44	0.9500
C12—C13	1.389 (3)	C44—C45	1.376 (4)
C13—H13	0.9500	C45—H45	0.9500
C13—C14	1.379 (4)	C45—C46	1.391 (3)
C14—H14	0.9500	C46—H46	0.9500

## Selected geometric parameters (°)

N2A—N1A—C1	118.4 (2)	C14—C15—C16	120.3 (2)
C3A—N1A—N2A	112.5 (2)	C16—C15—H15	119.9
C3A—N1A—C1	128.6 (2)	C11—C16—C15	122.6 (2)
C1B—N1B—C1	125.5 (2)	C11—C16—H16	118.7
C1B—N1B—C3B	109.52 (19)	C15—C16—H16	118.7
C3B—N1B—C1	124.8 (2)	C22—C21—B1	120.69 (19)
N2C—N1C—C2	118.7 (2)	C26—C21—C22	114.4 (2)
C3C—N1C—N2C	112.3 (2)	C26—C21—B1	124.71 (19)
C3C—N1C—C2	128.7 (2)	C21—C22—H22	118.5
C1A—N2A—N1A	103.5 (2)	C23—C22—C21	123.0 (2)
C1B—N2B—C2	123.7 (2)	C23—C22—H22	118.5
C1B—N2B—C2B	109.3 (2)	C22—C23—H23	119.8
C2B—N2B—C2	126.1 (2)	C22—C23—C24	120.3 (2)
C1C—N2C—N1C	103.7 (2)	C24—C23—H23	119.8
N1A—C1—N1B	111.31 (18)	C23—C24—H24	120.6
N1A—C1—H1A	109.4	C25—C24—C23	118.8 (2)
N1A—C1—H1B	109.4	C25—C24—H24	120.6
N1B—C1—H1A	109.4	C24—C25—H25	119.9
N1B—C1—H1B	109.4	C24—C25—C26	120.2 (2)
H1A—C1—H1B	108.0	C26—C25—H25	119.9
N2A—C1A—H1AA	124.0	C21—C26—H26	118.4
N2A—C1A—C2A	112.0 (3)	C25—C26—C21	123.1 (2)

C2A—C1A—H1AA	124.0	C25—C26—H26	118.4
N1B—C1B—N2B	107.6 (2)	C32—C31—C36	115.27 (18)
N1B—C1B—H1BA	126.2	C32—C31—B1	124.00 (18)
N2B—C1B—H1BA	126.2	C36—C31—B1	120.64 (19)
N2C—C1C—H1C	123.8	C31—C32—H32	118.7
N2C—C1C—C2C	112.3 (3)	C33—C32—C31	122.5 (2)
C2C—C1C—H1C	123.8	C33—C32—H32	118.7
N1C—C2—N2B	108.9 (2)	C32—C33—H33	119.7
N1C—C2—H2A	109.9	C34—C33—C32	120.6 (2)
N1C—C2—H2B	109.9	C34—C33—H33	119.7
N2B—C2—H2A	109.9	C33—C34—H34	120.7
N2B—C2—H2B	109.9	C33—C34—C35	118.6 (2)
H2A—C2—H2B	108.3	C35—C34—H34	120.7
C1A—C2A—H2AA	127.3	C34—C35—H35	119.9
C3A—C2A—C1A	105.4 (3)	C36—C35—C34	120.2 (2)
C3A—C2A—H2AA	127.3	C36—C35—H35	119.9
N2B—C2B—H2BA	126.6	C31—C36—H36	118.6
C3B—C2B—N2B	106.9 (2)	C35—C36—C31	122.8 (2)
C3B—C2B—H2BA	126.6	C35—C36—H36	118.6
C1C—C2C—H2C	127.6	C42—C41—C46	115.15 (19)
C3C—C2C—C1C	104.9 (2)	C42—C41—B1	125.10 (18)
C3C—C2C—H2C	127.6	C46—C41—B1	119.74 (19)
N1A—C3A—C2A	106.6 (3)	C41—C42—H42	118.5
N1A—C3A—H3A	126.7	C43—C42—C41	123.0 (2)
C2A—C3A—H3A	126.7	C43—C42—H42	118.5
N1B—C3B—H3B	126.7	C42—C43—H43	120.0
C2B—C3B—N1B	106.7 (2)	C44—C43—C42	119.9 (2)
C2B—C3B—H3B	126.7	C44—C43—H43	120.0
N1C—C3C—C2C	106.9 (2)	C43—C44—H44	120.4
N1C—C3C—H3C	126.6	C45—C44—C43	119.3 (2)
C2C—C3C—H3C	126.6	C45—C44—H44	120.4
C12—C11—B1	119.6 (2)	C44—C45—H45	119.9
C16—C11—C12	115.0 (2)	C44—C45—C46	120.3 (2)
C16—C11—B1	125.4 (2)	C46—C45—H45	119.9
C11—C12—H12	118.6	C41—C46—H46	118.8
C13—C12—C11	122.8 (2)	C45—C46—C41	122.4 (2)
C13—C12—H12	118.6	C45—C46—H46	118.8
C12—C13—H13	119.9	C11—B1—C31	109.86 (17)
C14—C13—C12	120.1 (3)	C11—B1—C41	108.07 (16)
C14—C13—H13	119.9	C21—B1—C11	113.13 (18)
C13—C14—H14	120.4	C21—B1—C31	103.43 (16)

C15—C14—C13	119.1 (2)	C21—B1—C41	110.39 (18)
C15—C14—H14	120.4	C41—B1—C31	111.99 (17)
C14—C15—H15	119.9		

## Selected geometric parameters, torsion angles (°)

N1A—N2A—C1A— C2A	-0.2 (3)	C22—C21—C26— C25	-0.9 (3)
N1C—N2C—C1C— C2C	0.0 (3)	C22—C21—B1—C11	57.0 (2)
N2A—N1A—C1— N1B	-81.2 (3)	C22—C21—B1—C31	-61.8 (2)
N2A—N1A—C3A— C2A	-0.9 (3)	C22—C21—B1—C41	178.21 (18)
N2A—C1A—C2A— C3A	-0.3 (3)	C22—C23—C24— C25	-1.0 (3)
N2B—C2B—C3B— N1B	-0.2 (3)	C23—C24—C25— C26	1.8 (3)
N2C—N1C—C2— N2B	62.2 (3)	C24—C25—C26— C21	-0.9 (3)
N2C—N1C—C3C— C2C	0.9 (3)	C26—C21—C22— C23	1.7 (3)
N2C—C1C—C2C— C3C	0.5 (4)	C26—C21—B1—C11	-127.8 (2)
C1—N1A—N2A— C1A	173.3 (2)	C26—C21—B1—C31	113.4 (2)
C1—N1A—C3A— C2A	-172.5 (2)	C26—C21—B1—C41	-6.6 (3)
C1—N1B—C1B— N2B	-176.9 (2)	C31—C32—C33— C34	0.0 (4)
C1—N1B—C3B— C2B	177.0 (2)	C32—C31—C36— C35	1.6 (3)
C1A—C2A—C3A— N1A	0.7 (3)	C32—C31—B1—C11	-9.9 (3)
C1B—N1B—C1— N1A	-124.7 (3)	C32—C31—B1—C21	111.1 (2)
C1B—N1B—C3B— C2B	0.4 (3)	C32—C31—B1—C41	-130.0 (2)
C1B—N2B—C2— N1C	-93.2 (3)	C32—C33—C34— C35	-0.5 (4)
C1B—N2B—C2B— C3B	0.0 (3)	C33—C34—C35— C36	1.6 (4)
C1C—C2C—C3C— N1C	-0.8 (3)	C34—C35—C36— C31	-2.2 (4)
C2—N1C—N2C— C1C	-174.5 (2)	C36—C31—C32— C33	-0.5 (3)
C2—N1C—C3C— C2C	174.0 (2)	C36—C31—B1—C11	173.8 (2)



C2—N2B—C1B— N1B	170.2 (2)	C36—C31—B1—C21	-65.2 (2)
C2—N2B—C2B— C3B	-169.7 (2)	C36—C31—B1—C41	53.7 (3)
C2B—N2B—C1B— N1B	0.2 (3)	C41—C42—C43— C44	0.3 (3)
C2B—N2B—C2— N1C	75.1 (3)	C42—C41—C46— C45	-1.6 (3)
C3A—N1A—N2A— C1A	0.7 (3)	C42—C41—B1—C11	-118.2 (2)
C3A—N1A—C1— N1B	90.0 (3)	C42—C41—B1—C21	117.6 (2)
C3B—N1B—C1— N1A	59.3 (3)	C42—C41—B1—C31	3.0 (3)
C3B—N1B—C1B— N2B	-0.4 (3)	C42—C43—C44— C45	-0.9 (3)
C3C—N1C—N2C— C1C	-0.6 (3)	C43—C44—C45— C46	0.2 (4)
C3C—N1C—C2— N2B	-110.6 (3)	C44—C45—C46— C41	1.1 (4)
C11—C12—C13— C14	0.8 (4)	C46—C41—C42— C43	0.9 (3)
C12—C11—C16— C15	1.1 (3)	C46—C41—B1—C11	62.1 (3)
C12—C11—B1—C21	176.16 (18)	C46—C41—B1—C21	-62.1 (2)
C12—C11—B1—C31	-68.8 (2)	C46—C41—B1—C31	-176.73 (19)
C12—C11—B1—C41	53.6 (2)	B1—C11—C12—C13	176.6 (2)
C12—C13—C14— C15	0.6 (4)	B1—C11—C16—C15	-177.0 (2)
C13—C14—C15— C16	-1.1 (4)	B1—C21—C22—C23	177.4 (2)
C14—C15—C16— C11	0.3 (4)	B1—C21—C26—C25	-176.35 (19)
C16—C11—C12— C13	-1.6 (3)	B1—C31—C32—C33	-177.0 (2)
C16—C11—B1—C21	-5.9 (3)	B1—C31—C36—C35	178.2 (2)
C16—C11—B1—C31	109.1 (2)	B1—C41—C42—C43	-178.8 (2)
C16—C11—B1—C41	-128.4 (2)	B1—C41—C46—C45	178.1 (2)
C21—C22—C23— C24	-0.8 (3)		

## 7.1.2. Crystal data for ligand 1c

## Selected geometric parameters (Å)

N1A—N2A	1.3534 (18)	C13—H13	0.9500
---------	-------------	---------	--------

N1A—C1	1.4502 (19)	C13—C14	1.387 (2)
N1A—C3A	1.3495 (19)	C14—H14	0.9500
N1B—C1B	1.3280 (18)	C14—C15	1.379 (2)
N1B—C2	1.4690 (19)	C15—H15	0.9500
N1B—C3B	1.3814 (18)	C15—C16	1.391 (2)
N1C—N2C	1.3556 (19)	C16—H16	0.9500
N1C—C3C	1.348 (2)	C21—C22	1.404 (2)
N1C—C4	1.453 (2)	C21—C26	1.400 (2)
N2A—C1A	1.331 (2)	C21—B1	1.646 (2)
N2B—C1B	1.3235 (19)	C22—H22	0.9500
N2B—C2B	1.3777 (19)	C22—C23	1.389 (2)
N2B—C3	1.4603 (19)	C23—H23	0.9500
N2C—C1C	1.329 (2)	C23—C24	1.376 (2)
C1—H1A	0.9900	C24—H24	0.9500
C1—H1B	0.9900	C24—C25	1.383 (2)
C1—C2	1.510 (2)	C25—H25	0.9500
C1A—H1AA	0.9500	C25—C26	1.393 (2)
C1A—C2A	1.387 (2)	C26—H26	0.9500
C1B—H1BA	0.9500	C31—C32	1.400 (2)
C1C—H1C	0.9500	C31—C36	1.405 (2)
C1C—C2C	1.392 (3)	C31—B1	1.643 (2)
C2—H2A	0.9900	C32—H32	0.9500
C2—H2B	0.9900	C32—C33	1.393 (2)
C2A—H2AA	0.9500	C33—H33	0.9500
C2A—C3A	1.366 (2)	C33—C34	1.381 (2)
C2B—H2BA	0.9500	C34—H34	0.9500
C2B—C3B	1.341 (2)	C34—C35	1.383 (2)
C2C—H2C	0.9500	C35—H35	0.9500
C2C—C3C	1.370 (3)	C35—C36	1.389 (2)
C3—H3A	0.9900	C36—H36	0.9500
C3—H3B	0.9900	C41—C42	1.398 (2)
C3—C4	1.516 (2)	C41—C46	1.400 (2)
C3A—H3AA	0.9500	C41—B1	1.642 (2)
C3B—H3BA	0.9500	C42—H42	0.9500
C3C—H3C	0.9500	C42—C43	1.393 (2)
C4—H4A	0.9900	C43—H43	0.9500
C4—H4B	0.9900	C43—C44	1.379 (2)
C11—C12	1.402 (2)	C44—H44	0.9500
C11—C16	1.403 (2)	C44—C45	1.383 (2)
C11—B1	1.644 (2)	C45—H45	0.9500
C12—H12	0.9500	C45—C46	1.385 (2)

C12—C13	1.391 (2)	C46—H46	0.9500
---------	-----------	---------	--------

**Selected geometric parameters (°)**

N2A—N1A—C1	119.50 (12)	C14—C13—C12	120.12 (15)
C3A—N1A—N2A	112.19 (13)	C14—C13—H13	119.9
C3A—N1A—C1	127.94 (13)	C13—C14—H14	120.6
C1B—N1B—C2	124.65 (12)	C15—C14—C13	118.88 (15)
C1B—N1B—C3B	108.28 (13)	C15—C14—H14	120.6
C3B—N1B—C2	126.82 (12)	C14—C15—H15	119.8
N2C—N1C—C4	119.49 (13)	C14—C15—C16	120.41 (15)
C3C—N1C—N2C	111.85 (14)	C16—C15—H15	119.8
C3C—N1C—C4	127.90 (15)	C11—C16—H16	118.7
C1A—N2A—N1A	103.98 (13)	C15—C16—C11	122.61 (15)
C1B—N2B—C2B	108.50 (13)	C15—C16—H16	118.7
C1B—N2B—C3	125.58 (13)	C22—C21—B1	121.60 (13)
C2B—N2B—C3	125.81 (13)	C26—C21—C22	114.85 (13)
C1C—N2C—N1C	104.38 (14)	C26—C21—B1	123.16 (13)
N1A—C1—H1A	109.1	C21—C22—H22	118.5
N1A—C1—H1B	109.1	C23—C22—C21	122.99 (15)
N1A—C1—C2	112.46 (13)	C23—C22—H22	118.5
H1A—C1—H1B	107.8	C22—C23—H23	119.8
C2—C1—H1A	109.1	C24—C23—C22	120.31 (15)
C2—C1—H1B	109.1	C24—C23—H23	119.8
N2A—C1A—H1AA	124.0	C23—C24—H24	120.6
N2A—C1A—C2A	112.06 (15)	C23—C24—C25	118.83 (15)
C2A—C1A—H1AA	124.0	C25—C24—H24	120.6
N1B—C1B—H1BA	125.6	C24—C25—H25	119.8
N2B—C1B—N1B	108.84 (13)	C24—C25—C26	120.36 (16)
N2B—C1B—H1BA	125.6	C26—C25—H25	119.8
N2C—C1C—H1C	124.0	C21—C26—H26	118.7
N2C—C1C—C2C	111.90 (16)	C25—C26—C21	122.65 (15)
C2C—C1C—H1C	124.0	C25—C26—H26	118.7
N1B—C2—C1	113.24 (12)	C32—C31—C36	114.91 (13)
N1B—C2—H2A	108.9	C32—C31—B1	122.76 (13)
N1B—C2—H2B	108.9	C36—C31—B1	122.11 (13)
C1—C2—H2A	108.9	C31—C32—H32	118.5
C1—C2—H2B	108.9	C33—C32—C31	123.04 (15)
H2A—C2—H2B	107.7	C33—C32—H32	118.5
C1A—C2A—H2AA	127.5	C32—C33—H33	120.0
C3A—C2A—C1A	105.05 (14)	C34—C33—C32	120.08 (16)

C3A—C2A—H2AA	127.5	C34—C33—H33	120.0
N2B—C2B—H2BA	126.4	C33—C34—H34	120.6
C3B—C2B—N2B	107.28 (13)	C33—C34—C35	118.82 (15)
C3B—C2B—H2BA	126.4	C35—C34—H34	120.6
C1C—C2C—H2C	127.6	C34—C35—H35	119.8
C3C—C2C—C1C	104.79 (16)	C34—C35—C36	120.47 (15)
C3C—C2C—H2C	127.6	C36—C35—H35	119.8
N2B—C3—H3A	109.2	C31—C36—H36	118.7
N2B—C3—H3B	109.2	C35—C36—C31	122.66 (15)
N2B—C3—C4	111.88 (13)	C35—C36—H36	118.7
H3A—C3—H3B	107.9	C42—C41—C46	115.17 (13)
C4—C3—H3A	109.2	C42—C41—B1	125.96 (13)
C4—C3—H3B	109.2	C46—C41—B1	118.73 (12)
N1A—C3A—C2A	106.72 (15)	C41—C42—H42	118.9
N1A—C3A—H3AA	126.6	C43—C42—C41	122.22 (14)
C2A—C3A—H3AA	126.6	C43—C42—H42	118.9
N1B—C3B—H3BA	126.5	C42—C43—H43	119.7
C2B—C3B—N1B	107.10 (13)	C44—C43—C42	120.67 (14)
C2B—C3B—H3BA	126.5	C44—C43—H43	119.7
N1C—C3C—C2C	107.07 (16)	C43—C44—H44	120.6
N1C—C3C—H3C	126.5	C43—C44—C45	118.72 (14)
C2C—C3C—H3C	126.5	C45—C44—H44	120.6
N1C—C4—C3	109.05 (13)	C44—C45—H45	120.0
N1C—C4—H4A	109.9	C44—C45—C46	120.03 (14)
N1C—C4—H4B	109.9	C46—C45—H45	120.0
C3—C4—H4A	109.9	C41—C46—H46	118.4
C3—C4—H4B	109.9	C45—C46—C41	123.16 (14)
H4A—C4—H4B	108.3	C45—C46—H46	118.4
C12—C11—C16	115.18 (13)	C11—B1—C21	112.20 (11)
C12—C11—B1	120.17 (13)	C31—B1—C11	110.81 (12)
C16—C11—B1	124.58 (13)	C31—B1—C21	103.41 (11)
C11—C12—H12	118.6	C41—B1—C11	105.56 (11)
C13—C12—C11	122.74 (15)	C41—B1—C21	111.57 (12)
C13—C12—H12	118.6	C41—B1—C31	113.48 (11)
C12—C13—H13	119.9		

## Selected geometric parameters, torsion angles (°)

N1A—N2A—C1A— C2A	0.07 (18)	C21—C22—C23— C24	-1.2 (2)
N1A—C1—C2—N1B	65.58 (17)	C22—C21—C26— C25	0.3 (2)

N1C—N2C—C1C— C2C	0.42 (18)	C22—C21—B1—C11	43.49 (18)
N2A—N1A—C1—C2	-101.96 (15)	C22—C21—B1—C31	-75.97 (16)
N2A—N1A—C3A— C2A	-0.48 (18)	C22—C21—B1—C41	161.71 (13)
N2A—C1A—C2A— C3A	-0.3 (2)	C22—C23—C24— C25	0.4 (2)
N2B—C2B—C3B— N1B	0.44 (17)	C23—C24—C25— C26	0.7 (3)
N2B—C3—C4—N1C	-177.50 (12)	C24—C25—C26— C21	-1.1 (3)
N2C—N1C—C3C— C2C	1.00 (19)	C26—C21—C22— C23	0.9 (2)
N2C—N1C—C4—C3	93.56 (16)	C26—C21—B1—C11	-144.01 (14)
N2C—C1C—C2C— C3C	0.2 (2)	C26—C21—B1—C31	96.53 (16)
C1—N1A—N2A— C1A	173.85 (13)	C26—C21—B1—C41	-25.79 (19)
C1—N1A—C3A— C2A	-173.40 (15)	C31—C32—C33— C34	-0.7 (2)
C1A—C2A—C3A— N1A	0.48 (19)	C32—C31—C36— C35	2.1 (2)
C1B—N1B—C2—C1	118.84 (16)	C32—C31—B1—C11	-21.50 (18)
C1B—N1B—C3B— C2B	-0.41 (17)	C32—C31—B1—C21	98.91 (15)
C1B—N2B—C2B— C3B	-0.32 (17)	C32—C31—B1—C41	-140.05 (13)
C1B—N2B—C3—C4	-101.15 (17)	C32—C33—C34— C35	1.1 (2)
C1C—C2C—C3C— N1C	-0.68 (19)	C33—C34—C35— C36	0.1 (2)
C2—N1B—C1B— N2B	174.85 (13)	C34—C35—C36— C31	-1.7 (2)
C2—N1B—C3B— C2B	-174.90 (14)	C36—C31—C32— C33	-0.8 (2)
C2B—N2B—C1B— N1B	0.06 (17)	C36—C31—B1—C11	164.24 (12)
C2B—N2B—C3—C4	83.07 (18)	C36—C31—B1—C21	-75.35 (15)
C3—N2B—C1B— N1B	-176.33 (13)	C36—C31—B1—C41	45.69 (18)
C3—N2B—C2B— C3B	176.06 (14)	C41—C42—C43— C44	-1.6 (2)
C3A—N1A—N2A— C1A	0.25 (17)	C42—C41—C46— C45	-0.6 (2)
C3A—N1A—C1—C2	70.5 (2)	C42—C41—B1—C11	-108.34 (15)
C3B—N1B—C1B— N2B	0.21 (17)	C42—C41—B1—C21	129.53 (15)

C3B—N1B—C2—C1	-67.52 (19)	C42—C41—B1—C31	13.2 (2)
C3C—N1C—N2C—C1C	-0.87 (17)	C42—C43—C44—C45	0.0 (2)
C3C—N1C—C4—C3	-75.6 (2)	C43—C44—C45—C46	1.3 (2)
C4—N1C—N2C—C1C	-171.68 (13)	C44—C45—C46—C41	-1.0 (2)
C4—N1C—C3C—C2C	170.84 (15)	C46—C41—C42—C43	1.9 (2)
C11—C12—C13—C14	0.6 (2)	C46—C41—B1—C11	67.03 (16)
C12—C11—C16—C15	2.6 (2)	C46—C41—B1—C21	-55.11 (17)
C12—C11—B1—C21	-164.95 (12)	C46—C41—B1—C31	-171.44 (12)
C12—C11—B1—C31	-49.92 (17)	B1—C11—C12—C13	-179.52 (13)
C12—C11—B1—C41	73.32 (16)	B1—C11—C16—C15	179.58 (14)
C12—C13—C14—C15	1.2 (2)	B1—C21—C22—C23	173.95 (14)
C13—C14—C15—C16	-1.0 (2)	B1—C21—C26—C25	-172.66 (15)
C14—C15—C16—C11	-1.0 (2)	B1—C31—C32—C33	-175.48 (13)
C16—C11—C12—C13	-2.4 (2)	B1—C31—C36—C35	176.73 (13)
C16—C11—B1—C21	18.23 (19)	B1—C41—C42—C43	177.39 (14)
C16—C11—B1—C31	133.26 (14)	B1—C41—C46—C45	-176.44 (14)
C16—C11—B1—C41	-103.50 (15)		

### 7.1.3. Crystal data for complex 2

#### Selected geometric parameters (Å)

Ag1A—C1B1	2.080 (4)	N1C6—C2S	1.430 (5)
Ag1A—C1B2	2.078 (4)	N1C6—C3C6	1.359 (5)
N1A1—N2A1	1.361 (4)	N2A6—C1A6	1.317 (5)
N1A1—C1P	1.434 (5)	N2B6—C1B6	1.355 (5)
N1A1—C3A1	1.349 (5)	N2B6—C2S	1.462 (5)
N1A2—N2A2	1.348 (4)	N2B6—C3B6	1.378 (4)
N1A2—C1P'	1.438 (5)	N2C6—C1C6	1.314 (5)
N1A2—C3A2	1.336 (5)	C1A6—H1A6	0.9500
N1B1—C1B1	1.363 (4)	C1A6—C2A6	1.375 (5)
N1B1—C1P	1.467 (5)	C1C6—H1C6	0.9500
N1B1—C2B1	1.380 (4)	C1C6—C2C6	1.379 (6)
N1B2—C1B2	1.360 (5)	C1S—H1SA	0.9900

N1B2—C1P'	1.461 (5)	C1S—H1SB	0.9900
N1B2—C2B2	1.379 (4)	C2A6—H2A6	0.9500
N1C1—N2C1	1.366 (4)	C2A6—C3A6	1.360 (5)
N1C1—C2P	1.444 (5)	C2B6—H2B6	0.9500
N1C1—C3C1	1.344 (5)	C2B6—C3B6	1.332 (5)
N1C2—N2C2	1.359 (4)	C2C6—H2C6	0.9500
N1C2—C2P'	1.433 (5)	C2C6—C3C6	1.349 (6)
N1C2—C3C2	1.364 (5)	C2S—H2SA	0.9900
N2A1—C1A1	1.317 (5)	C2S—H2SB	0.9900
N2A2—C1A2	1.328 (5)	C3A6—H3A6	0.9500
N2B1—C1B1	1.357 (5)	C3B6—H3B6	0.9500
N2B1—C2P	1.458 (5)	C3C6—H3C6	0.9500
N2B1—C3B1	1.381 (4)	C11M—C12M	1.407 (5)
N2B2—C1B2	1.351 (4)	C11M—C16M	1.403 (5)
N2B2—C2P'	1.461 (5)	C11M—B1M	1.661 (5)
N2B2—C3B2	1.383 (4)	C12M—H12M	0.9500
N2C1—C1C1	1.309 (6)	C12M—C13M	1.396 (5)
N2C2—C1C2	1.320 (5)	C13M—H13M	0.9500
C1A1—H1A1	0.9500	C13M—C14M	1.388 (5)
C1A1—C2A1	1.392 (6)	C14M—H14M	0.9500
C1A2—H1A2	0.9500	C14M—C15M	1.381 (5)
C1A2—C2A2	1.377 (7)	C15M—H15M	0.9500
C1C1—H1C1	0.9500	C15M—C16M	1.381 (5)
C1C1—C2C1	1.356 (7)	C16M—H16M	0.9500
C1C2—H1C2	0.9500	C21M—C22M	1.398 (5)
C1C2—C2C2	1.390 (6)	C21M—C26M	1.407 (5)
C1P—H1PA	0.9900	C21M—B1M	1.641 (6)
C1P—H1PB	0.9900	C22M—H22M	0.9500
C1P'—H1PC	0.9900	C22M—C23M	1.396 (5)
C1P'—H1PD	0.9900	C23M—H23M	0.9500
C2A1—H2A1	0.9500	C23M—C24M	1.379 (7)
C2A1—C3A1	1.355 (5)	C24M—H24M	0.9500
C2A2—H2A2	0.9500	C24M—C25M	1.376 (7)
C2A2—C3A2	1.340 (6)	C25M—H25M	0.9500
C2B1—H2B1	0.9500	C25M—C26M	1.387 (6)
C2B1—C3B1	1.327 (5)	C26M—H26M	0.9500
C2B2—H2B2	0.9500	C31M—C32M	1.406 (5)
C2B2—C3B2	1.337 (5)	C31M—C36M	1.397 (5)
C2C1—H2C1	0.9500	C31M—B1M	1.634 (6)
C2C1—C3C1	1.366 (6)	C32M—H32M	0.9500
C2C2—H2C2	0.9500	C32M—C33M	1.386 (5)

C2C2—C3C2	1.347 (6)	C33M—H33M	0.9500
C2P—H2PA	0.9900	C33M—C34M	1.377 (5)
C2P—H2PB	0.9900	C34M—H34M	0.9500
C2P'—H2PC	0.9900	C34M—C35M	1.378 (5)
C2P'—H2PD	0.9900	C35M—H35M	0.9500
C3A1—H3A1	0.9500	C35M—C36M	1.393 (5)
C3A2—H3A2	0.9500	C36M—H36M	0.9500
C3B1—H3B1	0.9500	C41M—C42M	1.407 (5)
C3B2—H3B2	0.9500	C41M—C46M	1.397 (5)
C3C1—H3C1	0.9500	C41M—B1M	1.655 (5)
C3C2—H3C2	0.9500	C42M—H42M	0.9500
Ag1C—C1B5 <sup>i</sup>	2.074 (4)	C42M—C43M	1.384 (5)
Ag1C—C1B5	2.074 (4)	C43M—H43M	0.9500
N1A5—N2A5	1.342 (4)	C43M—C44M	1.376 (5)
N1A5—C1R	1.442 (5)	C44M—H44M	0.9500
N1A5—C3A5	1.350 (5)	C44M—C45M	1.386 (5)
N1B5—C1B5	1.352 (5)	C45M—H45M	0.9500
N1B5—C1R	1.462 (5)	C45M—C46M	1.383 (5)
N1B5—C2B5	1.363 (5)	C46M—H46M	0.9500
N1C5—N2C5	1.361 (5)	C11O—C12O	1.407 (5)
N1C5—C2R	1.438 (6)	C11O—C16O	1.397 (5)
N1C5—C3C5	1.332 (7)	C11O—B11O	1.643 (5)
N2A5—C1A5	1.331 (5)	C12O—H12O	0.9500
N2B5—C1B5	1.351 (5)	C12O—C13O	1.390 (5)
N2B5—C2R	1.461 (5)	C13O—H13O	0.9500
N2B5—C3B5	1.370 (5)	C13O—C14O	1.361 (6)
N2C5—C1C5	1.324 (7)	C14O—H14O	0.9500
C1A5—H1A5	0.9500	C14O—C15O	1.379 (6)
C1A5—C2A5	1.398 (6)	C15O—H15O	0.9500
C1C5—H1C5	0.9500	C15O—C16O	1.379 (5)
C1C5—C2C5	1.391 (9)	C16O—H16O	0.9500
C1R—H1RA	0.9900	C21O—C22O	1.400 (5)
C1R—H1RB	0.9900	C21O—C26O	1.407 (5)
C2A5—H2A5	0.9500	C21O—B11O	1.636 (5)
C2A5—C3A5	1.357 (6)	C22O—H22O	0.9500
C2B5—H2B5	0.9500	C22O—C23O	1.386 (5)
C2B5—C3B5	1.343 (6)	C23O—H23O	0.9500
C2C5—H2C5	0.9500	C23O—C24O	1.382 (5)
C2C5—C3C5	1.368 (7)	C24O—H24O	0.9500
C2R—H2RA	0.9900	C24O—C25O	1.381 (5)
C2R—H2RB	0.9900	C25O—H25O	0.9500



C3A5—H3A5	0.9500	C25O—C26O	1.385 (5)
C3B5—H3B5	0.9500	C26O—H26O	0.9500
C3C5—H3C5	0.9500	C31O—C32O	1.412 (5)
Ag1B—C1B3	2.078 (4)	C31O—C36O	1.409 (5)
Ag1B—C1B4	2.070 (4)	C31O—B11O	1.647 (5)
N1A3—N2A3	1.353 (4)	C32O—H32O	0.9500
N1A3—C1Q	1.426 (5)	C32O—C33O	1.387 (5)
N1A3—C3A3	1.359 (5)	C33O—H33O	0.9500
N1A4—N2A4	1.350 (4)	C33O—C34O	1.383 (5)
N1A4—C1Q'	1.435 (5)	C34O—H34O	0.9500
N1A4—C3A4	1.350 (5)	C34O—C35O	1.376 (5)
N1B3—C1B3	1.356 (4)	C35O—H35O	0.9500
N1B3—C1Q	1.462 (5)	C35O—C36O	1.387 (5)
N1B3—C2B3	1.378 (5)	C36O—H36O	0.9500
N1B4—C1B4	1.347 (4)	C41O—C42O	1.403 (5)
N1B4—C1Q'	1.462 (5)	C41O—C46O	1.395 (5)
N1B4—C2B4	1.383 (5)	C41O—B11O	1.649 (6)
N1C3—N2C3	1.356 (5)	C42O—H42O	0.9500
N1C3—C2Q	1.428 (5)	C42O—C43O	1.383 (5)
N1C3—C3C3	1.342 (5)	C43O—H43O	0.9500
N1C4—N2C4	1.356 (5)	C43O—C44O	1.385 (5)
N1C4—C2Q'	1.436 (5)	C44O—H44O	0.9500
N1C4—C3C4	1.334 (6)	C44O—C45O	1.376 (5)
N2A3—C1A3	1.319 (5)	C45O—H45O	0.9500
N2A4—C1A4	1.314 (5)	C45O—C46O	1.392 (5)
N2B3—C1B3	1.353 (4)	C46O—H46O	0.9500
N2B3—C2Q	1.455 (4)	C11N—C12N	1.397 (5)
N2B3—C3B3	1.372 (5)	C11N—C16N	1.411 (5)
N2B4—C1B4	1.348 (5)	C11N—B1N	1.644 (5)
N2B4—C2Q'	1.460 (5)	C12N—H12N	0.9500
N2B4—C3B4	1.378 (5)	C12N—C13N	1.395 (5)
N2C3—C1C3	1.315 (6)	C13N—H13N	0.9500
N2C4—C1C4	1.325 (7)	C13N—C14N	1.372 (5)
C1A3—H1A3	0.9500	C14N—H14N	0.9500
C1A3—C2A3	1.394 (5)	C14N—C15N	1.385 (5)
C1A4—H1A4	0.9500	C15N—H15N	0.9500
C1A4—C2A4	1.387 (6)	C15N—C16N	1.379 (5)
C1C3—H1C3	0.9500	C16N—H16N	0.9500
C1C3—C2C3	1.373 (8)	C21N—C22N	1.406 (5)
C1C4—H1C4	0.9500	C21N—C26N	1.394 (5)
C1C4—C2C4	1.373 (8)	C21N—B1N	1.630 (5)

C1Q—H1Q	0.9500	C22N—H22N	0.9500
C1Q'—H1QA	0.9900	C22N—C23N	1.392 (5)
C1Q'—H1QB	0.9900	C23N—H23N	0.9500
C2A3—H2A3	0.9500	C23N—C24N	1.363 (6)
C2A3—C3A3	1.352 (6)	C24N—H24N	0.9500
C2A4—H2A4	0.9500	C24N—C25N	1.371 (6)
C2A4—C3A4	1.344 (6)	C25N—H25N	0.9500
C2B3—H2B3	0.9500	C25N—C26N	1.386 (5)
C2B3—C3B3	1.346 (6)	C26N—H26N	0.9500
C2B4—H2B4	0.9500	C31N—C32N	1.391 (5)
C2B4—C3B4	1.332 (5)	C31N—C36N	1.405 (5)
C2C3—H2C3	0.9500	C31N—B1N	1.645 (5)
C2C3—C3C3	1.367 (6)	C32N—H32N	0.9500
C2C4—H2C4	0.9500	C32N—C33N	1.391 (5)
C2C4—C3C4	1.370 (7)	C33N—H33N	0.9500
C2Q—H2QA	0.9900	C33N—C34N	1.380 (5)
C2Q—H2QB	0.9900	C34N—H34N	0.9500
C2Q'—H2QC	0.9900	C34N—C35N	1.392 (5)
C2Q'—H2QD	0.9900	C35N—H35N	0.9500
C3A3—H3A3	0.9500	C35N—C36N	1.387 (5)
C3A4—H3A4	0.9500	C36N—H36N	0.9500
C3B3—H3B3	0.9500	C41N—C42N	1.397 (5)
C3B4—H3B4	0.9500	C41N—C46N	1.400 (5)
C3C3—H3C3	0.9500	C41N—B1N	1.648 (6)
C3C4—H3C4	0.9500	C42N—H42N	0.9500
Ag1D—C1B6 <sup>ii</sup>	2.081 (4)	C42N—C43N	1.384 (5)
Ag1D—C1B6	2.081 (4)	C43N—H43N	0.9500
N1A6—N2A6	1.362 (4)	C43N—C44N	1.382 (5)
N1A6—C1S	1.438 (5)	C44N—H44N	0.9500
N1A6—C3A6	1.355 (5)	C44N—C45N	1.386 (5)
N1B6—C1B6	1.360 (5)	C45N—H45N	0.9500
N1B6—C1S	1.458 (5)	C45N—C46N	1.380 (5)
N1B6—C2B6	1.381 (4)	C46N—H46N	0.9500
N1C6—N2C6	1.359 (4)		

Symmetry code(s): (i)  $-x, -y+1, -z+2$ ; (ii)  $-x+1, -y+1, -z+3$ .

#### Selected geometric parameters (<sup>o</sup>)

C1B2—Ag1A—C1B1	174.32 (15)	C1B6—N2B6—C3B6	111.2 (3)
N2A1—N1A1—C1P	119.0 (3)	C3B6—N2B6—C2S	124.8 (3)
C3A1—N1A1—N2A1	111.8 (3)	C1C6—N2C6—N1C6	104.6 (4)

C3A1—N1A1—C1P	129.2 (4)	N2A6—C1A6—H1A 6	123.6
N2A2—N1A2—C1P'	119.1 (3)	N2A6—C1A6—C2A6	112.9 (4)
C3A2—N1A2—N2A 2	112.5 (4)	C2A6—C1A6—H1A 6	123.6
C3A2—N1A2—C1P'	128.4 (4)	N1B6—C1B6—Ag1D	126.0 (3)
C1B1—N1B1—C1P	124.2 (3)	N2B6—C1B6—Ag1D	130.5 (3)
C1B1—N1B1—C2B1	111.3 (3)	N2B6—C1B6—N1B6	103.4 (3)
C2B1—N1B1—C1P	124.3 (3)	N2C6—C1C6—H1C6	124.0
C1B2—N1B2—C1P'	123.6 (3)	N2C6—C1C6—C2C6	112.0 (4)
C1B2—N1B2—C2B2	111.6 (3)	C2C6—C1C6—H1C6	124.0
C2B2—N1B2—C1P'	124.8 (3)	N1A6—C1S—N1B6	113.2 (3)
N2C1—N1C1—C2P	119.1 (3)	N1A6—C1S—H1SA	108.9
C3C1—N1C1—N2C1	111.9 (4)	N1A6—C1S—H1SB	108.9
C3C1—N1C1—C2P	128.3 (4)	N1B6—C1S—H1SA	108.9
N2C2—N1C2—C2P'	119.8 (3)	N1B6—C1S—H1SB	108.9
N2C2—N1C2—C3C2	110.9 (4)	H1SA—C1S—H1SB	107.7
C3C2—N1C2—C2P'	129.1 (3)	C1A6—C2A6—H2A6	127.4
C1A1—N2A1—N1A 1	103.7 (3)	C3A6—C2A6—C1A6	105.1 (4)
C1A2—N2A2—N1A 2	102.4 (4)	C3A6—C2A6—H2A6	127.4
C1B1—N2B1—C2P	124.5 (3)	N1B6—C2B6—H2B6	126.9
C1B1—N2B1—C3B1	111.3 (3)	C3B6—C2B6—N1B6	106.1 (3)
C3B1—N2B1—C2P	124.1 (3)	C3B6—C2B6—H2B6	126.9
C1B2—N2B2—C2P'	123.5 (3)	C1C6—C2C6—H2C6	127.1
C1B2—N2B2—C3B2	111.5 (3)	C3C6—C2C6—C1C6	105.7 (4)
C3B2—N2B2—C2P'	124.9 (3)	C3C6—C2C6—H2C6	127.1
C1C1—N2C1—N1C1	103.4 (4)	N1C6—C2S—N2B6	112.3 (3)
C1C2—N2C2—N1C2	104.0 (3)	N1C6—C2S—H2SA	109.1
N2A1—C1A1—H1A 1	123.7	N1C6—C2S—H2SB	109.1
N2A1—C1A1—C2A1	112.7 (4)	N2B6—C2S—H2SA	109.1
C2A1—C1A1—H1A1	123.7	N2B6—C2S—H2SB	109.1
N2A2—C1A2—H1A 2	123.5	H2SA—C2S—H2SB	107.9
N2A2—C1A2—C2A2	113.1 (4)	N1A6—C3A6—C2A6	106.7 (4)
C2A2—C1A2—H1A2	123.5	N1A6—C3A6—H3A 6	126.6
N1B1—C1B1—Ag1A	128.2 (3)	C2A6—C3A6—H3A6	126.6
N2B1—C1B1—Ag1A	128.3 (3)	N2B6—C3B6—H3B6	126.2
N2B1—C1B1—N1B1	103.4 (3)	C2B6—C3B6—N2B6	107.5 (3)
N1B2—C1B2—Ag1A	127.0 (3)	C2B6—C3B6—H3B6	126.2
N2B2—C1B2—Ag1A	128.3 (3)	N1C6—C3C6—H3C6	126.6
N2B2—C1B2—N1B2	103.5 (3)	C2C6—C3C6—N1C6	106.8 (4)
N2C1—C1C1—H1C1	123.4	C2C6—C3C6—H3C6	126.6
N2C1—C1C1—C2C1	113.1 (5)	C12M—C11M—B1M	121.7 (3)
C2C1—C1C1—H1C1	123.4	C16M—C11M—	114.6 (3)

		C12M	
N2C2—C1C2—H1C2	123.6	C16M—C11M—B1M	123.7 (3)
N2C2—C1C2—C2C2	112.7 (4)	C11M—C12M—H12M	118.5
C2C2—C1C2—H1C2	123.6	C13M—C12M—C11M	122.9 (4)
N1A1—C1P—N1B1	112.0 (3)	C13M—C12M—H12M	118.5
N1A1—C1P—H1PA	109.2	C12M—C13M—H13M	120.0
N1A1—C1P—H1PB	109.2	C14M—C13M—C12M	120.0 (4)
N1B1—C1P—H1PA	109.2	C14M—C13M—H13M	120.0
N1B1—C1P—H1PB	109.2	C13M—C14M—H14M	120.7
H1PA—C1P—H1PB	107.9	C15M—C14M—C13M	118.7 (4)
N1A2—C1P'—N1B2	113.1 (3)	C15M—C14M—H14M	120.7
N1A2—C1P'—H1PC	108.9	C14M—C15M—H15M	119.7
N1A2—C1P'—H1PD	108.9	C14M—C15M—C16M	120.6 (4)
N1B2—C1P'—H1PC	108.9	C16M—C15M—H15M	119.7
N1B2—C1P'—H1PD	108.9	C11M—C16M—H16M	118.4
H1PC—C1P'—H1PD	107.8	C15M—C16M—C11M	123.2 (4)
C1A1—C2A1—H2A1	127.7	C15M—C16M—H16M	118.4
C3A1—C2A1—C1A1	104.6 (4)	C22M—C21M—C26M	115.3 (4)
C3A1—C2A1—H2A1	127.7	C22M—C21M—B1M	120.4 (4)
C1A2—C2A2—H2A2	127.8	C26M—C21M—B1M	124.3 (4)
C3A2—C2A2—C1A2	104.4 (5)	C21M—C22M—H22M	118.5
C3A2—C2A2—H2A2	127.8	C23M—C22M—C21M	123.1 (4)
N1B1—C2B1—H2B1	126.6	C23M—C22M—H22M	118.5
C3B1—C2B1—N1B1	106.9 (3)	C22M—C23M—H23M	120.4
C3B1—C2B1—H2B1	126.6	C24M—C23M—C22M	119.1 (5)
N1B2—C2B2—H2B2	126.7	C24M—C23M—H23M	120.4

C3B2—C2B2—N1B2	106.6 (3)	C23M—C24M— H24M	120.0
C3B2—C2B2—H2B2	126.7	C25M—C24M— C23M	120.0 (5)
C1C1—C2C1—H2C1	127.1	C25M—C24M— H24M	120.0
C1C1—C2C1—C3C1	105.9 (5)	C24M—C25M— H25M	119.9
C3C1—C2C1—H2C1	127.1	C24M—C25M— C26M	120.2 (5)
C1C2—C2C2—H2C2	127.7	C26M—C25M— H25M	119.9
C3C2—C2C2—C1C2	104.7 (4)	C21M—C26M— H26M	118.9
C3C2—C2C2—H2C2	127.7	C25M—C26M— C21M	122.2 (5)
N1C1—C2P—N2B1	111.8 (3)	C25M—C26M— H26M	118.9
N1C1—C2P—H2PA	109.3	C32M—C31M—B1M	121.1 (3)
N1C1—C2P—H2PB	109.3	C36M—C31M— C32M	114.3 (4)
N2B1—C2P—H2PA	109.3	C36M—C31M—B1M	124.5 (3)
N2B1—C2P—H2PB	109.3	C31M—C32M— H32M	118.5
H2PA—C2P—H2PB	107.9	C33M—C32M— C31M	123.1 (4)
N1C2—C2P'—N2B2	112.0 (3)	C33M—C32M— H32M	118.5
N1C2—C2P'—H2PC	109.2	C32M—C33M— H33M	119.7
N1C2—C2P'—H2PD	109.2	C34M—C33M— C32M	120.6 (4)
N2B2—C2P'—H2PC	109.2	C34M—C33M— H33M	119.7
N2B2—C2P'—H2PD	109.2	C33M—C34M— H34M	120.8
H2PC—C2P'—H2PD	107.9	C33M—C34M— C35M	118.5 (4)
N1A1—C3A1—C2A1	107.2 (4)	C35M—C34M— H34M	120.8
N1A1—C3A1—H3A 1	126.4	C34M—C35M— H35M	119.8
C2A1—C3A1—H3A1	126.4	C34M—C35M— C36M	120.4 (4)
N1A2—C3A2—C2A2	107.6 (4)	C36M—C35M— H35M	119.8
N1A2—C3A2—H3A 2	126.2	C31M—C36M— H36M	118.4

C2A2—C3A2—H3A2	126.2	C35M—C36M—C31M	123.1 (4)
N2B1—C3B1—H3B1	126.4	C35M—C36M—H36M	118.4
C2B1—C3B1—N2B1	107.1 (3)	C42M—C41M—B1M	124.7 (3)
C2B1—C3B1—H3B1	126.4	C46M—C41M—C42M	114.2 (3)
N2B2—C3B2—H3B2	126.6	C46M—C41M—B1M	121.1 (3)
C2B2—C3B2—N2B2	106.8 (3)	C41M—C42M—H42M	118.4
C2B2—C3B2—H3B2	126.6	C43M—C42M—C41M	123.3 (4)
N1C1—C3C1—C2C1	105.6 (5)	C43M—C42M—H42M	118.4
N1C1—C3C1—H3C1	127.2	C42M—C43M—H43M	119.9
C2C1—C3C1—H3C1	127.2	C44M—C43M—C42M	120.2 (4)
N1C2—C3C2—H3C2	126.2	C44M—C43M—H43M	119.9
C2C2—C3C2—N1C2	107.6 (4)	C43M—C44M—H44M	120.6
C2C2—C3C2—H3C2	126.2	C43M—C44M—C45M	118.7 (4)
C1B5 <sup>i</sup> —Ag1C—C1B5	180.00 (8)	C45M—C44M—H44M	120.6
N2A5—N1A5—C1R	119.2 (3)	C44M—C45M—H45M	119.9
N2A5—N1A5—C3A5	113.1 (4)	C46M—C45M—C44M	120.2 (4)
C3A5—N1A5—C1R	127.6 (4)	C46M—C45M—H45M	119.9
C1B5—N1B5—C1R	124.3 (3)	C41M—C46M—H46M	118.3
C1B5—N1B5—C2B5	112.0 (4)	C45M—C46M—C41M	123.4 (4)
C2B5—N1B5—C1R	123.7 (4)	C45M—C46M—H46M	118.3
N2C5—N1C5—C2R	119.0 (5)	C21M—B1M—C11M	109.1 (3)
C3C5—N1C5—N2C5	112.4 (5)	C21M—B1M—C41M	110.3 (3)
C3C5—N1C5—C2R	128.6 (5)	C31M—B1M—C11M	107.8 (3)
C1A5—N2A5—N1A5	103.4 (3)	C31M—B1M—C21M	110.6 (3)
C1B5—N2B5—C2R	124.5 (3)	C31M—B1M—C41M	110.1 (3)
C1B5—N2B5—C3B5	111.7 (4)	C41M—B1M—C11M	108.9 (3)
C3B5—N2B5—C2R	123.7 (4)	C12O—C11O—B11O	122.4 (3)
C1C5—N2C5—N1C5	104.0 (5)	C16O—C11O—C12O	115.4 (3)
N2A5—C1A5—H1A5	123.9	C16O—C11O—B11O	121.5 (3)

N2A5—C1A5—C2A5	112.2 (4)	C11O—C12O—H12O	119.2
C2A5—C1A5—H1A5	123.9	C13O—C12O—C11O	121.6 (4)
N1B5—C1B5—Ag1C	127.8 (3)	C13O—C12O—H12O	119.2
N2B5—C1B5—Ag1C	128.6 (3)	C12O—C13O—H13O	119.6
N2B5—C1B5—N1B5	103.3 (3)	C14O—C13O—C12O	120.8 (4)
N2C5—C1C5—H1C5	124.2	C14O—C13O—H13O	119.6
N2C5—C1C5—C2C5	111.6 (6)	C13O—C14O—H14O	120.2
C2C5—C1C5—H1C5	124.2	C13O—C14O—C15O	119.5 (4)
N1A5—C1R—N1B5	112.6 (3)	C15O—C14O—H14O	120.2
N1A5—C1R—H1RA	109.1	C14O—C15O—H15O	120.2
N1A5—C1R—H1RB	109.1	C16O—C15O—C14O	119.7 (4)
N1B5—C1R—H1RA	109.1	C16O—C15O—H15O	120.2
N1B5—C1R—H1RB	109.1	C11O—C16O—H16O	118.5
H1RA—C1R—H1RB	107.8	C15O—C16O—C11O	123.0 (4)
C1A5—C2A5—H2A5	127.7	C15O—C16O—H16O	118.5
C3A5—C2A5—C1A5	104.7 (4)	C22O—C21O—C26O	114.3 (3)
C3A5—C2A5—H2A5	127.7	C22O—C21O—B11O	123.9 (3)
N1B5—C2B5—H2B5	126.7	C26O—C21O—B11O	121.8 (3)
C3B5—C2B5—N1B5	106.5 (4)	C21O—C22O—H22O	118.5
C3B5—C2B5—H2B5	126.7	C23O—C22O—C21O	123.1 (4)
C1C5—C2C5—H2C5	127.4	C23O—C22O—H22O	118.5
C3C5—C2C5—C1C5	105.1 (6)	C22O—C23O—H23O	119.8
C3C5—C2C5—H2C5	127.4	C24O—C23O—C22O	120.3 (4)
N1C5—C2R—N2B5	111.3 (3)	C24O—C23O—H23O	119.8
N1C5—C2R—H2RA	109.4	C23O—C24O—H24O	120.6
N1C5—C2R—H2RB	109.4	C25O—C24O—C23O	118.8 (4)
N2B5—C2R—H2RA	109.4	C25O—C24O—H24O	120.6
N2B5—C2R—H2RB	109.4	C24O—C25O—H25O	120.0
H2RA—C2R—H2RB	108.0	C24O—C25O—C26O	120.0 (4)
N1A5—C3A5—C2A5	106.6 (4)	C26O—C25O—H25O	120.0
N1A5—C3A5—H3A5	126.7	C21O—C26O—H26O	118.4
C2A5—C3A5—H3A5	126.7	C25O—C26O—C21O	123.3 (4)
N2B5—C3B5—H3B5	126.8	C25O—C26O—H26O	118.4
C2B5—C3B5—N2B5	106.5 (4)	C32O—C31O—B11O	121.8 (3)
C2B5—C3B5—H3B5	126.8	C36O—C31O—C32O	115.0 (3)
N1C5—C3C5—C2C5	106.8 (6)	C36O—C31O—B11O	123.2 (3)
N1C5—C3C5—H3C5	126.6	C31O—C32O—H32O	118.6
C2C5—C3C5—H3C5	126.6	C33O—C32O—C31O	122.8 (4)
C1B4—Ag1B—C1B3	175.61 (15)	C33O—C32O—H32O	118.6
N2A3—N1A3—C1Q	120.0 (3)	C32O—C33O—H33O	120.0
N2A3—N1A3—C3A3	111.8 (3)	C34O—C33O—C32O	120.0 (4)

C3A3—N1A3—C1Q	127.9 (4)	C34O—C33O—H33O	120.0
N2A4—N1A4—C1Q'	120.2 (3)	C33O—C34O—H34O	120.5
N2A4—N1A4—C3A4	111.8 (4)	C35O—C34O—C33O	119.0 (4)
C3A4—N1A4—C1Q'	127.9 (4)	C35O—C34O—H34O	120.5
C1B3—N1B3—C1Q	124.0 (3)	C34O—C35O—H35O	119.5
C1B3—N1B3—C2B3	111.3 (4)	C34O—C35O—C36O	121.0 (4)
C2B3—N1B3—C1Q	124.7 (3)	C36O—C35O—H35O	119.5
C1B4—N1B4—C1Q'	125.3 (3)	C31O—C36O—H36O	119.0
C1B4—N1B4—C2B4	111.9 (3)	C35O—C36O—C31O	122.1 (4)
C2B4—N1B4—C1Q'	122.8 (3)	C35O—C36O—H36O	119.0
N2C3—N1C3—C2Q	119.2 (4)	C42O—C41O—B11O	118.5 (3)
C3C3—N1C3—N2C3	111.9 (4)	C46O—C41O—C42O	114.5 (3)
C3C3—N1C3—C2Q	128.8 (4)	C46O—C41O—B11O	126.5 (3)
N2C4—N1C4—C2Q'	118.8 (4)	C41O—C42O—H42O	118.1
C3C4—N1C4—N2C4	112.4 (4)	C43O—C42O—C41O	123.8 (4)
C3C4—N1C4—C2Q'	128.6 (4)	C43O—C42O—H42O	118.1
C1A3—N2A3—N1A3	104.2 (3)	C42O—C43O—H43O	120.2
C1A4—N2A4—N1A4	103.5 (3)	C42O—C43O—C44O	119.6 (4)
C1B3—N2B3—C2Q	124.7 (3)	C44O—C43O—H43O	120.2
C1B3—N2B3—C3B3	111.4 (3)	C43O—C44O—H44O	120.6
C3B3—N2B3—C2Q	123.7 (3)	C45O—C44O—C43O	118.8 (4)
C1B4—N2B4—C2Q'	124.2 (3)	C45O—C44O—H44O	120.6
C1B4—N2B4—C3B4	112.0 (3)	C44O—C45O—H45O	119.7
C3B4—N2B4—C2Q'	123.8 (3)	C44O—C45O—C46O	120.7 (4)
C1C3—N2C3—N1C3	104.3 (5)	C46O—C45O—H45O	119.7
C1C4—N2C4—N1C4	103.2 (5)	C41O—C46O—H46O	118.7
N2A3—C1A3—H1A3	124.0	C45O—C46O—C41O	122.7 (4)
N2A3—C1A3—C2A3	112.0 (4)	C45O—C46O—H46O	118.7
C2A3—C1A3—H1A3	124.0	C11O—B11O—C31O	112.2 (3)
N2A4—C1A4—H1A4	123.5	C11O—B11O—C41O	102.2 (3)
N2A4—C1A4—C2A4	112.9 (4)	C21O—B11O—C11O	112.9 (3)
C2A4—C1A4—H1A4	123.5	C21O—B11O—C31O	106.7 (3)
N1B3—C1B3—Ag1B	128.0 (3)	C21O—B11O—C41O	113.6 (3)
N2B3—C1B3—Ag1B	127.9 (3)	C31O—B11O—C41O	109.3 (3)
N2B3—C1B3—N1B3	104.0 (3)	C12N—C11N—C16N	114.5 (3)
N1B4—C1B4—Ag1B	126.0 (3)	C12N—C11N—B1N	123.9 (3)
N1B4—C1B4—N2B4	103.3 (3)	C16N—C11N—B1N	121.7 (3)
N2B4—C1B4—Ag1B	130.6 (3)	C11N—C12N—H12N	118.2
N2C3—C1C3—H1C3	124.0	C13N—C12N—C11N	123.6 (4)
N2C3—C1C3—C2C3	112.1 (5)	C13N—C12N—H12N	118.2
C2C3—C1C3—H1C3	124.0	C12N—C13N—H13N	120.2



N2C4—C1C4—H1C4	123.5	C14N—C13N—C12N	119.6 (4)
N2C4—C1C4—C2C4	113.0 (6)	C14N—C13N—H13N	120.2
C2C4—C1C4—H1C4	123.5	C13N—C14N—H14N	120.5
N1A3—C1Q—N1B3	112.2 (3)	C13N—C14N—C15N	119.1 (4)
N1A3—C1Q—H1Q	123.9	C15N—C14N—H14N	120.5
N1B3—C1Q—H1Q	123.9	C14N—C15N—H15N	119.7
N1A4—C1Q'—N1B4	112.2 (3)	C16N—C15N—C14N	120.7 (4)
N1A4—C1Q'—H1QA	109.2	C16N—C15N—H15N	119.7
N1A4—C1Q'—H1QB	109.2	C11N—C16N—H16N	118.7
N1B4—C1Q'—H1QA	109.2	C15N—C16N—C11N	122.6 (4)
N1B4—C1Q'—H1QB	109.2	C15N—C16N—H16N	118.7
H1QA—C1Q'—H1QB	107.9	C22N—C21N—B1N	123.5 (3)
C1A3—C2A3—H2A3	127.4	C26N—C21N—C22N	114.8 (3)
C3A3—C2A3—C1A3	105.3 (4)	C26N—C21N—B1N	121.4 (3)
C3A3—C2A3—H2A3	127.4	C21N—C22N—H22N	118.8
C1A4—C2A4—H2A4	127.8	C23N—C22N—C21N	122.4 (4)
C3A4—C2A4—C1A4	104.4 (4)	C23N—C22N—H22N	118.8
C3A4—C2A4—H2A4	127.8	C22N—C23N—H23N	119.9
N1B3—C2B3—H2B3	126.8	C24N—C23N—C22N	120.2 (4)
C3B3—C2B3—N1B3	106.4 (4)	C24N—C23N—H23N	119.9
C3B3—C2B3—H2B3	126.8	C23N—C24N—H24N	120.2
N1B4—C2B4—H2B4	126.8	C23N—C24N—C25N	119.6 (4)
C3B4—C2B4—N1B4	106.4 (4)	C25N—C24N—H24N	120.2
C3B4—C2B4—H2B4	126.8	C24N—C25N—H25N	120.0
C1C3—C2C3—H2C3	127.3	C24N—C25N—C26N	120.0 (4)
C3C3—C2C3—C1C3	105.5 (5)	C26N—C25N—H25N	120.0
C3C3—C2C3—H2C3	127.3	C21N—C26N—H26N	118.5
C1C4—C2C4—H2C4	127.8	C25N—C26N—C21N	123.0 (4)
C3C4—C2C4—C1C4	104.4 (6)	C25N—C26N—H26N	118.5
C3C4—C2C4—H2C4	127.8	C32N—C31N—C36N	114.6 (3)
N1C3—C2Q—N2B3	111.3 (3)	C32N—C31N—B1N	125.5 (4)
N1C3—C2Q—H2QA	109.4	C36N—C31N—B1N	119.9 (3)
N1C3—C2Q—H2QB	109.4	C31N—C32N—H32N	118.3
N2B3—C2Q—H2QA	109.4	C33N—C32N—C31N	123.3 (4)
N2B3—C2Q—H2QB	109.4	C33N—C32N—H32N	118.3
H2QA—C2Q—H2QB	108.0	C32N—C33N—H33N	119.9
N1C4—C2Q'—N2B4	111.4 (3)	C34N—C33N—C32N	120.2 (4)
N1C4—C2Q'—H2QC	109.3	C34N—C33N—H33N	119.9
N1C4—C2Q'—H2QD	109.3	C33N—C34N—H34N	120.6
N2B4—C2Q'—H2QC	109.3	C33N—C34N—C35N	118.8 (4)
N2B4—C2Q'—H2QD	109.3	C35N—C34N—H34N	120.6

H2QC—C2Q'—H2QD	108.0	C34N—C35N—H35N	120.2
N1A3—C3A3—H3A3	126.7	C36N—C35N—C34N	119.7 (4)
C2A3—C3A3—N1A3	106.6 (4)	C36N—C35N—H35N	120.2
C2A3—C3A3—H3A3	126.7	C31N—C36N—H36N	118.3
N1A4—C3A4—H3A4	126.3	C35N—C36N—C31N	123.4 (4)
C2A4—C3A4—N1A4	107.4 (4)	C35N—C36N—H36N	118.3
C2A4—C3A4—H3A4	126.3	C42N—C41N—C46N	114.6 (3)
N2B3—C3B3—H3B3	126.5	C42N—C41N—B1N	127.0 (3)
C2B3—C3B3—N2B3	107.0 (4)	C46N—C41N—B1N	118.3 (3)
C2B3—C3B3—H3B3	126.5	C41N—C42N—H42N	118.4
N2B4—C3B4—H3B4	126.8	C43N—C42N—C41N	123.2 (4)
C2B4—C3B4—N2B4	106.5 (4)	C43N—C42N—H42N	118.4
C2B4—C3B4—H3B4	126.8	C42N—C43N—H43N	119.8
N1C3—C3C3—C2C3	106.2 (5)	C44N—C43N—C42N	120.4 (4)
N1C3—C3C3—H3C3	126.9	C44N—C43N—H43N	119.8
C2C3—C3C3—H3C3	126.9	C43N—C44N—H44N	120.9
N1C4—C3C4—C2C4	107.0 (6)	C43N—C44N—C45N	118.2 (4)
N1C4—C3C4—H3C4	126.5	C45N—C44N—H44N	120.9
C2C4—C3C4—H3C4	126.5	C44N—C45N—H45N	119.8
C1B6—Ag1D—C1B6 <sup>ii</sup>	180.0	C46N—C45N—C44N	120.5 (4)
N2A6—N1A6—C1S	119.7 (3)	C46N—C45N—H45N	119.8
C3A6—N1A6—N2A6	111.4 (3)	C41N—C46N—H46N	118.4
C3A6—N1A6—C1S	128.9 (3)	C45N—C46N—C41N	123.1 (4)
C1B6—N1B6—C1S	124.4 (3)	C45N—C46N—H46N	118.4
C1B6—N1B6—C2B6	111.8 (3)	C11N—B1N—C31N	106.6 (3)
C2B6—N1B6—C1S	123.8 (3)	C11N—B1N—C41N	109.2 (3)
N2C6—N1C6—C2S	120.4 (3)	C21N—B1N—C11N	112.4 (3)
N2C6—N1C6—C3C6	110.9 (4)	C21N—B1N—C31N	112.9 (3)
C3C6—N1C6—C2S	128.7 (3)	C21N—B1N—C41N	103.7 (3)
C1A6—N2A6—N1A6	103.9 (3)	C31N—B1N—C41N	112.1 (3)
C1B6—N2B6—C2S	124.0 (3)		

Symmetry code(s): (i)  $-x, -y+1, -z+2$ ; (ii)  $-x+1, -y+1, -z+3$ .

#### Selected geometric parameters, torsion angles ( $^{\circ}$ )

N1A1—N2A1— C1A1—C2A1	0.2 (5)	C1C6—C2C6— C3C6—N1C6	-0.2 (5)
N1A2—N2A2— C1A2—C2A2	-0.5 (5)	C1S—N1A6— N2A6—C1A6	-179.1 (3)
N1B1—C2B1— C3B1—N2B1	-0.2 (4)	C1S—N1A6— C3A6—C2A6	178.8 (4)
N1B2—C2B2—	0.4 (4)	C1S—N1B6—C1B6—	-6.7 (5)

C3B2—N2B2		Ag1D	
N1C1—N2C1— C1C1—C2C1	-0.2 (6)	C1S—N1B6—C1B6— N2B6	177.4 (3)
N1C2—N2C2— C1C2—C2C2	0.6 (5)	C1S—N1B6—C2B6— C3B6	-177.9 (3)
N2A1—N1A1— C1P—N1B1	-96.4 (4)	C2B6—N1B6— C1B6—Ag1D	175.1 (3)
N2A1—N1A1— C3A1—C2A1	0.0 (5)	C2B6—N1B6— C1B6—N2B6	-0.8 (4)
N2A1—C1A1— C2A1—C3A1	-0.2 (5)	C2B6—N1B6—C1S— N1A6	-104.8 (4)
N2A2—N1A2— C1P—N1B2	86.0 (4)	C2S—N1C6— N2C6—C1C6	176.6 (4)
N2A2—N1A2— C3A2—C2A2	-0.5 (5)	C2S—N1C6—C3C6— C2C6	-176.2 (4)
N2A2—C1A2— C2A2—C3A2	0.3 (6)	C2S—N2B6—C1B6— Ag1D	3.7 (5)
N2C1—N1C1— C2P—N2B1	-80.6 (4)	C2S—N2B6—C1B6— N1B6	179.3 (3)
N2C1—N1C1— C3C1—C2C1	-2.0 (5)	C2S—N2B6—C3B6— C2B6	-179.2 (3)
N2C1—C1C1— C2C1—C3C1	-1.0 (7)	C3A6—N1A6— N2A6—C1A6	-0.7 (4)
N2C2—N1C2— C2P—N2B2	78.9 (4)	C3A6—N1A6— C1S—N1B6	96.1 (5)
N2C2—N1C2— C3C2—C2C2	-0.1 (5)	C3B6—N2B6— C1B6—Ag1D	-174.6 (3)
N2C2—C1C2— C2C2—C3C2	-0.7 (6)	C3B6—N2B6— C1B6—N1B6	1.0 (4)
C1A1—C2A1— C3A1—N1A1	0.1 (5)	C3B6—N2B6—C2S— N1C6	70.0 (5)
C1A2—C2A2— C3A2—N1A2	0.1 (6)	C3C6—N1C6— N2C6—C1C6	-0.3 (5)
C1B1—N1B1—C1P— N1A1	71.1 (5)	C3C6—N1C6—C2S— N2B6	92.2 (5)
C1B1—N1B1— C2B1—C3B1	0.4 (4)	C11M—C12M— C13M—C14M	0.0 (5)
C1B1—N2B1—C2P— N1C1	-96.2 (4)	C12M—C11M— C16M—C15M	-0.8 (5)
C1B1—N2B1— C3B1—C2B1	-0.1 (4)	C12M—C11M— B1M—C21M	-156.6 (3)
C1B2—N1B2— C1P—N1A2	-97.0 (4)	C12M—C11M— B1M—C31M	-36.5 (4)
C1B2—N1B2— C2B2—C3B2	-0.8 (4)	C12M—C11M— B1M—C41M	83.0 (4)
C1B2—N2B2— C2P—N1C2	104.7 (4)	C12M—C13M— C14M—C15M	-1.8 (5)
C1B2—N2B2—	0.2 (4)	C13M—C14M—	2.2 (6)

C3B2—C2B2		C15M—C16M	
C1C1—C2C1— C3C1—N1C1	1.8 (6)	C14M—C15M— C16M—C11M	-0.9 (6)
C1C2—C2C2— C3C2—N1C2	0.4 (5)	C16M—C11M— C12M—C13M	1.3 (5)
C1P—N1A1— N2A1—C1A1	-179.1 (4)	C16M—C11M— B1M—C21M	25.1 (5)
C1P—N1A1— C3A1—C2A1	178.8 (4)	C16M—C11M— B1M—C31M	145.2 (3)
C1P—N1B1—C1B1— Ag1A	-9.1 (5)	C16M—C11M— B1M—C41M	-95.3 (4)
C1P—N1B1—C1B1— N2B1	174.1 (3)	C21M—C22M— C23M—C24M	-2.1 (6)
C1P—N1B1—C2B1— C3B1	-174.1 (3)	C22M—C21M— C26M—C25M	-0.2 (6)
C1P <sup>+</sup> —N1A2— N2A2—C1A2	179.2 (3)	C22M—C21M— B1M—C11M	-76.7 (4)
C1P <sup>+</sup> —N1A2— C3A2—C2A2	-179.0 (4)	C22M—C21M— B1M—C31M	164.8 (3)
C1P <sup>+</sup> —N1B2— C1B2—Ag1A	15.6 (5)	C22M—C21M— B1M—C41M	42.9 (5)
C1P <sup>+</sup> —N1B2— C1B2—N2B2	-176.2 (3)	C22M—C23M— C24M—C25M	1.2 (7)
C1P <sup>+</sup> —N1B2— C2B2—C3B2	176.2 (3)	C23M—C24M— C25M—C26M	0.1 (7)
C2B1—N1B1— C1B1—Ag1A	176.3 (3)	C24M—C25M— C26M—C21M	-0.6 (7)
C2B1—N1B1— C1B1—N2B1	-0.5 (4)	C26M—C21M— C22M—C23M	1.6 (6)
C2B1—N1B1—C1P— N1A1	-115.0 (4)	C26M—C21M— B1M—C11M	102.1 (4)
C2B2—N1B2— C1B2—Ag1A	-167.3 (3)	C26M—C21M— B1M—C31M	-16.3 (5)
C2B2—N1B2— C1B2—N2B2	0.9 (4)	C26M—C21M— B1M—C41M	-138.3 (4)
C2B2—N1B2— C1P <sup>+</sup> —N1A2	86.3 (4)	C31M—C32M— C33M—C34M	-0.6 (6)
C2P—N1C1— N2C1—C1C1	172.7 (4)	C32M—C31M— C36M—C35M	-0.8 (5)
C2P—N1C1—C3C1— C2C1	-172.4 (4)	C32M—C31M— B1M—C11M	-51.1 (4)
C2P—N2B1—C1B1— Ag1A	-0.1 (5)	C32M—C31M— B1M—C21M	68.1 (4)
C2P—N2B1—C1B1— N1B1	176.7 (3)	C32M—C31M— B1M—C41M	-169.8 (3)
C2P—N2B1—C3B1— C2B1	-176.5 (3)	C32M—C33M— C34M—C35M	-0.3 (6)
C2P <sup>+</sup> —N1C2—	-176.8 (4)	C33M—C34M—	0.7 (6)

N2C2—C1C2		C35M—C36M	
C2P <sup>i</sup> —N1C2—	176.0 (4)	C34M—C35M—	-0.1 (6)
C3C2—C2C2		C36M—C31M	
C2P <sup>i</sup> —N2B2—	-15.3 (5)	C36M—C31M—	1.1 (6)
C1B2—Ag1A		C32M—C33M	
C2P <sup>i</sup> —N2B2—	176.8 (3)	C36M—C31M—	131.3 (4)
C1B2—N1B2		B1M—C11M	
C2P <sup>i</sup> —N2B2—	-177.2 (3)	C36M—C31M—	-109.5 (4)
C3B2—C2B2		B1M—C21M	
C3A1—N1A1—	-0.1 (4)	C36M—C31M—	12.6 (5)
N2A1—C1A1		B1M—C41M	
C3A1—N1A1—	84.9 (5)	C41M—C42M—	-2.1 (6)
C1P—N1B1		C43M—C44M	
C3A2—N1A2—	0.6 (5)	C42M—C41M—	-0.8 (6)
N2A2—C1A2		C46M—C45M	
C3A2—N1A2—	-95.6 (5)	C42M—C41M—	139.4 (4)
C1P <sup>i</sup> —N1B2		B1M—C11M	
C3B1—N2B1—	-176.4 (3)	C42M—C41M—	19.7 (5)
C1B1—Ag1A		B1M—C21M	
C3B1—N2B1—	0.4 (4)	C42M—C41M—	-102.5 (4)
C1B1—N1B1		B1M—C31M	
C3B1—N2B1—C2P—	79.7 (4)	C42M—C43M—	1.3 (6)
N1C1		C44M—C45M	
C3B2—N2B2—	167.3 (3)	C43M—C44M—	-0.4 (6)
C1B2—Ag1A		C45M—C46M	
C3B2—N2B2—	-0.7 (4)	C44M—C45M—	0.2 (6)
C1B2—N1B2		C46M—C41M	
C3B2—N2B2—	-78.3 (4)	C46M—C41M—	1.7 (5)
C2P <sup>i</sup> —N1C2		C42M—C43M	
C3C1—N1C1—	1.3 (5)	C46M—C41M—	-42.3 (5)
N2C1—C1C1		B1M—C11M	
C3C1—N1C1—C2P—	89.2 (5)	C46M—C41M—	-162.0 (3)
N2B1		B1M—C21M	
C3C2—N1C2—	-0.3 (5)	C46M—C41M—	75.7 (4)
N2C2—C1C2		B1M—C31M	
C3C2—N1C2—	-96.8 (5)	B1M—C11M—	-177.2 (3)
C2P <sup>i</sup> —N2B2		C12M—C13M	
N1A5—N2A5—	0.0 (5)	B1M—C11M—	177.6 (3)
C1A5—C2A5		C16M—C15M	
N1B5—C2B5—	-0.9 (6)	B1M—C21M—	-179.5 (4)
C3B5—N2B5		C22M—C23M	
N1C5—N2C5—	-1.2 (7)	B1M—C21M—	-179.1 (4)
C1C5—C2C5		C26M—C25M	
N2A5—N1A5—	-95.7 (4)	B1M—C31M—	-176.7 (4)
C1R—N1B5		C32M—C33M	
N2A5—N1A5—	-0.2 (5)	B1M—C31M—	177.0 (3)
C3A5—C2A5		C36M—C35M	
N2A5—C1A5—	-0.1 (5)	B1M—C41M—	-179.9 (4)

C2A5—C3A5		C42M—C43M	
N2C5—N1C5— C2R—N2B5	-89.1 (5)	B1M—C41M— C46M—C45M	-179.2 (4)
N2C5—N1C5— C3C5—C2C5	0.0 (6)	C11O—C12O— C13O—C14O	-2.6 (7)
N2C5—C1C5— C2C5—C3C5	1.2 (7)	C12O—C11O— C16O—C15O	1.1 (6)
C1A5—C2A5— C3A5—N1A5	0.2 (5)	C12O—C11O— B11O—C21O	-148.8 (3)
C1B5—N1B5— C1R—N1A5	74.5 (5)	C12O—C11O— B11O—C31O	-28.2 (5)
C1B5—N1B5— C2B5—C3B5	0.7 (6)	C12O—C11O— B11O—C41O	88.8 (4)
C1B5—N2B5— C2R—N1C5	-115.5 (4)	C12O—C13O— C14O—C15O	2.7 (8)
C1B5—N2B5— C3B5—C2B5	0.8 (6)	C13O—C14O— C15O—C16O	-1.0 (7)
C1C5—C2C5— C3C5—N1C5	-0.7 (6)	C14O—C15O— C16O—C11O	-0.9 (7)
C1R—N1A5— N2A5—C1A5	178.4 (4)	C16O—C11O— C12O—C13O	0.6 (6)
C1R—N1A5— C3A5—C2A5	-178.3 (4)	C16O—C11O— B11O—C21O	41.3 (5)
C1R—N1B5— C1B5—Ag1C	-6.5 (6)	C16O—C11O— B11O—C31O	162.0 (3)
C1R—N1B5— C1B5—N2B5	179.3 (3)	C16O—C11O— B11O—C41O	-81.1 (4)
C1R—N1B5— C2B5—C3B5	-178.8 (4)	C21O—C22O— C23O—C24O	-1.0 (6)
C2B5—N1B5— C1B5—Ag1C	174.0 (3)	C22O—C21O— C26O—C25O	-3.7 (5)
C2B5—N1B5— C1B5—N2B5	-0.2 (5)	C22O—C21O— B11O—C11O	18.9 (5)
C2B5—N1B5— C1R—N1A5	-106.0 (5)	C22O—C21O— B11O—C31O	-104.8 (4)
C2R—N1C5— N2C5—C1C5	178.5 (4)	C22O—C21O— B11O—C41O	134.7 (4)
C2R—N1C5— C3C5—C2C5	-177.5 (4)	C22O—C23O— C24O—C25O	-1.6 (6)
C2R—N2B5— C1B5—Ag1C	8.7 (6)	C23O—C24O— C25O—C26O	1.4 (6)
C2R—N2B5— C1B5—N1B5	-177.1 (4)	C24O—C25O— C26O—C21O	1.3 (6)
C2R—N2B5— C3B5—C2B5	177.6 (4)	C26O—C21O— C22O—C23O	3.5 (5)
C3A5—N1A5— N2A5—C1A5	0.1 (5)	C26O—C21O— B11O—C11O	-162.3 (3)
C3A5—N1A5—	82.3 (5)	C26O—C21O—	74.0 (4)

C1R—N1B5		B11O—C31O	
C3B5—N2B5—	-174.5 (3)	C26O—C21O—	-46.5 (5)
C1B5—Ag1C		B11O—C41O	
C3B5—N2B5—	-0.3 (5)	C31O—C32O—	1.8 (5)
C1B5—N1B5		C33O—C34O	
C3B5—N2B5—	68.1 (6)	C32O—C31O—	1.6 (5)
C2R—N1C5		C36O—C35O	
C3C5—N1C5—	0.7 (6)	C32O—C31O—	-39.3 (5)
N2C5—C1C5		B11O—C11O	
C3C5—N1C5—	88.3 (6)	C32O—C31O—	84.9 (4)
C2R—N2B5		B11O—C21O	
N1A3—N2A3—	-0.4 (5)	C32O—C31O—	-151.9 (3)
C1A3—C2A3		B11O—C41O	
N1A4—N2A4—	-0.4 (5)	C32O—C33O—	-0.3 (5)
C1A4—C2A4		C34O—C35O	
N1B3—C2B3—	0.1 (5)	C33O—C34O—	-0.5 (5)
C3B3—N2B3		C35O—C36O	
N1B4—C2B4—	-0.4 (5)	C34O—C35O—	-0.2 (5)
C3B4—N2B4		C36O—C31O	
N1C3—N2C3—	0.5 (7)	C36O—C31O—	-2.3 (5)
C1C3—C2C3		C32O—C33O	
N1C4—N2C4—	-1.4 (6)	C36O—C31O—	142.2 (3)
C1C4—C2C4		B11O—C11O	
N2A3—N1A3—	93.0 (4)	C36O—C31O—	-93.6 (4)
C1Q—N1B3		B11O—C21O	
N2A3—N1A3—	1.1 (5)	C36O—C31O—	29.6 (5)
C3A3—C2A3		B11O—C41O	
N2A3—C1A3—	1.0 (5)	C41O—C42O—	0.9 (6)
C2A3—C3A3		C43O—C44O	
N2A4—N1A4—	-97.3 (4)	C42O—C41O—	1.1 (5)
C1Q'—N1B4		C46O—C45O	
N2A4—N1A4—	-0.8 (5)	C42O—C41O—	-62.3 (4)
C3A4—C2A4		B11O—C11O	
N2A4—C1A4—	0.0 (6)	C42O—C41O—	175.8 (3)
C2A4—C3A4		B11O—C21O	
N2C3—N1C3—	86.5 (4)	C42O—C41O—	56.8 (4)
C2Q—N2B3		B11O—C31O	
N2C3—N1C3—	0.2 (5)	C42O—C43O—	1.2 (6)
C3C3—C2C3		C44O—C45O	
N2C3—C1C3—	-0.4 (7)	C43O—C44O—	-2.0 (6)
C2C3—C3C3		C45O—C46O	
N2C4—N1C4—	-95.1 (4)	C44O—C45O—	0.8 (6)
C2Q'—N2B4		C46O—C41O	
N2C4—N1C4—	-0.3 (6)	C46O—C41O—	-2.0 (5)
C3C4—C2C4		C42O—C43O	
N2C4—C1C4—	1.2 (7)	C46O—C41O—	108.9 (4)
C2C4—C3C4		B11O—C11O	
C1A3—C2A3—	-1.2 (5)	C46O—C41O—	-13.0 (5)

C3A3—N1A3		B11O—C21O	
C1A4—C2A4—	0.5 (5)	C46O—C41O—	-132.1 (4)
C3A4—N1A4		B11O—C31O	
C1B3—N1B3—	-72.2 (5)	B11O—C11O—	-169.8 (4)
C1Q—N1A3		C12O—C13O	
C1B3—N1B3—	-0.2 (5)	B11O—C11O—	171.6 (4)
C2B3—C3B3		C16O—C15O	
C1B3—N2B3—	118.5 (4)	B11O—C21O—	-177.6 (4)
C2Q—N1C3		C22O—C23O	
C1B3—N2B3—	0.1 (5)	B11O—C21O—	177.4 (3)
C3B3—C2B3		C26O—C25O	
C1B4—N1B4—	82.4 (5)	B11O—C31O—	179.1 (3)
C1Q'—N1A4		C32O—C33O	
C1B4—N1B4—	0.2 (5)	B11O—C31O—	-179.8 (3)
C2B4—C3B4		C36O—C35O	
C1B4—N2B4—	-113.6 (4)	B11O—C41O—	170.2 (3)
C2Q'—N1C4		C42O—C43O	
C1B4—N2B4—	0.4 (5)	B11O—C41O—	-170.3 (3)
C3B4—C2B4		C46O—C45O	
C1C3—C2C3—	0.1 (6)	C11N—C12N—	-0.6 (6)
C3C3—N1C3		C13N—C14N	
C1C4—C2C4—	-0.5 (6)	C12N—C11N—	2.3 (5)
C3C4—N1C4		C16N—C15N	
C1Q—N1A3—	-175.5 (3)	C12N—C11N—	-138.3 (4)
N2A3—C1A3		B1N—C21N	
C1Q—N1A3—	175.7 (4)	C12N—C11N—	97.4 (4)
C3A3—C2A3		B1N—C31N	
C1Q—N1B3—	4.9 (5)	C12N—C11N—	-23.9 (5)
C1B3—Ag1B		B1N—C41N	
C1Q—N1B3—	-179.3 (3)	C12N—C13N—	1.4 (6)
C1B3—N2B3		C14N—C15N	
C1Q—N1B3—	179.3 (3)	C13N—C14N—	-0.3 (6)
C2B3—C3B3		C15N—C16N	
C1Q'—N1A4—	175.8 (3)	C14N—C15N—	-1.7 (6)
N2A4—C1A4		C16N—C11N	
C1Q'—N1A4—	-175.4 (4)	C16N—C11N—	-1.2 (5)
C3A4—C2A4		C12N—C13N	
C1Q'—N1B4—	-4.4 (6)	C16N—C11N—	43.7 (5)
C1B4—Ag1B		B1N—C21N	
C1Q'—N1B4—	179.4 (3)	C16N—C11N—	-80.6 (4)
C1B4—N2B4		B1N—C31N	
C1Q'—N1B4—	-179.2 (4)	C16N—C11N—	158.1 (3)
C2B4—C3B4		B1N—C41N	
C2B3—N1B3—	-175.5 (3)	C21N—C22N—	0.9 (7)
C1B3—Ag1B		C23N—C24N	
C2B3—N1B3—	0.3 (4)	C22N—C21N—	0.8 (6)
C1B3—N2B3		C26N—C25N	
C2B3—N1B3—	108.2 (4)	C22N—C21N—	19.2 (5)



C1Q—N1A3		B1N—C11N	
C2B4—N1B4—	176.2 (3)	C22N—C21N—	139.8 (4)
C1B4—Ag1B		B1N—C31N	
C2B4—N1B4—	0.0 (4)	C22N—C21N—	-98.6 (4)
C1B4—N2B4		B1N—C41N	
C2B4—N1B4—	-98.3 (4)	C22N—C23N—	-0.3 (7)
C1Q'—N1A4		C24N—C25N	
C2Q—N1C3—	-176.5 (4)	C23N—C24N—	0.0 (7)
N2C3—C1C3		C25N—C26N	
C2Q—N1C3—	175.8 (4)	C24N—C25N—	-0.3 (7)
C3C3—C2C3		C26N—C21N	
C2Q—N2B3—	-9.0 (5)	C26N—C21N—	-1.1 (6)
C1B3—Ag1B		C22N—C23N	
C2Q—N2B3—	175.1 (3)	C26N—C21N—	-168.3 (3)
C1B3—N1B3		B1N—C11N	
C2Q—N2B3—	-175.3 (3)	C26N—C21N—	-47.7 (5)
C3B3—C2B3		B1N—C31N	
C2Q'—N1C4—	176.4 (4)	C26N—C21N—	73.9 (4)
N2C4—C1C4		B1N—C41N	
C2Q'—N1C4—	-175.1 (4)	C31N—C32N—	1.5 (6)
C3C4—C2C4		C33N—C34N	
C2Q'—N2B4—	3.7 (6)	C32N—C31N—	2.6 (5)
C1B4—Ag1B		C36N—C35N	
C2Q'—N2B4—	179.7 (3)	C32N—C31N—	112.3 (4)
C1B4—N1B4		B1N—C11N	
C2Q'—N2B4—	-179.6 (4)	C32N—C31N—	-11.6 (5)
C3B4—C2B4		B1N—C21N	
C3A3—N1A3—	-0.4 (4)	C32N—C31N—	-128.2 (4)
N2A3—C1A3		B1N—C41N	
C3A3—N1A3—	-81.3 (5)	C32N—C33N—	0.8 (6)
C1Q—N1B3		C34N—C35N	
C3A4—N1A4—	0.7 (5)	C33N—C34N—	-1.2 (6)
N2A4—C1A4		C35N—C36N	
C3A4—N1A4—	76.9 (5)	C34N—C35N—	-0.6 (6)
C1Q'—N1B4		C36N—C31N	
C3B3—N2B3—	175.6 (3)	C36N—C31N—	-3.1 (6)
C1B3—Ag1B		C32N—C33N	
C3B3—N2B3—	-0.3 (4)	C36N—C31N—	-65.2 (4)
C1B3—N1B3		B1N—C11N	
C3B3—N2B3—	-66.7 (5)	C36N—C31N—	170.9 (3)
C2Q—N1C3		B1N—C21N	
C3B4—N2B4—	-176.2 (3)	C36N—C31N—	54.2 (4)
C1B4—Ag1B		B1N—C41N	
C3B4—N2B4—	-0.2 (4)	C41N—C42N—	0.2 (6)
C1B4—N1B4		C43N—C44N	
C3B4—N2B4—	66.3 (5)	C42N—C41N—	0.1 (5)
C2Q'—N1C4		C46N—C45N	
C3C3—N1C3—	-0.4 (6)	C42N—C41N—	123.1 (4)

N2C3—C1C3		B1N—C11N	
C3C3—N1C3— C2Q—N2B3	-88.8 (5)	C42N—C41N— B1N—C21N	-116.9 (4)
C3C4—N1C4— N2C4—C1C4	1.0 (5)	C42N—C41N— B1N—C31N	5.2 (5)
C3C4—N1C4— C2Q'—N2B4	79.4 (5)	C42N—C43N— C44N—C45N	0.4 (6)
N1A6—N2A6— C1A6—C2A6	0.6 (5)	C43N—C44N— C45N—C46N	-0.8 (6)
N1B6—C2B6— C3B6—N2B6	0.4 (4)	C44N—C45N— C46N—C41N	0.5 (6)
N1C6—N2C6— C1C6—C2C6	0.1 (5)	C46N—C41N— C42N—C43N	-0.5 (5)
N2A6—N1A6— C1S—N1B6	-85.7 (4)	C46N—C41N— B1N—C11N	-60.7 (4)
N2A6—N1A6— C3A6—C2A6	0.6 (5)	C46N—C41N— B1N—C21N	59.3 (4)
N2A6—C1A6— C2A6—C3A6	-0.2 (5)	C46N—C41N— B1N—C31N	-178.6 (3)
N2C6—N1C6— C2S—N2B6	-84.0 (4)	B1N—C11N— C12N—C13N	-179.3 (3)
N2C6—N1C6— C3C6—C2C6	0.3 (5)	B1N—C11N— C16N—C15N	-179.5 (3)
N2C6—C1C6— C2C6—C3C6	0.1 (6)	B1N—C21N— C22N—C23N	171.9 (4)
C1A6—C2A6— C3A6—N1A6	-0.2 (5)	B1N—C21N— C26N—C25N	-172.3 (4)
C1B6—N1B6—C1S— N1A6	77.2 (5)	B1N—C31N— C32N—C33N	179.2 (4)
C1B6—N1B6— C2B6—C3B6	0.3 (4)	B1N—C31N— C36N—C35N	-179.5 (3)
C1B6—N2B6—C2S— N1C6	-108.0 (4)	B1N—C41N— C42N—C43N	175.8 (3)
C1B6—N2B6— C3B6—C2B6	-0.9 (4)	B1N—C41N— C46N—C45N	-176.5 (3)

#### 7.1.4. Crystal data for complex 3

##### Selected geometric parameters (Å)

Ru1—C1AA	2.179 (11)	C79—H79	0.9500
Ru1—Cl7	2.397 (2)	C79—C137	1.387 (11)
Ru1—N26	2.091 (8)	C79—C146	1.392 (12)
Ru1—C102	2.185 (9)	C80—H80	0.9500
Ru1—C114	2.040 (9)	C80—C92	1.371 (15)

Ru1—C150	2.236 (9)	C80—C131	1.370 (14)
Ru1—C184	2.233 (9)	C81—H81	0.9500
Ru1—C0AA	2.171 (10)	C81—C155	1.365 (13)
Ru1—C2AA	2.201 (11)	C81—C161	1.413 (12)
Ru3—Cl8	2.392 (2)	C82—C139	1.402 (12)
Ru3—N7	2.016 (8)	C82—C152	1.392 (12)
Ru3—C10	2.169 (9)	C82—B191	1.649 (13)
Ru3—N12	2.083 (7)	C84—H84	0.9500
Ru3—C84	2.199 (8)	C84—C94	1.378 (13)
Ru3—C94	2.197 (9)	C84—C149	1.435 (13)
Ru3—C149	2.240 (9)	C86—H86	0.9500
Ru3—C176	2.168 (9)	C86—C103	1.424 (12)
Ru3—C190	2.246 (8)	C86—C133	1.396 (12)
C1AA—H1AA	0.9500	C85—H85	0.9500
C1AA—C0AA	1.400 (15)	C87—H87	0.9500
C1AA—C2AA	1.421 (14)	C87—C154	1.414 (12)
Ru2—Cl1X	2.404 (2)	C88—H88A	0.9900
Ru2—C2	2.175 (9)	C88—H88B	0.9900
Ru2—N32	2.100 (8)	C88—N148	1.449 (12)
Ru2—N34	2.036 (9)	C89—H89	0.9500
Ru2—C40	2.202 (9)	C90—H90	0.9500
Ru2—C89	2.191 (9)	B91—C93	1.630 (12)
Ru2—C101	2.172 (9)	C92—H92	0.9500
Ru2—C105	2.235 (8)	C93—C157	1.400 (11)
Ru2—C160	2.249 (9)	C94—H94	0.9500
Ru4—Cl5	2.398 (2)	C94—C176	1.410 (13)
Ru4—N3	2.029 (8)	C95—H95	0.9500
Ru4—N4	2.082 (7)	N96—N148	1.383 (11)
Ru4—C8	2.193 (8)	N96—C185	1.323 (14)
Ru4—C14	2.173 (9)	C97—H97	0.9500
Ru4—C65	2.247 (9)	C97—C164	1.404 (13)
Ru4—C87	2.200 (8)	C98—C108	1.412 (12)
Ru4—C154	2.203 (8)	C98—B208	1.645 (14)
Ru4—C201	2.249 (10)	C100—H100	0.9500
C2—H2	0.9500	C100—C158	1.372 (13)
C2—C89	1.416 (14)	C100—C195	1.393 (12)
C2—C101	1.369 (14)	C99—H99	0.9500
N3—N13	1.364 (10)	C99—C3	1.413 (13)
N3—N1X	1.342 (10)	C101—H101	0.9500
N4—N11	1.361 (9)	C101—C160	1.428 (13)
N4—C61	1.339 (11)	C102—H102	0.9500

N5—C99	1.313 (11)	C102—C150	1.411 (14)
N5—N215	1.342 (9)	C102—C2AA	1.406 (14)
N6—N52	1.349 (10)	C103—B191	1.640 (13)
N6—C165	1.326 (11)	C103—C195	1.418 (12)
N7—N19	1.363 (10)	C104—H10A	0.9900
N7—N2X	1.362 (10)	C104—H10B	0.9900
C8—H8	0.9500	C105—H105	0.9500
C8—C14	1.388 (12)	C105—C160	1.387 (13)
C8—C154	1.418 (12)	C107—C110	1.400 (12)
C9—H9	0.9500	C107—B191	1.637 (13)
C9—N19	1.378 (11)	C107—C198	1.409 (12)
C9—C109	1.320 (13)	C106—H106	0.9500
C10—H10	0.9500	C106—C141	1.368 (14)
C10—C176	1.390 (12)	C109—H109	0.9500
C10—C190	1.418 (13)	C108—H108	0.9500
N11—C47	1.442 (11)	C110—H110	0.9500
N11—C159	1.351 (10)	C110—C121	1.385 (12)
N12—N29	1.373 (10)	C111—H111	0.9500
N12—C156	1.312 (11)	C112—H112	0.9500
N13—C18	1.373 (11)	C112—C165	1.395 (13)
N13—C47	1.450 (10)	C113—H113	0.9500
C14—H14	0.9500	C113—C164	1.376 (15)
C14—C201	1.448 (13)	C113—C193	1.379 (15)
N15—N34	1.362 (11)	C115—H115	0.9500
N15—C67	1.386 (12)	C115—C152	1.380 (13)
N15—C119	1.456 (12)	C115—C188	1.375 (14)
N17—N34	1.351 (11)	C116—H116	0.9500
N17—C118	1.449 (11)	C117—H117	0.9500
N17—C123	1.386 (11)	C117—C122	1.324 (14)
C18—H18	0.9500	C118—H11A	0.9900
C18—C90	1.341 (13)	C118—H11B	0.9900
N19—C25	1.461 (11)	C119—H11C	0.9900
C21—H21	0.9500	C119—H11D	0.9900
C21—C61	1.392 (12)	C120—H120	0.9500
C21—C159	1.360 (13)	C120—C173	1.382 (14)
C22—H22	0.9500	C120—C175	1.371 (14)
C22—C62	1.409 (12)	C121—H121	0.9500
C22—C77	1.372 (12)	C121—C129	1.401 (13)
N2X—C27	1.482 (11)	C122—H122	0.9500
N2X—C109	1.375 (10)	C123—H123	0.9500
N24—C104	1.449 (11)	C125—H125	0.9500

N24—C114	1.352 (11)	C125—C132	1.386 (12)
N24—C117	1.379 (12)	C125—C137	1.408 (12)
C25—H25A	0.9900	C126—H126	0.9500
C25—H25B	0.9900	C126—C180	1.386 (13)
C25—N29	1.444 (11)	B127—C136	1.620 (12)
N26—N41	1.356 (10)	B127—C147	1.647 (12)
N26—C192	1.322 (13)	C128—H128	0.9500
C27—H27A	0.9900	C128—C183	1.391 (14)
C27—H27B	0.9900	C129—H129	0.9500
C27—N52	1.469 (11)	C129—C172	1.380 (13)
C28—H28	0.9500	C130—H130	0.9500
C28—C85	1.386 (12)	C130—C151	1.362 (15)
C28—C111	1.394 (13)	C131—H131	0.9500
N29—C76	1.325 (11)	C132—H132	0.9500
C30—C85	1.373 (12)	C132—C169	1.389 (13)
C30—B91	1.649 (12)	C133—H133	0.9500
C30—C144	1.420 (12)	C133—C158	1.385 (14)
N31—C33	1.349 (12)	C135—H135	0.9500
N31—N54	1.355 (10)	C135—C182	1.396 (14)
N31—C118	1.473 (12)	C136—C168	1.398 (12)
N32—N44	1.364 (10)	C137—B208	1.641 (13)
N32—C131	1.332 (12)	C138—H138	0.9500
C33—H33	0.9500	C138—C151	1.397 (15)
C33—C38	1.360 (14)	C138—C168	1.379 (13)
N1X—C71	1.459 (10)	C139—H139	0.9500
N1X—C90	1.385 (11)	C139—C163	1.405 (13)
C37—C60	1.403 (12)	C140—H140	0.9500
C37—C183	1.403 (13)	C141—H141	0.9500
C37—B191	1.642 (13)	C142—H142	0.9500
C38—H38	0.9500	C142—C166	1.376 (13)
C38—C181	1.377 (14)	C144—H144	0.9500
C39—H39	0.9500	C146—H146	0.9500
C39—C66	1.356 (13)	C146—C169	1.383 (13)
C39—C69	1.390 (13)	C147—C162	1.393 (12)
C40—H40	0.9500	N148—C4	1.335 (13)
C40—C89	1.403 (12)	C149—H149	0.9500
C40—C105	1.420 (13)	C149—C190	1.393 (13)
N41—C104	1.460 (12)	C150—H150	0.9500
N41—C179	1.342 (12)	C150—C184	1.387 (13)
C42—C46	1.411 (12)	C151—H151	0.9500
C42—B91	1.658 (13)	C152—H152	0.9500

C42—C189	1.393 (12)	C153—H153	0.9500
C43—C50	1.394 (12)	C153—C180	1.373 (12)
C43—C97	1.405 (12)	C154—H154	0.9500
C43—B127	1.644 (12)	C155—H155	0.9500
N44—C92	1.366 (12)	C155—C187	1.385 (14)
N44—C119	1.432 (12)	C156—H156	0.9500
N45—C88	1.454 (11)	C156—C167	1.379 (13)
N45—C114	1.354 (11)	C157—H157	0.9500
N45—C122	1.388 (11)	C158—H158	0.9500
C46—H46	0.9500	C159—H159	0.9500
C46—C173	1.397 (13)	C160—H160	0.9500
C47—H47A	0.9900	C162—H162	0.9500
C47—H47B	0.9900	C161—C171	1.394 (12)
C48—H48	0.9500	C161—B208	1.655 (12)
C48—C141	1.385 (14)	C163—H163	0.9500
C48—C162	1.381 (13)	C163—C188	1.379 (14)
C50—H50	0.9500	C164—H164	0.9500
C50—C193	1.400 (13)	C165—H165	0.9500
N52—C55	1.336 (11)	C166—H166	0.9500
C53—H53	0.9500	C167—H167	0.9500
C53—C157	1.377 (12)	C168—H168	0.9500
C53—C166	1.371 (13)	C169—H169	0.9500
N54—C181	1.319 (12)	C171—H171	0.9500
C55—H55	0.9500	C171—C174	1.392 (13)
C55—C112	1.370 (13)	C172—H172	0.9500
C56—H56	0.9500	C172—C198	1.392 (13)
C56—C130	1.424 (13)	C173—H173	0.9500
C56—C136	1.391 (12)	C174—H174	0.9500
C57—H57	0.9500	C174—C187	1.353 (14)
C57—C72	1.387 (13)	C175—H175	0.9500
C57—C135	1.371 (12)	C175—C189	1.378 (12)
C58—C116	1.404 (12)	C176—H176	0.9500
C58—C140	1.409 (12)	C179—H179	0.9500
C58—B208	1.640 (12)	C179—C197	1.375 (15)
C60—H60	0.9500	C180—H180	0.9500
C60—C202	1.369 (14)	C181—H181	0.9500
C61—H61	0.9500	C182—H182	0.9500
C62—B127	1.636 (12)	C182—C200	1.390 (15)
C62—C153	1.416 (11)	C183—H183	0.9500
C63—H63	0.9500	C184—H184	0.9500
C63—C93	1.411 (11)	C184—C0AA	1.403 (14)

C63—C142	1.395 (12)	C185—H185	0.9500
C64—H64	0.9500	C185—C207	1.409 (17)
C64—C106	1.395 (13)	C187—H187	0.9500
C64—C147	1.408 (12)	C188—H188	0.9500
C65—H65	0.9500	C189—H189	0.9500
C65—C87	1.428 (13)	C190—H190	0.9500
C65—C201	1.359 (13)	C192—H192	0.9500
C66—H66	0.9500	C192—C197	1.385 (15)
C66—C116	1.390 (12)	C193—H193	0.9500
C67—H67	0.9500	C194—H194	0.9500
C67—C123	1.326 (14)	C194—C200	1.397 (13)
C68—H68	0.9500	C195—H195	0.9500
C68—C128	1.378 (15)	C197—H197	0.9500
C68—C202	1.373 (15)	C198—H198	0.9500
C69—H69	0.9500	C200—H200	0.9500
C69—C140	1.366 (12)	C201—H201	0.9500
C70—H70	0.9500	C202—H202	0.9500
C70—N215	1.376 (11)	C207—H207	0.9500
C70—C3	1.358 (14)	C207—C4	1.375 (15)
C71—H71A	0.9900	C0AA—H0AA	0.9500
C71—H71B	0.9900	C3—H3	0.9500
C71—N215	1.462 (11)	C2AA—H2AA	0.9500
C72—B91	1.632 (12)	C4—H4	0.9500
C72—C194	1.421 (12)	O1—H1	0.8400
C73—H73	0.9500	O1—C4AA	1.399 (12)
C73—C95	1.373 (13)	O2—H2A	0.8400
C73—C108	1.406 (13)	O2—C5AA	1.401 (13)
C74—H74	0.9500	C4AA—H4AA	0.9800
C74—C111	1.381 (12)	C4AA—H4AB	0.9800
C74—C144	1.388 (12)	C4AA—H4AC	0.9800
C75—H75	0.9500	O8—H8A	0.8400
C75—C78	1.387 (13)	O8—C3AA	1.477 (19)
C75—C95	1.385 (13)	C5AA—H5AA	0.9800
C76—H76	0.9500	C5AA—H5AB	0.9800
C76—C167	1.364 (14)	C5AA—H5AC	0.9800
C77—H77	0.9500	C3AA—H3AA	0.9800
C77—C126	1.395 (13)	C3AA—H3AB	0.9800
C78—H78	0.9500	C3AA—H3AC	0.9800
C78—C98	1.396 (12)		

## Selected geometric parameters (°)

C1AA—Ru1—Cl7	162.3 (3)	N148—C88—H88A	109.4
C1AA—Ru1—C102	67.6 (4)	N148—C88—H88B	109.4
C1AA—Ru1—C150	79.2 (4)	Ru2—C89—H89	130.0
C1AA—Ru1—C184	67.0 (4)	C2—C89—Ru2	70.5 (5)
C1AA—Ru1—C2AA	37.8 (4)	C2—C89—H89	120.2
N26—Ru1—C1AA	111.9 (4)	C40—C89—Ru2	71.8 (5)
N26—Ru1—Cl7	85.5 (2)	C40—C89—C2	119.7 (9)
N26—Ru1—C102	161.9 (4)	C40—C89—H89	120.2
N26—Ru1—C150	124.8 (3)	C18—C90—N1X	106.7 (8)
N26—Ru1—C184	96.4 (3)	C18—C90—H90	126.7
N26—Ru1—C0AA	89.8 (4)	N1X—C90—H90	126.7
N26—Ru1—C2AA	148.8 (3)	C30—B91—C42	111.2 (7)
C102—Ru1—Cl7	94.9 (3)	C72—B91—C30	102.7 (7)
C102—Ru1—C150	37.2 (4)	C72—B91—C42	114.0 (7)
C102—Ru1—C184	66.3 (4)	C93—B91—C30	110.5 (6)
C102—Ru1—C2AA	37.4 (4)	C93—B91—C42	106.2 (7)
C114—Ru1—C1AA	96.1 (4)	C93—B91—C72	112.3 (7)
C114—Ru1—Cl7	88.9 (2)	N44—C92—C80	107.7 (9)
C114—Ru1—N26	83.1 (3)	N44—C92—H92	126.1
C114—Ru1—C102	115.0 (4)	C80—C92—H92	126.1
C114—Ru1—C150	151.5 (4)	C63—C93—B91	121.3 (7)
C114—Ru1—C184	161.6 (4)	C157—C93—C63	114.9 (7)
C114—Ru1—C0AA	124.6 (4)	C157—C93—B91	123.8 (7)
C114—Ru1—C2AA	91.8 (4)	Ru3—C94—H94	131.0
C150—Ru1—Cl7	88.3 (3)	C84—C94—Ru3	71.8 (5)
C184—Ru1—Cl7	109.4 (3)	C84—C94—H94	119.8
C184—Ru1—C150	36.2 (3)	C84—C94—C176	120.3 (9)
C0AA—Ru1—C1AA	37.5 (4)	C176—C94—Ru3	70.0 (5)
C0AA—Ru1—Cl7	145.4 (3)	C176—C94—H94	119.8
C0AA—Ru1—C102	79.6 (4)	C73—C95—C75	119.0 (9)
C0AA—Ru1—C150	66.6 (4)	C73—C95—H95	120.5
C0AA—Ru1—C184	37.1 (4)	C75—C95—H95	120.5
C0AA—Ru1—C2AA	67.9 (4)	C185—N96—N148	103.5 (9)
C2AA—Ru1—Cl7	125.3 (3)	C43—C97—H97	118.9
C2AA—Ru1—C150	67.2 (4)	C164—C97—C43	122.2 (9)
C2AA—Ru1—C184	79.1 (4)	C164—C97—H97	118.9
N7—Ru3—Cl8	86.9 (2)	C78—C98—C108	115.2 (8)
N7—Ru3—C10	120.7 (3)	C78—C98—B208	122.7 (8)
N7—Ru3—N12	84.5 (3)	C108—C98—B208	121.9 (8)



N7—Ru3—C84	117.7 (3)	C158—C100—H100	118.9
N7—Ru3—C94	93.8 (3)	C158—C100—C195	122.2 (9)
N7—Ru3—C149	155.3 (3)	C195—C100—H100	118.9
N7—Ru3—C176	94.8 (3)	N5—C99—H99	123.9
N7—Ru3—C190	158.1 (3)	N5—C99—C3	112.1 (8)
C10—Ru3—Cl8	151.4 (3)	C3—C99—H99	123.9
C10—Ru3—C84	80.5 (3)	Ru2—C101—H101	126.9
C10—Ru3—C94	67.9 (3)	C2—C101—Ru2	71.8 (6)
C10—Ru3—C149	66.8 (3)	C2—C101—H101	119.2
C10—Ru3—C190	37.4 (3)	C2—C101—C160	121.5 (9)
N12—Ru3—Cl8	84.5 (2)	C160—C101—Ru2	74.1 (5)
N12—Ru3—C10	90.5 (3)	C160—C101—H101	119.2
N12—Ru3—C84	157.6 (3)	Ru1—C102—H102	127.4
N12—Ru3—C94	153.8 (3)	C150—C102—Ru1	73.4 (5)
N12—Ru3—C149	119.9 (3)	C150—C102—H102	119.4
N12—Ru3—C176	116.3 (3)	C2AA—C102—Ru1	72.0 (6)
N12—Ru3—C190	93.4 (3)	C2AA—C102—H102	119.4
C84—Ru3—Cl8	93.7 (3)	C2AA—C102—C150	121.3 (9)
C84—Ru3—C149	37.7 (3)	C86—C103—B191	123.0 (8)
C84—Ru3—C190	67.1 (3)	C195—C103—C86	114.2 (8)
C94—Ru3—Cl8	121.6 (2)	C195—C103—B191	122.3 (8)
C94—Ru3—C84	36.5 (3)	N24—C104—N41	109.4 (7)
C94—Ru3—C149	66.2 (3)	N24—C104—H10A	109.8
C94—Ru3—C190	78.5 (3)	N24—C104—H10B	109.8
C149—Ru3—Cl8	91.4 (2)	N41—C104—H10A	109.8
C149—Ru3—C190	36.2 (3)	N41—C104—H10B	109.8
C176—Ru3—Cl8	159.3 (2)	H10A—C104—H10B	108.3
C176—Ru3—C10	37.4 (3)	Ru2—C105—H105	131.1
C176—Ru3—C84	67.3 (3)	C40—C105—Ru2	70.1 (5)
C176—Ru3—C94	37.7 (3)	C40—C105—H105	119.2
C176—Ru3—C149	78.4 (3)	C160—C105—Ru2	72.5 (5)
C176—Ru3—C190	66.6 (3)	C160—C105—C40	121.7 (8)
C190—Ru3—Cl8	114.7 (3)	C160—C105—H105	119.2
Ru1—C1AA—H1AA	129.6	C110—C107—B191	122.3 (8)
C0AA—C1AA—Ru1	70.9 (6)	C110—C107—C198	114.9 (8)
C0AA—C1AA— H1AA	120.0	C198—C107—B191	122.6 (7)
C0AA—C1AA— C2AA	119.9 (10)	C64—C106—H106	119.7
C2AA—C1AA—Ru1	71.9 (6)	C141—C106—C64	120.5 (9)
C2AA—C1AA— H1AA	120.0	C141—C106—H106	119.7

C2—Ru2—Cl1X	161.9 (3)	C9—C109—N2X	107.3 (8)
C2—Ru2—C40	67.7 (3)	C9—C109—H109	126.3
C2—Ru2—C89	37.8 (4)	N2X—C109—H109	126.3
C2—Ru2—C105	78.6 (3)	C73—C108—C98	122.0 (8)
C2—Ru2—C160	66.9 (4)	C73—C108—H108	119.0
N32—Ru2—Cl1X	85.4 (2)	C98—C108—H108	119.0
N32—Ru2—C2	112.5 (4)	C107—C110—H110	118.8
N32—Ru2—C40	162.7 (3)	C121—C110—C107	122.4 (8)
N32—Ru2—C89	149.3 (3)	C121—C110—H110	118.8
N32—Ru2—C101	90.9 (3)	C28—C111—H111	121.5
N32—Ru2—C105	125.4 (3)	C74—C111—C28	117.1 (8)
N32—Ru2—C160	96.9 (3)	C74—C111—H111	121.5
N34—Ru2—Cl1X	89.0 (2)	C55—C112—H112	127.9
N34—Ru2—C2	95.4 (4)	C55—C112—C165	104.1 (8)
N34—Ru2—N32	83.1 (3)	C165—C112—H112	127.9
N34—Ru2—C40	114.2 (3)	C164—C113—H113	120.5
N34—Ru2—C89	91.1 (3)	C164—C113—C193	119.0 (9)
N34—Ru2—C101	123.4 (3)	C193—C113—H113	120.5
N34—Ru2—C105	151.1 (4)	N24—C114—Ru 1	122.2 (7)
N34—Ru2—C160	160.9 (3)	N24—C114—N45	104.0 (8)
C40—Ru2—Cl1X	94.6 (2)	N45—C114—Ru 1	133.8 (6)
C40—Ru2—C105	37.3 (3)	C152—C115—H115	119.5
C40—Ru2—C160	66.8 (3)	C188—C115—H115	119.5
C89—Ru2—Cl1X	124.8 (2)	C188—C115—C152	120.9 (9)
C89—Ru2—C40	37.2 (3)	C58—C116—H116	119.2
C89—Ru2—C105	66.6 (3)	C66—C116—C58	121.6 (8)
C89—Ru2—C160	79.1 (3)	C66—C116—H116	119.2
C101—Ru2—Cl1X	146.7 (3)	N24—C117—H117	126.7
C101—Ru2—C2	36.7 (4)	C122—C117—N24	106.6 (8)
C101—Ru2—C40	79.6 (3)	C122—C117—H117	126.7
C101—Ru2—C89	67.2 (4)	N17—C118—N31	110.2 (7)
C101—Ru2—C105	66.3 (3)	N17—C118—H11A	109.6
C101—Ru2—C160	37.6 (3)	N17—C118—H11B	109.6
C105—Ru2—Cl1X	89.1 (2)	N31—C118—H11A	109.6
C105—Ru2—C160	36.0 (3)	N31—C118—H11B	109.6
C160—Ru2—Cl1X	110.0 (2)	H11A—C118—H11B	108.1
N3—Ru4—Cl5	87.6 (2)	N15—C119—H11C	109.8
N3—Ru4—N4	84.7 (3)	N15—C119—H11D	109.8
N3—Ru4—C8	93.3 (3)	N44—C119—N15	109.4 (7)
N3—Ru4—C14	120.8 (3)	N44—C119—H11C	109.8
N3—Ru4—C65	152.9 (3)	N44—C119—H11D	109.8

N3—Ru4—C87	115.6 (3)	H11C—C119—H11D	108.2
N3—Ru4—C154	91.1 (3)	C173—C120—H120	120.4
N3—Ru4—C201	158.9 (3)	C175—C120—H120	120.4
N4—Ru4—Cl5	85.0 (2)	C175—C120—C173	119.2 (9)
N4—Ru4—C8	113.6 (3)	C110—C121—H121	119.3
N4—Ru4—C14	90.2 (3)	C110—C121—C129	121.4 (8)
N4—Ru4—C65	122.3 (3)	C129—C121—H121	119.3
N4—Ru4—C87	159.7 (3)	N45—C122—H122	126.3
N4—Ru4—C154	150.7 (3)	C117—C122—N45	107.4 (8)
N4—Ru4—C201	95.1 (3)	C117—C122—H122	126.3
C8—Ru4—Cl5	161.5 (2)	N17—C123—H123	126.3
C8—Ru4—C65	78.8 (3)	C67—C123—N17	107.4 (9)
C8—Ru4—C87	67.9 (3)	C67—C123—H123	126.3
C8—Ru4—C154	37.6 (3)	C132—C125—H125	118.7
C8—Ru4—C201	67.4 (3)	C132—C125—C137	122.7 (8)
C14—Ru4—Cl5	150.6 (2)	C137—C125—H125	118.7
C14—Ru4—C8	37.1 (3)	C77—C126—H126	121.0
C14—Ru4—C65	66.4 (3)	C180—C126—C77	118.0 (9)
C14—Ru4—C87	79.9 (3)	C180—C126—H126	121.0
C14—Ru4—C154	67.3 (3)	C43—B127—C147	110.3 (7)
C14—Ru4—C201	38.2 (3)	C62—B127—C43	103.9 (6)
C65—Ru4—Cl5	92.0 (2)	C62—B127—C147	112.2 (7)
C65—Ru4—C201	35.2 (3)	C136—B127—C43	115.1 (7)
C87—Ru4—Cl5	95.0 (3)	C136—B127—C62	112.8 (7)
C87—Ru4—C65	37.4 (3)	C136—B127—C147	102.7 (6)
C87—Ru4—C154	37.5 (3)	C68—C128—H128	119.9
C87—Ru4—C201	66.2 (3)	C68—C128—C183	120.3 (10)
C154—Ru4—Cl5	123.9 (2)	C183—C128—H128	119.9
C154—Ru4—C65	66.8 (3)	C121—C129—H129	121.3
C154—Ru4—C201	78.8 (3)	C172—C129—C121	117.5 (8)
C201—Ru4—Cl5	113.4 (3)	C172—C129—H129	121.3
Ru2—C2—H2	129.3	C56—C130—H130	120.0
C89—C2—Ru2	71.7 (5)	C151—C130—C56	120.0 (10)
C89—C2—H2	119.9	C151—C130—H130	120.0
C101—C2—Ru2	71.5 (6)	N32—C131—C80	112.1 (10)
C101—C2—H2	119.9	N32—C131—H131	123.9
C101—C2—C89	120.2 (9)	C80—C131—H131	123.9
N13—N3—Ru4	123.5 (6)	C125—C132—H132	119.8
N1X—N3—Ru4	132.8 (6)	C125—C132—C169	120.4 (8)
N1X—N3—N13	103.7 (7)	C169—C132—H132	119.8
N11—N4—Ru4	123.6 (5)	C86—C133—H133	119.4

C61—N4—Ru4	130.6 (6)	C158—C133—C86	121.3 (9)
C61—N4—N11	105.7 (7)	C158—C133—H133	119.4
C99—N5—N215	104.0 (7)	C57—C135—H135	120.1
C165—N6—N52	103.4 (7)	C57—C135—C182	119.8 (9)
N19—N7—Ru3	124.0 (6)	C182—C135—H135	120.1
N2X—N7—Ru3	132.8 (6)	C56—C136—B127	124.5 (8)
N2X—N7—N19	103.1 (7)	C56—C136—C168	114.9 (8)
Ru4—C8—H8	129.9	C168—C136—B127	120.4 (8)
C14—C8—Ru4	70.7 (5)	C79—C137—C125	115.1 (8)
C14—C8—H8	120.3	C79—C137—B208	123.3 (7)
C14—C8—C154	119.4 (8)	C125—C137—B208	121.5 (7)
C154—C8—Ru4	71.6 (5)	C151—C138—H138	120.2
C154—C8—H8	120.3	C168—C138—H138	120.2
N19—C9—H9	126.4	C168—C138—C151	119.5 (10)
C109—C9—H9	126.4	C82—C139—H139	118.2
C109—C9—N19	107.1 (8)	C82—C139—C163	123.5 (9)
Ru3—C10—H10	125.9	C163—C139—H139	118.2
C176—C10—Ru3	71.3 (5)	C58—C140—H140	118.6
C176—C10—H10	120.4	C69—C140—C58	122.8 (8)
C176—C10—C190	119.3 (9)	C69—C140—H140	118.6
C190—C10—Ru3	74.3 (5)	C48—C141—H141	120.9
C190—C10—H10	120.4	C106—C141—C48	118.2 (9)
N4—N11—C47	119.5 (7)	C106—C141—H141	120.9
C159—N11—N4	110.3 (7)	C63—C142—H142	119.8
C159—N11—C47	129.3 (7)	C166—C142—C63	120.4 (9)
N29—N12—Ru3	124.3 (6)	C166—C142—H142	119.8
C156—N12—Ru3	130.8 (6)	C30—C144—H144	118.6
C156—N12—N29	104.8 (7)	C74—C144—C30	122.9 (8)
N3—N13—C18	111.5 (7)	C74—C144—H144	118.6
N3—N13—C47	121.6 (7)	C79—C146—H146	119.7
C18—N13—C47	126.9 (7)	C169—C146—C79	120.5 (8)
Ru4—C14—H14	126.2	C169—C146—H146	119.7
C8—C14—Ru4	72.2 (5)	C64—C147—B127	122.7 (8)
C8—C14—H14	119.7	C162—C147—C64	113.2 (8)
C8—C14—C201	120.7 (8)	C162—C147—B127	123.7 (8)
C201—C14—Ru4	73.8 (5)	N96—N148—C88	119.1 (8)
C201—C14—H14	119.7	C4—N148—C88	129.2 (9)
N34—N15—C67	110.5 (8)	C4—N148—N96	111.7 (9)
N34—N15—C119	122.4 (8)	Ru3—C149—H149	131.3
C67—N15—C119	127.0 (8)	C84—C149—Ru3	69.6 (5)
N34—N17—C118	125.3 (7)	C84—C149—H149	119.7

N34—N17—C123	110.6 (8)	C190—C149—Ru3	72.2 (5)
C123—N17—C118	124.0 (8)	C190—C149—C84	120.6 (8)
N13—C18—H18	126.7	C190—C149—H149	119.7
C90—C18—N13	106.5 (7)	Ru1—C150—H150	131.2
C90—C18—H18	126.7	C102—C150—Ru1	69.4 (5)
N7—N19—C9	111.2 (7)	C102—C150—H150	120.3
N7—N19—C25	121.4 (7)	C184—C150—Ru1	71.8 (5)
C9—N19—C25	127.4 (7)	C184—C150—C102	119.5 (9)
C61—C21—H21	127.2	C184—C150—H150	120.3
C159—C21—H21	127.2	C130—C151—C138	119.2 (9)
C159—C21—C61	105.6 (8)	C130—C151—H151	120.4
C62—C22—H22	118.2	C138—C151—H151	120.4
C77—C22—H22	118.2	C82—C152—H152	118.5
C77—C22—C62	123.7 (8)	C115—C152—C82	123.0 (9)
N7—N2X—C27	124.9 (7)	C115—C152—H152	118.5
N7—N2X—C109	111.3 (7)	C62—C153—H153	118.1
C109—N2X—C27	123.8 (7)	C180—C153—C62	123.8 (8)
C114—N24—C104	122.6 (8)	C180—C153—H153	118.1
C114—N24—C117	111.5 (8)	Ru4—C154—H154	130.7
C117—N24—C104	125.8 (7)	C8—C154—Ru4	70.8 (5)
N19—C25—H25A	109.5	C8—C154—H154	120.0
N19—C25—H25B	109.5	C87—C154—Ru4	71.1 (5)
H25A—C25—H25B	108.1	C87—C154—C8	120.0 (8)
N29—C25—N19	110.7 (7)	C87—C154—H154	120.0
N29—C25—H25A	109.5	C81—C155—H155	119.7
N29—C25—H25B	109.5	C81—C155—C187	120.6 (9)
N41—N26—Ru1	123.2 (6)	C187—C155—H155	119.7
C192—N26—Ru1	132.2 (7)	N12—C156—H156	124.1
C192—N26—N41	104.6 (8)	N12—C156—C167	111.8 (8)
N2X—C27—H27A	109.6	C167—C156—H156	124.1
N2X—C27—H27B	109.6	C53—C157—C93	122.9 (8)
H27A—C27—H27B	108.1	C53—C157—H157	118.6
N52—C27—N2X	110.4 (7)	C93—C157—H157	118.6
N52—C27—H27A	109.6	C100—C158—C133	117.6 (8)
N52—C27—H27B	109.6	C100—C158—H158	121.2
C85—C28—H28	119.7	C133—C158—H158	121.2
C85—C28—C111	120.7 (8)	N11—C159—C21	108.0 (8)
C111—C28—H28	119.7	N11—C159—H159	126.0
N12—N29—C25	118.7 (7)	C21—C159—H159	126.0
C76—N29—N12	110.6 (7)	Ru2—C160—H160	131.9
C76—N29—C25	130.5 (8)	C101—C160—Ru2	68.3 (5)

C85—C30—B91	122.7 (7)	C101—C160—H160	121.1
C85—C30—C144	113.8 (7)	C105—C160—Ru 2	71.4 (5)
C144—C30—B91	123.3 (7)	C105—C160—C101	117.9 (9)
C33—N31—N54	112.9 (8)	C105—C160—H160	121.1
C33—N31—C118	127.6 (8)	C48—C162—C147	124.4 (9)
N54—N31—C118	119.4 (7)	C48—C162—H162	117.8
N44—N32—Ru2	121.9 (6)	C147—C162—H162	117.8
C131—N32—Ru 2	132.7 (7)	C81—C161—B208	121.1 (8)
C131—N32—N44	105.4 (8)	C171—C161—C81	114.6 (8)
N31—C33—H33	127.4	C171—C161—B208	123.8 (8)
N31—C33—C38	105.1 (9)	C139—C163—H163	120.6
C38—C33—H33	127.4	C188—C163—C139	118.8 (9)
N15—N34—Ru2	121.9 (7)	C188—C163—H163	120.6
N17—N34—Ru2	133.7 (6)	C97—C164—H164	119.8
N17—N34—N15	104.5 (8)	C113—C164—C97	120.4 (10)
N3—N1X—C71	125.7 (7)	C113—C164—H164	119.8
N3—N1X—C90	111.5 (7)	N6—C165—C112	112.5 (8)
C90—N1X—C71	122.8 (8)	N6—C165—H165	123.7
C60—C37—C183	114.5 (9)	C112—C165—H165	123.7
C60—C37—B191	121.2 (8)	C53—C166—C142	118.9 (9)
C183—C37—B191	124.1 (8)	C53—C166—H166	120.5
C33—C38—H38	126.7	C142—C166—H166	120.5
C33—C38—C181	106.5 (9)	C76—C167—C156	104.8 (8)
C181—C38—H38	126.7	C76—C167—H167	127.6
C66—C39—H39	120.8	C156—C167—H167	127.6
C66—C39—C69	118.3 (8)	C136—C168—H168	118.0
C69—C39—H39	120.8	C138—C168—C136	124.0 (9)
Ru2—C40—H40	128.0	C138—C168—H168	118.0
C89—C40—Ru2	70.9 (5)	C132—C169—H169	120.9
C89—C40—H40	120.5	C146—C169—C132	118.2 (8)
C89—C40—C105	119.0 (8)	C146—C169—H169	120.9
C105—C40—Ru2	72.6 (5)	C161—C171—H171	118.6
C105—C40—H40	120.5	C174—C171—C161	122.8 (9)
N26—N41—C104	119.6 (7)	C174—C171—H171	118.6
C179—N41—N26	111.5 (9)	C129—C172—H172	119.6
C179—N41—C104	128.8 (8)	C129—C172—C198	120.8 (9)
C46—C42—B91	121.9 (7)	C198—C172—H172	119.6
C189—C42—C46	115.7 (8)	C46—C173—H173	120.0
C189—C42—B91	122.4 (8)	C120—C173—C46	120.0 (9)
C50—C43—C97	115.4 (8)	C120—C173—H173	120.0
C50—C43—B127	124.0 (8)	C171—C174—H174	119.8

Chapter 7: Appendices

C97—C43—B127	120.6 (7)	C187—C174—C171	120.4 (9)
N32—N44—C92	109.6 (8)	C187—C174—H174	119.8
N32—N44—C119	120.9 (7)	C120—C175—H175	119.7
C92—N44—C119	129.4 (8)	C120—C175—C189	120.5 (9)
C114—N45—C88	125.4 (8)	C189—C175—H175	119.7
C114—N45—C122	110.5 (8)	Ru3—C176—H176	129.4
C122—N45—C88	124.0 (8)	C10—C176—Ru3	71.3 (5)
C42—C46—H46	119.2	C10—C176—C94	121.0 (9)
C173—C46—C42	121.6 (9)	C10—C176—H176	119.5
C173—C46—H46	119.2	C94—C176—Ru3	72.3 (5)
N11—C47—N13	110.3 (7)	C94—C176—H176	119.5
N11—C47—H47A	109.6	N41—C179—H179	126.4
N11—C47—H47B	109.6	N41—C179—C197	107.2 (9)
N13—C47—H47A	109.6	C197—C179—H179	126.4
N13—C47—H47B	109.6	C126—C180—H180	119.8
H47A—C47—H47B	108.1	C153—C180—C126	120.5 (9)
C141—C48—H48	119.9	C153—C180—H180	119.8
C162—C48—H48	119.9	C38—C181—H181	124.1
C162—C48—C141	120.2 (9)	N54—C181—C38	111.7 (9)
C43—C50—H50	118.6	N54—C181—H181	124.1
C43—C50—C193	122.7 (9)	C135—C182—H182	120.7
C193—C50—H50	118.6	C200—C182—C135	118.6 (9)
N6—N52—C27	121.7 (8)	C200—C182—H182	120.7
C55—N52—N6	113.0 (8)	C37—C183—H183	118.8
C55—N52—C27	125.2 (8)	C128—C183—C37	122.4 (9)
C157—C53—H53	119.6	C128—C183—H183	118.8
C166—C53—H53	119.6	Ru1—C184—H184	131.9
C166—C53—C157	120.8 (8)	C150—C184—Ru1	72.0 (5)
C181—N54—N31	103.7 (8)	C150—C184—H184	119.9
N52—C55—H55	126.6	C150—C184—C0AA	120.2 (10)
N52—C55—C112	106.9 (9)	C0AA—C184—Ru1	69.0 (5)
C112—C55—H55	126.6	C0AA—C184—H184	119.9
C130—C56—H56	118.8	N96—C185—H185	123.5
C136—C56—H56	118.8	N96—C185—C207	113.1 (10)
C136—C56—C130	122.4 (9)	C207—C185—H185	123.5
C72—C57—H57	117.6	C155—C187—H187	120.5
C135—C57—H57	117.6	C174—C187—C155	119.1 (9)
C135—C57—C72	124.8 (9)	C174—C187—H187	120.5
C116—C58—C140	115.0 (8)	C115—C188—C163	119.2 (9)
C116—C58—B208	123.0 (8)	C115—C188—H188	120.4
C140—C58—B208	121.7 (8)	C163—C188—H188	120.4

C37—C60—H60	118.3	C42—C189—H189	118.7
C202—C60—C37	123.4 (10)	C175—C189—C42	122.7 (9)
C202—C60—H60	118.3	C175—C189—H189	118.7
N4—C61—C21	110.4 (8)	Ru3—C190—H190	132.8
N4—C61—H61	124.8	C10—C190—Ru3	68.3 (5)
C21—C61—H61	124.8	C10—C190—H190	120.2
C22—C62—B127	122.3 (7)	C149—C190—Ru3	71.7 (5)
C22—C62—C153	113.4 (8)	C149—C190—C10	119.6 (9)
C153—C62—B127	124.1 (7)	C149—C190—H190	120.2
C93—C63—H63	119.0	C37—B191—C82	112.1 (7)
C142—C63—H63	119.0	C103—B191—C37	109.6 (7)
C142—C63—C93	122.0 (8)	C103—B191—C82	102.9 (7)
C106—C64—H64	118.3	C107—B191—C37	106.1 (7)
C106—C64—C147	123.4 (9)	C107—B191—C82	111.8 (7)
C147—C64—H64	118.3	C107—B191—C103	114.5 (7)
Ru4—C65—H65	131.8	N26—C192—H192	123.9
C87—C65—Ru4	69.5 (5)	N26—C192—C197	112.2 (10)
C87—C65—H65	119.3	C197—C192—H192	123.9
C201—C65—Ru4	72.5 (6)	C50—C193—H193	119.9
C201—C65—H65	119.3	C113—C193—C50	120.2 (9)
C201—C65—C87	121.5 (9)	C113—C193—H193	119.9
C39—C66—H66	119.2	C72—C194—H194	118.8
C39—C66—C116	121.6 (9)	C200—C194—C72	122.3 (9)
C116—C66—H66	119.2	C200—C194—H194	118.8
N15—C67—H67	126.5	C100—C195—C103	122.2 (8)
C123—C67—N15	106.9 (8)	C100—C195—H195	118.9
C123—C67—H67	126.5	C103—C195—H195	118.9
C128—C68—H68	120.6	C179—C197—C192	104.5 (10)
C202—C68—H68	120.6	C179—C197—H197	127.8
C202—C68—C128	118.9 (10)	C192—C197—H197	127.8
C39—C69—H69	119.7	C107—C198—H198	118.5
C140—C69—C39	120.6 (9)	C172—C198—C107	123.0 (8)
C140—C69—H69	119.7	C172—C198—H198	118.5
N215—C70—H70	127.4	C182—C200—C194	120.2 (9)
C3—C70—H70	127.4	C182—C200—H200	119.9
C3—C70—N215	105.1 (8)	C194—C200—H200	119.9
N1X—C71—H71A	109.5	Ru4—C201—H201	131.9
N1X—C71—H71B	109.5	C14—C201—Ru4	68.1 (5)
N1X—C71—N215	110.6 (7)	C14—C201—H201	120.4
H71A—C71—H71B	108.1	C65—C201—Ru4	72.3 (6)
N215—C71—H71A	109.5	C65—C201—C14	119.1 (9)



N215—C71—H71B	109.5	C65—C201—H201	120.4
C57—C72—B91	122.5 (8)	C60—C202—C68	120.5 (10)
C57—C72—C194	114.4 (8)	C60—C202—H202	119.7
C194—C72—B91	122.8 (8)	C68—C202—H202	119.7
C95—C73—H73	119.8	C185—C207—H207	128.3
C95—C73—C108	120.4 (8)	C4—C207—C185	103.4 (10)
C108—C73—H73	119.8	C4—C207—H207	128.3
C111—C74—H74	119.4	C58—B208—C98	111.4 (7)
C111—C74—C144	121.1 (8)	C58—B208—C137	111.8 (7)
C144—C74—H74	119.4	C58—B208—C161	103.8 (6)
C78—C75—H75	119.8	C98—B208—C161	112.0 (7)
C95—C75—H75	119.8	C137—B208—C98	106.5 (7)
C95—C75—C78	120.5 (9)	C137—B208—C161	111.5 (7)
N29—C76—H76	126.0	N5—N215—C70	113.3 (7)
N29—C76—C167	108.0 (8)	N5—N215—C71	121.9 (7)
C167—C76—H76	126.0	C70—N215—C71	124.7 (7)
C22—C77—H77	119.7	Ru1—C0AA—H0AA	126.9
C22—C77—C126	120.5 (9)	C1AA—C0AA—Ru1	71.6 (6)
C126—C77—H77	119.7	C1AA—C0AA—C184	120.6 (10)
C75—C78—H78	118.6	C1AA—C0AA— H0AA	119.7
C75—C78—C98	122.9 (9)	C184—C0AA—Ru1	73.8 (6)
C98—C78—H78	118.6	C184—C0AA—H0AA	119.7
C137—C79—H79	118.5	C70—C3—C99	105.4 (8)
C137—C79—C146	123.0 (8)	C70—C3—H3	127.3
C146—C79—H79	118.5	C99—C3—H3	127.3
C92—C80—H80	127.4	Ru1—C2AA—H2AA	130.8
C131—C80—H80	127.4	C1AA—C2AA—Ru1	70.2 (6)
C131—C80—C92	105.1 (9)	C1AA—C2AA— H2AA	120.8
C155—C81—H81	118.7	C102—C2AA—Ru1	70.7 (6)
C155—C81—C161	122.5 (9)	C102—C2AA—C1AA	118.4 (10)
C161—C81—H81	118.7	C102—C2AA—H2AA	120.8
C139—C82—B191	119.4 (8)	N148—C4—C207	108.4 (10)
C152—C82—C139	114.5 (8)	N148—C4—H4	125.8
C152—C82—B191	125.4 (8)	C207—C4—H4	125.8
Ru3—C84—H84	127.1	C4AA—O1—H1	109.5
C94—C84—Ru3	71.6 (5)	C5AA—O2—H2A	109.5
C94—C84—H84	120.5	O1—C4AA—H4AA	109.5
C94—C84—C149	119.0 (8)	O1—C4AA—H4AB	109.5
C149—C84—Ru3	72.7 (5)	O1—C4AA—H4AC	109.5
C149—C84—H84	120.5	H4AA—C4AA—	109.5

		H4AB	
C103—C86—H86	118.8	H4AA—C4AA— H4AC	109.5
C133—C86—H86	118.8	H4AB—C4AA— H4AC	109.5
C133—C86—C103	122.5 (9)	C3AA—O8—H8A	109.5
C28—C85—H85	117.8	O2—C5AA—H5AA	109.5
C30—C85—C28	124.4 (8)	O2—C5AA—H5AB	109.5
C30—C85—H85	117.8	O2—C5AA—H5AC	109.5
Ru4—C87—H87	127.0	H5AA—C5AA— H5AB	109.5
C65—C87—Ru4	73.1 (5)	H5AA—C5AA— H5AC	109.5
C65—C87—H87	120.5	H5AB—C5AA— H5AC	109.5
C154—C87—Ru4	71.4 (5)	O8—C3AA—H3AA	109.5
C154—C87—C65	119.0 (8)	O8—C3AA—H3AB	109.5
C154—C87—H87	120.5	O8—C3AA—H3AC	109.5
N45—C88—H88A	109.4	H3AA—C3AA— H3AB	109.5
N45—C88—H88B	109.4	H3AA—C3AA— H3AC	109.5
H88A—C88—H88B	108.0	H3AB—C3AA— H3AC	109.5
N148—C88—N45	111.0 (8)		

### Selected geometric parameters (°)

Ru1—C1AA— C0AA—C184	57.4 (9)	C89—C40—C105— C160	-2.3 (13)
Ru1—C1AA— C2AA—C102	-53.6 (8)	C90—N1X—C71— N215	-94.1 (10)
Ru1—N26—N41— C104	0.2 (11)	B91—C30—C85— C28	175.5 (8)
Ru1—N26—N41— C179	-179.5 (6)	B91—C30—C144— C74	-175.9 (8)
Ru1—N26—C192— C197	179.0 (7)	B91—C42—C46— C173	179.5 (8)
Ru1—C102—C150— C184	-53.4 (8)	B91—C42—C189— C175	-178.5 (8)
Ru1—C102—C2AA— C1AA	53.4 (8)	B91—C72—C194— C200	173.2 (8)
Ru1—C150—C184— C0AA	-51.4 (9)	B91—C93—C157— C53	-179.0 (8)
Ru1—C184—C0AA— C1AA	-56.4 (9)	C92—N44—C119— N15	122.7 (10)
Ru3—N7—N19—C9	-178.6 (6)	C92—C80—C131—	-3.0 (12)

		N32	
Ru3—N7—N19—C25	0.7 (11)	C93—C63—C142— C166	-2.7 (13)
Ru3—N7—N2X— C27	-4.6 (13)	C94—C84—C149— Ru3	-56.6 (7)
Ru3—N7—N2X— C109	178.3 (7)	C94—C84—C149— C190	-3.5 (13)
Ru3—C10—C176— C94	54.7 (7)	C95—C73—C108— C98	0.8 (13)
Ru3—C10—C190— C149	-52.1 (8)	C95—C75—C78— C98	-3.3 (14)
Ru3—N12—N29— C25	8.9 (10)	N96—N148—C4— C207	1.6 (12)
Ru3—N12—N29— C76	-176.5 (6)	N96—C185—C207— C4	0.6 (14)
Ru3—N12—C156— C167	176.9 (6)	C97—C43—C50— C193	2.0 (13)
Ru3—C84—C94— C176	-52.5 (7)	C97—C43—B127— C62	-70.6 (10)
Ru3—C84—C149— C190	53.2 (8)	C97—C43—B127— C136	165.5 (8)
Ru3—C94—C176— C10	-54.3 (8)	C97—C43—B127— C147	49.8 (10)
Ru3—C149—C190— C10	50.6 (7)	C99—N5—N215— C70	1.2 (10)
Ru2—C2—C89—C40	54.3 (7)	C99—N5—N215— C71	178.2 (8)
Ru2—C2—C101— C160	-57.3 (8)	C101—C2—C89— Ru2	-54.6 (8)
Ru2—N32—N44— C92	-177.3 (6)	C101—C2—C89— C40	-0.3 (13)
Ru2—N32—N44— C119	-0.4 (11)	C102—C150— C184—Ru1	52.3 (8)
Ru2—N32—C131— C80	178.4 (7)	C102—C150— C184—C0AA	0.9 (14)
Ru2—C40—C89—C2	-53.7 (7)	C103—C86—C133— C158	1.5 (13)
Ru2—C40—C105— C160	53.3 (8)	C104—N24—C114— Ru1	1.0 (12)
Ru2—C101—C160— C105	-53.2 (7)	C104—N24—C114— N45	-178.6 (8)
Ru2—C105—C160— C101	51.7 (7)	C104—N24—C117— C122	178.6 (9)
Ru4—N3—N13—C18	-176.2 (6)	C104—N41—C179— C197	-179.7 (9)
Ru4—N3—N13—C47	3.0 (10)	C105—C40—C89— Ru2	56.4 (7)
Ru4—N3—N1X—	-5.0 (12)	C105—C40—C89—	2.7 (12)

Chapter 7: Appendices

C71			C2		
Ru4—N3—N1X—	176.3 (6)		C107—C110—	1.1 (14)	
C90			C121—C129		
Ru4—N4—N11—C47	12.8 (10)		C106—C64—C147—	172.1 (8)	
			B127		
Ru4—N4—N11—	-177.2 (6)		C106—C64—C147—	-0.2 (12)	
C159			C162		
Ru4—N4—C61—C21	176.4 (6)		C109—C9—N19—N7	-0.4 (11)	
Ru4—C8—C14—	-57.9 (8)		C109—C9—N19—	-179.7 (8)	
C201			C25		
Ru4—C8—C154—	53.4 (7)		C109—N2X—C27—	-96.2 (9)	
C87			N52		
Ru4—C14—C201—	-53.2 (8)		C108—C73—C95—	0.1 (13)	
C65			C75		
Ru4—C65—C87—	-56.6 (7)		C108—C98—B208—	-151.4 (7)	
C154			C58		
Ru4—C65—C201—	51.2 (7)		C108—C98—B208—	86.5 (9)	
C14			C137		
Ru4—C87—C154—	-53.2 (7)		C108—C98—B208—	-35.7 (11)	
C8			C161		
C2—C101—C160—	56.2 (8)		C110—C107—	77.7 (10)	
Ru2			B191—C37		
C2—C101—C160—	3.0 (13)		C110—C107—	-44.7 (12)	
C105			B191—C82		
N3—N13—C18—C90	-1.7 (10)		C110—C107—	-161.3 (8)	
			B191—C103		
N3—N13—C47—N11	52.1 (10)		C110—C107—	2.0 (14)	
			C198—C172		
N3—N1X—C71—	87.3 (10)		C110—C121—	-0.1 (14)	
N215			C129—C172		
N3—N1X—C90—	0.9 (10)		C111—C28—C85—	1.5 (13)	
C18			C30		
N4—N11—C47—N13	-59.9 (10)		C111—C74—C144—	-0.8 (13)	
			C30		
N4—N11—C159—	1.0 (10)		C114—N24—C104—	-55.7 (11)	
C21			N41		
N5—C99—C3—C70	2.9 (12)		C114—N24—C117—	1.3 (11)	
			C122		
N6—N52—C55—	0.1 (10)		C114—N45—C88—	-102.4 (10)	
C112			N148		
N7—N19—C25—N29	53.7 (10)		C114—N45—C122—	0.1 (11)	
			C117		
N7—N2X—C27—	87.1 (10)		C116—C58—C140—	-1.7 (12)	
N52			C69		
N7—N2X—C109—	1.0 (10)		C116—C58—B208—	31.7 (11)	
C9			C98		
C8—C14—C201—	57.1 (8)		C116—C58—B208—	150.7 (8)	
Ru4			C137		

C8—C14—C201— C65	3.9 (13)	C116—C58—B208— C161	-88.9 (10)
C9—N19—C25—N29	-127.2 (9)	C117—N24—C104— N41	127.3 (9)
N11—N4—C61—C21	0.5 (10)	C117—N24—C114— Ru1	178.4 (6)
N12—N29—C76— C167	-0.8 (10)	C117—N24—C114— N45	-1.3 (10)
N12—C156—C167— C76	-1.0 (11)	C118—N17—N34— Ru2	-3.7 (13)
N13—N3—N1X— C71	176.8 (7)	C118—N17—N34— N15	176.1 (7)
N13—N3—N1X— C90	-1.9 (9)	C118—N17—C123— C67	-176.1 (8)
N13—C18—C90— N1X	0.5 (9)	C118—N31—C33— C38	-174.6 (9)
C14—C8—C154— Ru4	-54.0 (7)	C118—N31—N54— C181	175.4 (8)
C14—C8—C154— C87	-0.6 (12)	C119—N15—N34— Ru2	-0.1 (11)
N15—C67—C123— N17	-0.2 (10)	C119—N15—N34— N17	-180.0 (8)
C18—N13—C47— N11	-128.8 (8)	C119—N15—C67— C123	-179.9 (8)
N19—N7—N2X— C27	175.9 (7)	C119—N44—C92— C80	-177.7 (9)
N19—N7—N2X— C109	-1.2 (9)	C120—C175— C189—C42	-4.1 (14)
N19—C9—C109— N2X	-0.3 (10)	C121—C129— C172—C198	0.2 (15)
N19—C25—N29— N12	-57.4 (10)	C122—N45—C88— N148	81.6 (11)
N19—C25—N29— C76	129.2 (9)	C122—N45—C114— Ru1	-178.9 (7)
C22—C62—B127— C43	-82.6 (9)	C122—N45—C114— N24	0.7 (10)
C22—C62—B127— C136	42.8 (11)	C123—N17—N34— Ru2	179.9 (7)
C22—C62—B127— C147	158.2 (8)	C123—N17—N34— N15	-0.2 (9)
C22—C62—C153— C180	-3.0 (13)	C123—N17—C118— N31	-87.4 (10)
C22—C77—C126— C180	-2.1 (14)	C125—C132— C169—C146	1.6 (14)
N2X—N7—N19—C9	1.0 (9)	C125—C137— B208—C58	-34.9 (11)
N2X—N7—N19— C25	-179.7 (7)	C125—C137— B208—C98	87.0 (9)

Chapter 7: Appendices

N2X—C27—N52— N6	37.1 (11)	C125—C137— B208—C161	-150.6 (8)
N2X—C27—N52— C55	-145.1 (9)	B127—C43—C50— C193	-175.8 (8)
N24—C117—C122— N45	-0.8 (10)	B127—C43—C97— C164	177.3 (8)
C25—N29—C76— C167	173.1 (9)	B127—C62—C153— C180	-177.7 (8)
N26—N41—C104— N24	53.6 (11)	B127—C136— C168—C138	-174.9 (8)
N26—N41—C179— C197	0.0 (11)	B127—C147— C162—C48	-171.3 (8)
N26—C192—C197— C179	1.7 (13)	C128—C68—C202— C60	1.4 (15)
C27—N2X—C109— C9	-176.2 (8)	C129—C172— C198—C107	-1.2 (16)
C27—N52—C55— C112	-177.9 (8)	C130—C56—C136— B127	174.4 (8)
N29—N12—C156— C167	0.6 (10)	C130—C56—C136— C168	0.5 (12)
N29—C76—C167— C156	1.1 (11)	C131—N32—N44— C92	-0.7 (10)
C30—B91—C93— C63	-146.8 (7)	C131—N32—N44— C119	176.2 (9)
C30—B91—C93— C157	34.1 (11)	C131—C80—C92— N44	2.4 (11)
N31—C33—C38— C181	-0.6 (12)	C132—C125— C137—C79	-2.3 (13)
N31—N54—C181— C38	-0.2 (11)	C132—C125— C137—B208	-178.3 (8)
N32—N44—C92— C80	-1.1 (11)	C133—C86—C103— B191	-173.0 (8)
N32—N44—C119— N15	-53.6 (11)	C133—C86—C103— C195	-1.6 (12)
C33—N31—N54— C181	-0.2 (10)	C135—C57—C72— B91	-174.7 (8)
C33—N31—C118— N17	-132.4 (9)	C135—C57—C72— C194	-0.8 (13)
C33—C38—C181— N54	0.5 (13)	C135—C182— C200—C194	-1.0 (14)
N34—N15—C67— C123	0.1 (10)	C136—C56—C130— C151	0.1 (14)
N34—N15—C119— N44	55.3 (11)	C136—B127— C147—C64	-99.9 (9)
N34—N17—C118— N31	96.7 (10)	C136—B127— C147—C162	71.5 (9)
N34—N17—C123— C67	0.3 (10)	C137—C79—C146— C169	-1.1 (14)

Chapter 7: Appendices

N1X—N3—N13— C18	2.2 (9)	C137—C125— C132—C169	0.2 (14)
N1X—N3—N13— C47	-178.5 (7)	C139—C82—C152— C115	-1.6 (12)
N1X—C71—N215— N5	37.8 (11)	C139—C82—B191— C37	52.0 (10)
N1X—C71—N215— C70	-145.6 (8)	C139—C82—B191— C103	-65.7 (10)
C37—C60—C202— C68	0.2 (15)	C139—C82—B191— C107	171.0 (7)
C39—C66—C116— C58	-2.1 (13)	C139—C163— C188—C115	-0.5 (13)
C39—C69—C140— C58	-0.3 (13)	C140—C58—C116— C66	2.8 (12)
C40—C105—C160— Ru2	-52.2 (8)	C140—C58—B208— C98	-154.8 (8)
C40—C105—C160— C101	-0.5 (13)	C140—C58—B208— C137	-35.7 (11)
N41—N26—C192— C197	-1.7 (12)	C140—C58—B208— C161	84.6 (9)
N41—C179—C197— C192	-0.9 (12)	C141—C48—C162— C147	-1.8 (14)
C42—C46—C173— C120	2.1 (14)	C142—C63—C93— B91	-178.8 (8)
C42—B91—C93— C63	92.5 (9)	C142—C63—C93— C157	0.4 (12)
C42—B91—C93— C157	-86.7 (9)	C144—C30—C85— C28	0.6 (12)
C43—C50—C193— C113	-2.6 (15)	C144—C30—B91— C42	-29.9 (11)
C43—C97—C164— C113	-0.2 (15)	C144—C30—B91— C72	92.5 (9)
C43—B127—C136— C56	136.9 (8)	C144—C30—B91— C93	-147.6 (8)
C43—B127—C136— C168	-49.5 (10)	C144—C74—C111— C28	2.9 (12)
C43—B127—C147— C64	23.3 (11)	C146—C79—C137— C125	2.8 (13)
C43—B127—C147— C162	-165.2 (8)	C146—C79—C137— B208	178.7 (8)
N44—N32—C131— C80	2.3 (11)	C147—C64—C106— C141	0.4 (14)
N45—C88—N148— N96	-57.2 (11)	C147—B127— C136—C56	-103.1 (9)
N45—C88—N148— C4	123.4 (10)	C147—B127— C136—C168	70.5 (9)
C46—C42—B91— C30	145.6 (8)	N148—N96—C185— C207	0.3 (12)

Chapter 7: Appendices

C46—C42—B91— C72	30.0 (11)	C149—C84—C94— Ru3	57.2 (7)
C46—C42—B91— C93	-94.2 (9)	C149—C84—C94— C176	4.6 (13)
C46—C42—C189— C175	2.0 (13)	C150—C102— C2AA—Ru1	-56.6 (8)
C47—N11—C159— C21	169.8 (8)	C150—C102— C2AA—C1AA	-3.3 (14)
C47—N13—C18— C90	179.1 (8)	C150—C184— C0AA—Ru1	52.8 (9)
C50—C43—C97— C164	-0.6 (13)	C150—C184— C0AA—C1AA	-3.6 (15)
C50—C43—B127— C62	107.1 (9)	C151—C138— C168—C136	0.3 (14)
C50—C43—B127— C136	-16.8 (12)	C152—C82—C139— C163	1.1 (12)
C50—C43—B127— C147	-132.5 (8)	C152—C82—B191— C37	-137.3 (8)
N52—N6—C165— C112	0.1 (10)	C152—C82—B191— C103	105.0 (9)
N52—C55—C112— C165	0.0 (10)	C152—C82—B191— C107	-18.3 (12)
N54—N31—C33— C38	0.5 (11)	C152—C115— C188—C163	0.0 (14)
N54—N31—C118— N17	52.8 (10)	C153—C62—B127— C43	91.6 (10)
C55—C112—C165— N6	-0.1 (11)	C153—C62—B127— C136	-143.0 (8)
C56—C130—C151— C138	-0.5 (14)	C153—C62—B127— C147	-27.6 (11)
C56—C136—C168— C138	-0.7 (12)	C154—C8—C14— Ru4	54.4 (7)
C57—C72—B91— C30	84.6 (9)	C154—C8—C14— C201	-3.5 (13)
C57—C72—B91— C42	-154.9 (8)	C155—C81—C161— C171	-0.8 (13)
C57—C72—B91— C93	-34.1 (11)	C155—C81—C161— B208	171.7 (8)
C57—C72—C194— C200	-0.7 (13)	C156—N12—N29— C25	-174.5 (8)
C57—C135—C182— C200	-0.4 (14)	C156—N12—N29— C76	0.1 (10)
C60—C37—C183— C128	2.4 (13)	C157—C53—C166— C142	-0.6 (14)
C60—C37—B191— C82	-164.7 (8)	C158—C100— C195—C103	-0.9 (13)
C60—C37—B191— C103	-51.1 (11)	C159—N11—C47— N13	132.2 (9)



C60—C37—B191— C107	73.0 (10)	C159—C21—C61— N4	0.1 (11)
C61—N4—N11—C47	-171.0 (7)	C162—C48—C141— C106	1.8 (13)
C61—N4—N11— C159	-1.0 (9)	C161—C81—C155— C187	1.1 (15)
C61—C21—C159— N11	-0.7 (10)	C161—C171— C174—C187	-0.3 (14)
C62—C22—C77— C126	-1.3 (14)	C164—C113— C193—C50	1.7 (15)
C62—B127—C136— C56	17.8 (11)	C165—N6—N52— C27	177.9 (7)
C62—B127—C136— C168	-168.6 (7)	C165—N6—N52— C55	-0.1 (10)
C62—B127—C147— C64	138.7 (8)	C166—C53—C157— C93	-1.7 (14)
C62—B127—C147— C162	-49.8 (11)	C168—C138— C151—C130	0.3 (14)
C62—C153—C180— C126	-0.1 (15)	C171—C161— B208—C58	88.5 (10)
C63—C93—C157— C53	1.8 (13)	C171—C161— B208—C98	-31.7 (11)
C63—C142—C166— C53	2.8 (13)	C171—C161— B208—C137	-150.9 (8)
C64—C106—C141— C48	-1.2 (13)	C171—C174— C187—C155	0.6 (14)
C64—C147—C162— C48	0.9 (12)	C173—C120— C175—C189	5.0 (14)
C65—C87—C154— Ru4	57.5 (7)	C175—C120— C173—C46	-4.1 (15)
C65—C87—C154— C8	4.3 (12)	C176—C10—C190— Ru3	57.3 (7)
C66—C39—C69— C140	1.1 (13)	C176—C10—C190— C149	5.2 (13)
C67—N15—N34— Ru2	180.0 (6)	C179—N41—C104— N24	-126.8 (9)
C67—N15—N34— N17	0.1 (9)	C183—C37—C60— C202	-2.1 (13)
C67—N15—C119— N44	-124.8 (9)	C183—C37—B191— C82	20.1 (12)
C68—C128—C183— C37	-0.9 (15)	C183—C37—B191— C103	133.8 (8)
C69—C39—C66— C116	0.0 (13)	C183—C37—B191— C107	-102.2 (9)
C71—N1X—C90— C18	-177.8 (7)	C185—N96—N148— C88	179.3 (8)
C72—C57—C135— C182	1.4 (14)	C185—N96—N148— C4	-1.2 (11)

C72—B91—C93— C63	-32.7 (11)	C185—C207—C4— N148	-1.3 (12)
C72—B91—C93— C157	148.1 (8)	C188—C115— C152—C82	1.1 (14)
C72—C194—C200— C182	1.6 (14)	C189—C42—C46— C173	-1.0 (13)
C75—C78—C98— C108	4.0 (12)	C189—C42—B91— C30	-33.9 (11)
C75—C78—C98— B208	179.3 (8)	C189—C42—B91— C72	-149.5 (8)
C77—C22—C62— B127	178.5 (8)	C189—C42—B91— C93	86.4 (9)
C77—C22—C62— C153	3.7 (13)	C190—C10—C176— Ru3	-58.8 (8)
C77—C126—C180— C153	2.7 (14)	C190—C10—C176— C94	-4.1 (13)
C78—C75—C95— C73	1.1 (13)	B191—C37—C60— C202	-177.7 (8)
C78—C98—C108— C73	-2.7 (12)	B191—C37—C183— C128	177.8 (9)
C78—C98—B208— C58	33.6 (11)	B191—C82—C139— C163	172.8 (8)
C78—C98—B208— C137	-88.6 (9)	B191—C82—C152— C115	-172.7 (8)
C78—C98—B208— C161	149.2 (8)	B191—C103— C195—C100	172.7 (8)
C79—C137—B208— C58	149.4 (8)	B191—C107— C110—C121	-176.7 (8)
C79—C137—B208— C98	-88.7 (10)	B191—C107— C198—C172	176.7 (9)
C79—C137—B208— C161	33.7 (12)	C192—N26—N41— C104	-179.3 (8)
C79—C146—C169— C132	-1.2 (14)	C192—N26—N41— C179	1.0 (10)
C81—C155—C187— C174	-1.0 (14)	C193—C113— C164—C97	-0.4 (15)
C81—C161—C171— C174	0.3 (12)	C194—C72—B91— C30	-88.8 (9)
C81—C161—B208— C58	-83.2 (9)	C194—C72—B91— C42	31.7 (11)
C81—C161—B208— C98	156.6 (8)	C194—C72—B91— C93	152.4 (8)
C81—C161—B208— C137	37.3 (11)	C195—C100— C158—C133	0.7 (13)
C82—C139—C163— C188	-0.1 (13)	C195—C103— B191—C37	164.3 (8)
C84—C94—C176— Ru3	53.4 (7)	C195—C103— B191—C82	-76.3 (9)

C84—C94—C176— C10	-0.9 (13)	C195—C103— B191—C107	45.3 (11)
C84—C149—C190— Ru3	-52.0 (7)	C198—C107— C110—C121	-1.9 (13)
C84—C149—C190— C10	-1.4 (13)	C198—C107— B191—C37	-96.7 (10)
C86—C103—B191— C37	-25.0 (11)	C198—C107— B191—C82	140.9 (9)
C86—C103—B191— C82	94.4 (9)	C198—C107— B191—C103	24.3 (13)
C86—C103—B191— C107	-144.1 (8)	C201—C65—C87— Ru4	52.7 (8)
C86—C103—C195— C100	1.3 (12)	C201—C65—C87— C154	-3.9 (13)
C86—C133—C158— C100	-1.0 (13)	C202—C68—C128— C183	-1.1 (15)
C85—C28—C111— C74	-3.2 (12)	B208—C58—C116— C66	176.8 (8)
C85—C30—B91— C42	155.7 (8)	B208—C58—C140— C69	-175.7 (8)
C85—C30—B91— C72	-82.0 (9)	B208—C98—C108— C73	-178.2 (8)
C85—C30—B91— C93	38.0 (11)	B208—C161— C171—C174	-171.9 (8)
C85—C30—C144— C74	-1.0 (12)	N215—N5—C99—C3	-2.5 (11)
C87—C65—C201— Ru4	-51.4 (8)	N215—C70—C3— C99	-1.9 (10)
C87—C65—C201— C14	-0.2 (13)	C0AA—C1AA— C2AA—Ru1	54.2 (9)
C88—N45—C114— Ru1	4.7 (14)	C0AA—C1AA— C2AA—C102	0.6 (14)
C88—N45—C114— N24	-175.7 (8)	C3—C70—N215—N5	0.5 (11)
C88—N45—C122— C117	176.5 (8)	C3—C70—N215— C71	-176.3 (8)
C88—N148—C4— C207	-179.0 (9)	C2AA—C1AA— C0AA—Ru1	-54.7 (9)
C89—C2—C101— Ru2	54.7 (8)	C2AA—C1AA— C0AA—C184	2.8 (15)
C89—C2—C101— C160	-2.6 (14)	C2AA—C102— C150—Ru1	56.0 (8)
C89—C40—C105— Ru2	-55.6 (7)	C2AA—C102— C150—C184	2.5 (14)

## 7.1.5. Crystal data for complex 4a

## Selected geometric parameters (Å)

Ru01—Cl02	2.4080 (6)	C3A—H3A	0.9500
Ru01—N2A	2.086 (2)	C3B—H3B	0.9500
Ru01—C1B	2.046 (2)	C3C—H3C	0.9500
Ru01—C1D	2.236 (3)	C3D—H3D	0.9500
Ru01—C2D	2.225 (2)	C3D—C4D	1.431 (3)
Ru01—C3D	2.242 (2)	C4D—C5D	1.402 (3)
Ru01—C4D	2.226 (2)	C4D—C8D	1.514 (4)
Ru01—C5D	2.182 (2)	C5D—H5D	0.9500
Ru01—C6D	2.195 (2)	C5D—C6D	1.416 (4)
N1A—N2A	1.355 (3)	C6D—H6D	0.9500
N1A—C1	1.452 (3)	C7D—H7DA	0.9800
N1A—C3A	1.340 (3)	C7D—H7DB	0.9800
N1B—C1	1.450 (3)	C7D—H7DC	0.9800
N1B—C1B	1.350 (3)	C8D—H8D	1.0000
N1B—C2B	1.394 (3)	C8D—C9D	1.540 (4)
N1C—N2C	1.350 (3)	C8D—C10D	1.511 (4)
N1C—C2	1.443 (3)	C9D—H9DA	0.9800
N1C—C3C	1.349 (3)	C9D—H9DB	0.9800
N2A—C1A	1.334 (3)	C9D—H9DC	0.9800
N2B—C1B	1.350 (3)	C10D—H10A	0.9800
N2B—C2	1.467 (3)	C10D—H10B	0.9800
N2B—C3B	1.390 (3)	C10D—H10C	0.9800
N2C—C1C	1.321 (4)	O1—B1	1.485 (3)
C1—H1A	0.9900	O1—B2	1.342 (3)
C1—H1B	0.9900	O2—B2	1.388 (3)
C1A—H1AA	0.9500	O2—B3	1.384 (3)
C1A—C2A	1.392 (4)	O3—B1	1.477 (3)
C1C—H1C	0.9500	O3—B3	1.350 (3)
C1C—C2C	1.390 (4)	O4—H4	0.864 (17)
C1D—C2D	1.429 (4)	O4—B2	1.358 (3)
C1D—C6D	1.395 (4)	O5—H5	0.857 (17)
C1D—C7D	1.497 (4)	O5—B3	1.354 (3)
C2—H2A	0.9900	O6—B1	1.454 (3)
C2—H2B	0.9900	O6—B5	1.340 (3)
C2A—H2AA	0.9500	O7—B1	1.463 (3)
C2A—C3A	1.371 (4)	O7—B4	1.338 (4)
C2B—H2BA	0.9500	O8—B4	1.373 (4)
C2B—C3B	1.336 (4)	O8—B5	1.387 (4)
C2C—H2C	0.9500	O9—H9	0.909 (17)

C2C—C3C	1.359 (4)	O9—B5	1.357 (4)
C2D—H2D	0.9500	O10—H10	0.8400
C2D—C3D	1.383 (4)	O10—B4	1.366 (3)

## Selected geometric parameters (°)

N2A—Ru01—Cl02	84.44 (5)	C1D—C2D—H2D	119.1
N2A—Ru01—C1D	158.31 (9)	C3D—C2D—Ru01	72.61 (14)
N2A—Ru01—C2D	121.01 (9)	C3D—C2D—C1D	121.8 (2)
N2A—Ru01—C3D	94.98 (8)	C3D—C2D—H2D	119.1
N2A—Ru01—C4D	92.61 (8)	N1A—C3A—C2A	107.2 (2)
N2A—Ru01—C5D	117.22 (9)	N1A—C3A—H3A	126.4
N2A—Ru01—C6D	154.70 (9)	C2A—C3A—H3A	126.4
C1B—Ru01—Cl02	87.89 (6)	N2B—C3B—H3B	126.4
C1B—Ru01—N2A	83.50 (8)	C2B—C3B—N2B	107.3 (2)
C1B—Ru01—C1D	117.90 (10)	C2B—C3B—H3B	126.4
C1B—Ru01—C2D	155.05 (10)	N1C—C3C—C2C	107.4 (2)
C1B—Ru01—C3D	158.45 (9)	N1C—C3C—H3C	126.3
C1B—Ru01—C4D	121.10 (9)	C2C—C3C—H3C	126.3
C1B—Ru01—C5D	94.77 (9)	Ru01—C3D—H3D	130.7
C1B—Ru01—C6D	93.77 (9)	C2D—C3D—Ru01	71.33 (14)
C1D—Ru01—Cl02	92.41 (7)	C2D—C3D—H3D	119.9
C1D—Ru01—C3D	66.56 (10)	C2D—C3D—C4D	120.2 (2)
C2D—Ru01—Cl02	89.90 (7)	C4D—C3D—Ru01	70.72 (13)
C2D—Ru01—C1D	37.37 (10)	C4D—C3D—H3D	119.9
C2D—Ru01—C3D	36.06 (9)	C3D—C4D—Ru01	71.91 (13)
C2D—Ru01—C4D	66.46 (9)	C3D—C4D—C8D	122.1 (2)
C3D—Ru01—Cl02	113.42 (7)	C5D—C4D—Ru01	69.78 (14)
C4D—Ru01—Cl02	150.41 (6)	C5D—C4D—C3D	118.4 (2)
C4D—Ru01—C1D	79.59 (9)	C5D—C4D—C8D	119.3 (2)
C4D—Ru01—C3D	37.36 (9)	C8D—C4D—Ru01	134.90 (17)
C5D—Ru01—Cl02	158.33 (7)	Ru01—C5D—H5D	127.7
C5D—Ru01—C1D	67.34 (10)	C4D—C5D—Ru01	73.15 (14)
C5D—Ru01—C2D	78.66 (10)	C4D—C5D—H5D	119.7
C5D—Ru01—C3D	66.73 (9)	C4D—C5D—C6D	120.7 (2)
C5D—Ru01—C4D	37.07 (9)	C6D—C5D—Ru01	71.63 (14)
C5D—Ru01—C6D	37.74 (10)	C6D—C5D—H5D	119.7
C6D—Ru01—Cl02	120.68 (7)	Ru01—C6D—H6D	129.2
C6D—Ru01—C1D	36.68 (10)	C1D—C6D—Ru01	73.26 (15)
C6D—Ru01—C2D	66.25 (10)	C1D—C6D—C5D	121.3 (2)

C6D—Ru01—C3D	78.42 (9)	C1D—C6D—H6D	119.3
C6D—Ru01—C4D	67.25 (10)	C5D—C6D—Ru01	70.63 (14)
N2A—N1A—C1	119.92 (19)	C5D—C6D—H6D	119.3
C3A—N1A—N2A	111.3 (2)	C1D—C7D—H7DA	109.5
C3A—N1A—C1	128.7 (2)	C1D—C7D—H7DB	109.5
C1B—N1B—C1	122.05 (19)	C1D—C7D—H7DC	109.5
C1B—N1B—C2B	112.2 (2)	H7DA—C7D—H7DB	109.5
C2B—N1B—C1	125.7 (2)	H7DA—C7D—H7DC	109.5
N2C—N1C—C2	120.0 (2)	H7DB—C7D—H7DC	109.5
C3C—N1C—N2C	111.5 (2)	C4D—C8D—H8D	107.7
C3C—N1C—C2	128.4 (2)	C4D—C8D—C9D	105.9 (2)
N1A—N2A—Ru01	123.94 (14)	C9D—C8D—H8D	107.7
C1A—N2A—Ru01	130.45 (17)	C10D—C8D—C4D	116.2 (2)
C1A—N2A—N1A	105.6 (2)	C10D—C8D—H8D	107.7
C1B—N2B—C2	125.25 (19)	C10D—C8D—C9D	111.3 (3)
C1B—N2B—C3B	111.33 (19)	C8D—C9D—H9DA	109.5
C3B—N2B—C2	123.41 (19)	C8D—C9D—H9DB	109.5
C1C—N2C—N1C	104.5 (2)	C8D—C9D—H9DC	109.5
N1A—C1—H1A	109.8	H9DA—C9D—H9DB	109.5
N1A—C1—H1B	109.8	H9DA—C9D—H9DC	109.5
N1B—C1—N1A	109.49 (18)	H9DB—C9D—H9DC	109.5
N1B—C1—H1A	109.8	C8D—C10D—H10A	109.5
N1B—C1—H1B	109.8	C8D—C10D—H10B	109.5
H1A—C1—H1B	108.2	C8D—C10D—H10C	109.5
N2A—C1A—H1AA	124.8	H10A—C10D—H10B	109.5
N2A—C1A—C2A	110.4 (2)	H10A—C10D—H10C	109.5
C2A—C1A—H1AA	124.8	H10B—C10D—H10C	109.5
N1B—C1B—Ru01	123.36 (16)	B2—O1—B1	123.55 (18)
N1B—C1B—N2B	103.62 (19)	B3—O2—B2	119.17 (19)
N2B—C1B—Ru01	133.01 (17)	B3—O3—B1	123.04 (18)
N2C—C1C—H1C	123.9	B2—O4—H4	109.6 (17)
N2C—C1C—C2C	112.2 (2)	B3—O5—H5	112.1 (19)
C2C—C1C—H1C	123.9	B5—O6—B1	122.6 (2)
C2D—C1D—Ru01	70.90 (14)	B4—O7—B1	122.5 (2)
C2D—C1D—C7D	120.7 (2)	B4—O8—B5	118.3 (2)
C6D—C1D—Ru01	70.06 (15)	B5—O9—H9	107.4 (18)
C6D—C1D—C2D	117.6 (2)	B4—O10—H10	109.5
C6D—C1D—C7D	121.7 (3)	O3—B1—O1	109.61 (19)
C7D—C1D—Ru01	131.26 (19)	O6—B1—O1	108.11 (19)
N1C—C2—N2B	110.3 (2)	O6—B1—O3	109.08 (19)
N1C—C2—H2A	109.6	O6—B1—O7	112.2 (2)

N1C—C2—H2B	109.6	O7—B1—O1	107.83 (18)
N2B—C2—H2A	109.6	O7—B1—O3	109.93 (19)
N2B—C2—H2B	109.6	O1—B2—O2	120.9 (2)
H2A—C2—H2B	108.1	O1—B2—O4	123.0 (2)
C1A—C2A—H2AA	127.2	O4—B2—O2	116.1 (2)
C3A—C2A—C1A	105.6 (2)	O3—B3—O2	121.0 (2)
C3A—C2A—H2AA	127.2	O3—B3—O5	123.0 (2)
N1B—C2B—H2BA	127.2	O5—B3—O2	116.0 (2)
C3B—C2B—N1B	105.6 (2)	O7—B4—O8	122.2 (2)
C3B—C2B—H2BA	127.2	O7—B4—O10	119.5 (3)
C1C—C2C—H2C	127.8	O10—B4—O8	118.2 (3)
C3C—C2C—C1C	104.5 (3)	O6—B5—O8	121.7 (2)
C3C—C2C—H2C	127.8	O6—B5—O9	122.6 (3)
Ru01—C2D—H2D	129.0	O9—B5—O8	115.8 (2)
C1D—C2D—Ru01	71.73 (15)		

## Selected geometric parameters, torsion angles (°)

Ru01—N2A—C1A— C2A	-178.55 (16)	C3B—N2B—C1B— Ru01	179.17 (17)
Ru01—C1D—C2D— C3D	-54.9 (2)	C3B—N2B—C1B— N1B	0.3 (2)
Ru01—C1D—C6D— C5D	54.0 (2)	C3B—N2B—C2— N1C	-50.1 (3)
Ru01—C2D—C3D— C4D	-53.2 (2)	C3C—N1C—N2C— C1C	-0.7 (3)
Ru01—C3D—C4D— C5D	-53.84 (19)	C3C—N1C—C2— N2B	-73.9 (3)
Ru01—C3D—C4D— C8D	132.2 (2)	C3D—C4D—C5D— Ru01	54.87 (19)
Ru01—C4D—C5D— C6D	-55.8 (2)	C3D—C4D—C5D— C6D	-0.9 (3)
Ru01—C4D—C8D— C9D	179.6 (2)	C3D—C4D—C8D— C9D	83.4 (3)
Ru01—C4D—C8D— C10D	55.4 (3)	C3D—C4D—C8D— C10D	-40.8 (3)
Ru01—C5D—C6D— C1D	-55.2 (2)	C4D—C5D—C6D— Ru01	56.5 (2)
N1A—N2A—C1A— C2A	-0.3 (2)	C4D—C5D—C6D— C1D	1.3 (4)
N1B—C2B—C3B— N2B	0.7 (3)	C5D—C4D—C8D— C9D	-90.5 (3)
N1C—N2C—C1C— C2C	1.0 (4)	C5D—C4D—C8D— C10D	145.3 (2)

N2A—N1A—C1— N1B	56.1 (3)	C6D—C1D—C2D— Ru01	54.0 (2)
N2A—N1A—C3A— C2A	-0.1 (3)	C6D—C1D—C2D— C3D	-0.9 (4)
N2A—C1A—C2A— C3A	0.3 (3)	C7D—C1D—C2D— Ru01	-127.3 (2)
N2C—N1C—C2— N2B	102.5 (2)	C7D—C1D—C2D— C3D	177.8 (2)
N2C—N1C—C3C— C2C	0.2 (3)	C7D—C1D—C6D— Ru01	126.9 (2)
N2C—C1C—C2C— C3C	-0.9 (4)	C7D—C1D—C6D— C5D	-179.1 (2)
C1—N1A—N2A— Ru01	-5.2 (3)	C8D—C4D—C5D— Ru01	-131.0 (2)
C1—N1A—N2A— C1A	176.44 (19)	C8D—C4D—C5D— C6D	173.2 (2)
C1—N1A—C3A— C2A	-175.9 (2)	B1—O1—B2—O2	-4.5 (4)
C1—N1B—C1B— Ru01	1.4 (3)	B1—O1—B2—O4	175.7 (2)
C1—N1B—C1B— N2B	-179.55 (19)	B1—O3—B3—O2	11.3 (4)
C1—N1B—C2B— C3B	179.1 (2)	B1—O3—B3—O5	-171.2 (2)
C1A—C2A—C3A— N1A	-0.1 (3)	B1—O6—B5—O8	7.8 (4)
C1B—N1B—C1— N1A	-55.1 (3)	B1—O6—B5—O9	-171.3 (3)
C1B—N1B—C2B— C3B	-0.6 (3)	B1—O7—B4—O8	-2.9 (4)
C1B—N2B—C2— N1C	128.3 (2)	B1—O7—B4—O10	172.9 (2)
C1B—N2B—C3B— C2B	-0.7 (3)	B2—O1—B1—O3	15.6 (3)
C1C—C2C—C3C— N1C	0.4 (3)	B2—O1—B1—O6	134.3 (2)
C1D—C2D—C3D— Ru01	54.5 (2)	B2—O1—B1—O7	-104.1 (2)
C1D—C2D—C3D— C4D	1.3 (4)	B2—O2—B3—O3	2.1 (3)
C2—N1C—N2C— C1C	-177.7 (2)	B2—O2—B3—O5	-175.5 (2)
C2—N1C—C3C— C2C	176.9 (2)	B3—O2—B2—O1	-5.5 (3)
C2—N2B—C1B— Ru01	0.6 (3)	B3—O2—B2—O4	174.3 (2)
C2—N2B—C1B— N1B	-178.3 (2)	B3—O3—B1—O1	-18.9 (3)



C2—N2B—C3B— C2B	177.9 (2)	B3—O3—B1—O6	-137.1 (2)
C2B—N1B—C1— N1A	125.2 (2)	B3—O3—B1—O7	99.5 (2)
C2B—N1B—C1B— Ru01	-178.83 (16)	B4—O7—B1—O1	-113.7 (2)
C2B—N1B—C1B— N2B	0.2 (2)	B4—O7—B1—O3	126.9 (2)
C2D—C1D—C6D— Ru01	-54.4 (2)	B4—O7—B1—O6	5.3 (3)
C2D—C1D—C6D— C5D	-0.4 (4)	B4—O8—B5—O6	-4.6 (4)
C2D—C3D—C4D— Ru01	53.4 (2)	B4—O8—B5—O9	174.6 (3)
C2D—C3D—C4D— C5D	-0.4 (3)	B5—O6—B1—O1	111.1 (3)
C2D—C3D—C4D— C8D	-174.4 (2)	B5—O6—B1—O3	-129.8 (2)
C3A—N1A—N2A— Ru01	178.65 (15)	B5—O6—B1—O7	-7.7 (3)
C3A—N1A—N2A— C1A	0.3 (2)	B5—O8—B4—O7	2.1 (4)
C3A—N1A—C1— N1B	-128.5 (2)	B5—O8—B4—O10	-173.7 (3)

### 7.1.6. Crystal data for complex 5

#### Selected geometric parameters (Å)

Ru1A—H	1.50 (4)	C12'—C13'	1.269 (17)
Ru1A—P1A	2.3683 (12)	C12C—H12C	0.9500
Ru1A—P1B	2.3697 (11)	C12C—C13C	1.382 (7)
Ru1A—N2E	2.123 (5)	C12D—H12D	0.9500
Ru1A—C1F	1.812 (6)	C12D—C13D	1.385 (7)
Ru1A—C7E	2.121 (6)	C12G—H12G	0.9500
P1A—C11A	1.829 (5)	C12G—C13G	1.280 (13)
P1A—C21A	1.835 (6)	C13'—H13'	0.9500
P1A—C31A	1.816 (5)	C13C—H13C	0.9500
P1B—C11B	1.853 (5)	C13C—C14C	1.390 (7)
P1B—C21B	1.833 (5)	C13D—H13D	0.9500
P1B—C31B	1.815 (5)	C13D—C14D	1.378 (7)
O1F—C1F	1.171 (5)	C13G—H13G	0.9500
N1E—N2E	1.377 (5)	C14C—H14C	0.9500
N1E—C5E	1.353 (7)	C14C—C15C	1.389 (7)
N1E—C6E	1.444 (6)	C14D—H14D	0.9500

N2E—C3E	1.333 (7)	C14D—C15D	1.388 (7)
N3E—C6E	1.439 (6)	C15C—H15C	0.9500
N3E—C7E	1.384 (6)	C15C—C16C	1.378 (7)
N3E—C8E	1.376 (7)	C15D—H15D	0.9500
N4E—C7E	1.377 (6)	C15D—C16D	1.374 (7)
N4E—C9E	1.409 (7)	C16C—H16C	0.9500
N4E—C10E	1.453 (6)	C16D—H16D	0.9500
N5E—N6E	1.365 (6)	C21C—C22C	1.385 (6)
N5E—C10E	1.454 (6)	C21C—C26C	1.391 (6)
N5E—C13E	1.360 (7)	C21D—C22D	1.391 (6)
N6E—C11E	1.345 (7)	C21D—C26D	1.389 (7)
C3E—H3E	0.9500	C22C—H22C	0.9500
C3E—C4E	1.387 (7)	C22C—C23C	1.397 (7)
C4E—H4E	0.9500	C22D—H22D	0.9500
C4E—C5E	1.340 (8)	C22D—C23D	1.386 (7)
C5E—H5E	0.9500	C23C—H23C	0.9500
C6E—H6EA	0.9900	C23C—C24C	1.368 (7)
C6E—H6EB	0.9900	C23D—H23D	0.9500
C8E—H8E	0.9500	C23D—C24D	1.388 (7)
C8E—C9E	1.298 (7)	C24C—H24C	0.9500
C9E—H9E	0.9500	C24C—C25C	1.378 (7)
C10E—H10E	0.9900	C24D—H24D	0.9500
C10E—H10F	0.9900	C24D—C25D	1.384 (7)
C11A—C12A	1.405 (7)	C25C—H25C	0.9500
C11A—C16A	1.383 (7)	C25C—C26C	1.394 (7)
C11B—C12B	1.394 (6)	C25D—H25D	0.9500
C11B—C16B	1.363 (7)	C25D—C26D	1.368 (7)
C11E—H11E	0.9500	C26C—H26C	0.9500
C11E—C12E	1.388 (8)	C26D—H26D	0.9500
C12A—H12A	0.9500	C31C—C32C	1.392 (6)
C12A—C13A	1.389 (7)	C31C—C36C	1.383 (7)
C12B—H12B	0.9500	C31D—C32D	1.403 (7)
C12B—C13B	1.368 (7)	C31D—C36D	1.387 (6)
C12E—H12E	0.9500	C32C—H32C	0.9500
C12E—C13E	1.356 (8)	C32C—C33C	1.380 (7)
C13A—H13A	0.9500	C32D—H32D	0.9500
C13A—C14A	1.378 (7)	C32D—C33D	1.371 (6)
C13B—H13B	0.9500	C33C—H33C	0.9500
C13B—C14B	1.363 (8)	C33C—C34C	1.384 (7)
C13E—H13E	0.9500	C33D—H33D	0.9500
C14A—H14A	0.9500	C33D—C34D	1.394 (7)

C14A—C15A	1.367 (8)	C34C—H34C	0.9500
C14B—H14B	0.9500	C34C—C35C	1.380 (7)
C14B—C15B	1.379 (7)	C34D—H34D	0.9500
C15A—H15A	0.9500	C34D—C35D	1.367 (7)
C15A—C16A	1.382 (7)	C35C—H35C	0.9500
C15B—H15B	0.9500	C35C—C36C	1.383 (7)
C15B—C16B	1.364 (8)	C35D—H35D	0.9500
C16A—H16A	0.9500	C35D—C36D	1.422 (7)
C16B—H16B	0.9500	C36C—H36C	0.9500
C21A—C22A	1.371 (7)	C36D—H36D	0.9500
C21A—C26A	1.397 (7)	C11M—C12M	1.391 (8)
C21B—C22B	1.392 (7)	C11M—C16M	1.402 (7)
C21B—C26B	1.406 (7)	C11M—B1M	1.641 (9)
C22A—H22A	0.9500	C12M—H12M	0.9500
C22A—C23A	1.376 (8)	C12M—C13M	1.399 (8)
C22B—H22B	0.9500	C13M—H13M	0.9500
C22B—C23B	1.376 (7)	C13M—C14M	1.370 (8)
C23A—H23A	0.9500	C14M—H14M	0.9500
C23A—C24A	1.376 (8)	C14M—C15M	1.373 (8)
C23B—H23B	0.9500	C15M—H15M	0.9500
C23B—C24B	1.383 (7)	C15M—C16M	1.404 (8)
C24A—H24A	0.9500	C16M—H16M	0.9500
C24A—C25A	1.377 (8)	C21M—C22M	1.413 (7)
C24B—H24B	0.9500	C21M—C26M	1.378 (7)
C24B—C25B	1.391 (8)	C21M—B1M	1.627 (8)
C25A—H25A	0.9500	C22M—H22M	0.9500
C25A—C26A	1.390 (7)	C22M—C23M	1.376 (8)
C25B—H25B	0.9500	C23M—H23M	0.9500
C25B—C26B	1.367 (7)	C23M—C24M	1.384 (8)
C26A—H26A	0.9500	C24M—H24M	0.9500
C26B—H26B	0.9500	C24M—C25M	1.361 (8)
C31A—C32A	1.404 (6)	C25M—H25M	0.9500
C31A—C36A	1.401 (7)	C25M—C26M	1.399 (8)
C31B—C32B	1.387 (7)	C26M—H26M	0.9500
C31B—C36B	1.402 (7)	C31M—C32M	1.408 (7)
C32A—H32A	0.9500	C31M—C36M	1.386 (7)
C32A—C33A	1.400 (8)	C31M—B1M	1.674 (7)
C32B—H32B	0.9500	C32M—H32M	0.9500
C32B—C33B	1.395 (7)	C32M—C33M	1.388 (7)
C33A—H33A	0.9500	C33M—H33M	0.9500
C33A—C34A	1.381 (8)	C33M—C34M	1.375 (7)

C33B—H33B	0.9500	C34M—H34M	0.9500
C33B—C34B	1.385 (8)	C34M—C35M	1.384 (7)
C34A—H34A	0.9500	C35M—H35M	0.9500
C34A—C35A	1.389 (8)	C35M—C36M	1.375 (7)
C34B—H34B	0.9500	C36M—H36M	0.9500
C34B—C35B	1.364 (8)	C41M—C42M	1.398 (8)
C35A—H35A	0.9500	C41M—C46M	1.389 (7)
C35A—C36A	1.376 (7)	C41M—B1M	1.654 (8)
C35B—H35B	0.9500	C42M—H42M	0.9500
C35B—C36B	1.409 (7)	C42M—C43M	1.401 (8)
C36A—H36A	0.9500	C43M—H43M	0.9500
C36B—H36B	0.9500	C43M—C44M	1.378 (8)
Ru1B—HA	1.71 (4)	C44M—H44M	0.9500
Ru1B—P1C	2.3784 (11)	C44M—C45M	1.364 (8)
Ru1B—P1D	2.3758 (11)	C45M—H45M	0.9500
Ru1B—N2G	2.164 (4)	C45M—C46M	1.402 (8)
Ru1B—C1H	1.813 (6)	C46M—H46M	0.9500
Ru1B—C7G	2.114 (5)	C11N—C12N	1.398 (7)
P1C—C11C	1.826 (5)	C11N—C16N	1.403 (6)
P1C—C21C	1.838 (5)	C11N—B1N	1.655 (7)
P1C—C31C	1.843 (5)	C12N—H12N	0.9500
P1D—C11D	1.827 (5)	C12N—C13N	1.389 (6)
P1D—C21D	1.840 (5)	C13N—H13N	0.9500
P1D—C31D	1.825 (5)	C13N—C14N	1.379 (7)
O1H—C1H	1.170 (5)	C14N—H14N	0.9500
N1G—N2G	1.364 (5)	C14N—C15N	1.360 (7)
N1G—C5G	1.344 (6)	C15N—H15N	0.9500
N1G—C6G	1.453 (6)	C15N—C16N	1.401 (7)
N2G—C3G	1.344 (6)	C16N—H16N	0.9500
N3G—C6G	1.433 (6)	C21N—C22N	1.411 (7)
N3G—C7G	1.385 (6)	C21N—C26N	1.390 (7)
N3G—C9G	1.374 (6)	C21N—B1N	1.637 (7)
N4G—C7G	1.378 (6)	C22N—H22N	0.9500
N4G—C8G	1.386 (6)	C22N—C23N	1.396 (7)
N4G—C10G	1.445 (6)	C23N—H23N	0.9500
N5G—N6G	1.341 (9)	C23N—C24N	1.374 (7)
N5G—C10G	1.558 (8)	C24N—H24N	0.9500
N5G—C13G	1.338 (13)	C24N—C25N	1.365 (7)
N5G'—N6G'	1.305 (17)	C25N—H25N	0.9500
N5G'—C10G	1.408 (14)	C25N—C26N	1.393 (7)
N5G'—C13'	1.380 (16)	C26N—H26N	0.9500

N6G—C11G	1.374 (10)	C31N—C32N	1.395 (7)
N6G'—C11'	1.347 (18)	C31N—C36N	1.397 (7)
C3G—H3G	0.9500	C31N—B1N	1.634 (8)
C3G—C4G	1.375 (7)	C32N—H32N	0.9500
C4G—H4G	0.9500	C32N—C33N	1.393 (7)
C4G—C5G	1.385 (8)	C33N—H33N	0.9500
C5G—H5G	0.9500	C33N—C34N	1.378 (7)
C6G—H6GA	0.9900	C34N—H34N	0.9500
C6G—H6GB	0.9900	C34N—C35N	1.373 (7)
C8G—H8G	0.9500	C35N—H35N	0.9500
C8G—C9G	1.341 (7)	C35N—C36N	1.393 (7)
C9G—H9G	0.9500	C36N—H36N	0.9500
C10G—H10A	0.9900	C41N—C42N	1.419 (6)
C10G—H10B	0.9900	C41N—C46N	1.385 (7)
C10G—H10C	0.9900	C41N—B1N	1.654 (7)
C10G—H10D	0.9900	C42N—H42N	0.9500
C11'—H11'	0.9500	C42N—C43N	1.401 (7)
C11'—C12'	1.482 (17)	C43N—H43N	0.9500
C11C—C12C	1.393 (7)	C43N—C44N	1.367 (7)
C11C—C16C	1.393 (6)	C44N—H44N	0.9500
C11D—C12D	1.380 (6)	C44N—C45N	1.390 (7)
C11D—C16D	1.391 (7)	C45N—H45N	0.9500
C11G—H11G	0.9500	C45N—C46N	1.402 (6)
C11G—C12G	1.441 (11)	C46N—H46N	0.9500
C12'—H12'	0.9500		

## Selected geometric parameters (°)

P1A—Ru1A—H	80.9 (12)	C16C—C11C—P1C	121.8 (4)
P1A—Ru1A—P1B	168.78 (5)	C16C—C11C—C12C	119.8 (5)
P1B—Ru1A—H	88.0 (12)	C12D—C11D—P1D	123.9 (4)
N2E—Ru1A—H	87.7 (13)	C12D—C11D—C16D	118.6 (5)
N2E—Ru1A—P1A	92.80 (10)	C16D—C11D—P1D	117.4 (4)
N2E—Ru1A—P1B	88.27 (10)	N6G—C11G—H11G	126.5
C1F—Ru1A—H	86.9 (13)	N6G—C11G—C12G	107.0 (8)
C1F—Ru1A—P1A	89.31 (13)	C12G—C11G—H11G	126.5
C1F—Ru1A—P1B	88.54 (13)	C11'—C12'—H12'	128.4
C1F—Ru1A—N2E	173.8 (2)	C13'—C12'—C11'	103.2 (14)
C1F—Ru1A—C7E	99.0 (2)	C13'—C12'—H12'	128.4
C7E—Ru1A—H	173.7 (13)	C11C—C12C—H12C	120.1

C7E—Ru1A—P1A	96.89 (12)	C13C—C12C—C11C	119.7 (5)
C7E—Ru1A—P1B	94.32 (12)	C13C—C12C—H12C	120.1
C7E—Ru1A—N2E	86.5 (2)	C11D—C12D—H12D	119.9
C11A—P1A—Ru1A	112.31 (15)	C11D—C12D—C13D	120.2 (5)
C11A—P1A—C21A	102.1 (2)	C13D—C12D—H12D	119.9
C21A—P1A—Ru1A	118.11 (16)	C11G—C12G—H12G	126.3
C31A—P1A—Ru1A	115.79 (16)	C13G—C12G—C11G	107.4 (11)
C31A—P1A—C11A	102.7 (2)	C13G—C12G—H12G	126.3
C31A—P1A—C21A	103.8 (2)	N5G'—C13'—H13'	123.7
C11B—P1B—Ru1A	116.32 (16)	C12'—C13'—N5G'	112.5 (15)
C21B—P1B—Ru1A	116.01 (15)	C12'—C13'—H13'	123.7
C21B—P1B—C11B	101.7 (2)	C12C—C13C—H13C	119.8
C31B—P1B—Ru1A	115.03 (15)	C12C—C13C—C14C	120.5 (6)
C31B—P1B—C11B	102.7 (2)	C14C—C13C—H13C	119.8
C31B—P1B—C21B	103.0 (2)	C12D—C13D—H13D	119.7
N2E—N1E—C6E	119.7 (4)	C14D—C13D—C12D	120.6 (5)
C5E—N1E—N2E	112.2 (5)	C14D—C13D—H13D	119.7
C5E—N1E—C6E	127.2 (5)	N5G—C13G—H13G	125.6
N1E—N2E—Ru1A	125.2 (4)	C12G—C13G—N5G	108.7 (12)
C3E—N2E—Ru1A	130.4 (4)	C12G—C13G—H13G	125.6
C3E—N2E—N1E	103.6 (5)	C13C—C14C—H14C	120.2
C7E—N3E—C6E	123.4 (5)	C15C—C14C—C13C	119.6 (5)
C8E—N3E—C6E	123.3 (5)	C15C—C14C—H14C	120.2
C8E—N3E—C7E	112.8 (5)	C13D—C14D—H14D	120.1
C7E—N4E—C9E	112.2 (5)	C13D—C14D—C15D	119.7 (5)
C7E—N4E—C10E	126.3 (5)	C15D—C14D—H14D	120.1
C9E—N4E—C10E	121.3 (5)	C14C—C15C—H15C	119.8
N6E—N5E—C10E	119.3 (5)	C16C—C15C—C14C	120.3 (5)
C13E—N5E—N6E	112.1 (5)	C16C—C15C—H15C	119.8
C13E—N5E—C10E	128.5 (5)	C14D—C15D—H15D	120.4
C11E—N6E—N5E	102.7 (5)	C16D—C15D—C14D	119.2 (5)
O1F—C1F—Ru1A	176.5 (5)	C16D—C15D—H15D	120.4
N2E—C3E—H3E	124.6	C11C—C16C—H16C	119.9
N2E—C3E—C4E	110.7 (6)	C15C—C16C—C11C	120.1 (5)
C4E—C3E—H3E	124.6	C15C—C16C—H16C	119.9
C3E—C4E—H4E	126.2	C11D—C16D—H16D	119.2
C5E—C4E—C3E	107.7 (6)	C15D—C16D—C11D	121.6 (5)
C5E—C4E—H4E	126.2	C15D—C16D—H16D	119.2
N1E—C5E—H5E	127.1	C22C—C21C—P1C	122.0 (4)
C4E—C5E—N1E	105.8 (6)	C22C—C21C—C26C	118.7 (5)
C4E—C5E—H5E	127.1	C26C—C21C—P1C	119.2 (4)

N1E—C6E—H6EA	109.2	C22D—C21D—P1D	121.1 (4)
N1E—C6E—H6EB	109.2	C26D—C21D—P1D	121.1 (4)
N3E—C6E—N1E	112.3 (4)	C26D—C21D—C22D	117.8 (5)
N3E—C6E—H6EA	109.2	C21C—C22C—H22C	120.1
N3E—C6E—H6EB	109.2	C21C—C22C—C23C	119.8 (5)
H6EA—C6E—H6EB	107.9	C23C—C22C—H22C	120.1
N3E—C7E—Ru1A	122.8 (4)	C21D—C22D—H22D	119.1
N4E—C7E—Ru1A	136.5 (4)	C23D—C22D—C21D	121.8 (5)
N4E—C7E—N3E	100.5 (5)	C23D—C22D—H22D	119.1
N3E—C8E—H8E	126.0	C22C—C23C—H23C	119.3
C9E—C8E—N3E	107.9 (6)	C24C—C23C—C22C	121.4 (5)
C9E—C8E—H8E	126.0	C24C—C23C—H23C	119.3
N4E—C9E—H9E	126.7	C22D—C23D—H23D	120.5
C8E—C9E—N4E	106.6 (6)	C22D—C23D—C24D	119.1 (5)
C8E—C9E—H9E	126.7	C24D—C23D—H23D	120.5
N4E—C10E—N5E	110.8 (4)	C23C—C24C—H24C	120.4
N4E—C10E—H10E	109.5	C23C—C24C—C25C	119.1 (5)
N4E—C10E—H10F	109.5	C25C—C24C—H24C	120.4
N5E—C10E—H10E	109.5	C23D—C24D—H24D	120.3
N5E—C10E—H10F	109.5	C25D—C24D—C23D	119.5 (5)
H10E—C10E—H10F	108.1	C25D—C24D—H24D	120.3
C12A—C11A—P1A	118.0 (4)	C24C—C25C—H25C	119.9
C16A—C11A—P1A	123.3 (4)	C24C—C25C—C26C	120.3 (5)
C16A—C11A—C12A	118.6 (5)	C26C—C25C—H25C	119.9
C12B—C11B—P1B	120.9 (4)	C24D—C25D—H25D	119.6
C16B—C11B—P1B	122.0 (4)	C26D—C25D—C24D	120.9 (5)
C16B—C11B—C12B	117.1 (5)	C26D—C25D—H25D	119.6
N6E—C11E—H11E	123.4	C21C—C26C—C25C	120.7 (5)
N6E—C11E—C12E	113.1 (6)	C21C—C26C—H26C	119.7
C12E—C11E—H11E	123.4	C25C—C26C—H26C	119.7
C11A—C12A—H12A	119.6	C21D—C26D—H26D	119.5
C13A—C12A—C11A	120.9 (5)	C25D—C26D—C21D	121.0 (5)
C13A—C12A—H12A	119.6	C25D—C26D—H26D	119.5
C11B—C12B—H12B	119.7	C32C—C31C—P1C	122.1 (4)
C13B—C12B—C11B	120.7 (5)	C36C—C31C—P1C	120.0 (4)
C13B—C12B—H12B	119.7	C36C—C31C—C32C	117.7 (5)
C11E—C12E—H12E	127.7	C32D—C31D—P1D	118.9 (4)
C13E—C12E—C11E	104.6 (6)	C36D—C31D—P1D	121.7 (4)
C13E—C12E—H12E	127.7	C36D—C31D—C32D	119.2 (4)
C12A—C13A—H13A	120.5	C31C—C32C—H32C	119.3
C14A—C13A—C12A	119.1 (6)	C33C—C32C—C31C	121.4 (5)

C14A—C13A—H13A	120.5	C33C—C32C—H32C	119.3
C12B—C13B—H13B	119.2	C31D—C32D—H32D	119.6
C14B—C13B—C12B	121.5 (5)	C33D—C32D—C31D	120.7 (5)
C14B—C13B—H13B	119.2	C33D—C32D—H32D	119.6
N5E—C13E—H13E	126.3	C32C—C33C—H33C	120.1
C12E—C13E—N5E	107.5 (6)	C32C—C33C—C34C	119.7 (5)
C12E—C13E—H13E	126.3	C34C—C33C—H33C	120.1
C13A—C14A—H14A	119.8	C32D—C33D—H33D	119.8
C15A—C14A—C13A	120.5 (5)	C32D—C33D—C34D	120.4 (5)
C15A—C14A—H14A	119.8	C34D—C33D—H33D	119.8
C13B—C14B—H14B	121.0	C33C—C34C—H34C	120.2
C13B—C14B—C15B	118.0 (6)	C35C—C34C—C33C	119.7 (5)
C15B—C14B—H14B	121.0	C35C—C34C—H34C	120.2
C14A—C15A—H15A	119.5	C33D—C34D—H34D	120.0
C14A—C15A—C16A	121.0 (6)	C35D—C34D—C33D	119.9 (5)
C16A—C15A—H15A	119.5	C35D—C34D—H34D	120.0
C14B—C15B—H15B	119.7	C34C—C35C—H35C	120.1
C16B—C15B—C14B	120.5 (6)	C34C—C35C—C36C	119.9 (6)
C16B—C15B—H15B	119.7	C36C—C35C—H35C	120.1
C11A—C16A—H16A	120.0	C34D—C35D—H35D	119.8
C15A—C16A—C11A	120.0 (5)	C34D—C35D—C36D	120.3 (5)
C15A—C16A—H16A	120.0	C36D—C35D—H35D	119.8
C11B—C16B—C15B	122.2 (6)	C31C—C36C—C35C	121.5 (5)
C11B—C16B—H16B	118.9	C31C—C36C—H36C	119.3
C15B—C16B—H16B	118.9	C35C—C36C—H36C	119.3
C22A—C21A—P1A	122.5 (4)	C31D—C36D—C35D	119.4 (5)
C22A—C21A—C26A	117.3 (5)	C31D—C36D—H36D	120.3
C26A—C21A—P1A	120.2 (4)	C35D—C36D—H36D	120.3
C22B—C21B—P1B	123.0 (4)	C12M—C11M— C16M	114.3 (6)
C22B—C21B—C26B	117.7 (5)	C12M—C11M—B1M	124.2 (5)
C26B—C21B—P1B	119.4 (4)	C16M—C11M—B1M	121.3 (5)
C21A—C22A—H22A	119.0	C11M—C12M— H12M	118.0
C21A—C22A—C23A	122.1 (6)	C11M—C12M— C13M	124.0 (6)
C23A—C22A—H22A	119.0	C13M—C12M— H12M	118.0
C21B—C22B—H22B	119.7	C12M—C13M— H13M	120.3
C23B—C22B—C21B	120.6 (5)	C14M—C13M— C12M	119.5 (6)
C23B—C22B—H22B	119.7	C14M—C13M—	120.3



Chapter 7: Appendices

		H13M	
C22A—C23A—H23A	119.9	C13M—C14M—H14M	120.3
C24A—C23A—C22A	120.3 (6)	C13M—C14M—C15M	119.4 (7)
C24A—C23A—H23A	119.9	C15M—C14M—H14M	120.3
C22B—C23B—H23B	119.1	C14M—C15M—H15M	119.9
C22B—C23B—C24B	121.8 (6)	C14M—C15M—C16M	120.3 (6)
C24B—C23B—H23B	119.1	C16M—C15M—H15M	119.9
C23A—C24A—H24A	120.3	C11M—C16M—C15M	122.6 (6)
C23A—C24A—C25A	119.3 (6)	C11M—C16M—H16M	118.7
C25A—C24A—H24A	120.3	C15M—C16M—H16M	118.7
C23B—C24B—H24B	121.2	C22M—C21M—B1M	122.3 (5)
C23B—C24B—C25B	117.6 (6)	C26M—C21M—C22M	113.8 (6)
C25B—C24B—H24B	121.2	C26M—C21M—B1M	123.2 (5)
C24A—C25A—H25A	120.1	C21M—C22M—H22M	118.7
C24A—C25A—C26A	119.9 (6)	C23M—C22M—C21M	122.5 (6)
C26A—C25A—H25A	120.1	C23M—C22M—H22M	118.7
C24B—C25B—H25B	119.3	C22M—C23M—H23M	119.5
C26B—C25B—C24B	121.4 (6)	C22M—C23M—C24M	120.9 (6)
C26B—C25B—H25B	119.3	C24M—C23M—H23M	119.5
C21A—C26A—H26A	119.4	C23M—C24M—H24M	120.6
C25A—C26A—C21A	121.2 (5)	C25M—C24M—C23M	118.8 (6)
C25A—C26A—H26A	119.4	C25M—C24M—H24M	120.6
C21B—C26B—H26B	119.6	C24M—C25M—H25M	120.4
C25B—C26B—C21B	120.8 (5)	C24M—C25M—C26M	119.2 (6)
C25B—C26B—H26B	119.6	C26M—C25M—H25M	120.4
C32A—C31A—P1A	124.2 (5)	C21M—C26M—	124.7 (6)

Chapter 7: Appendices

		C25M	
C36A—C31A—P1A	117.5 (4)	C21M—C26M— H26M	117.7
C36A—C31A—C32A	118.3 (5)	C25M—C26M— H26M	117.7
C32B—C31B—P1B	119.3 (4)	C32M—C31M—B1M	122.3 (5)
C32B—C31B—C36B	117.4 (5)	C36M—C31M— C32M	114.6 (5)
C36B—C31B—P1B	123.3 (4)	C36M—C31M—B1M	123.1 (5)
C31A—C32A—H32A	120.6	C31M—C32M— H32M	118.7
C33A—C32A—C31A	118.8 (6)	C33M—C32M— C31M	122.6 (5)
C33A—C32A—H32A	120.6	C33M—C32M— H32M	118.7
C31B—C32B—H32B	119.1	C32M—C33M— H33M	119.9
C31B—C32B—C33B	121.9 (5)	C34M—C33M— C32M	120.2 (6)
C33B—C32B—H32B	119.1	C34M—C33M— H33M	119.9
C32A—C33A—H33A	119.3	C33M—C34M— H34M	120.6
C34A—C33A—C32A	121.4 (6)	C33M—C34M— C35M	118.8 (5)
C34A—C33A—H33A	119.3	C35M—C34M— H34M	120.6
C32B—C33B—H33B	119.9	C34M—C35M— H35M	120.0
C34B—C33B—C32B	120.2 (6)	C36M—C35M— C34M	120.0 (5)
C34B—C33B—H33B	119.9	C36M—C35M— H35M	120.0
C33A—C34A—H34A	119.9	C31M—C36M— H36M	118.1
C33A—C34A—C35A	120.2 (6)	C35M—C36M— C31M	123.8 (6)
C35A—C34A—H34A	119.9	C35M—C36M— H36M	118.1
C33B—C34B—H34B	120.5	C42M—C41M—B1M	123.6 (5)
C35B—C34B—C33B	119.1 (6)	C46M—C41M— C42M	114.0 (5)
C35B—C34B—H34B	120.5	C46M—C41M—B1M	122.4 (5)
C34A—C35A—H35A	120.7	C41M—C42M— H42M	118.0
C36A—C35A—C34A	118.7 (6)	C41M—C42M— C43M	124.0 (6)
C36A—C35A—H35A	120.7	C43M—C42M—	118.0

		H42M	
C34B—C35B—H35B	119.4	C42M—C43M—H43M	120.5
C34B—C35B—C36B	121.3 (6)	C44M—C43M—C42M	119.1 (6)
C36B—C35B—H35B	119.4	C44M—C43M—H43M	120.5
C31A—C36A—H36A	118.7	C43M—C44M—H44M	120.3
C35A—C36A—C31A	122.6 (5)	C45M—C44M—C43M	119.4 (6)
C35A—C36A—H36A	118.7	C45M—C44M—H44M	120.3
C31B—C36B—C35B	120.3 (5)	C44M—C45M—H45M	119.8
C31B—C36B—H36B	119.9	C44M—C45M—C46M	120.4 (6)
C35B—C36B—H36B	119.9	C46M—C45M—H45M	119.8
P1C—Ru1B—HA	91.1 (11)	C41M—C46M—C45M	123.2 (6)
P1D—Ru1B—HA	78.6 (11)	C41M—C46M—H46M	118.4
P1D—Ru1B—P1C	169.30 (5)	C45M—C46M—H46M	118.4
N2G—Ru1B—HA	88.9 (12)	C11M—B1M—C31M	111.9 (4)
N2G—Ru1B—P1C	88.00 (10)	C11M—B1M—C41M	109.9 (5)
N2G—Ru1B—P1D	94.75 (10)	C21M—B1M—C11M	112.2 (5)
C1H—Ru1B—HA	87.0 (12)	C21M—B1M—C31M	106.5 (5)
C1H—Ru1B—P1C	89.61 (13)	C21M—B1M—C41M	108.2 (5)
C1H—Ru1B—P1D	86.87 (13)	C41M—B1M—C31M	108.1 (4)
C1H—Ru1B—N2G	175.2 (2)	C12N—C11N—C16N	114.8 (4)
C1H—Ru1B—C7G	99.2 (2)	C12N—C11N—B1N	123.4 (4)
C7G—Ru1B—HA	170.8 (12)	C16N—C11N—B1N	121.4 (5)
C7G—Ru1B—P1C	95.63 (11)	C11N—C12N—H12N	118.4
C7G—Ru1B—P1D	94.91 (11)	C13N—C12N—C11N	123.2 (5)
C7G—Ru1B—N2G	85.18 (19)	C13N—C12N—H12N	118.4
C11C—P1C—Ru1B	114.18 (15)	C12N—C13N—H13N	120.0
C11C—P1C—C21C	103.1 (2)	C14N—C13N—C12N	119.9 (5)
C11C—P1C—C31C	103.2 (2)	C14N—C13N—H13N	120.0
C21C—P1C—Ru1B	117.23 (14)	C13N—C14N—H14N	120.4
C21C—P1C—C31C	100.4 (2)	C15N—C14N—C13N	119.2 (5)
C31C—P1C—Ru1B	116.64 (15)	C15N—C14N—H14N	120.4
C11D—P1D—Ru1B	114.46 (15)	C14N—C15N—H15N	119.6
C11D—P1D—C21D	103.9 (2)	C14N—C15N—C16N	120.8 (5)

C21D—P1D—Ru 1B	119.47 (16)	C16N—C15N—H15N	119.6
C31D—P1D—Ru 1B	113.35 (15)	C11N—C16N—H16N	119.0
C31D—P1D—C11D	102.7 (2)	C15N—C16N—C11N	122.0 (5)
C31D—P1D—C21D	100.8 (2)	C15N—C16N—H16N	119.0
N2G—N1G—C6G	119.9 (4)	C22N—C21N—B1N	123.6 (5)
C5G—N1G—N2G	112.2 (4)	C26N—C21N—C22N	114.1 (5)
C5G—N1G—C6G	126.7 (4)	C26N—C21N—B1N	122.3 (5)
N1G—N2G—Ru 1B	124.6 (3)	C21N—C22N—H22N	118.8
C3G—N2G—Ru 1B	131.0 (4)	C23N—C22N—C21N	122.4 (5)
C3G—N2G—N1G	103.8 (4)	C23N—C22N—H22N	118.8
C7G—N3G—C6G	123.7 (5)	C22N—C23N—H23N	119.5
C9G—N3G—C6G	122.9 (4)	C24N—C23N—C22N	121.0 (5)
C9G—N3G—C7G	113.1 (5)	C24N—C23N—H23N	119.5
C7G—N4G—C8G	113.5 (5)	C23N—C24N—H24N	121.0
C7G—N4G—C10G	124.5 (4)	C25N—C24N—C23N	118.0 (5)
C8G—N4G—C10G	122.0 (5)	C25N—C24N—H24N	121.0
N6G—N5G—C10G	123.8 (7)	C24N—C25N—H25N	119.5
C13G—N5G—N6G	112.6 (8)	C24N—C25N—C26N	121.1 (6)
C13G—N5G—C10G	123.6 (7)	C26N—C25N—H25N	119.5
N6G'—N5G'—C10G	116.9 (13)	C21N—C26N—C25N	123.3 (5)
N6G'—N5G'—C13'	108.5 (14)	C21N—C26N—H26N	118.4
C13'—N5G'—C10G	134.6 (12)	C25N—C26N—H26N	118.4
N5G—N6G—C11G	104.3 (8)	C32N—C31N—C36N	114.1 (5)
N5G'—N6G'—C11'	107.9 (15)	C32N—C31N—B1N	122.4 (5)
O1H—C1H—Ru 1B	176.5 (5)	C36N—C31N—B1N	123.5 (5)
N2G—C3G—H3G	123.9	C31N—C32N—H32N	118.3
N2G—C3G—C4G	112.1 (5)	C33N—C32N—C31N	123.4 (5)
C4G—C3G—H3G	123.9	C33N—C32N—H32N	118.3
C3G—C4G—H4G	127.4	C32N—C33N—H33N	120.0
C3G—C4G—C5G	105.3 (5)	C34N—C33N—C32N	120.0 (5)
C5G—C4G—H4G	127.4	C34N—C33N—H33N	120.0
N1G—C5G—C4G	106.6 (5)	C33N—C34N—H34N	120.4
N1G—C5G—H5G	126.7	C35N—C34N—C33N	119.2 (6)
C4G—C5G—H5G	126.7	C35N—C34N—H34N	120.4
N1G—C6G—H6GA	109.1	C34N—C35N—H35N	120.2
N1G—C6G—H6GB	109.1	C34N—C35N—C36N	119.6 (5)
N3G—C6G—N1G	112.3 (4)	C36N—C35N—H35N	120.2
N3G—C6G—H6GA	109.1	C31N—C36N—H36N	118.1
N3G—C6G—H6GB	109.1	C35N—C36N—C31N	123.8 (5)
H6GA—C6G—H6GB	107.9	C35N—C36N—H36N	118.1
N3G—C7G—Ru 1B	123.2 (4)	C42N—C41N—B1N	118.7 (5)

N4G—C7G—Ru1B	136.3 (4)	C46N—C41N—C42N	115.9 (4)
N4G—C7G—N3G	100.5 (4)	C46N—C41N—B1N	124.3 (4)
N4G—C8G—H8G	127.1	C41N—C42N—H42N	119.4
C9G—C8G—N4G	105.9 (5)	C43N—C42N—C41N	121.1 (5)
C9G—C8G—H8G	127.1	C43N—C42N—H42N	119.4
N3G—C9G—H9G	126.5	C42N—C43N—H43N	119.6
C8G—C9G—N3G	107.0 (5)	C44N—C43N—C42N	120.7 (5)
C8G—C9G—H9G	126.5	C44N—C43N—H43N	119.6
N4G—C10G—N5G	111.3 (4)	C43N—C44N—H44N	120.0
N4G—C10G—H10A	109.4	C43N—C44N—C45N	120.1 (5)
N4G—C10G—H10B	109.4	C45N—C44N—H44N	120.0
N4G—C10G—H10C	110.0	C44N—C45N—H45N	120.7
N4G—C10G—H10D	110.0	C44N—C45N—C46N	118.7 (5)
N5G—C10G—H10A	109.4	C46N—C45N—H45N	120.7
N5G—C10G—H10B	109.4	C41N—C46N—C45N	123.5 (5)
N5G—C10G—N4G	108.3 (7)	C41N—C46N—H46N	118.3
N5G—C10G—H10C	110.0	C45N—C46N—H46N	118.3
N5G—C10G—H10D	110.0	C21N—B1N—C11N	110.3 (4)
H10A—C10G—H10B	108.0	C21N—B1N—C41N	106.1 (4)
H10C—C10G—H10D	108.4	C31N—B1N—C11N	107.3 (4)
N6G—C11'—H11'	126.3	C31N—B1N—C21N	112.0 (4)
N6G—C11'—C12'	107.4 (14)	C31N—B1N—C41N	110.0 (4)
C12'—C11'—H11'	126.3	C41N—B1N—C11N	111.2 (4)
C12C—C11C—P1C	118.5 (4)		

## Selected geometric parameters, torsion angles (°)

Ru1A—P1A— C11A—C12A	51.1 (4)	C10G—N4G—C8G— C9G	-179.6 (4)
Ru1A—P1A— C11A—C16A	-130.5 (4)	C10G—N5G—N6G— C11G	178.7 (6)
Ru1A—P1A— C21A—C22A	-126.8 (4)	C10G—N5G— C13G—C12G	-176.7 (7)
Ru1A—P1A— C21A—C26A	54.4 (5)	C10G—N5G'— N6G'—C11'	-176.2 (15)
Ru1A—P1A— C31A—C32A	-130.1 (4)	C10G—N5G'—C13'— C12'	-178.7 (15)
Ru1A—P1A— C31A—C36A	47.6 (4)	C11'—C12'—C13'— N5G'	-4 (2)
Ru1A—P1B—C11B— C12B	154.8 (4)	C11C—P1C—C21C— C22C	-7.8 (4)
Ru1A—P1B—C11B—	-26.9 (5)	C11C—P1C—C21C—	170.0 (4)

C16B			C26C		
Ru1A—P1B—C21B— C22B	105.5 (4)		C11C—P1C—C31C— C32C	-88.2 (4)	
Ru1A—P1B—C21B— C26B	-74.5 (4)		C11C—P1C—C31C— C36C	86.8 (4)	
Ru1A—P1B—C31B— C32B	-48.1 (4)		C11C—C12C— C13C—C14C	-0.4 (8)	
Ru1A—P1B—C31B— C36B	128.2 (4)		C11D—P1D— C21D—C22D	92.6 (4)	
Ru1A—N2E—C3E— C4E	170.4 (3)		C11D—P1D— C21D—C26D	-89.8 (4)	
P1A—C11A— C12A—C13A	178.1 (4)		C11D—P1D— C31D—C32D	175.8 (4)	
P1A—C11A— C16A—C15A	-177.4 (4)		C11D—P1D— C31D—C36D	-8.9 (5)	
P1A—C21A— C22A—C23A	179.8 (5)		C11D—C12D— C13D—C14D	-0.1 (7)	
P1A—C21A— C26A—C25A	179.9 (4)		C11G—C12G— C13G—N5G	-3.1 (13)	
P1A—C31A— C32A—C33A	175.2 (4)		C12C—C11C— C16C—C15C	1.1 (7)	
P1A—C31A— C36A—C35A	-177.0 (4)		C12C—C13C— C14C—C15C	0.1 (8)	
P1B—C11B—C12B— C13B	179.1 (4)		C12D—C11D— C16D—C15D	0.9 (7)	
P1B—C11B—C16B— C15B	-177.7 (5)		C12D—C13D— C14D—C15D	1.6 (8)	
P1B—C21B—C22B— C23B	-179.6 (4)		C13'—N5G'—N6G'— C11'	5 (2)	
P1B—C21B—C26B— C25B	179.0 (4)		C13'—N5G'—C10G— N4G	97.6 (17)	
P1B—C31B—C32B— C33B	176.1 (4)		C13C—C14C— C15C—C16C	0.8 (8)	
P1B—C31B—C36B— C35B	-175.6 (4)		C13D—C14D— C15D—C16D	-1.9 (8)	
N1E—N2E—C3E— C4E	1.2 (5)		C13G—N5G—N6G— C11G	-0.1 (10)	
N2E—N1E—C5E— C4E	0.6 (6)		C13G—N5G— C10G—N4G	83.2 (9)	
N2E—N1E—C6E— N3E	-60.5 (6)		C14C—C15C— C16C—C11C	-1.4 (8)	
N2E—C3E—C4E— C5E	-0.9 (6)		C14D—C15D— C16D—C11D	0.6 (8)	
N3E—C8E—C9E— N4E	0.2 (6)		C16C—C11C— C12C—C13C	-0.1 (7)	
N5E—N6E—C11E— C12E	0.0 (7)		C16D—C11D— C12D—C13D	-1.2 (7)	
N6E—N5E—C10E—	-96.0 (6)		C21C—P1C—C11C—	77.4 (4)	

N4E		C12C	
N6E—N5E—C13E— C12E	0.2 (7)	C21C—P1C—C11C— C16C	-103.5 (4)
N6E—C11E—C12E— C13E	0.1 (8)	C21C—P1C—C31C— C32C	18.0 (5)
C3E—C4E—C5E— N1E	0.1 (6)	C21C—P1C—C31C— C36C	-167.0 (4)
C5E—N1E—N2E— Ru1A	-171.1 (3)	C21C—C22C— C23C—C24C	-0.4 (8)
C5E—N1E—N2E— C3E	-1.1 (5)	C21D—P1D— C11D—C12D	5.8 (5)
C5E—N1E—C6E— N3E	131.8 (5)	C21D—P1D— C11D—C16D	-178.2 (4)
C6E—N1E—N2E— Ru1A	19.6 (5)	C21D—P1D— C31D—C32D	-77.1 (4)
C6E—N1E—N2E— C3E	-170.5 (4)	C21D—P1D— C31D—C36D	98.2 (4)
C6E—N1E—C5E— C4E	169.0 (5)	C21D—C22D— C23D—C24D	0.1 (8)
C6E—N3E—C7E— Ru1A	-10.0 (6)	C22C—C21C— C26C—C25C	-0.6 (7)
C6E—N3E—C7E— N4E	173.4 (4)	C22C—C23C— C24C—C25C	-1.3 (8)
C6E—N3E—C8E— C9E	-173.4 (5)	C22D—C21D— C26D—C25D	-0.4 (7)
C7E—N3E—C6E— N1E	56.1 (6)	C22D—C23D— C24D—C25D	0.0 (8)
C7E—N3E—C8E— C9E	-0.5 (6)	C23C—C24C— C25C—C26C	2.1 (8)
C7E—N4E—C9E— C8E	0.2 (6)	C23D—C24D— C25D—C26D	-0.3 (8)
C7E—N4E—C10E— N5E	108.0 (5)	C24C—C25C— C26C—C21C	-1.2 (7)
C8E—N3E—C6E— N1E	-131.8 (5)	C24D—C25D— C26D—C21D	0.5 (8)
C8E—N3E—C7E— Ru1A	177.2 (3)	C26C—C21C— C22C—C23C	1.4 (7)
C8E—N3E—C7E— N4E	0.6 (5)	C26D—C21D— C22D—C23D	0.1 (7)
C9E—N4E—C7E— Ru1A	-176.3 (4)	C31C—P1C—C11C— C12C	-178.4 (4)
C9E—N4E—C7E— N3E	-0.5 (5)	C31C—P1C—C11C— C16C	0.7 (4)
C9E—N4E—C10E— N5E	-66.4 (6)	C31C—P1C—C21C— C22C	-114.1 (4)
C10E—N4E—C7E— Ru1A	8.9 (7)	C31C—P1C—C21C— C26C	63.7 (4)
C10E—N4E—C7E—	-175.3 (4)	C31C—C32C—	-3.8 (8)

N3E		C33C—C34C	
C10E—N4E—C9E— C8E	175.3 (4)	C31D—P1D— C11D—C12D	110.5 (4)
C10E—N5E—N6E— C11E	176.6 (5)	C31D—P1D— C11D—C16D	-73.5 (4)
C10E—N5E—C13E— C12E	-176.2 (5)	C31D—P1D— C21D—C22D	-13.6 (4)
C11A—P1A— C21A—C22A	-3.1 (5)	C31D—P1D— C21D—C26D	164.0 (4)
C11A—P1A— C21A—C26A	178.1 (4)	C31D—C32D— C33D—C34D	-0.5 (8)
C11A—P1A— C31A—C32A	107.2 (4)	C32C—C31C— C36C—C35C	-1.9 (8)
C11A—P1A— C31A—C36A	-75.2 (4)	C32C—C33C— C34C—C35C	0.0 (9)
C11A—C12A— C13A—C14A	0.2 (8)	C32D—C31D— C36D—C35D	-0.3 (7)
C11B—P1B—C21B— C22B	-127.2 (4)	C32D—C33D— C34D—C35D	1.7 (8)
C11B—P1B—C21B— C26B	52.7 (4)	C33C—C34C— C35C—C36C	2.7 (9)
C11B—P1B—C31B— C32B	-175.5 (4)	C33D—C34D— C35D—C36D	-2.2 (8)
C11B—P1B—C31B— C36B	0.8 (5)	C34C—C35C— C36C—C31C	-1.8 (9)
C11B—C12B— C13B—C14B	-0.9 (9)	C34D—C35D— C36D—C31D	1.5 (8)
C11E—C12E— C13E—N5E	-0.2 (7)	C36C—C31C— C32C—C33C	4.7 (8)
C12A—C11A— C16A—C15A	0.9 (8)	C36D—C31D— C32D—C33D	-0.2 (8)
C12A—C13A— C14A—C15A	-0.6 (9)	C11M—C12M— C13M—C14M	-0.8 (9)
C12B—C11B— C16B—C15B	0.7 (9)	C12M—C11M— C16M—C15M	-1.6 (8)
C12B—C13B— C14B—C15B	-0.3 (10)	C12M—C11M— B1M—C21M	151.6 (5)
C13A—C14A— C15A—C16A	1.2 (9)	C12M—C11M— B1M—C31M	32.0 (7)
C13B—C14B— C15B—C16B	1.7 (10)	C12M—C11M— B1M—C41M	-88.0 (6)
C13E—N5E—N6E— C11E	-0.1 (6)	C12M—C13M— C14M—C15M	0.3 (9)
C13E—N5E—C10E— N4E	80.1 (7)	C13M—C14M— C15M—C16M	-0.6 (9)
C14A—C15A— C16A—C11A	-1.4 (8)	C14M—C15M— C16M—C11M	1.3 (9)
C14B—C15B—	-1.9 (11)	C16M—C11M—	1.4 (8)



C16B—C11B		C12M—C13M	
C16A—C11A— C12A—C13A	-0.3 (8)	C16M—C11M— B1M—C21M	-33.2 (7)
C16B—C11B— C12B—C13B	0.7 (8)	C16M—C11M— B1M—C31M	-152.8 (5)
C21A—P1A— C11A—C12A	-76.4 (4)	C16M—C11M— B1M—C41M	87.2 (6)
C21A—P1A— C11A—C16A	101.9 (5)	C21M—C22M— C23M—C24M	1.3 (10)
C21A—P1A— C31A—C32A	1.1 (5)	C22M—C21M— C26M—C25M	-0.8 (9)
C21A—P1A— C31A—C36A	178.7 (4)	C22M—C21M— B1M—C11M	-37.1 (7)
C21A—C22A— C23A—C24A	0.5 (10)	C22M—C21M— B1M—C31M	85.6 (6)
C21B—P1B—C11B— C12B	27.8 (5)	C22M—C21M— B1M—C41M	-158.4 (5)
C21B—P1B—C11B— C16B	-153.9 (5)	C22M—C23M— C24M—C25M	-0.4 (10)
C21B—P1B—C31B— C32B	79.1 (4)	C23M—C24M— C25M—C26M	-1.1 (10)
C21B—P1B—C31B— C36B	-104.6 (4)	C24M—C25M— C26M—C21M	1.8 (10)
C21B—C22B— C23B—C24B	-0.2 (8)	C26M—C21M— C22M—C23M	-0.7 (9)
C22A—C21A— C26A—C25A	1.0 (8)	C26M—C21M— B1M—C11M	153.2 (5)
C22A—C23A— C24A—C25A	0.8 (10)	C26M—C21M— B1M—C31M	-84.2 (6)
C22B—C21B— C26B—C25B	-1.1 (7)	C26M—C21M— B1M—C41M	31.8 (7)
C22B—C23B— C24B—C25B	0.4 (8)	C31M—C32M— C33M—C34M	0.2 (8)
C23A—C24A— C25A—C26A	-1.2 (9)	C32M—C31M— C36M—C35M	-0.2 (8)
C23B—C24B— C25B—C26B	-1.0 (8)	C32M—C31M— B1M—C11M	106.8 (6)
C24A—C25A— C26A—C21A	0.3 (8)	C32M—C31M— B1M—C21M	-16.1 (7)
C24B—C25B— C26B—C21B	1.4 (8)	C32M—C31M— B1M—C41M	-132.1 (5)
C26A—C21A— C22A—C23A	-1.4 (9)	C32M—C33M— C34M—C35M	0.7 (8)
C26B—C21B— C22B—C23B	0.5 (7)	C33M—C34M— C35M—C36M	-1.3 (9)
C31A—P1A— C11A—C12A	176.2 (4)	C34M—C35M— C36M—C31M	1.1 (9)
C31A—P1A—	-5.5 (5)	C36M—C31M—	-0.5 (8)

C11A—C16A		C32M—C33M	
C31A—P1A— C21A—C22A	103.4 (5)	C36M—C31M— B1M—C11M	-75.1 (7)
C31A—P1A— C21A—C26A	-75.4 (4)	C36M—C31M— B1M—C21M	162.0 (5)
C31A—C32A— C33A—C34A	2.0 (8)	C36M—C31M— B1M—C41M	46.0 (7)
C31B—P1B—C11B— C12B	-78.6 (5)	C41M—C42M— C43M—C44M	0.6 (10)
C31B—P1B—C11B— C16B	99.7 (5)	C42M—C41M— C46M—C45M	0.2 (8)
C31B—P1B—C21B— C22B	-21.0 (5)	C42M—C41M— B1M—C11M	149.8 (5)
C31B—P1B—C21B— C26B	158.9 (4)	C42M—C41M— B1M—C21M	-87.4 (6)
C31B—C32B— C33B—C34B	0.1 (8)	C42M—C41M— B1M—C31M	27.5 (8)
C32A—C31A— C36A—C35A	0.8 (8)	C42M—C43M— C44M—C45M	-0.9 (10)
C32A—C33A— C34A—C35A	0.1 (9)	C43M—C44M— C45M—C46M	0.8 (10)
C32B—C31B— C36B—C35B	0.8 (7)	C44M—C45M— C46M—C41M	-0.5 (9)
C32B—C33B— C34B—C35B	0.0 (8)	C46M—C41M— C42M—C43M	-0.2 (9)
C33A—C34A— C35A—C36A	-1.7 (9)	C46M—C41M— B1M—C11M	-31.2 (7)
C33B—C34B— C35B—C36B	0.4 (8)	C46M—C41M— B1M—C21M	91.5 (6)
C34A—C35A— C36A—C31A	1.3 (8)	C46M—C41M— B1M—C31M	-153.5 (5)
C34B—C35B— C36B—C31B	-0.8 (8)	B1M—C11M— C12M—C13M	176.9 (5)
C36A—C31A— C32A—C33A	-2.4 (7)	B1M—C11M— C16M—C15M	-177.3 (5)
C36B—C31B— C32B—C33B	-0.5 (7)	B1M—C21M— C22M—C23M	-171.4 (6)
Ru1B—P1C—C11C— C12C	-50.9 (4)	B1M—C21M— C26M—C25M	169.7 (6)
Ru1B—P1C—C11C— C16C	128.3 (4)	B1M—C31M— C32M—C33M	177.8 (5)
Ru1B—P1C—C21C— C22C	118.5 (4)	B1M—C31M— C36M—C35M	-178.5 (5)
Ru1B—P1C—C21C— C26C	-63.7 (4)	B1M—C41M— C42M—C43M	178.8 (6)
Ru1B—P1C—C31C— C32C	145.8 (4)	B1M—C41M— C46M—C45M	-178.9 (5)
Ru1B—P1C—C31C—	-39.2 (5)	C11N—C12N—	0.4 (8)

C36C		C13N—C14N	
Ru1B—P1D— C11D—C12D	-126.2 (4)	C12N—C11N— C16N—C15N	-2.6 (8)
Ru1B—P1D— C11D—C16D	49.8 (4)	C12N—C11N— B1N—C21N	154.7 (5)
Ru1B—P1D— C21D—C22D	-138.4 (4)	C12N—C11N— B1N—C31N	-83.1 (6)
Ru1B—P1D— C21D—C26D	39.2 (4)	C12N—C11N— B1N—C41N	37.2 (7)
Ru1B—P1D— C31D—C32D	51.8 (4)	C12N—C13N— C14N—C15N	-1.4 (9)
Ru1B—P1D— C31D—C36D	-132.9 (4)	C13N—C14N— C15N—C16N	0.3 (9)
Ru1B—N2G—C3G— C4G	173.2 (3)	C14N—C15N— C16N—C11N	1.8 (9)
P1C—C11C—C12C— C13C	179.0 (4)	C16N—C11N— C12N—C13N	1.6 (8)
P1C—C11C—C16C— C15C	-178.1 (4)	C16N—C11N— B1N—C21N	-32.1 (7)
P1C—C21C—C22C— C23C	179.1 (4)	C16N—C11N— B1N—C31N	90.1 (6)
P1C—C21C—C26C— C25C	-178.4 (4)	C16N—C11N— B1N—C41N	-149.6 (5)
P1C—C31C—C32C— C33C	179.9 (4)	C21N—C22N— C23N—C24N	0.7 (8)
P1C—C31C—C36C— C35C	-177.2 (4)	C22N—C21N— C26N—C25N	-2.4 (8)
P1D—C11D— C12D—C13D	174.8 (4)	C22N—C21N— B1N—C11N	-95.9 (5)
P1D—C11D— C16D—C15D	-175.3 (4)	C22N—C21N— B1N—C31N	144.7 (5)
P1D—C21D— C22D—C23D	177.7 (4)	C22N—C21N— B1N—C41N	24.7 (6)
P1D—C21D— C26D—C25D	-178.1 (4)	C22N—C23N— C24N—C25N	-1.2 (8)
P1D—C31D— C32D—C33D	175.2 (4)	C23N—C24N— C25N—C26N	0.0 (9)
P1D—C31D— C36D—C35D	-175.6 (4)	C24N—C25N— C26N—C21N	2.0 (9)
N1G—N2G—C3G— C4G	1.9 (5)	C26N—C21N— C22N—C23N	1.0 (7)
N2G—N1G—C5G— C4G	1.2 (6)	C26N—C21N— B1N—C11N	82.7 (6)
N2G—N1G—C6G— N3G	-60.0 (5)	C26N—C21N— B1N—C31N	-36.7 (6)
N2G—C3G—C4G— C5G	-1.2 (6)	C26N—C21N— B1N—C41N	-156.7 (5)
N4G—C8G—C9G—	0.6 (5)	C31N—C32N—	0.1 (8)

N3G		C33N—C34N	
N5G—N6G—C11G— C12G	-1.8 (9)	C32N—C31N— C36N—C35N	-0.4 (7)
N5G'—N6G'—C11'— C12'	-7 (2)	C32N—C31N— B1N—C11N	-151.6 (5)
N6G—N5G—C10G— N4G	-95.4 (7)	C32N—C31N— B1N—C21N	-30.4 (6)
N6G—N5G—C13G— C12G	2.1 (13)	C32N—C31N— B1N—C41N	87.3 (6)
N6G—C11G— C12G—C13G	3.1 (11)	C32N—C33N— C34N—C35N	1.1 (9)
N6G'—N5G'— C10G—N4G	-80.7 (16)	C33N—C34N— C35N—C36N	-1.9 (9)
N6G'—N5G'—C13'— C12'	0 (2)	C34N—C35N— C36N—C31N	1.6 (8)
N6G'—C11'—C12'— C13'	7 (2)	C36N—C31N— C32N—C33N	-0.5 (7)
C3G—C4G—C5G— N1G	0.0 (6)	C36N—C31N— B1N—C11N	29.3 (6)
C5G—N1G—N2G— Ru1B	-174.0 (3)	C36N—C31N— B1N—C21N	150.4 (4)
C5G—N1G—N2G— C3G	-1.9 (5)	C36N—C31N— B1N—C41N	-91.8 (5)
C5G—N1G—C6G— N3G	133.3 (5)	C41N—C42N— C43N—C44N	0.1 (8)
C6G—N1G—N2G— Ru1B	17.5 (5)	C42N—C41N— C46N—C45N	-1.0 (7)
C6G—N1G—N2G— C3G	-170.4 (4)	C42N—C41N— B1N—C11N	-158.1 (4)
C6G—N1G—C5G— C4G	168.8 (5)	C42N—C41N— B1N—C21N	81.9 (5)
C6G—N3G—C7G— Ru1B	-4.6 (5)	C42N—C41N— B1N—C31N	-39.4 (6)
C6G—N3G—C7G— N4G	174.6 (4)	C42N—C43N— C44N—C45N	-1.2 (8)
C6G—N3G—C9G— C8G	-174.7 (4)	C43N—C44N— C45N—C46N	1.2 (8)
C7G—N3G—C6G— N1G	53.7 (6)	C44N—C45N— C46N—C41N	0.0 (8)
C7G—N3G—C9G— C8G	-1.2 (5)	C46N—C41N— C42N—C43N	1.0 (7)
C7G—N4G—C8G— C9G	0.1 (5)	C46N—C41N— B1N—C11N	34.1 (6)
C7G—N4G—C10G— N5G	111.6 (5)	C46N—C41N— B1N—C21N	-85.9 (6)
C7G—N4G—C10G— N5G'	159.0 (7)	C46N—C41N— B1N—C31N	152.8 (4)
C8G—N4G—C7G—	178.2 (3)	B1N—C11N—	175.2 (5)

Ru1B		C12N—C13N	
C8G—N4G—C7G— N3G	-0.8 (5)	B1N—C11N— C16N—C15N	-176.4 (5)
C8G—N4G—C10G— N5G	-68.7 (6)	B1N—C21N— C22N—C23N	179.7 (5)
C8G—N4G—C10G— N5G'	-21.3 (8)	B1N—C21N— C26N—C25N	178.9 (5)
C9G—N3G—C6G— N1G	-133.5 (4)	B1N—C31N— C32N—C33N	-179.7 (5)
C9G—N3G—C7G— Ru1B	-178.0 (3)	B1N—C31N— C36N—C35N	178.8 (5)
C9G—N3G—C7G— N4G	1.2 (4)	B1N—C41N— C42N—C43N	-167.8 (5)
C10G—N4G—C7G— Ru1B	-2.1 (7)	B1N—C41N— C46N—C45N	167.1 (4)
C10G—N4G—C7G— N3G	178.9 (4)		

## 7.1.7. Crystal data for complex 7

## Selected geometric parameters (Å)

Ru01—N1C	2.076 (4)	C2—H2D	0.9900
Ru01—N1C <sup>i</sup>	2.076 (4)	C11—C16	1.390 (6)
Ru01—N2A <sup>i</sup>	2.088 (3)	C11—C12	1.407 (6)
Ru01—N2A	2.088 (3)	C11—B1	1.631 (7)
Ru01—C1B	2.043 (4)	C1C—H1C	0.9500
Ru01—C1B <sup>i</sup>	2.043 (4)	C3B—H3B	0.9500
N1C—N2C	1.376 (5)	C23—H23	0.9500
N1C—C3C	1.334 (5)	C23—C22	1.389 (6)
N2A—N1A	1.371 (5)	C23—C24	1.369 (7)
N2A—C1A	1.328 (5)	C43—H43	0.9500
N1B—C1B	1.346 (5)	C43—C44	1.375 (7)
N1B—C2B	1.395 (6)	C16—H16	0.9500
N1B—C1	1.444 (6)	C3A—H3A	0.9500
N1A—C3A	1.346 (6)	C3A—C2A	1.366 (6)
N1A—C1	1.470 (6)	C1—H1B	0.9900
N2C—C2	1.464 (5)	C1—H1D	0.9900
N2C—C1C	1.341 (6)	C22—H22	0.9500
N2B—C1B	1.369 (5)	C44—H44	0.9500
N2B—C2	1.437 (6)	C44—C45	1.378 (7)

N2B—C3B	1.385 (6)	C12—H12	0.9500
C21—C22	1.381 (6)	C12—C13	1.377 (6)
C21—C26	1.400 (7)	C36—H36	0.9500
C21—B1	1.641 (7)	C36—C35	1.395 (7)
C15—H15	0.9500	C46—H46	0.9500
C15—C16	1.395 (6)	C46—C45	1.379 (7)
C15—C14	1.379 (6)	C45—H45	0.9500
C2C—H2C	0.9500	C35—H35	0.9500
C2C—C3C	1.373 (6)	C35—C34	1.375 (8)
C2C—C1C	1.360 (6)	C14—H14	0.9500
C42—H42	0.9500	C14—C13	1.366 (7)
C42—C41	1.388 (6)	C32—H32	0.9500
C42—C43	1.378 (7)	C32—C33	1.390 (7)
C3C—H3C	0.9500	C26—H26	0.9500
C1A—H1A	0.9500	C26—C25	1.389 (7)
C1A—C2A	1.380 (6)	C13—H13	0.9500
C2B—H2B	0.9500	C2A—H2AA	0.9500
C2B—C3B	1.324 (7)	C33—H33	0.9500
C41—C46	1.399 (6)	C33—C34	1.374 (8)
C41—B1	1.658 (7)	C34—H34	0.9500
C31—C36	1.393 (7)	C24—H24	0.9500
C31—C32	1.402 (7)	C24—C25	1.377 (8)
C31—B1	1.651 (7)	C25—H25	0.9500
C2—H2A	0.9900		

Symmetry code(s): (i)  $-x, -y, -z+2$ .

#### Selected geometric parameters (°)

N1C—Ru01—N1C <sup>i</sup>	180.0	N2B—C3B—H3B	126.4
N1C <sup>i</sup> —Ru01—N2A <sup>i</sup>	90.51 (14)	C2B—C3B—N2B	107.1 (4)
N1C—Ru01—N2A <sup>i</sup>	89.49 (14)	C2B—C3B—H3B	126.4
N1C <sup>i</sup> —Ru01—N2A	89.49 (14)	C22—C23—H23	120.7
N1C—Ru01—N2A	90.51 (14)	C24—C23—H23	120.7
N2A—Ru01—N2A <sup>i</sup>	180.0	C24—C23—C22	118.7 (5)
C1B—Ru01—N1C <sup>i</sup>	95.88 (15)	C42—C43—H43	119.6
C1B <sup>i</sup> —Ru01—N1C <sup>i</sup>	84.12 (15)	C44—C43—C42	120.8 (5)
C1B <sup>i</sup> —Ru01—N1C	95.88 (15)	C44—C43—H43	119.6
C1B—Ru01—N1C	84.12 (15)	C15—C16—H16	118.7
C1B—Ru01—N2A <sup>i</sup>	97.90 (15)	C11—C16—C15	122.6 (4)
C1B <sup>i</sup> —Ru01—N2A	97.90 (15)	C11—C16—H16	118.7

C1B <sup>i</sup> —Ru01—N2A <sup>i</sup>	82.10 (15)	N1A—C3A—H3A	126.5
C1B—Ru01—N2A	82.10 (15)	N1A—C3A—C2A	107.0 (4)
C1B <sup>i</sup> —Ru01—C1B	180.0 (2)	C2A—C3A—H3A	126.5
N2C—N1C—Ru01	123.5 (3)	N1B—C1—N1A	108.6 (4)
C3C—N1C—Ru01	132.8 (3)	N1B—C1—H1B	110.0
C3C—N1C—N2C	103.6 (4)	N1B—C1—H1D	110.0
N1A—N2A—Ru01	124.0 (3)	N1A—C1—H1B	110.0
C1A—N2A—Ru01	132.0 (3)	N1A—C1—H1D	110.0
C1A—N2A—N1A	103.5 (4)	H1B—C1—H1D	108.3
C1B—N1B—C2B	112.6 (4)	C21—C22—C23	124.1 (4)
C1B—N1B—C1	119.1 (4)	C21—C22—H22	118.0
C2B—N1B—C1	125.8 (4)	C23—C22—H22	118.0
N2A—N1A—C1	120.7 (4)	C43—C44—H44	120.7
C3A—N1A—N2A	111.8 (4)	C43—C44—C45	118.5 (5)
C3A—N1A—C1	127.5 (4)	C45—C44—H44	120.7
N1C—N2C—C2	121.0 (4)	C11—C12—H12	118.3
C1C—N2C—N1C	110.9 (4)	C13—C12—C11	123.4 (5)
C1C—N2C—C2	128.0 (4)	C13—C12—H12	118.3
C1B—N2B—C2	119.6 (4)	C31—C36—H36	118.4
C1B—N2B—C3B	111.7 (4)	C31—C36—C35	123.3 (5)
C3B—N2B—C2	127.3 (4)	C35—C36—H36	118.4
N1B—C1B—Ru01	128.0 (3)	C41—C46—H46	118.2
N1B—C1B—N2B	102.5 (4)	C45—C46—C41	123.6 (5)
N2B—C1B—Ru01	126.2 (3)	C45—C46—H46	118.2
C22—C21—C26	115.2 (4)	C44—C45—C46	119.7 (5)
C22—C21—B1	120.9 (4)	C44—C45—H45	120.1
C26—C21—B1	123.8 (4)	C46—C45—H45	120.1
C16—C15—H15	119.9	C36—C35—H35	120.4
C14—C15—H15	119.9	C34—C35—C36	119.3 (6)
C14—C15—C16	120.3 (5)	C34—C35—H35	120.4
C3C—C2C—H2C	127.5	C15—C14—H14	120.5
C1C—C2C—H2C	127.5	C13—C14—C15	119.0 (5)
C1C—C2C—C3C	105.0 (4)	C13—C14—H14	120.5
C41—C42—H42	118.5	C31—C32—H32	118.4
C43—C42—H42	118.5	C33—C32—C31	123.1 (5)
C43—C42—C41	122.9 (5)	C33—C32—H32	118.4
N1C—C3C—C2C	112.5 (4)	C21—C26—H26	119.1
N1C—C3C—H3C	123.8	C25—C26—C21	121.9 (5)
C2C—C3C—H3C	123.8	C25—C26—H26	119.1
N2A—C1A—H1A	123.7	C12—C13—H13	119.9
N2A—C1A—C2A	112.6 (4)	C14—C13—C12	120.2 (5)

C2A—C1A—H1A	123.7	C14—C13—H13	119.9
N1B—C2B—H2B	127.0	C1A—C2A—H2AA	127.4
C3B—C2B—N1B	106.0 (4)	C3A—C2A—C1A	105.2 (4)
C3B—C2B—H2B	127.0	C3A—C2A—H2AA	127.4
C42—C41—C46	114.5 (5)	C32—C33—H33	120.3
C42—C41—B1	124.5 (4)	C34—C33—C32	119.5 (6)
C46—C41—B1	120.9 (4)	C34—C33—H33	120.3
C36—C31—C32	114.7 (5)	C35—C34—H34	120.0
C36—C31—B1	120.7 (4)	C33—C34—C35	120.1 (6)
C32—C31—B1	124.6 (5)	C33—C34—H34	120.0
N2C—C2—H2A	109.8	C21—B1—C41	109.5 (4)
N2C—C2—H2D	109.8	C21—B1—C31	105.4 (4)
N2B—C2—N2C	109.5 (4)	C31—B1—C41	111.5 (4)
N2B—C2—H2A	109.8	C11—B1—C21	110.3 (4)
N2B—C2—H2D	109.8	C11—B1—C41	107.0 (4)
H2A—C2—H2D	108.2	C11—B1—C31	113.1 (4)
C16—C11—C12	114.5 (4)	C23—C24—H24	120.0
C16—C11—B1	123.5 (4)	C23—C24—C25	120.0 (5)
C12—C11—B1	121.8 (4)	C25—C24—H24	120.0
N2C—C1C—C2C	107.9 (4)	C26—C25—H25	119.9
N2C—C1C—H1C	126.0	C24—C25—C26	120.2 (6)
C2C—C1C—H1C	126.0	C24—C25—H25	119.9

Symmetry code(s): (i)  $-x, -y, -z+2$ .

#### Selected geometric parameters (<sup>g</sup>)

Ru01—N1C—N2C— C2	-6.2 (5)	C43—C42—C41— C46	1.1 (7)
Ru01—N1C—N2C— C1C	176.4 (3)	C43—C42—C41—B1	-176.0 (4)
Ru01—N1C—C3C— C2C	-175.6 (3)	C43—C44—C45— C46	0.6 (7)
Ru01—N2A—N1A— C3A	-172.0 (3)	C16—C15—C14— C13	-0.6 (7)
Ru01—N2A—N1A— C1	6.6 (5)	C16—C11—C12— C13	-1.7 (7)
Ru01—N2A—C1A— C2A	171.4 (3)	C16—C11—B1—C21	6.1 (6)
N1C—N2C—C2— N2B	56.8 (5)	C16—C11—B1—C41	-113.0 (5)



N1C—N2C—C1C— C2C	-0.3 (5)	C16—C11—B1—C31	123.9 (5)
N2A—N1A—C3A— C2A	-0.5 (5)	C3A—N1A—C1— N1B	120.9 (5)
N2A—N1A—C1— N1B	-57.5 (5)	C1—N1B—C1B— Ru01	-3.6 (6)
N2A—C1A—C2A— C3A	-0.2 (6)	C1—N1B—C1B— N2B	-163.8 (4)
N1B—C2B—C3B— N2B	0.9 (5)	C1—N1B—C2B— C3B	161.7 (4)
N1A—N2A—C1A— C2A	-0.1 (5)	C1—N1A—C3A— C2A	-179.0 (4)
N1A—C3A—C2A— C1A	0.4 (5)	C22—C21—C26— C25	-0.1 (8)
N2C—N1C—C3C— C2C	0.1 (5)	C22—C21—B1—C41	-165.3 (4)
C1B—N1B—C2B— C3B	-0.1 (6)	C22—C21—B1—C31	-45.2 (6)
C1B—N1B—C1— N1A	55.9 (6)	C22—C21—B1—C11	77.2 (5)
C1B—N2B—C2— N2C	-57.6 (5)	C22—C23—C24— C25	0.5 (9)
C1B—N2B—C3B— C2B	-1.4 (6)	C12—C11—C16— C15	0.2 (7)
C21—C26—C25— C24	0.3 (10)	C12—C11—B1—C21	-177.9 (4)
C15—C14—C13— C12	-0.9 (8)	C12—C11—B1—C41	63.0 (6)
C42—C41—C46— C45	-0.8 (7)	C12—C11—B1—C31	-60.1 (6)
C42—C41—B1—C21	93.8 (5)	C36—C31—C32— C33	-1.5 (7)
C42—C41—B1—C31	-22.5 (6)	C36—C31—B1—C21	-51.0 (6)
C42—C41—B1—C11	-146.6 (4)	C36—C31—B1—C41	67.7 (5)
C42—C43—C44— C45	-0.4 (7)	C36—C31—B1—C11	-171.6 (4)
C3C—N1C—N2C— C2	177.5 (4)	C36—C35—C34— C33	-0.1 (8)
C3C—N1C—N2C— C1C	0.1 (5)	C46—C41—B1—C21	-83.1 (5)
C3C—C2C—C1C— N2C	0.3 (5)	C46—C41—B1—C31	160.6 (4)
C1A—N2A—N1A— C3A	0.4 (5)	C46—C41—B1—C11	36.5 (6)
C1A—N2A—N1A— C1	179.0 (4)	C14—C15—C16— C11	1.0 (7)
C2B—N1B—C1B— Ru01	159.5 (3)	C32—C31—C36— C35	2.7 (7)

C2B—N1B—C1B— N2B	-0.7 (5)	C32—C31—B1—C21	126.3 (5)
C2B—N1B—C1— N1A	-104.9 (5)	C32—C31—B1—C41	-115.0 (5)
C41—C42—C43— C44	-0.5 (7)	C32—C31—B1—C11	5.6 (6)
C41—C46—C45— C44	0.0 (8)	C32—C33—C34— C35	1.2 (8)
C31—C36—C35— C34	-2.0 (8)	C26—C21—C22— C23	0.1 (7)
C31—C32—C33— C34	-0.4 (8)	C26—C21—B1—C41	15.7 (7)
C2—N2C—C1C— C2C	-177.5 (4)	C26—C21—B1—C31	135.7 (5)
C2—N2B—C1B— Ru01	7.9 (6)	C26—C21—B1—C11	-101.9 (6)
C2—N2B—C1B— N1B	168.6 (4)	B1—C21—C22—C23	-179.0 (4)
C2—N2B—C3B— C2B	-167.6 (5)	B1—C21—C26—C25	179.0 (6)
C11—C12—C13— C14	2.1 (8)	B1—C41—C46—C45	176.3 (4)
C1C—N2C—C2— N2B	-126.2 (5)	B1—C31—C36—C35	-179.8 (4)
C1C—C2C—C3C— N1C	-0.3 (6)	B1—C31—C32—C33	-178.9 (4)
C3B—N2B—C1B— Ru01	-159.4 (3)	B1—C11—C16—C15	176.5 (4)
C3B—N2B—C1B— N1B	1.2 (5)	B1—C11—C12—C13	-178.1 (5)
C3B—N2B—C2— N2C	107.6 (5)	C24—C23—C22— C21	-0.3 (8)
C23—C24—C25— C26	-0.5 (10)		

## 7.1.8. Crystal data for complex 6

## Selected geometric parameters (Å)

P3—C16	1.824 (2)	C18—C40	1.392 (3)
P3—C18	1.825 (2)	C21—C52	1.387 (4)
P3—C29	1.8158 (18)	C23—C4aa	1.390 (3)
P3—Ru2	2.3819 (6)	C24—C25	1.379 (3)
P5—C8	1.816 (2)	C24—C32	1.386 (3)
P5—C17	1.824 (2)	C25—C38	1.391 (3)

P5—Ru1	2.3690 (6)	C29—C32	1.397 (3)
P5—C6	1.8170 (19)	C30—C42	1.380 (3)
C7—C29	1.396 (3)	C40—C50	1.379 (3)
C7—C38	1.391 (3)	C42—C49	1.383 (4)
C8—C43	1.393 (3)	C43—C5	1.373 (3)
C8—C52	1.401 (3)	C49—C50	1.394 (4)
C9—C11	1.396 (3)	Ru2—Cl2 <sup>i</sup>	2.7642 (7)
C9—C19	1.387 (3)	Ru2—Cl2	2.5367 (7)
C10—C22	1.386 (4)	Ru2—Ru1	3.3796 (5)
C10—C4aa	1.395 (4)	Ru2—Cl3	2.6765 (7)
C11—C14	1.387 (3)	Cl2—Ru1	2.7182 (7)
C12—C21	1.391 (4)	Ru1—Cl3	2.6550 (7)
C12—C5	1.382 (4)	Ru1—Cl3 <sup>i</sup>	2.5620 (6)
C14—C20	1.384 (3)	C2aa—C3aa	1.396 (3)
C15—C17	1.399 (3)	C2aa—C13	1.377 (4)
C15—C22	1.391 (3)	C6—C3aa	1.402 (3)
C16—C19	1.387 (3)	C6—C0aa	1.385 (3)
C16—C20	1.396 (3)	C1aa—C0aa	1.394 (3)
C17—C23	1.398 (3)	C1aa—C13	1.390 (4)
C18—C30	1.398 (3)		

Symmetry code(s): (i)  $-x+2, y, -z+1/2$ .

#### Selected geometric parameters (°)

C18—P3—C16	105.20 (9)	C42—C30—C18	120.8 (2)
C29—P3—C16	102.94 (9)	C29—C32—C24	120.2 (2)
C29—P3—C18	105.60 (9)	C25—C38—C7	119.8 (2)
Ru2—P3—C16	112.15 (7)	C50—C40—C18	121.1 (2)
Ru2—P3—C18	109.79 (7)	C49—C42—C30	120.2 (2)
Ru2—P3—C29	119.97 (6)	C5—C43—C8	120.4 (2)
C17—P5—C8	104.23 (9)	C50—C49—C42	119.7 (2)
Ru1—P5—C8	112.64 (6)	C49—C50—C40	119.9 (2)
Ru1—P5—C17	114.89 (7)	C21—C52—C8	120.0 (2)
C6—P5—C8	103.92 (9)	Cl2 <sup>i</sup> —Ru2—P3	108.911 (15)
C6—P5—C17	103.46 (9)	Cl2—Ru2—P3	137.247 (16)
C6—P5—Ru1	116.31 (7)	Ru1—Ru2—P3	150.735 (13)
C38—C7—C29	120.33 (19)	Ru1—Ru2—Cl2	52.374 (11)
C43—C8—P5	124.14 (16)	Ru1—Ru2—Cl2 <sup>i</sup>	96.988 (11)
C52—C8—P5	116.74 (16)	Cl3—Ru2—P3	116.611 (17)
C52—C8—C43	119.1 (2)	Cl3—Ru2—Cl2	101.589 (16)
C19—C9—C11	120.3 (2)	Cl3—Ru2—Cl2 <sup>i</sup>	86.218 (13)

C4aa—C10—C22	120.1 (2)	Cl3—Ru2—Ru1	50.382 (12)
C14—C11—C9	119.3 (2)	Ru1—Cl2—Ru2	79.969 (14)
C5—C12—C21	119.7 (2)	Ru1—Cl2—Ru2 <sup>i</sup>	88.262 (13)
C20—C14—C11	120.28 (19)	Ru2—Ru1—P5	122.809 (14)
C22—C15—C17	120.1 (2)	Cl2—Ru1—P5	112.062 (15)
C19—C16—P3	123.13 (14)	Cl2—Ru1—Ru2	47.657 (11)
C20—C16—P3	117.70 (16)	Cl3 <sup>i</sup> —Ru1—P5	139.652 (18)
C20—C16—C19	119.16 (19)	Cl3—Ru1—P5	119.728 (17)
C15—C17—P5	118.19 (16)	Cl3 <sup>i</sup> —Ru1—Ru2	97.101 (11)
C23—C17—P5	122.80 (15)	Cl3—Ru1—Ru2	50.944 (10)
C23—C17—C15	119.0 (2)	Cl3 <sup>i</sup> —Ru1—Cl2	89.490 (14)
C30—C18—P3	117.67 (16)	Cl3—Ru1—Cl2	97.518 (15)
C40—C18—P3	123.93 (16)	Ru1 <sup>i</sup> —Cl3—Ru2	93.537 (14)
C40—C18—C30	118.32 (19)	Ru1—Cl3—Ru2	78.674 (14)
C16—C19—C9	120.4 (2)	C13—C2aa—C3aa	120.3 (2)
C16—C20—C14	120.5 (2)	C3aa—C6—P5	121.64 (16)
C52—C21—C12	120.1 (2)	C0aa—C6—P5	118.62 (15)
C15—C22—C10	120.4 (2)	C0aa—C6—C3aa	119.62 (18)
C4aa—C23—C17	120.9 (2)	C13—C1aa—C0aa	119.5 (2)
C32—C24—C25	120.4 (2)	C6—C3aa—C2aa	119.5 (2)
C38—C25—C24	120.11 (19)	C1aa—C0aa—C6	120.5 (2)
C7—C29—P3	123.94 (14)	C43—C5—C12	120.7 (2)
C32—C29—P3	116.75 (14)	C1aa—C13—C2aa	120.5 (2)
C32—C29—C7	119.13 (17)	C23—C4aa—C10	119.4 (2)

Symmetry code(s): (i)  $-x+2, y, -z+1/2$ .

### 7.1.9. Crystal data for complex 8

#### Selected geometric parameters (Å)

Ni1—Cl1	2.2001 (12)	C12B—H12B	0.9500
Ni1—N1A	1.887 (3)	C12B—C13B	1.398 (6)
Ni1—N1C	1.907 (3)	C13B—H13B	0.9500
Ni1—C1B	1.848 (4)	C13B—C14B	1.376 (7)
N1A—N2A	1.368 (4)	C14B—H14B	0.9500
N1A—C3A	1.338 (5)	C14B—C15B	1.379 (7)
N1B—C0AA	1.454 (5)	C15B—H15B	0.9500
N1B—C1B	1.337 (5)	C15B—C16B	1.384 (6)

N1B—C3B	1.377 (5)	C16B—H16B	0.9500
N1C—N2C	1.362 (5)	C21B—C22B	1.389 (6)
N1C—C3C	1.342 (5)	C21B—C26B	1.407 (6)
N2A—C0AA	1.450 (5)	C21B—B1B	1.656 (6)
N2A—C1A	1.329 (5)	C22B—H22B	0.9500
N2B—C1B	1.348 (5)	C22B—C23B	1.394 (5)
N2B—C2	1.457 (5)	C23B—H23B	0.9500
N2B—C2B	1.391 (5)	C23B—C24B	1.384 (6)
N2C—C1C	1.348 (5)	C24B—H24B	0.9500
N2C—C2	1.452 (5)	C24B—C25B	1.383 (6)
C0AA—H0AA	0.9900	C25B—H25B	0.9500
C0AA—H0AB	0.9900	C25B—C26B	1.401 (5)
C1A—H1A	0.9500	C26B—H26B	0.9500
C1A—C2A	1.367 (6)	C31B—C32B	1.409 (5)
C1C—H1C	0.9500	C31B—C36B	1.406 (5)
C1C—C2C	1.361 (6)	C31B—B1B	1.629 (6)
C2—H2A	0.9900	C32B—H32B	0.9500
C2—H2B	0.9900	C32B—C33B	1.383 (6)
C2A—H2AA	0.9500	C33B—H33B	0.9500
C2A—C3A	1.391 (6)	C33B—C34B	1.383 (6)
C2B—H2BA	0.9500	C34B—H34B	0.9500
C2B—C3B	1.347 (6)	C34B—C35B	1.391 (6)
C2C—H2C	0.9500	C35B—H35B	0.9500
C2C—C3C	1.389 (6)	C35B—C36B	1.395 (6)
C3A—H3A	0.9500	C36B—H36B	0.9500
C3B—H3B	0.9500	C41B—C42B	1.411 (5)
C3C—H3C	0.9500	C41B—C46B	1.410 (5)
O1AC—C2AC	1.190 (7)	C41B—B1B	1.639 (6)
C1AC—H1AA	0.9800	C42B—H42B	0.9500
C1AC—H1AB	0.9800	C42B—C43B	1.391 (6)
C1AC—H1AC	0.9800	C43B—H43B	0.9500
C1AC—C2AC	1.439 (8)	C43B—C44B	1.376 (6)
C2AC—C3AC	1.493 (11)	C44B—H44B	0.9500
C2AC—C1	1.644 (17)	C44B—C45B	1.380 (6)
C2AC—O2	1.26 (2)	C45B—H45B	0.9500
C3AC—H3AA	0.9800	C45B—C46B	1.386 (6)
C3AC—H3AB	0.9800	C46B—H46B	0.9500
C3AC—H3AC	0.9800	C1—H1B	0.9800
C11B—C12B	1.398 (6)	C1—H1D	0.9800
C11B—C16B	1.397 (6)	C1—H1E	0.9800
C11B—B1B	1.651 (6)		

Selected geometric parameters (<sup>o</sup>)

N1A—Ni1—Cl1	90.93 (11)	C16B—C11B—B1B	120.0 (4)
N1A—Ni1—N1C	177.07 (15)	C11B—C12B—H12B	119.0
N1C—Ni1—Cl1	91.48 (11)	C13B—C12B—C11B	122.1 (5)
C1B—Ni1—Cl1	176.03 (13)	C13B—C12B—H12B	119.0
C1B—Ni1—N1A	88.11 (16)	C12B—C13B—H13B	119.8
C1B—Ni1—N1C	89.59 (16)	C14B—C13B—C12B	120.4 (5)
N2A—N1A—Ni1	125.2 (3)	C14B—C13B—H13B	119.8
C3A—N1A—Ni1	129.3 (3)	C13B—C14B—H14B	120.5
C3A—N1A—N2A	105.0 (3)	C13B—C14B—C15B	118.9 (4)
C1B—N1B—C0AA	120.9 (3)	C15B—C14B—H14B	120.5
C1B—N1B—C3B	111.2 (3)	C14B—C15B—H15B	119.9
C3B—N1B—C0AA	127.8 (4)	C14B—C15B—C16B	120.2 (5)
N2C—N1C—Ni1	124.3 (3)	C16B—C15B—H15B	119.9
C3C—N1C—Ni1	129.4 (3)	C11B—C16B—H16B	118.5
C3C—N1C—N2C	105.7 (3)	C15B—C16B—C11B	123.0 (4)
N1A—N2A—C0AA	120.3 (3)	C15B—C16B—H16B	118.5
C1A—N2A—N1A	110.9 (4)	C22B—C21B—C26B	114.9 (4)
C1A—N2A—C0AA	128.6 (4)	C22B—C21B—B1B	124.8 (4)
C1B—N2B—C2	120.4 (3)	C26B—C21B—B1B	120.1 (4)
C1B—N2B—C2B	111.1 (3)	C21B—C22B—H22B	118.1
C2B—N2B—C2	128.4 (4)	C21B—C22B—C23B	123.8 (4)
N1C—N2C—C2	121.2 (3)	C23B—C22B—H22B	118.1
C1C—N2C—N1C	110.6 (4)	C22B—C23B—H23B	120.2
C1C—N2C—C2	127.7 (4)	C24B—C23B—C22B	119.5 (4)
N1B—C0AA—H0AA	110.0	C24B—C23B—H23B	120.2
N1B—C0AA—H0AB	110.0	C23B—C24B—H24B	120.5
N2A—C0AA—N1B	108.5 (3)	C25B—C24B—C23B	119.1 (4)
N2A—C0AA—H0AA	110.0	C25B—C24B—H24B	120.5
N2A—C0AA—H0AB	110.0	C24B—C25B—H25B	119.9
H0AA—C0AA—H0AB	108.4	C24B—C25B—C26B	120.2 (4)
N2A—C1A—H1A	125.9	C26B—C25B—H25B	119.9
N2A—C1A—C2A	108.3 (4)	C21B—C26B—H26B	118.8
C2A—C1A—H1A	125.9	C25B—C26B—C21B	122.3 (4)
N1B—C1B—Ni1	127.4 (3)	C25B—C26B—H26B	118.8
N1B—C1B—N2B	104.9 (3)	C32B—C31B—B1B	122.4 (3)
N2B—C1B—Ni1	127.6 (3)	C36B—C31B—C32B	115.1 (4)
N2C—C1C—H1C	126.2	C36B—C31B—B1B	122.2 (4)
N2C—C1C—C2C	107.5 (4)	C31B—C32B—H32B	118.6

C2C—C1C—H1C	126.2	C33B—C32B—C31B	122.8 (4)
N2B—C2—H2A	110.2	C33B—C32B—H32B	118.6
N2B—C2—H2B	110.2	C32B—C33B—H33B	119.7
N2C—C2—N2B	107.8 (3)	C34B—C33B—C32B	120.6 (4)
N2C—C2—H2A	110.2	C34B—C33B—H33B	119.7
N2C—C2—H2B	110.2	C33B—C34B—H34B	120.6
H2A—C2—H2B	108.5	C33B—C34B—C35B	118.7 (4)
C1A—C2A—H2AA	127.5	C35B—C34B—H34B	120.6
C1A—C2A—C3A	105.0 (4)	C34B—C35B—H35B	119.9
C3A—C2A—H2AA	127.5	C34B—C35B—C36B	120.2 (4)
N2B—C2B—H2BA	127.2	C36B—C35B—H35B	119.9
C3B—C2B—N2B	105.6 (4)	C31B—C36B—H36B	118.8
C3B—C2B—H2BA	127.2	C35B—C36B—C31B	122.5 (4)
C1C—C2C—H2C	126.9	C35B—C36B—H36B	118.8
C1C—C2C—C3C	106.1 (4)	C42B—C41B—B1B	124.3 (4)
C3C—C2C—H2C	126.9	C46B—C41B—C42B	114.4 (4)
N1A—C3A—C2A	110.8 (4)	C46B—C41B—B1B	121.0 (4)
N1A—C3A—H3A	124.6	C41B—C42B—H42B	118.6
C2A—C3A—H3A	124.6	C43B—C42B—C41B	122.8 (4)
N1B—C3B—H3B	126.4	C43B—C42B—H42B	118.6
C2B—C3B—N1B	107.2 (4)	C42B—C43B—H43B	119.7
C2B—C3B—H3B	126.4	C44B—C43B—C42B	120.6 (4)
N1C—C3C—C2C	110.0 (4)	C44B—C43B—H43B	119.7
N1C—C3C—H3C	125.0	C43B—C44B—H44B	120.7
C2C—C3C—H3C	125.0	C43B—C44B—C45B	118.6 (4)
H1AA—C1AC— H1AB	109.5	C45B—C44B—H44B	120.7
H1AA—C1AC— H1AC	109.5	C44B—C45B—H45B	119.6
H1AB—C1AC— H1AC	109.5	C44B—C45B—C46B	120.8 (4)
C2AC—C1AC— H1AA	109.5	C46B—C45B—H45B	119.6
C2AC—C1AC— H1AB	109.5	C41B—C46B—H46B	118.6
C2AC—C1AC— H1AC	109.5	C45B—C46B—C41B	122.8 (4)
O1AC—C2AC— C1AC	124.2 (7)	C45B—C46B—H46B	118.6
O1AC—C2AC— C3AC	118.3 (8)	C11B—B1B—C21B	104.6 (3)
C1AC—C2AC— C3AC	111.1 (6)	C31B—B1B—C11B	111.9 (3)
C1AC—C2AC—C1	100.6 (9)	C31B—B1B—C21B	111.4 (3)

O2—C2AC—C1AC	147.3 (13)	C31B—B1B—C41B	104.4 (3)
O2—C2AC—C1	109.4 (13)	C41B—B1B—C11B	112.4 (3)
C2AC—C3AC— H3AA	109.5	C41B—B1B—C21B	112.3 (3)
C2AC—C3AC— H3AB	109.5	C2AC—C1—H1B	109.5
C2AC—C3AC— H3AC	109.5	C2AC—C1—H1D	109.5
H3AA—C3AC— H3AB	109.5	C2AC—C1—H1E	109.5
H3AA—C3AC— H3AC	109.5	H1B—C1—H1D	109.5
H3AB—C3AC— H3AC	109.5	H1B—C1—H1E	109.5
C12B—C11B—B1B	124.3 (4)	H1D—C1—H1E	109.5
C16B—C11B—C12B	115.4 (4)		

## Selected geometric parameters (°)

Ni1—N1A—N2A— C0AA	-11.2 (5)	C12B—C11B— B1B—C41B	23.8 (5)
Ni1—N1A—N2A— C1A	172.8 (3)	C12B—C13B— C14B—C15B	-0.9 (7)
Ni1—N1A—C3A— C2A	-172.5 (3)	C13B—C14B— C15B—C16B	1.0 (7)
Ni1—N1C—N2C— C1C	172.9 (3)	C14B—C15B— C16B—C11B	-0.2 (7)
Ni1—N1C—N2C—C2	-14.4 (5)	C16B—C11B— C12B—C13B	0.8 (6)
Ni1—N1C—C3C— C2C	-172.3 (3)	C16B—C11B— B1B—C21B	75.5 (4)
Cl1—Ni1—N1A— N2A	149.3 (3)	C16B—C11B— B1B—C31B	-45.2 (5)
Cl1—Ni1—N1A— C3A	-40.5 (4)	C16B—C11B— B1B—C41B	-162.4 (4)
N1A—Ni1—C1B— N1B	33.0 (3)	C21B—C22B— C23B—C24B	2.4 (6)
N1A—Ni1—C1B— N2B	-151.7 (3)	C22B—C21B— C26B—C25B	1.7 (6)
N1A—N2A—C0AA— N1B	52.4 (4)	C22B—C21B— B1B—C11B	94.5 (4)
N1A—N2A—C1A— C2A	-0.2 (5)	C22B—C21B— B1B—C31B	-144.5 (4)
N1C—Ni1—C1B— N1B	-148.8 (3)	C22B—C21B— B1B—C41B	-27.7 (5)
N1C—Ni1—C1B—	26.5 (3)	C22B—C23B—	0.2 (6)



N2B		C24B—C25B	
N1C—N2C—C1C— C2C	-1.0 (5)	C23B—C24B— C25B—C26B	-1.6 (6)
N1C—N2C—C2— N2B	54.7 (5)	C24B—C25B— C26B—C21B	0.6 (6)
N2A—N1A—C3A— C2A	-0.8 (5)	C26B—C21B— C22B—C23B	-3.2 (6)
N2A—C1A—C2A— C3A	-0.3 (5)	C26B—C21B— B1B—C11B	-80.9 (4)
N2B—C2B—C3B— N1B	-0.1 (4)	C26B—C21B— B1B—C31B	40.1 (5)
N2C—N1C—C3C— C2C	-1.6 (5)	C26B—C21B— B1B—C41B	156.8 (4)
N2C—C1C—C2C— C3C	0.0 (6)	C31B—C32B— C33B—C34B	-1.6 (6)
C0AA—N1B—C1B— Ni1	-0.2 (5)	C32B—C31B— C36B—C35B	-1.1 (6)
C0AA—N1B—C1B— N2B	-176.3 (3)	C32B—C31B— B1B—C11B	149.3 (4)
C0AA—N1B—C3B— C2B	175.7 (4)	C32B—C31B— B1B—C21B	32.7 (5)
C0AA—N2A—C1A— C2A	-175.8 (4)	C32B—C31B— B1B—C41B	-88.8 (4)
C1A—N2A—C0AA— N1B	-132.4 (4)	C32B—C33B— C34B—C35B	0.9 (6)
C1A—C2A—C3A— N1A	0.7 (5)	C33B—C34B— C35B—C36B	-0.3 (6)
C1B—Ni1—N1A— N2A	-26.8 (3)	C34B—C35B— C36B—C31B	0.5 (6)
C1B—Ni1—N1A— C3A	143.4 (4)	C36B—C31B— C32B—C33B	1.7 (6)
C1B—N1B—C0AA— N2A	-47.1 (5)	C36B—C31B— B1B—C11B	-36.6 (5)
C1B—N1B—C3B— C2B	0.6 (4)	C36B—C31B— B1B—C21B	-153.2 (4)
C1B—N2B—C2— N2C	-51.2 (5)	C36B—C31B— B1B—C41B	85.3 (4)
C1B—N2B—C2B— C3B	-0.4 (4)	C41B—C42B— C43B—C44B	-0.1 (7)
C1C—N2C—C2— N2B	-134.1 (4)	C42B—C41B— C46B—C45B	2.2 (6)
C1C—C2C—C3C— N1C	1.1 (6)	C42B—C41B— B1B—C11B	-145.6 (4)
C2—N2B—C1B—Ni1	7.5 (5)	C42B—C41B— B1B—C21B	-27.9 (6)
C2—N2B—C1B— N1B	-176.4 (3)	C42B—C41B— B1B—C31B	92.9 (4)
C2—N2B—C2B—	176.5 (4)	C42B—C43B—	2.1 (7)

C3B		C44B—C45B	
C2—N2C—C1C— C2C	-173.0 (4)	C43B—C44B— C45B—C46B	-1.8 (7)
C2B—N2B—C1B— Ni1	-175.3 (3)	C44B—C45B— C46B—C41B	-0.4 (7)
C2B—N2B—C1B— N1B	0.8 (4)	C46B—C41B— C42B—C43B	-2.0 (6)
C2B—N2B—C2— N2C	132.1 (4)	C46B—C41B— B1B—C11B	41.0 (5)
C3A—N1A—N2A— C0AA	176.7 (3)	C46B—C41B— B1B—C21B	158.6 (4)
C3A—N1A—N2A— C1A	0.7 (5)	C46B—C41B— B1B—C31B	-80.5 (5)
C3B—N1B—C0AA— N2A	138.2 (4)	B1B—C11B— C12B—C13B	174.9 (4)
C3B—N1B—C1B— Ni1	175.3 (3)	B1B—C11B— C16B—C15B	-175.1 (4)
C3B—N1B—C1B— N2B	-0.9 (4)	B1B—C21B— C22B—C23B	-178.9 (4)
C3C—N1C—N2C— C1C	1.6 (5)	B1B—C21B— C26B—C25B	177.6 (4)
C3C—N1C—N2C— C2	174.3 (4)	B1B—C31B— C32B—C33B	176.1 (4)
C11B—C12B— C13B—C14B	0.0 (6)	B1B—C31B— C36B—C35B	-175.6 (4)
C12B—C11B— C16B—C15B	-0.7 (6)	B1B—C41B— C42B—C43B	-175.8 (4)
C12B—C11B— B1B—C21B	-98.4 (4)	B1B—C41B— C46B—C45B	176.3 (4)
C12B—C11B— B1B—C31B	140.9 (4)		

## 7.1.10. Crystal data for complex 9

## Selected geometric parameters (Å)

Ni01—Cl01	2.2199 (9)	N04—C01	1.347 (2)
Ni01—N06	1.9016 (19)	N04—C03	1.391 (3)
Ni01—N01	1.8996 (18)	N04—C04	1.455 (3)
Ni01—C01	1.847 (2)	C02—H02	0.9500
P01—F02	1.6073 (16)	C02—C03	1.355 (3)
P01—F01	1.5993 (15)	C11—H11	0.9500
P01—F03	1.5974 (17)	C11—C10	1.395 (3)
P01—F05	1.6032 (17)	C08—H08	0.9500
P01—F06	1.6023 (15)	C08—C07	1.400 (3)

P01—F04	1.6017 (17)	C05—H05A	0.9900
N06—N05	1.364 (2)	C05—H05B	0.9900
N06—C08	1.333 (3)	C03—H03	0.9500
N03—C02	1.390 (2)	C09—H09	0.9500
N03—C01	1.344 (3)	C09—C10	1.380 (3)
N03—C05	1.453 (3)	C04—H04A	0.9900
N01—N02	1.365 (2)	C04—H04B	0.9900
N01—C11	1.344 (3)	C10—H10	0.9500
N02—C05	1.451 (2)	C07—H07	0.9500
N02—C09	1.347 (3)	C07—C06	1.370 (4)
N05—C04	1.446 (3)	C06—H06	0.9500
N05—C06	1.351 (3)		

### Selected geometric parameters (°)

N06—Ni01—C101	90.68 (6)	N03—C02—H02	126.9
N01—Ni01—C101	92.31 (6)	C03—C02—N03	106.29 (18)
N01—Ni01—N06	175.68 (7)	C03—C02—H02	126.9
C01—Ni01—C101	178.86 (6)	N01—C11—H11	124.5
C01—Ni01—N06	88.40 (9)	N01—C11—C10	110.98 (18)
C01—Ni01—N01	88.64 (9)	C10—C11—H11	124.5
F01—P01—F02	90.07 (9)	N03—C01—Ni01	128.01 (15)
F01—P01—F05	89.28 (10)	N03—C01—N04	104.72 (16)
F01—P01—F06	179.19 (10)	N04—C01—Ni01	127.27 (15)
F01—P01—F04	90.11 (9)	N06—C08—H08	124.8
F03—P01—F02	89.48 (9)	N06—C08—C07	110.4 (2)
F03—P01—F01	90.45 (10)	C07—C08—H08	124.8
F03—P01—F05	179.13 (10)	N03—C05—H05A	110.1
F03—P01—F06	90.34 (10)	N03—C05—H05B	110.1
F03—P01—F04	89.93 (10)	N02—C05—N03	108.05 (15)
F05—P01—F02	89.69 (9)	N02—C05—H05A	110.1
F06—P01—F02	89.78 (8)	N02—C05—H05B	110.1
F06—P01—F05	89.92 (10)	H05A—C05—H05B	108.4
F04—P01—F02	179.38 (9)	N04—C03—H03	126.9
F04—P01—F05	90.91 (10)	C02—C03—N04	106.10 (18)
F04—P01—F06	90.05 (9)	C02—C03—H03	126.9
N05—N06—Ni01	124.19 (15)	N02—C09—H09	126.3
C08—N06—Ni01	129.52 (16)	N02—C09—C10	107.33 (18)
C08—N06—N05	105.91 (18)	C10—C09—H09	126.3
C02—N03—C05	128.28 (17)	N05—C04—N04	108.45 (17)
C01—N03—C02	111.48 (17)	N05—C04—H04A	110.0
C01—N03—C05	120.13 (16)	N05—C04—H04B	110.0

N02—N01—Ni01	124.85 (13)	N04—C04—H04A	110.0
C11—N01—Ni01	129.10 (14)	N04—C04—H04B	110.0
C11—N01—N02	105.00 (17)	H04A—C04—H04B	108.4
N01—N02—C05	120.12 (17)	C11—C10—H10	127.4
C09—N02—N01	111.42 (16)	C09—C10—C11	105.26 (18)
C09—N02—C05	128.07 (17)	C09—C10—H10	127.4
N06—N05—C04	121.40 (18)	C08—C07—H07	127.2
C06—N05—N06	110.6 (2)	C06—C07—C08	105.5 (2)
C06—N05—C04	127.8 (2)	C06—C07—H07	127.2
C01—N04—C03	111.41 (17)	N05—C06—C07	107.6 (2)
C01—N04—C04	120.60 (17)	N05—C06—H06	126.2
C03—N04—C04	127.99 (17)	C07—C06—H06	126.2

### 7.1.11. Crystal data for complex 10

#### Selected geometric parameters (Å)

Ni1D—C2D	1.885 (11)	C41A—B1A	1.681 (12)
Ni1D—C2D <sup>i</sup>	1.885 (10)	C46A—H46A	0.9500
Ni1D—C8D	1.928 (9)	C46A—C45A	1.3900
Ni1D—C8D <sup>i</sup>	1.928 (9)	C45A—H45A	0.9500
N1D—C2D	1.344 (12)	C45A—C44A	1.3900
N1D—C3D	1.410 (15)	C44A—H44A	0.9500
N1D—C1AA	1.373 (15)	C44A—C43A	1.3900
C2D—C1D	1.292 (13)	C43A—H43A	0.9500
N3D—C5D	1.500 (15)	C43A—C42A	1.3900
N3D—C6D	1.395 (15)	C42A—H42A	0.9500
N3D—C8D	1.358 (11)	C11B—C12B	1.3900
C4D—C7D	1.372 (15)	C11B—C15B	1.3900
C4D—C8D	1.333 (13)	C11B—B1B	1.697 (12)
C4D—C9D	1.462 (16)	C12B—H12B	0.9500
C1D—C0AA	1.394 (14)	C12B—C13B	1.3900
C1D—C6	1.446 (15)	C13B—H13B	0.9500
C0AA—H0AA	0.9500	C13B—C14B	1.3900
C0AA—C3D	1.336 (17)	C14B—H14B	0.9500
C3D—H3D	0.9500	C14B—C16B	1.3900
C1AA—H1AA	0.9900	C16B—H16B	0.9500
C1AA—H1AB	0.9900	C16B—C15B	1.3900
C1AA—C5D	1.360 (18)	C15B—H15B	0.9500
C5D—H5DA	0.9900	C21B—C26B	1.3900
C5D—H5DB	0.9900	C21B—C22B	1.3900
C6D—H6D	0.9500	C21B—B1B	1.671 (13)

C6D—C7D	1.343 (15)	C26B—H26B	0.9500
C7D—H7D	0.9500	C26B—C25B	1.3900
C9D—H9DA	0.9900	C25B—H25B	0.9500
C9D—H9DB	0.9900	C25B—C1	1.3900
C9D—C8	1.485 (18)	C1—H1	0.9500
Ni1C—C2C <sup>ii</sup>	1.884 (11)	C1—C24B	1.3900
Ni1C—C2C	1.884 (11)	C24B—H24B	0.9500
Ni1C—N8C <sup>ii</sup>	1.922 (12)	C24B—C22B	1.3900
Ni1C—N8C	1.922 (12)	C22B—H22B	0.9500
N0AA—C2C	1.315 (13)	C31B—C36B	1.3900
N0AA—C3C	1.374 (15)	C31B—C32B	1.3900
N0AA—C4C	1.509 (16)	C31B—B1B	1.646 (13)
C2C—N1C	1.483 (19)	C36B—H36B	0.9500
N3C—C5C	1.47 (2)	C36B—C35B	1.3900
N3C—N8C	1.392 (15)	C35B—H35B	0.9500
N3C—C10	1.454 (19)	C35B—C34B	1.3900
N1C—C8AA	1.32 (2)	C34B—H34B	0.9500
C8AA—H8AA	0.9500	C34B—C33B	1.3900
C8AA—C3C	1.30 (2)	C33B—H33B	0.9500
C3C—H3C	0.9500	C33B—C32B	1.3900
C4C—H4CA	0.9900	C32B—H32B	0.9500
C4C—H4CB	0.9900	C41B—C42B	1.3900
C4C—C5C	1.373 (18)	C41B—C46B	1.3900
C5C—H5CA	0.9900	C41B—B1B	1.704 (13)
C5C—H5CB	0.9900	C42B—H42B	0.9500
C7C—N8C	1.42 (2)	C42B—C43B	1.3900
C7C—C12	1.40 (2)	C43B—C44B	1.3900
C11A—C12A	1.3900	C44B—H44B	0.9500
C11A—C16A	1.3900	C44B—C45B	1.3900
C11A—B1A	1.693 (13)	C45B—H45B	0.9500
C12A—H12A	0.9500	C45B—C46B	1.3900
C12A—C13A	1.3900	C46B—H46B	0.9500
C13A—H13A	0.9500	C6—H6A	0.9900
C13A—C14A	1.3900	C6—H6B	0.9900
C14A—H14A	0.9500	C6—C4AA	1.497 (17)
C14A—C15A	1.3900	C8—H8A	0.9900
C15A—H15A	0.9500	C8—H8B	0.9900
C15A—C16A	1.3900	C8—N9AA	1.51 (3)
C16A—H16A	0.9500	N4—N2	1.4200
C21A—C22A	1.3900	N4—C7	1.4200
C21A—C26A	1.3900	N4—C4AA	1.58 (3)

C21A—B1A	1.686 (12)	N2—C3AA	1.4200
C22A—C23A	1.3900	C3AA—H3AA	0.9500
C23A—C24A	1.3900	C3AA—C2AA	1.4200
C24A—C25A	1.3900	C2AA—H2AA	0.9500
C25A—C26A	1.3900	C2AA—C7	1.4200
C31A—C32A	1.3900	C7—H7	0.9500
C31A—C36A	1.3900	C4AA—H4AA	0.9900
C31A—B1A	1.675 (12)	C4AA—H4AB	0.9900
C32A—H32A	0.9500	C10—H10	0.9500
C32A—C33A	1.3900	C10—C12	1.56 (3)
C33A—H33A	0.9500	N9AA—N4CA	1.4200
C33A—C34A	1.3900	N9AA—C1BA	1.4200
C34A—H34A	0.9500	N4CA—C3CA	1.4200
C34A—C35A	1.3900	C3CA—H3CA	0.9500
C35A—H35A	0.9500	C3CA—C2CA	1.4200
C35A—C36A	1.3900	C2CA—H2CA	0.9500
C36A—H36A	0.9500	C2CA—C1BA	1.4200
C41A—C46A	1.3900	C1BA—H1BA	0.9500
C41A—C42A	1.3900	C12—H12	0.9500

Symmetry code(s): (i)  $-x-2, -y, -z-2$ ; (ii)  $-x-2, -y+1, -z-3$ .

#### Selected geometric parameters (°)

C2D—Ni1D—C2D <sup>i</sup>	180.0	C46A—C45A—C44A	120.0
C2D <sup>i</sup> —Ni1D—C8D <sup>i</sup>	92.5 (4)	C44A—C45A—H45A	120.0
C2D—Ni1D—C8D <sup>i</sup>	87.5 (4)	C45A—C44A—H44A	120.0
C2D <sup>i</sup> —Ni1D—C8D	87.5 (4)	C43A—C44A—C45A	120.0
C2D—Ni1D—C8D	92.5 (4)	C43A—C44A—H44A	120.0
C8D—Ni1D—C8D <sup>i</sup>	180.0	C44A—C43A—H43A	120.0
C2D—N1D—C3D	109.5 (11)	C44A—C43A—C42A	120.0
C2D—N1D—C1AA	124.3 (11)	C42A—C43A—H43A	120.0
C1AA—N1D—C3D	126.1 (11)	C41A—C42A—H42A	120.0
N1D—C2D—Ni1D	122.7 (9)	C43A—C42A—C41A	120.0
C1D—C2D—Ni1D	131.4 (8)	C43A—C42A—H42A	120.0
C1D—C2D—N1D	105.8 (10)	C11A—B1A—C41A	109.6 (7)
C6D—N3D—C5D	122.3 (11)	C21A—B1A—C11A	110.0 (7)
C8D—N3D—C5D	128.8 (11)	C21A—B1A—C41A	108.1 (7)
C8D—N3D—C6D	108.9 (10)	C31A—B1A—C11A	112.5 (7)
C7D—C4D—C9D	123.9 (14)	C31A—B1A—C21A	107.6 (7)
C8D—C4D—C7D	110.7 (10)	C31A—B1A—C41A	109.0 (7)

C8D—C4D—C9D	124.7 (13)	C12B—C11B—C15B	120.0
C2D—C1D—C0AA	112.9 (10)	C12B—C11B—B1B	119.8 (6)
C2D—C1D—C6	119.2 (12)	C15B—C11B—B1B	120.1 (6)
C0AA—C1D—C6	127.7 (13)	C11B—C12B—H12B	120.0
C1D—C0AA—H0AA	127.4	C11B—C12B—C13B	120.0
C3D—C0AA—C1D	105.2 (12)	C13B—C12B—H12B	120.0
C3D—C0AA—H0AA	127.4	C12B—C13B—H13B	120.0
N1D—C3D—H3D	126.7	C14B—C13B—C12B	120.0
C0AA—C3D—N1D	106.5 (11)	C14B—C13B—H13B	120.0
C0AA—C3D—H3D	126.7	C13B—C14B—H14B	120.0
N1D—C1AA—H1AA	107.1	C13B—C14B—C16B	120.0
N1D—C1AA—H1AB	107.1	C16B—C14B—H14B	120.0
H1AA—C1AA— H1AB	106.8	C14B—C16B—H16B	120.0
C5D—C1AA—N1D	120.8 (15)	C15B—C16B—C14B	120.0
C5D—C1AA—H1AA	107.1	C15B—C16B—H16B	120.0
C5D—C1AA—H1AB	107.1	C11B—C15B—H15B	120.0
N3D—C5D—H5DA	106.7	C16B—C15B—C11B	120.0
N3D—C5D—H5DB	106.7	C16B—C15B—H15B	120.0
C1AA—C5D—N3D	122.4 (12)	C26B—C21B—C22B	120.0
C1AA—C5D—H5DA	106.7	C26B—C21B—B1B	117.5 (6)
C1AA—C5D—H5DB	106.7	C22B—C21B—B1B	122.4 (7)
H5DA—C5D—H5DB	106.6	C21B—C26B—H26B	120.0
N3D—C6D—H6D	126.5	C25B—C26B—C21B	120.0
C7D—C6D—N3D	106.9 (11)	C25B—C26B—H26B	120.0
C7D—C6D—H6D	126.5	C26B—C25B—H25B	120.0
C4D—C7D—H7D	126.4	C26B—C25B—C1	120.0
C6D—C7D—C4D	107.1 (12)	C1—C25B—H25B	120.0
C6D—C7D—H7D	126.4	C25B—C1—H1	120.0
N3D—C8D—Ni1D	125.8 (7)	C24B—C1—C25B	120.0
C4D—C8D—Ni1D	127.9 (8)	C24B—C1—H1	120.0
C4D—C8D—N3D	106.3 (9)	C1—C24B—H24B	120.0
C4D—C9D—H9DA	108.0	C1—C24B—C22B	120.0
C4D—C9D—H9DB	108.0	C22B—C24B—H24B	120.0
C4D—C9D—C8	117 (2)	C21B—C22B—H22B	120.0
H9DA—C9D—H9DB	107.2	C24B—C22B—C21B	120.0
C8—C9D—H9DA	108.0	C24B—C22B—H22B	120.0
C8—C9D—H9DB	108.0	C36B—C31B—C32B	120.0
C2C <sup>ii</sup> —Ni1C—C2C	180.0	C36B—C31B—B1B	122.7 (5)
C2C <sup>ii</sup> —Ni1C—N8C	91.6 (5)	C32B—C31B—B1B	117.3 (5)
C2C <sup>ii</sup> —Ni1C—N8C <sup>ii</sup>	88.4 (5)	C31B—C36B—H36B	120.0

C2C—Ni1C—N8C <sup>ii</sup>	91.6 (5)	C31B—C36B—C35B	120.0
C2C—Ni1C—N8C	88.4 (5)	C35B—C36B—H36B	120.0
N8C <sup>ii</sup> —Ni1C—N8C	180.0 (8)	C36B—C35B—H35B	120.0
C2C—N0AA—C3C	112.5 (12)	C34B—C35B—C36B	120.0
C2C—N0AA—C4C	125.1 (11)	C34B—C35B—H35B	120.0
C3C—N0AA—C4C	121.5 (11)	C35B—C34B—H34B	120.0
N0AA—C2C—Ni1C	133.1 (9)	C35B—C34B—C33B	120.0
N0AA—C2C—N1C	100.4 (11)	C33B—C34B—H34B	120.0
N1C—C2C—Ni1C	123.2 (10)	C34B—C33B—H33B	120.0
N8C—N3C—C5C	122.1 (13)	C32B—C33B—C34B	120.0
N8C—N3C—C10	102.6 (14)	C32B—C33B—H33B	120.0
C10—N3C—C5C	135.1 (13)	C31B—C32B—H32B	120.0
C8AA—N1C—C2C	109.0 (15)	C33B—C32B—C31B	120.0
N1C—C8AA—H8AA	125.5	C33B—C32B—H32B	120.0
C3C—C8AA—N1C	109.0 (17)	C42B—C41B—C46B	120.0
C3C—C8AA—H8AA	125.5	C42B—C41B—B1B	120.5 (5)
N0AA—C3C—H3C	126.1	C46B—C41B—B1B	119.4 (5)
C8AA—C3C—N0AA	107.8 (14)	C41B—C42B—H42B	120.0
C8AA—C3C—H3C	126.1	C41B—C42B—C43B	120.0
N0AA—C4C—H4CA	108.1	C43B—C42B—H42B	120.0
N0AA—C4C—H4CB	108.1	C44B—C43B—C42B	120.0
H4CA—C4C—H4CB	107.3	C43B—C44B—H44B	120.0
C5C—C4C—N0AA	116.7 (12)	C43B—C44B—C45B	120.0
C5C—C4C—H4CA	108.1	C45B—C44B—H44B	120.0
C5C—C4C—H4CB	108.1	C44B—C45B—H45B	120.0
N3C—C5C—H5CA	108.1	C44B—C45B—C46B	120.0
N3C—C5C—H5CB	108.1	C46B—C45B—H45B	120.0
C4C—C5C—N3C	116.9 (16)	C41B—C46B—H46B	120.0
C4C—C5C—H5CA	108.1	C45B—C46B—C41B	120.0
C4C—C5C—H5CB	108.1	C45B—C46B—H46B	120.0
H5CA—C5C—H5CB	107.3	C11B—B1B—C41B	108.0 (7)
N8C—C7C—C12	112.0 (18)	C21B—B1B—C11B	110.8 (7)
N3C—N8C—Ni1C	118.4 (11)	C21B—B1B—C41B	108.8 (7)
N3C—N8C—C7C	112.8 (13)	C31B—B1B—C11B	106.9 (7)
C7C—N8C—Ni1C	128.6 (11)	C31B—B1B—C21B	110.2 (8)
C12A—C11A—C16A	120.0	C31B—B1B—C41B	112.2 (7)
C12A—C11A—B1A	120.6 (5)	C1D—C6—H6A	108.9
C16A—C11A—B1A	119.3 (5)	C1D—C6—H6B	108.9
C11A—C12A—H12A	120.0	C1D—C6—C4AA	113.2 (18)
C11A—C12A—C13A	120.0	H6A—C6—H6B	107.7
C13A—C12A—H12A	120.0	C4AA—C6—H6A	108.9



C12A—C13A—H13A	120.0	C4AA—C6—H6B	108.9
C12A—C13A—C14A	120.0	C9D—C8—H8A	110.1
C14A—C13A—H13A	120.0	C9D—C8—H8B	110.1
C13A—C14A—H14A	120.0	H8A—C8—H8B	108.4
C15A—C14A—C13A	120.0	N9AA—C8—C9D	108 (2)
C15A—C14A—H14A	120.0	N9AA—C8—H8A	110.1
C14A—C15A—H15A	120.0	N9AA—C8—H8B	110.1
C14A—C15A—C16A	120.0	N2—N4—C7	108.0
C16A—C15A—H15A	120.0	N2—N4—C4AA	121.1 (17)
C11A—C16A—H16A	120.0	C7—N4—C4AA	130.6 (17)
C15A—C16A—C11A	120.0	C3AA—N2—N4	108.0
C15A—C16A—H16A	120.0	N2—C3AA—H3AA	126.0
C22A—C21A—C26A	120.0	N2—C3AA—C2AA	108.0
C22A—C21A—B1A	121.6 (6)	C2AA—C3AA— H3AA	126.0
C26A—C21A—B1A	118.4 (6)	C3AA—C2AA— H2AA	126.0
C23A—C22A—C21A	120.0	C7—C2AA—C3AA	108.0
C22A—C23A—C24A	120.0	C7—C2AA—H2AA	126.0
C23A—C24A—C25A	120.0	N4—C7—H7	126.0
C24A—C25A—C26A	120.0	C2AA—C7—N4	108.0
C25A—C26A—C21A	120.0	C2AA—C7—H7	126.0
C32A—C31A—C36A	120.0	C6—C4AA—N4	108.4 (18)
C32A—C31A—B1A	122.5 (6)	C6—C4AA—H4AA	110.0
C36A—C31A—B1A	117.3 (6)	C6—C4AA—H4AB	110.0
C31A—C32A—H32A	120.0	N4—C4AA—H4AA	110.0
C31A—C32A—C33A	120.0	N4—C4AA—H4AB	110.0
C33A—C32A—H32A	120.0	H4AA—C4AA— H4AB	108.4
C32A—C33A—H33A	120.0	N3C—C10—H10	124.1
C34A—C33A—C32A	120.0	C12—C10—N3C	111.7 (14)
C34A—C33A—H33A	120.0	C12—C10—H10	124.1
C33A—C34A—H34A	120.0	N4CA—N9AA—C8	133 (2)
C33A—C34A—C35A	120.0	C1BA—N9AA—C8	119 (2)
C35A—C34A—H34A	120.0	C1BA—N9AA— N4CA	108.0
C34A—C35A—H35A	120.0	N9AA—N4CA— C3CA	108.0
C34A—C35A—C36A	120.0	N4CA—C3CA— H3CA	126.0
C36A—C35A—H35A	120.0	C2CA—C3CA— N4CA	108.0
C31A—C36A—H36A	120.0	C2CA—C3CA—	126.0

		H3CA	
C35A—C36A—C31A	120.0	C3CA—C2CA—H2CA	126.0
C35A—C36A—H36A	120.0	C3CA—C2CA—C1BA	108.0
C46A—C41A—C42A	120.0	C1BA—C2CA—H2CA	126.0
C46A—C41A—B1A	122.1 (6)	N9AA—C1BA—C2CA	108.0
C42A—C41A—B1A	117.8 (5)	N9AA—C1BA—H1BA	126.0
C41A—C46A—H46A	120.0	C2CA—C1BA—H1BA	126.0
C41A—C46A—C45A	120.0	C7C—C12—H12	130.2
C45A—C46A—H46A	120.0	C10—C12—C7C	100 (2)
C46A—C45A—H45A	120.0	C10—C12—H12	130.2

Symmetry code(s): (i)  $-x-2, -y, -z-2$ ; (ii)  $-x-2, -y+1, -z-3$ .

#### Selected geometric parameters, torsion angles (°)

Ni1D—C2D—C1D—C0AA	-177.2 (9)	C36A—C31A—B1A—C21A	-76.4 (7)
Ni1D—C2D—C1D—C6	-1.0 (18)	C36A—C31A—B1A—C41A	40.6 (9)
N1D—C2D—C1D—C0AA	-0.3 (14)	C41A—C46A—C45A—C44A	0.0
N1D—C2D—C1D—C6	175.9 (12)	C46A—C41A—C42A—C43A	0.0
N1D—C1AA—C5D—N3D	44 (3)	C46A—C41A—B1A—C11A	95.0 (8)
C2D—N1D—C3D—C0AA	2.7 (17)	C46A—C41A—B1A—C21A	-24.8 (9)
C2D—N1D—C1AA—C5D	-73 (2)	C46A—C41A—B1A—C31A	-141.5 (6)
C2D—C1D—C0AA—C3D	2.0 (16)	C46A—C45A—C44A—C43A	0.0
C2D—C1D—C6—C4AA	119.6 (18)	C45A—C44A—C43A—C42A	0.0
N3D—C6D—C7D—C4D	1.3 (16)	C44A—C43A—C42A—C41A	0.0
C4D—C9D—C8—N9AA	76 (3)	C42A—C41A—C46A—C45A	0.0
C1D—C0AA—C3D—N1D	-2.7 (16)	C42A—C41A—B1A—C11A	-82.1 (7)
C1D—C6—C4AA—	-70 (2)	C42A—C41A—	158.1 (5)

N4		B1A—C21A	
C0AA—C1D—C6— C4AA	-65 (2)	C42A—C41A— B1A—C31A	41.4 (9)
C3D—N1D—C2D— Ni1D	175.8 (9)	B1A—C11A— C12A—C13A	175.5 (6)
C3D—N1D—C2D— C1D	-1.4 (14)	B1A—C11A— C16A—C15A	-175.5 (6)
C3D—N1D—C1AA— C5D	111.8 (18)	B1A—C21A— C22A—C23A	179.2 (7)
C1AA—N1D—C2D— Ni1D	0.1 (18)	B1A—C21A— C26A—C25A	-179.2 (6)
C1AA—N1D—C2D— C1D	-177.1 (13)	B1A—C31A— C32A—C33A	-175.0 (7)
C1AA—N1D—C3D— C0AA	178.2 (14)	B1A—C31A— C36A—C35A	175.2 (7)
C5D—N3D—C6D— C7D	178.0 (14)	B1A—C41A— C46A—C45A	-177.1 (7)
C5D—N3D—C8D— Ni1D	2 (2)	B1A—C41A— C42A—C43A	177.2 (7)
C5D—N3D—C8D— C4D	-178.0 (14)	C11B—C12B— C13B—C14B	0.0
C6D—N3D—C5D— C1AA	-163.9 (17)	C12B—C11B— C15B—C16B	0.0
C6D—N3D—C8D— Ni1D	-178.2 (9)	C12B—C11B— B1B—C21B	-151.2 (6)
C6D—N3D—C8D— C4D	2.1 (14)	C12B—C11B— B1B—C31B	88.7 (8)
C7D—C4D—C8D— Ni1D	179.0 (9)	C12B—C11B— B1B—C41B	-32.2 (9)
C7D—C4D—C8D— N3D	-1.3 (14)	C12B—C13B— C14B—C16B	0.0
C7D—C4D—C9D— C8	60 (3)	C13B—C14B— C16B—C15B	0.0
C8D—Ni1D—C2D— N1D	60.7 (10)	C14B—C16B— C15B—C11B	0.0
C8D <sup>i</sup> —Ni1D—C2D— N1D	-119.3 (10)	C15B—C11B— C12B—C13B	0.0
C8D—Ni1D—C2D— C1D	-122.8 (11)	C15B—C11B— B1B—C21B	32.6 (10)
C8D <sup>i</sup> —Ni1D—C2D— C1D	57.2 (11)	C15B—C11B— B1B—C31B	-87.5 (8)
C8D—N3D—C5D— C1AA	16 (3)	C15B—C11B— B1B—C41B	151.6 (5)
C8D—N3D—C6D— C7D	-2.1 (16)	C21B—C26B— C25B—C1	0.0
C8D—C4D—C7D— C6D	0.0 (16)	C26B—C21B— C22B—C24B	0.0
C8D—C4D—C9D—	-110 (2)	C26B—C21B—	-90.6 (8)

C8		B1B—C11B	
C9D—C4D—C7D— C6D	-171.6 (16)	C26B—C21B— B1B—C31B	27.5 (9)
C9D—C4D—C8D— Ni1D	-9 (2)	C26B—C21B— B1B—C41B	150.8 (6)
C9D—C4D—C8D— N3D	170.2 (15)	C26B—C25B—C1— C24B	0.0
C9D—C8—N9AA— N4CA	-122 (3)	C25B—C1—C24B— C22B	0.0
C9D—C8—N9AA— C1BA	66 (3)	C1—C24B—C22B— C21B	0.0
Ni1C—C2C—N1C— C8AA	-172.3 (15)	C22B—C21B— C26B—C25B	0.0
N0AA—C2C—N1C— C8AA	-10 (2)	C22B—C21B— B1B—C11B	86.1 (9)
N0AA—C4C—C5C— N3C	49 (2)	C22B—C21B— B1B—C31B	-155.8 (6)
C2C—N0AA—C3C— C8AA	-9 (2)	C22B—C21B— B1B—C41B	-32.5 (9)
C2C—N0AA—C4C— C5C	27 (2)	C31B—C36B— C35B—C34B	0.0
C2C—N1C—C8AA— C3C	6 (3)	C36B—C31B— C32B—C33B	0.0
N3C—C10—C12— C7C	-11 (2)	C36B—C31B— B1B—C11B	-5.1 (9)
N1C—C8AA—C3C— N0AA	1 (2)	C36B—C31B— B1B—C21B	-125.6 (6)
C3C—N0AA—C2C— Ni1C	170.4 (14)	C36B—C31B— B1B—C41B	113.1 (6)
C3C—N0AA—C2C— N1C	11.3 (17)	C36B—C35B— C34B—C33B	0.0
C3C—N0AA—C4C— C5C	-165.1 (15)	C35B—C34B— C33B—C32B	0.0
C4C—N0AA—C2C— Ni1C	-21 (2)	C34B—C33B— C32B—C31B	0.0
C4C—N0AA—C2C— N1C	-179.8 (12)	C32B—C31B— C36B—C35B	0.0
C4C—N0AA—C3C— C8AA	-178.3 (16)	C32B—C31B— B1B—C11B	173.6 (5)
C5C—N3C—N8C— Ni1C	-8.1 (17)	C32B—C31B— B1B—C21B	53.2 (8)
C5C—N3C—N8C— C7C	177.6 (16)	C32B—C31B— B1B—C41B	-68.2 (8)
C5C—N3C—C10— C12	-169.6 (18)	C41B—C42B— C43B—C44B	0.0
N8C <sup>ii</sup> —Ni1C—C2C— N0AA	136.3 (17)	C42B—C41B— C46B—C45B	0.0
N8C—Ni1C—C2C—	-43.7 (17)	C42B—C41B—	130.4 (6)

N0AA		B1B—C11B	
N8C <sup>ii</sup> —Ni1C—C2C— N1C	-68.5 (15)	C42B—C41B— B1B—C21B	-109.3 (7)
N8C—Ni1C—C2C— N1C	111.5 (15)	C42B—C41B— B1B—C31B	12.9 (10)
N8C—N3C—C5C— C4C	-77.4 (19)	C42B—C43B— C44B—C45B	0.0
N8C—N3C—C10— C12	5.9 (18)	C43B—C44B— C45B—C46B	0.0
N8C—C7C—C12— C10	11 (3)	C44B—C45B— C46B—C41B	0.0
C11A—C12A— C13A—C14A	0.0	C46B—C41B— C42B—C43B	0.0
C12A—C11A— C16A—C15A	0.0	C46B—C41B— B1B—C11B	-52.6 (9)
C12A—C11A— B1A—C21A	125.6 (6)	C46B—C41B— B1B—C21B	67.7 (8)
C12A—C11A— B1A—C31A	-114.6 (6)	C46B—C41B— B1B—C31B	-170.1 (6)
C12A—C11A— B1A—C41A	6.9 (9)	B1B—C11B— C12B—C13B	-176.2 (8)
C12A—C13A— C14A—C15A	0.0	B1B—C11B— C15B—C16B	176.2 (7)
C13A—C14A— C15A—C16A	0.0	B1B—C21B— C26B—C25B	176.8 (7)
C14A—C15A— C16A—C11A	0.0	B1B—C21B— C22B—C24B	-176.6 (7)
C16A—C11A— C12A—C13A	0.0	B1B—C31B— C36B—C35B	178.7 (7)
C16A—C11A— B1A—C21A	-58.9 (8)	B1B—C31B— C32B—C33B	-178.8 (6)
C16A—C11A— B1A—C31A	60.9 (8)	B1B—C41B— C42B—C43B	176.9 (7)
C16A—C11A— B1A—C41A	-177.6 (5)	B1B—C41B— C46B—C45B	-177.0 (7)
C21A—C22A— C23A—C24A	0.0	C6—C1D—C0AA— C3D	-173.8 (15)
C22A—C21A— C26A—C25A	0.0	C8—N9AA—N4CA— C3CA	-173 (3)
C22A—C21A— B1A—C11A	-6.1 (9)	C8—N9AA—C1BA— C2CA	174 (2)
C22A—C21A— B1A—C31A	-128.8 (6)	N4—N2—C3AA— C2AA	0.0
C22A—C21A— B1A—C41A	113.5 (7)	N2—N4—C7—C2AA	0.0
C22A—C23A— C24A—C25A	0.0	N2—N4—C4AA—C6	-73 (2)
C23A—C24A—	0.0	N2—C3AA—C2AA—	0.0

C25A—C26A		C7	
C24A—C25A—	0.0	C3AA—C2AA—C7—	0.0
C26A—C21A		N4	
C26A—C21A—	0.0	C7—N4—N2—C3AA	0.0
C22A—C23A			
C26A—C21A—	173.1 (5)	C7—N4—C4AA—C6	101 (2)
B1A—C11A			
C26A—C21A—	50.4 (8)	C4AA—N4—N2—	174.9 (18)
B1A—C31A		C3AA	
C26A—C21A—	-67.3 (8)	C4AA—N4—C7—	-174 (2)
B1A—C41A		C2AA	
C31A—C32A—	0.0	C10—N3C—C5C—	97.4 (19)
C33A—C34A		C4C	
C32A—C31A—	0.0	C10—N3C—N8C—	175.7 (9)
C36A—C35A		Ni1C	
C32A—C31A—	-22.5 (9)	C10—N3C—N8C—	1.3 (18)
B1A—C11A		C7C	
C32A—C31A—	98.7 (7)	N9AA—N4CA—	0.0
B1A—C21A		C3CA—C2CA	
C32A—C31A—	-144.3 (6)	N4CA—N9AA—	0.0
B1A—C41A		C1BA—C2CA	
C32A—C33A—	0.0	N4CA—C3CA—	0.0
C34A—C35A		C2CA—C1BA	
C33A—C34A—	0.0	C3CA—C2CA—	0.0
C35A—C36A		C1BA—N9AA	
C34A—C35A—	0.0	C1BA—N9AA—	0.0
C36A—C31A		N4CA—C3CA	
C36A—C31A—	0.0	C12—C7C—N8C—	177.5 (15)
C32A—C33A		Ni1C	
C36A—C31A—	162.4 (5)	C12—C7C—N8C—	-9 (3)
B1A—C11A		N3C	

Symmetry code(s): (i)  $-x-2, -y, -z-2$ ; (ii)  $-x-2, -y+1, -z-3$ .

### 7.1.12. Crystal data for complex 11

Table 2. Selected geometric parameters (Å, °)

Au1—Cl2	2.2854 (11)	C11—C12	1.331 (6)
Au1—C3	1.973 (4)	C11—H111	0.922
C3—N4	1.359 (5)	C12—N13	1.389 (6)
C3—N13	1.349 (5)	C12—H121	0.934
N4—C5	1.463 (6)	N13—C14	1.458 (5)
N4—C11	1.390 (6)	C14—N15	1.428 (6)
C5—N6	1.445 (5)	C14—H142	0.977

C5—H52	0.976	C14—H141	0.983
C5—H51	0.988	N15—N16	1.358 (5)
N6—N7	1.355 (5)	N15—C19	1.349 (5)
N6—C10	1.360 (5)	N16—C17	1.332 (6)
N7—C8	1.331 (6)	C17—C18	1.398 (8)
C8—C9	1.390 (7)	C17—H171	0.927
C8—H81	0.935	C18—C19	1.354 (7)
C9—C10	1.348 (6)	C18—H181	0.947
C9—H91	0.922	C19—H191	0.942
C10—H101	0.944		
Cl2—Au1—C3	177.16 (11)	N6—C10—C9	106.6 (4)
Au1—C3—N4	126.9 (3)	N4—C11—C12	106.8 (4)
Au1—C3—N13	128.4 (3)	C11—C12—N13	107.1 (4)
N4—C3—N13	104.5 (4)	C12—N13—C3	110.9 (3)
C3—N4—C5	124.7 (4)	C12—N13—C14	123.9 (4)
C3—N4—C11	110.7 (3)	C3—N13—C14	125.2 (4)
C5—N4—C11	124.6 (4)	N13—C14—N15	111.7 (3)
N4—C5—N6	112.4 (3)	C14—N15—N16	119.2 (3)
C5—N6—N7	120.0 (4)	C14—N15—C19	128.7 (4)
C5—N6—C10	127.9 (4)	N16—N15—C19	111.9 (3)
N7—N6—C10	112.1 (4)	N15—N16—C17	103.6 (4)
N6—N7—C8	103.8 (4)	N16—C17—C18	112.4 (4)
N7—C8—C9	111.8 (4)	C17—C18—C19	104.3 (4)
C8—C9—C10	105.7 (4)	C18—C19—N15	107.8 (4)

## Selected hydrogen-bond parameters

$D-H\cdots A$	$D-H$ (Å)	$H\cdots A$ (Å)	$D\cdots A$ (Å)	$D-H\cdots A$ (°)
C5—H52 $\cdots$ N16 <sup>i</sup>	0.976	2.433	3.297 (7)	147.31 (14)

Symmetry code(s): (i)  $x+1/2, -y+1/2, z+1/2$ .

## 7.1.13. Crystal data for complex 12

## Selected geometric parameters (Å, °)

Au1—Cl2	2.2807 (7)	N12—C13	1.331 (4)
Au1—Cl3	2.3116 (7)	C13—C14	1.389 (5)
Au1—Cl4	2.2780 (7)	C13—H131	0.897
Au1—C5	2.007 (2)	C14—C15	1.361 (4)

C5—N6	1.346 (3)	C14—H141	0.944
C5—N9	1.342 (3)	C15—H151	0.972
N6—C7	1.388 (3)	C16—N17	1.432 (3)
N6—C16	1.468 (3)	C16—H162	1.024
C7—C8	1.342 (3)	C16—H161	0.984
C7—H71	0.914	N17—N18	1.354 (3)
C8—N9	1.387 (3)	N17—C21	1.356 (3)
C8—H81	0.981	N18—C19	1.325 (3)
N9—C10	1.470 (3)	C19—C20	1.390 (4)
C10—N11	1.435 (3)	C19—H191	0.997
C10—H101	0.947	C20—C21	1.364 (4)
C10—H102	0.900	C20—H201	0.969
N11—N12	1.346 (3)	C21—H211	0.906
N11—C15	1.357 (3)		
Cl2—Au1—Cl3	91.47 (3)	N9—C10—N11	111.30 (18)
Cl2—Au1—Cl4	177.44 (2)	C10—N11—N12	119.9 (2)
Cl3—Au1—Cl4	90.13 (3)	C10—N11—C15	127.8 (2)
Cl2—Au1—C5	89.37 (7)	N12—N11—C15	112.4 (2)
Cl3—Au1—C5	179.11 (6)	N11—N12—C13	103.8 (2)
Cl4—Au1—C5	89.02 (6)	N12—C13—C14	112.3 (3)
Au1—C5—N6	127.06 (16)	C13—C14—C15	104.9 (3)
Au1—C5—N9	127.00 (17)	C14—C15—N11	106.6 (3)
N6—C5—N9	105.91 (19)	N6—C16—N17	111.26 (18)
C5—N6—C7	110.20 (19)	C16—N17—N18	119.37 (19)
C5—N6—C16	125.97 (19)	C16—N17—C21	127.7 (2)
C7—N6—C16	123.8 (2)	N18—N17—C21	112.7 (2)
N6—C7—C8	106.7 (2)	N17—N18—C19	103.6 (2)
C7—C8—N9	106.9 (2)	N18—C19—C20	112.4 (2)
C8—N9—C5	110.23 (19)	C19—C20—C21	105.2 (2)
C8—N9—C10	123.84 (19)	C20—C21—N17	106.1 (2)
C5—N9—C10	125.9 (2)		

## Selected hydrogen-bond parameters

$D-H\cdots A$	$D-H$ (Å)	$H\cdots A$ (Å)	$D\cdots A$ (Å)	$D-H\cdots A$ (°)
C8—H81 $\cdots$ N18 <sup>i</sup>	0.981	2.581	3.495 (4)	155.06 (7)
C16— H162 $\cdots$ N12 <sup>ii</sup>	1.024	2.545	3.504 (4)	155.78 (7)

Symmetry code(s): (i)  $x-1, y, z$ ; (ii)  $-x+1, -y+1, -z+2$ .



## 7.2. Catalysis data

## 7.2.1. Catalysis data for chapter 2

## 7.2.1.1. Catalysed transfer hydrogenation of acetophenone using Ru(II) complexes

3-6.

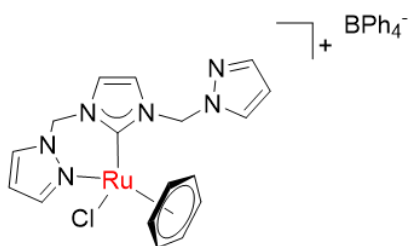
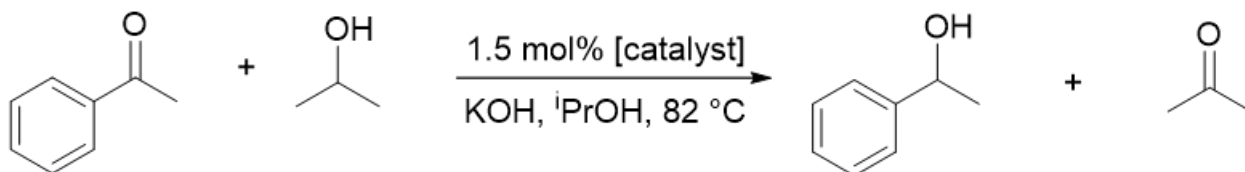


Table 7.1 Catalysed transfer hydrogenation of acetophenone using 3.

Time (h)	% conversion
0.5	80
4	84

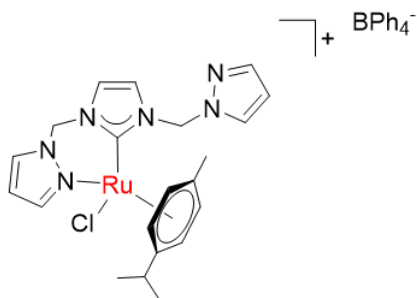
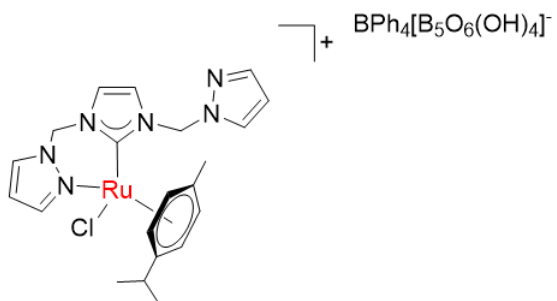
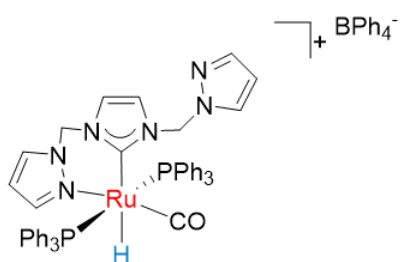


Table 7.2 Catalysed transfer hydrogenation of acetophenone using 4

Time (h)	% conversion
0.5	39
1	55
1.5	67
2	82
2.5	88
3	92
3.5	94
4	100

**Table 7.3** Catalysed transfer hydrogenation of acetophenone using **4a**

Time (h)	% conversion
0.5	91
1	96
1.5	96
2	96
2.5	97
4	100

**Table 7.4** Catalysed transfer hydrogenation of acetophenone using **5**

Time (h)	% conversion
3.5	24
4	35
27	100

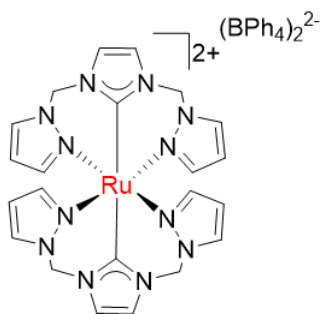
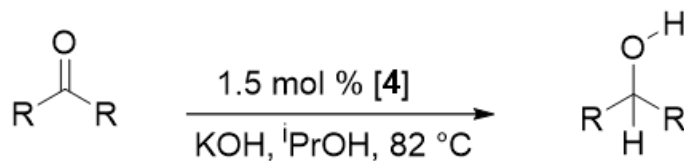


Table 7.5 Catalysed transfer hydrogenation of acetophenone using 7

Time (h)	% conversion
0.5	6
4	14
22.5	25

7.2.1.2. Catalysed transfer hydrogenation of a range of ketone substrates using complex 4.



Substrate = Benzophenone

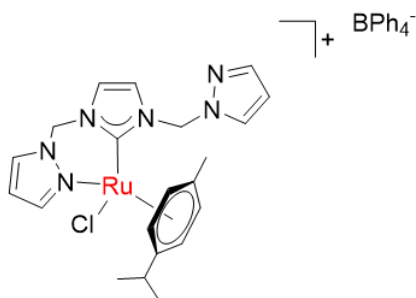
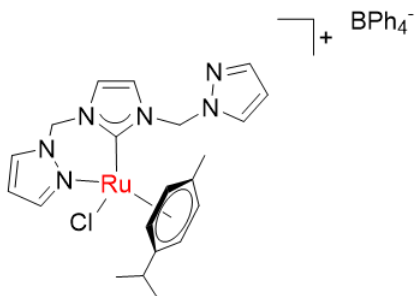


Table 7.6 Catalysed transfer hydrogenation of benzophenone using 4

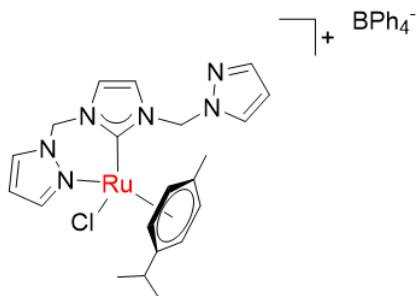
Time (h)	% conversion
0.16	49
0.33	59
0.5	69
1	80
1.5	90
2	97
2.5	99
3	100

Substrate = 4- nitro-acetophenone

**Table 7.7** Catalysed transfer hydrogenation of 4-nitro-acetophenone using **4**

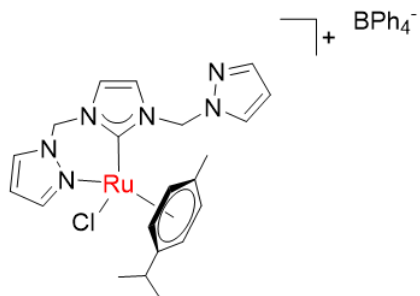
Time (h)	% conversion
0.5	0
4	0

Substrate = Cyclohexanone

**Table 7.8** Catalysed transfer hydrogenation of cyclohexanone using **4**

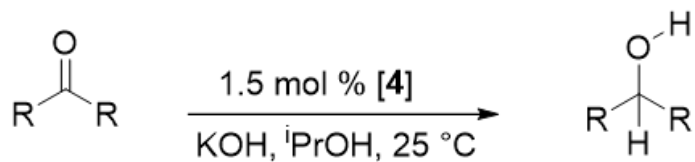
Time (h)	% conversion
0.16	51
0.33	63
0.5	72
1	86
1.5	96
2	100

Substrate = 2-hexanone

**Table 7.9** Catalysed transfer hydrogenation of 2-hexanone using **4**

Time (h)	% conversion
0.16	22
0.33	34
0.5	44
1	66
1.5	76
2	78
2.5	86
3	92
3.5	100

7.2.1.3. Catalysed transfer hydrogenation of a range of ketone substrates using complex 4 at room temperature conditions.



Substrate = Benzophenone

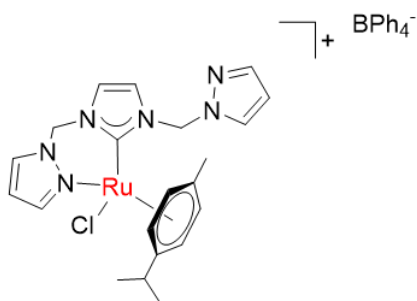
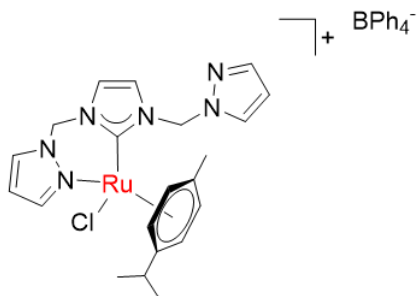


**Table 7.10** Catalysed transfer hydrogenation of benzophenone at r.t. using 4

Time (h)	% conversion
0.5	0
4	0

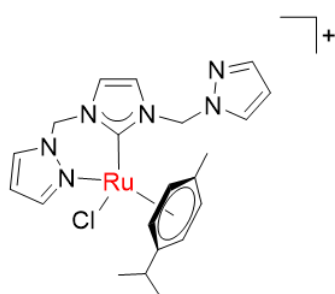


Substrate = 4- nitro-acetophenone

**Table 7.11** Catalysed transfer hydrogenation of 4-nitro-acetophenone at r.t. using 4

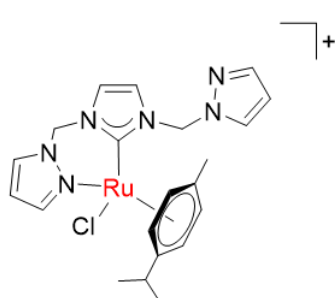
Time (h)	% conversion
0.5	0
4	0

Substrate = Cyclohexanone

+ BPh<sub>4</sub><sup>-</sup>**Table 7.12** Catalysed transfer hydrogenation of cyclohexanone at r.t. using **4**

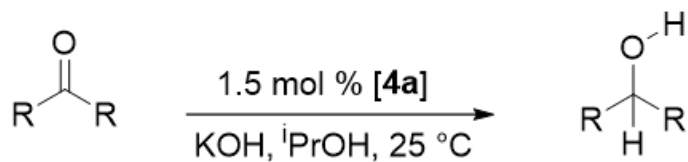
Time (h)	% conversion
0.5	0
4	0

Substrate = 2-hexanone

+ BPh<sub>4</sub><sup>-</sup>**Table 7.13** Catalysed transfer hydrogenation of 2-hexanone at r.t. using **4**

Time (h)	% conversion
0.5	0
4	0

7.2.1.4. Catalysed transfer hydrogenation of a range of ketone substrates using **4a** at room temperature conditions



Substrate = acetophenone

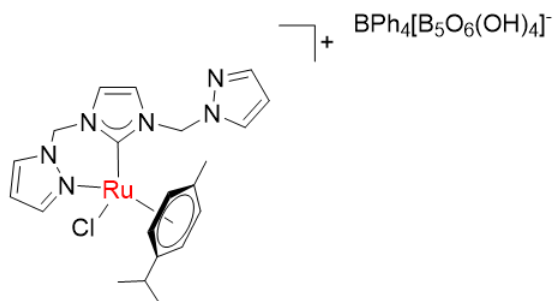
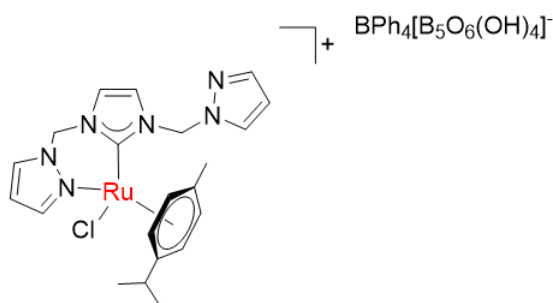


**Table 7.14** Catalysed transfer hydrogenation of acetophenone at r.t. using **4a**

Time (h)	% conversion
0.5	3
1	5
1.5	8
2	8
2.5	10
3	12
24	51

Substrate = Benzophenone

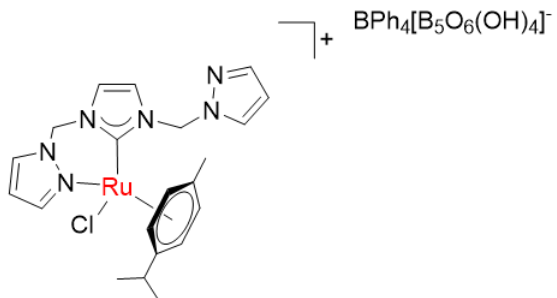
**Table 7.15** Catalysed transfer hydrogenation of benzophenone at r.t. using **4a**



Time (h)	% conversion
4	12
24	41

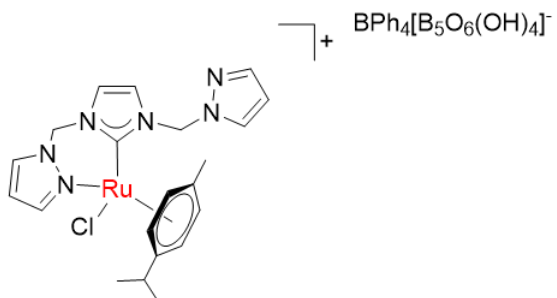


Substrate = 4-nitro-acetophenone

**Table 7.16** Catalysed transfer hydrogenation of 4-nitro-acetophenone at r.t. using **4a**

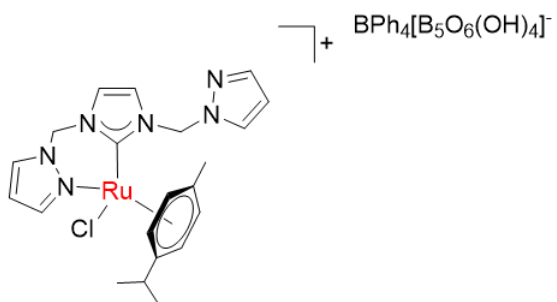
Time (h)	% conversion
0.5	0
4	0

Substrate = Cyclohexanone

**Table 7.17** Catalysed transfer hydrogenation of cyclohexanone at r.t. using **4a**

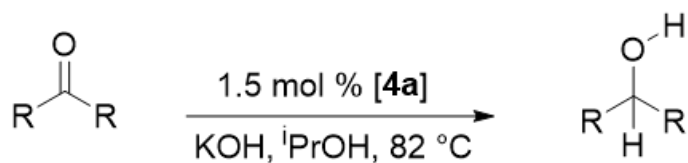
Time (h)	% conversion
0.5	3
1	7
1.5	8
4	10
24	59

Substrate = 2-hexanone

**Table 7.18** Catalysed transfer hydrogenation of 2-hexanone at r.t. using **4a**

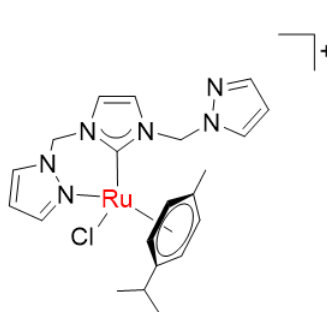
Time (h)	% conversion
0.5	0
4	0

## 7.2.1.5. Catalysed transfer hydrogenation of a range of ketone substrates using 4a.

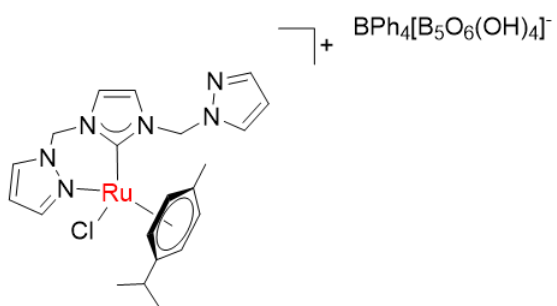


Substrate = Benzophenone

**Table 7.19** Catalysed transfer hydrogenation of benzophenone using 4a

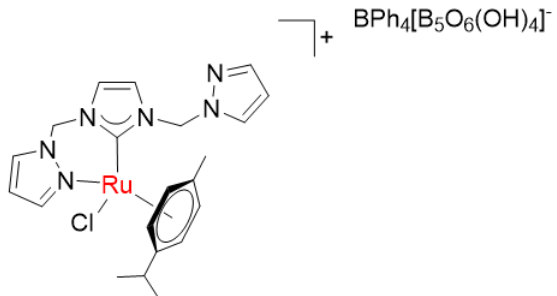
	$\text{BPh}_4[\text{B}_5\text{O}_6(\text{OH})_4]^-$	Time (h)	% conversion
		0.16	66
		0.33	83
		0.5	91
		1	91
		1.5	91
		2	100

Substrate = 4-nitro-acetophenone

**Table 7.20** Catalysed transfer hydrogenation of 4-nitro-acetophenone at using 4a

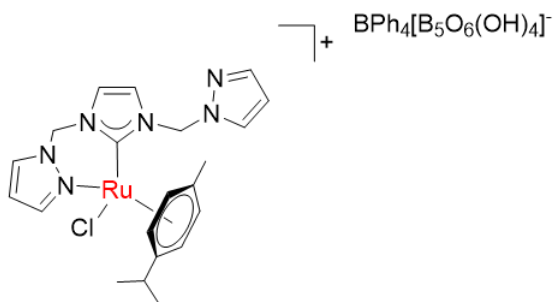
Time (h)	% conversion
0.5	0
4	0

Substrate = Cyclohexanone

**Table 7.21** Catalysed transfer hydrogenation of cyclohexanone at using **4a**

Time (h)	% conversion
0.16	58
0.33	82
0.5	92
1	100

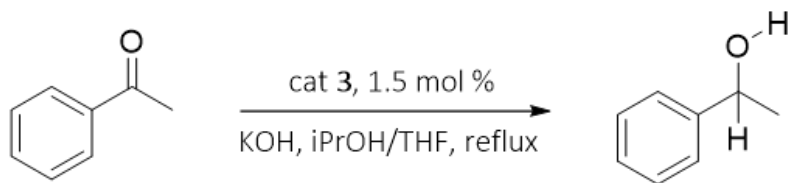
Substrate = 2-hexanone

**Table 7.22** Catalysed transfer hydrogenation of 2-hexanone at using **4a**

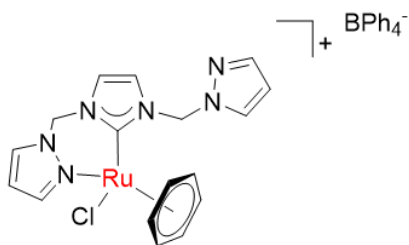
Time (h)	% conversion
0.5	0
4	0

## 7.2.1.6. Catalysed transfer hydrogenation of acetophenone using 3 with THF/iPrOH

solvent mix.



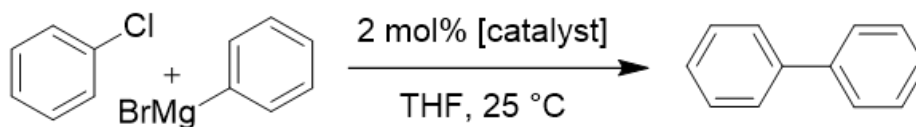
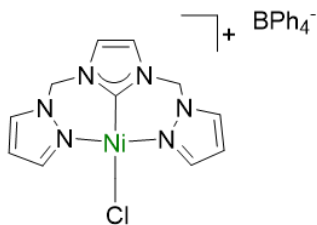
Substrate = acetophenone

**Table 7.23** Catalysed transfer hydrogenation of acetophenone with THF/iPrOH using 4

Time (h)	% conversion
0.16	47
0.33	61
0.5	87
1	91
1.5	97
2	100

## 7.2.2. Catalysis data for chapter 3

## 7.2.2.1. Catalysed Kumada Cross Coupling of chlorobenzene with phenylmagnesium bromide using complexes 8, 9 and 10.

Table 7.24 Catalysed Kumada Cross Coupling of chlorobenzene using **8**

Time (h)	% conversion
0.25	17
0.5	20
0.75	23
1	28
1.25	39
1.75	58
2.25	60
2.75	66
3.25	74
4	89
6	99

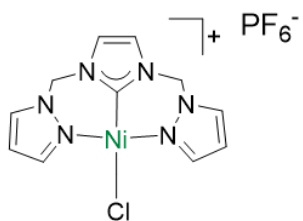
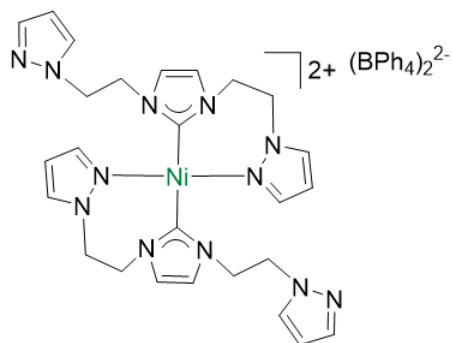


Table 7.25 Catalysed Kumada Cross Coupling of chlorobenzene using 9

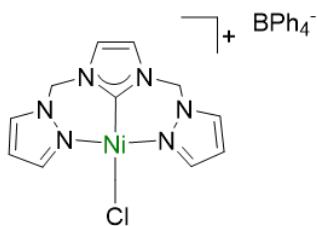
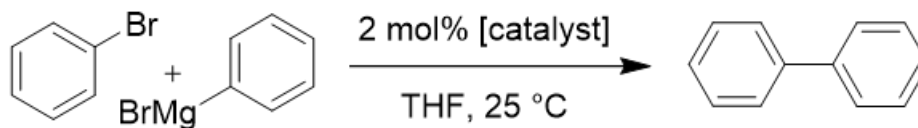
Time (h)	% conversion
0.25	9
0.5	9
0.75	9
1.75	15
6	40
20	40

Table 7.26 Catalysed Kumada Cross Coupling of chlorobenzene using 10



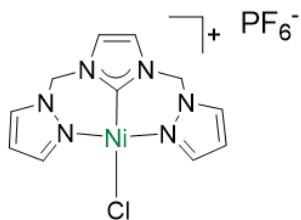
Time (h)	% conversion
0.25	40
0.5	40
4	40

7.2.2.2. Catalysed Kumada Cross Coupling of bromobenzene and phenylmagnesium bromide using complexes 8, 9 and 10.

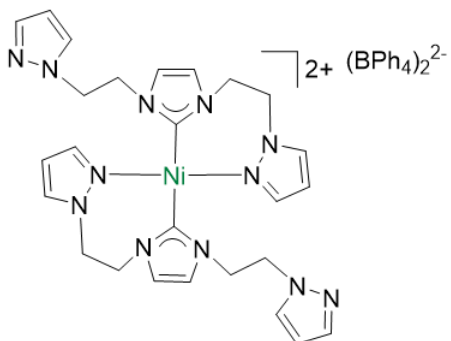


**Table 7.27** Catalysed Kumada Cross Coupling of bromobenzene using **8**

Time (h)	% conversion
0.25	50
0.5	50
0.75	65
1	69
1.25	72
1.75	74
2.25	80
2.75	87
3.25	87

**Table 7.28** Catalysed Kumada Cross Coupling of bromobenzene using **9**

Time (h)	% conversion
0.25	10
0.5	18
0.75	25
1	27
1.25	27
1.75	46
2.25	68
2.75	80
3.25	84
4	87
5.75	89
24	100

**Table 7.29** Catalysed Kumada Cross Coupling of bromobenzene using **10**

Time (h)	% conversion
0.25	17
0.5	28
1	40
4	40



7.2.2.3. Catalysed Kumada Cross Coupling reaction of iodobenzene with phenylmagnesium bromide using **8**.

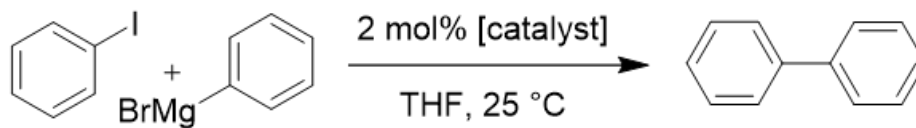
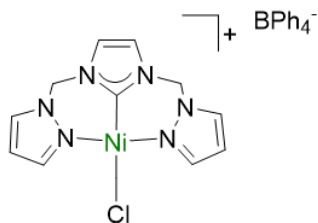
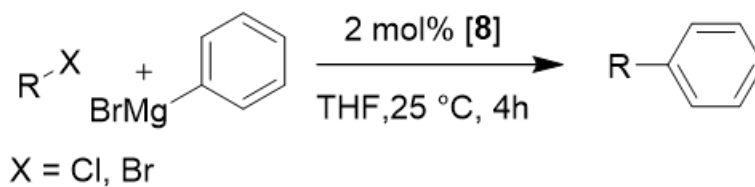


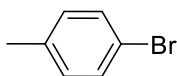
**Table 7.30** Catalysed Kumada Cross Coupling of iodobenzene using **8**



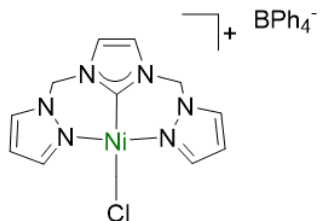
Time (h)	% conversion
0.16	57
0.5	74
1.25	97
1.75	100

7.2.2.4. Catalysed Kumada Cross Coupling of a range of halogenated substrates with phenylmagnesium bromide using **8**.

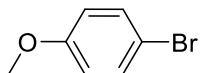




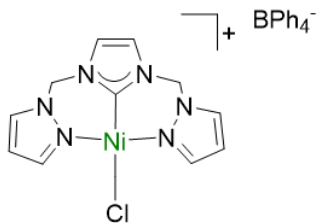
**Table 7.31** Catalysed Kumada Cross Coupling of tolylbromide using **8**



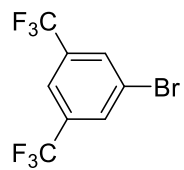
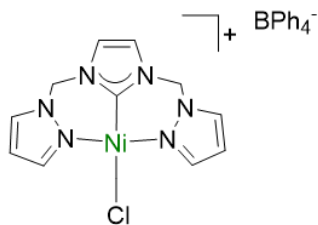
Time (h)	% conversion
0.5	39
0.75	58
1	60
1.25	63
1.5	70
2	73
2.25	78
4	78



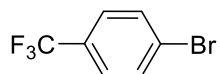
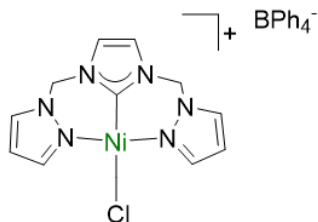
**Table 7.32** Catalysed Kumada Cross Coupling of 4-methoxy-phenylbromide using **8**



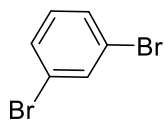
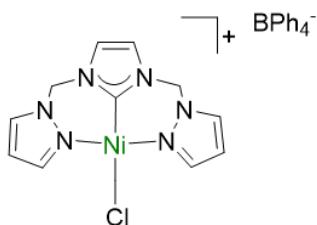
Time (h)	% conversion
0.25	17
3	50

**Table 7.33** Catalysed Kumada Cross Coupling of 1,3-difluoromethyl-phenylbromide using **8**

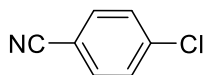
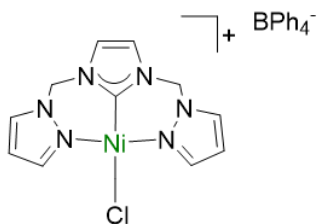
Time (h)	% conversion
0.25	2
1.25	29
3	68

**Table 7.34** Catalysed Kumada Cross Coupling of 4-fluoromethyl-phenylbromide using **8**

Time (h)	% conversion
1.25	13
3	16

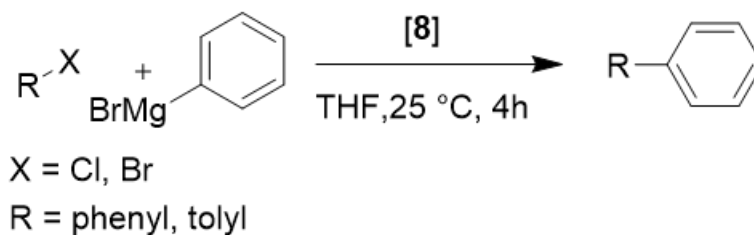
**Table 7.35** Catalysed Kumada Cross Coupling of 1,3-dibromobenzene using **8**

Time (h)	% conversion
3	67
6	67

**Table 7.36** Catalysed Kumada Cross Coupling of 4-cyano-phenylchloride using **8**

Time (h)	% conversion
0.5	0
3	0
4	0

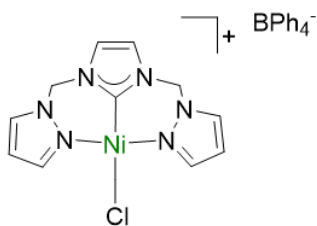
7.2.2.5. Catalysed Kumada Cross Coupling of a range of substrates with phenylmagnesium bromide using **8** at different catalyst loadings



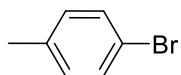
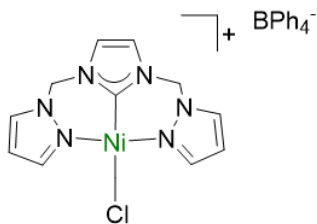
1 mol% catalyst **8**

**Table 7.37** Catalysed Kumada Cross Coupling of chlorobenzene using **8** at 1mol% catalyst loading

Substrate = Chlorobenzene

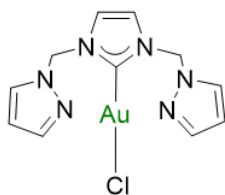
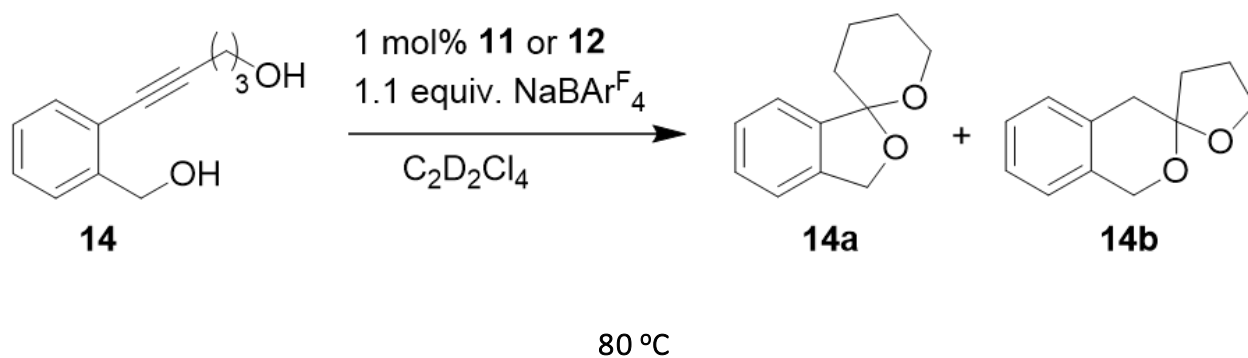


Time (h)	% conversion
0.25	35
1.25	39
4	43

5 mol% catalyst **8****Table 7.38** Catalysed Kumada Cross Coupling of tolylbromide using **8** at 5 mol% catalyst loading

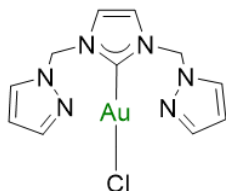
Time (h)	% conversion
0.5	34
0.75	56
1	60
1.25	63
1.5	71
1.75	72
2.25	75
4	75

## 7.2.3. Catalysis data for chapter 4

7.2.3.1. Catalysed dihydroalkoxylation reactions of **14** using complexes **11** or **12**.**Table 7.39** Catalysed dihydroalkoxylation of **14** using **11** at 80 °C.

Time(h)	%conversion
0	0
0.0225	91.24828467
0.033888889	98.17357504
0.041666667	99.28325695
0.049444444	99.69360836
0.057222222	99.76894767
0.065	99.9225853
0.0725	99.85434797

100 °C

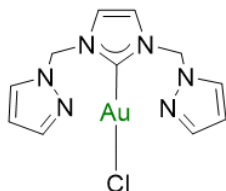
**Table 7.40** Catalysed dihydroalkoxylation of **14** using **11** at 100 °C.

Time (h)	% conv.
0	0
0.035833333	53.26479
0.045555556	59.42211
0.053055556	62.41782
0.060833333	65.21566
0.068611111	67.12119
0.076111111	70.3251
0.083888889	70.94524
0.091666667	73.025
0.099166667	74.26086
0.106944444	75.72667
0.114444444	74.42903
0.122222222	77.13883
0.131111111	78.45597
0.140277778	79.68174
0.149444444	79.73344
0.158611111	79.21114
0.167777778	80.63124
0.176666667	80.76303
0.185833333	80.94895
0.194722222	81.49323
0.203888889	80.64978
0.213055556	81.49763
0.2275	80.79814
0.242222222	81.53135
0.256944444	82.64867
0.271666667	82.33742
0.286388889	82.99134
0.300833333	84.21906
0.315555556	82.63602
0.330277778	81.30751
0.344722222	83.59704
0.359444444	84.07445
0.3825	85.27523
0.405555556	85.07555
0.428333333	83.45988
0.451388889	85.09716
0.474166667	85.33655
0.497222222	85.99142



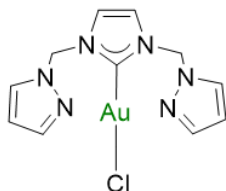
0.520277778	86.34445
0.543333333	84.88706
0.566111111	85.81258
0.589166667	86.8089
0.628888889	87.00545
0.668333333	84.26898
0.708055556	86.46764
0.747777778	87.48134

70 °C

**Table 7.41** Catalysed dihydroalkoxylation of **14** using **11** at 70 °C.

Time(h)	%conversion
0.006667	20.54232
0.013333	29.53276
0.02	37.0868
0.026667	44.50796
0.033056	51.54905
0.039722	58.42841
0.046667	64.63631
0.053056	70.28231
0.059722	75.21691
0.066389	79.65203
0.073056	83.3559
0.081111	86.86407
0.089167	89.90064
0.097222	92.17501
0.105278	93.95854
0.113333	95.36354
0.121389	96.40939
0.129444	97.24073
0.137222	97.79392
0.145278	98.30438
0.153333	98.63678
0.166944	99.09167
0.180556	99.33176
0.194167	99.47234
0.207778	99.5873
0.221389	99.67362
0.235	99.80683
0.248333	99.90566
0.261944	99.84319
0.275556	99.90628

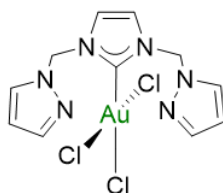
25 °C

**Table 7.42** Catalysed dihydroalkoxylation of **14** using **11** at 25 °C.

Time(h)	%conv
0	0%
0.017778	26%
0.017778	31%
0.024444	35%
0.031111	38%
0.037778	40%
0.044167	43%
0.050833	44%
0.0575	47%
0.064167	49%
0.070556	52%
0.077222	52%
0.083889	55%
0.091944	57%
0.1	59%
0.108056	60%
0.115833	62%
0.123889	63%
0.131944	64%
0.14	65%
0.148056	67%
0.156111	68%
0.163889	69%
0.1775	71%
0.191111	73%
0.204722	74%
0.218333	75%
0.231944	76%
0.245556	77%
0.258889	78%
0.2725	79%
0.286111	80%
0.299722	82%
0.338333	84%
0.377222	86%
0.415833	87%
0.454444	88%
0.493056	89%
0.531667	90%

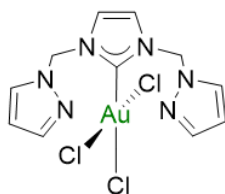
0.570556	91%
0.609167	92%
0.647778	92%
0.686389	93%
0.775	95%
0.863611	95%
0.9525	96%
1.041111	97%
1.129722	98%
1.218333	98%
1.306944	98%
1.395556	98%

70 °C

**Table 7.43** Catalysed dihydroalkoxylation of **14** using **12** at 70 °C.

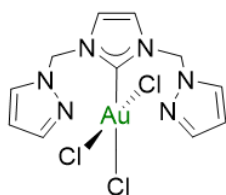
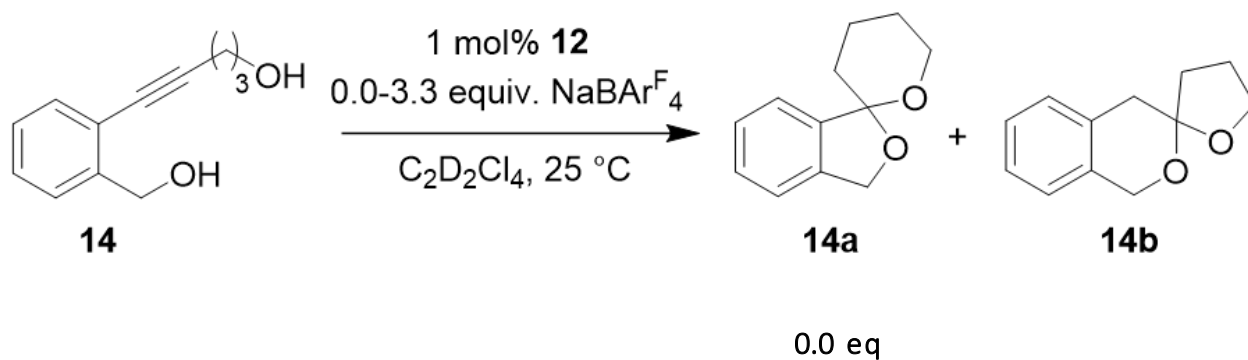
Time(h)	%conv
0	0%
0.017778	100%

25 °C

**Table 7.44** Catalysed dihydroalkoxylation of **14** using **12** at 25 °C.

Time(h)	%conv
0	0%
0.014444	55%
0.028889	66%
0.040278	74%
0.051667	81%
0.062778	86%
0.074167	90%
0.085556	93%
0.096667	95%
0.108056	96%
0.119444	97%
0.130833	98%
0.141944	99%
0.154722	99%
0.1675	100%

0.18	100%
0.192778	100%

7.2.3.2. Catalysed dihydroalkoxylation of **14** using **12** with differing NaBAr<sup>F</sup><sub>4</sub> loadings

**Table 7.45** Catalysed dihydroalkoxylation of **14** using **12** and 0.0 eq NaBAr<sup>F</sup><sub>4</sub> at 25 °C.

Time(h)	%conv
0	0
0.017778	26%
0.017778	31%
0.024444	35%
0.031111	38%
0.037778	40%
0.044167	43%
0.050833	44%
0.0575	47%
0.064167	49%
0.070556	52%
0.077222	52%
0.083889	55%
0.091944	57%
0.1	59%
0.108056	60%
0.115833	62%
0.123889	63%
0.131944	64%
0.14	65%
0.148056	67%
0.156111	68%
0.163889	69%
0.1775	71%

0.191111	73%
0.204722	74%
0.218333	75%
0.231944	76%
0.245556	77%
0.258889	78%
0.2725	79%
0.286111	80%
0.299722	82%
0.338333	84%
0.377222	86%
0.415833	87%
0.454444	88%
0.493056	89%
0.531667	90%
0.570556	91%
0.609167	92%
0.647778	92%
0.686389	93%
0.775	95%
0.863611	95%
0.9525	96%
1.041111	97%
1.129722	98%
1.218333	98%
1.306944	98%
1.395556	98%

2.2 eq

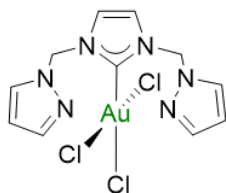


**Table 7.46** Catalysed dihydroalkoxylation of **14** using **12** and 2.2 eq NaBAr<sup>F</sup><sub>4</sub> at 25 °C.

time(h)	%conv
0	0%
0.017778	58%
0.024444	63%
0.031111	68%
0.037778	70%
0.044167	73%
0.050833	75%
0.0575	77%
0.064167	80%

0.070556	81%
0.077222	83%
0.083889	85%
0.091944	86%
0.1	88%
0.108056	89%
0.115833	90%
0.123889	92%
0.131944	94%
0.14	95%
0.148056	96%
0.156111	97%
0.163889	98%
0.1775	99%

3.3 eq

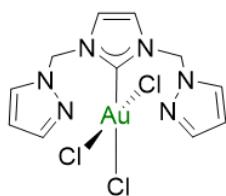
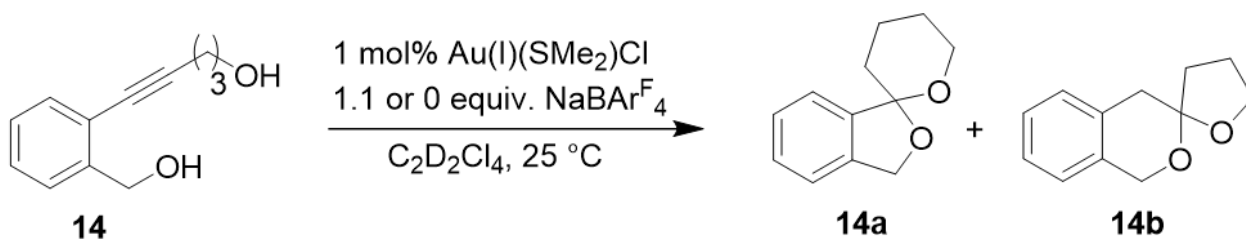


**Table 7.47** Catalysed dihydroalkoxylation of **14** using **12** and 3.3 eq NaBAr<sup>F</sup><sub>4</sub> at 25 °C.

time(h)	%conv
0	0%
0.017222	67%
0.023889	73%
0.030556	78%
0.037222	84%
0.043611	86%
0.050278	89%
0.056944	93%
0.063611	95%
0.07	97%
0.076667	99%
0.083333	100%

7.2.3.3. Catalysed dihydroalkoxylation of **14** using Au(I)(SMe<sub>2</sub>)Cl



0.0 eq NaBArF<sub>4</sub>**Table 7.48** Catalysed dihydroalkoxylation of **14** using Au(I)(SMe<sub>2</sub>)Cl and 0.0 eq NaBArF<sub>4</sub> at 25 °C.

Time(h)	%conv
0	0%
0.018056	16%
0.024722	19%
0.031111	21%
0.037778	24%
0.044444	26%
0.051111	27%
0.057778	29%
0.064444	31%
0.071111	32%
0.077778	33%
0.084167	34%
0.092222	36%
0.100278	37%
0.108333	38%
0.116389	39%
0.124444	39%
0.1325	40%
0.140556	42%
0.148611	42%
0.156667	43%
0.164444	43%
0.178056	44%
0.191667	45%
0.205278	46%
0.218889	47%
0.2325	47%
0.245833	48%
0.259444	49%
0.273056	49%
0.286667	50%
0.300278	50%
0.338889	52%
0.3775	54%
0.416111	55%
0.455	55%
0.493611	57%
0.532222	57%



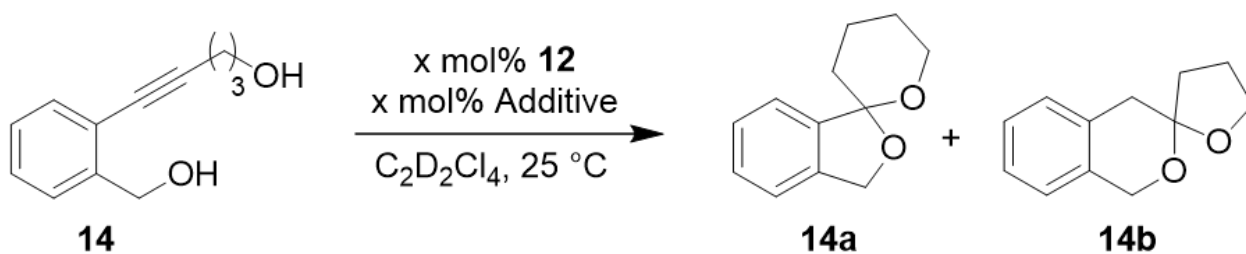
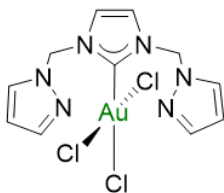
0.570833	58%
0.609444	59%
0.648056	59%
0.686944	60%
0.775556	61%
0.864167	62%
0.952778	64%
1.041389	65%
1.13	66%
1.218611	67%
1.3075	68%
1.396111	68%
1.484722	69%
2.778611	70%

1.1 eq NaBAr<sup>F</sup><sub>4</sub>

**Table 7.49** Catalysed dihydroalkoxylation of **14** using Au(I)(SMe<sub>2</sub>)Cl and 1.1 eq NaBAr<sup>F</sup><sub>4</sub> at 25 °C.

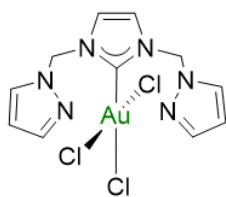
Time(h)	%conv
0	0%
0.044722	15%
0.051389	18%
0.058333	22%
0.064722	22%
0.071389	23%
0.078056	25%
0.084722	27%
0.091389	32%
0.098056	31%
0.104722	35%
0.111389	37%
0.119444	41%
0.127222	45%
0.135278	46%
0.143333	48%
0.151389	53%
0.159444	56%
0.167778	61%
0.175556	65%

0.183611	70%
0.191667	75%
0.205278	84%
0.218889	92%
0.2325	97%
0.246111	98%
0.259722	100%

7.2.3.4. Catalysed dihydroalkoxylation of **14** using **12** at reduced catalytic loadings0.1 mol% **12**, 0.11 mol% NaBAr<sup>F</sup><sub>4</sub>**Table 7.50** Catalysed dihydroalkoxylation of **14** using 0.1 mol% **12** and 1.1 eq NaBAr<sup>F</sup><sub>4</sub> at 25 °C.

Time(h)	%conv
0	0%
0.036667	30%
0.043333	30%
0.05	30%
0.056667	30%
0.063333	31%
0.07	31%
0.076389	31%
0.083056	32%
0.089722	31%
0.096389	31%
0.103056	31%
0.111111	32%
0.118889	32%
0.126944	32%
0.135	32%
0.143056	32%

0.151111	33%
0.158611	32%
0.166667	32%
0.174722	32%
0.182778	33%
0.196111	32%
0.209722	33%
0.223333	33%
0.236944	33%
0.250556	33%
0.264167	33%
0.277778	33%
0.291389	33%
0.304722	33%
0.318333	34%
0.356944	33%
0.395833	34%
0.434444	34%
0.473056	34%
0.511667	34%
0.550278	35%
0.588889	35%
0.6275	35%

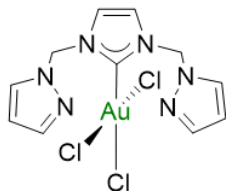


0.01mol% **12**, 0.011 mol% NaBAr<sup>F</sup><sub>4</sub>

**Table 7.51** Catalysed dihydroalkoxylation of **14** using 0.01 mol% **12** and 1.1 eq NaBAr<sup>F</sup><sub>4</sub> at 25 °C.

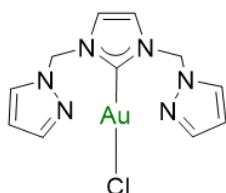
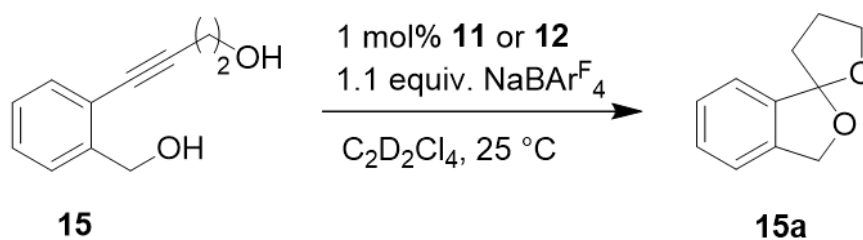
Time(h)	%conv
0	0%
0.035	6%
0.041667	9%
0.048333	9%

0.055	10%
0.068333	10%
0.075	10%

1 mol% **12**, 1.1 mol% AgSbF<sub>6</sub>**Table 7.52** Catalysed dihydroalkoxylation of **14** using 1 mol% **12** and 1.1 eq AgSbF<sub>6</sub> at 25 °C.

Time(h)	%conv
0	0%
0.035	69%
0.041667	71%
0.048333	73%
0.055	75%
0.061667	76%
0.068333	77%
0.075	79%
0.081667	79%
0.088333	81%
0.095	81%
0.101667	82%
0.109722	83%
0.117778	84%
0.125833	84%
0.133611	85%
0.141667	85%
0.149722	86%
0.157778	86%
0.165833	87%
0.173889	87%
0.181944	87%
0.195556	88%
0.208889	88%
0.2225	89%
0.236111	89%
0.249722	89%
0.263333	90%
0.276944	90%
0.290278	90%
0.303889	90%
0.3175	91%
0.356389	91%
0.395	91%
0.433611	92%
0.472222	92%
0.510833	92%
0.549722	92%
0.588333	92%

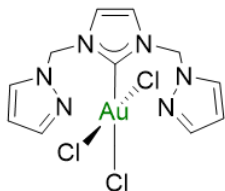
0.626944	92%
0.665556	93%
0.704167	93%
0.792778	93%
0.881389	93%
0.97	93%
1.058889	93%
1.1475	93%
1.236111	93%
1.324722	93%
1.413333	93%
1.501944	93%

7.2.3.5. Catalysed dihydroalkoxylation of **15** using **11** or **12**

**Table 7.53** Catalysed dihydroalkoxylation of **15** using **11** and 1.1 eq NaBArF<sub>4</sub> at 25 °C.

Time(h)	%conv
0	0%
0.034722	7%
0.041389	7%
0.048056	9%
0.054722	11%
0.061111	10%
0.067778	12%
0.074444	13%
0.081111	14%
0.087778	15%
0.094444	15%
0.101111	17%
0.109167	17%
0.116944	21%

0.125	22%
0.133056	23%
0.141111	24%
0.149167	22%
0.157222	26%
0.165278	26%
0.173333	27%
0.181111	29%
0.194722	30%
0.208333	30%
0.221944	29%
0.235556	34%
0.249167	35%
0.2625	36%
0.276389	34%
0.289722	38%
0.303333	39%
0.316944	40%
0.355556	44%
0.394167	47%
0.432778	50%
0.471389	52%
0.510278	54%
0.548889	57%
0.5875	59%
0.626111	62%
0.664722	62%
0.703611	64%
0.792222	69%
0.880833	74%
0.969444	78%
1.058056	81%
1.146667	84%
1.235556	87%
1.324167	89%
1.412778	90%
1.501389	91%
1.625556	93%
1.953333	96%

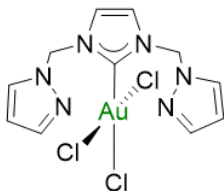
Table 7.54 Catalysed dihydroalkoxylation of **15** using **12** and 1.1 eq NaBARF<sub>4</sub> at 25 °C.

time(h)	%conv
0	0%
0.035	44%
0.041667	55%
0.048333	63%
0.055	69%
0.061667	73%
0.068333	76%
0.075	79%
0.081389	81%
0.088056	83%
0.094722	85%
0.101389	86%
0.109444	88%
0.1175	89%
0.125556	90%
0.133611	91%
0.141667	92%
0.149722	93%
0.1575	94%
0.165556	95%
0.173611	95%
0.181667	96%
0.195278	97%
0.208889	97%
0.2225	98%
0.236111	98%
0.249444	99%
0.263056	99%
0.276667	99%



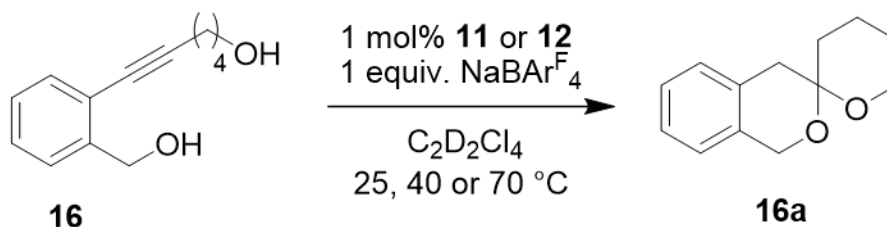
1 mol% **12**, 1.1 eq AgSbF<sub>6</sub>**Table 7.55** Catalysed dihydroalkoxylation of **15** using **12** and 1.1 eq AgSbF<sub>6</sub> at

25 °C.

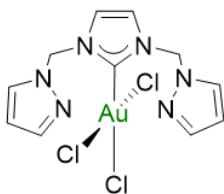


Time(h)	%conv
0	0%
0.033611	33%
0.04	37%
0.046667	41%
0.053333	43%
0.06	46%
0.066667	49%
0.073333	52%
0.08	55%
0.086667	56%
0.093333	59%
0.1	60%
0.108056	63%
0.116111	65%
0.124167	66%
0.132222	69%
0.140278	70%
0.148056	72%
0.156111	73%
0.164167	74%
0.172222	75%
0.180278	76%
0.193889	78%
0.2075	80%
0.220833	81%
0.234444	82%
0.248056	83%
0.261667	84%
0.275278	86%
0.288889	86%
0.302222	87%
0.315833	88%
0.354444	90%
0.393333	91%
0.431944	92%
0.470556	93%

0.509167	94%
0.547778	95%
0.586389	95%
0.625278	96%
0.663889	96%
0.7025	96%
0.791111	97%
0.879722	97%
0.968333	98%
1.056944	98%
1.145833	98%
1.234444	98%
1.323056	98%
1.411667	99%
1.500278	99%

7.2.3.6. Catalysed dihydroalkoxylation of **16** using **11** or **12**.

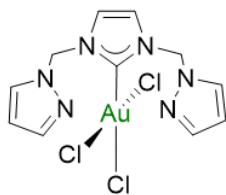
70 °C

**Table 7.56** Catalysed dihydroalkoxylation of **16** using **11** and 1.1 eq NaBARF<sub>4</sub> at 70 °C.

Time(h)	%conversion
0.005556	0.246159
0.012222	0.29028
0.018889	2.157607
0.025556	1.091563
0.032222	2.284552
0.038889	3.334587
0.045556	2.10126
0.052222	4.277357
0.058889	5.451882

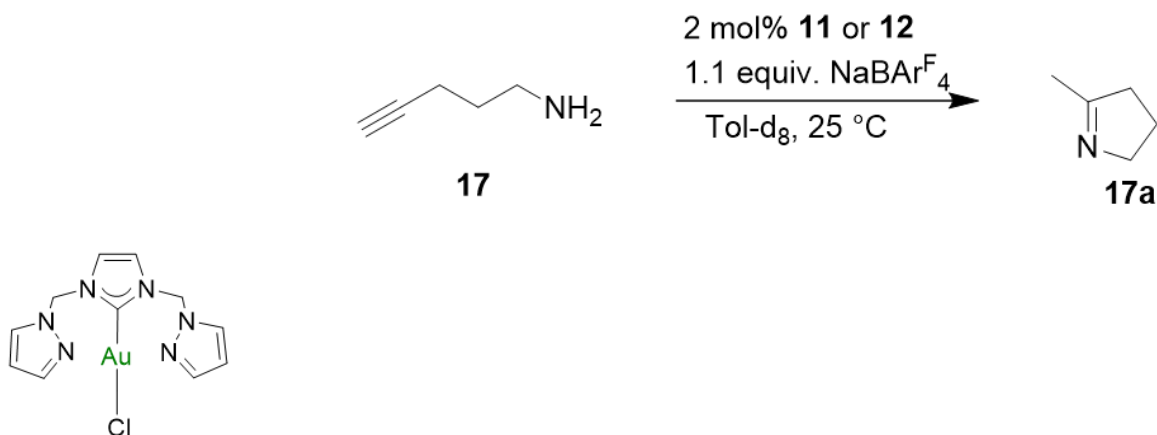
0.065556	5.072372
0.072222	8.117413
0.080278	9.904641
0.088333	10.83527
0.096111	13.86294
0.104167	14.65435
0.112222	17.11979
0.120278	18.36399
0.128333	18.50275
0.136389	19.99718
0.144444	20.66332
0.1525	20.55118
0.166111	21.83937
0.179722	22.29341
0.193333	21.06399
0.206944	22.9386
0.220556	21.92043
0.234167	23.34503
0.247778	23.48182
0.261389	23.5908
0.275	23.70938
0.288611	23.84087
0.327222	22.54701
0.365833	24.27542
0.404722	24.46038
0.443333	23.30172
0.481944	23.66627
0.520556	23.71367
0.559167	23.63021
0.598056	23.91652
0.636667	25.24997
0.675556	24.09889
0.764167	25.50791

40 °C



**Table 7.57** Catalysed dihydroalkoxylation of **16** using **12** and 1.1 eq NaBAR<sub>4</sub><sup>F</sup> at 40 °C.

Time(h)	%conv
0	0%
0.051389	38%
0.058056	38%
0.064722	37%
0.071389	38%
0.078056	37%
0.084722	37%
0.091111	37%
0.097778	36%
0.104444	37%
0.111111	36%
0.117778	37%
0.125833	36%
0.133889	37%
0.141944	36%
0.15	36%
0.158056	37%
0.165833	37%
0.173889	37%
0.181944	37%
0.19	37%
0.198056	35%
0.211667	36%
0.225278	36%
0.238889	36%
0.2525	36%
0.266111	36%
0.279722	37%
0.293333	36%

7.2.3.7. Catalysed hydroamination of **17** using **11** or **12**.**Table 7.58** Catalysed hydroamination of **17** using **11** at 25 °C.

Time(h)	%conv
0	0%
0.050556	3%
0.056944	4%
0.063611	4%
0.070278	4%
0.076944	5%
0.083611	6%
0.090278	5%
0.096667	5%
0.103333	5%
0.11	5%
0.116667	5%
0.124722	6%
0.132778	6%
0.140833	7%
0.148889	6%
0.156944	6%
0.164722	6%
0.172778	6%
0.180833	7%
0.188889	7%
0.196944	7%
0.210278	7%
0.223889	7%
0.2375	8%
0.251111	8%
0.264722	8%
0.278333	9%

0.291667	9%
0.305278	9%
0.318889	9%
0.3325	9%
0.371111	9%
0.41	10%
0.448611	11%
0.487222	11%
0.525833	12%
0.564444	12%
0.603333	13%
0.641944	13%
0.680556	13%
0.719167	13%
0.808056	14%
0.896667	15%
0.985278	15%
1.073889	16%
1.1625	16%
1.251111	17%
1.339722	17%
1.428611	18%
1.517222	18%

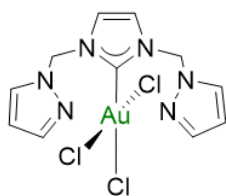


**Table 7.59** Catalysed hydroamination of **17** using **12** at 25 °C.

Time(h)	%conv
0	0%
0.075556	3%
0.082222	3%
0.088889	4%
0.095556	4%
0.101944	4%
0.108889	6%
0.115556	6%
0.122222	6%
0.128611	6%
0.135278	6%
0.141944	6%
0.15	6%

0.158056	7%
0.165833	7%
0.173889	7%
0.181944	8%
0.19	8%
0.197778	8%
0.205833	9%
0.213889	9%
0.221944	9%
0.235556	9%
0.249167	10%
0.262778	10%
0.276111	10%
0.289722	11%
0.303333	11%
0.316944	11%
0.330556	12%
0.343889	12%
0.357778	12%
0.396389	13%
0.435	14%
0.473611	15%
0.512222	15%
0.550833	16%
0.589444	16%
0.628333	17%
0.666944	17%
0.705556	18%
0.744167	18%
0.832778	19%
0.921389	20%
1.01	21%
1.098611	22%
1.187222	23%
1.275833	23%
1.364722	24%
1.453056	24%
1.541667	25%

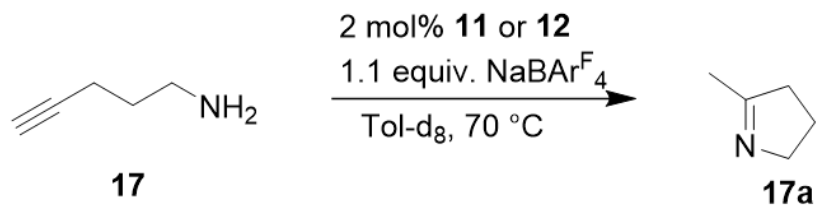
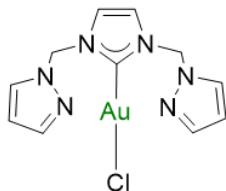


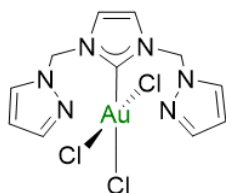
**Table 7.60** Catalysed hydroamination of **17** using **11** at 70 °C.



Time(h)	%conv
0	0%
0.005	11%
0.005	18%
0.011667	22%
0.018333	26%
0.025	29%
0.031667	31%
0.038333	33%
0.045	35%
0.051667	37%
0.058333	39%
0.064722	40%
0.071389	41%
0.079444	43%
0.0875	44%
0.095556	45%
0.103611	46%
0.111389	47%
0.119444	48%
0.1275	49%
0.135556	50%
0.143611	51%
0.151389	52%
0.165	53%
0.178611	54%
0.192222	55%
0.205833	56%
0.219444	57%
0.233056	59%



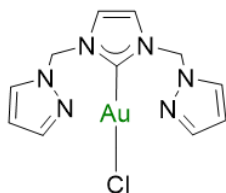
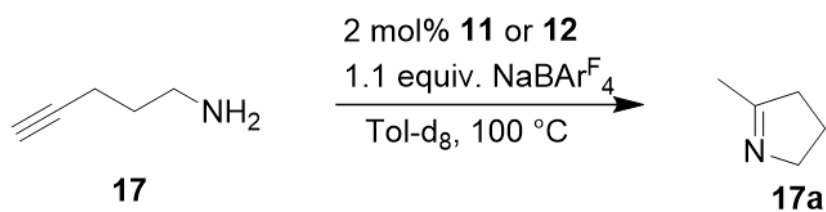
0.246667	59%
0.260278	60%
0.273889	60%
0.2875	62%
0.326111	64%
0.364722	66%
0.403333	67%
0.441944	68%
0.480833	69%



**Table 7.61** Catalysed hydroamination of **17** using **12** at 70 °C.

Time(h)	%conv
0	0%
0.007222	7%
0.013889	12%
0.020556	17%
0.027222	20%
0.033889	22%
0.040556	25%
0.047222	26%
0.053611	28%
0.060556	29%
0.066944	30%
0.073611	31%
0.081667	32%
0.089722	34%
0.097778	35%
0.105556	36%
0.113611	37%
0.121667	38%
0.129722	38%
0.1375	39%
0.145556	40%
0.153611	41%
0.167222	42%
0.180833	43%
0.194444	45%
0.207778	46%
0.221389	47%
0.235	48%
0.248611	49%
0.262222	49%

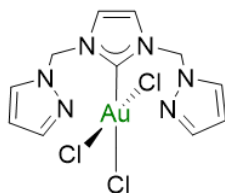
0.275556	50%
0.289167	51%
0.327778	53%
0.366667	55%
0.405278	57%
0.443889	59%
0.4825	60%
0.521111	62%
0.559722	63%
0.598611	65%
0.637222	66%
0.675833	67%
0.764444	70%
0.853056	71%
0.941944	73%
1.030556	75%
1.119167	76%
1.207778	78%
1.296389	79%
1.385	81%



**Table 7.62** Catalysed hydroamination of **17** using **11** at 100 °C.

time(h)	%conv
0	0
0	0%
0.015	58%
0.022778	65%
0.030833	70%
0.038611	73%
0.046944	76%

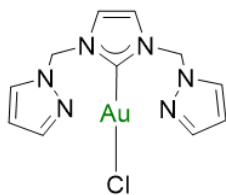
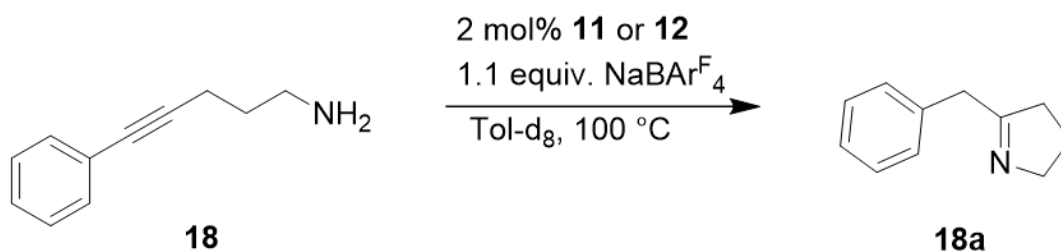
0.055278	79%
0.063056	81%
0.070833	82%
0.079167	83%
0.086667	84%
0.095833	86%
0.105	86%
0.114444	86%
0.123611	88%
0.132778	88%
0.141944	89%
0.151111	89%
0.16	90%
0.169167	90%
0.178333	90%
0.193333	91%
0.208056	91%
0.222778	91%
0.237778	91%
0.2525	92%
0.2675	92%
0.2825	92%
0.296944	93%
0.311944	91%
0.326667	93%
0.35	93%



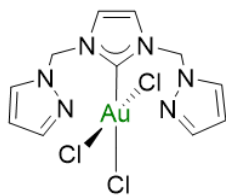
**Table 7.63** Catalysed hydroamination of **17** using **12** at 100 °C.

Time(h)	%conv
0	0%
0.007778	39%
0.015556	51%
0.023333	60%
0.031389	67%
0.039167	71%
0.046944	75%
0.054722	78%
0.0625	81%
0.070278	82%

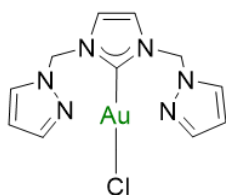
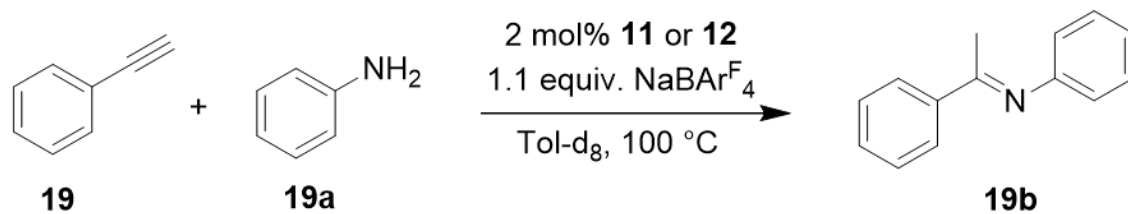
0.078333	85%
0.085833	86%
0.095	87%
0.104167	89%
0.113611	89%
0.122778	91%
0.131667	92%
0.140833	92%
0.150278	94%
0.159722	94%
0.170278	94%
0.179444	95%
0.195	95%
0.209722	96%
0.224722	96%
0.239444	96%
0.254444	97%

7.2.3.8. Catalysed hydroamination of **18** using **11** or **12**.Table 7.64 Catalysed hydroamination of **18** using **11** at 100 °C.

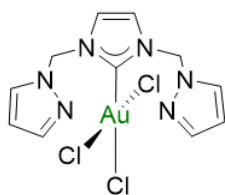
Time(h)	%conv
0	0%
0.033333	50%
0.066667	61%
0.1	76%
0.15	88%
0.233333	94%
0.4	98%
	0.00%

Table 7.65 Catalysed hydroamination of **18** using **12** at 100 °C.

time(h)	%conv
0	0%
0.033333	69%
0.066667	81%
0.1	89%
0.15	95%
0.233333	98%
0.4	100%

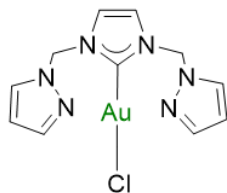
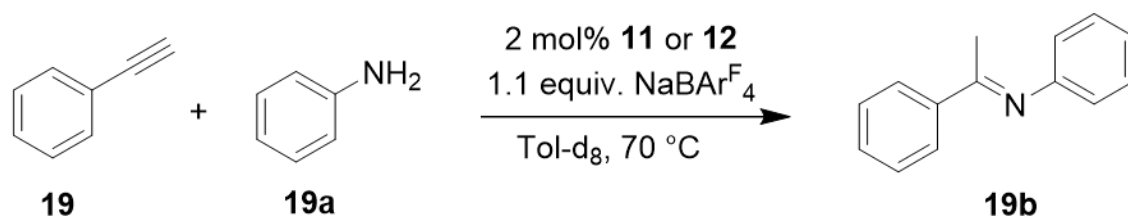
7.2.3.9. Catalysed intermolecular hydroamination of **19** with **19a** using **11** or **12**Table 7.66 Catalysed intermolecular hydroamination of **19** with **19a** using **11** at 100 °C.

Time(h)	%conv
0	0
0.033	17
0.066	20
0.15	24
0.5	27
1	28
20	31

**Table 7.67** Catalysed intermolecular hydroamination of **19** with **19a** using **12** at

100 °C.

Time(h)	%conv
0	0
0.033	9
0.066	12
0.15	16
0.5	19
1	21
20	26

**Table 7.68** Catalysed intermolecular hydroamination of **19** with **19a** using **11**

at 70 °C.

Time(h)	%conv
0	0
0.033	24
0.066	26
0.15	28
0.5	29
1	30
20	30

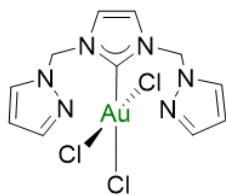


**Table 7.69** Catalysed intermolecular hydroamination of **19** with **19a** using **12** at 70 °C.

Time(h)	%conv
0	0
0.033	8
0.066	21
0.15	24
0.5	26
1	26
20	26

**7.3. References:**

- (1) Bruker, A., *Bruker AXS Inc., Madison, WI*, **2007**.
- (2) Sheldrick, G. M. *Acta Crystallogr. Sect. A: Found. Crystallogr.* **2007**, 64, 112.
- (3) Macrae, C. F.; Edgington, P. R.; McCabe, P.; Pidcock, E.; Shields, G. P. *J. Appl. Crystallogr.* **2006**, 39, 453.